

Seagate Pretrial Exhibit C

REDACTED

**IN THE UNITED STATES DISTRICT COURT
FOR THE WESTERN DISTRICT OF PENNSYLVANIA**

LAMBETH MAGNETIC STRUCTURES,)	
LLC,)	
)	
Plaintiff,)	
)	Case No. 2:16-cv-00538-CB
)	
v.)	
)	
SEAGATE TECHNOLOGY (US))	
HOLDINGS, INC. and SEAGATE)	
TECHNOLOGY LLC,)	
)	
Defendants.)	

EXPERT REPORT OF DR. ERIC E. FULLERTON

CONFIDENTIAL ATTORNEY EYES ONLY

Table of Contents

	Page
I. INTRODUCTION	1
II. QUALIFICATIONS AND EXPERIENCE	2
III. MATERIALS CONSIDERED	3
IV. SUMMARY OF OPINIONS	4
V. TECHNOLOGY BACKGROUND	5
A. Crystal Structures	5
1. Lattices and Unit Cells	5
2. Describing Planes and Directions in a Unit Cell: Miller Indices	10
3. Describing a Crystal's Orientation	14
4. Single Crystals and Polycrystalline Structures	18
B. Growing Crystals: Epitaxial Growth and Variants	19
1. Templates and Crystal Mismatches	19
2. Crystal Variants	21
C. Measuring the Crystallographic Properties of Materials	23
1. Transmission Electron Microscopy (TEM)	23
(a) Diffraction Mode and Diffraction Patterns	24
(b) Imaging Mode	35
2. X-Ray Diffraction (XRD)	37
D. Magnetism	42
1. Magnetic Anisotropy	43
2. Sources of Magnetic Anisotropy	43
3. Uniaxial Anisotropy	45
E. Measuring the Magnetic Properties of Materials	45
F. Hard Disk Drives	48
G. Write Heads	50
VI. THE '988 PATENT	54
A. Overview	54
B. Asserted Claims	60
C. Claim Construction of the Asserted Claims	61
VII. THE ACCUSED SEAGATE PRODUCTS	62
A. Overview of the Accused Products	63
B. [REDACTED]	66
C. [REDACTED]	75
D. [REDACTED]	81
VIII. LEGAL STANDARDS	83
A. Literal Infringement	83
B. Infringement Under the Doctrine of Equivalents	83
C. Indirect Infringement (Induced Infringement)	84
D. Person of Ordinary Skill in the Art	84
E. Other Legal Matters	85
IX. NON-INFRINGEMENT ANALYSIS	86
A. The Accused [REDACTED] Products Do Not Infringe Claims 1 and 27	87

1.	The [REDACTED] products do not have “at least one layer providing a (111) textured hexagonal atomic template disposed between said substrate and said bcc-d layer”	87
(a)	“layer that is predominately (111) hexagonal”	89
(i)	Dr. Clark’s FFT data for S0GPPC does not show any (111) textured NiFe layer	89
(ii)	Dr. Clark’s FFT data for S2MMMC does not show a (111) textured NiFe layer	107
(iii)	Dr. Clark’s other measurements are inconsistent with a (111) textured NiFe layer.....	120
(iv)	The extreme thinness of the NiFe layers prevents a predominate crystallographic orientation from forming	123
(b)	layer that provides “an atomic pattern upon which material is grown and which is used to direct the growth of an overlying layer”	124
2.	The [REDACTED] products do not have “at least one bcc-d layer which is magnetic, forming a uniaxial symmetry broken structure”	125
(a)	“a structure consisting of unequal volumes or unequal amounts of the bcc-d variants of a six variant system” (symmetry broken structure).....	127
(i)	Drs. Coffey & Clark fail to show the existence of any “bcc-d variants of a six variant system” in the FeCo layers	127
a)	Dr. Clark’s microbeam diffraction data does not show “bcc-d variants of a six variant system”	129
i)	Sample S0GPPC	129
ii)	Sample S2MMMC.....	140
b)	Dr. Clark’s FFT data does not show “bcc-d variants of a six variant system”	147
c)	Dr. Clark’s microbeam diffraction, ring diffraction, and dark field image data all consistently show FeCo layers with many non-(110) crystals	149
(ii)	Under LMS’s erroneous construction of “variant,” the FeCo layers contain many more than six bcc-d variants	151
a)	Microbeam Diffraction Data.....	152
i)	Sample S0GPPC	152
ii)	Sample S2MMMC.....	156
b)	Dark Field Image Data.....	157
c)	Diffraction Ring.....	162

(b)	“having an anisotropy energy density function with only a single maximum and a single minimum as the magnetization angle is rotated by 180 degrees from a physical axis” (uniaxial).....	163
(i)	Dr. Coffey cites no magnetic data whatsoever in his report.....	163
(ii)	Dr. Coffey erroneously conflates “uniaxial” with “uniaxial symmetry broken structure”—completely ignoring all other sources of magnetic anisotropy.....	168
(iii)	In lieu of relying on any magnetic data, Dr. Coffey erroneously relies on the doctrine of equivalents.....	171
(c)	“a structure that is uniaxial as a result of the structure being symmetry broken” (uniaxial symmetry broken structure).....	173
(i)	Overview of Dr. Coffey’s method of calculating anisotropy.....	175
(ii)	Dr. Coffey erroneously assumes that Dr. Clark’s dark field image data depicts only bcc-d(110) crystals.....	179
(iii)	Dr. Coffey ignores the actual empirical data, and instead calculates anisotropy using made up data that guarantees a uniaxial outcome.....	184
(iv)	Dr. Coffey makes additional errors in his anisotropy calculation, which is purely theoretical.....	185
B.	The Accused [REDACTED] Products Do Not Infringe Claims 1 and 27.....	190
1.	The [REDACTED] products do not have “at least one layer providing a (111) textured hexagonal atomic template disposed between said substrate and said bcc-d layer”.....	190
(a)	“layer that is predominately (111) hexagonal”.....	191
(i)	Dr. Clark’s FFT data for SBRD8K does not show a (111) textured NiFe layer.....	192
(ii)	Dr. Clark’s other measurements are inconsistent with a (111) textured NiFe layer.....	203
(iii)	The extreme thinness of the NiFe layers prevents a predominate crystallographic orientation from forming.....	205
(b)	layer that provides “an atomic pattern upon which material is grown and which is used to direct the growth of an overlying layer”.....	206

2.	The [REDACTED] products do not have “at least one bcc-d layer which is magnetic, forming a uniaxial symmetry broken structure”	207
(a)	“a structure consisting of unequal volumes or unequal amounts of the bcc-d variants of a six variant system” (symmetry broken structure).....	209
(i)	Drs. Coffey & Clark fail to show the existence of any “variants” in the FeCo layers.....	209
a)	Dr. Clark’s microbeam diffraction data does not show any “bcc-d variants of a six variant system”	210
b)	Dr. Clark’s FFT data does not show “bcc-d variants of a six variant system”	215
c)	Dr. Clark’s microbeam diffraction and dark field image data consistently show FeCo layers with many non-(110) crystals	217
(ii)	Under LMS’s erroneous construction of “variant,” the FeCo layers contain many more than six bcc-d variants	218
a)	Microbeam Diffraction Data.....	218
b)	Dark Field Image Data.....	220
(b)	“having an anisotropy energy density function with only a single maximum and a single minimum as the magnetization angle is rotated by 180 degrees from a physical axis” (uniaxial).....	223
(i)	Dr. Coffey cites no magnetic data whatsoever in his report	223
(ii)	Dr. Coffey erroneously conflates “uniaxial” with “uniaxial symmetry broken structure”—completely ignoring all other sources of magnetic anisotropy	227
(iii)	In lieu of relying on any magnetic data, Dr. Coffey erroneously relies on the doctrine of equivalents	230
(c)	“a structure that is uniaxial as a result of the structure being symmetry broken” (uniaxial symmetry broken structure).....	233
(i)	Overview of Dr. Coffey’s method of calculating anisotropy	234
(ii)	Dr. Coffey erroneously assumes that Dr. Clark’s dark field image data depicts only bcc-d(110) crystals	238

	(iii) Dr. Coffey ignores the actual empirical data, and instead calculates anisotropy using made up data that guarantees a uniaxial outcome	242
	(iv) Dr. Coffey makes additional errors in his anisotropy calculation, which is purely theoretical	243
C.	The Accused [REDACTED] Products Do Not Infringe Claims 1 and 27.....	248
1.	The [REDACTED] products do not have “at least one layer providing a (111) textured hexagonal atomic template disposed between said substrate and said bcc-d layer”	248
2.	The [REDACTED] products do not have “at least one bcc-d layer which is magnetic, forming a uniaxial symmetry broken structure”	251
D.	The Accused Products Do Not Infringe the Other Asserted Claims of the '988 Patent.....	254
X.	ANALYSIS REGARDING INDIRECT INFRINGEMENT	254
XI.	ANALYSIS REGARDING DAMAGES ISSUES	255
A.	PMR.....	255
B.	Comparability of Certain Licensed Patents to the '988 Patent.....	261
1.	“Jülich” Patent	261
2.	“Censtor” Patents.....	264
3.	Carnegie Mellon University Patents	267
4.	Syndia License	269
5.	White License	270
6.	“Dual Stripe MR Technology”	271

I. INTRODUCTION

1. I have been retained by Seagate Technology (US) Holdings, Inc. and Seagate Technology, LLC (“Seagate”) as an independent expert witness in connection with the patent litigation brought by Lambeth Magnetic Structures, LLC (“LMS”) against Seagate. I have been asked to provide a report and to testify in this case on certain topics including, among other things, whether certain Seagate products infringe U.S. Patent No. 7,128,988 (“the ’988 Patent”).

2. My opinions and the bases for my opinions are contained in the remainder of this report. If Seagate calls me as a witness in this matter, I currently expect that my testimony will relate to the issues described in this report, including: the subject matter of the ’988 Patent, the function and development of the accused Seagate products, and whether any accused Seagate product infringes any of the asserted claims of the ’988 Patent, either literally or under the doctrine of equivalents. I generally refer to the accused Seagate products at issue here as the “Accused Products.”

3. I am being compensated for my work on this matter at a rate of \$350 per hour, with reimbursement for actual reasonable expenses. I have no other interest in this matter, and my compensation does not depend on the outcome of this case.

4. If I am called to testify in this matter, I may use as exhibits various documents produced in this matter that refer or relate to the matters discussed in this report. I may also use as exhibits photos, videos, or other graphical or multimedia presentations depicting or illustrating the matters discussed in my report. I may also use as exhibits physical samples of materials referred to in this report. I have not yet selected the particular exhibits that might be used. In addition, I reserve the right to and may create or assist in the creation of certain demonstrative exhibits or summaries of my findings and opinions to assist me in testifying.

5. I may testify as an expert regarding additional matters, including (i) to rebut positions that LMS takes, including opinions of their experts and materials they discuss or rely upon, (ii) based on any Orders from the Court, (iii) based on documents or other discovery that LMS or other parties have not yet produced or that were produced too late to be fully considered before my report was due, or (iv) based on recent depositions or other deposition or witness testimony which has not yet been

given. I reserve the right to supplement or amend this report based on such materials and information.

II. QUALIFICATIONS AND EXPERIENCE

6. My qualifications for forming the opinions set forth in this report are summarized here and are presented more fully in my curriculum vitae, which is attached as Exhibit B to this report.

7. I am a Professor at the University of California, San Diego (“UCSD”) in the Department of Electrical and Computer Engineering and in the Department of NanoEngineering. I also am the Director of the Center for Memory and Recording Research (“CMRR”) at UCSD. CMRR has five endowed professorships, more than ten post-doctoral researchers, and over 65 graduate student researchers that focus on the scientific and engineering disciplines underlying modern information storage technologies: magnetic materials and devices; micromagnetics and recording physics; mechanical interfaces and tribology; and information theory, coding, and signal processing. While at UCSD, my research has focused on thin film magnetic and nano-materials, thin film superlattice growth, magnetic recording and memory technologies, and x-ray and neutron scattering.

8. I earned a Bachelor of Science degree (1984) in Physics at Harvey Mudd College. I earned both a Master of Science degree (1986) and a Ph.D. in Physics (1991) from the University of California, San Diego. My Ph.D. thesis related to the structural characterization of crystalline superlattices.

9. Before joining UCSD, I held a variety of professional and academic positions. I was a postdoctoral appointee and then physicist at the Argonne National Laboratory. I then joined the IBM Almaden Research Center as a research staff member, where my division eventually became part of Hitachi Global Storage Technologies. I continued to work in this division for several years as a senior manager and research scientist, with a focus on the development of high density magnetic recording media based on ferromagnetic thin films.

10. I am a member of numerous professional societies and organizations, including the Materials Research Society and the American Vacuum Society. I also am a Fellow of the American Physical Society and IEEE. I am a past winner of the Exceptional Achievement Award at Argonne National Laboratory, the IBM Outstanding Achievement Award, the IBM Fourth Plateau Invention Achievement Award, and the American Institute of Physics Prize for Industrial Applications of Physics. I recently was elected as a member of the National Academy of Engineering class of 2018.

11. I have published over 300 papers in the field of thin films, crystalline materials, magnetic materials, and nano-engineering, and have edited books and contributed chapters of books in several of these areas.

12. I also am an inventor on 51 issued U.S. Patents, including U.S. Patent No. 6,280,813 entitled Magnetic Recording Media with Antiferromagnetically Coupled Ferromagnetic Films as the Recording Layer, which was selected as one of the *Five Patents to Watch* by the Massachusetts Institute of Technology's Technology Review magazine and ranked as among the top 10% most valuable IBM patents. I was awarded the Hitachi Global Storage gold patent award twice.

13. My curriculum vitae (Exhibit B) contains further details on my education, experience, publications, patents, and other qualifications. In the preceding four years, I have not testified as an expert at trial or by deposition in any other matter.

III. MATERIALS CONSIDERED

14. In forming my opinions and writing my report for this case, I have reviewed the '988 Patent, including the '988 Patent's claims, specification, drawings, and prosecution histories (for both the U.S. and European applications). I also have reviewed documents and things produced by Lambeth and Seagate in this case, as well as deposition testimony, discovery responses, public web sites, and the Court's Claim Construction Order, among other things.

15. I have extensively reviewed LMS's Infringement Contentions and Amended Infringement Contentions, as well as the expert reports submitted by Dr. Kevin Coffey and Dr. William Clark. In addition, I have extensively reviewed testing

data and other materials produced in connection with Dr. Coffey's and Dr. Clark's reports. Examples of such materials are cited throughout my report.

16. I also have reviewed testing data provided by Dr. Eric Stach as described in his expert report. I believe that Dr. Stach's additional discussion of the technology is accurate and I agree with his opinions and conclusions, which I have considered in forming my own opinions.

17. A summary of materials I reviewed or considered in connection with this report is set forth in Exhibit D. I may rely on those materials, in addition to materials specifically cited as supportive examples in particular sections of this report, as support for my report and my opinions. In addition, I may rely on my own prior industry and technical experience, and my professional and academic expertise in the fields of thin film science and magnetism. I reserve the right to supplement and amend my opinions as more information or documents are received.

IV. SUMMARY OF OPINIONS

18. I expect to testify on issues pertaining to the '988 Patent, and in particular regarding my opinions as to whether Seagate infringes any of the Asserted Claims of the '988 Patent. I may also provide a tutorial (including physical samples, photos, videos, or other graphical or multimedia presentations depicting or illustrating the matters discussed in my report) on the technology relating to the '988 Patent. I also expect to testify regarding the development, manufacture, operation, properties, and other aspects of the Accused Products.

19. Based on my investigation and review of the information made available to me in this matter and my own investigation, combined with my knowledge and experience, I have developed an understanding of the Accused Products. I have been asked to analyze whether the Accused Products infringe any of the asserted claims of the '988 Patent. The details of my analysis are provided below.

20. It is my opinion that the Accused Products do not infringe any of the following claims of the '988 Patent, which I refer to as the "Asserted Claims": 1, 3, 6, 7,

9, 17, 19, 27, 28, and 29. It is my opinion that none of the Accused Products infringe any of the Asserted Claims either literally or under the doctrine of equivalents.

21. In addition, I express further opinions in the remainder of my report.

22. All of my opinions, and the bases of those opinions, are true and correct to the best of my knowledge and belief, including those related to scientific issues, which I believe are true and correct to a reasonable degree of scientific certainty.

V. TECHNOLOGY BACKGROUND

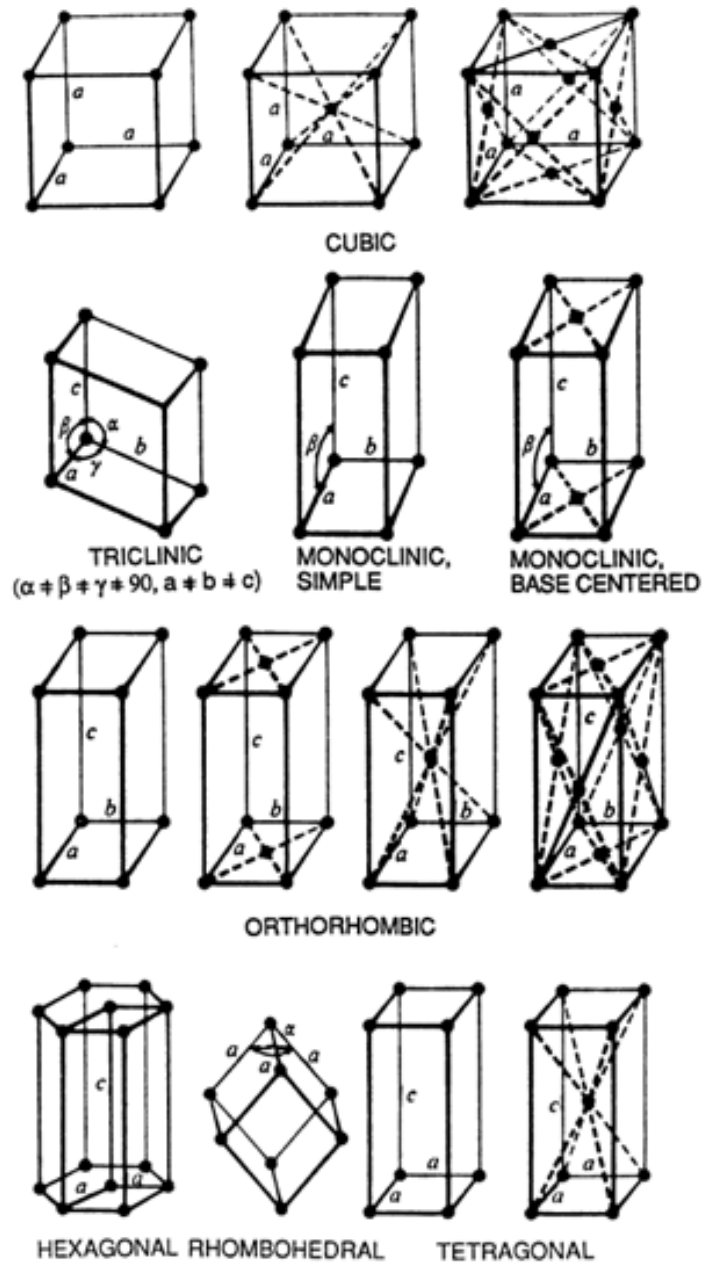
23. In this section, I describe technology related to the '988 Patent, hard disk drives, and related matters.¹

A. Crystal Structures

1. Lattices and Unit Cells

24. A crystal structure is a structure formed from a repeating pattern of atoms that are organized in a particular way. Crystal structures are characterized by a long range geometric order on the atomic scale. This highly ordered geometry takes the shape of a three-dimensional repeating pattern of atoms that is often referred to as a crystal lattice. There are many different types of crystal lattices that repeat a basic pattern outward in each direction. A single building block representing the pattern in the lattice is referred to a "unit cell." Examples of a number of different types of unit cells are shown in the illustration below:

¹ In preparing this section, I adapted portions of the declaration I previously prepared in connection with the Court's claim construction hearing, along with new material. In addition, I have reviewed and adapted certain descriptions of the technology found in the expert reports of Dr. Caroline Ross and Dr. Eric Stach, both of which contain accurate and helpful overviews of some of the technology at issue in my non-infringement analysis. For example, I use certain graphics and sources that also appear in Dr. Ross's and/or Dr. Stach's reports where appropriate.



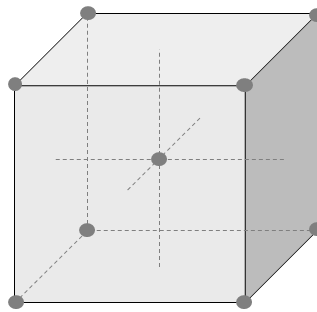
(M. Ohring, MATERIALS SCIENCE OF THIN FILMS (2nd ed. 2001) (“Ohring”), at 3.)

25. The simplest type of crystal lattice is the cubic lattice, shown as a unit cell in the top row in the illustrations above. A cubic lattice will have atoms arranged at the corners of the cube. The dimensions of the cubic unit cell are labeled as “a” above in the illustration above. This dimension is known as a “lattice parameter.” For non-cubic lattices, the lattice parameters will have different dimensions—represented above by “a,”

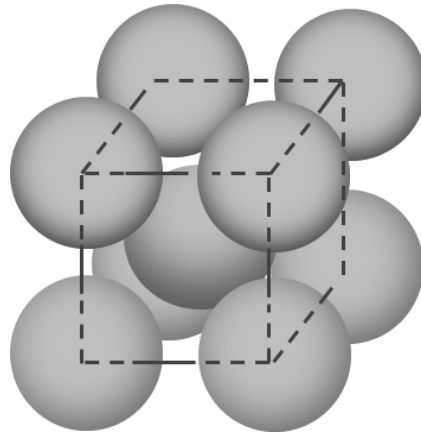
“b,” and “c” for some of the unit cells shown above. The unit cell shown in the lower left of the illustration above is for a hexagonal lattice. In this lattice, the atoms are arranged at the vertices of a hexagonal prism and in center of the face of each hexagon.

26. When no long-range repeating atomic structure is present in a material—so that the distances between atoms do not regularly repeat or if they become randomly distributed—the material is no longer considered crystalline. Such random networks of atoms are described as amorphous structures.

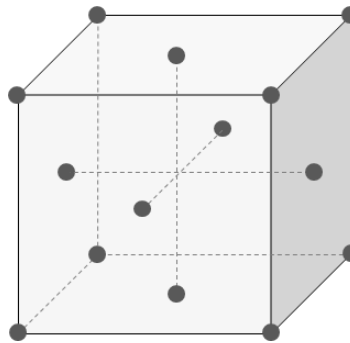
27. There are several types of lattices that are most pertinent to this case. One of those is the body centered cubic (bcc) lattice, which is shown below as a unit cell:



28. In the above illustration, the gray atoms are located at each corner of the cube, and a single atom is also located in the center of the body of the cube (hence “body centered cubic”). While the above illustration makes it easier to envision the cubic nature of the crystal lattice, in reality, there are no lines between the corner atoms (the lines represent atomic bonds) and the atoms are much larger, as shown in the illustration below:

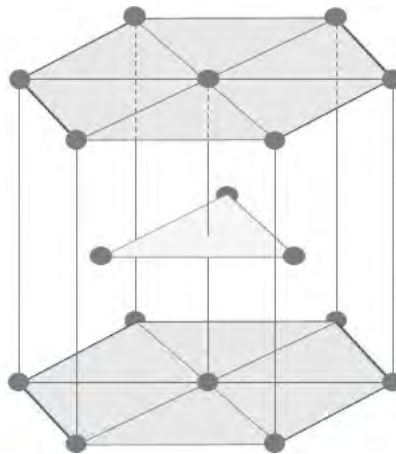


29. Another type of cubic crystal lattice pertinent to this case is a face centered cubic (fcc) lattice, which is shown as a unit cell below.

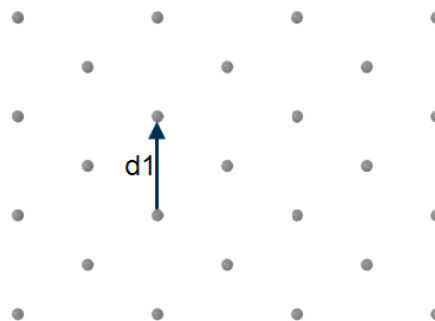


30. Like the bcc lattice, the fcc unit cell also has atoms at each corner of the unit cell. In contrast to the bcc lattice, the fcc unit cell contains atoms centered in each face of the unit cell cube.

31. A third type of crystalline lattice pertinent to this case is the hexagonal close-pack lattice, which has a unit cell that appears as follows:



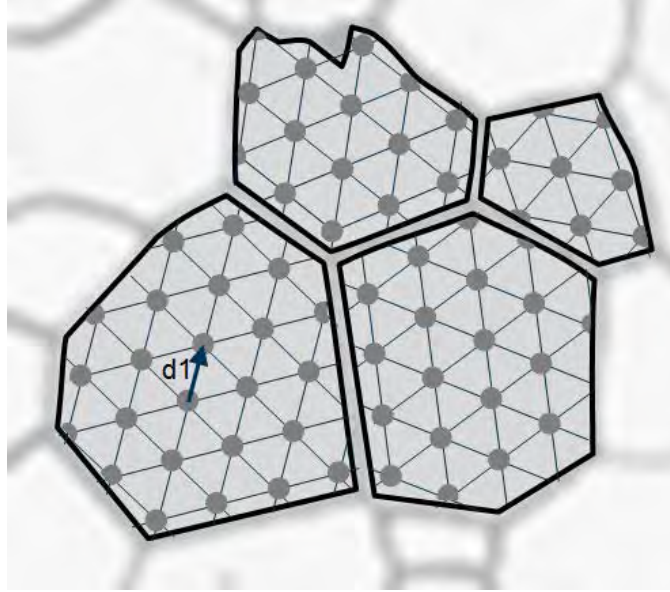
32. As noted above, the dimensions of the unit cell are referred to as “lattice parameters.” Single crystals have regular, repeating atomic spacings in all directions across the entire crystal. This is referred to as “translational periodicity.” As shown in the figure below, translational periodicity means that a single crystal will have a common distance between its atoms in any given direction:



33. For example, the distance $d1$, represented above by lattice parameter $d1$, will be replicated between atoms in that direction throughout the crystalline lattice.

34. A polycrystalline structure is a structure comprising multiple single crystals. Polycrystalline structures will have local translational periodicity, but will not have translational periodicity across the entire structure. In other words, the translational periodicity is changed when moving from one crystal to the next within the structure. The crystals in a polycrystalline structure are often referred to as “grains.” The illustration below shows an example of a material with a polycrystalline structure, with

four grains outlined in black. Each grain has translational periodicity within the boundaries of the grain:

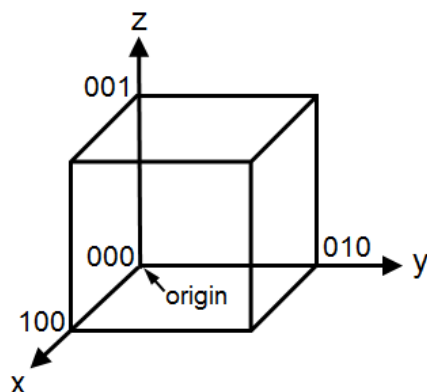


35. Materials that are amorphous will not have regular, periodic long-range spacing. In these types of materials, an atom cannot necessarily be found at a certain distance in a given direction from another atom

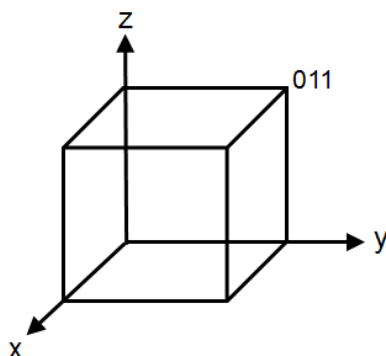
2. Describing Planes and Directions in a Unit Cell: Miller Indices

36. While unit cells are helpful in conceptualizing the relative distances and arrangement of atoms in a crystal, unit cells by themselves do not describe the *orientation* of the crystal lattice as it grows and repeats itself. Therefore, a three-dimensional coordinate system called the Miller index was developed to describe a crystal lattice's orientation, including specific planes and directions within the crystal lattice.

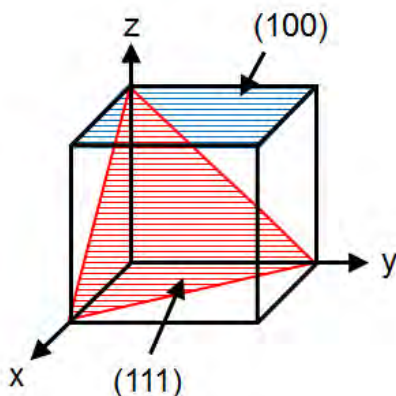
37. Here is how that system works for a cubic crystal. First, the origin (0,0,0) of the coordinate system is selected by choosing one of the corners of the cube, with the x, y, and z axes lying along the edges of the cube, as shown in the example below. In this example, the origin is in the lower back left corner of the unit cube, and is represented by (x, y, z) coordinates as (0,0,0):



38. Once that selection is made, each corner of the cube is represented by the appropriate (x, y, z) coordinates. For example, the upper right corner of the cube is located at 0 on the x-axis, 1 on the y-axis, and 1 on the z-axis, so the coordinates (011) would refer to that corner, as shown below:



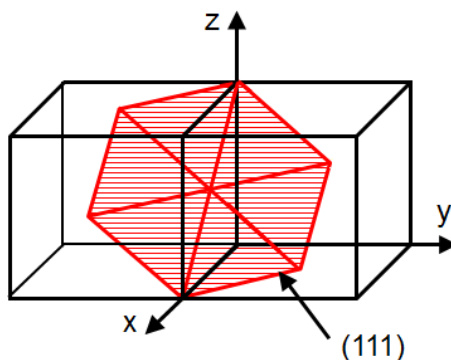
39. The same coordinate system is used to represent planes in a crystal lattice. The three steps to determine the coordinates for a plane using the Miller index are as follows: (1) determine the intercepts of the plane on the three axes (x, y, z) of the unit cell; (2) take the reciprocals of those numbers; and (3) reduce those reciprocals to the smallest integer by clearing fractions. (Ohring, at 5.) Two exemplary planes are shown below: the (001) plane on the top of the unit cell appears in blue, and the (111) plane, a triangle with vertices at corners of the unit cell appears in red:



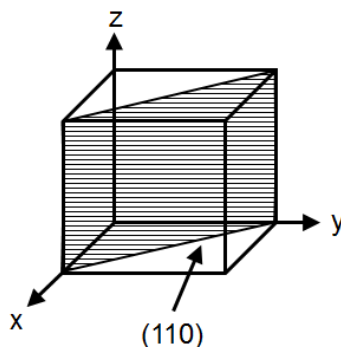
40. As can be seen in the illustration above, the (001) plane intersects the z-axis at 1. However, the (001) plane does not intersect the x or y axes at all, a condition which is represented by 0. The reciprocal of the z-axis intercept is $1/1$, which reduces to 1. As there are no fractions to clear, we are left with (001) to describe the top plane of the unit cube, which is shown in blue above.

41. Similarly, with the (111) plane, we see that it intersects the x-axis and 1, the y-axis at 1, and the z-axis at 1. The reciprocal of 1 is 1, and there are no fractions to clear, so we are left with (111) for the triangular plane, which is shown in red above.

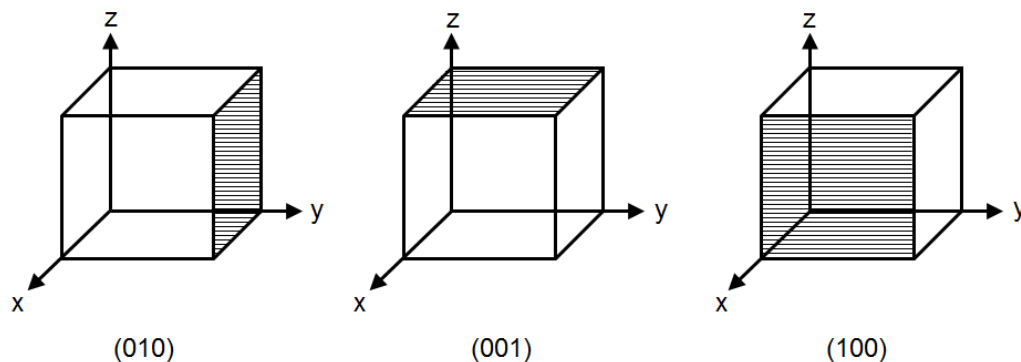
42. The (111) plane can also be viewed as hexagonal, by selecting six of the above triangular planes intersecting multiple unit cells:



43. Another example of a crystal plane is the (110) plane. As can be seen in the illustration below, the (110) plane intersects the x-axis at 1, and the y-axis at 1, but does not intersect the z-axis, producing a Miller index of (110) for this plane:



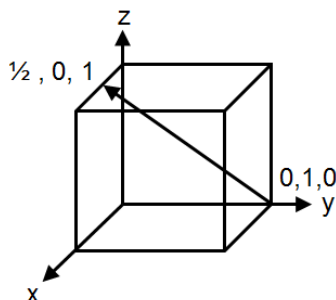
44. In the Miller index system, parentheses () are used to indicate a single plane, while a family of planes is indicated by braces { }. Planes within the same family are related by the symmetry of the lattice. For example, the faces of a cubic unit cell, which are (010), (001), and (100), are all part of the same {100} family of planes, as shown below:



In general, in a cubic system, the three Miller Index digits are interchangeable within the same family. For example, as long as you have two “zeroes” and one “one,” you are in the {100} family of planes. Likewise, as long as you have two “ones” and one “zero,” you are in the {110} family of planes. Thus, (110), (101), and (011) are all in the same family of planes, and are related via symmetry. In other words, there is no physical difference between the members of these family of planes, and the digits can be exchanged because in a cubic structure their order is based on a wholly arbitrary choice of the initial unit axes, a, b and c.

45. The Miller index can also be used to describe directions within crystalline structures. A single direction is indicated with brackets [], while a family of directions

is indicated by angle brackets $\langle \rangle$. In order to describe a direction, the coordinates of the starting point are subtracted from the end point, as shown below for the direction $[122]$:



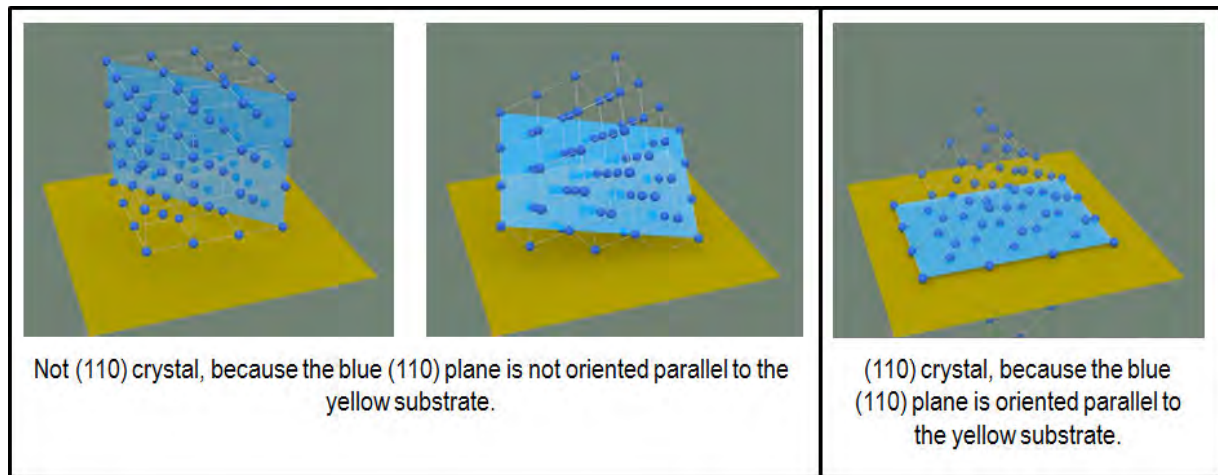
46. Subtracting the starting point from the ending point results in $\frac{1}{2} - 0$, then $0 - 1$, and finally $1 - 0$, producing $[\frac{1}{2}, -1, 1]$. Clearing the fractions produces $[1, -2, 2]$, which is written as $[1\bar{2}2]$, where the bar over the number represents a negative number.

47. Once a plane is identified, it is also possible to calculate the angle between two planes by calculating their vector dot product. Such calculations are useful, for example, in determining whether two planes are perpendicular to one another.

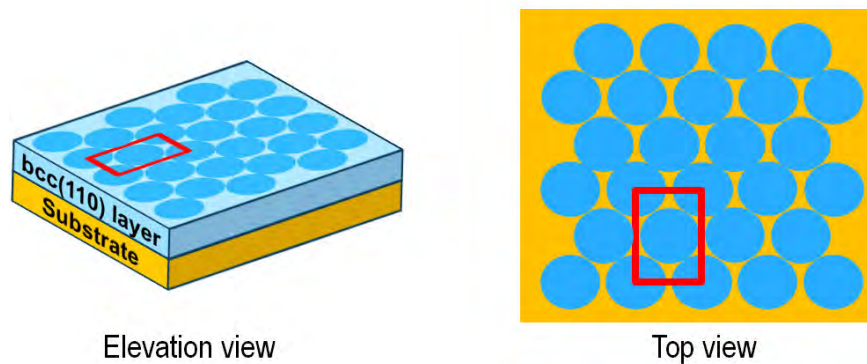
3. Describing a Crystal's Orientation

48. The planes and directions discussed above may be used to describe a particular crystal's orientation, such as with respect to the underlying crystal on which the crystal is grown.

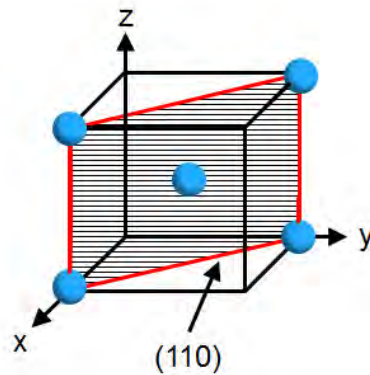
49. The illustration below shows how a bcc(110) plane, highlighted in blue in a bcc lattice, is rotated in order to be parallel to the substrate, shown in yellow:



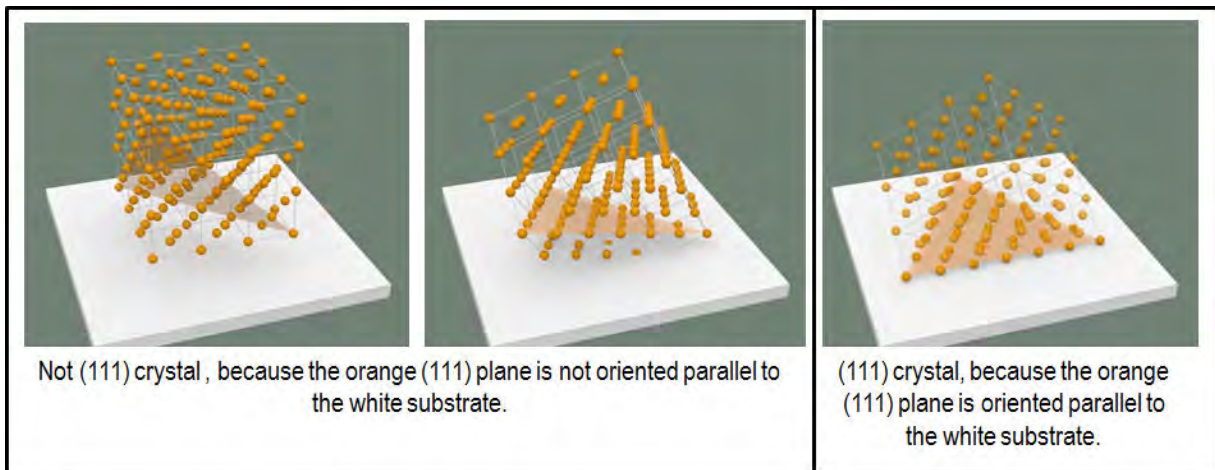
50. Another way of visualizing the bcc(110) texture is to view a single bcc (110) plane, and the atoms that define that bcc(110) plane, from an elevation view and a top down, or plan view perspective. This is shown below:



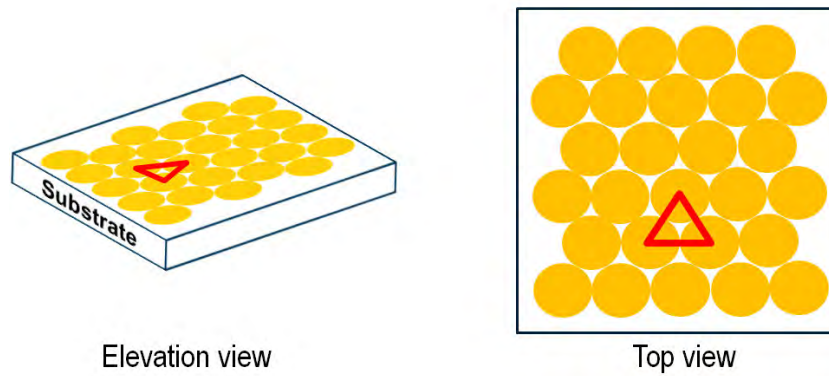
51. The bcc(110) plane for a single unit cell is highlighted in a red rectangle above. This is the same plane that was illustrated earlier (§ 43, *supra*) and is reproduced once again below, with the rectangular shape highlighted in red:



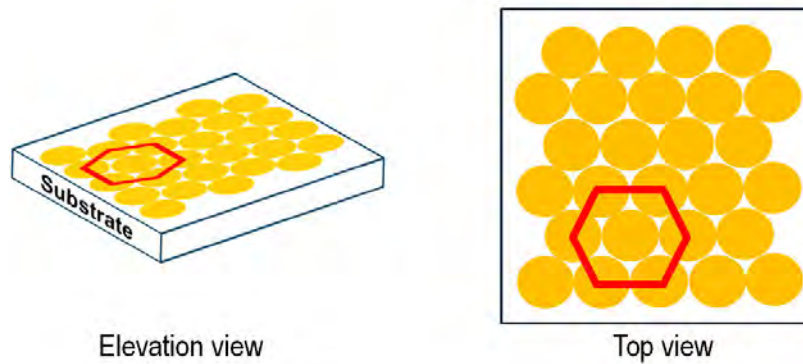
52. As another example, an fcc(111) textured material refers to a material in which the atoms are arranged in face-centered cubic unit cells *and* whose unit cells are predominantly oriented with their (111) plane parallel to the underlying layer (substrate). The illustration below shows how an fcc(111) plane, highlighted in orange in a fcc lattice, is rotated in order to be parallel to the substrate, shown in white:



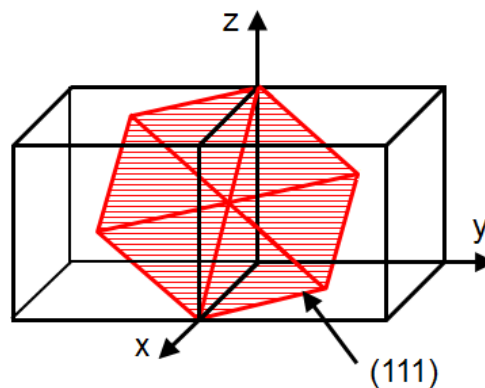
53. Another way of visualizing the fcc(111) texture is to view a single fcc(111) plane, and the atoms that define that fcc(111) plane, from an elevation view and a top down or plan view perspective, as follows:



54. The fcc(111) texture can also be visualized as a hexagon comprising multiple triangles, as shown below:



55. The fcc (111) plane for a single unit cell is highlighted in a red hexagon above. This is the same plane we saw earlier in discussing where this plane appears when viewed as a cubic cell, as reproduced below:

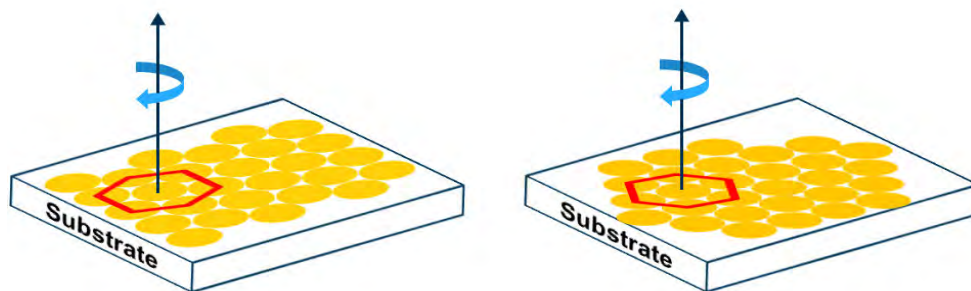


56. Some crystal structures may have multiple crystals with different orientations relative to the underlying substrate on which they are grown. When most of the crystals in a structure have the same orientation—*i.e.*, when a specific orientation predominates throughout the polycrystalline structure—we refer to that predominate orientation as the “crystal texture” (or simply “texture”). (*See, e.g.*, ’416 Patent at 2:36-40.) For example, a bcc(110) “textured” material refers to a material in which the atoms are arranged in body-centered cubic unit cells *and* whose unit cells are predominantly oriented with their (110) plane parallel to the underlying substrate.

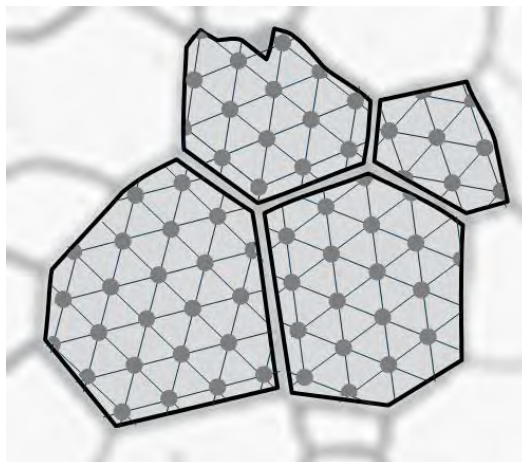
4. Single Crystals and Polycrystalline Structures

57. Crystal structures may also be made up of multiple crystals that have the same orientation relative to a substrate (*e.g.*, they may have be bcc(110) crystals), but different in-plane orientations. We refer to each crystal with a different in-plane orientation as a *grain*, and the boundary between two grains is called a grain boundary.

58. For example, an fcc(111) textured structure may have many different fcc(111) crystals (grains), each of which are rotated differently within the (111) plane. Rotation of an fcc(111) crystal within the plane is illustrated below, with the atoms of the fcc(111) crystal represented by the red hexagon rotated clockwise within the plane of the substrate:



59. For example, a polycrystalline structure with four fcc(111) grains with different in-plane orientations is shown below:



B. Growing Crystals: Epitaxial Growth and Variants

60. Epitaxial growth describes the process of growing crystals on top of an underlying material. The process of epitaxial growth can be accomplished using several techniques, including deposition of a material as a gas through sputtering, or deposition as a liquid using electroplating, on an underlying layer.

61. The interaction between the underlying material and the overlying crystal can be important in determining how the overlying crystal grows and develops, including how it orients itself relative to the underlying material. For example, if the overlying crystal has a different orientation than an underlying crystal layer, then the overlying crystalline lattice is often distorted as it attempts to match the atoms of the underlying lattice. The lattice mismatch between the overlying layer and the underlying material can therefore play a role in how the overlying layer grows. (*See, e.g.,* Ohring at 316-322.)

1. Templates and Crystal Mismatches

62. In epitaxial growth, when the underlying layer directs the growth of crystals in the layer grown on top of it, the underlying layer is often referred to as a “template.” (*See, e.g.,* Ohring, at 360-361.)

63. The interaction between the underlying and overlying material can be important in determining how the overlying crystal develops, including how it orients itself and its crystallographic properties relative to the underlying material. For example, when an overlying material is the same as the underlying material and grows

with the same crystallographic orientation as the underlying material (known as “homoepitaxy”), then the atoms of the overlying crystal will tend to align with the atoms of the underlying crystal. On the other hand, if the overlying crystal is a different material than the underlying crystal and grows with a preferred crystallographic orientation (known as “heteroepitaxy”), then the overlying crystal lattice is often distorted as it attempts to match the atoms of the underlying crystal. The lattice mismatch and the difference in crystalline symmetry between the overlying layer and the underlying material can therefore play a role in how the overlying layer grows. (*See, e.g.,* Ohring at 316-322.)

64. It is important to note that not all materials will function as a template—*i.e.*, not all materials will direct the growth of an overlying layer. For example, materials that have not formed a crystal structure will not direct the growth of an overlying layer and so do not function as a template. Materials can fail to form a crystal structure (thus disqualifying them from acting as template) for various reasons. For example, amorphous materials typically do not develop any crystal structure.

65. In addition, layers that are only a few atomic layers thick often exhibit no long-range crystal structure, as a crystal structure tends to develop and evolve as a layer grows in thickness. (*See, e.g.,* ’416 Patent at 11:6-9 (“The wetting layer 18 can be an amorphous material or a film too thin to have developed a crystalline texture, or a film whose texture provides a gross lattice mismatch for the ensuing layer.”); D. Lambeth et al., *Magnetic Media Performance: Control Methods for Crystalline Texture and Orientation*, Mat. Res. Soc. Symp. Proc. Vol. 517, p. 185 (1998) (“[B]elow 5 nm the Cr is so thin that little or no crystalline texture has evolved”); Patent Owner’s Preliminary Response to IPR2016-00013, at 42 (“One common feature in deposition of ultrathin films is that in many cases pseudomorphic growth occurs over several monolayers before the film converts into its usual crystal structure.”); *id.* at 43 (“In other words, an epitaxially grown ultrathin film will commonly have a pseudomorphic or metastable non-equilibrium crystalline structure for the first several monolayers. Such crystalline structures will not have formed into stable fcc or bcc structures. . . . Dr. Sinclair chose to ignore the fact that the layers at issue are ultrathin and therefore could

not have formed equilibrium crystalline structures.”); *id.* at 43-44 (distinguishing prior art: “Dill never described the crystalline structure of the interface layer . . . but the thickness of that interface layer (i.e., 0.4-2 nm) indicates that it was pseudomorphic fcc and could not have been in equilibrium crystalline phase.”); Ohring, at 529 (“Sometimes, texture evolves from random in initial deposits to strong orientation of low-energy planes parallel to the film surface, and finally, to changes in preferred texture as the film thickens further.”). As a result, very thin layers often feature no crystal structure and so do not function as a template for layers grown above them. (*See, e.g., id.*)

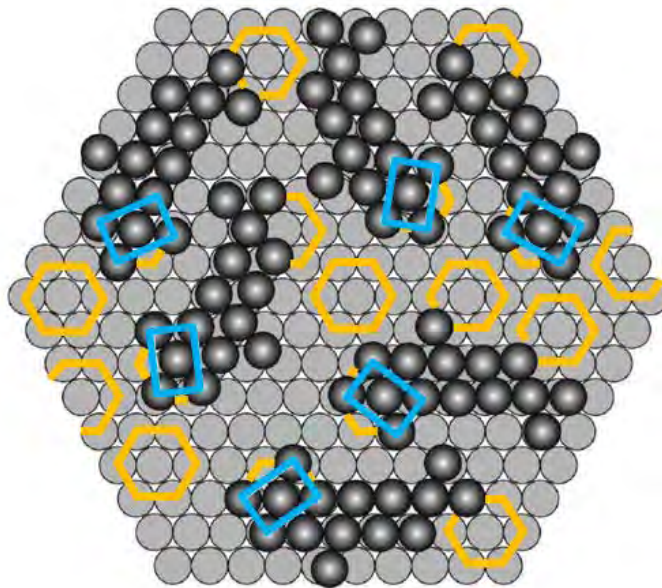
2. Crystal Variants

66. In epitaxial growth, there is often a mismatch between the crystal lattices and/or difference in the crystal symmetry of the materials. In these instances, this mismatch can cause the overlying crystals to form in multiple different orientations relative to the underlying crystal template. The '988 Patent calls a specific set of these possible crystals “variants.” (*See, e.g., '988 Patent at 23:38-41, 54-64.*) I understand that the Court construed the term “variant” to mean “one of a set of possible crystal orientations.”

67. Each variant has a different in-plane orientation relative to the orientation of the underlying template crystal. This orientational relationship between the variant and the underlying template defines the variant—*i.e.*, each variant is defined by an angle of rotation relative to the underlying crystal. What sets of variants can form in the overlying layer depends on a number of factors, including the crystal structure of each layer, the degree of lattice mismatch between the overlying and underlying layers, the film thickness of the overlayer, and deposition conditions such as temperature, deposition rates, and pressure. (*See, e.g., Dahmen, Orientation Relationships in Precipitation Systems, Acta Metallurgica, 30(1) 63-73 (1982)*) at 63; Gotoh, *Interpretation of the Epitaxial Orientation Relationship at bcc(110)/fcc(111) Interfaces, Applied Surface Science 33/34 443-49 (1988)*, at 443.)

68. The '988 Patent is directed to a “six-variant system,” *i.e.*, a system where there are six possible ways for bcc(110) crystals to form over an underlying (111)

textured hexagonal atomic template. (*See, e.g.*, '988 Patent at 14:48-52 (“By carefully controlling the epitaxial growth conditions of (110) crystalline extrude bcc or bcc derivative thin film materials on highly oriented (111) hexagonal atomic templates the applicant has invented a new set of six crystalline variants with special orientational relationships.”), FIG. 5, 13:39-42, 18:33-45 (defining the orientational relationships of the six variants).) To illustrate this concept, the diagram below shows a top-down representation of several crystal variants and their orientational relationship relative to a single underlying hexagonal crystal (*i.e.*, a single crystal template):



69. The light-gray circles represent atoms of an underlying hexagonal crystal template, and the yellow hexagons represent the orientation of that hexagonal crystal template. The dark-gray circles on top represent atoms of overlying bcc(110) crystals, and the blue rectangles depict the different bcc(110) crystals orientations that form with respect to the underlying template. The blue rectangles have different in-plane orientations relative to the underlying yellow hexagons. Each of the rectangles is a bcc(110) crystal variant, meaning it is one of the six possible ways in which a blue rectangle (variant) can orient itself relative to the underlying yellow hexagonal crystals (the template). This therefore shows the six-variant system of the '988 Patent— there

are six bcc(110) variants that can form, each with a different orientational relationship with respect to the underlying hexagonal atomic template.

70. As discussed in more detail below (*see* Section VI.A), the central feature of the '988 Patent is its theory that growing particular exchange-coupled combinations of these six crystal variants in the magnetic layer of a thin film will result in certain desirable magnetic properties.

C. Measuring the Crystallographic Properties of Materials

71. A number of methods can be used to test for and measure the crystallographic properties of the layers in a thin film, including its crystal structure, the presence of any texture, and the nature and orientation of its variants.

72. A common method for determining the crystal structure of a material is to measure the translational periodicity of the material's atoms. This can be done through x-ray or electron beam diffraction. X-rays and electron beams have particular wavelengths and they interact with the atoms in the material when traveling through the material. When the lattice planes are aligned at specific angles to the incoming x-ray or electron beams they will scatter with increased intensity. For example, with a single crystal, the periodic spacing of the atoms will cause the x-ray or electron beam to diffract at specific angles and intensities.

1. Transmission Electron Microscopy (TEM)

73. TEM is used to view materials at extremely high magnification levels. Instead of using light, as optical microscopes do, TEM uses electrons to image a sample. In essence, TEM transmits electrons through a very thin slice of material onto a screen, and then an imaging device creates an image of the electrons that passed through the sample or collects a diffraction pattern from where the electrons have scattered from the sample. TEM takes advantage of the exceptionally short wave length of electrons to produce images or scattering patterns of objects with better than 1 nm spatial resolution.

74. There are several basic modes of TEM operation, including image mode and diffraction mode. Image mode produces a black and white image, much like the image produced by a light microscope. Diffraction mode, in contrast, produces a pattern

of spots that can be analyzed to determine the crystal structure (if any) of the sample. An example of each is shown below:

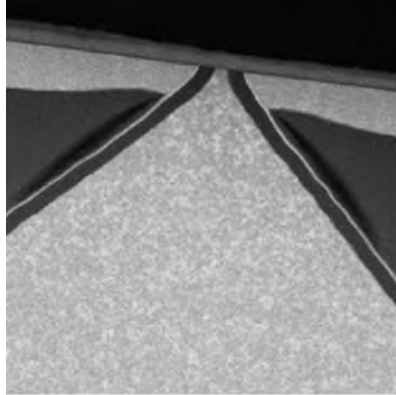
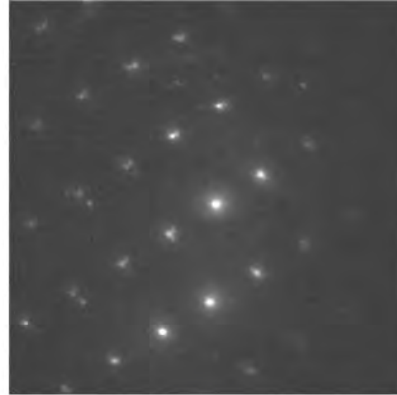


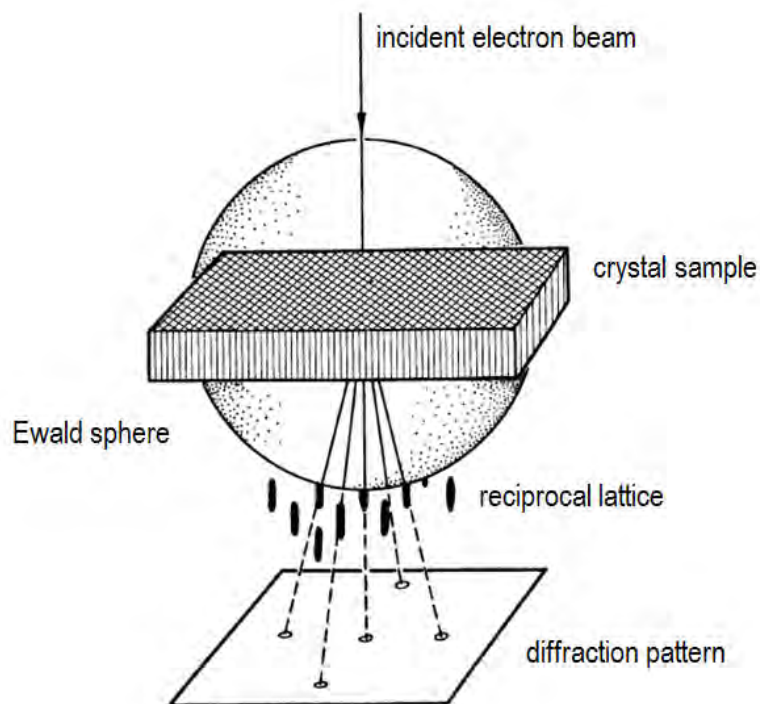
Image Mode



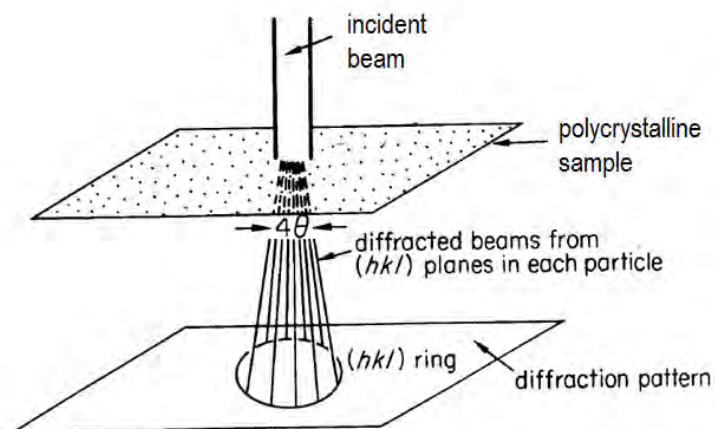
Diffraction Mode

(a) Diffraction Mode and Diffraction Patterns

75. Diffraction patterns, as explained above, are a pattern of regularly repeating spots that reflect the particular structure and shape of the sample's crystal lattice. Diffraction patterns provide information about the arrangement of atoms in the material, which is related to the crystal structure. Diffraction patterns are formed in "reciprocal space." Because there is a 'reciprocal' relationship between the location of atoms in real space and the diffraction pattern, there thus exists a 'reciprocal space' wherein the information about potential diffraction events is contained. The particular pattern of spots formed in this reciprocal space depends on the particular orientation relationship between the incident electron beam and the crystal orientation: this orientation relationship thus determines the diffraction pattern that is formed. An illustration of a beam passing through a sample and creating a series of spots in reciprocal space is illustrated below:



76. In a single crystal sample, the resulting diffraction pattern will be a series of spots. In a polycrystalline sample, however, the diffraction pattern will be a series of rings, each centered on the incident beam of electrons. If the polycrystalline sample is randomly oriented, each plane will produce an evenly distributed ring, as shown below:



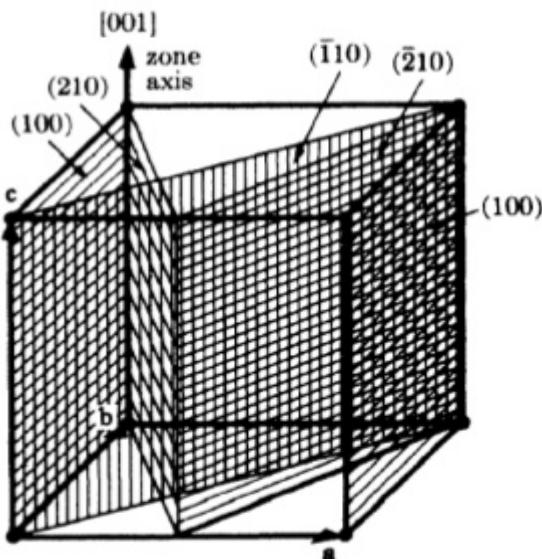
77. A typical electron diffraction spot pattern from a single crystalline material is shown below. In this illustration, the center bright spot labeled with a “T” is the location of where the electron beam is transmitted, and the spots labeled “D” are selected diffracted spots. The square pattern is formed as a result of diffraction from a cubic crystal along the 001 orientation of the crystal:



(J.W. Edington, *Practical Electron Microscopy in Materials Science*, at 32 (1976).)

78. The crystal producing the 001 pattern shown above might produce a different diffraction pattern if the beam transmitting the electrons is aligned differently.

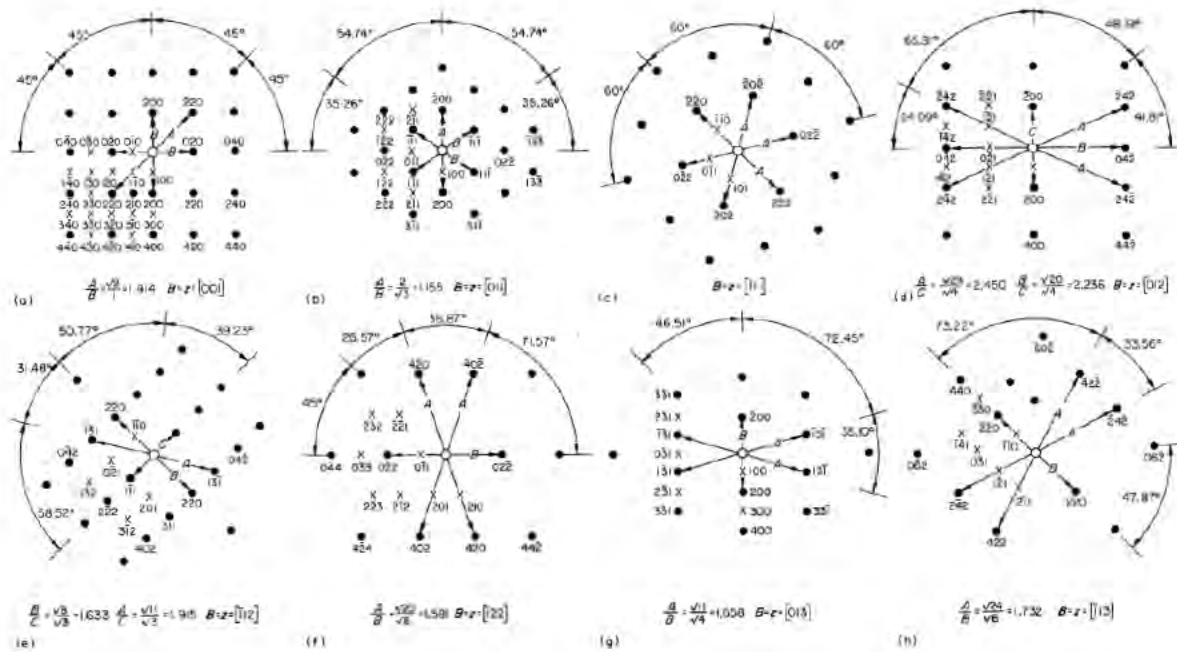
79. When the beam is aligned along a direction that has different planes diffracting at the same time, we refer to that as the “zone axis.” These are generally directions that have a high degree of symmetry. For example, the 001 zone axis in a cubic crystal is commonly used because it has several planes that are parallel to the beam, and thus diffract the beam, as shown below:



80. The 001 zone axis is the vertical line at the back left of the above cubic unit cell, and all of the shaded planes (100, 210, 110, 210) are parallel to the 001 zone axis, and accordingly will diffract a beam sent into the crystal along the 001 zone axis.

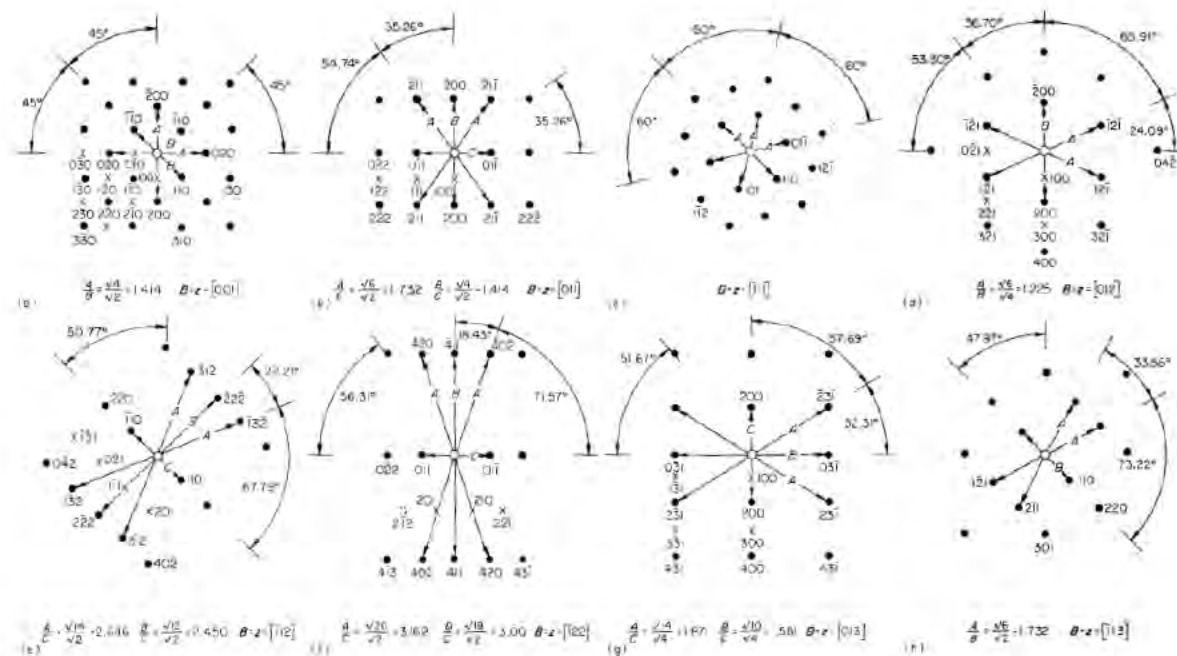
81. The diffraction patterns obtained from testing a material can be compared to *standard diffraction patterns* to determine the crystal structure (if any) of the material. When comparing measurements to these standard diffraction patterns, it is important to understand the direction of the electron beam relative to the sample.

82. In this case, the standard diffraction patterns for fcc crystals and bcc crystals are relevant. Standard diffraction patterns for the eight most common zone axes for fcc and bcc crystals are shown below:



(J.W. Edington, *Practical Electron Microscopy in Materials Science*, at 32 (1976))

(FCC zone axes)



(J.W. Edington, *Practical Electron Microscopy in Materials Science*, at 304-306 (1976))
(BCC zone axes)

83. The zone axis for each standard pattern is noted below the pattern. For example, in upper leftmost pattern for fcc and bcc, the zone axis is indicated as [001]. (See generally (J.W. Edington, *Practical Electron Microscopy in Materials Science* 44-45, 283-84 (1976).)

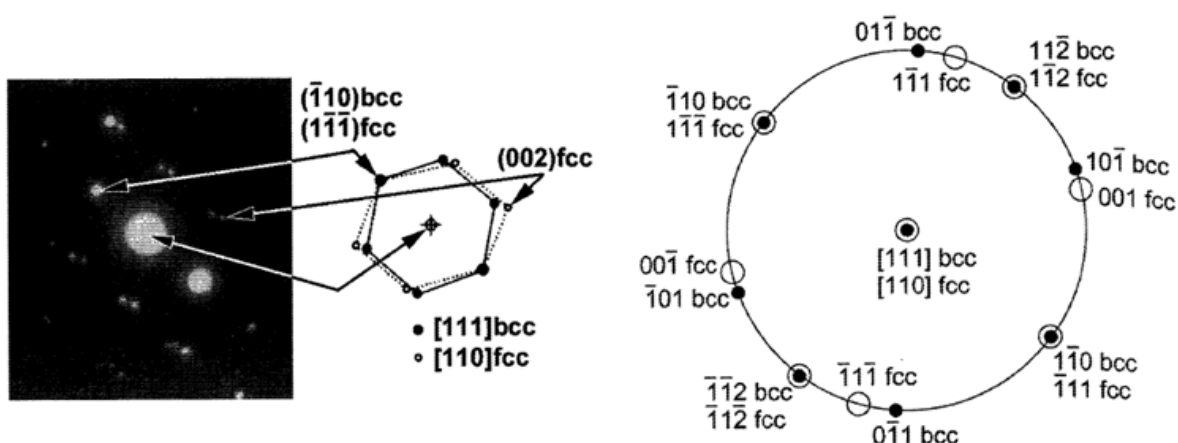
84. Critically, the standard diffraction patterns depict the exact ratio of distances between spots and the center spot, as well as the exact angle between spots and the center spot. For example, for the [001] zone axis in a bcc crystal, the above image lists a ratio between distance A and B as $A/B = 1.414$. It is worth noting that this is measured to three significant figures after the decimal. As another example, the angle shown between two spots and the center spot for a bcc [111] zone axis is 60 degrees. The angle shown for an fcc [011] zone axis is 54.74 degrees. Thus, while both the bcc [111] and the fcc [011] zone axes have spot patterns that are roughly hexagonal, a difference of 5.36 degrees in angle can indicate an entirely different crystal structure: *e.g.*, bcc vs. fcc.

85. Thus, care must be taken when making comparisons to standard diffraction patterns to ensure that the ratios between diffraction spots and angles between diffraction spots are exactly as shown in the standard diffraction patterns. Failure to align the patterns with the correct atomic spacing will lead to inaccurate, misleading, and unreliable results. (B. Fultz and J. Howe, *Transmission Electron Microscopy and Diffractometry of Materials* 290-292 (2013) (noting accuracy should be within 3% for measuring the ratio of atomic distances).)

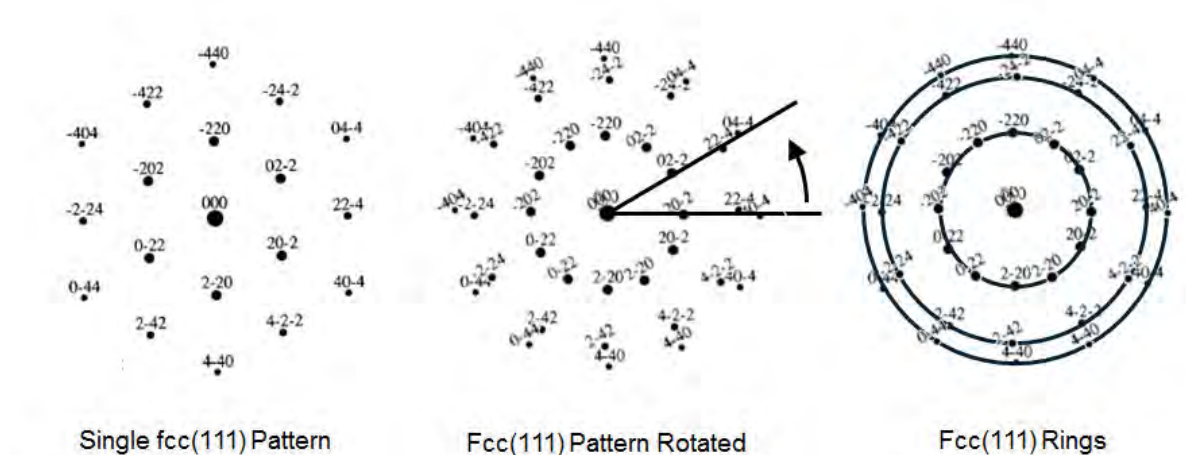
86. To compare measured diffraction patterns with the standard diffraction patterns, one typically determines the spacings and angles of the measured diffraction pattern and then compares those spacings and angles to a standard diffraction pattern. This can also sometimes be shown by overlaying the standard diffraction pattern onto the diffraction image to determine any differences in spacings and angles. (See J.W. Edington, *Practical Electron Microscopy in Materials Science* 47 (1976); B. Fultz and J. Howe, *Transmission Electron Microscopy and Diffractometry of Materials* 292 (2013)

(“The easy way to index this diffraction pattern is to look it up in Appendix A.6 of this book.”). I note that Dr. Stach provides a good example of this analysis in his report. (See Stach, ¶¶ 73-79.)

87. One can also use TEM diffraction patterns to examine the orientational relationship between crystals. For example, if a plan view is used for the electron beam direction, one can plot a bcc(110) crystal’s orientation relative to an underlying fcc(111) crystal using the resulting TEM diffraction patterns that should appear for both crystals. Shown below, for example, is a TEM diffraction pattern showing a bcc(110) crystal oriented over an fcc(111) hexagonal crystal, like that shown in Figure 5 of the ’988 Patent:

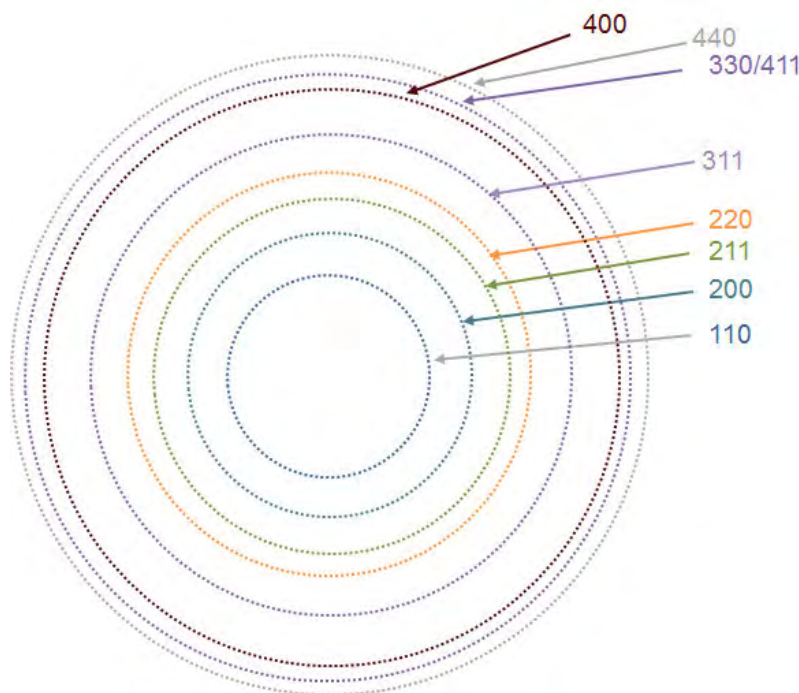


88. If a measured sample contains multiple grains (*e.g.*, fcc(111) crystals with different in-plane orientations), the diffraction pattern will not be a series of spots, but rather a series of rings. This reflects the fact that the beam is intersecting multiple crystal grains, each with a different orientation within the plane. As a result of these different orientations, the resulting diffraction pattern is a series of rings centered around the beam. This can be seen below, by rotating an example diffraction pattern of a single fcc(111) crystal:



89. As shown above, as the fcc [111] zone axis pattern is rotated about the center beam, the diffraction spots form a series of rings, each at a certain radius. The radius of each ring is related to the spacing between the planes forming each ring in the sample crystal. As shown above, for example, the innermost ring is formed from the {220} set of planes, the second ring is formed from the {422} set of planes, and the outermost ring is formed from the {440} set of planes.

90. Shown below, for example, is a simulated ring diffraction Dr. Stach created for a sample composed entirely of bcc(110) crystals, randomly oriented about the electron beam direction:

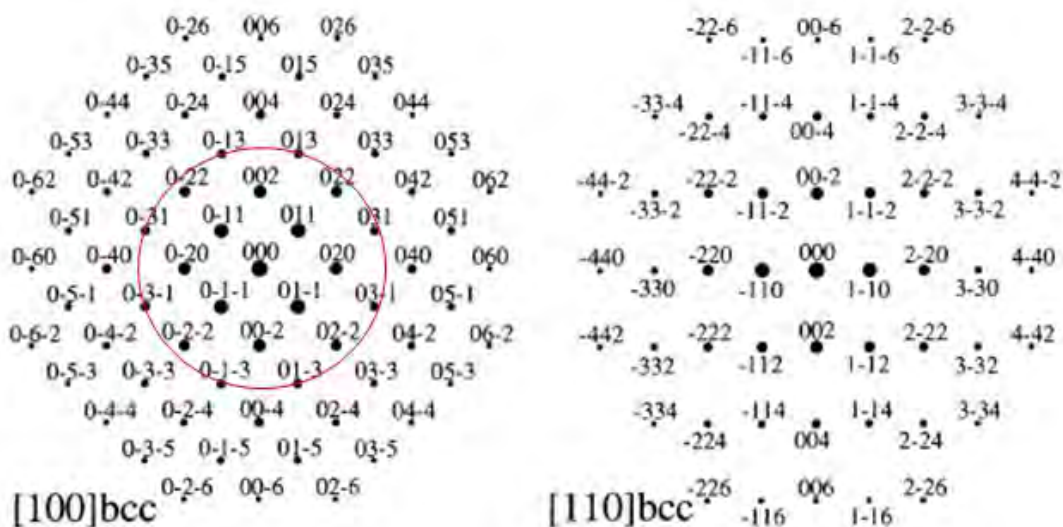


(Ring Pattern for BCC(110) Crystals)

91. Each of the rings above is labeled with the crystalline planes that contributed to that particular ring. It is important to notice that a crystal with a single texture, in this case bcc(110), will have rings in addition to the ring labeled 110 above, including the 200, 211, 220, 330/411 (which overlap as they have nearly the same d-spacing), 400, and 440 rings. This is because while the name “bcc(110) crystal” indicates that one particular plane, the (110) plane, is parallel to the substrate, other planes within a bcc crystal will also diffract the electron beam and thus produce rings in the diffraction pattern.

92. The rings in a given pattern can be indexed and compared to standard diffraction patterns, so as to identify the crystal(s) contributing to the diffraction. While many different crystals may contribute to certain rings, there are also rings that are unique to certain crystals. These unique rings may allow us to identify the crystals present in a sample. For example, while a bcc crystal studied using [110] zone axis will have a 110 ring, a bcc crystal studied using [100] zone axis will also have a 110 ring. Yet only the [100] zone axis crystal will produce a 013 ring. This is apparent by

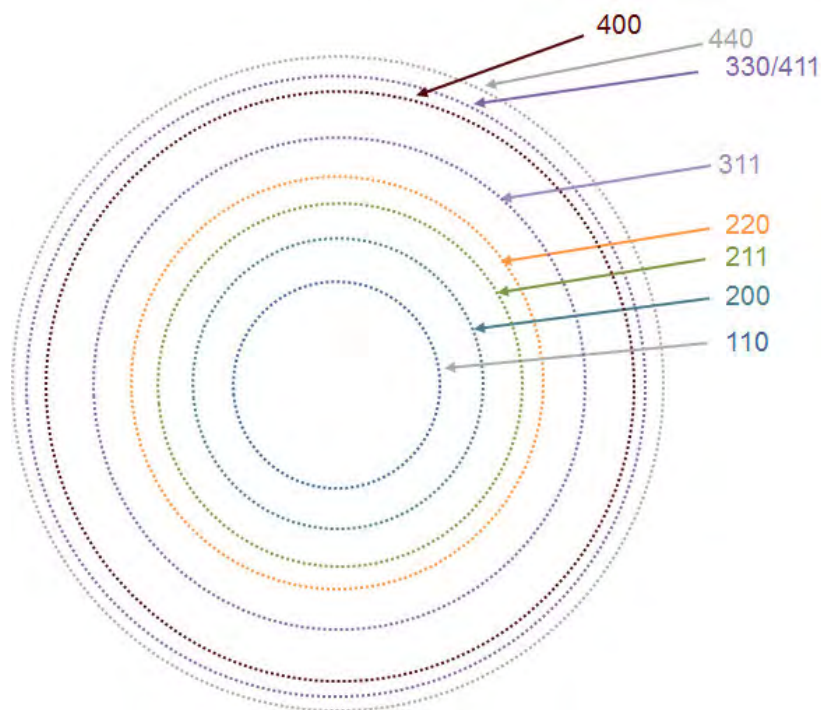
comparing the standard diffraction patterns for a bcc [100] zone axis (on the left) with a bcc [110] zone axis (on the right):



93. As shown above, only the bcc [100] zone axis pattern contains 013 spots. All of the equivalent 013 spots form the red circle drawn above on the [100] pattern. Due to the symmetry of a cubic crystal the following planes that form the red circle are all symmetrical: 013, 0-13, 0-31, 0-3-1, 01-3, 03-1, and 031.

94. Understanding these standard patterns allows us to identify the structure and orientation of the crystals in a measured material. If a diffraction pattern has a ring not associated with the standard ring pattern for a given crystal structure, we can definitively conclude that the given crystal structure did not contribute to the diffraction along that ring.

95. For example, if we measure a sample and find 310 and 213 rings, this tells us that the sample *cannot* contain only bcc(110) crystals, because bcc(110) crystals cannot cause diffraction producing the 310 and 213 rings:



(Ring Pattern for BCC(110) Crystals—**No 310 or 213 Rings**)

96. There thus *must* be other crystal orientations in the sample (*e.g.*, bcc(100) and/or bcc(310)). Bcc(100) crystals in particular will cause diffraction along the 310, 213, and 411 rings (among others).

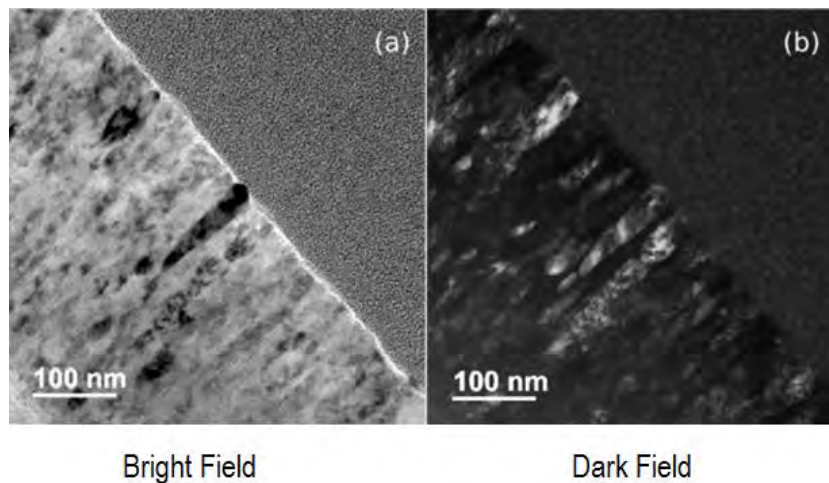
97. Furthermore, it is possible for the presence of a given set of rings to be consistent with more than one crystal orientation. For example, the presence of 200 diffraction rings is consistent with a number of different possible grain orientations, including 001, 011, 012, 013, 023, and 014. To be succinct, diffraction from 200 rings does not indicate 011 texture.

98. Microbeam Diffraction. Microbeam diffraction is a variation of TEM imaging in the diffraction mode, where a finely-focused beam is used to provide greater spatial resolution. The condenser lenses of the microscope are used to restrict the size of the electron beam that transmits through the sample. This limits the area from which the diffraction information will be obtained.

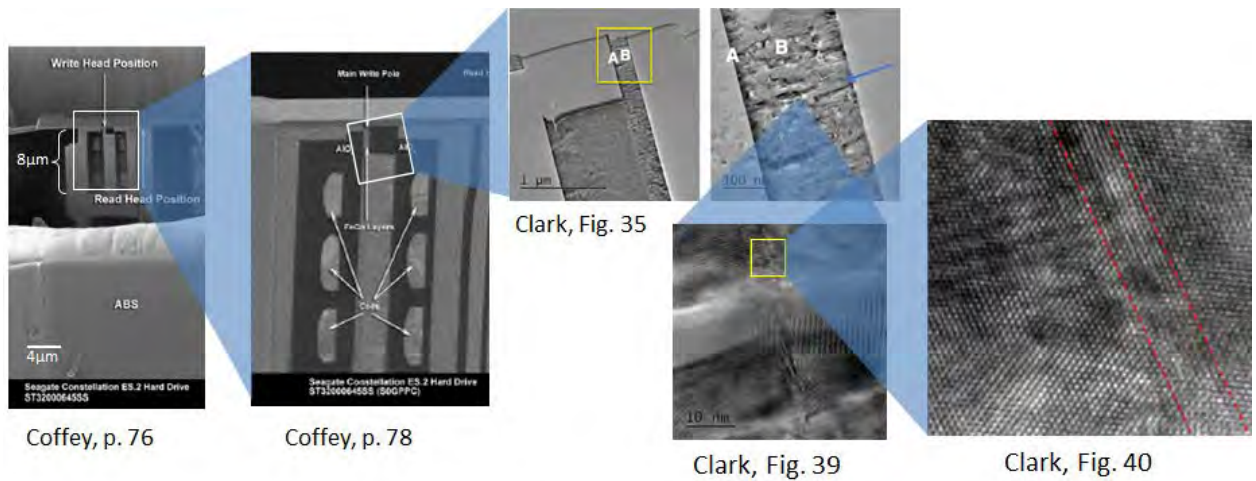
(b) Imaging Mode

99. As discussed above, image mode produces a grayscale image, much like the image produced by a light microscope. Below I discuss bright and dark field imaging mode, and high resolution phase-contrast images.

100. Bright and Dark Field Images: Two types of TEM imaging modes are bright field imaging and dark field imaging. Bright field imaging is created by placing an aperture below the objective lens which only allows the direct beam of electrons to pass through it. In contrast, in dark field imaging an aperture is placed below the objective lens such that it entirely blocks the direct beam of electrons, and instead only allows diffracted or indirect beams of electrons to pass through the aperture.



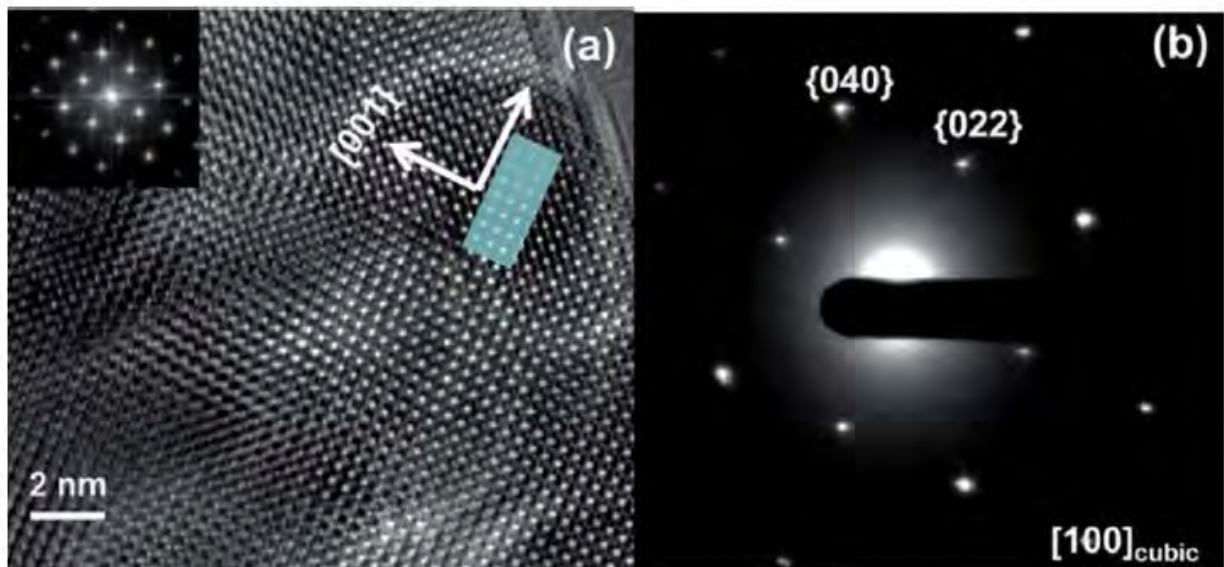
101. High Resolution Phase-Contrast Images. High resolution phase contrast images are formed by using a TEM in image mode (as opposed to diffraction mode) to create an image of a sample using the phase overlap of both the direct (transmitted) electron beam and one or more diffracted beams. An example of a series of TEM cross-section images from a Seagate HDD is shown below, compiled from Dr. Coffey and Dr. Clark's report, which show gradually increasing magnification. Dr. Clark's Figures 39 and 40 are examples of high resolution images:



102. The scale of these images also allows us to determine the relative size of the objects being imaged. For example, using the scale from the cross-section image on the far left, we can calculate that the size of Seagate's head is approximately 8 microns long in cross section, as can be seen on the cross section image on the far left. In contrast, the highly-magnified in high resolution image on the far right is only about 7 nm across.

103. FFTs. A Fast Fourier transform (FFT) is a computational method that can be used to reconstruct a diffraction pattern from a particular portion of a high-resolution image. FFTs can be used in certain cases to show the existence of particular crystal orientations by matching the FFT pattern with standard diffraction patterns in the manner described above.

104. For example, shown below on the left is a high-resolution TEM image for a crystal, with the accompanying FFT generated from that image cropped in the upper left corner. The TEM diffraction pattern for the same crystal is shown on the right:

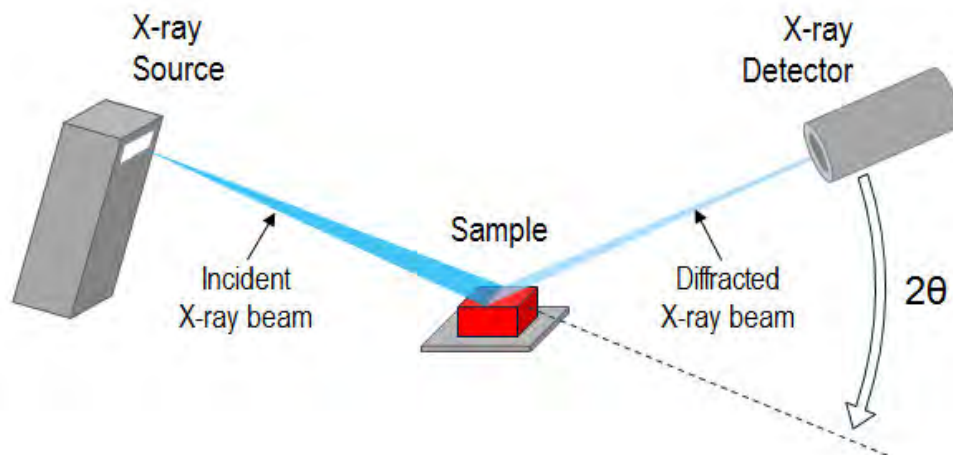


105. Thus, FFT images can sometimes be used to infer information about crystal structure and crystal orientation—but only for the specific crystal or crystals being imaged.

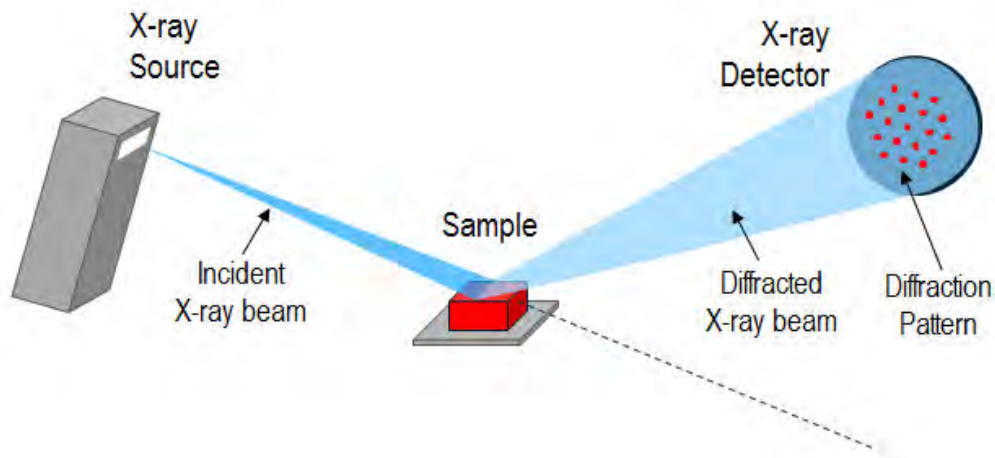
2. X-Ray Diffraction (XRD)

106. XRD is a technique that imparts x-rays on a sample, and then measures the x-rays diffracted by the sample.

107. X-ray diffraction is most often performed using an x-ray diffractometer. A standard x-ray diffractometer consists of three basic elements: (1) an x-ray source, (2) a sample holder (goniometer), and (3) an x-ray detector.

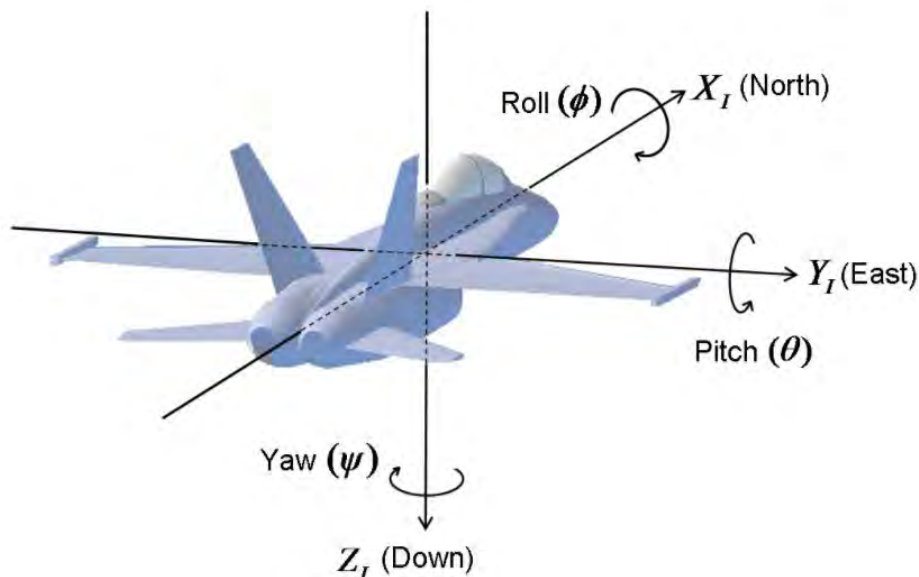


108. As shown above, in an x-ray diffraction measurement, a sample is mounted on the goniometer—an instrument that can be rotated along precise directions at precise angles. The x-ray source illuminates the sample along a certain direction. When the x-ray beam strikes the sample, the beam scatters and reflects off the sample at various angles and intensities, depending on the crystal structure and crystal orientation of the sample. The reflected x-rays are picked up by the x-ray detector in the form of a diffracted intensity or a “diffraction pattern,” as shown below for an area detector:



109. Then, with the x-ray beam still on, the goniometer gradually rotates the sample while the detector is kept fixed or rotates as well. As the sample is rotated, previous reflections disappear and new ones appear, causing the diffraction pattern to change. As the sample rotates, the resulting intensity and angles of the reflected x-rays (i.e., the diffraction patterns) are recorded as a function of the rotation.

110. Because the sample can be rotated relative to the incoming x-ray beam along three different directions (x, y, and z), these axes of rotation are denoted by the Greek letters θ (theta), ϕ (phi), and ψ (psi). These are known as Euler angles and may be visualized by imagining the ways in which an airplane can be rotated along the x, y, and z directions:



111. Just as the airplane can be rotated by some angle along any of the three axes of rotation, so too can an XRD sample be rotated relative to the incoming x-ray beam. The rotations one performs depends on what type of crystallographic information about the sample one wishes to obtain. In the context of the '988 Patent, two types of XRD measurements are relevant: (1) θ - 2θ and θ scans, which can be used to determine crystallographic texture (if any) of layers in the sample, and (2) pole figures, which can be used to determine the variants and symmetry breaking (if any) in the layers of the sample.

112. If we rotate the sample only along theta while fixing phi and psi, while the detector is fixed, we produce a θ scan. If we rotate the sample only along theta while fixing phi and psi and while the detector rotates twice the angle (2θ) we produce a θ - 2θ scan. In certain cases, θ - 2θ scans provide information about a material's texture—i.e., its predominant crystallographic orientation, if any. (*See, e.g.*, '988 Patent at 38:17-19 (“First we provide a perspective for the degree of texture obtained by observing a θ - 2θ x-ray diffraction scan”); '416 Patent at 17:62-19:35.) The theta scan can then be used to quantify the degree of texture for a highly textured film.

113. The idea behind θ - 2θ scans is that as the sample is rotated along θ (and the detector rotated at twice the angle) such that the incoming and outgoing x-rays make

an angle θ with the surface, a layer with a predominant crystallographic orientation will reflect x-rays very intensely at specific values of θ .

114. Two examples of XRD θ - 2θ scan data from the '416 Patent are shown below. The first plot (FIG. 27(a) of the '416 Patent) shows (111) textured NiFe on (111) Si since you only see (111) peaks and no other peaks of different orientations. The second plot (FIG. 29(b) from the '416 Patent) shows no (111) NiFe texture.

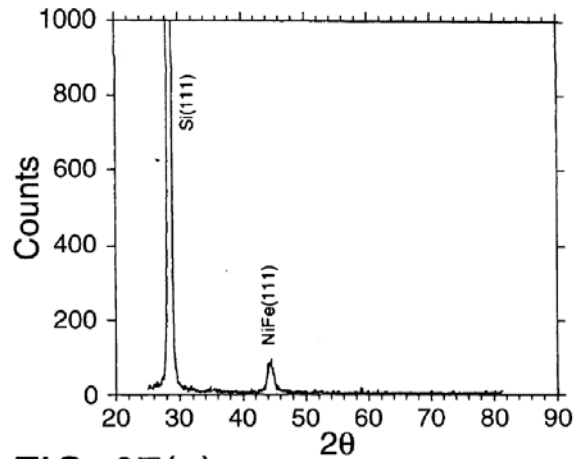


FIG. 27(a)

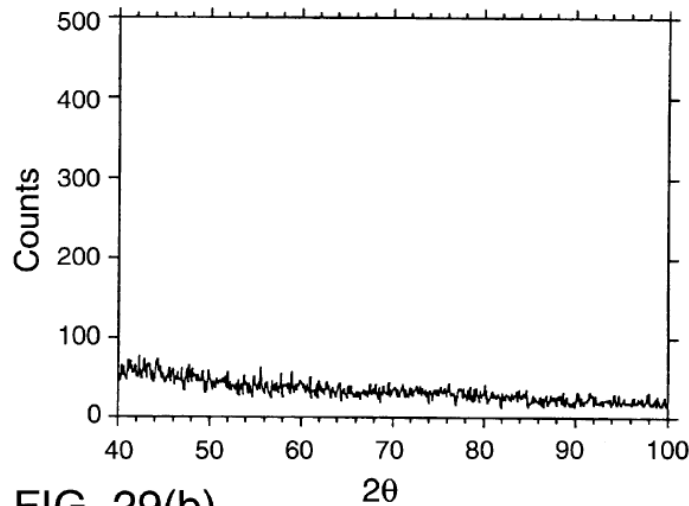


FIG. 29(b)

115. If we instead rotate the sample along phi, theta, and psi, while fixing the detector, we can produce a pole figure. Pole figures provide information about the in-

plane orientation of the crystals in a layer—provided you choose the detector angle to correspond to the scattering from the given set of atomic planes for a given material.

116. The '988 Patent contains one example of a pole figure in FIG. 14. I reproduce FIG. 14 from the patent below:

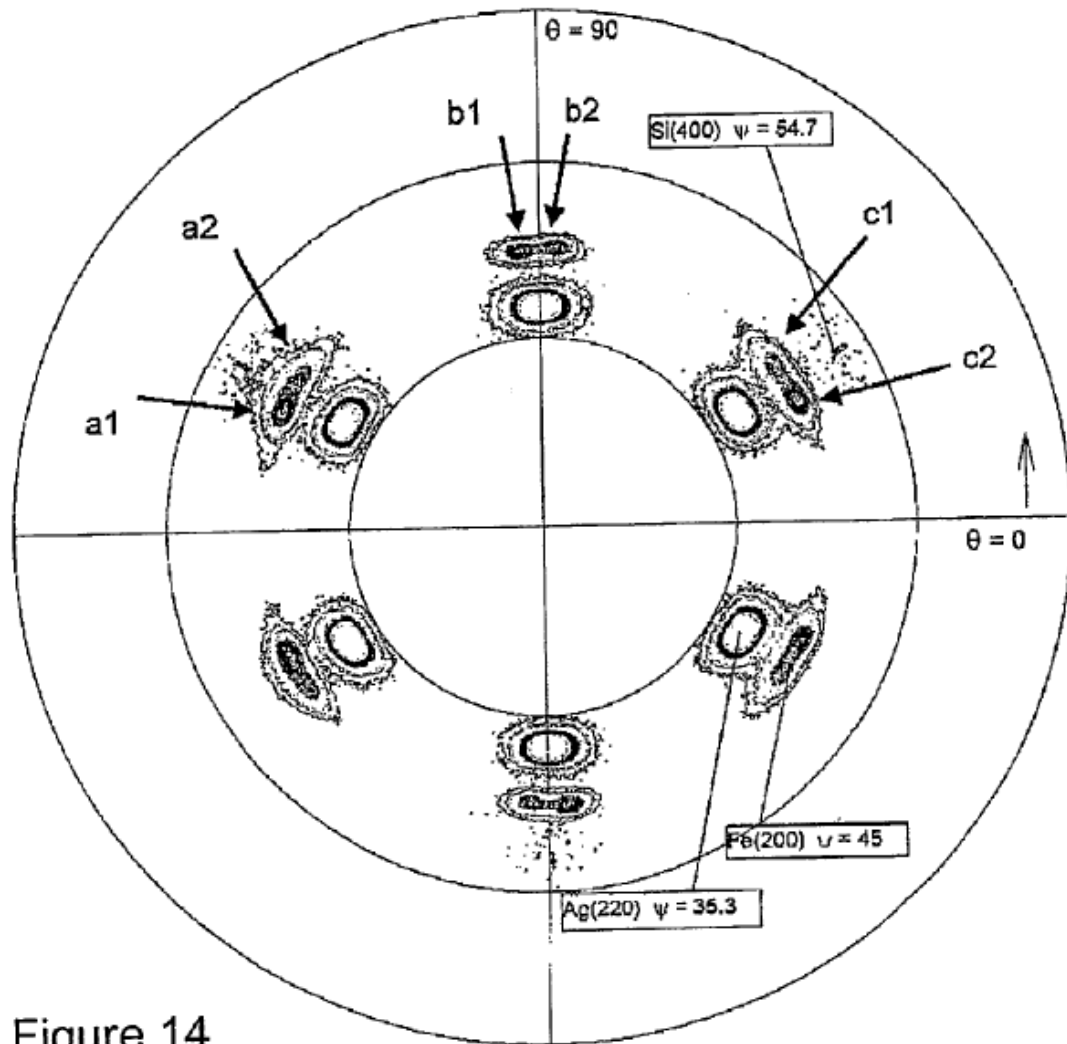


Figure 14

117. According to the '988 Patent, "FIG. 14 is X-ray pole figure data demonstrating the existence of six bcc-d (110) textured variants with $\delta=5.264$ where variant a1 and c2 dominate the other four variants to produce a symmetry broken structure. Also shown are the three Ag (220) peaks." ('988 Patent at 14:18-22.)

118. The '988 Patent explains how to analyze the pole figure data of FIG. 14 to determine whether the sample is a three-variant system (as observed in the prior art) or a six-variant system (as required of a symmetry broken structure):

[I]f there are only three possible variants then there should be three peaks observed for each 180 degrees of rotation and they would be equally spaced at 60 degree intervals. These would repeat during the second 180 of rotation. However, if there are six variants as advocated in this invention . . . six peaks would be seen per 180 degrees of rotation; and 12 would be seen during the full 360 degree rotation.

(*Id.* at 41:36-43.)

119. The '988 Patent thus states that because there are six peaks in the upper hemisphere (a 180-degree rotation) of FIG. 14, there are six variants. The six peaks correspond to the six variants of the patent, with each peak/variant labeled in FIG. 14 using the notations “a1,” “a2,” “b1,” “b2,” “c1,” and “c2.”

D. Magnetism

120. Magnetic fields are created by the movement of electrically charged particles (an electric current) or from the quantum mechanical spin of electrons. For example, the Earth has a magnetic field (which is why a compass points north—it is responding to the Earth's magnetic field). The Earth's magnetic field is caused by the movement of electrically charged liquid iron atoms swirling within the Earth's core.

121. Magnetic materials are materials that respond to some extent to an external magnetic field (*i.e.*, a magnetic field not caused by the object itself). The shape, material composition, defects, and crystal structure of an object can all affect how it the object responds to an external magnetic field.

122. A specific class of magnetic materials are ferromagnets, where quantum mechanical interactions can align electron spin and orbital (arising from the motion of electrons in current loops) moments such that the material has a saturation magnetization M_s defined as sum of the aligned local moments per unit volume.

123. Magnetization is defined by magnitude of the magnetization (M_s) and the direction of the magnetization. In an external magnetic field, the direction of magnetization will tend to align in the direction of the external field. This is the basic

operation of a compass where the magnetization of the needle aligns in the direction of an external magnetic field (usually, in the case of a compass, the Earth’s magnetic field).

1. Magnetic Anisotropy

124. “Anisotropy” describes a property that depends on direction. “Magnetic anisotropy” means that how an object responds to an external magnetic field depends on the direction (and magnitude) of that external magnetic field. More specifically, an object exhibits “magnetic anisotropy” when the energy (external magnetic field) needed to set the object’s magnetization direction depends on the direction.

125. An object has a preferred magnetization direction if less energy is needed to set the material’s magnetization along the preferred direction. The energy needed to set the magnetization away from the preferred direction will be higher than the energy needed to set the magnetization along the preferred direction. An object with one or more preferred magnetization directions therefore exhibits magnetic anisotropy, because less energy is required to magnetize the object along certain directions than others.

2. Sources of Magnetic Anisotropy

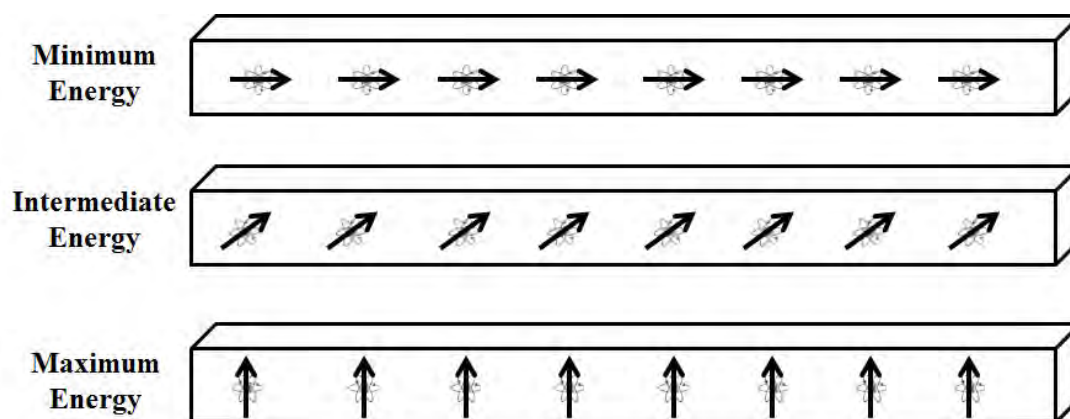
126. There are many potential sources of magnetic anisotropy—including, for example, magnetocrystalline anisotropy, atomic pair ordering, strain anisotropy, and shape anisotropy. (*See, e.g.*, B.D. Cullity and C.D. Graham, INTRODUCTION TO MAGNETIC MATERIALS, 2ND EDITION (2009), at 197-198 (listing the following sources of magnetic anisotropy: magnetocrystalline anisotropy; shape anisotropy; stress anisotropy; induced anisotropy by magnetic annealing, plastic deformation, and irradiation; and exchange anisotropy).) As Cullity explains: “Of these, only crystal anisotropy is intrinsic to the material. Strictly, then, all the others are extrinsic or ‘induced.’ . . . All the anisotropies [listed above] are important in practice, and any one may become predominant in special circumstances.” (*Id.* at 198.)

127. The crystal structure of a material can be a source of magnetic anisotropy because it sometimes takes more energy to magnetize a crystal along certain axes of its crystalline lattice—this is known as *magnetocrystalline anisotropy*.

128. *Atomic pair ordering* refers to magnetic anisotropy caused by a preferential arrangement of certain atomic pairs in a material, in which each atomic pair has a preferred magnetization direction.

129. *Strain anisotropy* is created by the imposition of strain on a crystal lattice, which distorts the lattice in a way that results in magnetic anisotropy.

130. *Shape anisotropy* arises from the internal magnetic fields that result from an elongated structure, which results in less energy needed to set the magnetization direction along the direction of elongation, and more energy to set the magnetization direction away from the elongated direction. This is illustrated below:



131. Shape anisotropy in particular is often a major source of magnetic anisotropy in thin films (which, by definition, are thin in at least one dimension, resulting in relative elongation along the non-thin dimensions). (*See, e.g.*, Cullity, at 234-237 (“shape alone can be a source of magnetic anisotropy”).) I note that Dr. Coffey acknowledges the significant impact of shape anisotropy in certain thin films: “for films having in-plane dimensions only 100 times greater than their thickness, the in-plane shape dependent demagnetization effects can be significant. . . . In this range of dimensions and for thin films that are not circular, the in-plane shape anisotropy effects can be significant to the magnetization directions of an object.” (Coffey, ¶ 55.)

132. The anisotropy energy density function of a material refers to a mathematical function that describes the material’s overall magnetic anisotropy—*i.e.*,

the sum of all these different sources of magnetic anisotropy. (*See, e.g.*, Cullity, at 197-198, 237-238.)

3. Uniaxial Anisotropy

133. “Uniaxial anisotropy” is a specific type of magnetic anisotropy in which a magnetic material has one preferred axis for its magnetic direction and no other locally preferred directions. That is, a material is “uniaxial” if the material’s anisotropy energy density function has only a single maximum and a single minimum as the magnetization angle is rotated by 180 degrees from a physical axis. (’988 Patent at 1:56-60; *see also* Coffey, ¶ 77 (“When a material has an anisotropy energy density function with only a single maximum and a single minimum as the magnetization angle is rotated by 180 degrees from a physical axis, the material is said to have ‘uniaxial’ anisotropy.” (citing ’988 Patent at 1:56-60).))

134. Measuring whether a material is “uniaxial”—*i.e.*, whether its anisotropy energy density function has only a single maximum and a single minimum as the magnetization angle is rotated by 180 degrees from a physical axis—is assessed by taking magnetic measurements of the material and analyzing the magnetic data. (*See, e.g.*, ’988 Patent, FIG. 15.)

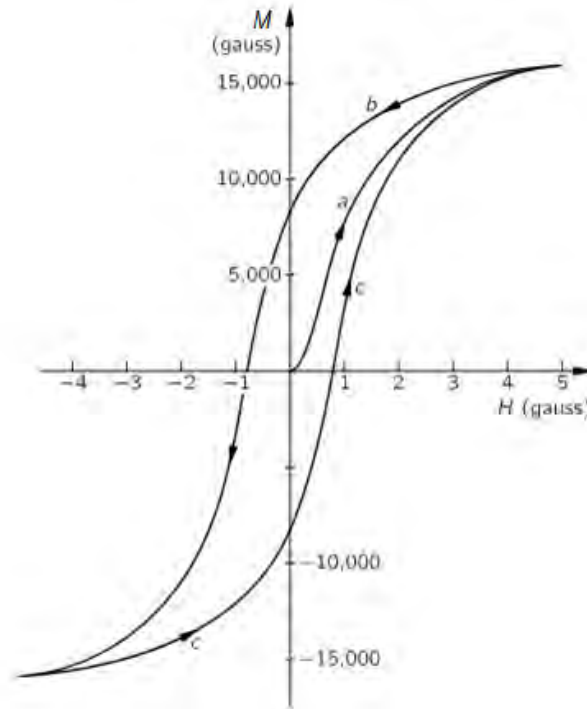
E. Measuring the Magnetic Properties of Materials

135. Several instruments and techniques exist for measuring the magnetic properties of materials, including for example vibrating sample magnetometers (VSM) and magneto-optical Kerr effect (MOKE) tools.

136. A VSM is an instrument used to measure a sample’s magnetic properties. The sample is placed on a sample holder (*e.g.* a glass or plastic rod) and vibrated between pickup coils, which inductively sense the magnetic moment of the sample. A magnetic field is applied, and the magnetic moment of the sample is detected as a function of the applied field. (*See generally* D. Jiles, INTRODUCTION TO MAGNETISM AND MAGNETIC MATERIALS (2015).)

137. Many magnetic measurement tools (including VSM and MOKE) can be used to generate data in the form of a “hysteresis loop,” which plots a sample’s magnetic

response to an external magnetic field as a function of the applied magnetic field's magnitude at a particular direction.



138. An example of a hysteresis loop (also sometimes referred to as an “M-H loop,” “magnetization curve,” or “magnetic response”) is shown above. The graph relates two quantities: the magnetization of the material, M , in response to an applied magnetic field, H .

139. The curve starts at the origin, indicating that with no external field applied (zero H), the material has no net magnetization (zero M).

140. As an external magnetic field is applied, we move along the part of the loop labeled “a.” This indicates that as the applied external field H increases in strength, the material’s magnetization M increases. Although an increase in H leads to an increase in M , we can see that their relationship is not linear—we call this a “nonlinear” magnetic response. For high enough fields the magnetization will saturate at a value called the “saturation magnetization” (M_s), which is when all the magnetization of the sample is aligned along the field direction.

141. If we then decrease the strength of the applied field H , we move along the curve labeled “b.” This indicates that as the applied field H is reduced, the material’s magnetization M decreases. Again, we see that the relationship between M and H is monotonic (a decrease in H leads to a decrease in M) but is not linear.

142. Continuing along the curve labeled “b,” we see that if we remove the applied field entirely ($H=0$), there is still some magnetization remaining in the material (i.e., $M \neq 0$). This tells us that the material not only becomes magnetized in response to the external field, but that even after the external field is completely removed, the material retains some of that magnetization. The magnetization that remains after the field is completely removed is known as the “remanent magnetization.”

143. Continuing along the curve labeled “b,” we see what happens if the applied field is not only removed but reversed in direction. As the applied field is reversed, the magnetization continues to decrease until it reaches zero. This tells us that completely demagnetizing the material after it has been magnetized requires an external field opposite the magnetization direction. The amount of external field needed to reset the magnetization varies by material. So-called “hard” magnetic materials are very resistant to changes in their magnetization and require very strong external fields to demagnetize, while “soft” magnetic materials require little external field to reset their magnetization. The strength of the external field needed to reset a material’s magnetization is known as the material’s “coercivity.”

144. Still continuing along the curve labeled “b,” we see that the magnetization M continues to decrease in a non-linear manner as H is decreased. At a high enough field it will saturate.

145. If we start to reduce the reverse (negative) field, H , we move along the curve labeled “c.” Again, we see that even once the field H is completely removed, the material retains some remanent magnetization. To remove the remanent magnetization, we must again apply a field H in the direction opposite the magnetization.

146. In sum, an M-H loop (or magnetization response) shows how a material's magnetization, M , changes in response to variations in the magnitude of an applied magnetic field, H .²

147. It is important to note that a single M-H loop depicts the material's magnetic response only for one particular direction. Thus, the M-H loop example I discuss above shows the magnetization response to an H-field applied in a single direction. Often, one is interested in understanding the magnetization response for multiple directions (*e.g.*, multiple directions across a 180-degree rotation). In those cases, one would measure the magnetic response (an M-H loop) for each direction of interest.

F. Hard Disk Drives

148. Because the Accused Products in this case involve the write heads of hard disk drives ("HDDs"), I have summarized in this section some of the basic components of hard disk drives and how they perform together, including the write head.

149. HDDs use a complex array of components, subassemblies, and electronics to magnetically store and retrieve data. At a high level, HDDs take the data from computers that are transmitted in bits—binary digits that can be thought of as representing either a "0" or a "1"—and store that data on magnetic media encoding the information in the direction of magnetization. Some of these components and subassemblies are shown in the illustration below:

² It is also common to plot B , the magnetic flux density, as a function of H , yielding a B-H loop. B-H loops are related to M-H loops and provide information about the coercivity and the remanent flux density of a material.



150. Among the key components and subassemblies are the disk or disks coated with a thin magnetic layer on which the data is stored; the spindle motor that spins the disk; and the slider that contains the write head and the read head.

151. The read head is a component of the slider with multiple thin films that work together to sense (*i.e.*, read) magnetic transitions on the disk. The write head is also a component of the slider. The write head consists of multiple components (*e.g.*, shields, write pole, coils) that work together to record magnetic transitions to the disk. The slider includes additional features such as a heater and an air bearing surface, both of which assist with maintaining a desired spacing between the slider and the disk. Sliders are manufactured on a wafer material, from which individual sliders are then cut. Each slider is mounted on a head gimbal assembly (“HGA”) that contains an arm assembly, a suspension, electronic components, and microactuators which help position the read head and the write head over a desired location of the disk. The HGA is mounted on an E-shaped arm assembly that is coupled to a voice coil motor actuator, which rotates the E-shaped arm assembly (and therefore HGA) over the disk.

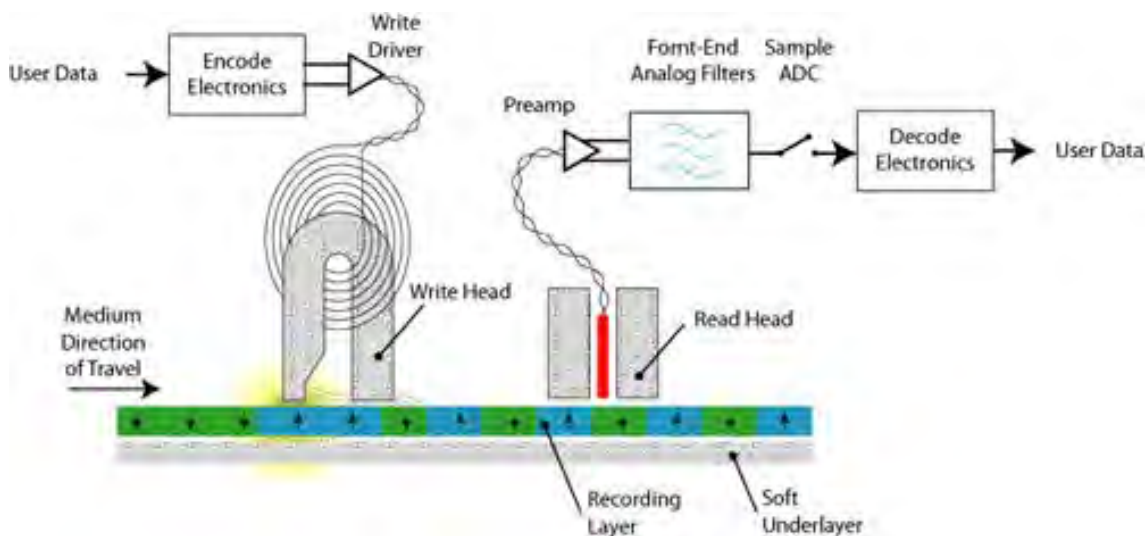
152. During operation, the write head writes data to the magnetic layers of the rotating disks, and the read head subsequently retrieves the recorded data. Upon instructions from the HDD’s electronic circuitry, the actuator guides the sliders (and therefore the read heads and the write heads) to the selected track of a disk where data is recorded or retrieved. Electronic components, including internal controllers using

application specific integrated circuits (ASICs) and ancillary electronic control chips, monitor and move the data within the HDD, provide signal processing, error correction, and other functions. For example, upon receiving instructions from the electronics, the voice coil motor actuator guides the read head and the write to the selected track of the disk where the data are recorded or retrieved.

153. The components and subassemblies described above are just a few of the mechanical and electronic parts and components that comprise an HDD and contribute to its overall performance. I have included in Exhibit C to my report a table summarizing many of these components and subassemblies. The summary is not intended to be comprehensive, but it provides a sense of the scale and complexity of the technology that goes into making HDDs. In the next section, I describe in more detail some of the components, materials, and design elements that go into the write head.

G. Write Heads

154. As mentioned above, write heads record data (“write”) to the media. The figure below shows a schematic of a write head and a read head positioned over a disk during the writing process.



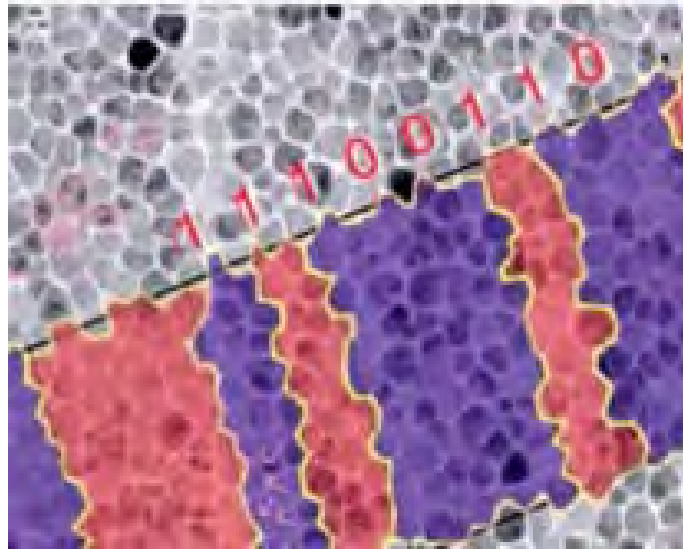
155. During the writing process, the write head flies above the disk and emanates a strong magnetic field from its tip to write data to the media. The magnetic field emanating from the tip changes the direction of magnetic grains in the media,

regions of which act as magnetic bits. The pattern of the magnetic bits determines whether the bit is read as a “0” or “1,” which represent data in the binary system used by computers.

156. I note that Dr. Coffey’s “simplified depiction of an HDD” (Coffey, ¶ 61) is inaccurate because it states that the “0s” and “1s” of binary data are represented by the direction of each magnetic bit. (*Id.* (“Basically, each bit acts like a small bar magnet, with the poles aligned in one direction for a 1 and the other for a 0.”); *see also id.* at ¶ 62 (“[D]ata will be recorded as the bit’s magnetic orientation will change and thus the data represented by that orientation also changes (*e.g.*, from a 0 to a 1).”).)

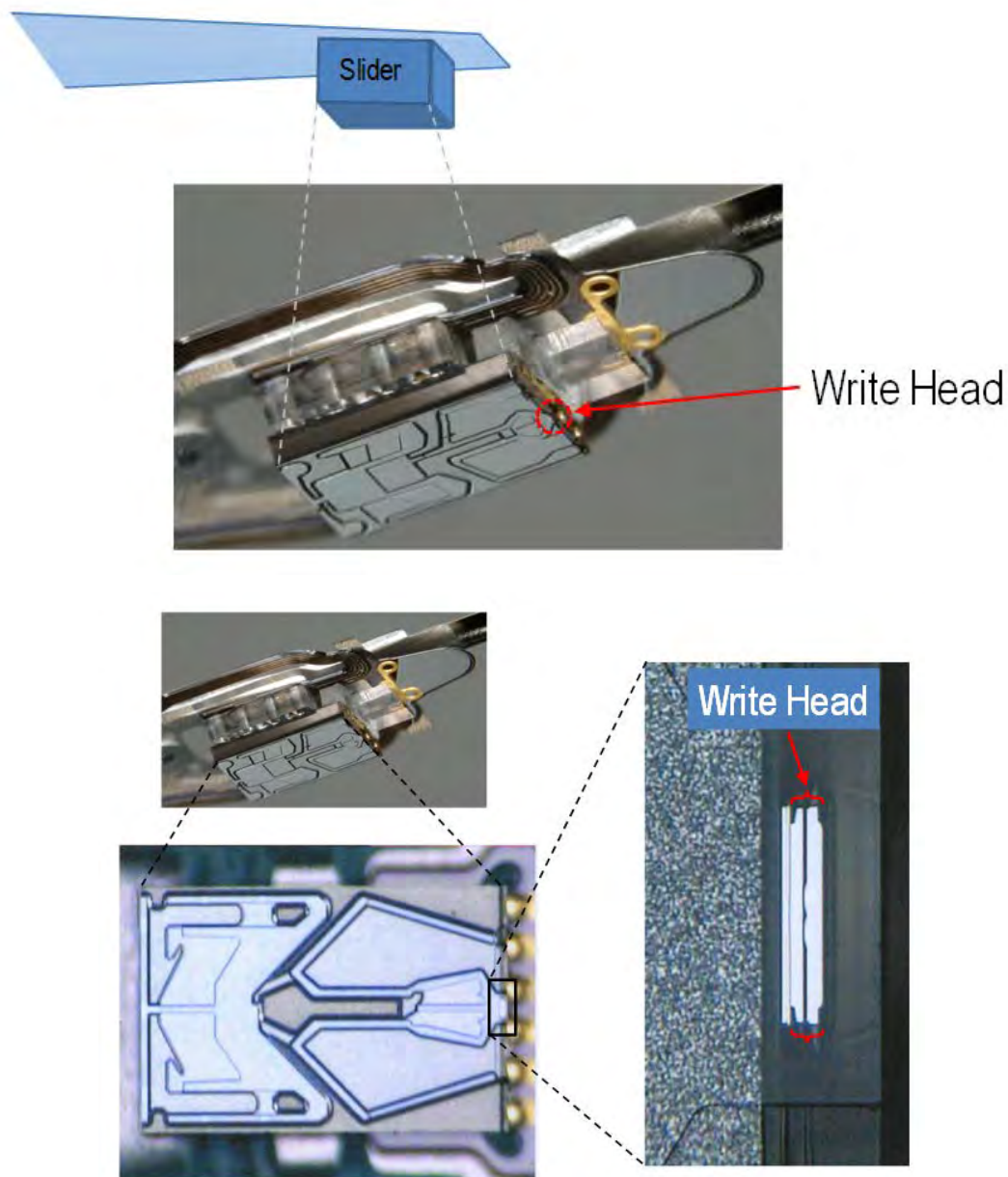
157. In fact, it is not the direction of the bits, but the **transition** in direction between bits, that determines whether data is stored as a “0” or “1.” A transition corresponds to a “1” while no transition corresponds to a “0.” (*See, e.g.*, O’Handley at 677 (“The presence or absence of a transition at expected intervals (called *bits*) is read as a ‘one’ or a ‘zero’ to represent binary coded information.”) (emphasis in original).)³ For example, the image below shows grains in the media magnetized up (red) or down (purple). Whether the data is read as a “1” or “0” does not depend on whether a region is red or purple, but whether there is a transition (“1”) or lack of transition (“0”):

³ Throughout this report, all emphases in cited materials have been added, unless otherwise noted.



158. To create the magnetic field responsible for writing data, the write head uses an electromagnet. As the name suggests, an “electro” magnet uses an electric current to produce a magnetic field. The electric current passes through a coil, which induces a strong magnetic flux in the head, which in turn generates the magnetic field at the write pole tip that writes to the media.

159. Write heads are sometimes referred to as “thin film” heads because the materials of the head comprise very thin layers—on the order of nanometers. To give a sense of how small write heads are, the pictures below show a series of progressively zoomed-in pictures of a write head on a slider.



160. A typical modern write head, comprising multiple layers of thin films, is usually several hundred nanometers thick, which is approximately 1/100th of the thickness of an average human hair. Individual thin film layers within a typical modern write head are often less than 1/1000th the thickness of a human hair.

161. Erase-after-write (“EAW”) refers generally to a number of phenomena that sometimes leads to the erasure or unintended overwriting of magnetic bits in the

media. There exist various strategies and design choices for mitigating EAW in HDDs (although some may come with tradeoffs in other respects).

162. Seagate, for example, uses a technique known as *degaussing* to effectively eliminate EAW. (See, e.g., SEA03129091.) Degaussing, which has nothing to do with uniaxial anisotropy, describes a technique where after the write head is done writing, rather than remove the write current entirely, a small alternating current is briefly applied at the end of the writing process. (*Id.*) Applying this alternating current helps the write head demagnetize faster than if the current was removed entirely. Seagate has found that this “Deguass feature of preamp [is] typically very effective in eliminating [conventional] EAW” and “Response to degauss is relatively strong.” (*Id.*) Degaussing is commonly used to deal with EAW since it is both effective at eliminating EAW and has no significant drawbacks.

163. I note that there are other techniques for avoiding EAW as well, including for example using antiferromagnetically coupled layers and/or optimizing write head geometry (neither of which have anything to do with uniaxial magnetic anisotropy). (See, e.g., D. Bai et. al, *Writer Pole Tip Remanence in Perpendicular Recording*, IEEE Transactions on Magnetics Vol. 42, No. 3 (March 2006), at 473-480 (discussing use of laminated and/or antiferromagnetically coupled poles to combat remanent erasure, *i.e.*, EAW); X. Shen and R.H. Victora, *Effect of Pole Tip Geometry on Remnant Field*, Journal of Applied Physics 103, 07F542-1 (2008) (discussing pole tip geometry design that “reduces the remnant field dramatically”).)

VI. THE '988 PATENT

A. Overview

164. The '988 Patent is entitled “Magnetic Material Structures, Devices and Methods,” and lists David N. Lambeth as its inventor.

165. In the Background section of the '988 Patent, the patent states that devices using magnetic materials will have “an improved performance if the magnetic properties can be better controlled during construction.” ('988 Patent at 1:29-31.) The '988 Patent posits that controlling the “magnetocrystalline anisotropy energy” of thin

films may create a “preferred direction, or directions, of orientation” for the magnetic material. (*Id.* at 1:36-38.)

166. The ’988 Patent contends that “good performance in device applications is almost always dependent upon there being a single preferred magnetic orientation or anisotropy direction and so in the manufacturing process one strives to achieve a desired uniaxial anisotropy.” (*Id.* at 1:45-49.) It states that: “[i]n general the anisotropy energy is a function of the orientation of the magnetization vector with respect to a given physical axis” and defines a “uniaxial” anisotropy to exist “if the anisotropy energy density function only contains a single maximum and a single minimum as the magnetization angle, θ , is rotated by 180 degrees from a physical axis.” (*Id.* at 1:56-60.)

167. The ’988 Patent states that others have suggested that uniaxial anisotropy results from certain phenomena such as (i) atomic pair ordering induced during a thermal treatment (known as annealing) and/or induced during deposition of a material in the presence of an applied magnetic field, (ii) strain anisotropy, and/or (iii) shape anisotropy. (*Id.* at 4:60-5:17, 6:15-34, 6:46-48; *see also, e.g.,* M. Takahashi and T. Kono, *Magnetic Anisotropy Induced by Magnetic and Stress Annealing in Co, Co-Ni and Co-Fe Alloys*, Japanese Journal of Applied Physics Volume 17 Number 2 (1978) (“The uniaxial magnetic anisotropy for induced by magnetic annealing has been studied for Co, Co-Ni alloys . . . and for Co-Fe, Fe-Ni alloys . . .”).) In contrast to the above-described mechanisms of uniaxial anisotropy, the ’988 Patent states that: “An objective of the present invention is to provide new mechanisms for controlling the magnetocrystalline anisotropy of thin magnetic films. By doing so the performance of almost all magnetic devices are envisioned to be improved.” (*Id.*, 1:49-53.)

168. The “new mechanism[] for controlling the magnetocrystalline anisotropy” posited by the ’988 Patent is to grow particular combinations of magnetic bcc-d(110) crystals with particular orientations—called “variants”—that, if exchange-coupled, may result in a uniaxial magnetocrystalline anisotropy.

169. In particular, the ’988 Patent states that growing a bcc-d magnetic material over a (111) textured hexagonal atomic under special conditions will result in six possible bcc-d variant crystals forming. The ’988 Patent posits that if one can induce

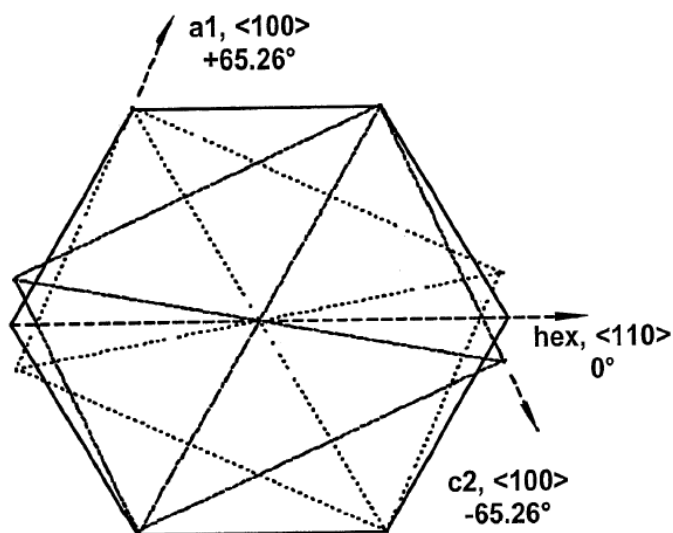
specific, exchange-coupled combinations of these six variants to grow in unequal amounts, the result is a “symmetry broken structure” that yields uniaxial magnetic anisotropy in the magnetic layer:

By carefully controlling the epitaxial growth conditions of (110) crystalline textured bcc or bcc derivative thin film materials on highly oriented (111) hexagonal atomic templates the applicant has invented a new set of six crystalline variants with special orientational relationships. By the selection and growth of a very special exchange coupled subset of these six orientational variants a symmetry broken uniaxial magnetic thin film is obtained.

(*Id.* at 14:48-55.)

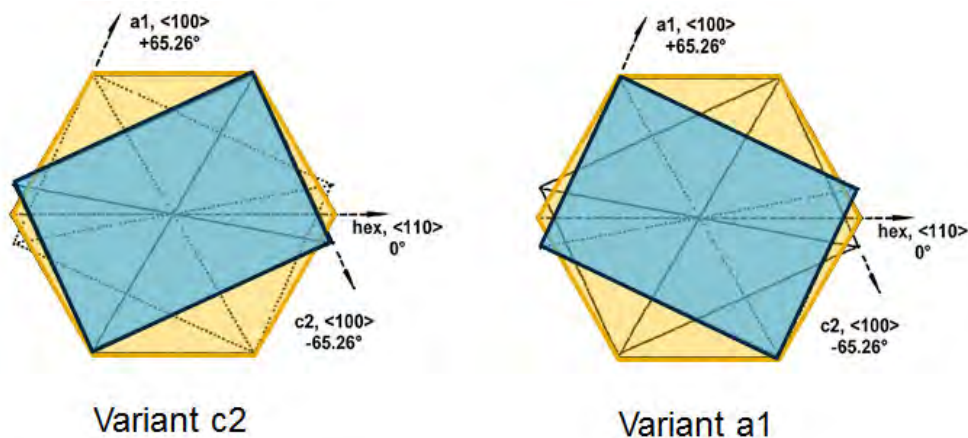
170. Because it is the variants’ orientations relative to the underlying hexagonal template that distinguishes them from one another, the ’988 Patent defines each of the six variants based on the variant’s orientation relative to the underlying hexagonal template that directed its growth. (*See, e.g.*, ’988 Patent at 18:33-45; *see also* 14:51-55 (“[T]he applicant has invented a uniaxial response by the combination of a set of six crystalline variants with special orientational relationships.”) The ’988 Patent labels each of the six bcc-d variants as “a1,” “a2,” “b1,” “b2,” “c1,” and “c2” and provides specific descriptions of their orientational relationships. (*Id.* at 18:33-45.)

171. For example, Figure 5 of the ’988 Patent depicts two of the six variants—“a1” and “c2”—based on their orientational relationship to an underlying (111) hexagonal template crystal. The ’988 Patent describes Figure 5 as showing “an illustration of two of the six possible orientational variants of the (110) crystal plane of a bcc-d crystal in comparison to the atomic arrangement of the (111) crystal plane of a hexagonal lattice template crystal.” (*Id.* at 13:39-42.)



('988 Patent, FIG. 5)

172. To see these orientational relationships more clearly, I have reproduced Figure 5 from the '988 Patent in two diagrams below to illustrate how each of these two variants is oriented:

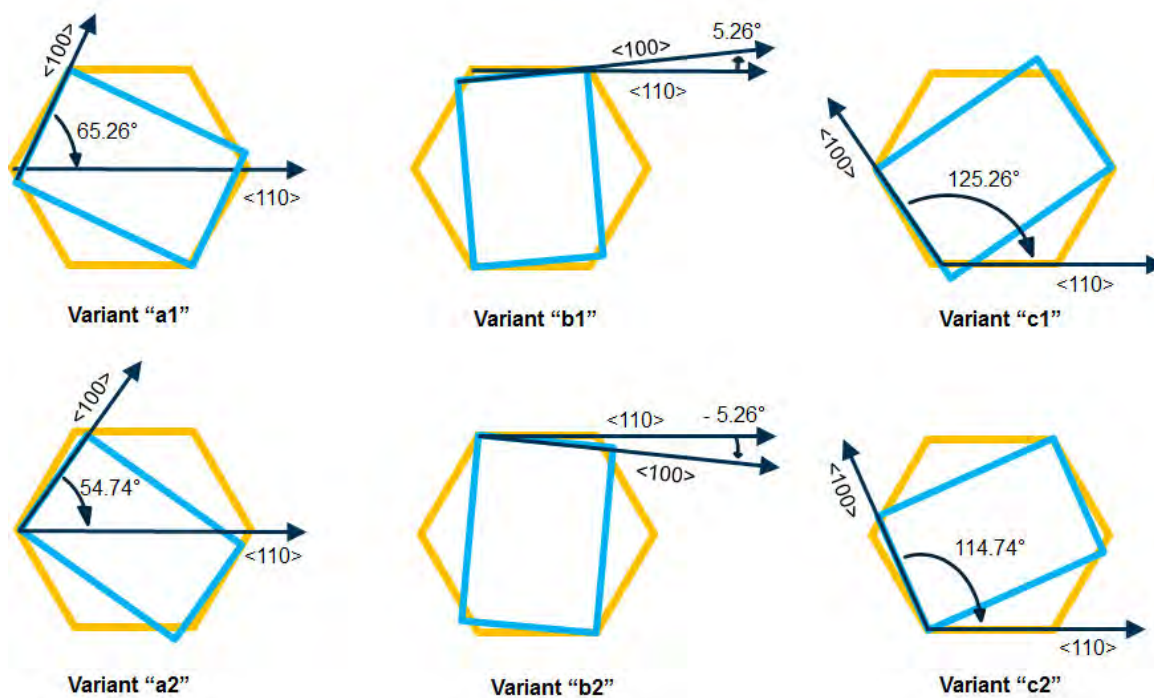


173. As shown in annotated Figure 5 above, atoms at the corners of the overlying rectangular bcc-d crystals will align with certain atoms on the surface of the underlying hexagonal template crystal. The variant labeled as “a1” is aligned with the underlying hexagonal crystal so as to share atoms at two points—creating an orientation in which a1’s $\langle 100 \rangle$ direction is 65.26 degrees relative to the $\langle 110 \rangle$ direction of the hexagonal crystal. Similarly, the other bcc-d variant (shown on the right) is identified as

“c2” and is aligned with two other points—creating an orientation in which c2’s $\langle 100 \rangle$ direction is -65.26 degrees (or equivalently, 114.74 degrees) relative to the $\langle 110 \rangle$ direction of the hexagonal crystal.

174. The particular rotational orientations of the bcc-d variants with respect to the underlying hexagonal crystal—specifically the orientation of the variant’s $\langle 100 \rangle$ direction relative to the hexagonal crystal’s $\langle 110 \rangle$ direction—is how the ’988 Patent describes and distinguishes the six variants of the magnetic layer. (*See id.* at 18:33-45.) The angle between (i) a variant’s $\langle 100 \rangle$ direction in the (110) plane and (ii) the $\langle 110 \rangle$ direction of the hexagonal template uniquely identifies each variant: “a1(60+ δ), a2(60- δ), b1(0+ δ), b2(0- δ), c1(120+ δ), and c2(120- δ).” (*Id.* at 18:36-38.)

175. The patent states posits that, because of slight variations in atomic spacing among materials, there will be a constant offset angle, δ . Shown below, for example, is each of the six possible variants where the offset is 5.26 degrees:



176. The ’988 Patent posits that certain combinations of the six variants will result in a symmetry broken structure that yields uniaxial anisotropy, while other

combinations will not. To deduce which combinations will work for variants grown on a single crystal hexagonal atomic template, the patent applies a simplified version of an equation from Soshin Chikazumi that describes the magnetic anisotropy energy density function of a bcc(110) crystal.

177. In particular, the '988 Patent states that “[t]o understand the magnetic properties of (110) textured magnetic bcc materials grown on a (111) texture fcc subst[r]ate we consider the expression for the cubic magnetocrystalline anisotropy energy when the magnetization is confined to the thin film plane of a single crystal of cubic material.” (*Id.* at 11:33-37.) The '988 Patent states that the energy density of a single bcc(110) crystal at a particular angle, θ , is given by the following equation (the “Chikazumi Equation”):

$$E_{110}(\theta) = K_1 \left\{ (1/4) \sin^4(\theta) + \sin^2(\theta) \cos^2(\theta) \right\} + K_2 \left\{ (1/4) \sin^4(\theta) \cos^2(\theta) \right\} + \text{higher } K \text{ terms.}$$

(*Id.* at 11:45-52.)

178. Although the '988 Patent cites the Chikazumi Equation shown above, it does not actually apply the Chikazumi Equation as written. Instead, the '988 Patent makes certain simplifying assumptions to the equation—namely, it assumes that $K_1 > 0$ and that higher order anisotropy constants such as K_2 and K_3 are all zero. (*See id.* at 11:56-58 (“The higher order energy terms are usually much smaller and are neglected.”).)

179. Using the simplified Chikazumi Equation, the '988 Patent purports to show mathematically that a single bcc(110) crystal by itself will not exhibit uniaxial anisotropy. (*See, e.g.*, FIG. 4; 12:48-54.) It theorizes, however, that while a single bcc(110) crystal by itself will not yield uniaxial anisotropy, growing certain exchange-coupled combinations of bcc(110) crystals of a six-variant system might yield uniaxial anisotropy. (*Id.* at 14:48-55; 20:14-23.) The '988 Patent applies the simplified Chikazumi Equation to predict and plot the energy density functions for various combinations of the six variants grown on a single crystal hexagonal atomic template. (*Id.* at FIG. 6, FIG. 7, FIG. 8, FIG. 10, FIG. 11.)

180. Of the 56 possible combinations of the six variants,⁴ the '988 Patent posits that “there are six possible balanced variant combinations that will yield exact Stoner-Wohlfarth like [uniaxial] energy curves . . . plus there are six possible balanced variant combinations that will yield uniaxial, but wavy energy density functions. All others yield non-uniaxial behavior.” (*Id.* at 20:18-23.) Therefore, when the '988 Patent states that “[b]y the selection and growth of a very special exchange coupled subset of these six orientational variants a symmetry broken uniaxial thin film is obtained” (*id.* at 14:52-55), it is referring to the variant combinations that it predicts will yield uniaxial anisotropy based on the simplified Chikazumi Equation.

B. Asserted Claims

181. I understand that LMS is asserting the following claims of the '988 Patent against Seagate: Independent claims 1 and 27, and dependent claims 3, 6, 7, 9, 17, 19, 28, and 29.

⁴ There are 56 combinations of variants possible when the variants are grown on a *single crystal* hexagonal template:

$$\binom{6}{2} + \binom{6}{3} + \binom{6}{4} + \binom{6}{5} = 56$$

For *polycrystalline* hexagonal templates, however, the number of possible variant combinations increases exponentially with the number of grains in the template.

For a polycrystalline template with just two grains, the number of possible variant combinations is 4,070:

$$\sum_{k=2}^{11} \binom{12}{k} = 4,070$$

Because it quickly becomes unworkable to apply the Chikazumi Equation to the millions or billions of possible variant combinations for most *polycrystalline* templates, the '988 Patent's calculations of variant combinations that yield uniaxial anisotropy are confined to variants grown on *single crystal* hexagonal atomic templates.

182. The two independent claims—1 and 27—are identical except for their preambles. Claim 1’s preamble recites “A magnetic material structure comprising,” while claim 27’s preamble recites “A magnetic device having incorporated therein a magnetic material structure comprising.” Because this difference in the claims’ preambles does not affect my non-infringement analysis, I analyze claims 1 and 27 together.

183. Claim 1 recites:

A magnetic material structure comprising
a substrate;
at least one bcc-d layer which is magnetic, forming a uniaxial
symmetry broken structure; and
at least one layer providing a (111) textured hexagonal atomic
template disposed between said substrate and said bcc-d layer.

C. Claim Construction of the Asserted Claims

184. I understand that the Court construed several of the terms found in the Asserted Claims in an Opinion and Order dated October 18, 2017 (“Claim Construction Order”). The Claim Construction Order construed the terms as follows:

	Term	Court’s Construction
1.	atomic template	An atomic pattern upon which material is grown and which is used to direct the growth of an overlying layer
2.	layer providing a (111) textured hexagonal atomic template	Layer that is predominately (111) hexagonal and that provides an atomic template
3.	symmetry broken structure	A structure consisting of unequal volumes or unequal amounts of the bcc-d variants of a six variant system
4.	variant/orientational variant	One of a set of possible crystal orientations

	Term	Court's Construction
	variants/orientational variants	Two or more of a set of possible crystal orientations
5.	uniaxial	Having an anisotropy energy density function with only a single maximum and a single minimum as the magnetization angle is rotated by 180 degrees from a physical axis
6.	uniaxial symmetry broken structure	A structure that is uniaxial as a result of the structure being symmetry broken
7.	bcc-d	Either a body centered cubic or a body centered cubic derivative crystal structure
8.	fcc-d	Either a face centered cubic or a face centered cubic derivative crystal structure

185. I have applied these claim constructions in forming my opinions in this case.

VII. THE ACCUSED SEAGATE PRODUCTS

186. In this section, I discuss the Seagate write head designs that LMS has accused of infringing the Asserted Claims of the '988 Patent, and more particularly the specific portions of those write heads that LMS's experts Dr. Coffey and Dr. Clark have focused on in their expert reports.

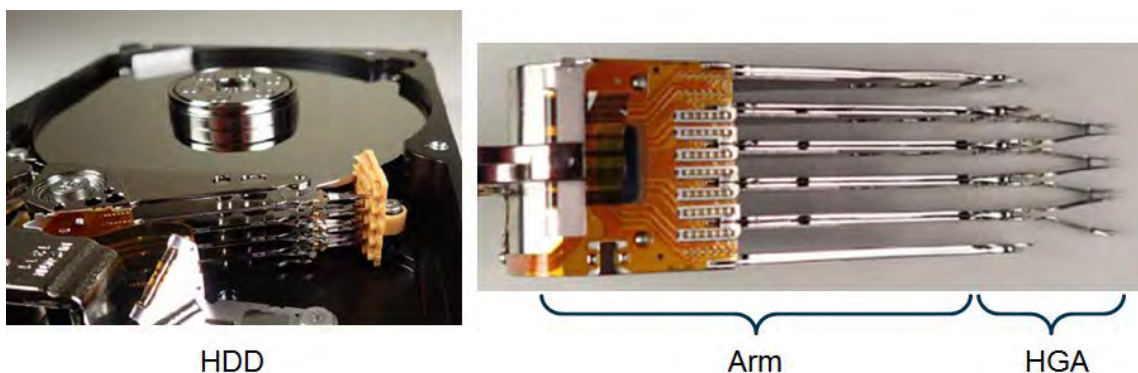
A. Overview of the Accused Products

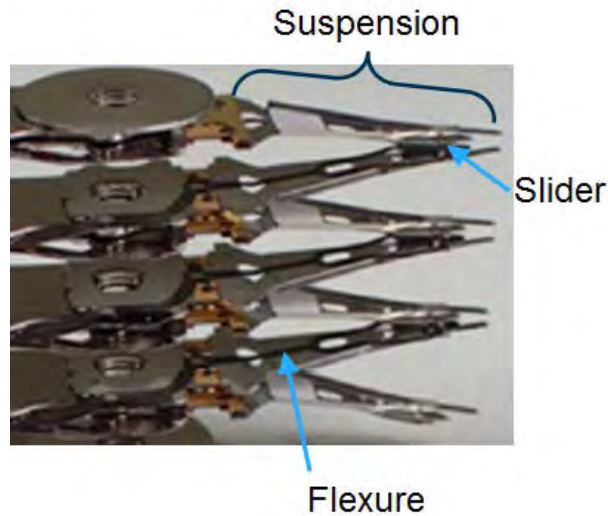
187. I understand that LMS contends that Seagate's hard disk drives containing write heads that use one of the following three Seagate designs infringe the Asserted Claims: [REDACTED] (*See, e.g., Coffey, ¶ 51.*)

188. Based on information in the documents and testimony that I have considered in the case, I understand that each of the write heads using one of these designs is a functional component that writes data to the media in Seagate hard disk drives. I understand that Seagate has supplied information about the Seagate HDD models that use one of these three write head designs.

189. In my opinion, each of these write heads is the smallest separate component that serves the function of writing data to the media in a hard disk drive. Each of these write heads, in turn, forms part of the slider in a hard disk drive, which is a larger component that also contains a read head. The read head is another separate functional component that reads data from the media of a hard disk drive. The slider containing both the write head and the read head is mounted on the head-gimbal assembly ("HGA") within the hard disk drive. As explained above, the HGA contains numerous components in addition to the slider (which contains the read and write head), including a suspension, flexures, and circuitry for controlling the HGA.

190. Set forth below are annotated photographs taken from Dr. Coffey's report showing each of these components in a sample Seagate hard disk drive:





191. Seagate began its independent research and development of PMR at its Pittsburgh research facility in the late 1990s. (SEA02887989; SEA01043275 at SEA01043284.) Seagate's Pittsburgh facility first demonstrated a PMR HDD on or around June 28, 2001 using PMR recording media to reach areal densities up to 35 GB/in². (SEA01043275 at SEA01043282.) The second PMR demonstration occurred shortly thereafter around July 6, 2001. (*Id.*) For the second demonstration, a solid pole PMR head comprising a single layer of a high-moment material was used to achieve areal densities up to 62 GB/in². (*Id.*) Seagate's third PMR demonstration occurred around October 8, 2001 using a "hybrid" PMR write head and reaching areal densities up to 83 GB/in². (*Id.*) The hybrid PMR write head included a write pole with a layer comprising a high-moment material (*i.e.*, 2.1T FeCoB) positioned on a layer comprising a low-moment material (*i.e.*, 0.5T NiFeCr). (SEA01043459 at SEA01043464–SEA01043465 & SEA01043480.)

192. In 2001, Seagate's Pittsburgh facility transferred responsibility for developing PMR HDDs to development teams in Bloomington, Minnesota and Fremont, California. (*See, e.g.*, SEA01043148.) As part of that transfer, Seagate's Pittsburgh team summarized their progress and findings in a report (SEA01043148), which was accompanied by five additional reports focusing on different technological aspects of PMR HDDs. The longest of the reports focused on the electronics used to support PMR.

(SEA01044086.) Another report discussed PMR media, modeling, and material science. (SEA01043618.) One report discussed modeling and testing the various PMR systems required to be integrated in a functioning PMR HDD. (SEA01043275.) Another report discussed the ability for PMR media and heads to magnetize and de-magnetize quickly. (SEA01043967.) Another report focused on PMR write head designs. (SEA01043459.)

193. The PMR write head report detailed various aspects of write heads the Pittsburgh team investigated for making a PMR write head. (SEA01043459 at SEA01043503–SEA01043505.) These aspects included write pole shapes (SEA01043459 at SEA01043473–SEA01043474); write pole layer thicknesses (SEA01043459 at SEA01043492); write head shield shapes, thicknesses, and positions (SEA01043459 at SEA01043475–SEA01043479); write head coil configurations (SEA01043459 at SEA01043484); manufacturing processes (SEA01043614; SEA01043459 at SEA01043505–SEA01043539); and write head modeling (SEA01043459 at SEA01043541–SEA01043552), among others.

194. The Seagate teams in Bloomington and Fremont continued optimizing aspects of PMR write heads. For example, the teams investigated the electronics, media, modeling, and various write head parameters (*e.g.*, write pole shapes, layer thicknesses, shield shapes and thicknesses, coil configurations, manufacturing). (SEA00026547.) As these and other features were optimized, Seagate continued demonstrating increased areal density, including 100 GB/in² in October 2002, 200 GB/in² in October 2004, and 300 GB/in² in December 2005. (SEA02887989.)

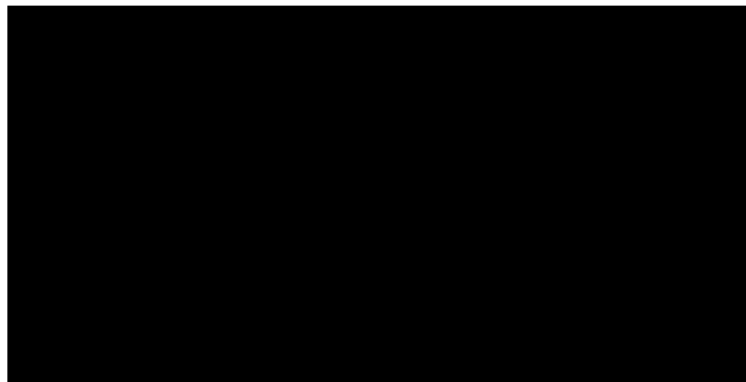
195. Seagate's first PMR HDD product was internally called "Pioneer," which was an enterprise drive released as test units to certain customers in 2004. (SEA00022942.) The first widely available PMR HDD was internally called "Venus," which was commercially released in December 2005 under the name Momentus 5400.3, a 2.5-inch notebook HDD with a capacity of 160 GB. (SEA02887989.) Seagate's first PMR HDDs used a write pole configuration internally referred to as "[REDACTED]," which was followed by "[REDACTED]," and then "[REDACTED]"

196. In the remainder of this section, I set forth my understanding of the three accused write head designs—[REDACTED]—and information provided by

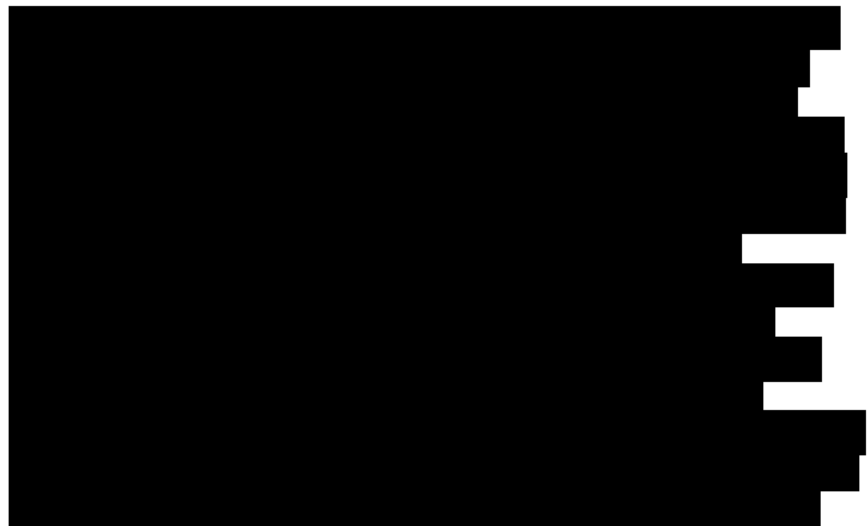
Seagate relating to those designs. I then describe the particular portions of these write head designs that LMS's experts Dr. Coffey and Dr. Clark have accused of practicing one or more limitations of the Asserted Claims. I explain in Section IX below why, in my opinion, the [REDACTED] write heads do not meet all the limitations of any Asserted Claim.

B. [REDACTED]

197. The write heads using the [REDACTED] design comprise thin films of particular materials. For their analyses, Dr. Coffey and Dr. Clark rely on descriptions from Seagate of the material compositions for these layers, which I also take to be true. In particular, the [REDACTED] design includes: a substrate, followed by layers of NiFe, FeCo, NiFe, and FeCo.



198. [REDACTED]



[REDACTED]

(Seagate's First Supplemental Response to LMS's Interrogatory No. 10, at 14-15.) I note that while nanowebers is a measure of magnetic flux, it can be converted to Angstroms (a measure of layer thickness), with 1000 Angstroms of FeCo (2.4T) equal to 45.5 nanowebers. (*Id.*)

199. Dr. Coffey describes in his report two particular [REDACTED] samples that he and Dr. Clark examined in forming their opinions.

200. Dr. Coffey states that reverse engineering was performed "at my direction on a representative [REDACTED] Product, specifically a hard disk drive bearing Seagate model no. ST32000645SS 6 TB and referred to as sample S0GPPC." (Coffey, ¶ 131.) Dr. Coffey included a photograph of this hard disk drive, which identifies the drive as a Constellation ES.2 Hard Drive. (*Id.*)

201. Dr. Coffey states that reverse engineering was also performed "at my direction on a second representative [REDACTED] Product, specifically a hard drive produced by Seagate bearing Seagate model no. ST3000NM0023 3TB and referred to as sample, S2MMMC." (*Id.* at ¶ 132.) Dr. Coffey included a photograph of this hard disk drive, which identified the drive as a Constellation ES.2 Hard Drive. (*Id.*)

202. I reproduce below the photographs from Dr. Coffey's report of the two hard disk drives considered by Dr. Coffey and Dr. Clark in their analyses of Seagate's [REDACTED] write head design:



Seagate HDD from Coffey p. 70, of sample S0GPPC, an [REDACTED] product.



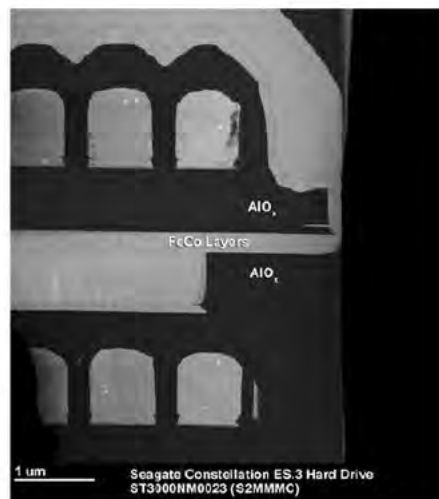
Seagate HDD from Coffey p. 71, of sample S2MMMC, an [REDACTED] product.

203. In their reports, Dr. Coffey and Dr. Clark provide a series of photographs showing various stages of the reverse engineering conducted to obtain the two samples (S0GPPC and S2MMMC)—one from each hard disk drive depicted above.

204. Cross-Section View of the Write Head. Among the photographs included in Dr. Coffey's report are TEM images showing a cross-section of sample S0GPPC (taken from the first hard disk drive), and another for sample S2MMMC (taken from the second hard disk drive), both of which are reproduced below. (*Id.* at ¶¶ 136-142.)



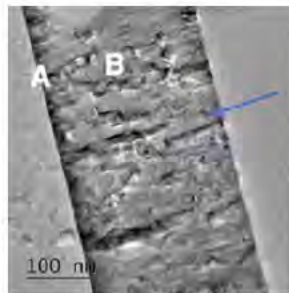
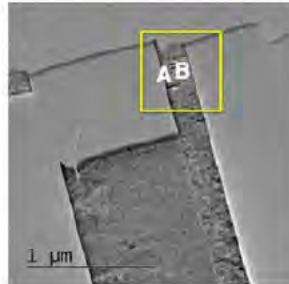
Cross section of sample S0GPPC, an [REDACTED] product, from Coffey p. 81.



Cross section of sample S2MMMC, an [REDACTED] product, from Coffey p. 81.

205. Dr. Coffey states in his report that “further TEM imaging at high resolution was performed on the cross-section of the write head prepared samples S0GPPC and S2MMMC, as described in Dr. Clark’s report.” (Coffey, ¶ 145.)

206. Those images, which Dr. Coffey reproduces from Dr. Clark’s report, are shown below:



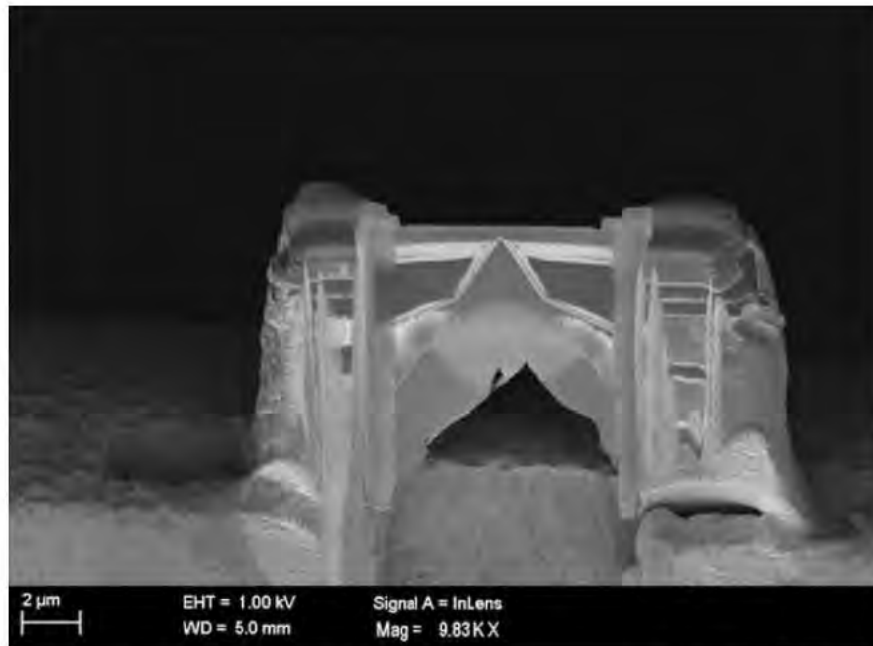
Cross section of sample S0GPPC, an [REDACTED] product, from Coffey p. 83.



Cross section of sample S2MMMC, an [REDACTED] product, from Coffey p. 84.

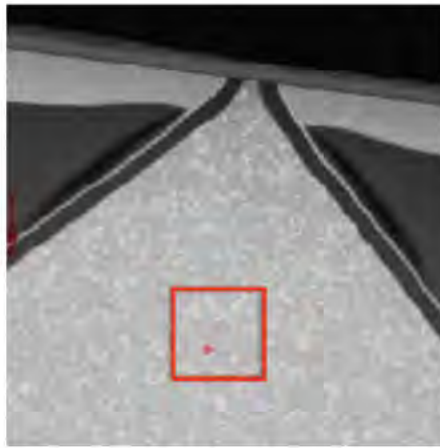
207. Dr. Clark describes the above images as a “TEM overview of S0GPPC, with regions where high resolution cross-sections were taken marked A and B.” (Clark, ¶ 81, Figure 35.) According to Dr. Clark, the TEM images were obtained using an “FEI Titan 80-300 S-Twin microscope (‘Titan’), operating in TEM mode at 300 kV, and fitted with an automated image corrector to enhance the spatial resolution.” (*Id.* at ¶ 81.)

208. Plan View of Write Head. Dr. Coffey next states that milling was done on the samples to form a plan view (top-down view) of the lower FeCo layer of sample S0GPPC. (*Id.* at ¶ 165-66.) The image below is described by Dr. Coffey in his report as “the sample of the lower FeCo layer [that] has been milled down to adequate transparency for further analysis.” (*Id.* at ¶ 171.)

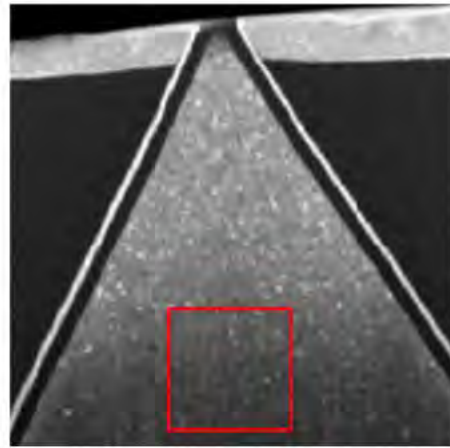


Lift-out Plan View of sample S0GPPC, an [REDACTED] from Coffey p. 101.

209. Microbeam Diffraction Measurements. This milled sample was tested by Dr. Clark using microbeam diffraction. In particular, Dr. Coffey states: “I understand that Dr. Clark performed microbeam diffraction analysis on the area of plan view samples from S0GPPC and S2MMMC as indicated by the red annotation on the TEM images below, which are reproduced from Dr. Clark’s report.” (*Id.* at ¶ 171.) According to Dr. Coffey, the first image below depicts sample S0GPPC, and the second image depicts sample S2MMMC:



Plan view of sample S0GPPC, an [REDACTED] product, from Coffey p. 106.



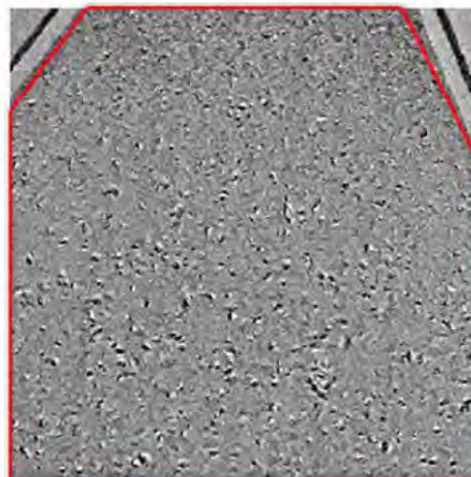
Plan view of sample S2MMMC, an [REDACTED] product, from Coffey p. 107.

210. I note that Dr. Clark, in his report, states that the areas designated by the red boxes shown in the photographs above are the areas where he performed microbeam diffraction. (*See, e.g.*, Clark, at p. 23 (“The red box on the left indicates the area in the sample from which the diffraction patterns were taken.”).)

211. Dark Field Imaging Measurements. Dr. Coffey in his report also describes dark field imaging performed by Dr. Clark on portions of the plan views for samples S0GPPC and S2MMMC. Dr. Coffey states: “I understand that Dr. Clark performed a dark field imaging analysis on the area of a plan view sample from samples S0GPPC and S2MMMC as indicated by the red annotation on the TEM image[s] below, which is reproduced from Dr. Clark’s report.” (Coffey, ¶ 187 (citing to Sections E.2.f, F.1.a.5, and F.1.b.5 of Clark’s report).) Based on this statement, the first image below depicts the lower FeCo layer of sample S0GPPC, and the second image depicts the same for sample S2MMMC. (Coffey, ¶ 187.)



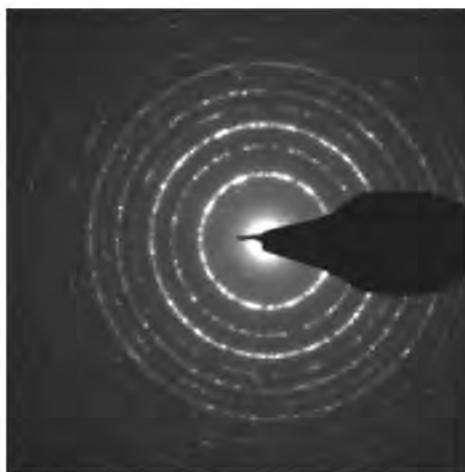
Plan view of sample S0GPPC, an asphalt product, from Coffey p. 109.



Plan View of sample S2MMMC, an asphalt product, from Coffey p. 109.

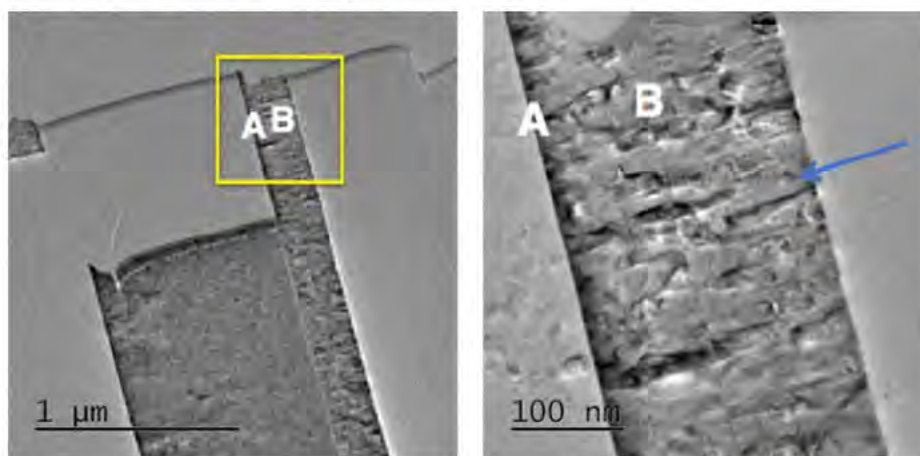
212. Dr. Coffey further states that the dark field images from these portions of samples S0GPPC and S2MMMC were used for calculating the relative area fractions of crystallites having aligned $\langle 100 \rangle$ directions as “a function of the measurement angle in the plane at 10 degree intervals from a physical axis for samples S0GPPC and S2MMMC” (citing to Sections F.1.a.5 and F.1.b.5 of Clark’s report). (*Id.* at ¶188.)

213. Diffraction Rings. I note that the area outlined in red for sample S0GPPC apparently was also used by Dr. Clark to obtain the diffraction “ring” pattern showing the various orientations of crystallites in the imaged area. (See Clark, ¶ 57 and Figure 19 (explaining that Figure 19 is a “[d]iffraction pattern taken from S0GPPC, and incorporating many crystallites”).) This ring pattern from Dr. Clark’s report is reproduced below:



Clark at p. 27, Figure 19

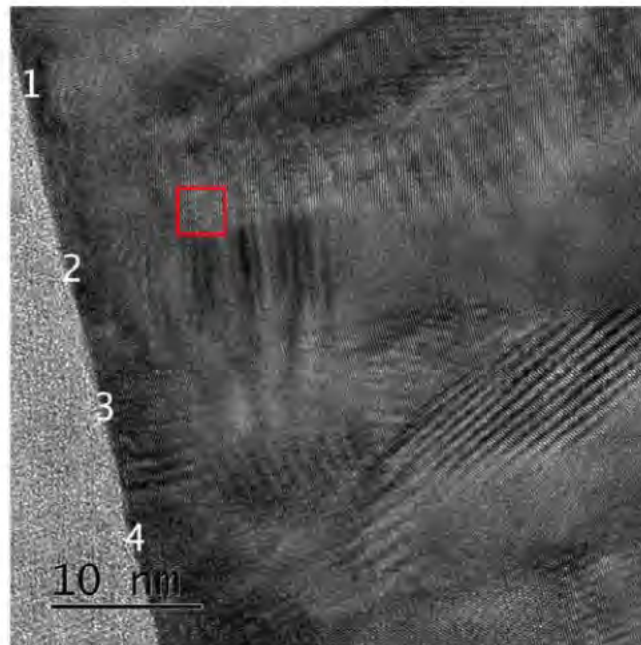
214. High-Resolution TEM Images. Dr. Clark's report contains additional high-resolution TEM cross-section images taken of samples S0GPPC and S2MMMC. (See, e.g., Clark, ¶¶ 62-65.) In particular, Dr. Clark states that "high resolution cross-section images were obtained from two regions of the write pole of S0GPPC as shown in Figure 35 below – at the left-hand edge (A), where the lower NiFe layer is, and in the center (B), where the upper NiFe is." (Clark, ¶ 81.) These images of cross-section images of sample S0GPPC are reproduced below:



Cross section of sample S0GPPC, an [REDACTED] product, from Clark p. 42.

215. FFTs. Dr. Clark also states in his report that additional "zoomed-in" images were taken from both regions A and B of this cross-section. (See, e.g., Clark, ¶¶ 83-86.) A specific zoomed-in area was selected for taking FFTs "at selected points in

high resolution cross-section images” from region A. (*Id.* at ¶ 87.) In particular, Dr. Clark states that FFTs were taken at four points “along the lower NiFe/lower FeCo interface” marked with numbers 1, 2, 3, and 4 in Figure 41 of his report. (*Id.*) These FFTs were taken “(a) in the lower NiFe layer at the location of the numbered points; and (b) in the lower FeCo immediately to the right of the numbered point.” (*Id.*) Figure 41 from Dr. Clark’s report showing each of these numbered points from region A is reproduced below:



Cross section of sample S0GPPC, an [REDACTED] product, from Clark p. 50.

(Clark, ¶ 87 and Figure 41.)

216. Dr. Clark allegedly also took FFTs at points other than at point 2. (*Id.* at ¶ 94 and n.17.)

217. Dr. Clark apparently undertook a similar process for taking FFTs in zoomed-in areas of the cross-section for sample S2MMMC. (*See, e.g.,* Clark, ¶¶ 131-134.) Figure 71 from Dr. Clark’s report, showing each of the numbered points from region A for sample S2MMMC at which FFTs were allegedly taken, is reproduced below:



Cross section of sample S2MMC, an [REDACTED] product, from Clark p. 84.

(Clark, ¶ 133 and Figure 71.)

218. Although there are other images that appear in Dr. Coffey's and Dr. Clark's reports that I address in my analysis below, the images set out above provide a basic framework for understanding the particular areas of samples S0GPPC and S2MMC that LMS contends meet the limitations of the Asserted Claims of the '988 Patent.

C. [REDACTED]

219. The write heads using the [REDACTED] design are made of thin films with a particular material structure. For their analyses, Dr. Coffey and Dr. Clark rely on descriptions from Seagate of the material compositions for these layers, which I also take to be true. In particular, the structure for the [REDACTED] design includes: a substrate, followed by layers of [REDACTED]

[REDACTED]

220. [REDACTED]

[REDACTED]

(Seagate's First Supplemental Response to LMS's Interrogatory No. 10, at 14.)

221. Dr. Coffey describes in his report the particular sample that was used in forming his and Dr. Clark's opinions regarding the thin film materials used in the write heads with the [REDACTED] design. In particular, Dr. Coffey states that reverse engineering was performed "at my direction on a representative [REDACTED] Product, specifically a hard disk drive bearing Seagate model no. ST500DM002-1BD142 500 GB and referred to as sample SBRD8K." (Coffey, ¶ 299.) Dr. Coffey included a photograph of this hard disk drive, which identifies the drive as a Barracuda Hard Drive. (*Id.*) I have included and reproduced below the photograph from Dr. Coffey's report of the specific hard disk drive used by Dr. Coffey and Dr. Clark in conducting their analyses of Seagate's [REDACTED] write head design:



Seagate HDD from Coffey p. 159, of sample SBRD8K, a [REDACTED] product

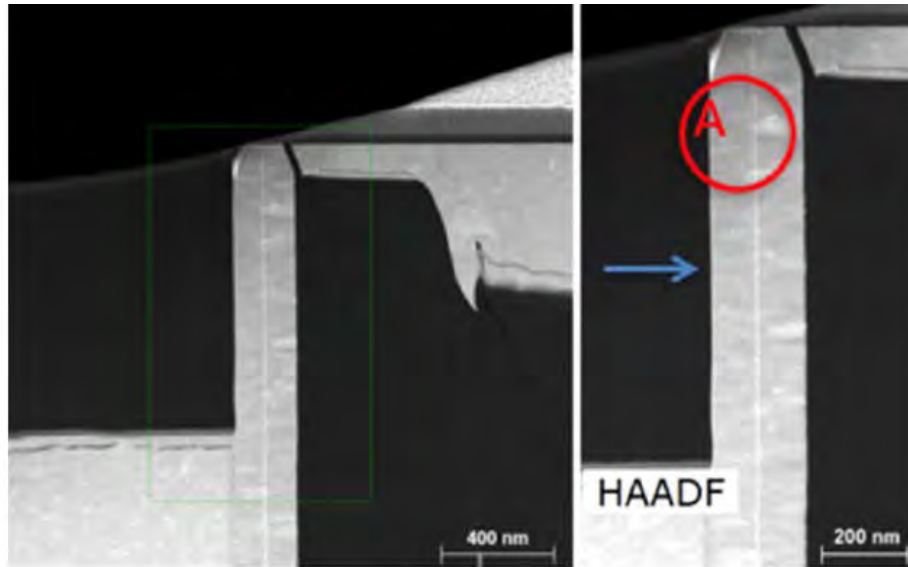
222. In his report, Dr. Coffey provides a series of photographs showing various stages of the reverse engineering allegedly conducted on a sample from the hard disk drive depicted above, on which testing was performed by Dr. Clark. Among the photographs included in Dr. Coffey's report were bright field images showing a cross-section of sample SBRD8K, reproduced below. (*Id.* at ¶¶ 300-304.)



Cross section of sample SBRD8K, a [REDACTED] product, from Coffey p. 164

223. Dr. Coffey then states in his report that “further TEM imaging at high resolution was performed on the cross-section of the write head prepared sample SBRD8K as described in Dr. Clark’s report” in sections E.2 and F.2.a.2. (Coffey, ¶

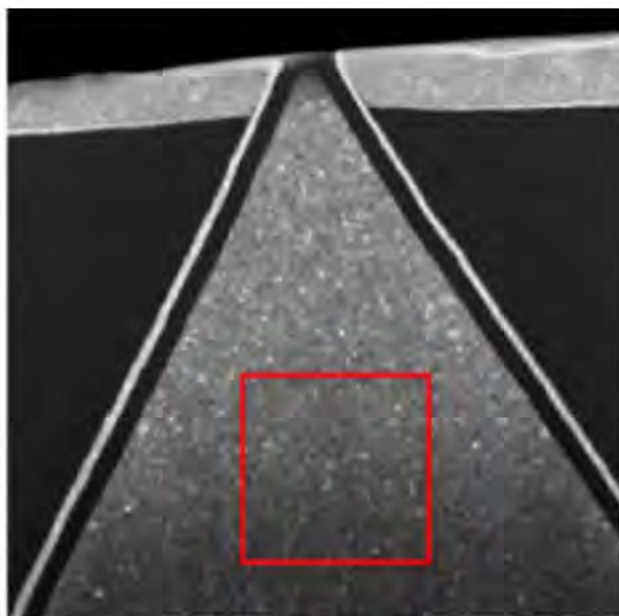
306.) Those images that Dr. Coffey reproduces from Dr. Clark's report are shown below:



Cross section of sample SBRD8K, a Hybrid X product, from Coffey p. 165

224. Dr. Clark describes these images as being obtained from “the circled region of the write pole of SBRD8K.” (Clark, ¶ 170 and Figure 96.) The TEM images allegedly were obtained using an “FEI Titan 80-300 S-Twin microscope (‘Titan’), operating in TEM mode at 300 kV, and fitted with an automated image corrector to enhance the spatial resolution.” (*Id.* at ¶ 179.)

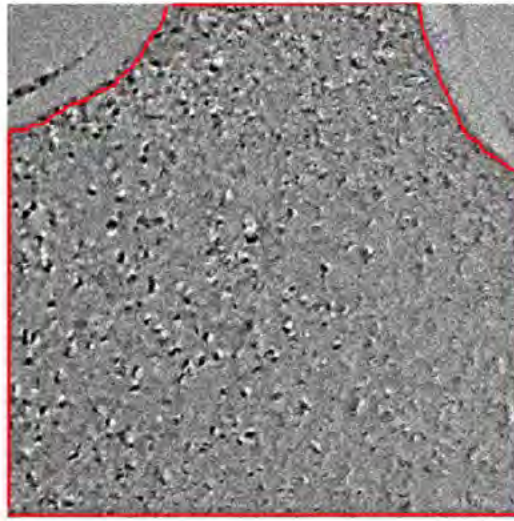
225. Dr. Coffey next states that milling similar to the one he described for the [REDACTED] samples was used on sample SBRD8K to form a plan view (top-down view) of the lower FeCo and NiFe layers of the write pole material in sample SBRD8K. (Coffey, ¶ 324.) This plan view sample was apparently tested by Dr. Clark using microbeam diffraction. In particular, Dr. Coffey states: “I understand that Dr. Clark performed microbeam diffraction analysis on the area of a plan view sample from SBRD8K as indicated by the red annotation on the TEM image below, which is reproduced from Dr. Clark’s report.” (*Id.* at ¶ 336.) This image is reproduced below from Dr. Coffey’s report at page 176:



Plan view of sample SBRD8K [REDACTED] product, from Coffey p. 176

226. I note that Dr. Clark, in his report, states that the area designated by the red box in the photograph above is the area in which he performed microbeam diffraction. (See Clark, p. 122 and Figure 16 (showing a red box for sample SBRD8K and stating that it depicts a “[p]lan view STEM image of SBRD8K near the pole tip of the write head (left). 1,600 diffraction patterns were taken from the area outlined in red.”).)

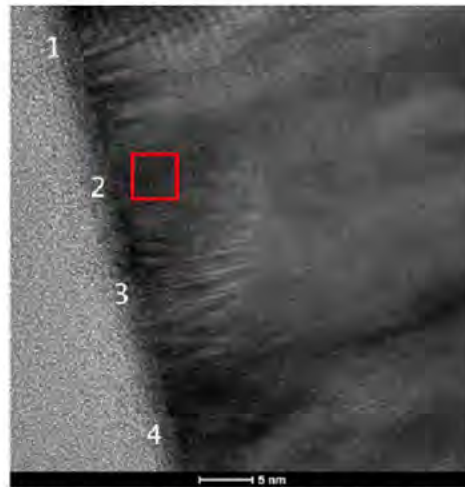
227. Dr. Coffey also describes dark field imaging that was performed by Dr. Clark on a portion of the plan view for sample SBRD8K. Dr. Coffey states: “I understand that Dr. Clark performed a dark field imaging analysis on the area of a plan view sample from sample SBRD8K as indicated by the red annotation on the TEM image below, which is reproduced from Dr. Clark’s report” (citing to Sections F.2.a.5. of Clark’s report). (*Id.* at ¶339; see also Clark at ¶¶ 202-205 and Figure 114 (explaining that Figure 114 shows the “[d]ark field image with area under analysis shown enclosed by the red box.”).) The image below apparently depicts the lower FeCo layer of sample SBRD8K. (Coffey at ¶ 339.)



Plan view of sample SBRD8K, a [REDACTED]
[REDACTED] product, from Coffey p. 178

228. Dr. Coffey further states that the dark field images from this portion of sample SBRD8K allegedly was used for calculating the relative area fractions of crystallites having aligned $\langle 100 \rangle$ directions as “a function of the measurement angle in the plane at 10 degree intervals from a physical axis for sample SBRD8K” (citing to Sections F.2.a.5 of Clark’s report). (*Id.* at ¶ 339.) Dr. Clark, in his report, confirmed that this was the area used to conduct his dark field image analysis. (Clark, ¶¶ 206-207 and Figure 116.)

229. Dr. Clark’s report contains additional high-resolution TEM cross-section images taken of sample SBRD8K. (*See, e.g.*, Clark, ¶¶ 172-176.) In particular, Dr. Clark states that “a high resolution cross-section image [was] taken in region A is shown in Figure 101 below, with a number of points along the lower NiFe/lower FeCo interface marked” with numbers 1, 2, 3, and 4. (*Id.* at ¶ 176.) According to Dr. Clark, FFTs were taken “(a) in the lower NiFe layer at the location of the numbered points; and (b) in the lower FeCo immediately to the left of the numbered point.” (*Id.*) Figure 101 from Dr. Clark’s report showing each of these numbered points from region A is reproduced below:



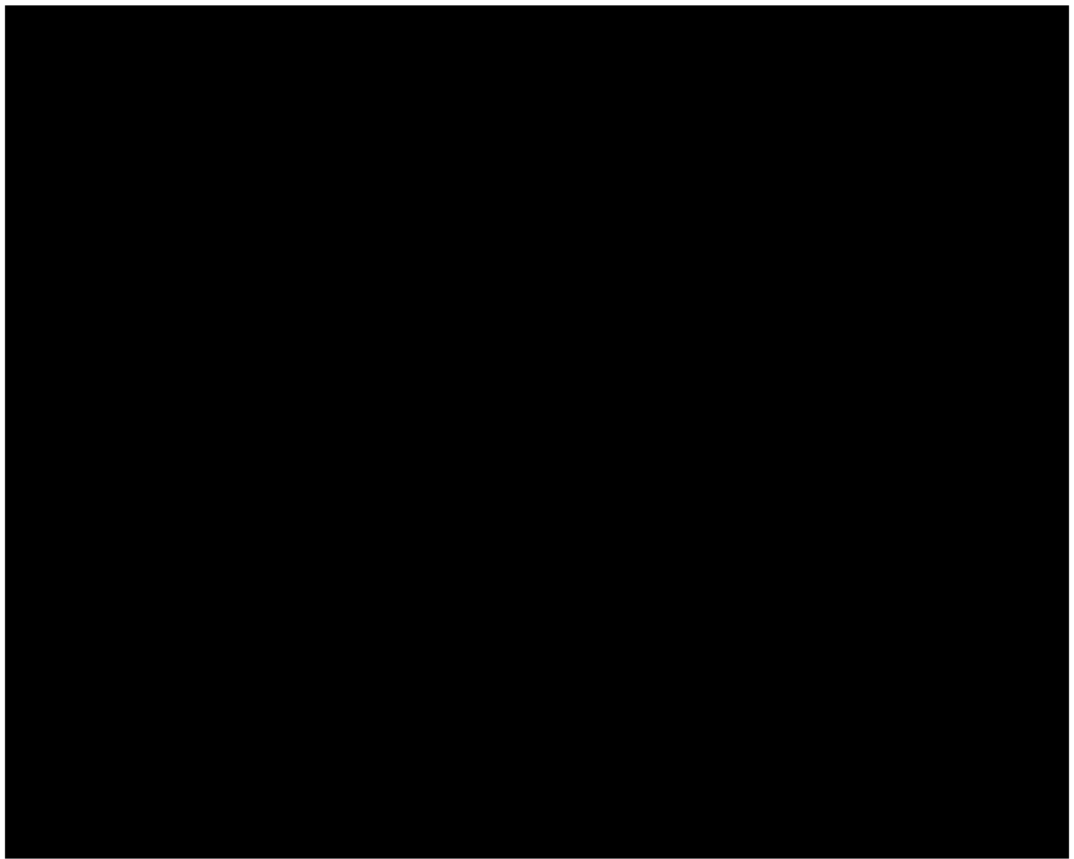
Cross section of sample SBRD8K, a [REDACTED] product, from Clark p. 176

230. Dr. Clark allegedly took FFTs at points other than point 2. (*Id.* at ¶183.)

231. Although there are other images that appear in Dr. Coffey's and Dr. Clark's reports that I address in my analysis below, the images set out above provide a basic framework for understanding the particular areas of sample SBRD8K that LMS accuses of infringing the Asserted Claims of the '988 Patent.

D. [REDACTED]

232. I understand that the write heads using the [REDACTED] design are no longer used by Seagate but that, when they were used, were made of thin films with a particular material structure. For their analyses, Dr. Coffey and Dr. Clark rely on descriptions from Seagate of the material compositions for these layers, which I also take to be true. (*See, e.g.*, Coffey at ¶ 459; Clark at ¶¶ 76-78.) In particular, the structure for the [REDACTED] design was a three-layer structure (from bottom to top) consisting of NiFe, FeCo, and aluminum oxide that repeated eight times.



233. According to Seagate, these materials had the following characteristics:



(Seagate's First Supplemental Response to LMS's Interrogatory No. 10, at 13-14.)

234. Dr. Coffey states in his report that he "was unable to obtain a sample of an [REDACTED] Product to reverse engineer." (Coffey, ¶ 460.) Despite not having any actual sample of a write head with the [REDACTED] design, Dr. Coffey states that "because of the substantial similarities between the lowest NiFe layer and the lowest FeCo layer in each of the [REDACTED] Products, I am able to rely on the same reverse engineering of these layers in the [REDACTED] Products in support of my infringement analysis for the [REDACTED] Products." (*Id.*)

235. Dr. Clark does not mention the [REDACTED] design and he did not conduct any tests or measurements of a sample write head using the [REDACTED] write head design.

VIII. LEGAL STANDARDS

236. Counsel for Seagate has informed me of general guidelines and rules for examining the claims of an issued patent to determine whether or not a claim is infringed by an accused product. I have been informed that the Court has construed various claim terms and set forth the Court's construction in a claim construction order. I understand infringement is determined by comparing what is accused of infringement to the claims as construed by the Court.

237. I understand that infringement is assessed on a claim-by-claim basis. Therefore, there may be infringement as to one claim but no infringement as to another.

238. I also understand that infringement of a dependent claim requires infringement of the independent claims on which the dependent claim depends, as well as infringement of any additional limitations in the dependent claim.

A. Literal Infringement

239. I understand that to prove literal infringement, the patentee must prove that it is more probable than not that the alleged infringer made, used, sold, offered for sale within, or imported into the United States a product that meets all the requirements of a claim.

240. For literal infringement, I understand that the accused product must contain each and every requirement of the asserted claim. If a device or product does not contain one or more requirement of a claim, I understand that device or product does not literally infringe the claim.

B. Infringement Under the Doctrine of Equivalents

241. For infringement under the doctrine of equivalents, I have been informed that the accused product must contain an element at least equivalent to each and every requirement of the asserted claim. I have been informed that a part of a product is equivalent to a requirement of an asserted claim if a person of ordinary skill in the art would think that the differences between the part and the requirement were insubstantial as of the time of the alleged infringement.

242. I understand that one may, but is not required to, use the function-way-result test to determine equivalence. I understand that under the function-way-result test, one analyzes whether, at the time of the alleged infringement, the accused product contains an element that performs substantially the same function in substantially the same way to achieve substantially the same result as the claim element.

243. I understand that a skilled practitioner's knowledge of the interchangeability between claimed and accused elements is also a factor in determining equivalence. I understand that the known interchangeability test looks to the knowledge of a person of ordinary skill in the art at the time of the alleged infringement to see whether that person would contemplate the interchange as a design choice. Evidence that the claimed and accused elements are not interchangeable alternatives weighs against a finding of equivalence.

244. I have been informed that, under the doctrine of prosecution history estoppel, a patentee may not use the doctrine of equivalents to capture any accused device that was disclaimed by a limiting amendment. I also understand that under the "all-limitations" rule the doctrine of equivalents cannot be applied so broadly as to effectively eliminate a claim element in its entirety.

C. Indirect Infringement (Induced Infringement)

245. I understand that the elements of an induced infringement claim are (1) proof that the indirect infringer knew of the patent during the alleged infringement, (2) proof that a third party directly infringed the patent, and (3) proof that the indirect infringer knowingly induced infringement and possessed specific intent to encourage the third party's infringement.

D. Person of Ordinary Skill in the Art

246. In my opinion, at the time of the invention, a person of ordinary skill in the art would have had a master's degree or a doctoral degree plus one or two years of experience, or a bachelor's degree plus five years of experience, in materials science and engineering, physics, electrical engineering, or a related field. This experience would include work on crystalline structures, magnetism, thin film science and technology, or a

related field. I am familiar with the level of skills of such persons based on my work in this field, including at the time of the invention of the '988 Patent.

247. I understand that Dr. Coffey has proposed the following definition of a person of ordinary skill in the art: “a person of ordinary skill in the art would have either (1) an advanced degree in physics, electrical engineering, or materials science, and at least five years of relevant post-graduate experience in magnetic materials, structures, and/or devices; or (2) an undergraduate degree in physics, electrical engineering, or materials science, and at least ten years of relevant experience in magnetic materials, structures, and/or devices.”

248. My opinions in this report do not depend on whether my definition of a person of ordinary skill in the art of the definition proposed by Dr. Coffey is applied. I believe that I am qualified to judge the capabilities and assess the perspective of a person of ordinary skill in the art under either definition.

E. Other Legal Matters

249. Priority Date of the '988 Patent. In forming my opinions in this case, I have assumed that the date of invention claimed in the '988 Patent is August 29, 2001, which is the earliest filing date for the application to which the '988 Patent claims priority. I understand that LMS has not provided any different date. I reserve the right to alter or amend my opinion if a different date of invention is found or asserted.

250. Standard for Expert Opinions. I understand that the standard for providing expert testimony under Rule 702 of the Federal Rules of Evidence provides that an expert may testify in the form of an opinion or otherwise if: (a) the expert's scientific, technical, or other specialized knowledge will help the trier of fact to understand the evidence or to determine a fact in issue; (b) the testimony is based on sufficient facts or data; (c) the testimony is the product of reliable principles and methods; and (d) the expert has reliably applied the principles and methods to the facts of the case. I understand that other relevant factors mentioned in the comments to Rule 702 and referred to as *Daubert* factors include (1) whether the expert's technique or theory can be or has been tested—that is, whether the expert's theory can be challenged

in some objective sense, or whether it is instead simply a subjective, conclusory approach that cannot reasonably be assessed for reliability; (2) whether the technique or theory has been subject to peer review and publication; (3) the known or potential rate of error of the technique or theory when applied; (4) the existence and maintenance of standards and controls; and (5) whether the technique or theory has been generally accepted in the scientific community.

IX. NON-INFRINGEMENT ANALYSIS

251. In this section, I discuss the accused Seagate products in further detail and compare the products to the Asserted Claims. Based on the analysis in this section, I conclude that the Accused Products do not infringe any of the Asserted Claims. I incorporate by reference the above discussion of the accused Seagate products in this analysis.

252. I have reviewed documents and other materials describing the manufacture, operation, properties, and other relevant aspects of the Accused Products. I have also reviewed deposition transcripts and discovery responses and inspected and/or operated certain versions of the Accused Products.

253. In Section IX.A, I explain why the Accused Products do not infringe claims 1 and 27 (the two asserted independent claims) of the '988 Patent.⁵ Specifically, I explain why the [REDACTED] write heads do not infringe claims 1 and 27 (Section IX.A), why the [REDACTED] write heads do not infringe claims 1 and 27 (Section IX.B), and why the [REDACTED] write heads do not infringe claims 1 and 27 (Section IX.C).

254. I understand that to infringe a dependent claim, one must infringe the independent claim upon which the dependent claim depends. Because I conclude that the asserted independent claims (claims 1 and 27) are not infringed by any Accused Product, I also conclude that the asserted dependent claims—of all of which depend on

⁵ Claims 1 and 27 differ only in their preambles. Because this difference in their preambles does not affect my non-infringement analysis, I analyze claims 1 and 27 together for purposes of non-infringement.

either claim 1 or 27—are also not infringed by any Accused Product. (*See* Section IX.D, *infra*.)

A. The Accused [REDACTED] Products Do Not Infringe Claims 1 and 27

255. In my opinion, the accused [REDACTED] products do not infringe claims 1 and 27 of the '988 Patent because the [REDACTED] write poles do not feature “at least one layer providing a (111) hexagonal atomic template.” (*See* Section IX.A.1, *infra*.)

256. In my opinion, the accused [REDACTED] products do not infringe claims 1 and 27 of the '988 Patent because the [REDACTED] write poles do not feature “at least one bcc-d layer which is magnetic, forming a uniaxial symmetry broken structure.” (*See* Section IX.A.2, *infra*.)

1. **The [REDACTED] products do not have “at least one layer providing a (111) textured hexagonal atomic template disposed between said substrate and said bcc-d layer”**

Term	Court's Construction
atomic template	“an atomic pattern upon which material is grown and which is used to direct the growth of an overlying layer”
layer providing a (111) textured hexagonal atomic template	“layer that is predominately (111) hexagonal and that provides an atomic template”

257. Dr. Coffey argues in ¶¶ 219-233 of his report that the accused [REDACTED] products have “at least one layer providing a (111) textured hexagonal atomic template disposed between said substrate and said bcc-d layer.” I have carefully considered Dr. Coffey's arguments and find his conclusion to be unfounded. None of Dr. Coffey's data supports his conclusion that the [REDACTED] products have “a layer that is predominately (111) hexagonal and that provides an atomic template.”

258. As discussed above, the [REDACTED] write heads comprise several layers, including [REDACTED], as depicted below:



259. I understand Dr. Coffey contends that the “lower layer of NiFe” is a “layer providing a (111) textured hexagonal atomic template disposed between said substrate and said bcc-d layer.” (*See, e.g.*, Coffey, ¶¶ 220, 222 (“I have concentrated my analysis on the lower (first-deposited) of the two layers of NiFe in the [REDACTED] Products . . .”).)⁶

260. I disagree. The lower NiFe layer in the [REDACTED] write heads does not meet this claim limitation because the lower NiFe layer is not a “(111) textured hexagonal atomic template.” The [REDACTED] write heads contain no NiFe layer that is “predominately (111) hexagonal.” Moreover, the [REDACTED] write heads contain no NiFe layer that directs the growth of an overlying layer.

⁶ I note that Dr. Coffey’s arguments in ¶¶ 219-231 focus exclusively on the lower NiFe layer—with no analysis of the upper NiFe layer. Nonetheless, Dr. Coffey asserts in conclusory fashion that “[w]hile my analysis concentrates on the lower NiFe layer and the lower FeCo layer, it is my opinion that all NiFe layers and FeCo layers in the write pole of the [REDACTED] products meet this limitation.” (Coffey, ¶ 232.)

To the extent Dr. Coffey argues that the upper NiFe layer meets the limitation of a “(111) textured hexagonal atomic template disposed between said substrate and said bcc-d layer,” that argument is flawed and unreasonable, for example because it is nothing more than a conclusion with no data or analysis to support it.

To the extent Dr. Coffey argues that either of the FeCo layers meets the limitation of a “(111) textured hexagonal atomic template disposed between said substrate and said bcc-d layer,” that argument is flawed and unreasonable, for example because the FeCo layers are not (111) textured, and in any event cannot serve as atomic templates for themselves.

(a) “layer that is predominately (111) hexagonal”

261. In my opinion, none of the data Dr. Coffey cites shows a NiFe layer that is “predominately (111) hexagonal,” as required by the Court’s claim construction.

262. Dr. Coffey’s argument for the “(111) texture” of the NiFe is limited to a single paragraph in his report. Specifically, Dr. Coffey states in ¶ 228 of his report that:

I understand that multiple FFTs were taken at various locations along the interface between the NiFe layers and the FeCo layers of samples S0GPPC and S2MMMC. I further understand Dr. Clark was able to conclude that the lower fcc NiFe layer has a (111) texture and that it is evident that the lower NiFe layer is predominately or predominantly (111) fcc.

(Coffey, ¶ 228 (citing Clark, ¶¶ 87-105 (S0GPPC sample), ¶¶ 133-150 (S2MMMC sample)).)

263. I note that Dr. Coffey does not claim to have undertaken his own review of Dr. Clark’s FFT data, but instead relies entirely on Dr. Clark’s report for this claim limitation.

264. Because Dr. Coffey’s only support for the “(111) texture” limitation comes from Dr. Clark’s report, I now turn to ¶¶ 87-105 (S0GPPC) and ¶¶ 133-150 (S2MMMC) of Dr. Clark’s report. Dr. Clark’s only basis for arguing that the lower NiFe layer is “(111) textured” comes from a handful of FFT images. (*See, e.g.*, Clark, ¶¶ 87-105, ¶¶ 133-150.) In my opinion, none of Dr. Clark’s FFT data supports his opinion that the NiFe layer is “(111) textured.” If anything, Dr. Clark’s FFT data shows that the imaged NiFe layers are not “(111) textured.”

(i) Dr. Clark’s FFT data for S0GPPC does not show any (111) textured NiFe layer

265. Dr. Clark sets out his basis for concluding that the S0GPPC samples contain a (111) textured NiFe layer in ¶¶ 87-105. Dr. Clark took FFT measurements from high resolution cross-section images of both the lower and upper NiFe layers of the S0GPPC sample. Specifically, Dr. Clark discusses the lower NiFe layer from ¶¶ 87-95 and the upper NiFe layer from ¶¶ 96-105. As I explain below, beginning with the lower

NiFe layer, Dr. Clark has no basis for concluding that either NiFe layer of sample S0GPPC is “predominately (111) hexagonal.”

266. **S0GPPC: Lower NiFe Layer.** Figure 42 of Dr. Clark’s report purportedly shows “FFT’s from the [lower] NiFe layer and [lower] FeCo layer.” (Clark, Figure 42 (p. 51).) According to Dr. Clark, “the two FFT patterns” shown in Figure 42 are “sufficient to determine the relative orientation of the lower NiFe layer and the lower FeCo layer above it. Therefore, the lower NiFe layer exhibits (111) texture, and the lower FeCo layer exhibits (110) texture.” (Clark, ¶ 91.)

267. In my opinion, Dr. Clark’s analysis of Figure 42 is flawed and unreasonable for at least three reasons.

268. First, Dr. Clark’s analysis of Figure 42 is based on an erroneous premise—namely, that the FFTs correspond to the diffraction patterns shown below them. Dr. Clark’s analysis hinges on the notion that Figure 42’s NiFe FFT matches a $\{110\}_{\text{FCC}}$ diffraction pattern, while Figure 42’s FeCo FFT matches a $\{111\}_{\text{BCC}}$ diffraction pattern. (Clark, ¶¶ 89-90.) They do not.

269. I reproduce Figure 42 of Dr. Clark’s report below:

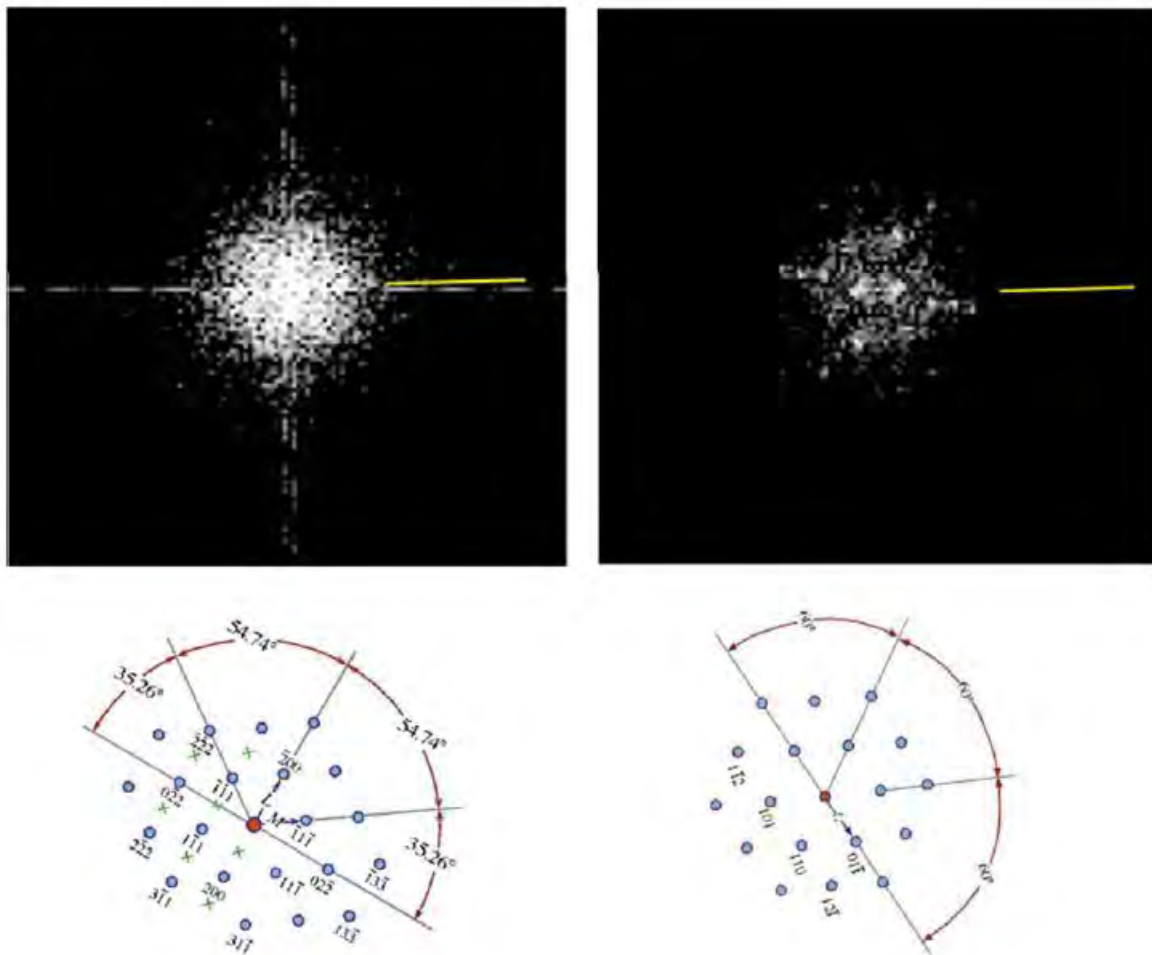


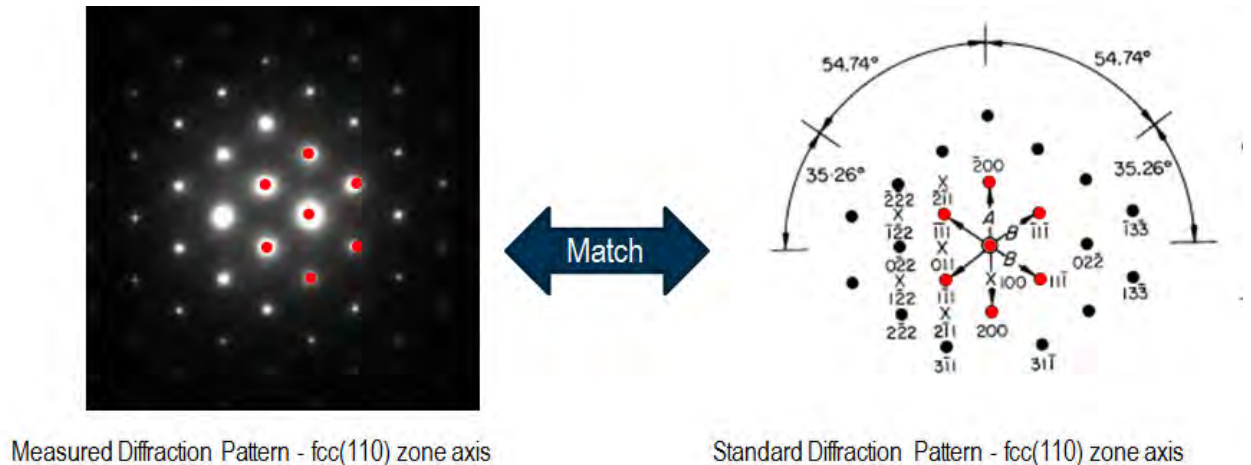
Figure 42: above: FFTs from the NiFe layer (left) and FeCo layer (right); below: standard diffraction patterns rotated into similar orientations as respective FFTs shown immediately above.

270. There is simply no basis for Dr. Clark's assertion that the NiFe FFT matches the $\{110\}_{\text{FCC}}$ diffraction pattern shown below it. Dr. Clark attempts to match the NiFe FFT to the $\{110\}_{\text{FCC}}$ diffraction pattern in order to argue that the NiFe layer contains one or more fcc crystals. (Clark, ¶ 89 ("[T]his FFT indicates that the crystal structure of the NiFe layer is FCC.")) But the NiFe FFT in Figure 42 clearly does not match the $\{110\}_{\text{FCC}}$ diffraction pattern needed for Dr. Clark to argue for the existence of fcc NiFe crystals. In other words, Dr. Clark's own FFT data does not show fcc crystals in the NiFe layer (let alone a predominance of fcc(111) crystals in that layer). For this

reason alone, Figure 42 does not support Dr. Clark's flawed and unreasonable conclusion that the lower NiFe layer is "predominately (111) hexagonal."

271. I note that Dr. Clark does not describe the methodology he used to compare the NiFe FFT to the $\{110\}_{\text{FCC}}$ diffraction pattern in Figure 42. For example, Dr. Clark does not attempt to identify the center diffraction peak, which is a critical step in this type of analysis (diffraction peak distances and angles are measured relative to the center diffraction peak). (*See, e.g.*, Stach, ¶ 77.) Nor does Dr. Clark attempt to overlay the $\{110\}_{\text{FCC}}$ diffraction pattern over the NiFe FFT—perhaps because doing so would make it even more clear that the NiFe FFT in no way matches any $\{110\}_{\text{FCC}}$ pattern.⁷ No reasonable scientist would agree with Dr. Clark's analysis of Figure 42, or the conclusions he draws from that flawed and unreasonable analysis.

272. To further highlight the contrast between the NiFe FFT and the $\{110\}_{\text{FCC}}$ diffraction pattern in Figure 42, shown below is an example of an empirical diffraction measurement that *actually* corresponds to a $\{110\}_{\text{FCC}}$ diffraction pattern:



⁷ I also disagree with Dr. Clark's assertion that the FeCo FFT matches a $\{111\}_{\text{BCC}}$ pattern. Attempting to overlay the $\{111\}_{\text{BCC}}$ pattern over the FeCo FFT produces a substantial mismatch.

273. The NiFe FFT in Figure 42 looks nothing like the example shown above. If anything, the NiFe FFT most closely resembles the diffraction pattern for an *amorphous* material—*i.e.*, a material with no crystal structure (and thus, no predominate crystallographic orientation).

274. I note it is not surprising that the NiFe FFT data in Figure 42 does not match any $\{110\}_{\text{FCC}}$ diffraction pattern given the thinness of the NiFe layer. [REDACTED]

[REDACTED] (See, e.g., '416 Patent at 11:6-9 (“The wetting layer 18 can be an amorphous material or a film too thin to have developed a crystalline texture, or a film whose texture provides a gross lattice mismatch for the ensuing layer.”); Patent Owner’s Preliminary Response to IPR2016-00013, at 42 (“One common feature in deposition of ultrathin films is that in many cases pseudomorphic growth occurs over several monolayers before the film converts into its usual crystal structure.”); *id.* at 43 (“In other words, an epitaxially grown ultrathin film will commonly have a pseudomorphic or metastable non-equilibrium crystalline structure for the first several monolayers. Such crystalline structures will not have formed into stable fcc or bcc structures. . . . Dr. Sinclair chose to ignore the fact that the layers at issue are ultrathin and therefore could not have formed equilibrium crystalline structures.”); *id.* at 43-44 (distinguishing prior art: “Dill never described the crystalline structure of the interface layer . . . but the thickness of that interface layer (*i.e.*, 0.4-2 nm) indicates that it was pseudomorphic fcc and could not have been in equilibrium crystalline phase.”); D. Lambeth et al., *Magnetic Media Performance: Control Methods for Crystalline Texture and Orientation*, Mat. Res. Soc. Symp. Proc. Vol. 517, p. 185 (1998) (“However, below 5 nm the Cr is so thin that little or no crystalline texture has evolved . . .”); M. Ohring, MATERIALS SCIENCE OF THIN FILMS 529, 562 (“Sometimes, texture evolves from random in initial deposits to strong orientation of low-energy planes parallel to the film surface, and finally, to changes in preferred texture as the film thickens further.”).)

275. In addition to Figure 42, Dr. Clark claims to have analyzed additional FFTs measured along other portions of the lower NiFe layer, apparently concluding that those additional FFTs match a $\{110\}_{\text{FCC}}$ diffraction pattern. (Clark, ¶ 94 (“Similar

analysis was performed on FFTs taken at [other points in the lower NiFe layer] and each showed similar results as described above [A]nnotated cross sections and their accompanying FFTs are also shown in Appendix C and also showed similar results as those described above, further confirming the orientational relationships and textures as described above.”.) They do not.

276. I note that Dr. Clark does not depict—let alone analyze—any of these additional FFTs in his report. Nevertheless, I have studied these additional FFTs of the lower NiFe layer, and I conclude that, like the NiFe FFT in Figure 42, none remotely match the $\{110\}_{\text{FCC}}$ diffraction pattern. I note that Dr. Stach has compiled an exhibit showing the extent of the mismatches between these FFTs and the standard diffraction patterns ($\{110\}_{\text{FCC}}$ and $\{112\}_{\text{FCC}}$). I have closely reviewed Dr. Stach’s exhibit, which I also include as Ex. D to this report, and I agree with Dr. Stach that because none of these additional FFTs match either the $\{110\}_{\text{FCC}}$ or the $\{112\}_{\text{FCC}}$ pattern, none of these additional FFTs depict any fcc NiFe crystals.

277. I note that Dr. Clark later appears to hedge by acknowledging that the NiFe FFTs of the lower NiFe layer do not match any $\{110\}_{\text{FCC}}$ diffraction pattern. Specifically, Dr. Clark asserts that “[t]o the extent that the FFT results for the lower NiFe layer are inconclusive, I conclude that the lower NiFe layer is FCC and exhibits a predominant (111) texture based further on the discussion of the upper NiFe / FeCo layers below.” (Clark, ¶ 95.) In my opinion, this argument is flawed and unreasonable because it purports to draw conclusions about the texture of the *lower* NiFe layer based on measurements of the *upper* NiFe layer—even though the lower and upper NiFe layer measurements do not match. (*Compare* Clark Figure 42, *with* Clark Figure 44.) Moreover, Dr. Clark’s analysis of the upper NiFe layer is also flawed and unreasonable for many of the same reasons. (*See* ¶¶ 290-313, *infra*.)

278. Second, Dr. Clark’s analysis of Figure 42 is further flawed and unreasonable because even assuming Dr. Clark’s NiFe FFT data actually matched the $\{110\}_{\text{FCC}}$ diffraction pattern (they clearly do not), merely matching a $\{110\}_{\text{FCC}}$ diffraction pattern is evidence of an fcc crystal in the NiFe layer—it is *not* evidence of a (111) crystal, and certainly not evidence of a predominance of fcc(111) crystals.

279. As I explained in the Technology Background, *crystal structure* (e.g., fcc, bcc) is a property distinct from *crystal orientation* (e.g., (111), (110)). (See Section V.A, *supra*.) Crystal structure refers to how the atoms are arranged in a unit cell, with an fcc crystal being a crystal whose atoms are arranged on the faces of a cubic unit cell. Crystal orientation refers to how a crystal is oriented relative to the substrate, with a (111) crystal being a crystal whose (111) plane is oriented parallel to the substrate. An fcc(111) crystal therefore describes (1) an fcc crystal (2) whose (111) plane is oriented parallel to the substrate. (See, e.g., Section V.A.2, *supra* (depicting both (111) and non-(111) fcc crystals).)

280. Even if Dr. Clark's NiFe FFTs matched a $\{110\}_{\text{FCC}}$ diffraction pattern (and they clearly do not), this would only be evidence of one or more fcc crystals in the NiFe layer. In order to properly conclude that any of these fcc crystals are fcc(111) crystals, the NiFe FFTs *must* not only (1) match the $\{110\}_{\text{FCC}}$ diffraction pattern *but also* (2) match the $\{110\}_{\text{FCC}}$ pattern such that the $\langle 111 \rangle_{\text{FCC}}$ direction is perpendicular to the substrate (a.k.a. the layer interface).

281. Dr. Clark acknowledges this requirement and simply asserts it—even though the NiFe FFT data of Figure 42 plainly contradicts him. In particular, Dr. Clark asserts that “when analyzing the pattern from the spot spacing and distribution, it can be seen that a $\langle 111 \rangle_{\text{FCC}}$ direction”—shown by the yellow line in Figure 42's NiFe FFT— “[is] also perpendicular to the lower NiFe/lower FeCo interface. . . . These mutual relationships are sufficient to determine the relative orientation of the lower NiFe layer and the lower FeCo layer above it. Therefore, the lower NiFe layer exhibits (111) texture” (Clark, ¶ 91.)

282. Dr. Clark's assertion that the yellow line in Figure 42's NiFe FFT—the $\langle 111 \rangle_{\text{FCC}}$ direction—is “perpendicular to the lower NiFe/lower FeCo interface” is contradicted by his own data. The $\langle 111 \rangle_{\text{FCC}}$ direction Dr. Clark draws in Figure 42 is not perpendicular to the interface shown in Figure 41, as demonstrated by the image below:

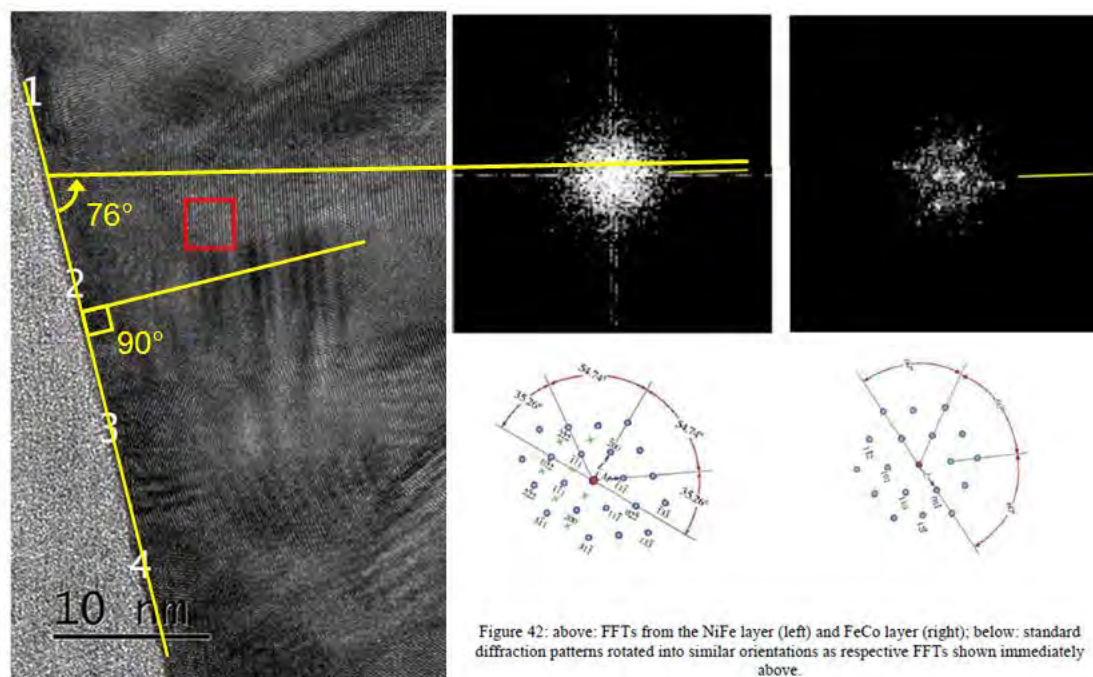


Figure 41: Example high resolution cross-section from region A. The numbered points indicate where FFTs were taken.

283. This comparison belies Dr. Clark’s claim that the $\langle 111 \rangle_{\text{FCC}}$ direction is “perpendicular to the lower NiFe/lower FeCo interface.” (Clark, ¶ 91.) The $\langle 111 \rangle_{\text{FCC}}$ direction is not perpendicular to the interface—as required of an fcc(111) crystal—but is instead about 76 degrees relative to the interface. Dr. Clark is wrong to assert in ¶ 91 that the $\langle 111 \rangle_{\text{FCC}}$ direction is perpendicular to the interface.

284. In sum, Dr. Clark’s NiFe FFT data does not match the $\{110\}_{\text{FCC}}$ diffraction pattern. But even assuming the NiFe FFT data matched the $\{110\}_{\text{FCC}}$ pattern as Dr. Clark claims, that match is inconsistent with a (111) crystal. The $\langle 111 \rangle_{\text{FCC}}$ direction is not perpendicular to the interface; Dr. Clark’s assertion that it is perpendicular contradicts the actual data. Dr. Clark’s analysis of Figure 42, and his conclusion that the FFT data somehow shows a (111) crystal (let alone a predominance of (111) crystals) in the lower NiFe layer, is therefore flawed and unreasonable for this reason as well.

285. Third, Dr. Clark’s analysis of Figure 42 and other FFT data is further flawed and unreasonable because, even if any of his FFT data actually matched a $\{110\}_{\text{FCC}}$ pattern with its $\langle 111 \rangle_{\text{FCC}}$ direction perpendicular to the NiFe/FeCo interface

(which is not remotely the case), such limited FFT data does not reasonably allow Dr. Clark to draw broad conclusions about the predominant crystal orientation (*i.e.*, texture) of the NiFe layer.

286. Dr. Clark's attempt to argue (111) texture based on a handful of FFT images (Clark, ¶ 92) is flawed and unreasonable because Dr. Clark's FFT data corresponds to a tiny fraction—only 1.1%—of the overall NiFe layer. Accordingly, there is no scientific basis for Dr. Clark to assert that the NiFe layer has any “predominate” crystal orientation (let alone a predominately (111) crystal orientation) after having measured only 1.1% of the overall layer. Such a conclusion is akin to a person concluding that a beach predominately comprises grains of black sand based on the fact that a single sample grain from that beach was found to be black.

287. In my opinion, it is scientifically unreasonable to conclude that a layer has any predominate crystal orientation based on a handful of select FFT measurements that correspond to only 1.1% of the total layer. I am not aware of any scientific publication in which the authors inferred a layer's predominant crystal orientation based on such a limited number of FFT measurements. In my opinion, no reasonable scientist would conclude anything about a layer's predominant crystal orientation based on a handful of FFT measurements spanning only 1.1% of the layer.

288. In sum, Dr. Clark argues that the lower NiFe layer is “(111) textured” based on a handful of FFT measurements of that layer. Because those FFT measurements do not match any $\{110\}_{\text{FCC}}$ diffraction pattern, do not feature any $\langle 111 \rangle_{\text{FCC}}$ direction perpendicular to the NiFe/FeCo interface, and comprise only 1.1% of the entire lower NiFe layer, those FFT measurements do not support Dr. Clark's conclusion that the lower NiFe layer features a “(111) texture.” If anything, Dr. Clark's FFT data contradicts, rather than supports, his claim that the lower NiFe layer is “predominately (111) hexagonal.”

289. For all these reasons, it is my opinion that Dr. Clark's FFT data completely fails to show that the lower NiFe layer of the [REDACTED] write heads is “predominately (111) hexagonal.”

290. **S0GPPC: Upper NiFe Layer.** Dr. Clark next proceeds to discuss FFT measurements purportedly done on the upper NiFe layer. Figure 44 purportedly shows “FFTs” from “(a) the upper FeCo layer,” “(b) in the upper NiFe layer,” and “(c) the lower FeCo layer.” (Clark, Figure 44 (p. 55).) According to Dr. Clark, Figure 44 “shows that the upper NiFe layer has a predominant (111) texture, and the upper FeCo layer has a predominant (110) texture.” (Clark, ¶ 100.)

291. In my opinion, Dr. Clark’s analysis of Figure 44 is flawed and unreasonable for at least three reasons (similar to how his analysis of Figure 42 was flawed and unreasonable).

292. First, Dr. Clark’s analysis of Figure 44 is based on an erroneous premise—namely, that the FFTs correspond to the diffraction patterns shown below them. Dr. Clark’s analysis hinges on the notion that Figure 44’s NiFe FFT matches a $\{110\}_{\text{FCC}}$ diffraction pattern, which it does not. (Clark, ¶ 98 (“the upper NiFe pattern is identified as $\{110\}_{\text{FCC}}$ ”).) I reproduce Figure 44 of Dr. Clark’s report below:

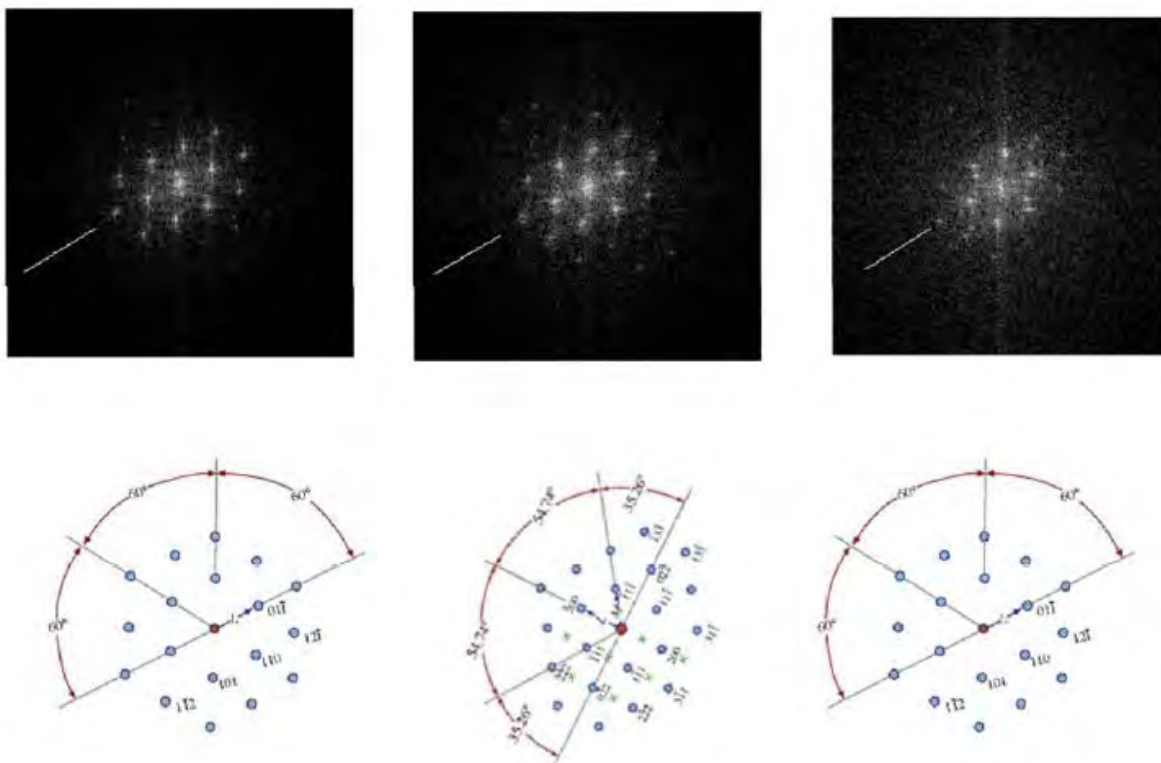


Figure 44: above: FFTs from: (a) the upper FeCo layer to the left of the upper NiFe layer (left); (b) in the upper NiFe layer (center); (c) the lower FeCo layer to the right of the NiFe layer (right); below: standard diffraction patterns rotated into similar orientations as respective FFTs shown immediately above.

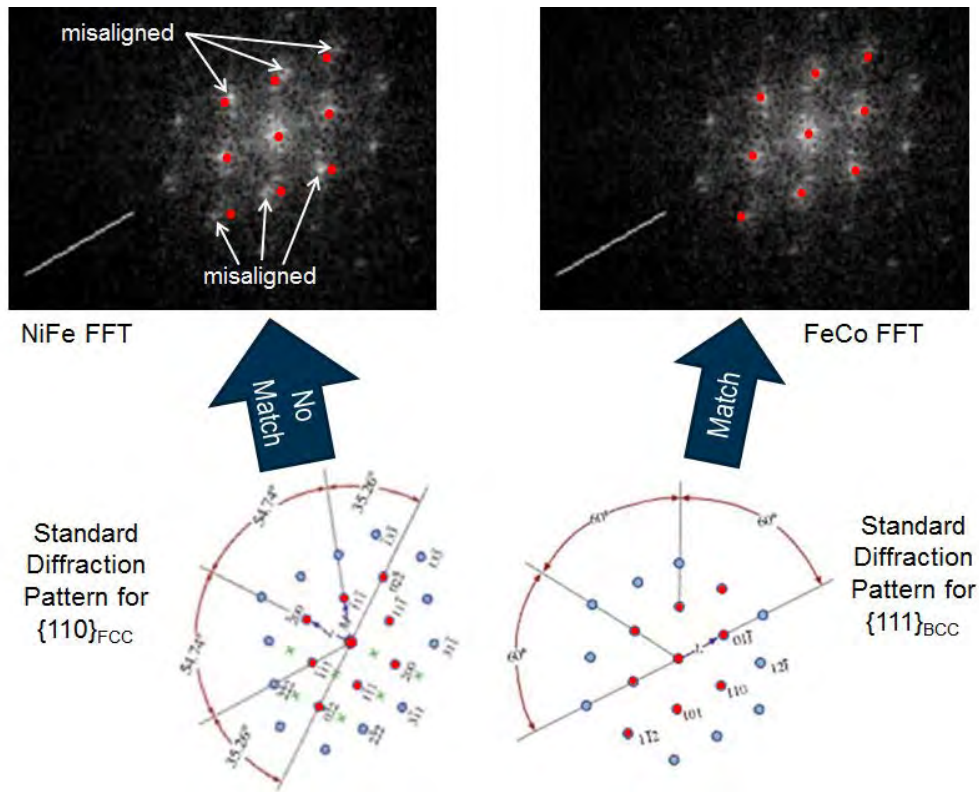
293. There is simply no basis for Dr. Clark’s assertion that the purported NiFe FFT matches the $\{110\}_{\text{FCC}}$ diffraction pattern shown below it. Dr. Clark attempts to match the NiFe FFT to the $\{110\}_{\text{FCC}}$ diffraction pattern in order to argue that the NiFe layer contains one or more fcc crystals. (Clark, ¶ 98.) But the NiFe FFT in Figure 44 clearly does not match the $\{110\}_{\text{FCC}}$ diffraction pattern needed for Dr. Clark to argue the existence of fcc NiFe crystals. In other words, Dr. Clark’s own FFT data does not show fcc crystals in the NiFe layer (let alone a predominance of fcc(111) crystals in that layer). For this reason alone, Figure 44 does not support Dr. Clark’s flawed and unreasonable conclusion that the upper NiFe layer is “predominately (111) hexagonal.”

294. I note that Dr. Clark does not describe the methodology he used to compare the NiFe FFT to the $\{110\}_{\text{FCC}}$ diffraction pattern in Figure 44. For example,

Dr. Clark does not attempt to identify the center diffraction peak, which is a critical step in this type of analysis (diffraction peak distances and angles are all measured relative to the center diffraction peak). (See, e.g., Stach, ¶ 77.) Nor does Dr. Clark attempt to overlay the $\{110\}_{\text{FCC}}$ diffraction pattern over the NiFe FFT—perhaps because doing so would make it even more clear that the NiFe FFT in no way matches the $\{110\}_{\text{FCC}}$ pattern. No reasonable scientist would agree with Dr. Clark’s analysis of Figure 44, or the conclusions he draws from that flawed and unreasonable analysis.

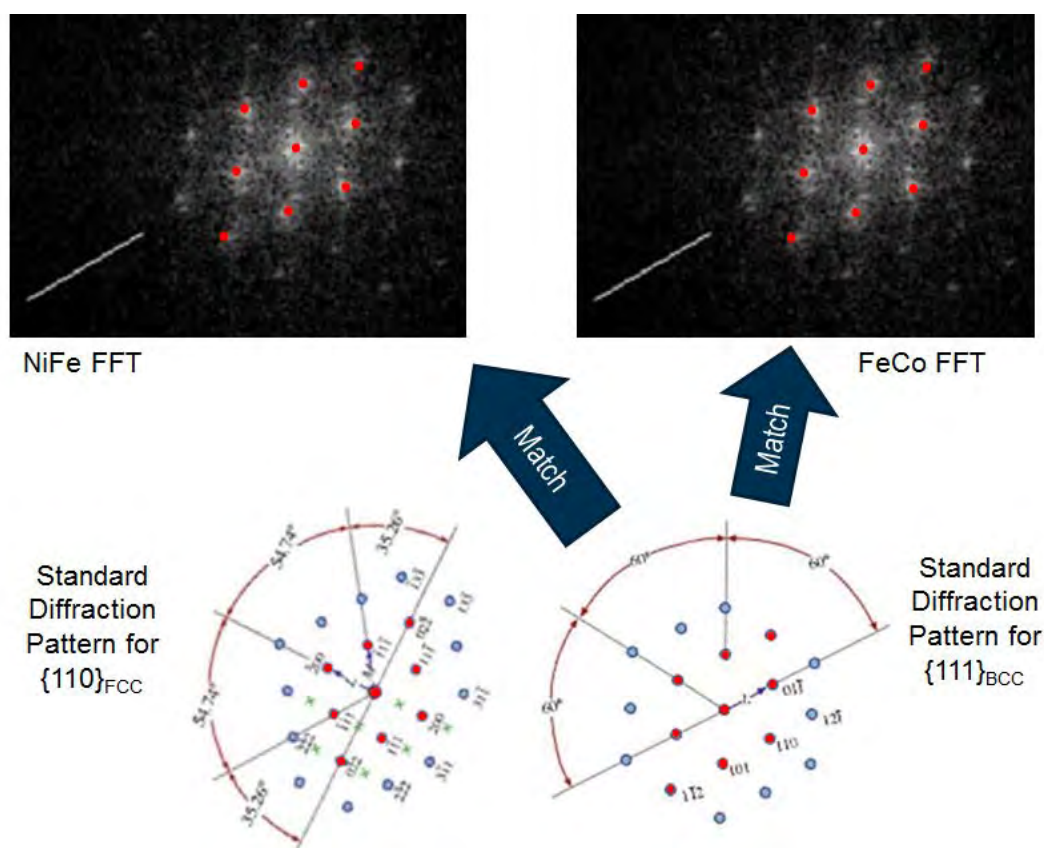
295. When one properly analyzes the NiFe FFT in Figure 44, one readily sees that the NiFe FFT in fact matches the $\{111\}_{\text{BCC}}$ diffraction pattern—not the $\{110\}_{\text{FCC}}$ diffraction as Dr. Clark claims.

296. Below is a modified version of Dr. Clark’s Figure 44 that illustrates how the NiFe FFT actually matches the $\{111\}_{\text{BCC}}$ diffraction pattern rather than the $\{110\}_{\text{FCC}}$ diffraction pattern. The image below depicts an attempt to match the $\{110\}_{\text{FCC}}$ diffraction pattern to the NiFe, and the $\{111\}_{\text{BCC}}$ diffraction pattern to the FeCo:

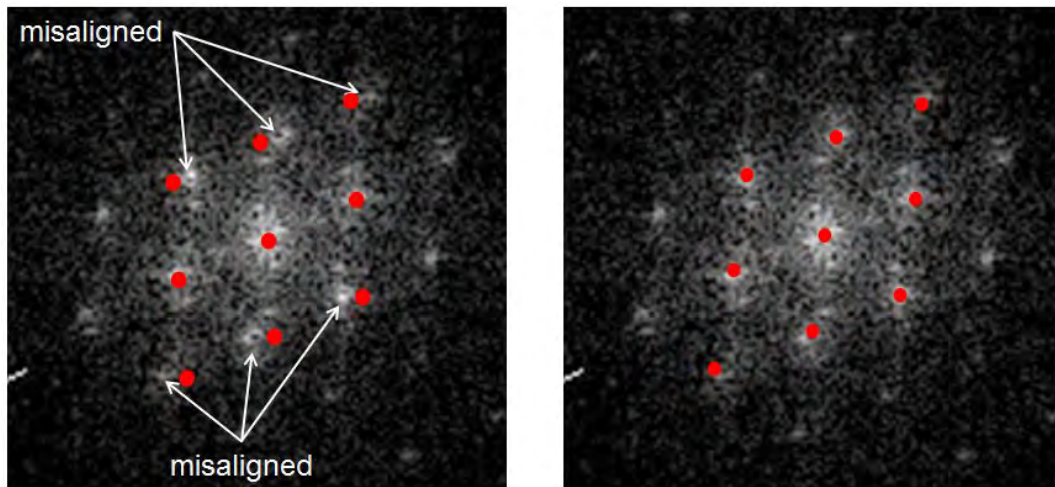


297. Based on the image above, I conclude that FeCo FFT matches the $\{111\}_{\text{BCC}}$ diffraction pattern. I conclude that the NiFe FFT does *not* match the $\{110\}_{\text{FCC}}$ diffraction pattern.

298. I further conclude that the $\{111\}_{\text{BCC}}$ pattern not only matches the FeCo FFT, the $\{111\}_{\text{BCC}}$ pattern also matches the NiFe FFT. The image below shows that the NiFe FFT matches the $\{111\}_{\text{BCC}}$ pattern:



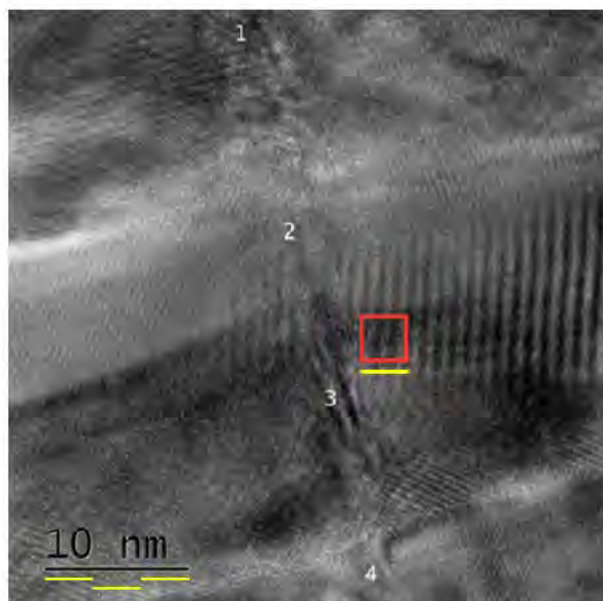
299. To further illustrate the extent of the mismatch between the NiFe FFT and the $\{110\}_{\text{FCC}}$ pattern, the image below shows two zoomed-in views of the NiFe FFT from Figure 44. The NiFe FFT on the left is overlaid with the $\{110\}_{\text{FCC}}$ pattern, showing substantial misalignment with that pattern. The NiFe FFT on the right is overlaid with the $\{111\}_{\text{BCC}}$ pattern, showing a match with no misalignment.



(Left: NiFe FFT misaligned with $\{110\}_{\text{FCC}}$. Right: NiFe FFT aligned with $\{111\}_{\text{BCC}}$.)

300. As is evident from these comparisons, Dr. Clark's claim that the NiFe FFT matches a $\{110\}_{\text{FCC}}$ pattern is unreasonable and incorrect, as a proper analysis shows a $\{111\}_{\text{BCC}}$ pattern instead. Such a $\{111\}_{\text{BCC}}$ pattern is evidence of a bcc crystal—not an fcc crystal—and therefore undermines Dr. Clark's assertion that the upper NiFe layer is "predominately (111) hexagonal."

301. Once again, I note it is not surprising that the NiFe FFT data in Figure 44 does not match any $\{110\}_{\text{FCC}}$ diffraction pattern given the thinness of the NiFe layer. The upper NiFe layer is only 1.5nm thick, whereas the size of Dr. Clark's FFT inputs (indicated by the red square below) is over 3nm x 3nm (indicated by the yellow lines drawn in to compare the size of the red square to the scale in the lower left):



302. Because the [REDACTED]—Dr. Clark appears to have been unable to isolate the upper NiFe layer from the FeCo layers above and below it for purposes of his FFT measurements. In other words, although Dr. Clark purports to have taken FFT measurements of the NiFe layer, [REDACTED]

This would explain why all three FFTs in Figure 44 match the $\{111\}_{\text{BCC}}$ pattern (not to mention each other)—they are likely all measurements of bcc FeCo crystals. There is no evidence of any crystal structure or orientation associated with the NiFe, which is too thin to have developed any predominate crystal structure or orientation.

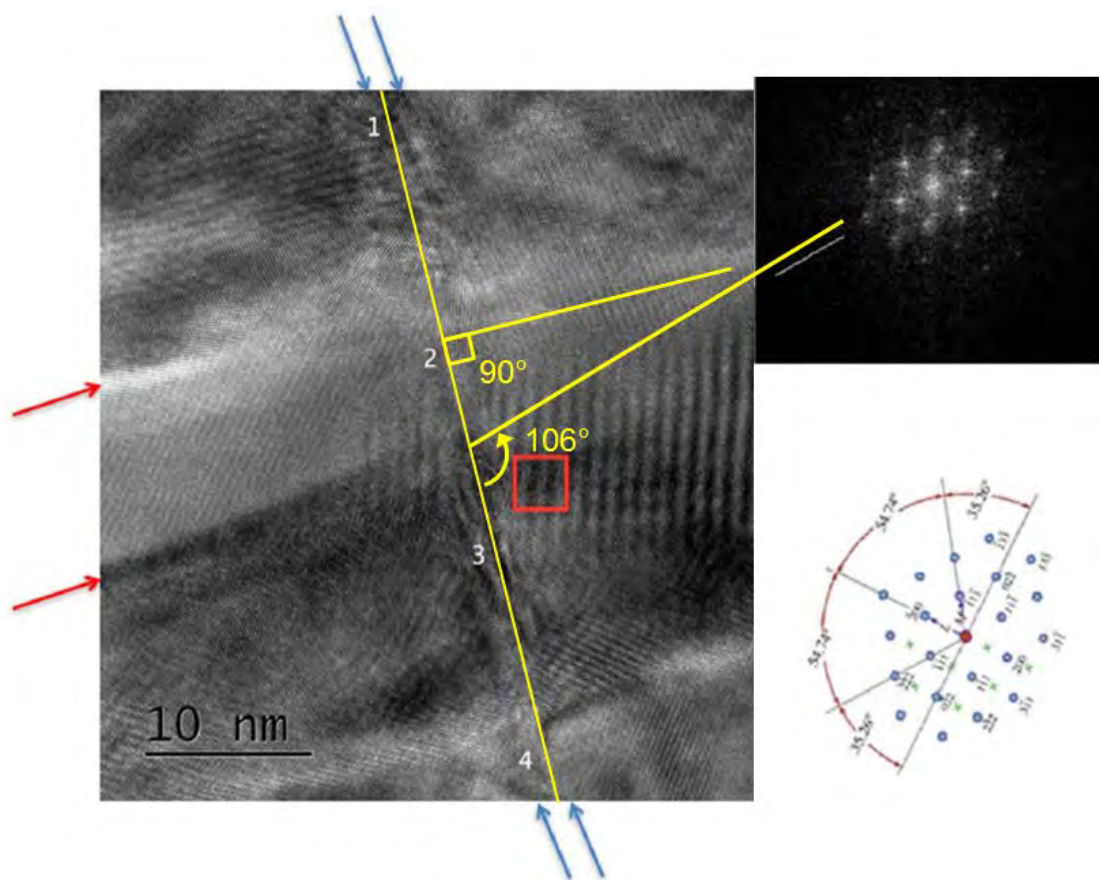
303. In addition to Figure 44, Dr. Clark claims to have analyzed additional FFTs purportedly measured along other portions of the upper NiFe layer, apparently concluding that those additional FFTs match a $\{110\}_{\text{FCC}}$ diffraction pattern. (Clark, ¶ 104 (“[S]imilar analysis was performed on FFTs taken at [other points in the upper NiFe layer] and each showed similar results as those described above . . . [A]nnotated cross sections and their accompanying FFTs are also shown in Appendix C and also showed similar results as those described above, further confirming the orientational relationships and textures as described above.”).) They do not.

304. I note that Dr. Clark does not depict—let alone analyze—any of these additional FFTs in his report. Nevertheless, I have studied these additional FFTs of the lower NiFe layer, and I conclude that, like the NiFe FFT in Figure 44, none remotely matches the $\{110\}_{\text{FCC}}$ diffraction pattern (or the $\{112\}_{\text{FCC}}$ diffraction pattern). Again, Dr. Stach has compiled an exhibit showing the extent of the mismatches between these FFTs and the standard diffraction patterns ($\{110\}_{\text{FCC}}$ and $\{112\}_{\text{FCC}}$). (See Ex. D.) I have closely reviewed Ex. D, and I agree with Dr. Stach that because none of these additional FFTs match either the $\{110\}_{\text{FCC}}$ or the $\{112\}_{\text{FCC}}$ pattern, none of these additional FFTs depict any fcc NiFe crystals.

305. Second, Dr. Clark’s analysis of Figure 44 is further flawed and unreasonable because even if Dr. Clark’s NiFe FFTs matched the $\{110\}_{\text{FCC}}$ diffraction pattern (they clearly do not), this would only be evidence of one or more fcc crystals in the NiFe layer. In order to properly conclude that any of these fcc crystals are fcc(111) crystals, the NiFe FFTs *must* not only (1) match the $\{110\}_{\text{FCC}}$ diffraction pattern *but also* (2) match the $\{110\}_{\text{FCC}}$ pattern such that the $\langle 111 \rangle_{\text{FCC}}$ direction is perpendicular to the substrate (a.k.a. the layer interface).

306. Dr. Clark acknowledges this requirement and simply asserts it—even though the purported NiFe FFT data of Figure 44 plainly contradicts him. In particular, Dr. Clark asserts that “the parallel directions in the FCC and BCC layers *normal to the interface* show repeatedly $\langle 110 \rangle$ direction in the BCC layers and $\langle 111 \rangle$ direction in the FCC layers. Therefore, this analysis shows that the upper NiFe layer has a predominant (111) texture” (Clark, ¶ 100; see also *id.* at ¶ 101 (incorrectly claiming that the $\langle 111 \rangle_{\text{FCC}}$ direction is “perpendicular to the upper NiFe/FeCo interfaces”).)

307. Dr. Clark’s assertion that the yellow line in Figure 44’s purported NiFe FFT—the $\langle 111 \rangle_{\text{FCC}}$ direction—is “perpendicular to the upper NiFe/FeCo interfaces” is plainly contradicted by his own data. The $\langle 111 \rangle_{\text{FCC}}$ direction Dr. Clark draws in Figure 44 is not perpendicular to the NiFe/FeCo interface shown in Figure 43, as demonstrated by the image below:



308. This comparison belies Dr. Clark's claim that the $\langle 111 \rangle_{\text{FCC}}$ direction is "perpendicular to the upper NiFe/FeCo interface." (Clark, ¶ 101.) The $\langle 111 \rangle_{\text{FCC}}$ direction is not perpendicular to the interface—as required of an fcc(111) crystal—but is instead about 106 degrees relative to the interface. Dr. Clark is simply wrong to assert in ¶¶ 100-101 that the $\langle 111 \rangle_{\text{FCC}}$ direction is perpendicular to the interface.

309. In sum, Dr. Clark's NiFe FFT data does not match any $\{110\}_{\text{FCC}}$ diffraction pattern. But even assuming the NiFe FFT data matched the $\{110\}_{\text{FCC}}$ pattern as Dr. Clark claims, that match is inconsistent with a (111) crystal. The $\langle 111 \rangle_{\text{FCC}}$ direction is not perpendicular to the interface; Dr. Clark's assertion that it is perpendicular contradicts the actual data. Dr. Clark's analysis of Figure 44, and his conclusion that the FFT data somehow shows a (111) crystal (let alone a predominance of (111) crystals) in the upper NiFe layer, is therefore flawed and unreasonable for this reason as well.

310. Third, Dr. Clark's analysis of Figure 44 and other FFT data is further flawed and unreasonable because, even if any of his FFT data actually matched a $\{110\}_{\text{FCC}}$ pattern with its $\langle 111 \rangle_{\text{FCC}}$ direction perpendicular to the NiFe/FeCo interface (which is not remotely the case), such limited FFT data does not reasonably allow Dr. Clark to draw broad conclusions about the predominant crystal orientation (*i.e.*, texture) of the NiFe layer.

311. Dr. Clark's attempt to argue (111) texture based on a handful of FFT images (Clark, ¶¶ 100-101) is flawed and unreasonable because Dr. Clark's FFT data corresponds to a tiny fraction—less than 1%—of the overall NiFe layer. Accordingly, there is no scientific basis for Dr. Clark to assert that the NiFe layer has any “predominate” crystal orientation (let alone a predominately (111) crystal orientation) after having measured less than 1% of the overall layer. Such a conclusion is akin to a person concluding that a beach predominately comprises grains of black sand based on the fact that a single sample grain from that beach was found to be black.

312. In my opinion, it is scientifically unreasonable to conclude that a layer has any predominate crystal orientation based on a handful of select FFT measurements that correspond to less than 1% of the total layer. I am not aware of any scientific publication in which the authors inferred a layer's predominant crystal orientation based on such a limited number of FFT measurements. In my opinion, no reasonable scientist would conclude anything about a layer's predominant crystal orientation based on a handful of FFT measurements spanning less than 1% of the layer.

313. In sum, Dr. Clark argues that the upper NiFe layer is “(111) textured” based on a handful of FFT measurements of that layer. Because those FFT measurements do not match any $\{110\}_{\text{FCC}}$ diffraction pattern, do not feature any $\langle 111 \rangle_{\text{FCC}}$ direction perpendicular to the NiFe/FeCo interface, and comprise less than 1% of the entire upper NiFe layer, those FFT measurements do not support Dr. Clark's conclusion that the upper NiFe layer features a “(111) texture.” If anything, Dr. Clark's FFT data contradicts, rather than supports, his claim that the upper NiFe layer is “predominately (111) hexagonal.”

314. For all these reasons, it is my opinion that Dr. Clark's FFT data completely fails to show that the upper NiFe layer of the [REDACTED] write heads is "predominately (111) hexagonal."

(ii) Dr. Clark's FFT data for S2MMMC does not show a (111) textured NiFe layer

315. **S2MMMC: Lower NiFe Layer.** Figure 72 of Dr. Clark's report purportedly shows "FFTs from the [lower] NiFe layer [] and [lower] FeCo layer." (Clark, p. 85.) According to Dr. Clark, "the two FFT patterns" shown in Figure 72 are "sufficient to determine the relative orientation of the lower NiFe layer and the lower FeCo layer above it. Therefore, the lower NiFe layer exhibits (111) texture, and the lower FeCo layer exhibits (110) texture." (Clark, ¶ 137.)

316. In my opinion, Dr. Clark's analysis of Figure 72 is flawed and unreasonable for at least three reasons.

317. First, Dr. Clark's analysis of Figure 72 is based on an erroneous premise—namely, that the FFTs correspond to standard diffraction patterns. Dr. Clark's analysis hinges on the notion that Figure 72's NiFe FFT matches the $\{110\}_{\text{FCC}}$ diffraction pattern. (Clark, ¶ 136.) It does not.

318. I reproduce Figure 72 of Dr. Clark's report below:

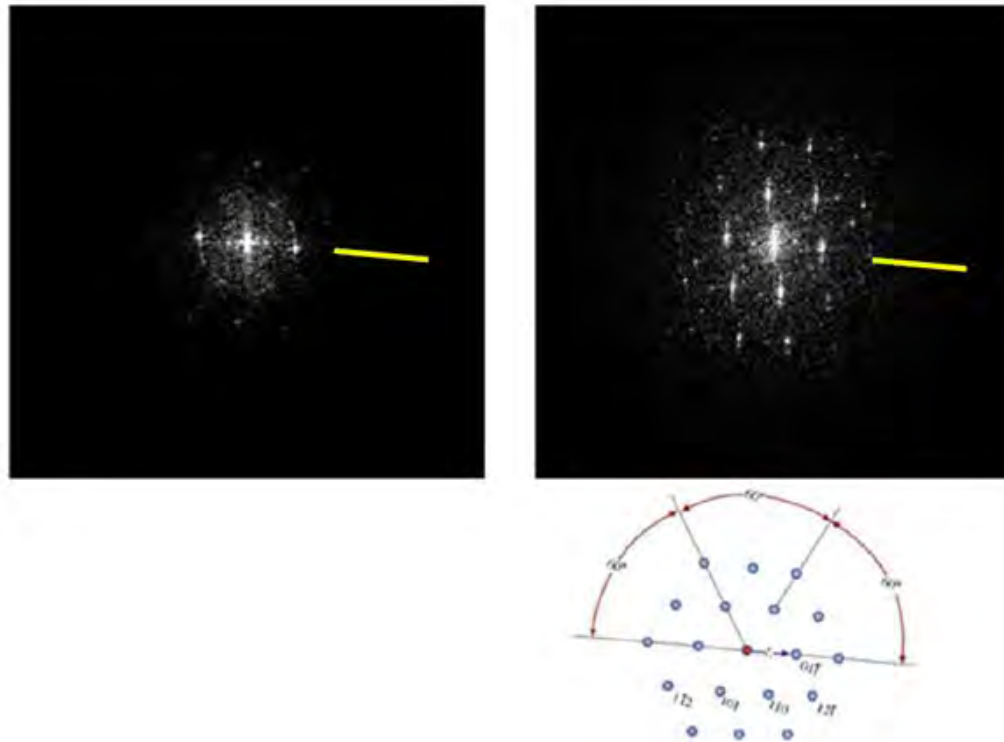


Figure 72: above: FFTs from the NiFe layer (left) and FeCo layer (right) – note that the NiFe pattern is indistinct; below: standard diffraction patterns rotated into similar orientations as respective FFTs shown immediately above.

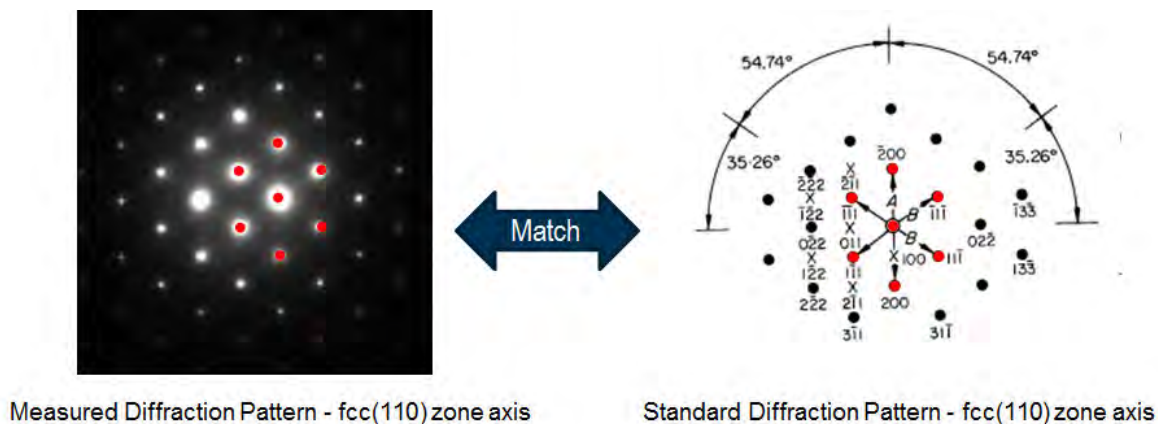
319. I note at the outset that (unlike Figures 42 and 44) Figure 72 does not even show the $\{110\}_{\text{FCC}}$ diffraction pattern underneath the NiFe FFT. Nevertheless, Dr. Clark argues that “[a]lthough the left hand FFT from the NiFe template is not distinct enough to analyze with certainty, the arrangement of the faint diffraction spots that are visible most closely resemble the $\{110\}_{\text{FCC}}$ pattern.” (Clark, ¶ 136.)

320. There is simply no basis for Dr. Clark’s assertion that the NiFe FFT resembles the $\{110\}_{\text{FCC}}$ diffraction pattern. Dr. Clark asserts the NiFe FFT resembles the $\{110\}_{\text{FCC}}$ diffraction pattern in order to argue that the NiFe layer contains one or more fcc crystals. (Clark, ¶¶ 136, 138.) But the NiFe FFT in Figure 72 clearly does not match the $\{110\}_{\text{FCC}}$ diffraction pattern needed for Dr. Clark to argue for the existence of fcc NiFe crystals. In other words, Dr. Clark’s own FFT data does not show fcc crystals in the NiFe layer (let alone a predominance of fcc(111) crystals in that layer). For this

reason alone, Figure 72 does not support Dr. Clark's flawed and unreasonable conclusion that the lower NiFe layer is "predominately (111) hexagonal."

321. I note that Dr. Clark does not describe the methodology he used to compare the NiFe FFT to the $\{110\}_{\text{FCC}}$ diffraction pattern in Figure 72, other than to claim in conclusory fashion that "the arrangement of the faint diffraction spots that are visible most closely resemble the $\{110\}_{\text{FCC}}$ pattern." (Clark, ¶ 136.) For example, Dr. Clark does not attempt to identify the center diffraction peak, which is a critical step in this type of analysis (diffraction peak distances and angles are all measured relative to the center diffraction peak). Nor does Dr. Clark attempt to overlay the $\{110\}_{\text{FCC}}$ diffraction pattern over the NiFe FFT—perhaps because doing so would make it even more clear that the NiFe FFT in no way matches any $\{110\}_{\text{FCC}}$ pattern. No reasonable scientist would agree with Dr. Clark's analysis of Figure 72, or the conclusions he draws from that flawed and unreasonable analysis.

322. To further highlight the contrast between the NiFe FFT and the $\{110\}_{\text{FCC}}$ diffraction pattern in Figure 72, shown below is an example of an empirical diffraction measurement that *actually* corresponds to a $\{110\}_{\text{FCC}}$ diffraction pattern:



323. The NiFe FFT in Figure 72 looks nothing like the example shown above.

324. I note it is not surprising that the NiFe FFT data in Figure 72 does not match any $\{110\}_{\text{FCC}}$ diffraction pattern given the thinness of the NiFe layer. [REDACTED]

[REDACTED]

[REDACTED]

325. In addition to Figure 72, Dr. Clark claims to have analyzed additional FFTs measured along other portions of the lower NiFe layer, apparently concluding that those additional FFTs match a $\{110\}_{\text{FCC}}$ diffraction pattern. (Clark, ¶ 140 (“Similar analysis was performed on FFTs taken at [other points in the lower NiFe layer] and each showed similar results as described above [A]nnotated cross sections and their accompanying FFTs are also shown in Appendix C and also showed similar results as those described above, further confirming the orientational relationships and textures as described above.”).) They do not.

326. I note that Dr. Clark does not depict—let alone analyze—any of these additional FFTs in his report. Nevertheless, I have studied these additional FFTs of the lower NiFe layer, and I conclude that, like the NiFe FFT in Figure 72, none remotely match the $\{110\}_{\text{FCC}}$ diffraction pattern (or the $\{112\}_{\text{FCC}}$ diffraction pattern). Again, Dr. Stach has compiled an exhibit showing the extent of the mismatch between these FFTs and the standard diffraction patterns ($\{110\}_{\text{FCC}}$ and $\{112\}_{\text{FCC}}$). (*See* Ex. D.) I have closely reviewed Ex. D, and I agree with Dr. Stach that because none of these additional FFTs match either the $\{110\}_{\text{FCC}}$ or the $\{112\}_{\text{FCC}}$ pattern, none of these additional FFTs depict any fcc NiFe crystals.

327. I note that Dr. Clark later appears to hedge by acknowledging that the NiFe FFTs of the lower NiFe layer do not match any $\{110\}_{\text{FCC}}$ diffraction pattern. Specifically, Dr. Clark admits that “the NiFe template is not distinct enough to analyze with certainty,” but he nevertheless argues that “[g]iven the evidence for the $\{110\}$ orientation in the NiFe layer in the mid-region of the sample discussed further below, I conclude that this pattern is $\{110\}_{\text{FCC}}$.” (Clark, ¶ 136.) In my opinion, this argument is flawed and unreasonable because it purports to draw conclusions about the texture of the *lower* NiFe layer based on measurements of the *upper* NiFe layer—even though the lower and upper NiFe layer measurements do not match. (*Compare* Clark Figure 72, *with* Clark Figure 74.) Moreover, Dr. Clark’s analysis of the upper NiFe layer is also flawed and unreasonable for many of the same reasons. (*See* ¶¶ 340-358, *infra*.)

328. Second, Dr. Clark’s analysis of Figure 72 is further flawed and unreasonable because even assuming Dr. Clark’s NiFe FFT data actually matched the

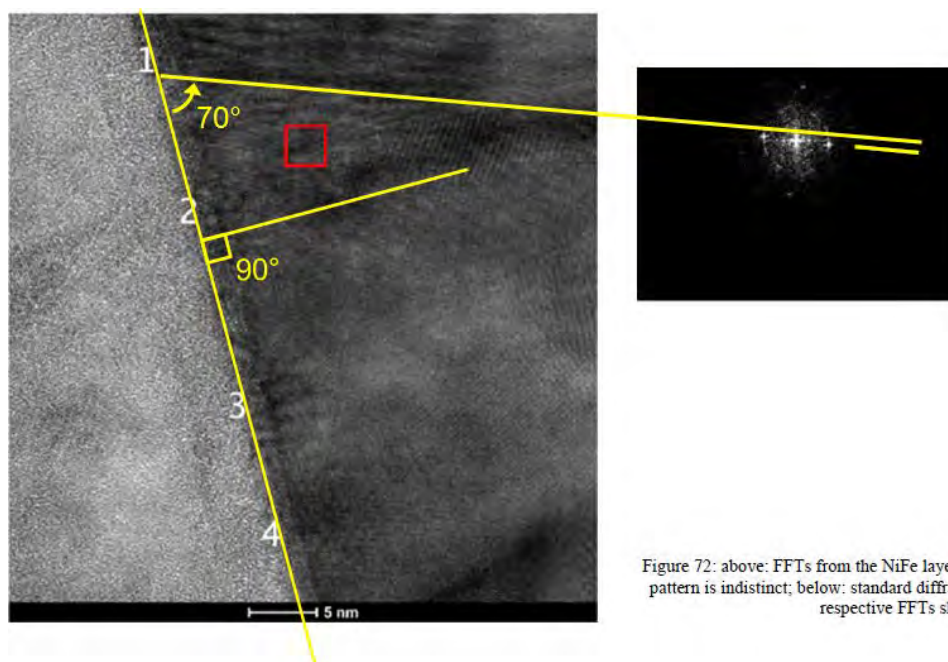
$\{110\}_{\text{FCC}}$ diffraction pattern (they clearly do not), merely matching a $\{110\}_{\text{FCC}}$ diffraction pattern is evidence of an fcc crystal in the NiFe layer—it is *not* evidence of a (111) crystal, and certainly not evidence of a predominance of fcc(111) crystals.

329. As I explained in the Technology Background, *crystal structure* (e.g., fcc, bcc) is a property distinct from *crystal orientation* (e.g., (111), (110)). An fcc(111) crystal describes (1) an fcc crystal (2) whose (111) plane is oriented parallel to the substrate. (See, e.g., Section V.A.2, *supra* (depicting both (111) and non-(111) fcc crystals).)

330. Even if Dr. Clark’s NiFe FFTs matched a $\{110\}_{\text{FCC}}$ diffraction pattern (and they clearly do not), this would only be evidence of one or more fcc crystals in the NiFe layer. In order to properly conclude that any of these fcc crystals are fcc(111) crystals, the NiFe FFTs *must* not only (1) match a $\{110\}_{\text{FCC}}$ diffraction pattern *but also* (2) match the $\{110\}_{\text{FCC}}$ pattern such that the $\langle 111 \rangle_{\text{FCC}}$ direction is perpendicular to the substrate (a.k.a. the layer interface).

331. Dr. Clark acknowledges this requirement and simply asserts it—even though the NiFe FFT data of Figure 72 plainly contradicts him. In particular, Dr. Clark asserts that “when analyzing the pattern from the spot spacing and distribution, it can be seen that a $\langle 111 \rangle_{\text{FCC}}$ direction in the NiFe”—shown by the yellow line in Figure 72’s NiFe FFT—“[is] also perpendicular to the lower NiFe/lower FeCo interface. . . . These mutual relationships are sufficient to determine the relative orientation of the lower NiFe layer and the lower FeCo layer above it. Therefore, the lower NiFe layer exhibits (111) texture” (Clark, ¶ 137.)

332. Dr. Clark’s assertion that the yellow line in Figure 72’s NiFe FFT—the $\langle 111 \rangle_{\text{FCC}}$ direction—is “perpendicular to the lower NiFe/lower FeCo interface” is contradicted by his own data. The $\langle 111 \rangle_{\text{FCC}}$ direction Dr. Clark draws in Figure 72 is not perpendicular to the interface shown in Figure 71, as demonstrated by the image below:



333. This comparison belies Dr. Clark’s claim that the $\langle 111 \rangle_{\text{FCC}}$ direction is “perpendicular to the lower NiFe/lower FeCo interface.” (Clark, ¶ 137.) The $\langle 111 \rangle_{\text{FCC}}$ direction is not perpendicular to the interface—as required of an fcc(111) crystal—but is instead about 70 degrees relative to the interface. Dr. Clark is simply wrong to assert in ¶ 137 that the $\langle 111 \rangle_{\text{FCC}}$ direction is perpendicular to the interface.

334. In sum, Dr. Clark’s NiFe FFT data does not match any $\{110\}_{\text{FCC}}$ diffraction pattern. But even assuming the NiFe FFT data matched the $\{110\}_{\text{FCC}}$ pattern as Dr. Clark claims, that match is inconsistent with a (111) crystal. The $\langle 111 \rangle_{\text{FCC}}$ direction is not perpendicular to the interface; Dr. Clark’s assertion that it is perpendicular contradicts the actual data. Dr. Clark’s analysis of Figure 72, and his conclusion that the FFT data somehow shows a (111) crystal (let alone a predominance of (111) crystals) in the lower NiFe layer, is therefore flawed and unreasonable for this reason as well.

335. Third, Dr. Clark’s analysis of Figure 72 and other FFT data is further flawed and unreasonable because, even if any of his FFT data actually matched a $\{110\}_{\text{FCC}}$ pattern with its $\langle 111 \rangle_{\text{FCC}}$ direction perpendicular to the NiFe/FeCo interface (which is not remotely the case), such limited FFT data does not reasonably allow Dr.

Clark to draw broad conclusions about the predominant crystal orientation (*i.e.*, texture) of the NiFe layer.

336. Dr. Clark's attempt to argue (111) texture based on a handful of FFT images (Clark, ¶ 138) is flawed and unreasonable because Dr. Clark's FFT data corresponds to a tiny fraction—less than 1%—of the overall NiFe layer. Accordingly, there is no scientific basis for Dr. Clark to assert that the NiFe layer has any “predominate” crystal orientation (let alone a predominately (111) crystal orientation) after having measured less than 1% of the overall layer. Such a conclusion is akin to a person concluding that a beach predominately comprises grains of black sand based on the fact that a single sample grain from that beach was found to be black.

337. In my opinion, it is scientifically unreasonable to conclude that a layer has any predominate crystal orientation based on a handful of select FFT measurements corresponding to less than 1% of the total layer. I am not aware of any scientific publication in which the authors inferred a layer's predominant crystal orientation based on such a limited number of FFT measurements. In my opinion, no reasonable scientist would conclude anything about a layer's predominant crystal orientation based on a handful of FFT measurements spanning less than 1% of the layer.

338. In sum, Dr. Clark argues that the lower NiFe layer is “(111) textured” based on a handful of FFT measurements of that layer. Because those FFT measurements do not match any $\{110\}_{\text{FCC}}$ diffraction pattern, do not feature any $\langle 111 \rangle_{\text{FCC}}$ direction perpendicular to the NiFe/FeCo interface, and comprise less than 1% of the entire lower NiFe layer, those FFT measurements do not support Dr. Clark's conclusion that the lower NiFe layer features a “(111) texture.” If anything, Dr. Clark's FFT data contradicts, rather than supports, his claim that the lower NiFe layer is “predominately (111) hexagonal.”

339. For all these reasons, it is my opinion that Dr. Clark's FFT data completely fails to show that the lower NiFe layer of the [REDACTED] write heads is “predominately (111) hexagonal.”

340. **S2MMC: Upper NiFe Layer.** Dr. Clark next proceeds to discuss FFT measurements purportedly done on the upper NiFe layer. Figure 74 purportedly shows

“FFTs” from “(a) the upper FeCo layer,” “(b) in the upper NiFe layer,” and “(c) the lower FeCo layer.” (Clark, Figure 74 (p. 89).) According to Dr. Clark, Figure 74 “shows that the upper NiFe layer has a predominant (111) texture.” (Clark, ¶ 146.)

341. In my opinion, Dr. Clark’s analysis of Figure 74 is flawed and unreasonable for at least three reasons (similar to how his analyses of Figures 42, 44, and 72 were flawed and unreasonable).

342. First, Dr. Clark’s analysis of Figure 74 is based on an erroneous premise—namely, that the FFTs correspond to the diffraction patterns shown below them. Dr. Clark’s analysis hinges on the notion that Figure 74’s NiFe FFT matches a $\{110\}_{\text{FCC}}$ diffraction pattern. (Clark, ¶ 144.) It does not.

343. I reproduce Figure 74 of Dr. Clark’s report below:

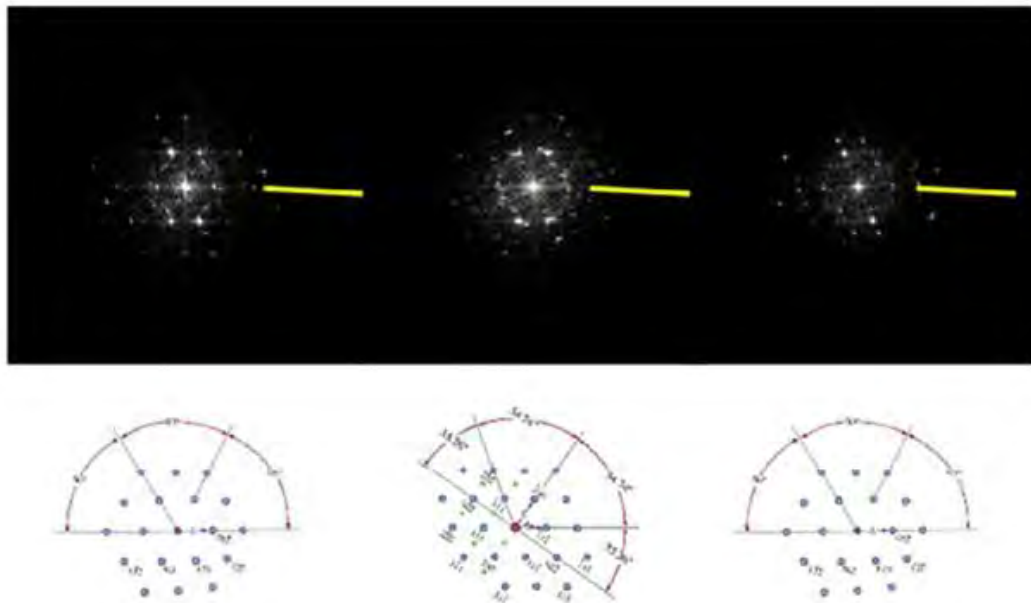


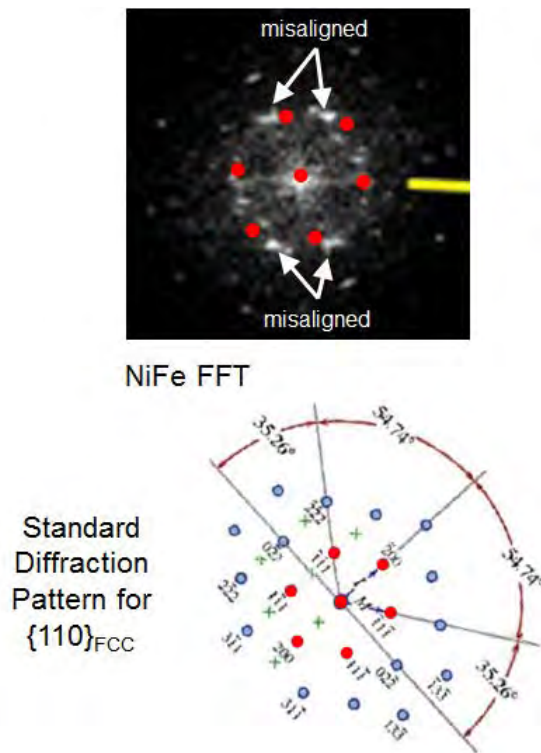
Figure 74: above: FFTs from point 1 from the FeCo layers (left and right) on either side of the upper NiFe layer (center). The FeCo patterns are $\{111\}_{\text{BCC}}$, as determined from the ratio of the lengths of the sides of the pattern motif, and the angles between directions, while the NiFe pattern is $\{111\}_{\text{FCC}}$.

344. There is simply no basis for Dr. Clark’s assertion that the NiFe FFT matches the $\{110\}_{\text{FCC}}$ diffraction pattern shown below it. Dr. Clark attempts to match

the NiFe FFT to the $\{110\}_{\text{FCC}}$ diffraction pattern in order to argue that the NiFe layer contains one or more fcc crystals. (Clark, ¶ 144.) But the NiFe FFT in Figure 74 clearly does not match the $\{110\}_{\text{FCC}}$ diffraction pattern needed for Dr. Clark to argue for the existence of fcc NiFe crystals. In other words, Dr. Clark's own FFT data does not show fcc crystals in the NiFe layer (let alone a predominance of fcc(111) crystals in that layer). For this reason alone, Figure 74 does not support Dr. Clark's flawed and unreasonable conclusion that the upper NiFe layer is "predominately (111) hexagonal."

345. I note that Dr. Clark does not describe the methodology he used to compare the NiFe FFT to the $\{110\}_{\text{FCC}}$ diffraction pattern in Figure 74. For example, Dr. Clark does not attempt to identify the center diffraction peak, which is a critical step in this type of analysis (diffraction peak distances and angles are all measured relative to the center diffraction peak). Nor does Dr. Clark attempt to overlay the $\{110\}_{\text{FCC}}$ diffraction pattern over the NiFe FFT—perhaps because doing so would make it even more clear that the NiFe FFT in no way matches any $\{110\}_{\text{FCC}}$ pattern. No reasonable scientist would agree with Dr. Clark's analysis of Figure 74, or the conclusions he draws from that flawed and unreasonable analysis.

346. When one properly analyzes the NiFe FFT in Figure 74, one readily sees that the NiFe FFT does not match the $\{110\}_{\text{FCC}}$ diffraction as Dr. Clark claims. Below is a modified version of Dr. Clark's Figure 74 that illustrates the substantial misalignment between the NiFe FFT and the $\{110\}_{\text{FCC}}$ diffraction pattern:



347. I note it is not surprising that the NiFe FFT data in Figure 74 does not match the $\{110\}_{\text{FCC}}$ diffraction pattern given the thinness of the NiFe layer. [REDACTED]

348. In addition to Figure 74, Dr. Clark claims to have analyzed additional “FFTs taken from various points along the NiFe layers, while they maintain a common direction with the FeCo layers normal to the interface, change significantly with position along the interface.” (Clark, ¶ 150.) To the extent Dr. Clark contends any of these additional NiFe FFTs match the $\{110\}_{\text{FCC}}$ diffraction pattern, they do not.

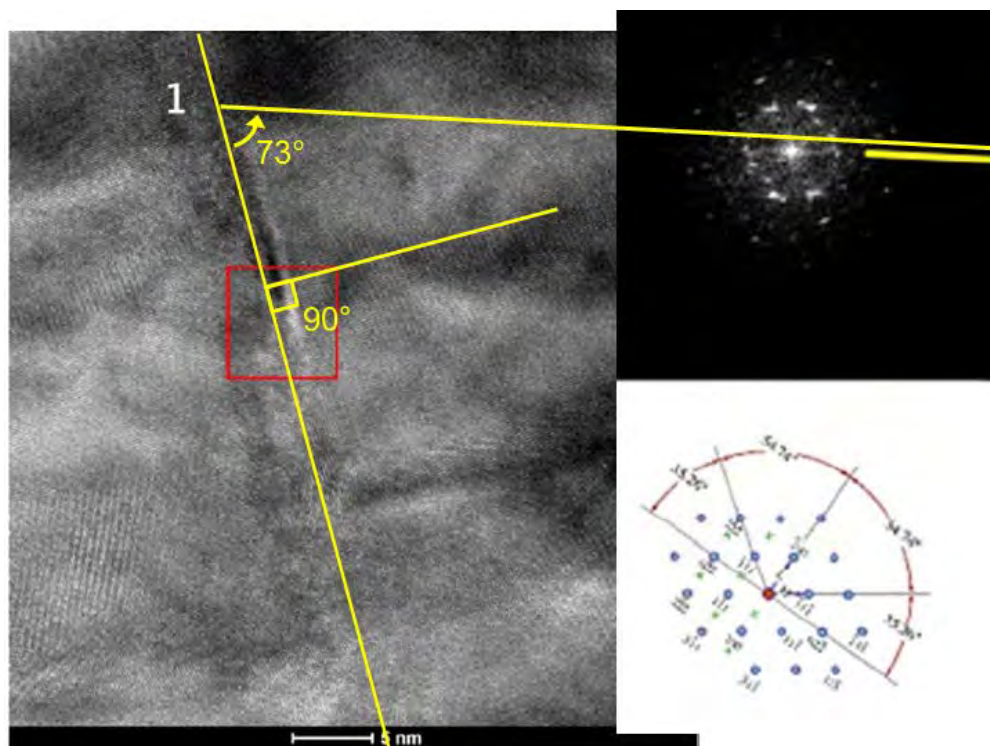
349. I note that Dr. Clark does not depict—let alone analyze—any of these additional FFTs in his report. Nevertheless, I have studied these additional FFTs of the lower NiFe layer, and I conclude that, like the NiFe FFT in Figure 74, none remotely match the $\{110\}_{\text{FCC}}$ diffraction pattern (or the $\{112\}_{\text{FCC}}$ diffraction pattern). Again, Dr. Stach has compiled an exhibit showing the extent of the mismatches between these FFTs and the standard diffraction patterns ($\{110\}_{\text{FCC}}$ and $\{112\}_{\text{FCC}}$). (See Ex. D.) I have

closely reviewed Ex. D, and I agree with Dr. Stach that because none of these additional FFTs match either the $\{110\}_{\text{FCC}}$ or the $\{112\}_{\text{FCC}}$ pattern, none of these additional FFTs depict any fcc NiFe crystals

350. Second, Dr. Clark's analysis of Figure 74 is further flawed and unreasonable because even assuming Dr. Clark's NiFe FFT data actually matched the $\{110\}_{\text{FCC}}$ diffraction pattern (and they clearly do not), merely matching a $\{110\}_{\text{FCC}}$ diffraction pattern is evidence of an fcc crystal in the NiFe layer—it is *not* evidence of a (111) crystal, and certainly not evidence of a predominance of fcc(111) crystals. In order to properly conclude that any of these fcc crystals are fcc(111) crystals, the NiFe FFTs *must* not only (1) match a $\{110\}_{\text{FCC}}$ diffraction pattern *but also* (2) match the $\{110\}_{\text{FCC}}$ pattern such that the $\langle 111 \rangle_{\text{FCC}}$ direction is perpendicular to the substrate (a.k.a. the layer interface).

351. Dr. Clark acknowledges this requirement and simply asserts it—even though the NiFe FFT data of Figure 74 plainly contradicts him. In particular, Dr. Clark asserts that “when analyzing the pattern from the spot spacing and distribution, it can be seen that a $\langle 111 \rangle_{\text{FCC}}$ direction in the NiFe”—shown by the yellow line in Figure 74's NiFe FFT—“[is] also perpendicular to the upper NiFe/FeCo interfaces.” (Clark, ¶ 147; *see also id.* at ¶ 148 (“The parallel directions in the FCC and BCC layers normal to the interface show repeatedly $\langle 110 \rangle$ direction in the BCC layers and $\langle 111 \rangle$ direction in the FCC layers. Therefore, this analysis shows that the lower NiFe layer has a predominant (111) texture”).)

352. Dr. Clark's assertion that the yellow line in Figure 74's NiFe FFT—the $\langle 111 \rangle_{\text{FCC}}$ direction—is “perpendicular to the upper NiFe/FeCo interfaces” is contradicted by his own data. The $\langle 111 \rangle_{\text{FCC}}$ direction Dr. Clark draws in Figure 74 is not perpendicular to the interface shown in Figure 73, as demonstrated by the image below:



353. This comparison belies Dr. Clark’s claim that the $\langle 111 \rangle_{\text{FCC}}$ direction is “perpendicular to the upper NiFe/FeCo interfaces.” (Clark, ¶ 147.) The $\langle 111 \rangle_{\text{FCC}}$ direction is not perpendicular to the interface—as required of an fcc(111) crystal—but is instead about 73 degrees relative to the interface. Dr. Clark is wrong to assert in ¶ 147 that the $\langle 111 \rangle_{\text{FCC}}$ direction is perpendicular to the interface.

354. In sum, Dr. Clark’s NiFe FFT data does not match any $\{110\}_{\text{FCC}}$ diffraction pattern. But even assuming the NiFe FFT data matched the $\{110\}_{\text{FCC}}$ pattern as Dr. Clark claims, that match is inconsistent with a (111) crystal. The $\langle 111 \rangle_{\text{FCC}}$ direction is not perpendicular to the interface; Dr. Clark’s assertion that it is perpendicular contradicts the actual data. Dr. Clark’s analysis of Figure 74, and his conclusion that the FFT data somehow shows a (111) crystal (let alone a predominance of (111) crystals) in the upper NiFe layer, is therefore flawed and unreasonable for this reason as well.

355. Third, Dr. Clark’s analysis of Figure 74 and other FFT data is further flawed and unreasonable because, even if any of his FFT data actually matched a $\{110\}_{\text{FCC}}$ pattern with its $\langle 111 \rangle_{\text{FCC}}$ direction perpendicular to the NiFe/FeCo interface

(which is not remotely the case), such limited FFT data does not reasonably allow Dr. Clark to draw broad conclusions about the predominant crystal orientation (*i.e.*, texture) of the NiFe layer.

356. Dr. Clark's attempt to argue (111) texture based on a handful of FFT images (Clark, ¶ 146) is flawed and unreasonable because Dr. Clark's FFT data corresponds to a tiny fraction—less than 1%—of the overall NiFe layer. Accordingly, there is no scientific basis for Dr. Clark to assert that the NiFe layer has any “predominate” crystal orientation (let alone a predominately (111) crystal orientation) after having measured less than 1% of the overall layer. Such a conclusion is akin to a person concluding that a beach predominately comprises grains of black sand based on the fact that a single sample grain from that beach was found to be black.

357. In my opinion, it is scientifically unreasonable to conclude that a layer has any predominate crystal orientation based on a handful of select FFT measurements corresponding to less than 1% of the total layer. I am not aware of any scientific publication in which the authors inferred a layer's predominant crystal orientation based on such a limited number of FFT measurements. In my opinion, no reasonable scientist would conclude anything about a layer's predominant crystal orientation based on a handful of FFT measurements spanning less than 1% of the layer.

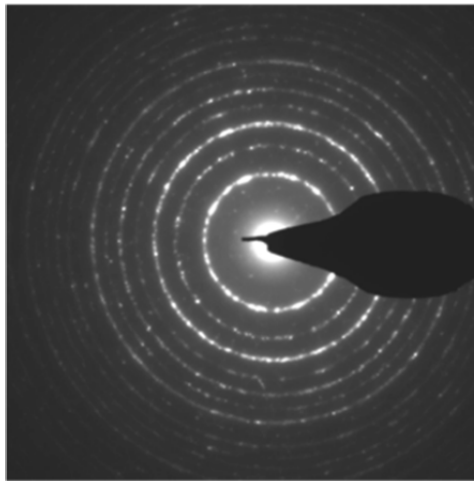
358. In sum, Dr. Clark argues that the upper NiFe layer is “(111) textured” based on a handful of FFT measurements of that layer. Because those FFT measurements do not match any $\{110\}_{\text{FCC}}$ diffraction pattern, do not feature any $\langle 111 \rangle_{\text{FCC}}$ direction perpendicular to the NiFe/FeCo interface, and comprise less than 1% of the entire upper NiFe layer, those FFT measurements do not support Dr. Clark's conclusion that the upper NiFe layer features a “(111) texture.” If anything, Dr. Clark's FFT data contradicts, rather than supports, his claim that the upper NiFe layer is “predominately (111) hexagonal.”

359. For all these reasons, it is my opinion that Dr. Clark's FFT data completely fails to show that the upper NiFe layer of the [REDACTED] write heads is “predominately (111) hexagonal.”

(iii) Dr. Clark's other measurements are inconsistent with a (111) textured NiFe layer

360. As explained above, none of Dr. Clark's FFT data remotely supports the conclusion that the NiFe layers in the [REDACTED] write heads are "predominately (111) hexagonal." In addition, none of Dr. Clark's other TEM measurements suggest any (111) texture to the NiFe layer(s). I note that, aside from the FFTs discussed above, Dr. Clark does not contend that any of his other TEM-based measurements evidence a (111) texture for any NiFe layer.

361. **Dr. Clark's Diffraction Ring Data Is Inconsistent With a (111) Textured NiFe Layer.**⁸ Dr. Clark took a diffraction ring measurement of the S0GPPC sample, shown below:



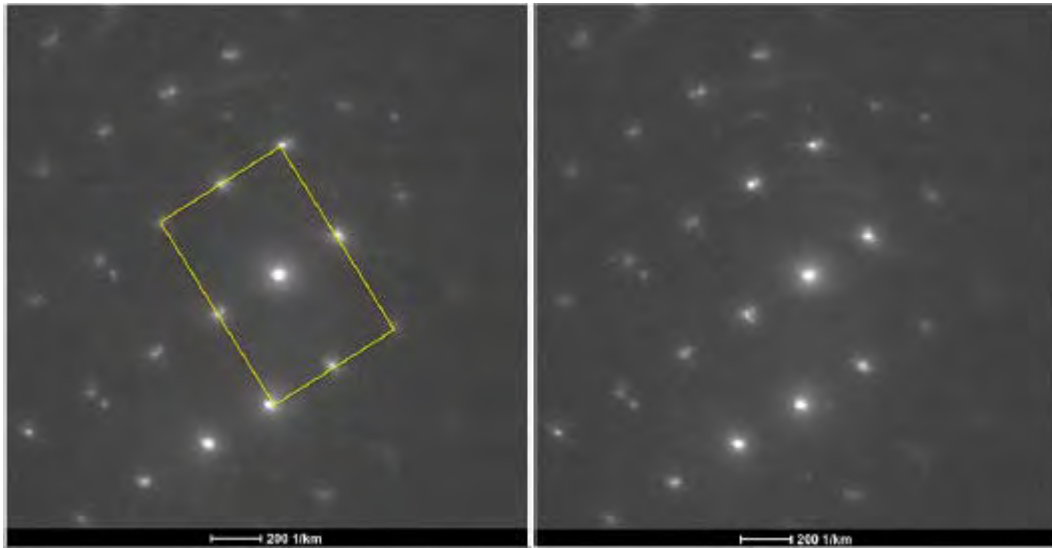
⁸ I note that Dr. Clark's diffraction ring data also contradicts his conclusory and incorrect claim that the FeCo layers are (110) textured. (*Contra* Clark, ¶ 91 ("the lower FeCo layer exhibits (110) texture"), ¶ 100 ("the upper FeCo layer has a predominant (110) texture"), ¶ 101 ("the lower FeCo layer exhibits (110) texture"), ¶ 146 ("the upper FeCo layer has a predominant (110) texture").)

This is because the 310 and 213 rings appear with substantial intensity, indicating that many non-(110) crystals *must* exist in the FeCo layers. A (110) textured FeCo layer—that is, one predominately comprising (110) crystals—would not have substantial diffraction along the 310 and 213 rings, which are necessarily caused by diffraction from *non*-(110) crystals. (See Section V.C.1(a), *supra*.)

362. As I explained in the Technology Background, different crystal orientations will cause diffraction along different rings. A layer with a predominantly (111) crystals would cause a specific set of diffraction rings to appear at specific distances from the center—yet these rings are not present in Dr. Clark’s diffraction ring pattern. I note that Dr. Clark does not mention or rely on his diffraction ring pattern as evidence of a (111) textured NiFe layer.

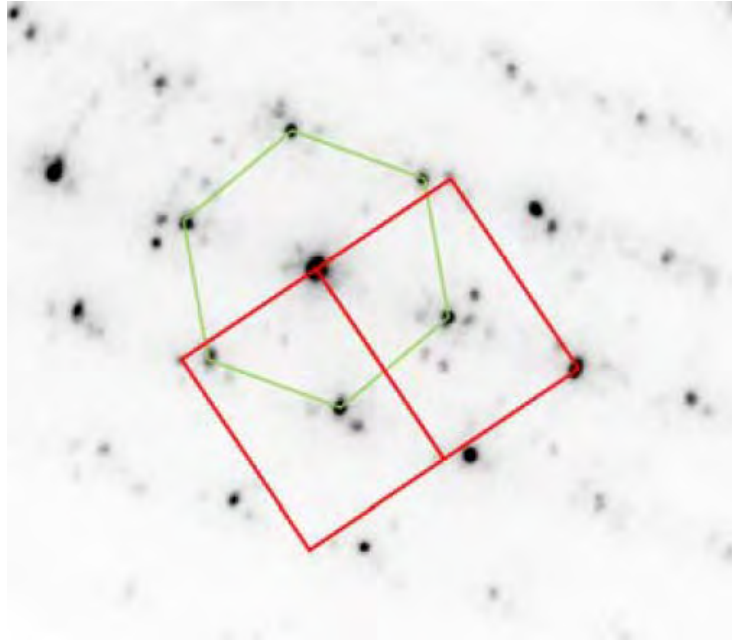
363. **Dr. Clark’s Microbeam Diffraction Data Is Inconsistent With a (111) Textured NiFe Layer.** Dr. Clark also took thousands of microbeam diffraction measurements (most of which he did not produce). These microbeam diffraction measurements also undermine Dr. Clark’s claim that a “(111) textured” NiFe layer exists in the accused [REDACTED] products.

364. For example, one of Dr. Clark’s microbeam diffraction patterns (from Figure 47) is shown below:



365. As I explained in the Technology Background, a (111) hexagonal crystal would, when measured with plan-view microbeam diffraction, produce a specific hexagonal diffraction pattern. Yet no such hexagonal diffraction pattern can be found in any of Dr. Clark’s microbeam diffraction measurements—further indicating that no (111) hexagonal crystals exist.

366. Specifically, a layer with predominantly (111) hexagonal crystals would manifest itself in plan-view microbeam diffraction as a hexagonal pattern, an example of which is shown below:



(LMS's Infringement Contentions (served on Toshiba on Oct. 9, 2015), at 9.)

367. I understand that the image above was prepared and submitted by LMS in its infringement contentions against Toshiba in another lawsuit. I understand that LMS cited this hexagonal template pattern in its infringement contentions against Toshiba as evidence of a "(111) textured hexagonal atomic template," among other things.

368. This hexagonal diffraction pattern—which corresponds to a (111) hexagonal crystal—cannot be found in any of Dr. Clark's microbeam diffraction measurements. Despite taking 1,600 microbeam diffraction measurements on the S0GPPC sample and 1,600 microbeam measurements on the S2MMMC sample—for a total of 3,200 microbeam diffraction measurements on the [REDACTED] write heads—Dr. Clark does not attempt to identify any such hexagonal pattern in any of his 3,200 microbeam diffraction measurements.

369. It is not possible to fit this hexagonal diffraction pattern to any of the microbeam diffraction measurements Dr. Clark produced. No matter how you position

the hexagonal template, it is not possible to align the diffraction peaks to the vertices of the hexagon.

370. It is therefore my opinion that Dr. Clark's microbeam diffraction data contradicts his opinion that the NiFe layers in the [REDACTED] write heads are "(111) textured." It is my opinion that Dr. Clark's microbeam diffraction data contradicts his opinion that the NiFe layers in the [REDACTED] write heads are "predominately (111) hexagonal."

(iv) The extreme thinness of the NiFe layers prevents a predominate crystallographic orientation from forming

371. As I explained in the Technology Background, layers that are only a few atomic layers thick generally exhibit no crystal structure, as a crystal structure tends to develop and evolve as a layer grows in thickness. As a result, very thin layers often feature no crystal structure—and therefore no predominant crystallographic orientation. (See, e.g., '416 Patent at 11:6-9 ("The wetting layer 18 can be an amorphous material or a film too thin to have developed a crystalline texture, or a film whose texture provides a gross lattice mismatch for the ensuing layer."); Patent Owner's Preliminary Response to IPR2016-00013, at 42 ("One common feature in deposition of ultrathin films is that in many cases pseudomorphic growth occurs over several monolayers before the film converts into its usual crystal structure."); *id.* at 43 ("In other words, an epitaxially grown ultrathin film will commonly have a pseudomorphic or metastable non-equilibrium crystalline structure for the first several monolayers. Such crystalline structures will not have formed into stable fcc or bcc structures. . . . Dr. Sinclair chose to ignore the fact that the layers at issue are ultrathin and therefore could not have formed equilibrium crystalline structures."); *id.* at 43-44 (distinguishing prior art: "Dill never described the crystalline structure of the interface layer . . . but the thickness of that interface layer (i.e., 0.4-2 nm) indicates that it was pseudomorphic fcc and could not have been in equilibrium crystalline phase."); D. Lambeth et al., *Magnetic Media Performance: Control Methods for Crystalline Texture and Orientation*, Mat. Res. Soc. Symp. Proc. Vol. 517, p. 185 (1998) ("However, below 5 nm the Cr is so thin that little or no crystalline texture has evolved . . ."); M. Ohring, MATERIALS SCIENCE OF THIN

FILMS 529, 562 (“Sometimes, texture evolves from random in initial deposits to strong orientation of low-energy planes parallel to the film surface, and finally, to changes in preferred texture as the film thickens further.”).)

372. In addition, I note that another method of measuring a layer’s texture (if any) is x-ray diffraction (XRD)—indeed this is how Dr. Lambeth measured texture in both the ’988 Patent and the ’416 Patent. (*See, e.g.*, ’988 Patent at 38:17-19 (“First we provide a perspective for the degree of texture obtained by observing a θ -2 θ x-ray diffraction scan”); ’416 Patent at FIG. 14, FIG. 21, FIG. 23, FIGs. 26-30.) I note that Dr. Clark and Dr. Coffey not analyze any XRD data in their reports.

373. I have also considered Dr. Coffey’s citations and characterizations of Seagate documents and deposition testimony on this issue (*see* Coffey ¶¶ 219-233) and find his characterizations of many of these documents to be flawed and unreasonable. Although Dr. Coffey string cites without explanation dozens of Seagate documents and testimony from ¶¶ 219-233 of his report—including citing over 20 Seagate documents for the undisputed “presence of the lower NiFe layer between the substrate and lower FeCo layer in all ██████ Products” (*id.* at ¶ 223)—none actually support his conclusion that the NiFe layer is (111) textured. None of the cited Seagate documents or testimony support Dr. Coffey’s conclusion that any NiFe layer is “predominately (111) hexagonal.”

374. For all these reasons, it is my opinion that the accused ██████ products do not meet this claim limitation. None of the NiFe layers in the ██████ write heads are “(111) textured.” None of the NiFe layers in the ██████ write heads are “predominately (111) hexagonal.”

(b) layer that provides “an atomic pattern upon which material is grown and which is used to direct the growth of an overlying layer”

375. In my opinion, the NiFe layers in the ██████ write heads do not provide an “atomic template,” *i.e.*, “an atomic pattern . . . which is used to direct the growth of an overlying layer.” Each of the NiFe layers in the ██████ write heads are so thin that they

have not developed any long-range crystal structure needed for epitaxial growth—they therefore cannot and do not “direct the growth of an overlying layer.”

376. In addition, I note that Dr. Clark himself provides examples of FeCo crystals growing irrespective of the NiFe layer. For example, Dr. Clark states that “[s]everal sets of lattice fringes are seen [in Figure 40], as are the FeCo/NiFe, which are marked with a red dashed line. The fringes that run parallel to the red dashed line are present on both sides of the NiFe, and in the NiFe layer itself, indicating that *the orientation of the FeCo is maintained on both sides of the NiFe.*” (Clark, ¶ 86 (interpreting Figure 40).) In other words, the crystals in the lower FeCo layer continue into the upper FeCo layer—the lower FeCo crystals are “growing through” the NiFe layer as if the NiFe layer was not there. This shows that the NiFe layer is not acting as an atomic template for the FeCo—*i.e.*, it is not “used to direct the growth of an overlying layer.”

377. For all these reasons, it is my opinion that the accused [REDACTED] products do not meet this claim limitation. None of the NiFe layers in the [REDACTED] write heads provide an “atomic template.” None of the NiFe layers in the [REDACTED] write heads are “used to direct the growth of an overlying layer.”

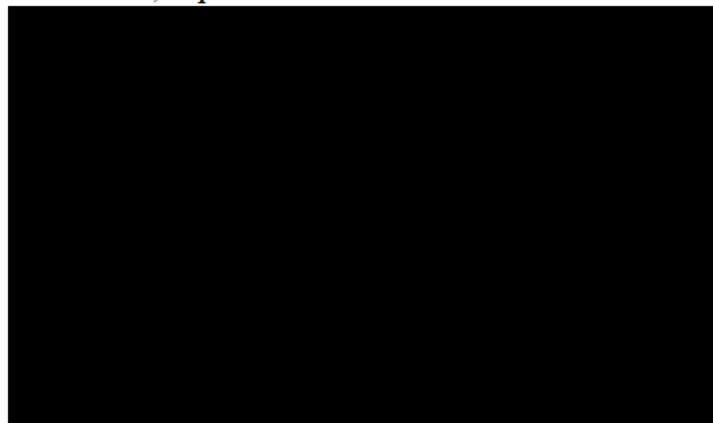
2. The [REDACTED] products do not have “at least one bcc-d layer which is magnetic, forming a uniaxial symmetry broken structure”

Term	Court’s Construction
uniaxial	“having an anisotropy energy density function with only a single maximum and a single minimum as the magnetization angle is rotated by 180 degrees from a physical axis”
symmetry broken structure	“a structure consisting of unequal volumes or unequal amounts of the bcc-d variants of a six variant system”
variant / orientational variant	“one of a set of possible crystal orientations”

Term	Court's Construction
variants / orientational variants	“two or more of a set of possible crystal orientations”
uniaxial symmetry broken structure	“a structure that is uniaxial as a result of the structure being symmetry broken”

378. Dr. Coffey argues in ¶¶ 159-218 of his report that the accused [REDACTED] products have “at least one bcc-d layer which is magnetic, forming a uniaxial symmetry broken structure.” I have carefully considered Dr. Coffey’s arguments and find his conclusion to be unfounded. Dr. Coffey’s data and analyses are flawed and unreasonable with respect to multiple claim limitations. Dr. Coffey’s data does not support his conclusion that the [REDACTED] products have “at least one bcc-d layer which is magnetic, forming a uniaxial symmetry broken structure.”

379. The [REDACTED] write heads comprise several layers, including two layers of NiFe and two layers of FeCo, depicted below:



380. I understand Dr. Coffey contends that “the lower (first-deposited) of the two layers of FeCo in the [REDACTED] Products” is “at least one bcc-d layer which is magnetic, forming a uniaxial symmetry broken structure.” (Coffey, ¶ 161.)

381. I disagree. Although the FeCo layers are magnetic bcc-d layers, neither the lower nor upper FeCo layers meets the remainder of this claim limitation. Neither the lower nor upper FeCo layer forms a “symmetry broken structure.” (See Section

IX.A.2(a).) Neither the lower nor upper FeCo layer is “uniaxial.” (See Section IX.A.2(b).) Neither the lower nor upper FeCo layer forms a “uniaxial symmetry broken structure.” (See Section IX.A.2(c).)

382. I understand that Dr. Coffey analyzes the “uniaxial symmetry broken structure” limitation as a single claim limitation.⁹ (See Coffey, ¶¶ 180-210.) As I understand the Court’s claim construction order, however, “symmetry broken structure,” “uniaxial,” and “uniaxial symmetry broken structure” each represents a claim limitation, and all three must be met for there to be infringement.

383. Because I understand that infringement requires a limitation-by-limitation analysis of each claim limitation, I separately analyze each claim limitation—“symmetry broken structure,” “uniaxial,” and “uniaxial symmetry broken structure”—below.

(a) “a structure consisting of unequal volumes or unequal amounts of the bcc-d variants of a six variant system” (symmetry broken structure)

384. In my opinion, the FeCo layers in the [REDACTED] products do not form a “symmetry broken structure”—*i.e.*, they do not form “a structure consisting of unequal volumes or unequal amounts of bcc-d variants of a six variant system.”

(i) Drs. Coffey & Clark fail to show the existence of any “bcc-d variants of a six variant system” in the FeCo layers

385. In my opinion, neither Dr. Coffey nor Dr. Clark offer any data showing that the FeCo layers in [REDACTED] form a six-variant system as taught by the ’988 Patent and required by the Court’s claim construction. As I discuss above, the ’988 Patent’s six variants refers to bcc-d(110) crystals oriented in one of six ways relative to an

⁹ Dr. Coffey ostensibly addresses the “uniaxial” limitation separately for purposes of asserting the doctrine of equivalents, but even here he appears to conflate multiple claim limitations in his analysis (namely, “uniaxial” and “uniaxial symmetry broken structure”). (See Coffey, ¶¶ 211-218.)

underlying (111) hexagonal template crystal. Neither Dr. Coffey nor Dr. Clark offer data showing the existence of any such variants.

386. A “variant” in the context of the ’988 Patent refers to a bcc-d(110) crystal with one of six orientations relative to an underlying (111) hexagonal template crystal. The Court construed “variants” to mean “two or more of a set of possible crystal orientations.” Whether two bcc-d crystals are the same variant or two different variants depends on their orientations relative to their underlying template crystals. If two bcc-d crystals have the same orientation relative to their underlying template crystals, they are the same “variant” (*i.e.*, they are “one of a set of possible orientations”). If two bcc-d crystals have different orientations relative to their underlying template crystal, they are two different variants (*i.e.*, they are “two . . . of a set of possible orientations”).

387. Because a “bcc-d variant” refers to a bcc-d(110) crystal with a particular orientation relative to an underlying (111) hexagonal template crystal, identifying a “bcc-d variant” requires identifying three things: (1) a bcc-d(110) crystal; (2) the underlying (111) hexagonal template crystal on which that bcc-d(110) crystal was grown; and (3) the orientation of the bcc-d(110) crystal relative to the template crystal.

388. Dr. Coffey and Dr. Clark fail to identify any “variants” (let alone variants of a six variant system) in any of the [REDACTED] layers.

389. Dr. Clark does attempt to identify bcc-d(110) crystals in the FeCo layers via microbeam diffraction measurements. But nowhere do Dr. Coffey or Dr. Clark attempt to identify any underlying (111) hexagonal template crystals—indeed, Dr. Clark’s own microbeam diffraction measurements show that no underlying (111) hexagonal template crystals exist. And nowhere do Dr. Coffey or Dr. Clark attempt to identify the orientation of any bcc-d crystal relative to an underlying (111) hexagonal template crystal (which, again, do not exist).

390. Because Dr. Coffey and Dr. Clark fail to identify any “bcc-d variants,” they fail to show that any [REDACTED] FeCo layer forms a “symmetry broken structure.”

a) Dr. Clark’s microbeam diffraction data does not show “bcc-d variants of a six variant system”

391. Dr. Coffey argues that: “I understand that microbeam diffraction analysis of representative samples of the [REDACTED] Products shows that the lower layer of FeCo in the write pole contains multiple bcc (110) crystalline grains that are members of the Kurdjumov-Sachs six variant system.” (Coffey, ¶ 183.) Dr. Coffey erroneously contends that Dr. Clark’s microbeam diffraction analysis is evidence of a Kurdjumov-Sachs six variant system. In fact, Dr. Clark’s microbeam diffraction data shows no variants because they consistently show that no (111) hexagonal template crystals exist.

392. Dr. Clark apparently took 3,200 microbeam diffraction measurements of the [REDACTED] FeCo layers. (*See, e.g.*, Clark, ¶ 106 (1,600 measurements on S0GPPC), ¶ 151 (1,600 measurements on S2MMC).) Of those 3,200 microbeam diffraction measurements, Dr. Clark contends that some show one, two, or three bcc-d(110) crystals (depending on the measurement) in the FeCo layer. But Dr. Clark never contends that any of these 3,200 microbeam diffraction measurements shows a (111) hexagonal template crystal (which I note is also compelling evidence that no (111) textured hexagonal atomic template exists in the accused [REDACTED] products). As a result, none of Dr. Clark’s microbeam diffraction measurements shows the existence of any “bcc-d variants”—let alone “bcc-d variants of a six variant system.”

i) Sample S0GPPC

393. Dr. Clark took 1,600 microbeam diffraction measurements of the S0GPPC sample. (Clark, ¶ 106.) According to Dr. Clark: “100 out of the 1600 diffraction patterns were selected using a random number generator. These 100 were categorized as either a) showing no recognizable pattern, b) showing a single {110} patterns, c) showing two or three {110} patterns, d) showing {110} twins, or e) showing a pattern other than {110}. The results show the following numbers in each category – 27 show no recognizable pattern, 30 showed a single {110} pattern, and 44 showed two or three {110} patterns (including twins).” (Clark, ¶ 114.)

394. This is precisely the point. Dr. Clark never contends that any of these microbeam diffraction measurements includes anything resembling a $\text{fcc}\{111\}$ pattern—*i.e.*, a pattern corresponding to a (111) hexagonal template crystal. I summarize in the table below Dr. Clark's own summary of his microbeam diffraction measurements:¹⁰

Summary of Microbeam Diffraction Measurements on S0GPPC (SP2X)		
<u># of Images</u>	<u>Pattern Dr. Clark Contends Exists</u>	<u>Meaning</u>
27	No Recognizable Pattern	27/100 microbeam diffraction measurements show no recognizable crystal structure
30	Single $\text{bcc}\{110\}$ Pattern	30/100 microbeam diffraction measurements show a single (110) crystal
44	Two or Three $\text{bcc}\{110\}$ Patterns	44/100 microbeam diffraction measurements show two or three (110) crystals
0	$\text{fcc}\{111\}$ Pattern	0/100 microbeam diffraction measurements show any (111) hexagonal template crystal(s)

395. Of the 1,600 microbeam diffraction measurements of the S0GPPC sample, Dr. Clark depicts eight of them in his report as Figures 47-52.

396. I reproduce Figure 47 of Dr. Clark's report below.

¹⁰ I note that Dr. Clark never produced most of the 1,600 microbeam diffraction patterns he purportedly took for sample S0GPPC. Indeed, of the 1,600 microbeam diffraction patterns Dr. Clark purportedly took, he produced just 29 in Appendix C to his report.

I also note that, although Dr. Clark purports to analyze and categorize a random sample of 100 microbeam diffraction patterns, when he categorizes them (Clark, ¶ 114), he ends up categorizing 101 patterns (*i.e.*, $27+30+44 = 101$).

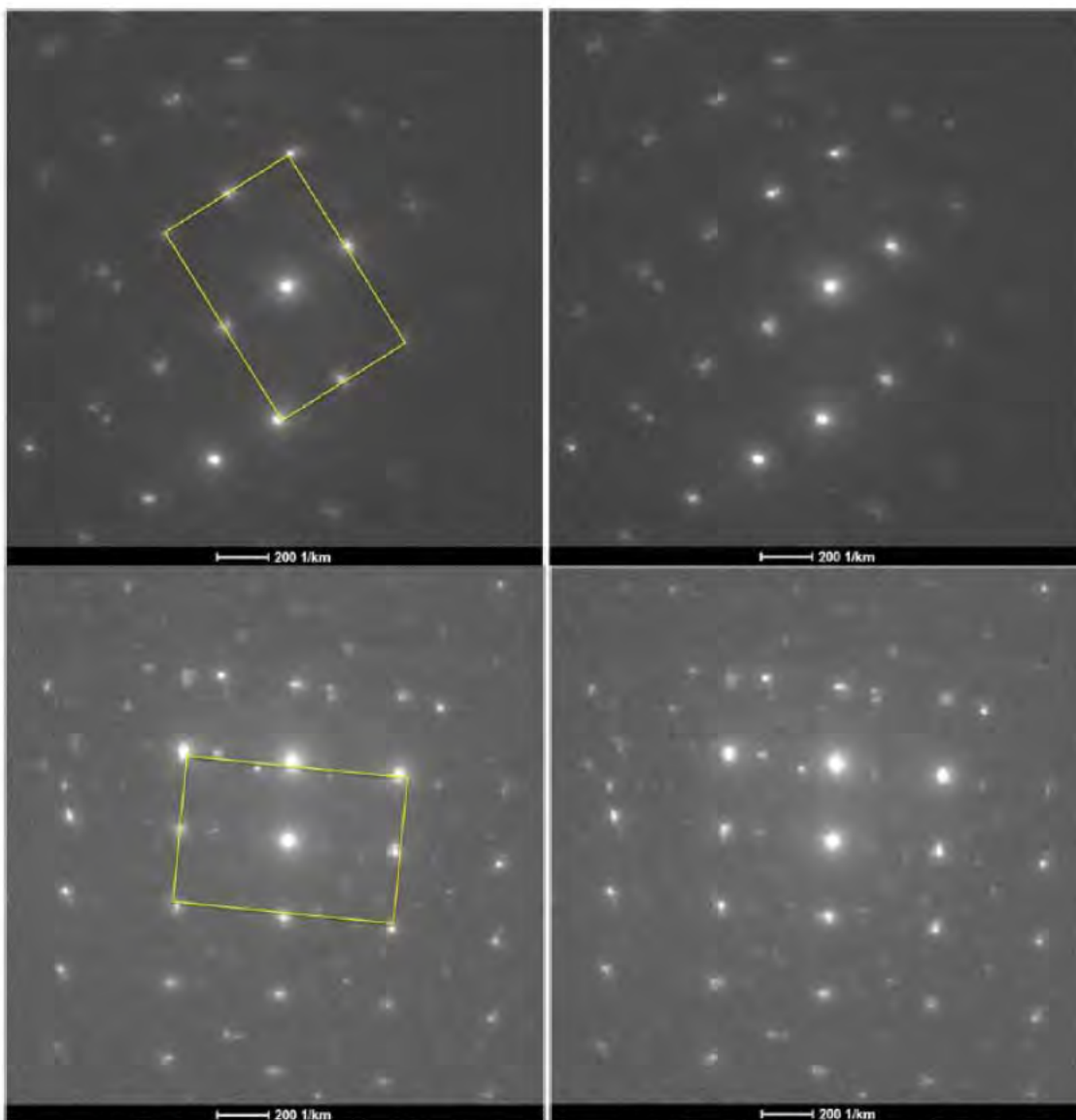
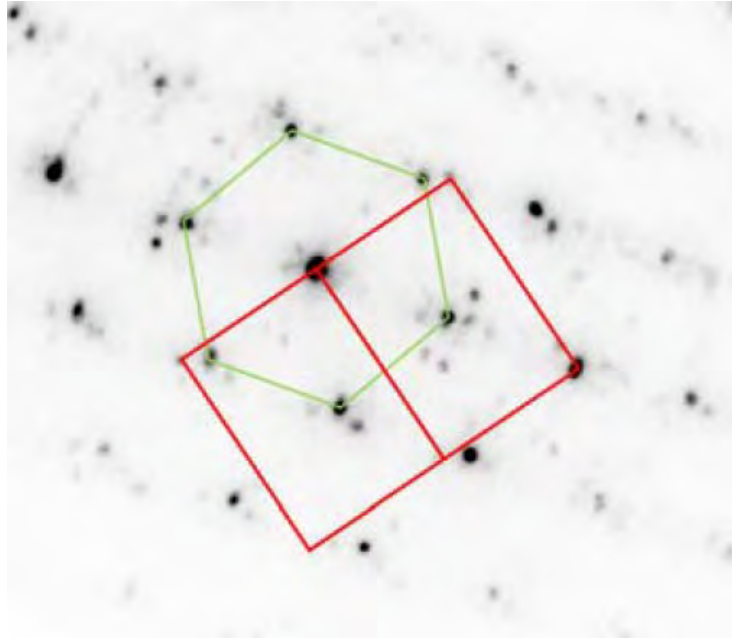


Figure 47: Single crystallite diffraction patterns, frames 722 (upper) and 417 (lower), in the (110) orientation. These patterns visually identify as standard (110)_{BCC} patterns.

397. According to Dr. Clark, “[t]ypical single crystal patterns obtained from this [microbeam diffraction] analysis are shown in Figure 47.” (Clark, ¶ 108.) Figure 47 shows two microbeam diffraction measurements—one in the upper half and one in the lower half. Dr. Clark says that these “patterns are readily identified and indexed as patterns in the (110)_{BCC} orientation.” (*Id.*)

398. But critically, nothing in Figure 47 corresponds to a (111) hexagonal template crystal. In order for a diffraction pattern to show a (111) hexagonal crystal, the

diffraction peaks must be spaced apart at regular repeating intervals so as to allow one to match a hexagon with particular dimensions on top. Specifically, the diffraction would match a hexagonal pattern where each of the six sides of the hexagon is exactly equal in length (with that length being determined by the lattice constant of the material). An example of such a pattern is shown below:



(LMS's Infringement Contentions (served on Toshiba on Oct. 9, 2015), at 9.)

399. Figure 47 clearly does not contain any such hexagonal pattern corresponding to a (111) hexagonal template crystal. Dr. Clark does not contend otherwise. As a result, Figure 47 does not identify "bcc-d variants" because it does not show any (111) hexagonal template crystal.

400. I reproduce Figure 48 of Dr. Clark's report below.

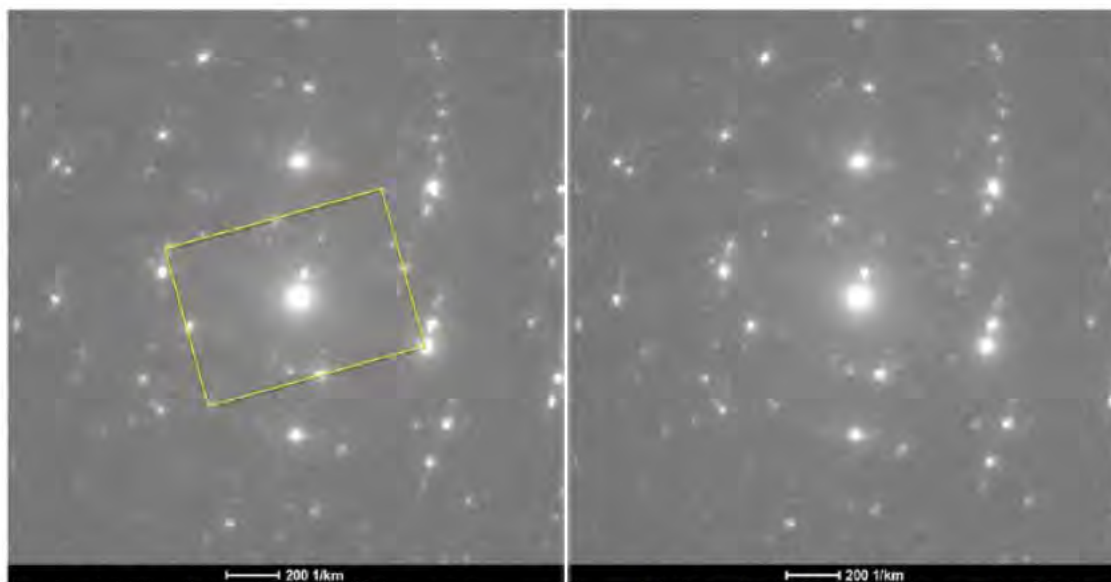


Figure 48: Single crystallite diffraction pattern, frame 837, in the (110) orientation. While there are additional or weak spots, this motif is readily identifiable as a (110)_{BCC} pattern.

401. According to Dr. Clark, “Figure 48 shows another example of a single crystallite (110)_{BCC} diffraction pattern.” (Clark, ¶ 109.) Figure 48 does not contain any hexagonal pattern corresponding to a (111) hexagonal template crystal. Indeed, Dr. Clark claims that “no orientation other than (110)_{BCC} is apparent.” (Clark, ¶ 109 (describing Figure 48).) As a result, Figure 48 does not identify “bcc-d variants” because it does not show any (111) hexagonal template crystal.

402. I reproduce Figure 49 of Dr. Clark’s report below.

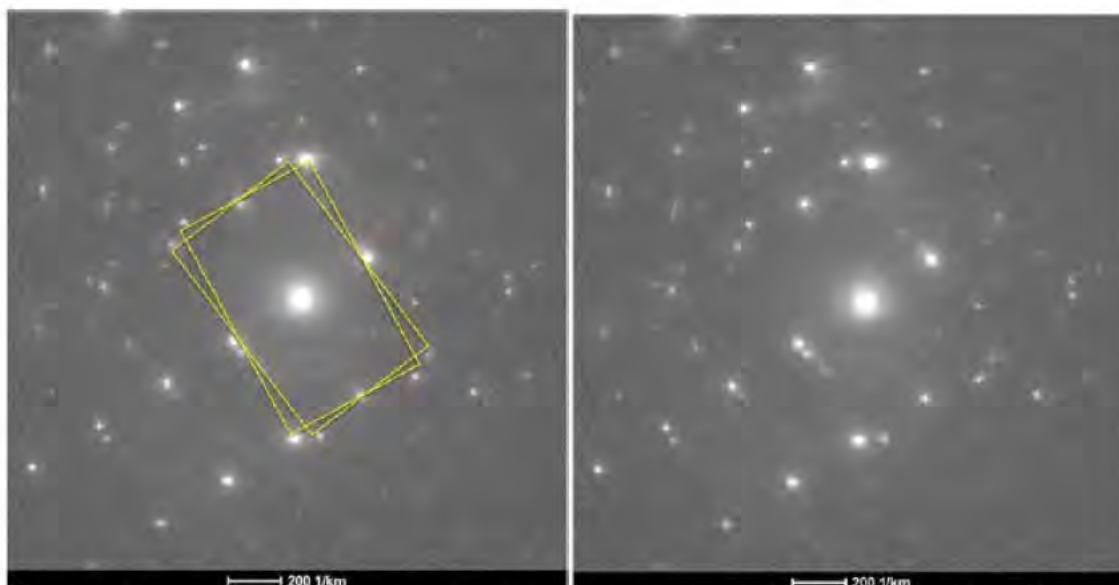


Figure 49: Two crystallites, both in the $(110)_{\text{BCC}}$ orientation, frame 721, rotated by $\sim 9^\circ$ about their common $[110]_{\text{BCC}}$ direction.

403. According to Dr. Clark, “Figure 49 [] shows an example diffraction pattern with two crystallites, both in the $(110)_{\text{BCC}}$ orientation, but rotated by $\sim 9^\circ$ about their common $[110]_{\text{BCC}}$ direction. This is the separation of two variants in the Kurdjumov-Sachs orientation.” (Clark, ¶ 110.)

404. As with Dr. Clark’s other microbeam diffraction patterns, Figure 49 does not contain any hexagonal pattern corresponding to a (111) hexagonal template crystal—and Dr. Clark does not contend otherwise. As a result, Figure 49 does not identify “bcc-d variants” because it does not show any (111) hexagonal template crystal.

405. Dr. Clark contends that Figure 49 shows “two crystallites” and that these two crystallites are “two variants in the Kurdjumov-Sachs orientation.” (Clark, ¶ 110.) This interpretation of Figure 49 is flawed and unreasonable. Neither of the two purported crystallites are “variants,” because neither crystallite is grown on any underlying (111) hexagonal template crystal. Because neither crystallite is a “variant,” the orientations of the two crystallites relative to one another is *irrelevant* (what would be relevant is the orientation of each crystallite relative to an underlying (111) hexagonal template crystal—if such a (111) crystal actually existed, which it does not). Without any evidence of the bcc-d crystallites’ orientations relative to underlying (111)

hexagonal template crystals—indeed, without any evidence that any (111) hexagonal template crystals even exist—it is incorrect and unreasonable for Dr. Clark to claim that Figure 49 shows “two variants in the Kurdjumov-Sachs orientation.” (Clark, ¶ 110.) Figure 49 does not identify any variants—let alone “two variants in the Kurdjumov-Sachs orientation”—because it does not show any (111) hexagonal template crystal.

406. I reproduce Figure 50 of Dr. Clark’s report below.

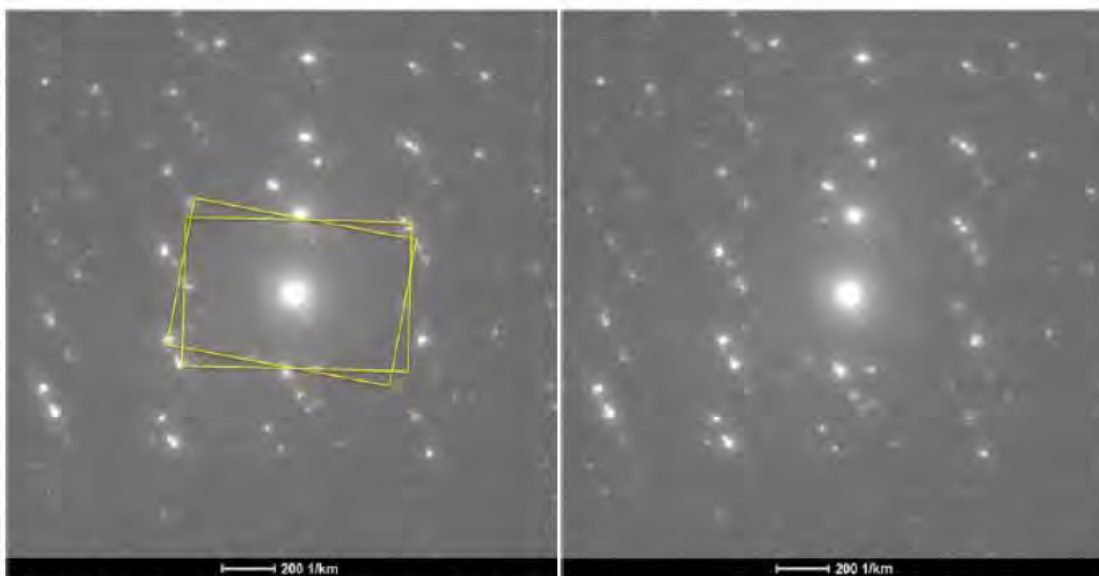


Figure 50: Two crystallites, both in the (110)_{BCC} orientation, frame 817, rotated by $\sim 9^\circ$ about their common [110]_{BCC} direction.

407. According to Dr. Clark, “Figure 50 [] shows another example diffraction pattern with two crystallites, both in the (110)_{BCC} orientation, but rotated by $\sim 11^\circ$ about their common [110]_{BCC} direction. This is also the separation of two variants in the Kurdjumov-Sachs orientation.” (Clark, ¶ 111.)

408. As with Dr. Clark’s other microbeam diffraction patterns, Figure 50 does not contain any hexagonal pattern corresponding to a (111) hexagonal template crystal—and Dr. Clark does not contend otherwise. As a result, Figure 50 does not identify “bcc-d variants” because it does not show any (111) hexagonal template crystal.

409. Dr. Clark contends that Figure 50 shows “two crystallites” and that these two crystallites are “two variants in the Kurdjumov-Sachs orientation.” (Clark, ¶ 111.) Dr. Clark’s interpretation of Figure 50 is flawed and unreasonable. Neither of the two

purported crystallites are “variants,” because neither crystallite is grown on any underlying (111) hexagonal template crystal. Because neither crystallite is a “variant,” the orientations of the two crystallites relative to one another is *irrelevant* (what would be relevant is the orientation of each crystallite relative to an underlying (111) hexagonal template crystal—if such a (111) crystal actually existed, which it does not). Without any evidence of the bcc-d crystallites’ orientations relative to underlying (111) hexagonal template crystals—indeed, without any evidence that any (111) hexagonal template crystals even exist—it is incorrect and unreasonable for Dr. Clark to claim that Figure 50 shows “two variants in the Kurdjumov-Sachs orientation.” (Clark, ¶ 111.) Figure 50 does not identify any variants—let alone “two variants in the Kurdjumov-Sachs orientation”—because it does not show any (111) hexagonal template crystal.

410. I reproduce Figure 51 of Dr. Clark’s report below.

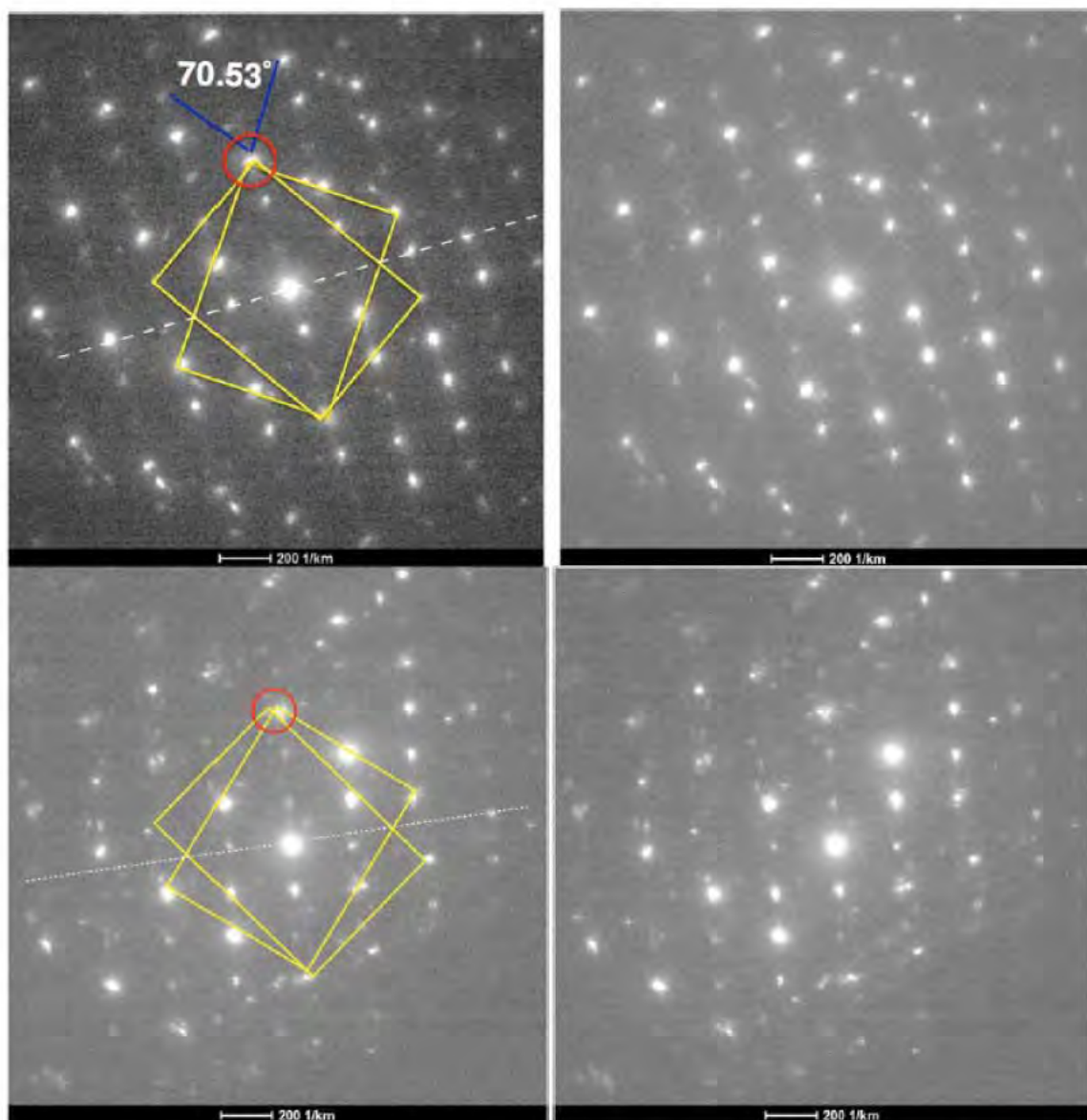


Figure 51: Both patterns, frames 726 (upper) and 802 (lower), show two crystallites both in the $(110)_{\text{BCC}}$ twin orientation, rotated by $\sim 70.53^\circ$ about their common $[110]_{\text{BCC}}$ direction

411. According to Dr. Clark, “Figure 51 shows two diffraction patterns each showing two crystallites both in the $(110)_{\text{BCC}}$ orientation, rotated about their common $[110]_{\text{BCC}}$ direction by $\sim 70.53^\circ$. This is also the separation of two variants in the Kurdjumov-Sachs orientation.” (Clark, ¶ 112.)

412. As with Dr. Clark’s other microbeam diffraction patterns, Figure 51 does not contain any hexagonal pattern corresponding to a (111) hexagonal template crystal—

and Dr. Clark does not contend otherwise. As a result, Figure 51 does not identify “bcc-d variants” because it does not show any (111) hexagonal template crystal.

413. Dr. Clark contends that each diffraction pattern in Figure 51 shows “two crystallites” and that each pair of crystallites are “two variants in the Kurdjumov-Sachs orientation.” (Clark, ¶ 112.) Dr. Clark’s interpretation of Figure 51 is flawed and unreasonable. Neither of the two purported crystallites are “variants,” because neither crystallite is grown on any underlying (111) hexagonal template crystal. Because neither crystallite is a variant, the orientations of the two crystallites relative to one another is *irrelevant* (what would be relevant is the orientation of each crystallite relative to an underlying (111) hexagonal template crystal—if such a (111) crystal actually existed, which it does not). Without any evidence of the bcc-d crystallites’ orientations relative to any underlying (111) hexagonal template crystals—indeed, without any evidence that any (111) hexagonal template crystals even exist—it is incorrect and unreasonable for Dr. Clark to claim that Figure 51 shows “two variants in the Kurdjumov-Sachs orientation.” (Clark, ¶ 112.) Figure 51 does not identify any variants—let alone “two variants in the Kurdjumov-Sachs orientation”—because it does not show any (111) hexagonal template crystal.

414. I reproduce Figure 52 of Dr. Clark’s report below.

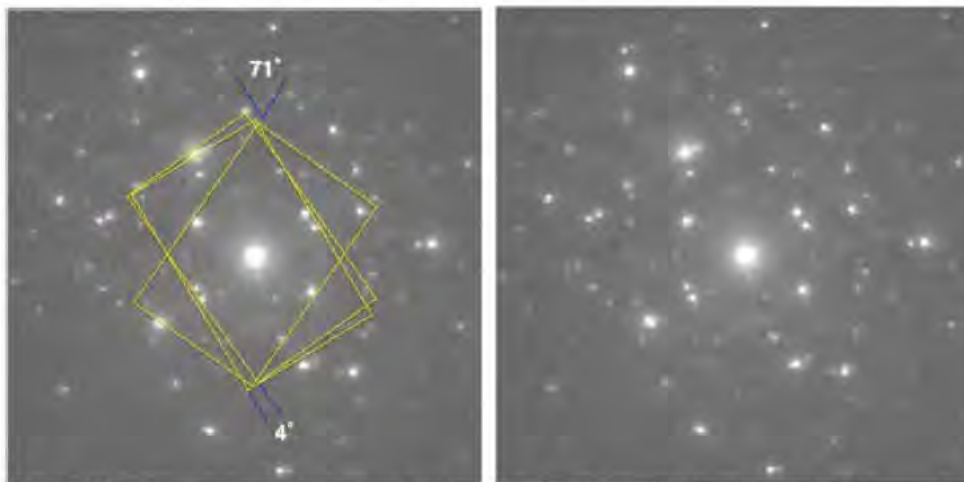


Figure 52: Diffraction pattern, frame 1487, showing three crystallites in the (110)_{BCC} orientation. Two crystallites are rotated with respect to each other by $\sim 4^\circ$, and the third is at $\sim 71^\circ$ from the first.

415. According to Dr. Clark, “Figure 52 shows a complex diffraction pattern, which arises when more than two crystallites contribute to the pattern. . . . [T]here are two variants of (110)_{BCC} rotated with respect to each other by $\sim 4^\circ$, and a third at $\sim 71^\circ$ from the first.” (Clark, ¶ 113.)

416. As with all of Dr. Clark’s microbeam diffraction patterns, Figure 52 does not contain any hexagonal pattern corresponding to a (111) hexagonal template crystal—and Dr. Clark does not contend otherwise. As a result, Figure 52 does not identify “bcc-d variants” because it does not show any (111) hexagonal template crystal.

417. Dr. Clark’s interpretation of Figure 52 is flawed and unreasonable. None of the crystallites are “variants,” because none of the crystallites are grown on any underlying (111) hexagonal template crystal. Because none of the crystallites is a variant, the orientations of the crystallites relative to one another is *irrelevant* (what would be relevant is the orientation of each crystallite relative to an underlying (111) hexagonal template crystal—which does not exist). Without any evidence of the bcc-d crystallites’ orientations relative to any underlying (111) hexagonal template crystals—indeed, without any evidence that any (111) hexagonal template crystals even exist—it is incorrect and unreasonable for Dr. Clark to claim that Figure 52 shows any variants.

418. I note that Dr. Clark does *not* contend that Figure 52 shows variants in a Kurdjumov-Sachs orientation. (See Clark, ¶ 113.)

419. I also note that, in addition to failing to show the presence of any (111) hexagonal template crystals in his microbeam diffraction patterns, Dr. Clark’s contention that his images show the presence of particular bcc(110) crystals is not supported in many of his examples. Dr. Stach and I have identified and analyzed some of these examples in Exhibit E, attached to this report.

420. In sum, *none* of Dr. Clark’s microbeam diffraction images show any (111) hexagonal template crystals. As a result, none of Dr. Clark’s microbeam diffraction images show any “bcc-d variants”—let alone “bcc-d variants of a six variant system.” If “bcc-d variants of a six variant system” actually existed in the measured SOGPPC sample, Dr. Clark’s microbeam imaging would have detected (111) hexagonal crystals underlying each of the bcc(110) crystallites. (Cf. LMS’s Infringement

Contentions (served on Toshiba on Oct. 9, 2015), at 9.) No such evidence of a “bcc-d variant” exists in any of Dr. Clark’s microbeam diffraction data.

421. In my opinion, the fact that Dr. Clark took 1,600 microbeam diffraction measurements of the S0GPPC sample yet found no evidence of (111) hexagonal template crystals shows that the S0GPPC sample’s FeCo layers do not consist of the “bcc-d variants of a six variant system” and therefore do not form any “symmetry broken structure.”

ii) Sample S2MMMC

422. Dr. Clark also took 1,600 microbeam diffraction measurements of the S2MMMC sample. (Clark, ¶ 151.) According to Dr. Clark: “100 out of the 1600 diffraction patterns were selected using a random number generator. These 100 were categorized as either a) showing no recognizable pattern, b) showing a single {110} patterns, c) showing two or three {110} patterns, d) showing {110} twins, or e) showing a pattern other than {110}. The results show the following numbers in each category – a) 86, b) 9, c) 0, d) 5, e) 0.” (Clark, ¶ 157.)

423. This is precisely the point. Dr. Clark never contends that any of these microbeam diffraction measurements includes anything resembling a fcc{111} pattern—*i.e.*, a pattern corresponding to a (111) hexagonal template crystal. I summarize in the table below Dr. Clark’s own summary of his microbeam diffraction measurements:¹¹

Summary of Microbeam Diffraction Measurements on S2MMMC (SP2X)		
<u># of Images</u>	<u>Pattern Dr. Clark Contends Exists</u>	<u>Meaning</u>
86	No Recognizable Pattern	86/100 microbeam diffraction

¹¹ I note that Dr. Clark did not produce most of the 1,600 microbeam diffraction patterns he purportedly took for the S2MMMC sample. Indeed, of the 1,600 microbeam diffraction patterns Dr. Clark purportedly took, he produced just 29 in Appendix C to his report.

		measurements show no recognizable crystal structure
9	Single bcc{110} Pattern	9/100 microbeam diffraction measurements show a single (110) crystal
5	Two or Three bcc{110} Patterns	5/100 microbeam diffraction measurements show two or three (110) crystals
0	fcc{111} Pattern	0/100 microbeam diffraction measurements show any (111) hexagonal template crystal(s)

424. Of the 1,600 microbeam diffraction measurements of the S2MMMC sample, Dr. Clark depicts six of them in his report as Figures 77-80.

425. I reproduce Figure 77 of Dr. Clark's report below.

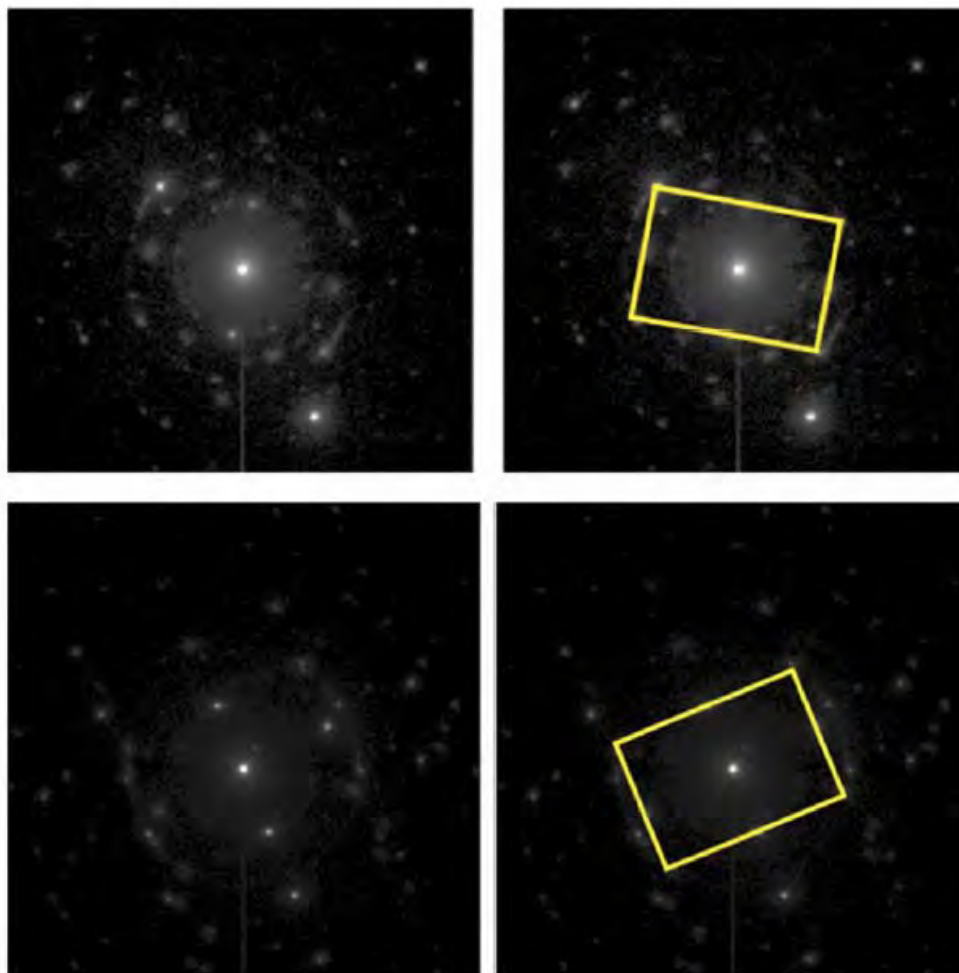


Figure 77: Single crystallite diffraction patterns, frames 419 (upper) and 836 (lower), in the (110) orientation. These patterns visually identify as standard (110)_{BCC} patterns.

426. According to Dr. Clark, “[t]ypical single crystal patterns obtained from this [microbeam diffraction] analysis are shown in Figure 77.” (Clark, ¶ 153.) Figure 47 shows two microbeam diffraction measurements—one on the upper half and one on the lower half. Dr. Clark says that these “patterns are readily identified and indexed as patterns in the (110)_{BCC} orientation.” (*Id.*)

427. Figure 77 clearly does not contain any hexagonal pattern corresponding to a (111) hexagonal template crystal. Dr. Clark does not contend otherwise. As a result, Figure 77 does not identify “bcc-d variants” because it does not show any (111) hexagonal template crystal.

428. I reproduce Figure 78 of Dr. Clark’s report below.

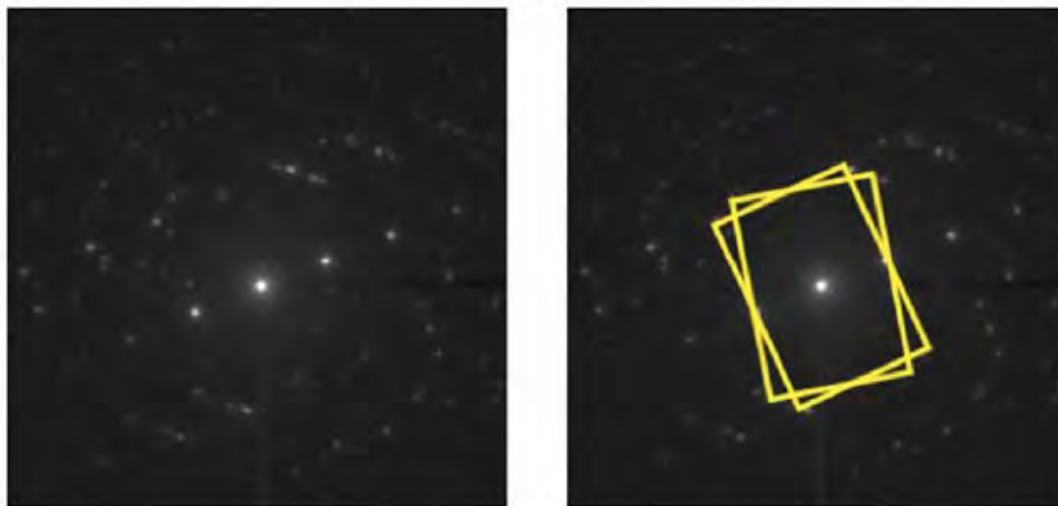


Figure 78: Two crystallites, both in the $(110)_{\text{BCC}}$ orientation, frame 137, rotated by $\sim 12^\circ$ about their common $[110]_{\text{BCC}}$ direction.

429. According to Dr. Clark, “Figure 78 shows an example diffraction pattern with two crystallites, both in the $(110)_{\text{BCC}}$ orientation, but rotated by $\sim 12^\circ$ about their common $[110]_{\text{BCC}}$ direction. This is the separation of two variants in the Kurdjumov-Sachs orientation.” (Clark, ¶ 154.)

430. As with Dr. Clark’s other microbeam diffraction patterns, Figure 78 does not contain any hexagonal pattern corresponding to a (111) hexagonal template crystal—and Dr. Clark does not contend otherwise. As a result, Figure 78 does not identify “bcc-d variants” because it does not show any (111) hexagonal template crystal.

431. Dr. Clark contends that Figure 78 shows “two crystallites” and that these two crystallites are “two variants in the Kurdjumov-Sachs orientation.” (Clark, ¶ 154.) This interpretation of Figure 78 is flawed and unreasonable. Neither of the two purported crystallites are “variants,” because neither crystallite is grown on any underlying (111) hexagonal template crystal. Because neither crystallite is a “variant,” the orientations of the two crystallites relative to one another is *irrelevant* (what would be relevant is the orientation of each crystallite relative to an underlying (111) hexagonal template crystal—if such a (111) crystal actually existed, which it does not). Without any evidence of the bcc-d crystallites’ orientations relative to any underlying (111) hexagonal template crystals—indeed, without any evidence that any (111) hexagonal

template crystals even exist—it is incorrect and unreasonable for Dr. Clark to claim that Figure 78 shows “two variants in the Kurdjumov-Sachs orientation.” (Clark, ¶ 154.) Figure 78 does not identify any variants—let alone “two variants in the Kurdjumov-Sachs orientation”—because it does not show any (111) hexagonal template crystal.

432. I reproduce Figure 79 of Dr. Clark’s report below.

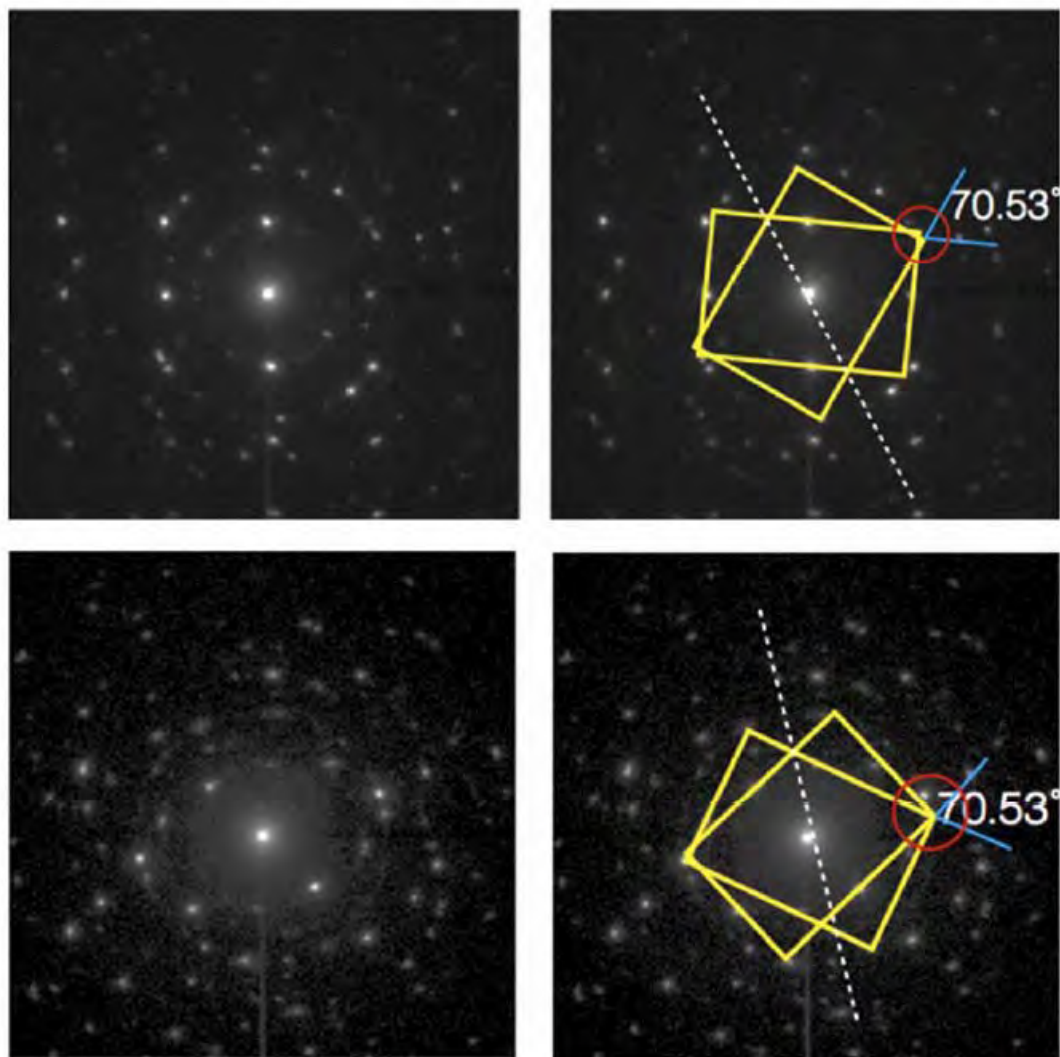


Figure 79: Both patterns, frames 120 (upper) and 669 (lower), show two crystallites both in the (110)_{BCC} twin orientation, rotated by $\sim 70.53^\circ$ about their common [110]_{BCC} direction

433. According to Dr. Clark, “Figure 79 [] shows two diffraction patterns each showing two crystallites both in the (110)_{BCC} orientation, rotated about their common

[110]_{BCC} direction by $\sim 70.53^\circ$. This is also the separation of two variants in the Kurdjumov-Sachs orientation.” (Clark, ¶ 155.)

434. As with Dr. Clark’s other microbeam diffraction patterns, Figure 79 does not contain any hexagonal pattern corresponding to a (111) hexagonal template crystal—and Dr. Clark does not contend otherwise. As a result, Figure 79 does not identify “bcc-d variants” because it does not show any (111) hexagonal template crystal.

435. Dr. Clark contends that Figure 79 shows “two crystallites” and that these two crystallites are “two variants in the Kurdjumov-Sachs orientation.” (Clark, ¶ 155.) Dr. Clark’s interpretation of Figure 79 is flawed and unreasonable. Neither of the two purported crystallites are “variants,” because neither crystallite is grown on any underlying (111) hexagonal template crystal. Because neither crystallite is a “variant,” the orientations of the two crystallites relative to one another is *irrelevant* (what would be relevant is the orientation of each crystallite relative to an underlying (111) hexagonal template crystal—if such a (111) crystal actually existed, which it does not). Without any evidence of the bcc-d crystallites’ orientations relative to any underlying (111) hexagonal template crystals—indeed, without any evidence that any (111) hexagonal template crystals even exist—it is incorrect and unreasonable for Dr. Clark to claim that Figure 79 shows “two variants in the Kurdjumov-Sachs orientation.” (Clark, ¶ 155.) Figure 79 does not identify any variants—let alone “two variants in the Kurdjumov-Sachs orientation”—because it does not show any (111) hexagonal template crystal.

436. I reproduce Figure 80 of Dr. Clark’s report below.

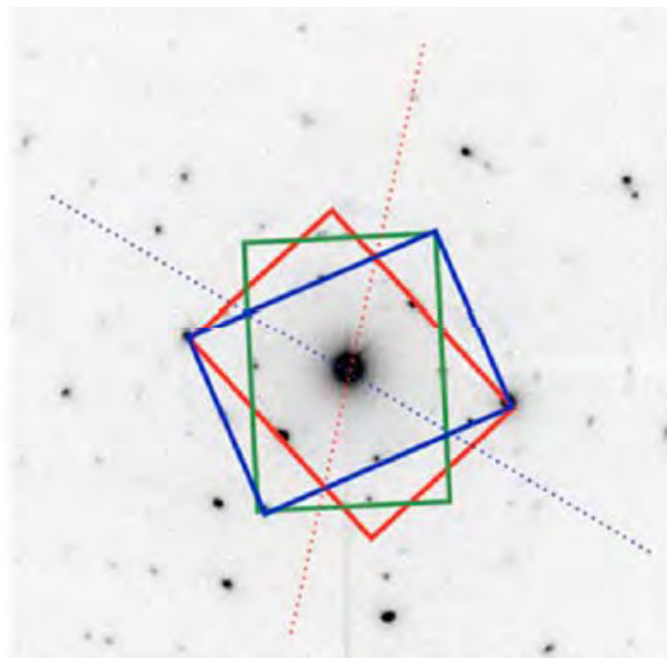


Figure 80: Diffraction pattern, frame 17, showing three crystallites in the $(110)_{\text{BCC}}$ orientation.

437. According to Dr. Clark, “Figure 80 [] shows a complex diffraction pattern, which arises when more than two crystallites contribute to the pattern. In the example of Figure 80[], there are two variants of $(110)_{\text{BCC}}$ rotated with respect to each other.” (Clark, ¶ 156; *but see* Clark, Figure 80 caption (“Diffraction pattern . . . showing three crystallites in the $(110)_{\text{BCC}}$ orientation”).)

438. As with all of Dr. Clark’s microbeam diffraction patterns, Figure 80 does not contain any hexagonal pattern corresponding to a (111) hexagonal template crystal—and Dr. Clark does not contend otherwise. As a result, Figure 80 does not identify “bcc-d variants” because it does not show any (111) hexagonal template crystal.

439. Dr. Clark’s interpretation of Figure 80 is flawed and unreasonable. Whether Dr. Clark contends Figure 80 shows two variants (Clark, ¶ 156) or three variants (Clark, Figure 80 caption), he is incorrect. None of the crystallites are “variants,” because none of the crystallites are grown on any underlying (111) hexagonal template crystal. Because none of the crystallites is a “variant,” the orientations of the crystallites relative to one another is *irrelevant* (what would be relevant is the orientation of each crystallite relative to an underlying (111) hexagonal template crystal—which

does not actually exist). Without any evidence of the bcc crystallites' orientations relative to any underlying (111) hexagonal template crystals—indeed, without any evidence that any (111) hexagonal template crystals even exist—it is incorrect and unreasonable for Dr. Clark to claim that Figure 80 shows any variants.

440. I note that Dr. Clark does *not* contend that Figure 80 shows variants in a Kurdjumov-Sachs orientation. (*See* Clark, ¶ 156.)

441. I also note that, in addition to failing to show the presence of any (111) hexagonal template crystals in his microbeam diffraction patterns, Dr. Clark's contention that his images show the presence of particular bcc(110) crystals is not supported in many of his examples. Dr. Stach and I have identified and analyzed some of these examples in Exhibit E, attached to this report.

442. In sum, *none* of Dr. Clark's microbeam diffraction images show any (111) hexagonal template crystals. As a result, none of Dr. Clark's microbeam diffraction images show any "bcc-d variants"—let alone "bcc-d variants of a six variant system." If "bcc-d variants of a six variant system" actually existed in the measured S2MMC sample, Dr. Clark's microbeam imaging would have detected (111) hexagonal crystals underlying each of the bcc(110) crystallites. (*Cf.* LMS's Infringement Contentions (served on Toshiba on Oct. 9, 2015), at 9.) No such evidence of a "bcc-d variant" exists in any of Dr. Clark's microbeam diffraction data.

443. In my opinion, the fact that Dr. Clark took 1,600 microbeam diffraction measurements of the S2MMC sample yet found no evidence of (111) hexagonal template crystals shows that the S2MMC sample's FeCo layers do not consist of the "bcc-d variants of a six variant system" and therefore do not form any "symmetry broken structure."

b) Dr. Clark's FFT data does not show "bcc-d variants of a six variant system"

444. Dr. Coffey argues that: "I further understand that there are unequal amounts of variants from the Kurdjumov-Sachs six-variant system in the lower layer of FeCo in sample S0GPPC based on high resolution cross-sectional imaging. Dr. Clark

used FFTs to analyze a cross-section sample from sample S0GPPC to confirm that the FeCo grains in the lower layer of FeCo and the lower layer of NiFe have an epitaxial $(111)\text{NiFe} \parallel (110)\text{FeCo}$ orientation relationship with the in-plane directions $\langle 111 \rangle_{\text{bcc}} \parallel \langle 110 \rangle_{\text{fcc}}$, which confirms that the FeCo grains are composed of variants from the Kurdjumov-Sachs six-variant system.” (Coffey, ¶ 184; *see also* Coffey, ¶ 185 (same statements for S2MMC).)

445. As I explained above, Dr. Clark’s interpretation of his FFTs is flawed, unreasonable, and incorrect for multiple reasons.

446. First, contrary to Dr. Clark’s claims, none of the FFT images for any NiFe layer remotely matches the $\{110\}_{\text{FCC}}$ diffraction pattern. (*See* Sections IX.A.1(a)(i) and IX.A.1(a)(ii), *supra*.)

447. Second, none of the FFT images show an epitaxial $(111)\text{NiFe} \parallel (110)\text{FeCo}$ orientation relationship because none of the FFTs purport to show any NiFe crystals with their $\langle 111 \rangle_{\text{FCC}}$ direction perpendicular to the NiFe/FeCo interface. In other words, even assuming Dr. Clark’s FFTs matched the diffraction patterns he claims they do (they do not), none of those FFTs show (111) NiFe crystals (*i.e.*, a NiFe crystal with its $\langle 111 \rangle_{\text{FCC}}$ direction perpendicular to the interface). (*See* Sections IX.A.1(a)(i) and IX.A.1(a)(ii), *supra*.)

448. Third, there is no valid scientific basis for Dr. Clark to make sweeping conclusions about the predominant crystallographic orientation of a NiFe layer based on a handful of FFT images that span less than 1.1% of the layer. (*See* Sections IX.A.1(a)(i) and IX.A.1(a)(ii), *supra*.)

449. In sum, Dr. Clark’s argument that his FFT data shows a “ $(111)\text{NiFe} \parallel (110)\text{FeCo}$ orientation relationship with the in-plane directions $\langle 111 \rangle_{\text{bcc}} \parallel \langle 110 \rangle_{\text{fcc}}$ ” is unreasonable and simply not supported by his FFT data. Dr. Clark’s FFTs show nothing of the sort, as is made plain when one actually examines the FFT data. (*See* Sections IX.A.1(a)(i) and IX.A.1(a)(ii), *supra*.)

450. Dr. Coffey nevertheless relies on Dr. Clark’s deeply flawed FFT analysis, and does not purport to offer any additional or independent analysis of his own. Dr. Coffey’s opinion that “there are unequal amounts of variants from the Kurdjumov-Sachs

six-variant system” is therefore based on nothing other than Dr. Clark’s deeply flawed and unreliable FFT analysis.

* * *

451. In sum, neither Dr. Coffey nor Dr. Clark offer any evidence of a (111) hexagonal template. Although Dr. Clark provides microbeam diffraction images, some of which may show the existence of one, two, or three bcc-d(110) crystals, none of those microbeam diffraction images indicate that any (111) hexagonal template crystal underlies any of these bcc-d(110) crystals. As for Dr. Clark’s FFT data, none of that data remotely shows any (111) hexagonal template crystal.

452. I have also considered Dr. Coffey’s citations and characterizations of Seagate documents and deposition testimony on this issue (*see* Coffey ¶¶ 180-210) and find his characterizations of many of those documents to be flawed and unreasonable. Although Dr. Coffey string cites without explanation dozens of Seagate documents and testimony from ¶¶ 180-210 of his report, none actually support his conclusion that the FeCo layer forms a symmetry broken structure—*i.e.*, “a structure consisting of unequal volumes or unequal amounts of the bcc-d variants of a six variant system.” For example, none of the cited Seagate documents or deposition testimony show any evidence of “bcc-d variants” because none show that any underlying (111) hexagonal template crystals exist in any accused Seagate products.

453. Because neither Dr. Coffey nor Dr. Clark offers any evidence of any (111) hexagonal template crystals underlying bcc-d(110) FeCo crystals, they have failed to show any “bcc-d variants”—let alone “bcc-d variants of a six variant system.” Without the “bcc-d variants of a six variant system,” neither FeCo layer can form a “symmetry broken structure.”

c) **Dr. Clark’s microbeam diffraction, ring diffraction, and dark field image data all consistently show FeCo layers with many *non*-(110) crystals**

454. Dr. Coffey and Dr. Clark fail to provide any evidence of bcc-d variants of a six variant system in any of Seagate’s FeCo layers. Indeed, Dr. Clark’s own data

repeatedly shows that Seagate's FeCo layers do not consist of six bcc(110) variants, and so do not form a "symmetry broken structure."

455. First, Dr. Clark obtained microbeam diffraction patterns for the lower FeCo layers of samples S0GPPC and S2MMMC. Dr. Clark claims he randomly selected and characterized 100 of those patterns for each sample. (Clark, ¶¶ 114, 157.)

Assuming Dr. Clark's characterization of those samples is correct (he did not include the images of those patterns in his report), he reports that for the first sample 27% of the diffraction patterns for the lower FeCo layer were not recognizable as bcc(110) crystals. (Clark, ¶ 114.) He reports for the second sample that 86% of the diffraction patterns in the lower FeCo layer were not recognizable as bcc(110) crystals. (Clark, ¶ 157.) This indicates that many (if not most) of the crystals in the lower FeCo layers Dr. Clark measured are *not* bcc(110).

456. Second, the ring diffraction pattern from Dr. Clark for the S0GPPC sample also shows that the sample has a significant number of FeCo crystals that are not bcc(110). This is because these ring patterns show significant diffraction into the 213 and 310 rings—diffraction that *cannot* come from a bcc(110) crystal. (*See* Section V.C.1(a), *supra*; *see also, e.g.*, SEA01944075 at 4077-78 (XRD measurement showing significant amounts of non-(110) crystals in the measured FeCo layer).)

457. Third, Dr. Clark's dark field imaging data show that most of the crystals in the FeCo layers he analyzed are not bcc(110) crystals. The crystallites he identified that are bcc(110) make up little more than 30-35% of the layers according to his own area-fraction data. (*See* Clark, Table 1 (pp. 70-71) and Table 2 (pp. 103-104).)

458. The presence of so many non-(110) crystals in the FeCo layers is inconsistent with the FeCo layers forming a "symmetry broken structure." Non-(110) crystals cannot form a six-variant system under the '988 Patent. (*E.g.*, '988 Patent at 12:66-13:2 ("[T]his invention deals with a structure to achieve uniaxial magnetocrystalline orientation via the use of the (110) texture of body centered cubic (BCC) or body centered cubic derivative crystal thin film structures.")). Because Seagate's FeCo layers contain many (if not mostly) non-(110) crystals, the FeCo layers do not consist of the bcc-d variants of a six variant system. Because Seagate's FeCo

layers contain many (if not mostly) non-(110) crystals, they do not form a symmetry broken structure.

459. In my opinion, the fact that Seagate's FeCo layers all contain a substantial number of non-(110) crystals—as consistently shown across multiple different measurements by Dr. Clark—is further evidence that the FeCo layers in Seagate's [REDACTED] products do not form a “symmetry broken structure” and therefore do not infringe the Asserted Claims of the '988 Patent.

460. For all these reasons, it is my opinion that none of the FeCo layers in the [REDACTED] write heads form “a structure consisting of unequal volumes or unequal amounts of the bcc-d variants of a six variant system” (*i.e.*, “a symmetry broken structure”).

(ii) Under LMS's erroneous construction of “variant,” the FeCo layers contain many more than six bcc-d variants

461. As I explained above, identifying a “bcc-d variant” requires identifying three things: (1) a bcc-d(110) crystal; (2) the underlying (111) hexagonal template crystal on which that bcc-d(110) crystal was grown; and (3) the orientation of the bcc-d(110) crystal relative to the template crystal.

462. Unable to show any underlying (111) hexagonal template crystals, Drs. Coffey and Clark ignore this requirement. Drs. Coffey and Clark implicitly—and incorrectly—construe “variant” so as to not require proof of any underlying (111) hexagonal template crystal. In particular, Drs. Coffey and Clark apparently have taken the position that *any* bcc-d(110) crystal is a “variant” (whether grown on an underlying (111) hexagonal template crystal or not), and two bcc-d(110) crystals with different orientations relative to each other are two different “variants.” (*See, e.g.*, Clark, ¶ 111; Coffey, ¶ 183.)

463. Although I disagree that a “bcc-d variant” merely refers to any bcc-d(110) crystal, in this section (IX.A.2(a)(ii)) I will apply Dr. Coffey's and Dr. Clark's flawed understanding of “variant” to show that, under their erroneous interpretation of “variant,” more than six bcc-d variants exist in the accused FeCo layers based on their own data.

a) **Microbeam Diffraction Data**

i) **Sample S0GPPC**

464. In describing Figure 49, Dr. Clark states that “Figure 49 shows an example diffraction pattern with **two crystallites, both in the (110)_{BCC} orientation**, but rotated by $\sim 9^\circ$ about their common $[110]_{\text{BCC}}$ direction. This is the separation of two variants in the Kurdjumov-Sachs orientation.” (Clark, ¶ 110.)

465. Dr. Clark apparently contends that Figure 49 shows two variants because it shows two $(110)_{\text{BCC}}$ crystallites. He contends that these two variants—these two $(110)_{\text{BCC}}$ crystallites—have a Kurdjumov Sachs-orientation because they are oriented roughly 9 degrees from one another. (*But see, e.g.,* Clark, ¶ 111 (claiming that 11 degrees “is also the separation of two variants in the Kurdjumov-Sachs orientation”); *id.* at ¶ 112 (claiming that 70.53 degrees “is also the separation of two variants in the Kurdjumov-Sachs orientation”); *id.* at ¶ 154 (claiming that 12 degrees is “the separation of two variants in the Kurdjumov-Sachs orientation”).)

466. Dr. Clark’s analysis therefore posits that each of these $(110)_{\text{BCC}}$ crystallites is a “variant.” As I explained above, this is an erroneous understanding of “variant,” because not all $(110)_{\text{BCC}}$ crystallites are variants. Specifically, in order to identify a “variant,” one *must* identify both a $(110)_{\text{BCC}}$ crystallite *and* the underlying (111) hexagonal template crystal.

467. Nevertheless, if one applies Dr. Clark’s understanding that any $(110)_{\text{BCC}}$ crystallite in a microbeam diffraction pattern is a “variant,” then Dr. Clark’s own microbeam diffraction patterns show more than six $(110)_{\text{BCC}}$ crystallites with different orientations—and therefore more than six “variants.” To the extent Dr. Clark contends that each $(110)_{\text{BCC}}$ crystallite is a “variant,” Dr. Clark’s own microbeam diffraction patterns show more than six “variants” in each FeCo layer. Because a “symmetry broken structure” requires a “six variant system,” a layer containing more than six “variants” cannot form a “symmetry broken structure.”

468. For example, under Dr. Clark's erroneous interpretation of "variant"—*i.e.*, where any two $(110)_{\text{BCC}}$ crystals with different in-plane orientations relative to each other are two "variants"—Figure 49 shows two "variants":

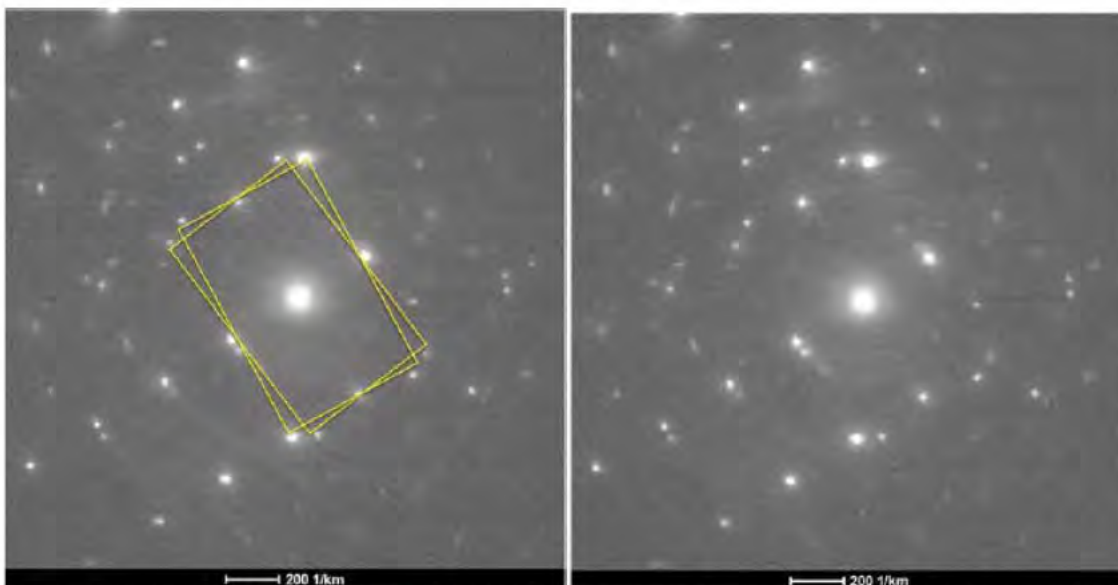


Figure 49: Two crystallites, both in the $(110)_{\text{BCC}}$ orientation, frame 721, rotated by $\sim 9^\circ$ about their common $[110]_{\text{BCC}}$ direction.

469. Under Dr. Clark's erroneous interpretation of "variant," Figure 50 shows two additional "variants":

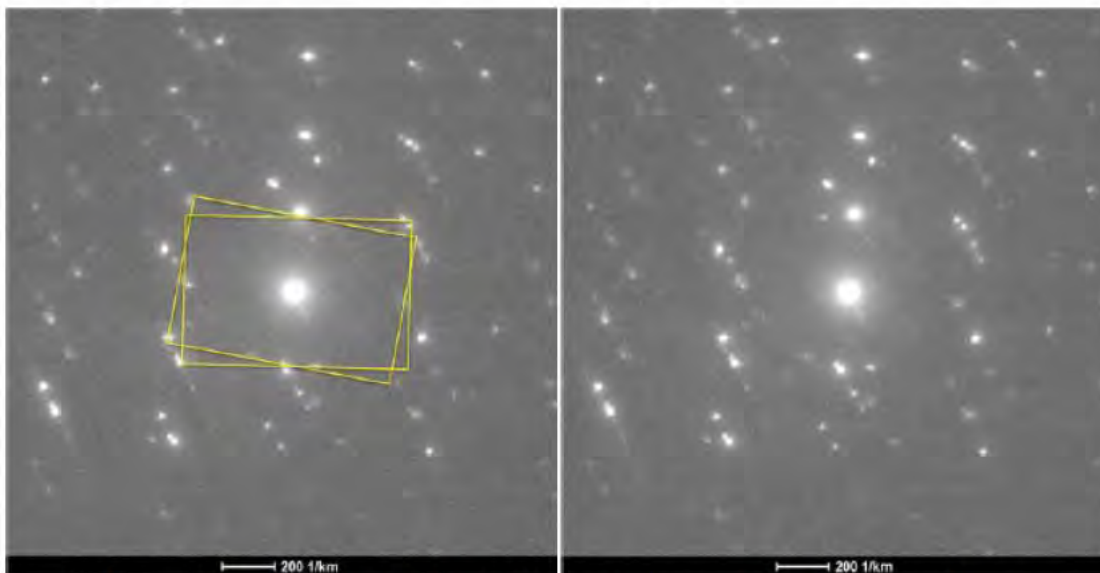


Figure 50: Two crystallites, both in the $(110)_{\text{BCC}}$ orientation, frame 817, rotated by $\sim 9^\circ$ about their common $[110]_{\text{BCC}}$ direction.

470. Under Dr. Clark's erroneous interpretation of "variant," Figure 51 shows two additional "variants":

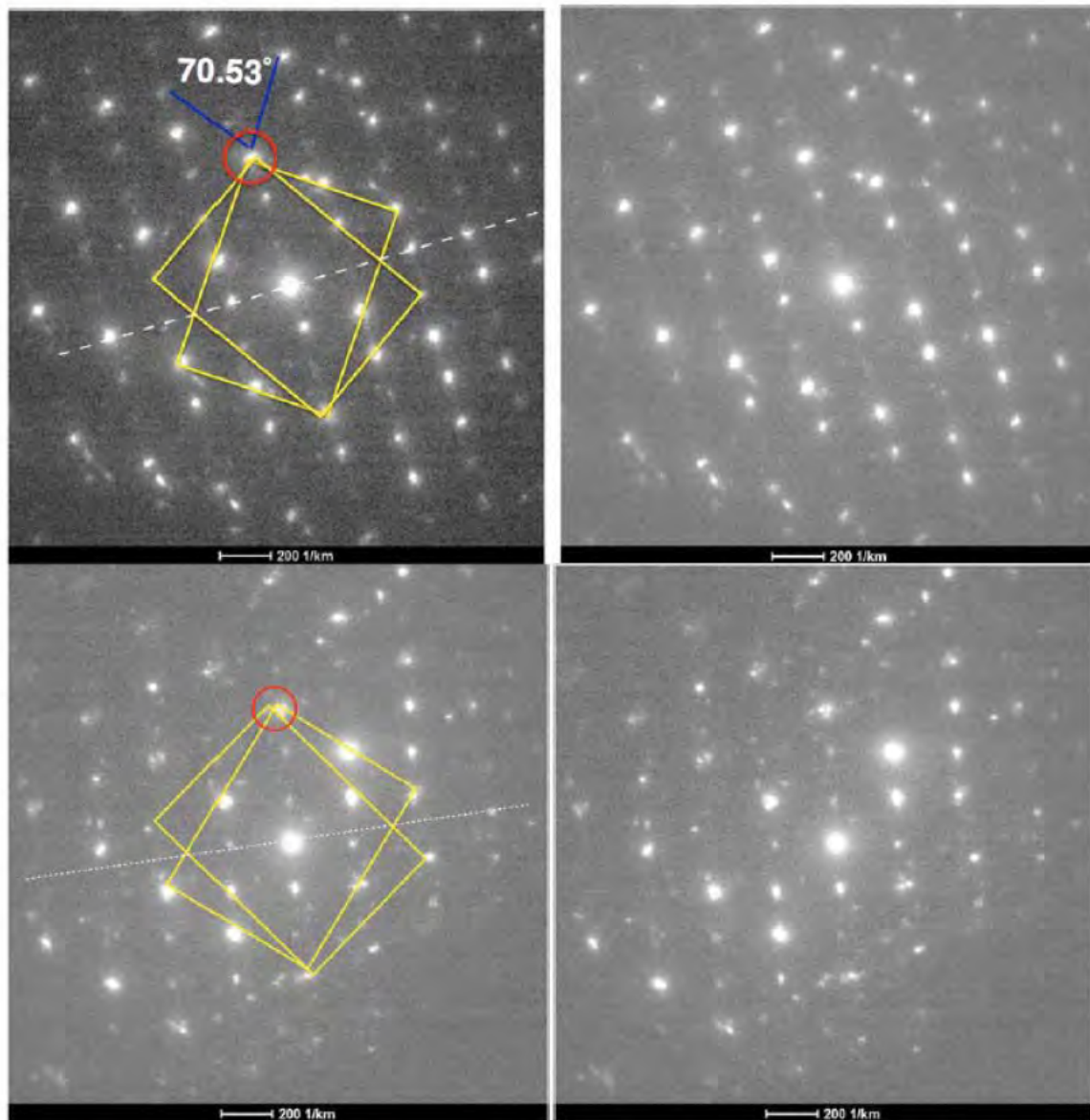


Figure 51: Both patterns, frames 726 (upper) and 802 (lower), show two crystallites both in the $(110)_{\text{BCC}}$ twin orientation, rotated by $\sim 70.53^\circ$ about their common $[110]_{\text{BCC}}$ direction

471. Under Dr. Clark's erroneous interpretation of "variant," Figure 52 shows three additional "variants":

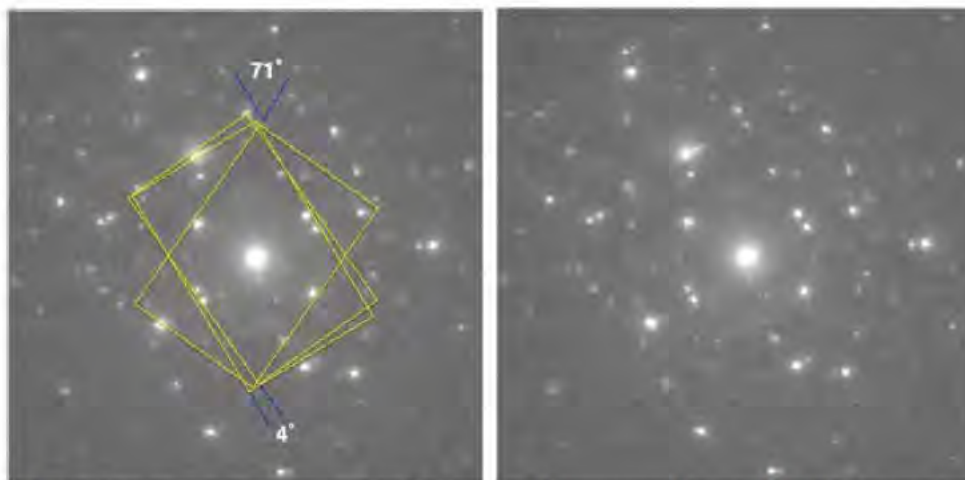


Figure 52: Diffraction pattern, frame 1487, showing three crystallites in the $(110)_{\text{BCC}}$ orientation. Two crystallites are rotated with respect to each other by $\sim 4^\circ$, and the third is at $\sim 71^\circ$ from the first.

472. Thus, Figures 49-52 alone show more than six $(110)_{\text{BCC}}$ crystallites—and therefore more than six “variants” under Dr. Coffey’s and Dr. Clark’s erroneous interpretation of that term.

473. Moreover, I note that Dr. Clark took 1600 microbeam diffraction patterns of sample S0GPPC—of those 1600, he produced less than 30 in Appendix C to his report. Of those 1600 microbeam patterns, Dr. Clark claims that, from a random sample of 100 patterns, he found that 44 showed two or three $(110)_{\text{BCC}}$ crystallites. (Clark, ¶ 114.) Assuming that Dr. Clark’s analysis of these microbeam diffraction patterns is correct—Dr. Clark did not actually produce the diffraction patterns needed to check his work—Dr. Clark’s own microbeam diffraction measurements show far more than six $(110)_{\text{BCC}}$ crystallites. If each $(110)_{\text{BCC}}$ crystallite is a “variant,” as Dr. Clark argues, then his own microbeam diffraction data shows the existence of far more than six “variants.”

474. I note Dr. Clark’s dark field image data measurements, which I discuss below, also show more than six variants under his erroneous interpretation of “variant.”

475. Because Dr. Clark’s own microbeam diffraction data shows that the FeCo layers of the measured S0GPPC sample contain more than six bcc(110) crystallites (“variants,” according to him), the FeCo layers cannot form a “symmetry broken structure.”

ii) Sample S2MMMC

476. In describing Figure 78, Dr. Clark states that “Figure 78 shows an example diffraction pattern with **two crystallites, both in the (110)_{BCC} orientation**, but rotated by $\sim 12^\circ$ about their common $[110]_{\text{BCC}}$ direction. This is the separation of two variants in the Kurdjumov-Sachs orientation.” (Clark, ¶ 154.)

477. Dr. Clark apparently contends that Figure 78 shows two variants because it shows two $(110)_{\text{BCC}}$ crystallites. He contends that these two variants—these two $(110)_{\text{BCC}}$ crystallites—have a Kurdjumov Sachs-orientation because they are oriented roughly 12 degrees from one another. (*But see, e.g.*, Clark, ¶ 110 (claiming that 9 degrees “is the separation of two variants in the Kurdjumov-Sachs orientation”); *id.* at ¶ 111 (claiming that 11 degrees “is also the separation of two variants in the Kurdjumov-Sachs orientation”); *id.* at 112 (claiming that 70.53 degrees “is also the separation of two variants in the Kurdjumov-Sachs orientation”).)

478. Dr. Clark’s analysis therefore posits that each of these $(110)_{\text{BCC}}$ crystallites is a “variant.” As I explained above, this is an erroneous understanding of “variant,” because not all $(110)_{\text{BCC}}$ crystallites are variants. Specifically, in order to identify a “variant,” one *must* identify both a $(110)_{\text{BCC}}$ crystallite *and* the underlying (111) hexagonal template crystal.

479. Nevertheless, if one applies Dr. Clark’s understanding that any $(110)_{\text{BCC}}$ crystallite in a microbeam diffraction pattern is a “variant,” then Dr. Clark’s own microbeam diffraction patterns show more than six $(110)_{\text{BCC}}$ crystallites with different orientations—and therefore more than six “variants.” To the extent Dr. Clark contends that each $(110)_{\text{BCC}}$ crystallite is a “variant,” Dr. Clark’s own microbeam diffraction patterns show more than six “variants” in each FeCo layer. Because a “symmetry broken structure” requires a “six variant system,” a layer containing more than six “variants” cannot form a “symmetry broken structure.”

480. For example, under Dr. Clark’s erroneous interpretation of “variant”—*i.e.*, where any two $(110)_{\text{BCC}}$ crystals with different in-plane orientations relative to each

other are two “variants”— Figures 77, 78, and 79 each shows two “variants” while Figure 80 shows three “variants.” (See Clark, Figures 77, 78, 79.)

481. Figures 77-80 alone show more than six $(110)_{\text{BCC}}$ crystallites—and therefore more than six “variants” under Dr. Coffey’s and Dr. Clark’s erroneous interpretation of that term.

482. Moreover, I note that Dr. Clark took 1600 microbeam diffraction patterns of sample S2MMMC—of those 1600, he produced less than 30 in Appendix C to his report. Of those 1600 microbeam patterns, Dr. Clark claims that, from a random sample of 100 patterns, he found that 5 showed two or three $(110)_{\text{BCC}}$ crystallites. (Clark, ¶ 157.) Assuming that Dr. Clark’s analysis of these microbeam diffraction patterns is correct—Dr. Clark did not actually produce the diffraction patterns needed to check his work—Dr. Clark’s own microbeam diffraction measurements show more than six $(110)_{\text{BCC}}$ crystallites. If each $(110)_{\text{BCC}}$ crystallite is a “variant,” as Dr. Clark argues, then his own microbeam diffraction data shows the existence of more than six “variants.”

483. I note Dr. Clark’s dark field image data measurements, which I discuss below, also show more than six variants under his erroneous interpretation of “variant.”

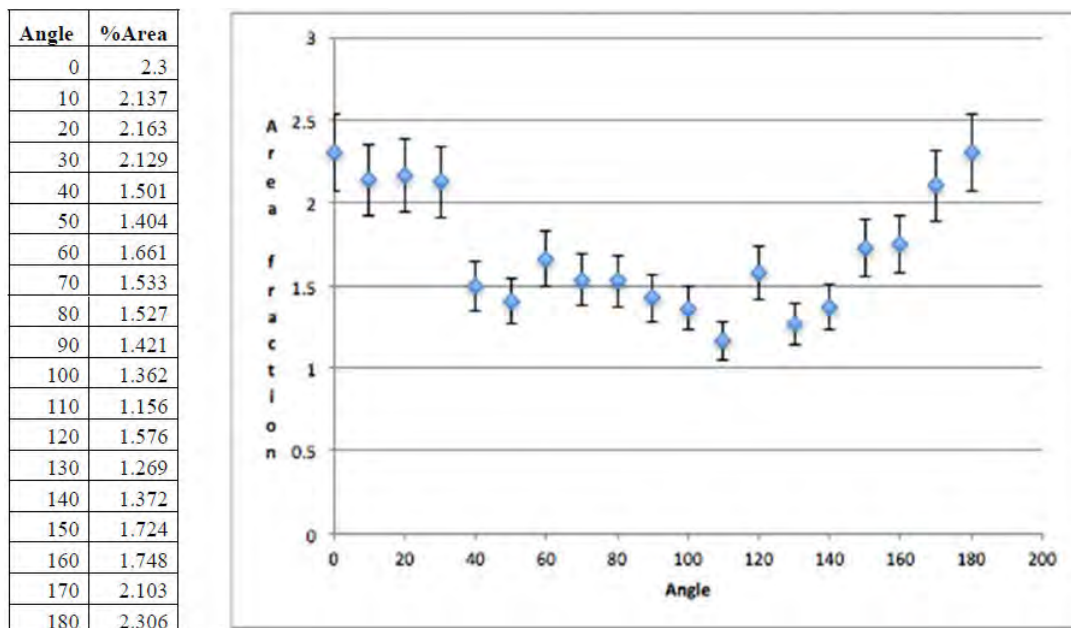
484. Because Dr. Clark’s own microbeam diffraction data shows that the FeCo layers of the measured S2MMMC sample contain more than six $\text{bcc}(110)$ crystallites (“variants,” according to him), the FeCo layers cannot form a “symmetry broken structure.”

b) Dark Field Image Data

485. Dr. Coffey states that “I also understand that dark field image analysis of samples S0GPPC and S2MMMC show symmetry breaking in the lower layer of FeCo in the write pole.” (Coffey, ¶ 187 (citing Clark, ¶¶ 56-60, 116-124, 159-167.)

486. Dr. Clark took dark field image measurements on the S0GPPC and S2MMMC write head samples. Specifically, Dr. Clark states that “a dark field image of an area of the lower FeCo layer is obtained . . . Where crystallites show up bright in the dark field image, in indicates that their $\{200\}$ planes are oriented so as to diffract into the direction enclosed by the objective aperture.” (Clark, ¶¶ 117, 160.)

487. For sample S0GPPC, Dr. Clark plots the “area fraction of white crystallites vs. angle” in Table 1 and Figure 59, which I reproduce below:



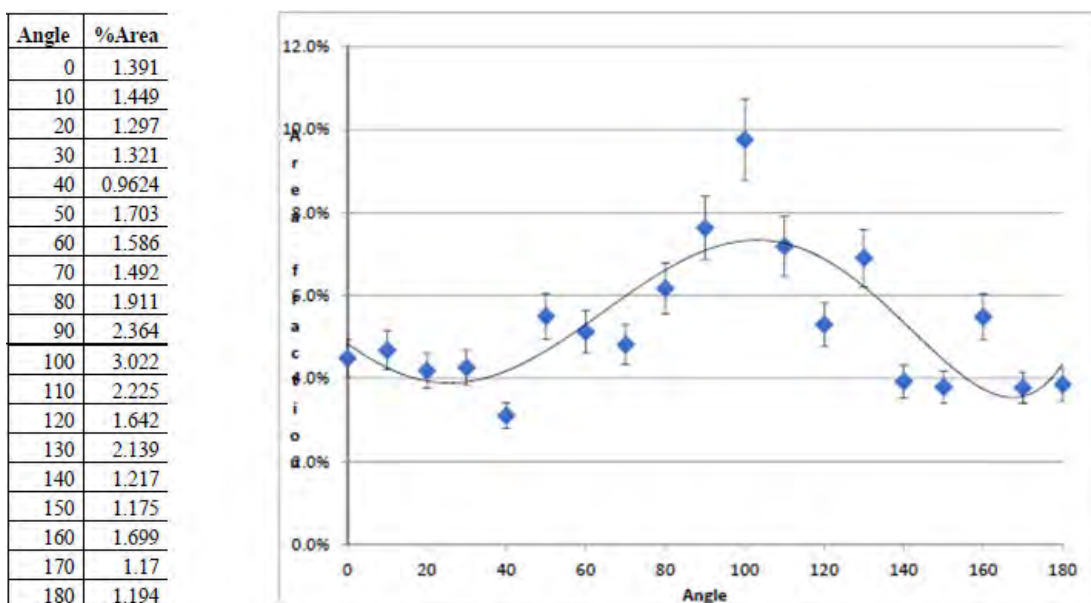
488. Dr. Coffey argues that Dr. Clark’s “dark field imaging analysis provides information on the fraction of crystallites with their easy axes substantially aligned toward each measured orientation and, *consequently, shows the presence of unequal amounts of variants* . . . because a greater amount of bcc-d crystallites are composed of variants with their easy axis aligned perpendicular to the long-axis of the write head (parallel to the ABS) than in other directions.” (Coffey, ¶ 188.)

489. According to Dr. Clark’s Figure 59 (his dark field image data), there appears to be a greater amount of bcc-d crystallites aligned at 0 and 180 degrees than in other directions. Dr. Coffey argues that this shows that bcc-d crystallites of different orientations—“variants”—exist in unequal amounts in the FeCo layer. (Coffey, ¶ 188.) Dr. Coffey takes the position that these bcc-d crystallites with different orientations are “variants” and that Figure 59 shows these “variants” exist in unequal amounts. (*Id.*)

490. But Figure 59 shows bcc-d crystallites with more than six different orientations. Because none of the area fractions is “0,” Figure 59 indicates that there exist FeCo crystallites with their <200> directions aligned at 0 degrees, 10 degrees, 20

degrees, 30 degrees, 40 degrees, 50 degrees, 60 degrees, 70 degrees, 80 degrees, 90 degrees, 100 degrees, 110 degrees, 120 degrees, 130 degrees, 140 degrees, 150 degrees, 160 degrees, and 170 degrees. Under Dr. Clark's and Dr. Coffey's expansive and erroneous interpretation of "variants," each of these crystallites is oriented differently and thus is a different "variant." Under Dr. Clark and Dr. Coffey's expansive and erroneous interpretation of "variants," Figure 59 shows far more than six "variants" in the measured FeCo layer.

491. For sample S2MMC, Dr. Clark plots the "area fraction of white crystallites vs. angle" in Table 2 and Figure 87, which I reproduce below:



492. Dr. Coffey argues that Dr. Clark's "dark field imaging analysis provides information on the fraction of crystallites with their easy axes substantially aligned toward each measured orientation and, *consequently, shows the presence of unequal amounts of variants* . . . because a greater amount of bcc-d crystallites are composed of variants with their easy axis aligned perpendicular to the long-axis of the write head (parallel to the ABS) than in other directions." (Coffey, ¶ 188.)

493. According to Dr. Clark's Figure 87 (his dark field image data), there appears to be a greater amount of bcc-d crystallites aligned at 0 and 180 degrees than in other directions. Dr. Coffey argues that this shows that bcc-d crystallites of different

orientations—“variants”—exist in unequal amounts in the FeCo layer. (Coffey, ¶ 188.) Dr. Coffey takes the position that these bcc-d crystallites with different orientations are “variants” and that Figure 87 shows these “variants” exist in unequal amounts. (*Id.*)

494. But Figure 87 shows bcc-d crystallites with more than six different orientations. Because none of the area fractions is “0,” Figure 87 indicates that there exist FeCo crystallites with their $\langle 200 \rangle$ directions aligned at 0 degrees, 10 degrees, 20 degrees, 30 degrees, 40 degrees, 50 degrees, 60 degrees, 70 degrees, 80 degrees, 90 degrees, 100 degrees, 110 degrees, 120 degrees, 130 degrees, 140 degrees, 150 degrees, 160 degrees, and 170 degrees. Under Dr. Clark and Dr. Coffey’s expansive and erroneous interpretation of “variants,” each of these crystallites is oriented differently and thus is a different “variant.” Under Dr. Clark and Dr. Coffey’s expansive and erroneous interpretation of “variants,” Figure 87 shows far more than six variants in the measured FeCo layer.

495. Because Dr. Clark’s own dark field imaging data show that the measured FeCo layers in the S0GPPC and S2MMMC samples each contain more than six “variants” (under Dr. Clark and Dr. Coffey’s erroneous definition of “variants”), the FeCo layers cannot and do not form a “symmetry broken structure.”

496. I also note that Dr. Clark’s dark field imaging is not a reliable technique for determining unequal amounts or unequal volumes of variants. According to the ’988 Patent, the proper technique for assessing a symmetry broken structure is a *pole figure*. (*See, e.g.*, ’988 Patent, FIG. 14.) Nowhere does the ’988 Patent contemplate or even mention assessing a “symmetry broken structure” using dark field imaging techniques. Nowhere does Dr. Clark or Dr. Coffey perform (let alone analyze) any pole figure data for any of the accused Seagate products.

497. Dr. Clark’s dark field imaging is also flawed because it is overinclusive in the crystallites it measures. Specifically, Dr. Clark’s dark field image data is only meaningful to the extent it records the orientation of bcc(110) crystallites—and not other bcc-d crystallites. That is not the case here. Due to how Dr. Clark ran his dark field image measurement (namely, by selecting to focus on the 200 ring), he counts not only

bcc(110) crystallites *but also* bcc(100) crystallites (as well as other possible crystallite orientations such as (012) and (013)).

498. In other words, both the bcc(110) and bcc(100) crystallite orientations will necessarily contribute scattering to the 200 ring. As a result, Dr. Clark's dark field imaging is flawed, and it is unreasonable to argue that there exists unequal amounts of bcc(110) crystallites when the data inherently counts both bcc(110) and bcc(100) crystallites.

499. Dr. Clark's dark field imaging is flawed in several other respects as well. These flaws cast doubt on the accuracy and reliability of his dark field image data, and also invalidate many of Dr. Clark's and Dr. Coffey's conclusions based on the dark field data.¹² For example, Dr. Clark double counts certain pixels (*i.e.*, the same pixels are counted as "white" for multiple different angles within 180 degrees).

500. Moreover, the area fraction of crystallites at 0 and 180 degrees should be the same, yet they are not. (*See, e.g.*, Clark, Figure 87 (1.391% area at 0 degrees vs. 1.194% area at 180 degrees); Clark, Figure 117 (1.994% area at 0 degrees vs. 0.807% area at 180 degrees).) The pronounced discrepancy between the area fraction of crystallites at 0 and the area fraction of crystallites at 180 suggests serious flaws with how Dr. Clark performed his dark field measurements.

501. In addition, the aperture Dr. Clark used to generate his dark field image data was not limited to the 200 ring (as Dr. Clark claims), but appears to have picked up diffraction from other rings. (*See, e.g.*, Clark, Figure 55 and Figure 113 (clearly depicting multiple rings in the aperture).) By including additional rings in the aperture, the resulting dark field image will include crystallites besides those that contribute to the 200 ring.

¹² I note that Dr. Stach, in his report, also articulates numerous flaws with Dr. Clark's dark field imaging. (*See, e.g.*, Stach, ¶¶ 374-391, 424-439, 476-493.) I have reviewed and agree with Dr. Stach's criticisms of Dr. Clark's dark field imaging.

502. This is *another* reason why Dr. Clark's dark field image data inherently counts more than just bcc(110) crystals. As discussed above, Dr. Clark's decision to focus on the 200 ring already results in him counting non-(110) crystals in the dark field data. But due to his flawed aperture, Dr. Clark in fact focused on multiple rings (not just the 200 ring), leading him to count *even more* non-(110) crystals in the dark field data.

503. It is unreasonable to argue that there exists unequal amounts of bcc(110) crystallites based on data that inherently counts non-(110) crystallites. I note this also renders all of Dr. Coffey's magnetic calculations mathematically flawed and incorrect, because those calculations assume that Dr. Clark's dark field image data counts only bcc(110) crystals, when in fact they do not. (See Section IX.A.2(c)(ii), *infra*.)

c) Diffraction Ring

504. Figure 19 of Dr. Clark's report shows a "diffraction pattern taken from SOGPPC, and incorporating many crystallites":

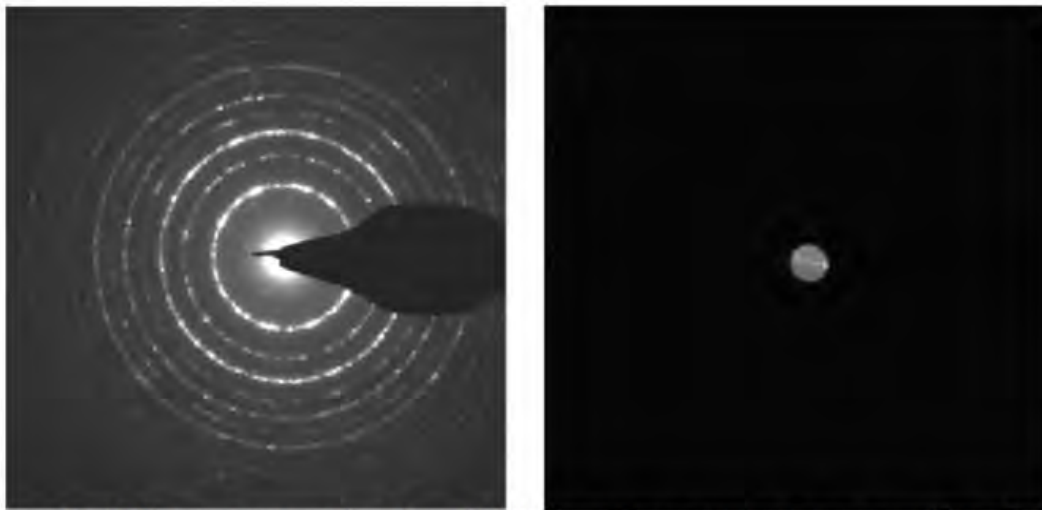


Figure 19: Diffraction pattern taken from SOGPPC, and incorporating many crystallites. On the right is an image of the objective aperture selecting the small segment of the 002 diffraction ring from which a dark field image is formed.

505. According to Dr. Coffey and Dr. Clark's interpretation of "variants," a six-variant system would manifest itself as six discrete diffraction peaks rather than the continuous rings shown in Figure 19. The continuous rings indicate that bcc-d crystallites exist with many—many more than six—different in-plane orientations.

* * *

506. In sum, a “variant” refers to a bcc-d(110) crystallite oriented in one of six possible ways relative to an underlying (111) hexagonal template crystal. But because Dr. Clark and Dr. Coffey are completely unable to find any evidence of underlying (111) hexagonal template crystals, they argue that a “variant” refers to any bcc-d(110) crystallite. Under this erroneous interpretation of “variant,” Dr. Clark’s own microbeam diffraction data, dark field image data, and diffraction ring data all show the existence of more than six “variants” in the accused FeCo layers. As a result, none of the accused FeCo layers form a “symmetry broken structure” because they do not consist of “bcc-d variants of a six-variant system.”

(b) “having an anisotropy energy density function with only a single maximum and a single minimum as the magnetization angle is rotated by 180 degrees from a physical axis” (uniaxial)

507. Dr. Coffey argues that “it is my opinion that the lower FeCo layer in the [REDACTED] Products is uniaxial as a result of the structure therein being symmetry broken, in accordance with the Court’s claim construction of claim 1 of the ‘988 patent.” (Coffey, ¶ 189.)

508. In my opinion, Dr. Coffey fails to show that any FeCo layer in the [REDACTED] Products is “uniaxial”—*i.e.*, that any FeCo layer “ha[s] an anisotropy energy density function with only a single maximum and a single minimum as the magnetization angle is rotated by 180 degrees from a physical axis.”

(i) Dr. Coffey cites no magnetic data whatsoever in his report

509. The ‘988 Patent defines “uniaxial” as follows:

Here, we define a “uniaxial” anisotropy to exist if the anisotropy energy density function only contains a single maximum and a single minimum as the magnetization angle, θ , is rotated by 180 degrees from a physical axis.

(‘988 Patent at 1:56-60.)

510. The Court construed “uniaxial” to mean “having an anisotropy energy density function with only a single maximum and a single minimum as the magnetization angle is rotated by 180 degrees from a physical axis.”

511. According to the '988 Patent, uniaxial materials and uniaxial thin films have various useful applications. (*See, e.g.*, '988 Patent at 2:8-19 (“[T]he device is constructed so that the applied field is directed along the hard magnetic axis of a uniaxial magnetic material.”); *id.* at 3:9-10 (criticizing non-uniaxial materials: “Multi-axis anisotropy materials always switch via wall motion and so suffer losses”); *id.* at 3:64-65 (“Uniaxial anisotropy is needed in such a device to achieve low losses.”).)

512. In describing its invention, the '988 Patent claims that “[m]aterials and device processing to achieve a desired orientation or anisotropy is commonly difficult and sometimes impossible, perhaps because heretofore the mechanism for achieving anisotropic orientation has not been well understood.” ('988 Patent at 1:62-66.) The '988 Patent purports to solve the problem of creating uniaxial thin films as follows: “[b]y the selection and growth of a very special exchange coupled subset of these six orientational variants a symmetry broken *uniaxial magnetic thin film* is obtained.” ('988 Patent at 14:52-55.) Thus, the '988 Patent purports to have invented a mechanism for achieving uniaxial magnetic anisotropy in certain materials—specifically, magnetic bcc-d layers. (*See* '988 Patent, Claim 1.)

513. “Uniaxial” is a magnetic property. Assessing whether a magnetic bcc-d layer is “uniaxial” requires magnetic testing and analysis of magnetic data. Assessing whether a magnetic bcc-d layer forms a “uniaxial” structure requires magnetic testing and analysis of magnetic data.

514. For example, the '988 Patent describes taking magnetic measurements of certain samples to assess whether those samples featured a uniaxial magnetic layer: “Magnetic response curve measurements were made for these samples. . . . FIG. 15 shows the Mx and My versus Hx response of one of the two variant exchange coupled, uniaxial symmetry broken samples” ('988 Patent at 43:49-50, 43:58-61.) The '988 Patent further states that “FIG. 15 clearly shows a non-linear uniaxial type of response function when the sample was driven into saturation and uniaxial result similar to the

ideal of FIG. 2.” (’988 Patent at 44:15-18; *see also id.* at 14:24-28 (“FIG. 15 shows a uniaxial magnetic hard axis response, M_x , function, and easy axis response function, M_y , data to an applied field along the hard axis, H_x , for an Fe ($K_1 > 0$) sample prepared with the easy axis along the hexagonal template $\langle 112 \rangle$ direction.”).)¹³

515. FIG. 15 of the ’988 Patent is data in the form of a “magnetic response curve measurement” (commonly referred to as a hysteresis loop) that was generated using a vibrating sample magnetometer (VSM). FIG. 15 of the ’988 Patent is shown below:

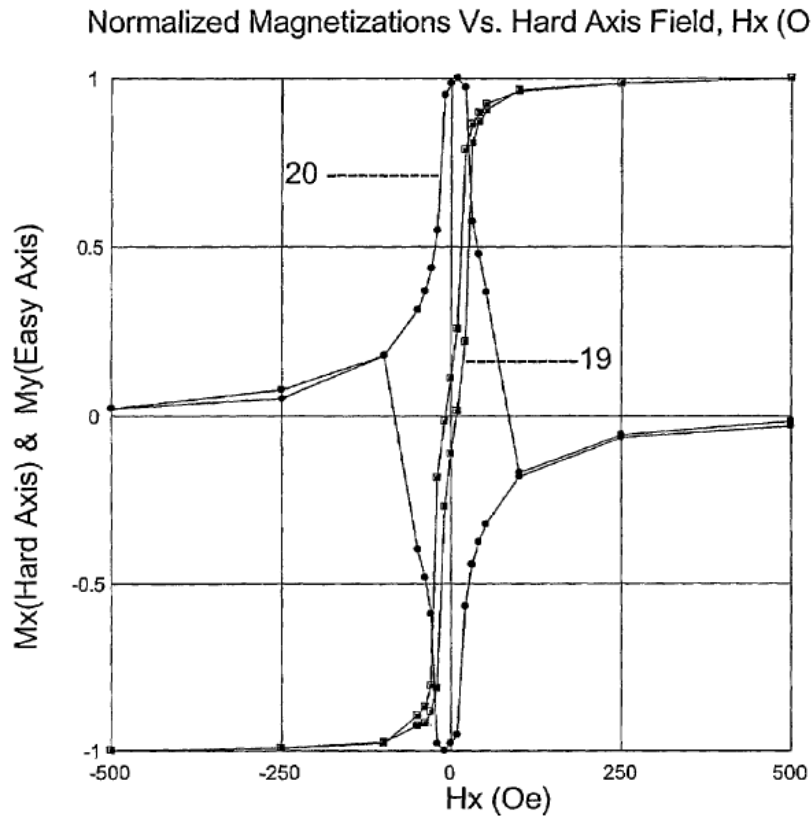


Figure 15

¹³ I note that, in my opinion, the magnetic data presented in FIG. 15 of the ’988 Patent is not sufficient to show uniaxial anisotropy in the measured material.

516. Because “uniaxial” is a *magnetic* property, assessing whether a structure has uniaxial anisotropy necessarily requires *magnetic* measurements and an analysis of *magnetic* data. The ’988 Patent took magnetic measurements (VSM) to generate the magnetic data (hysteresis loop) seen in FIG. 15.

517. Neither Dr. Coffey nor Dr. Clark cites, discusses, or analyzes *any actual magnetic measurements whatsoever* in their reports.

518. The ’988 Patent is a *magnetic* patent. It bears the title “*Magnetic Material Structures, Devices, and Methods.*” The first sentence of the specification states: “*This invention is directed to magnetic material structures, methods for making magnetic material structures, and devices made from magnetic material structures.*” (’988 Patent 1:8-10.) The “uniaxial” limitation of claim 1 is a *magnetic* claim limitation.

519. Yet neither Dr. Coffey nor Dr. Clark cites, discusses, nor analyzes *any magnetic measurements whatsoever* in their reports. Without such magnetic measurements, Dr. Coffey has no basis to conclude that the accused Seagate products meet the “uniaxial” limitation of claim 1. In my opinion, no reasonable scientist would accept Dr. Coffey’s conclusions about “uniaxial”—a *magnetic* claim limitation—without any magnetic measurements or data in his report.

520. Indeed, LMS apparently knew that magnetic testing was required to assess the “uniaxial” claim limitation—yet neither Dr. Coffey nor Dr. Clark cite any such magnetic testing in their reports. In its Amended Infringement Contentions against Seagate—dated November 29, 2017¹⁴—LMS wrote that:

[I]t is anticipated that magneto-optic Kerr effect (“MOKE”) measurements of plan-view samples of the FeCo-based layer of the write head will yield M-H loops at various angles of measurements. Upon obtaining multiple measurements at regular angular intervals, the magnetic anisotropy energy density function associated with the FeCo-based layer can be calculated and will confirm only a single maximum and a single minimum as the magnetization angle is rotated by 180 degrees from a physical axis.

¹⁴ I note that LMS served its Amended Infringement Contentions *after* the Court issued its claim construction order construing, among other things, the term “uniaxial.”

(LMS's Amended Infringement Contentions Ex. 2A, at 27.)

521. "MOKE" is a type of magnetic measurement that can be used to generate M-H loops (a.k.a. hysteresis loops or magnetization response curves). Had Dr. Coffey's report contained MOKE measurements as LMS described in its amended infringement contentions, one might reasonably analyze them to assess whether they correspond to a uniaxial magnetic layer in the accused Seagate products. But Dr. Coffey's report contained no MOKE measurements—or any magnetic measurements for that matter. It is simply unreasonable for Dr. Coffey to conclude that the accused Seagate products have a "uniaxial" FeCo layer when he conducts no magnetic measurements and analyzes no magnetic data to support that conclusion.

522. I understand that LMS asked Seagate to produce monitor wafers containing the accused [REDACTED] write heads, purportedly so that LMS could perform magnetic testing on those [REDACTED] write head materials. I understand that Seagate produced the monitor wafers to LMS as requested before the close of fact discovery. I understand this gave LMS over two months in which to perform magnetic measurements on these monitor wafers. Either Dr. Coffey did not take any magnetic measurements of the accused FeCo layers, or he took magnetic measurements and omitted them from his report.

523. In sum, it is not appropriate, reliable, or scientifically valid to conclude that an FeCo layer is uniaxial, or that an FeCo layer forms a "uniaxial" structure, without measuring the FeCo layer's actual magnetic properties. Dr. Coffey and Dr. Clark do not cite any magnetic measurements of any FeCo layers—let alone magnetic measurements showing an FeCo layer having an anisotropy energy density function with only a single maximum and a single minimum as the magnetization angle is rotated by 180 degrees from a physical axis.

524. Dr. Coffey and Dr. Clark therefore fail to show that any FeCo layer in the accused [REDACTED] Products is "uniaxial." Dr. Coffey and Dr. Clark fail to show that any FeCo layer in the accused [REDACTED] Products forms a "uniaxial" structure.

(ii) Dr. Coffey erroneously conflates “uniaxial” with “uniaxial symmetry broken structure”—completely ignoring all other sources of magnetic anisotropy

525. Rather than take magnetic measurements of the accused FeCo layers, Dr. Coffey instead purports to theoretically model a single source of magnetic anisotropy in the FeCo layers—namely, the layers’ magnetocrystalline anisotropy.¹⁵ Dr. Coffey concludes that because the FeCo layers purportedly have a uniaxial magnetocrystalline anisotropy (they do not), that is somehow the same as showing that the FeCo layers are uniaxial. In my opinion, Dr. Coffey inappropriately conflates the Court’s construction of “uniaxial” with “uniaxial symmetry broken structure.”

526. As I explain in the Technology Background—and as Dr. Coffey acknowledges—there are many sources of magnetic anisotropy, including shape anisotropy, strain anisotropy, magnetocrystalline anisotropy, and atomic pair ordering.

527. Whether a material is “uniaxial” involves the interaction of these different sources of magnetic anisotropy. In other words, “uniaxial” refers to a material where *the* anisotropy energy density function of the material contains only a single minimum and a single maximum as the magnetization is rotated by 180 degrees. A material has only one anisotropy energy density function: the total anisotropy due to shape anisotropy, strain anisotropy, magnetocrystalline anisotropy, atomic pair ordering, among other things.

528. When one takes a magnetic measurement of a material, one is measuring (directly or indirectly) the anisotropy energy density function of the material, *i.e.*, the total magnetic anisotropy. One can conclude that a material is “uniaxial” only if that

¹⁵ I note that magnetocrystalline anisotropy is *not* the same as anisotropy from symmetry breaking. Magnetocrystalline anisotropy refers to the anisotropy associated with the orientation of magnetic crystals generally, whereas the anisotropy that results from symmetry breaking refers only to the anisotropy associated with bcc-d (110) crystals grown on a (111) hexagonal atomic template crystal (*i.e.*, variants of a six-variant system). That is, the anisotropy that results from symmetry breaking is a subset of magnetocrystalline anisotropy.

anisotropy energy density function contains only a single maximum and a single minimum within a 180 degree rotation. Because Dr. Coffey never takes any magnetic measurements and never considers the anisotropy energy density function of any FeCo layer, his conclusion that any FeCo layer is “uniaxial” is flawed and unreasonable.

529. Rather than take magnetic measurements of the FeCo layers or consider the anisotropy energy density function of those layers, Dr. Coffey purports to theoretically model a single source of magnetic anisotropy in the FeCo layers—namely, the layers’ magnetocrystalline anisotropy. According to Dr. Coffey’s model, the FeCo layers feature a uniaxial magnetocrystalline anisotropy—a point on which he is mistaken. (*See* Section IX.A.2(c), *infra*.) But even assuming the FeCo layers featured a uniaxial magnetocrystalline anisotropy, it simply does not follow that the FeCo layers are therefore “uniaxial.” Because the anisotropy energy density function of the FeCo layers involves multiple components—multiple sources of anisotropy—one cannot ignore these other components when opining about whether the FeCo layers form a “uniaxial” structure. Yet that is what Dr. Coffey does.

530. A simple analogy exposes the flaw in Dr. Coffey’s reasoning. Dr. Coffey’s reasoning is analogous to reasoning that a paint mixture containing several different colors must be blue because one of the component paint colors is blue. That reasoning is flawed because one cannot ignore the other color components if one is to validly conclude anything about the color of the paint mixture. For example, if the paint mixture contains equal parts blue and yellow, the mixture is not blue, but green.

531. Shape anisotropy, in particular, plays a major role in the magnetic anisotropy of many thin film materials, including the FeCo layers at issue here. I note that Dr. Coffey acknowledges this fact. In discussing shape anisotropy, Dr. Coffey writes: “[F]or films having in-plane dimensions only 100 times greater than their thickness, the in-plane shape dependent demagnetization effects can be significant. . . . In this range of dimensions and for thin films that are not circular, the in-plane anisotropy effects can be significant to the magnetization directions of an object.” (Coffey, ¶ 50.)

532. The FeCo layers at issue here are “films having in-plane dimensions only 100 times greater than their thickness.” (Coffey, ¶ 50.) As Dr. Coffey acknowledges, “[i]n this range of dimensions and for thin films that are not circular, the in-plane shape anisotropy effects can be significant to the magnetization directions of an object.” (*Id.*)

533. Despite acknowledging the “significant” impact of shape on the magnetic anisotropy of the FeCo layers, Dr. Coffey’s report contains no analysis or consideration of those layers’ shape anisotropy—or for that matter, any source of magnetic anisotropy other than magnetocrystalline anisotropy.

534. Thus, to the extent Dr. Coffey concludes that the FeCo layers are “uniaxial” without considering any of these other sources of magnetic anisotropy, that conclusion is flawed and unreasonable. To the extent Dr. Coffey concludes that the FeCo layers form a “uniaxial” structure without considering any of these other sources of magnetic anisotropy, that conclusion is flawed and unreasonable.

535. I note that it would have been relatively straightforward for Dr. Coffey to have considered all these different sources of anisotropy—namely, by taking actual magnetic measurements of the accused FeCo layers. Such magnetic measurements would have measured (directly or indirectly) the magnetic anisotropy of the layers from all sources. That is how the ’988 Patent assessed the magnetic anisotropy of its samples: by taking VSM measurements and analyzing the resulting M-H loops. (*See, e.g.*, ’988 Patent, FIG. 15.) That is how LMS previously intended to assess the magnetic anisotropy of the FeCo layers, according to its amended infringement contentions: by taking MOKE measurements and analyzing the resulting M-H loops. (LMS’s Amended Infringement Contentions Ex. 2A, at 27.) Yet that is not what Dr. Coffey has done.

536. In sum, Dr. Coffey attempts to theoretically model the magnetocrystalline anisotropy of the FeCo layers and argues that according to his (deeply flawed) calculations, the magnetocrystalline anisotropy is uniaxial. In a leap of logic, Dr. Coffey then argues that because the magnetocrystalline anisotropy is uniaxial, the FeCo layers must be uniaxial. That simply does not follow. Shape anisotropy exerts a significant influence on the magnetic anisotropy of the FeCo layers. It is therefore flawed and unreasonable for Dr. Coffey to conclude that the magnetic anisotropy energy density

function of the FeCo layers contains only a single maximum and minimum within 180 degrees without having considered, *e.g.*, shape anisotropy, strain anisotropy, and atomic pair ordering. Moreover, both the '988 Patent and LMS's latest infringement contentions in this case make clear that the "uniaxial" limitation should have been assessed with magnetic measurements, none of which appear anywhere in Dr. Coffey's report. Either Dr. Coffey did not take any magnetic measurements of the accused FeCo layers, or he took magnetic measurements and omitted them from his report.

537. For all these reasons, Dr. Coffey's opinion that any FeCo layer in the accused [REDACTED] Products exhibits "uniaxial" anisotropy is flawed and unreasonable. For all these reasons, Dr. Coffey's opinion that any FeCo layer in the accused [REDACTED] Products forms a "uniaxial" structure is flawed and unreasonable.

(iii) In lieu of relying on any magnetic data, Dr. Coffey erroneously relies on the doctrine of equivalents

538. According to Dr. Coffey: "That the lower FeCo layer may have other contributors to its magnetic anisotropy, such as shape anisotropy or stress anisotropy, does not change the fact that the [REDACTED] Products achieve uniaxial magnetic properties as a result of symmetry breaking in the FeCo layer." (Coffey, ¶ 215.)

539. As I explained above, that is incorrect. It is unreasonable for Dr. Coffey to conclude that the "[REDACTED] Products achieve uniaxial magnetic properties" without any magnetic measurements or data to suggest that [REDACTED] Products are in fact uniaxial. Attempting to cloak this shortcoming under the guise of the doctrine of equivalents does not alter the basic fact that to prove "uniaxial magnetic properties" (Coffey, ¶ 215), one necessarily must perform magnetic measurements and analyze magnetic data.

540. According to Dr. Coffey: "I understand that Seagate may argue that, contrary to the Court's construction of 'uniaxial,' claim 1 requires that the bcc-d layer must exhibit uniaxial magnetic anisotropy due to symmetry breaking that dominates any other anisotropy that may be present or is the sole source of anisotropy." (Coffey, ¶ 212.)

541. To be clear: that is not my opinion, nor is it Seagate’s position. My opinion simply is that one cannot reasonably conclude that a bcc-d layer exhibits “uniaxial” anisotropy without actually measuring the layer’s magnetic properties. One cannot reasonably conclude that a bcc-d layer exhibits “uniaxial anisotropy” solely by modeling a single source of anisotropy (magnetocrystalline anisotropy) to the exclusion of all others. Doing so is contrary to the well-accepted physics of magnetic anisotropy. (*See, e.g.*, B.D. Cullity and C.D. Graham, INTRODUCTION TO MAGNETIC MATERIALS, 2ND EDITION (2009), at 197-98.) Doing so also improperly conflates the Court’s construction of “uniaxial” with the Court’s construction of “uniaxial symmetry broken structure” (causation).

542. In my opinion, Dr. Coffey fails to show that any FeCo layer in any [REDACTED] Product is “uniaxial.” Dr. Coffey fails to show that any FeCo layer in any [REDACTED] Product forms a “uniaxial” structure. In my opinion, an FeCo layer that is not uniaxial does not perform substantially the same function in substantially the same way to achieve substantially the same result as an FeCo layer that is uniaxial. I note that although Dr. Coffey appears to contend otherwise, his contention is entirely conclusory. (*See* Coffey, ¶ 211.) For example, Dr. Coffey does not identify or explain how an FeCo layer that is not uniaxial serves substantially the same function in substantially the same way to achieve substantially the same result as an FeCo layer that is uniaxial.

543. Indeed, the ’988 Patent draws a sharp distinction between uniaxial and non-uniaxial materials, criticizing the latter’s use in certain applications as leading to energy losses. (*See, e.g.*, ’988 Patent at 2:20-22 (“For example, a material, which has bi-axial anisotropy . . . will exhibit hysteresis and losses.”); *id.* at 3:9-10 (“Multi-axis anisotropy materials always switch via wall motion and so suffer losses.”).) The ’988

Patent itself therefore contradicts Dr. Coffey's claim that non-uniaxial materials are somehow equivalent to uniaxial materials.¹⁶

544. I have also considered Dr. Coffey's citations and characterizations of Seagate documents and deposition testimony on this issue (*see* Coffey ¶¶ 180-218) and find his characterizations of many of these documents to be flawed and unreasonable. Although Dr. Coffey string cites without explanation dozens of Seagate documents and testimony in ¶¶ 180-218 of his report, none actually support his conclusion that the FeCo layer forms a "uniaxial" structure—*i.e.*, a structure "having an anisotropy energy density function with only a single maximum and a single minimum as the magnetization angle is rotated by 180 degrees from a physical axis." For example, none of the cited Seagate documents or deposition testimony show any anisotropy energy density function for any FeCo layer, let alone an FeCo layer having an anisotropy energy density function with only a single maximum and a single minimum as the magnetization angle is rotated by 180 degrees from a physical axis.

545. For all these reasons, Dr. Coffey's opinion that any FeCo layer in the accused [REDACTED] Products meets the "uniaxial" claim limitation, either literally or under the doctrine of equivalents, is unreasonable, unsupported, and incorrect.

(c) "a structure that is uniaxial as a result of the structure being symmetry broken" (uniaxial symmetry broken structure)

546. In my opinion, the FeCo layers in the [REDACTED] products do not form a "uniaxial symmetry broken structure"—*i.e.*, they do not form "a structure that is uniaxial as a result of the structure being symmetry broken."

547. Dr. Coffey states that "it is my opinion that the lower FeCo layer of FeCo in the [REDACTED] Products is uniaxial because the anisotropy energy density function I

¹⁶ I understand counsel for Seagate asserts that, as a legal matter, the patent's explicit definition of "uniaxial" in precise mathematical terms bars LMS from applying the doctrine of equivalents to expand the scope of term beyond that explicit mathematical definition.

calculated solely due to the measured broken symmetry in representative samples of the [REDACTED] Products has a single maximum and a single minimum as the magnetization angle is rotated by 180 degrees from a physical axis.” (Coffey, ¶ 181.)

548. In my opinion, Dr. Coffey’s theoretical anisotropy calculation is severely flawed and unreliable in multiple respects.

549. First, although Dr. Coffey claims that he calculated “the anisotropy energy density function [] solely due to the measured broken symmetry,” that statement is factually incorrect. (Coffey, ¶ 181.)

550. A “symmetry broken structure” consists of unequal amounts or unequal volumes of the bcc-d variants of a six variant system. These six bcc-d variants refer to bcc-d(110) crystals oriented in one of six orientations relative to an underlying (111) hexagonal template crystal. Moreover, any crystals that are not (110) are not “variants” and do not comprise the “symmetry broken structure” of the ’988 Patent. Dr. Clark’s measurements consistently show that the measured FeCo layers include substantial amounts of non-(110) crystals—including, for example, bcc-d(100) crystals and bcc-d(211) crystals. (See Section IX.A.2(a)(i).c, *supra*; see also, e.g., SEA01944075 at 4077-78 (XRD measurement showing significant amounts of non-(110) crystals in the measured FeCo layer).) The magnetic anisotropy associated with these non-(110) crystals would not be magnetic anisotropy that results from a “symmetry broken structure.”

551. In order for Dr. Coffey to claim that “the anisotropy energy density function [he] calculated solely due to the measured broken symmetry . . . has a single maximum and a single minimum as the magnetization angle is rotated by 180 degrees from a physical axis,” he would have needed to calculate the anisotropy energy density function from only bcc-d(110) crystals—and *no other bcc-d crystals*. But Dr. Coffey’s calculations in fact count non-(110) bcc-d crystals, uprooting the entire premise of his theoretical calculations. (See Section IX.A.2(c)(ii), *infra*.)

552. Second, in addition to erroneously counting non-(110) bcc-d crystals in his anisotropy calculation, Dr. Coffey also ignores the empirical data as measured by Dr. Clark. Although Dr. Coffey purports to rely on Dr. Clark’s dark field image

measurements, he ultimately disregards those measurements. Specifically, when Dr. Coffey calculates anisotropy he does not use any of Dr. Clark's empirically measured data. Rather than use actual measured data as the input to his anisotropy calculation, Dr. Coffey substitutes in data that Dr. Coffey wished Dr. Clark had measured—not what Dr. Clark actually measured. (*See* Section IX.A.2(c)(iii), *infra*.)

553. Third, there are many serious additional flaws with Dr. Coffey's anisotropy model. Dr. Coffey makes unwarranted assumptions, errors in calculation, and unfounded conclusions. I discuss the other errors in Dr. Coffey's anisotropy model in Section IX.A.2(c)(iv), below.

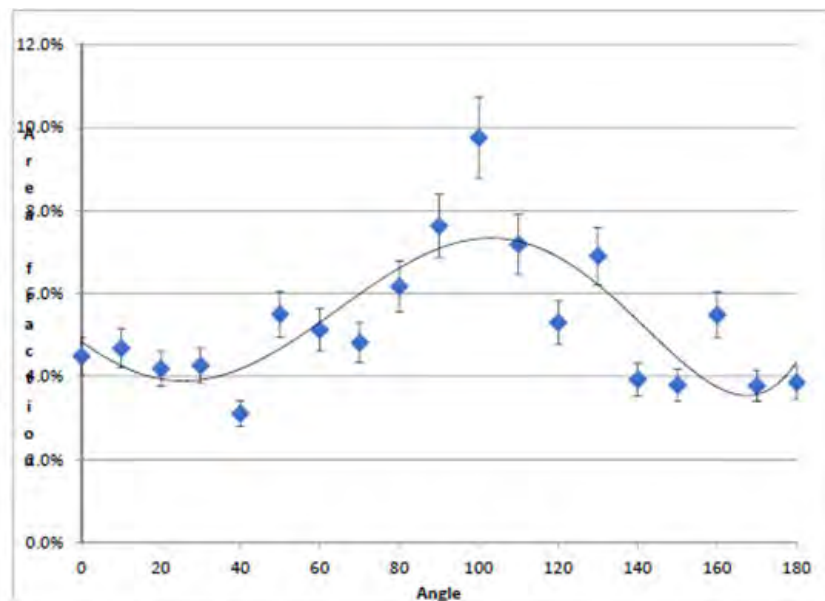
554. Dr. Coffey's anisotropy calculation is flawed and unreliable for all these reasons. In my opinion, Dr. Coffey's theoretical methodology for calculating anisotropy appears to be created solely for the purposes of this litigation. In my opinion, Dr. Coffey's theoretical methodology for calculating anisotropy contains no testable hypothesis, has never been subject to peer review, has no known or potential rate of error, is not controlled by scientific standards, is based on flawed and unreliable data, and is not reasonably grounded in established scientific methods.

(i) Overview of Dr. Coffey's method of calculating anisotropy

555. Before discussing the numerous flaws with Dr. Coffey's anisotropy calculation in more detail, I will summarize Dr. Coffey's method for calculating what he erroneously claims to be the anisotropy caused by symmetry breaking. Dr. Coffey's method can be broken down into a three-step process.

556. **Step 1**. Dr. Coffey plots the dark field image data from Dr. Clark, an example of which is shown below:

Angle	%Area
0	1.391
10	1.449
20	1.297
30	1.321
40	0.9624
50	1.703
60	1.586
70	1.492
80	1.911
90	2.364
100	3.022
110	2.225
120	1.642
130	2.139
140	1.217
150	1.175
160	1.699
170	1.17
180	1.194



557. Dr. Coffey erroneously contends that this plot of the dark field image data shows that “[t]he area fraction for the (110) bcc, six-variant crystallites is not independent of direction, rather it shows a pronounced variation as a function of angle.” (Coffey, ¶ 191.) In other words, Dr. Coffey believes, erroneously, that this graph plots the relative amounts of bcc(110) crystal orientations in the measured FeCo layer when in fact it does not. (See Section IX.A.2(c)(ii), *infra*.)

558. **Step 2.** Given what he believes to be the relative amounts of bcc(110) crystal orientations, Dr. Coffey attempts to calculate the magnetocrystalline anisotropy of these crystals. Dr. Coffey states that “the anisotropy energy density function for bcc-d crystals in the (110) plane is set forth in Chikazumi and referenced in the ‘988 patent. . . . Specifically, the equation is:”

$$E_{110}(\theta) = K_1\left\{\left(\frac{1}{4}\right)\sin^4(\theta) + \sin^2(\theta)\cos^2(\theta)\right\} + K_2\left\{\left(\frac{1}{4}\right)\sin^4(\theta)\cos^2(\theta)\right\} \\ + \text{higher } K \text{ terms}$$

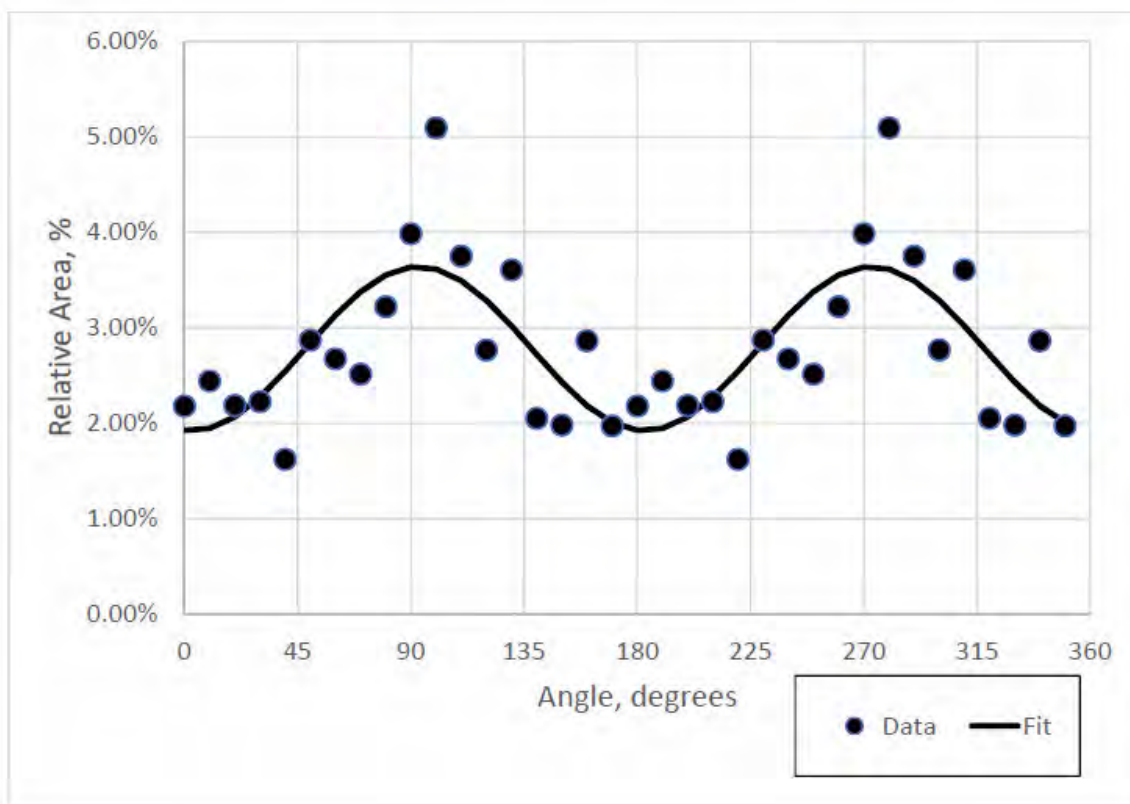
(Coffey, ¶ 192.)

559. Dr. Coffey relates the Chikazumi Equation to the dark field image data from Dr. Clark by writing that: “to determine the overall anisotropy energy density due to the symmetry breaking evidenced in the lower FeCo layer in the [REDACTED] Products it is

necessary to calculate the anisotropy energy density as an average over all the crystallites at different orientations in the sample.” (Coffey, ¶ 194.)

560. **Step 3.** With the dark field image data (which Dr. Coffey mistakenly believes to show the amounts of bcc(110) crystal orientations) and the Chikazumi Equation specifying the magnetocrystalline anisotropy of bcc(110) crystals, Dr. Coffey proceeds to calculate the anisotropy using the Chikazumi Equation. But rather than use the dark field image data from Dr. Clark as the input to the Chikazumi Equation, Dr. Coffey *discards* Dr. Clark’s measured data and replaces it with data forced to fit a perfect sinusoidal function. (Coffey, ¶¶ 190-191.)

561. For example, the graph below is taken from Dr. Coffey’s report:



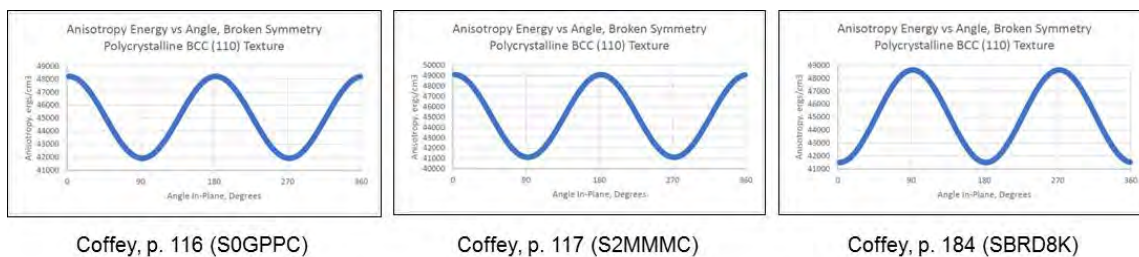
(Coffey, ¶ 191.)

562. The dots represent the empirical data as measured by Dr. Clark’s dark field image experiments. But those dots are not the values Dr. Coffey uses to calculate

the anisotropy. Instead, Coffey calculates anisotropy assuming that the crystal orientations fit *exactly* the superimposed sinusoidal curve shown above.

563. Dr. Coffey provides no reasonable justification for discarding Dr. Clark's empirical data in favor of a conveniently smooth, perfect sinusoidal fit. (See Coffey, ¶ 190.) I have shown mathematically that any set of data, if forced to fit Dr. Coffey's perfectly smooth sinusoidal function, will *always* generate a uniaxial result when plugged into the Chikazumi Equation. (Ex. F.)¹⁷ In other words, by discarding Dr. Clark's empirically measured crystal distribution data and substituting in a sinusoidal crystal distribution, Dr. Coffey *guarantees* a uniaxial outcome.

564. Dr. Coffey then performs the anisotropy calculation using the Chikazumi Equation and plots the result. (Coffey, ¶ 196.) Because Dr. Coffey's methodology of substituting sinusoidal values for actual measured values guarantees him a uniaxial result no matter the data, it comes as no surprise that Dr. Coffey's calculation yields a perfectly smooth, uniaxial energy density function for each of the samples "analyzed":



565. I note that all three energy density functions, although ostensibly calculated from three different samples, all fit a *perfect* \sin^2 function—*i.e.*, not only uniaxial, but uniaxial in the theoretical Stoner-Wohlfarth sense. (See, *e.g.*, '988 Patent at 2:63-66 ("Materials exhibiting the $\sin^2(\theta)$ energy density functional form are often referred to as having Stoner-Wohlfarth behavior after the famous ideal uniaxial single

¹⁷ In Ex. F, I first prove mathematically that Dr. Coffey's methodology guarantees him a uniaxial result. I then provide an example showing that even a randomly generated set of data, when analyzed using Dr. Coffey's methodology, yields a uniaxial energy density function.

domain magnetization theory.”.) This is not surprising since Dr. Coffey did not use any *actual* measured data in his analysis, but instead used data forced to fit a sinusoidal function, such that his calculations were guaranteed to generate perfectly uniaxial energy density functions. (*See* Ex. F.)

566. Having summarized Dr. Coffey’s method for purportedly calculating the anisotropy from symmetry breaking, I now explain in more detail the numerous flaws with his analysis.

(ii) Dr. Coffey erroneously assumes that Dr. Clark’s dark field image data depicts only bcc-d(110) crystals

567. Dr. Coffey’s anisotropy calculation incorrectly assumes that the only crystals measured in Dr. Clark’s dark field image data are bcc-d(110) crystals. Dr. Coffey calculates anisotropy using the Chikazumi Equation, which is an equation that describes the magnetic anisotropy energy density function of bcc-d(110) crystals—*but not any other kind of crystal*. The anisotropy energy density function of crystals with other orientations—such as a bcc-d(100) crystal—is *not* represented by the Chikazumi Equation. If one measured a sample containing bcc-d(100) crystals and calculated the anisotropy by applying the Chikazumi Equation, the result would be mathematically incorrect. Yet that is what Dr. Coffey does.

568. By focusing on the 200 ring in his dark field image measurements, Dr. Clark’s dark field image data necessarily includes not only bcc-d(110) crystals but also bcc-d(100) crystals (as well as a number of other possible bcc-d crystal orientations). Put another way, the pixels that “light up” in the dark field image data correspond to both bcc-d(110) and bcc-d(100) crystals.¹⁸

¹⁸ And likely other crystal orientations as well. As I note above, the aperture Dr. Clark used for his dark field imaging includes more than just the 200 ring. (*See* Section IX.A.2(a)(i)c, *supra*.) This results in even more non-(110) crystals being measured by Dr. Clark’s dark field imaging. (*Id.*)

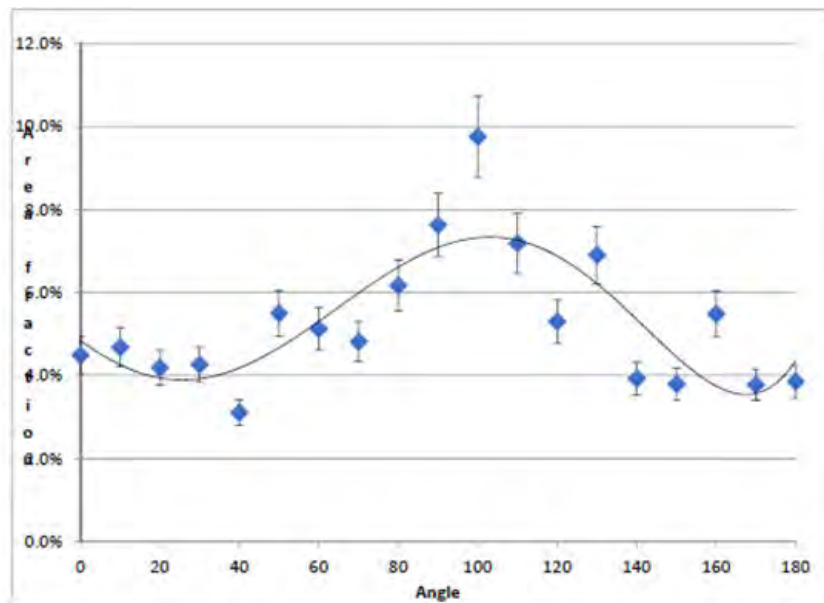
569. For example, the white pixels in the following dark field image data from Dr. Clark necessarily include both bcc-d(110) and bcc-d(100) crystals:



S0GPPC – 168-1

570. Dr. Clark's dark field image analysis plots the total amounts of bcc-d(110) crystals *and* bcc-d(100) crystals as a function of angle. For example, one such plot is shown below:

Angle	%Area
0	1.391
10	1.449
20	1.297
30	1.321
40	0.9624
50	1.703
60	1.586
70	1.492
80	1.911
90	2.364
100	3.022
110	2.225
120	1.642
130	2.139
140	1.217
150	1.175
160	1.699
170	1.17
180	1.194

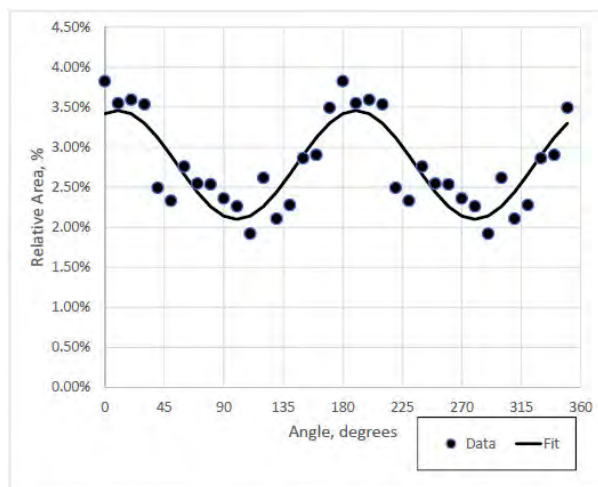


571. Although the plot says that 1.391% of the pixels “light up” at 0 degrees, that 1.391% of pixels includes *both* bcc-d(110) and bcc-d(100) crystals. For example, the 1.391% could be 1.0% bcc-d(110) and 0.391% bcc-d(100). Or it could be 0.391% bcc-d and 1.0% bcc-d(100). Based on the dark field image data alone, it is not possible

to quantify the breakdown of bcc-d(100) and bcc-d(110) crystals at any given angle. What is clear, however, is that there exists significant amounts of bcc-d(100) crystals throughout the accused FeCo layers—this is confirmed both by Dr. Clark’s microbeam diffraction data and Dr. Clark’s diffraction ring data. (*See, e.g.,* Section IX.A.2(a)(i)c, *supra.*)

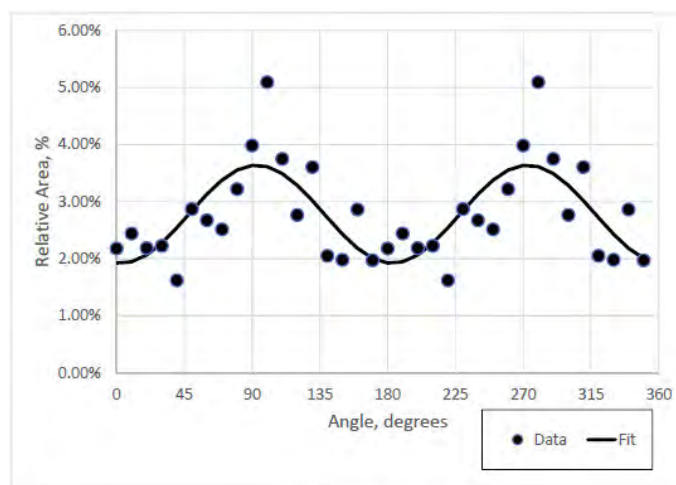
572. I also note that the sum of the total area from 0-170 degrees (or 10-180 degrees) is approximately 30%. This means that Dr. Clark’s dark field imaging counts only about 30% of the crystals in the layer (and of those 30%, some will be bcc(100), not bcc(110)). This is significant for two reasons. First, it shows that the majority of the FeCo layer (70%+) is in fact not bcc(110). (*See, e.g.,* Section IX.A.2(a)(i)c, *supra.*) Second, it means that about 70% of the crystals in the layer are *never accounted for* in any of Dr. Coffey’s calculations, making his calculation of the magnetocrystalline anisotropy of the FeCo layer incomplete, unreliable, and incorrect for this reason as well.

573. In sum, significant amounts of bcc-d(100) crystals exist throughout the accused FeCo layers, and Dr. Clark’s dark field image data necessarily includes those bcc-d(100) crystals in its measurement. Yet Dr. Coffey mistakenly calculates the anisotropy assuming that the only crystals represented in the dark field image data are bcc-d(110) crystals. This mistaken assumption is made explicit by Dr. Coffey himself when he refers to the dark field image plots, as well as when he performs his anisotropy calculation.



Coffey, p. 112

574. Dr. Coffey mistakenly describes the dark field image plot above as showing “[t]he area fraction for the (110) bcc, six-variant crystallites is not independent of direction, rather it shows a pronounced variation as a function of angle.” (Coffey, ¶ 190.) But the plotted values include non-bcc(110) crystals (such as bcc(100) crystals) and so this interpretation of the dark field image data is incorrect.



Coffey, p. 113

575. Dr. Coffey mistakenly describes the dark field image plot above as showing “[t]he area fraction for the (110) bcc, six-variant crystallites is not independent of direction, rather it shows a pronounced variation as a function of angle.” (Coffey, ¶

191.) But the plotted values include non-bcc(110) crystals (such as bcc(100) crystals) and so this interpretation of the dark field image data is incorrect.

576. Dr. Coffey's mistaken interpretation of Dr. Clark's dark field image data—namely, his mistaken assumption that the dark field image plots contain only bcc-d(110) crystals—is further made clear by how Dr. Coffey calculates the anisotropy energy density function. He writes that “the anisotropy energy density function *for bcc-d crystals in the (110) plane* is set forth in Chikazumi,” and then cites the Chikazumi Equation. (Coffey, ¶ 192.) But the Chikazumi Equation applies only to bcc-d(110) crystals—not bcc-d(100) crystals, or any other kind of crystal.

577. It would be proper to apply the Chikazumi Equation to a set of dark field image data only if the dark field image data measured *only* bcc-d(110) crystals. But because Dr. Clark's dark field image data includes other bcc-d crystals—including for example bcc-d(100) crystals—Dr. Coffey's application of the Chikazumi Equation to calculate anisotropy based on Dr. Clark's dark field image data is flawed, unreasonable, and leads to mathematically invalid results.

578. An analogy may help illustrate this critical flaw in Dr. Coffey's calculation. Suppose one has two kinds of socks: cotton socks and wool socks. There is an equation that says each cotton sock contains 10g of cotton. But this equation does not apply to wool socks (each wool socks contains only 1g of cotton). We know through measurements that we have a total of 500 socks—but these measurements do *not* tell us how many of those 500 socks are cotton and how many are wool. Nevertheless, we proceed by assuming that all 500 socks are cotton—erroneously applying the cotton sock equation to all 500 socks, and erroneously concluding that the 500 socks collectively contain $500 \times 10\text{g} = 5,000\text{g}$ of cotton.

579. Rather than socks, Dr. Coffey does this with bcc-d crystals. The Chikazumi Equation describes the anisotropy energy density function of bcc-d(110) crystals (cotton socks) *but not* bcc-d(100) crystals (wool socks). The dark field image data from Dr. Clark plots the total amount of bcc-d(110) and bcc-d(100) crystals as a function of angle (the amount of cotton and wool socks)—but does not distinguish how many of those crystals are bcc-d(110) and how many are bcc-d(100). Nevertheless, Dr.

Coffey proceeds by assuming that all the crystals are bcc-d(110)—he therefore erroneously applies the Chikazumi Equation to all the crystals, leading to a mathematically absurd outcome.

580. In sum, Dr. Coffey’s anisotropy calculation explicitly assumes that Dr. Clark’s dark field image data measures only bcc-d(110) crystals. (Coffey, ¶¶ 190-93.) Because Dr. Clark’s dark field image data measures additional bcc-d crystals—including bcc-d(100) crystals—this fundamental assumption underlying Dr. Coffey’s anisotropy calculation does not hold. This is a critical flaw in Dr. Coffey’s anisotropy calculation that, in my opinion, renders his conclusions about the anisotropy energy density function of the accused FeCo layers flawed, unreasonable, and mathematically incorrect.

(iii) Dr. Coffey ignores the actual empirical data, and instead calculates anisotropy using made up data that guarantees a uniaxial outcome

581. Although Dr. Coffey purports to rely on the dark field image data from Clark, he ends up discarding Dr. Clark’s data in favor of another set of data—data that Dr. Coffey made up to guarantee a uniaxial energy density function. (*See* Ex. F.)

582. Dr. Coffey’s methodology is therefore flawed and unreliable because it puts the cart before the horse. Rather than a methodology designed to measure the magnetic anisotropy of crystals, Dr. Coffey’s methodology is designed to consistently give one and only one result: uniaxial magnetic anisotropy. (*Id.*)

583. In engineering and computer science, there is a maxim that states “garbage in, garbage out.” This expresses the idea that if one inputs flawed and unreliable data (“garbage”) into a formula, the formula will give you flawed and unreliable data (“garbage”) as output. In other words, a calculation yields an invalid result if the input to that calculation is invalid.

584. That is the case here. Although Dr. Coffey claims to rely on Dr. Clark’s empirically measured dark field image data, he does not actually use it as the input to his anisotropy calculations. Instead, Dr. Coffey discards Clark’s empirical measurements, using as the input to his anisotropy calculation perfect sinusoidal data *guaranteed* to produce a uniaxial result. (*Id.*)

585. In my opinion, Dr. Coffey's use of made-up sinusoidal data is unreasonable and scientifically unjustified—*i.e.*, “garbage” input. In my opinion, this renders Dr. Coffey's calculations invalid, unreasonable, and scientifically incorrect—*i.e.*, “garbage” output.

(iv) Dr. Coffey makes additional errors in his anisotropy calculation, which is purely theoretical

586. Unreasonable Simplifications to the Chikazumi Equation. Dr. Coffey relies on the Chikazumi Equation from the '988 Patent to theoretically calculate energy density functions. As I explained above, use of the Chikazumi Equation is inappropriate here because that equation pertains *only* to bcc-d(110) crystals, not the bcc-d(100) and other crystals present in Dr. Clark's dark field measurements.

587. Dr. Coffey's application of the Chikazumi Equation is flawed for another reason as well: namely, the equation Dr. Coffey applies is not the actual Chikazumi Equation, but rather a simplified form of the equation.

588. This is the actual Chikazumi Equation as it appears in the '988 Patent:

$$E_{110}(\theta) = K_1 \left\{ (1/4) \sin^4(\theta) + \sin^2(\theta) \cos^2(\theta) \right\} + K_2 \left\{ (1/4) \sin^4(\theta) \cos^2(\theta) \right\} + \text{higher } K \text{ terms.}$$

589. This is also the equation Dr. Coffey cites in his report (albeit with a typo):

$$E_{110}(\theta) = K_1 \left\{ (1/4) \sin^4(\theta) + \sin^2(\theta) \cos^2(\theta) \right\} + K_2 \left\{ (1/4) \sin^4(\theta) \cos^2(\theta) \right\} \\ + \text{higher } K \text{ terms}$$

(Coffey, ¶ 192.)

590. But that is not the equation Dr. Coffey applies. Dr. Coffey simplifies the actual Chikazumi equation by assuming that $K_2=0$. (Coffey, ¶ 199.) He further assumes that all higher order anisotropy terms (e.g., K_3 , K_4) are also all also zero. (*Id.*) These simplifying assumptions are not justified or reasonable here.

591. The '988 Patent posits that K_2 and higher order anisotropy terms can be ignored (assumed to be zero) in instances where K_1 is many times larger than K_2 . Both the '988 Patent and Dr. Coffey fail to consider, however, that there are many instances where it is not appropriate to assume $K_1 \gg K_2$ —including cases involving FeCo alloys. Although pure Fe has a $K_1 > K_2$, as one adds Co to the Fe to create an FeCo alloy, the value of K_1 dramatically diminishes, as seen in the graph below:

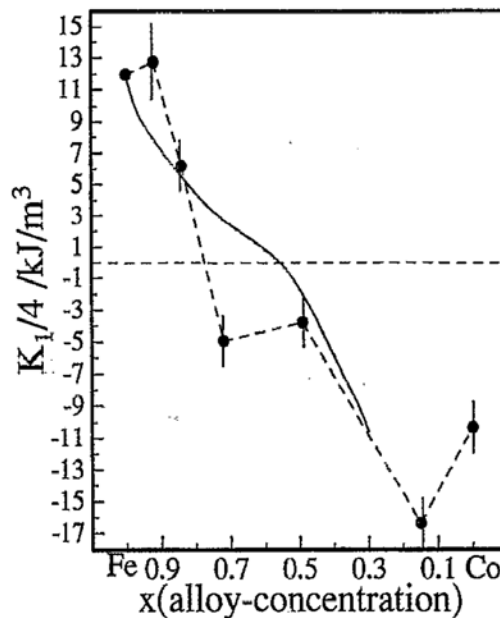


FIG. 7. Cubic anisotropy constant K_1 vs alloy concentration for $\text{Fe}_x\text{Co}_{1-x}$ films on MgO(001) substrates, as obtained from the MOKE hysteresis curves. A change of sign of the anisotropy constant occurs at an alloy concentration of $x=0.8$. The solid line reproduces the bulk behavior (Ref. 14).

592. As seen in the graph, K_1 rapidly decreases with increasing Co content. Eventually, K_1 reaches 0 and goes negative with increasing Co content—this happens around 60% Fe based on the previous research on bulk materials, and around 80% Fe for this study of FeCo films.

593. [REDACTED]

Any calculation that assumes that the magnitude of K_1 is many times greater than K_2 is therefore flawed and unreasonable.

594. Moreover, in many systems it is observed that K_1 and K_2 have very different temperature and composition dependence. The plot below shows the measured anisotropy for Co versus temperature:

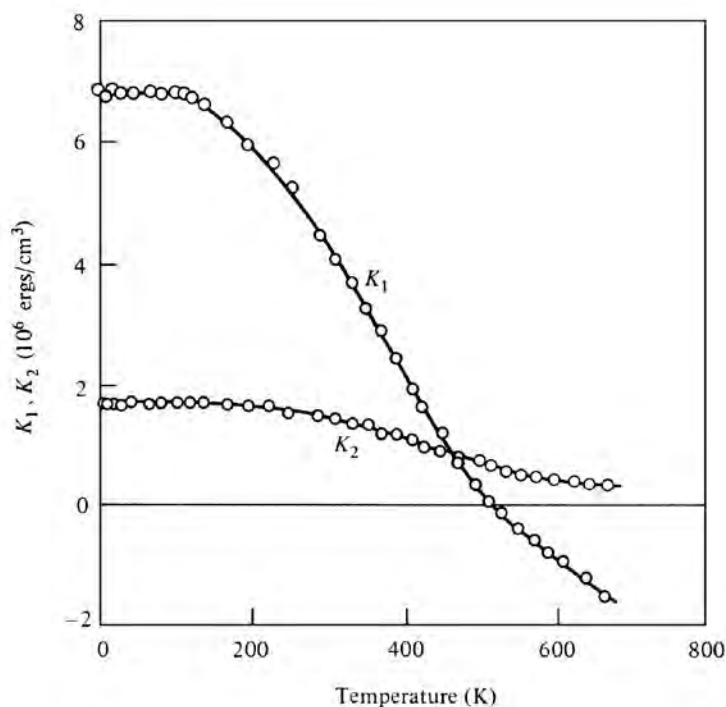


Fig. 7.25 Temperature dependence of anisotropy constants of cobalt [Y. Barnier, R. Pauthenet, and G. Rimet, *Cobalt*, 15 (1962) p. 1].

(Cullity, at 229.)

595. As can be seen, at elevated temperatures when K_1 changes sign, the magnitude of K_2 *exceeds* K_1 .

MATERIALS by J.M.D. Coey gives the following anisotropy constants for an alloy of Fe65Co35: $K_1 \approx 20 \text{ kJ m}^{-3}$ and $K_2 \approx -35 \text{ kJ m}^{-3}$ ($K_1 \approx 2 \times 10^5 \text{ erg cm}^{-3}$ and $K_2 \approx -3.5 \times 10^5 \text{ erg cm}^{-3}$)—so that the magnitude of K_2 is nearly twice that of K_1 .

596.

_____ . Any calculation that assumes

that K_1 is positive and many times greater in magnitude than K_2 is therefore flawed, unreasonable, and incorrect.

597. No Evidence or Mention of Exchange Coupling. I note that according to the '988 Patent, even when the correct variants of a six-variant system dominate (which is not remotely the case here), that alone is not enough to result in a “uniaxial symmetry broken structure” because “in order to achieve a uniaxial magnetic behavior the appropriate set of variants must be exchanged coupled.” ('988 Patent 22:62-66; *see also id.* at 41:14-15 (“exchange coupling [is] needed to cause uniaxial M-H curves”).) Nowhere does Dr. Coffey even consider—let alone show—that any purported “variants” are magnetically exchange coupled.

598. Moreover, Dr. Coffey states that the approach to calculate the “[t]he averaging of the anisotropy energy of individual crystals to determine an effective average anisotropy energy for a polycrystalline sample is described by G. Herzer, ‘Grain size dependence of coercivity and permeability in nanocrystalline ferromagnets,’ IEEE Trans. Magn., vol. 26, no. 5, pp. 1397-1402, Sept. 1990 (produced by Seagate at SEA01974948).” (Coffey, ¶ 346.)

599. Although Dr. Coffey cites Herzer as purported support for his methodology, Herzer in fact undermines Dr. Coffey’s average anisotropy calculation, which implicitly assumes that the crystals are all exchange coupled (*i.e.*, all the crystals’ magnetizations will rotate together in unison).

600. Herzer states that “[f]or very small grains . . . ferromagnetic exchange interaction more and more forces the magnetic moments to align parallel, thus, impeding the magnetization to follow the easy directions of each individual grain. As a consequence the effective anisotropy for the magnetic behavior is an average over several grains and, thus, reduced in magnitude.” But “[f]or large grains the magnetization can follow the easy magnetic directions in the single grains and domains can be formed within the grains.” Thus Herzer states that the way one averages the anisotropy depends on the size of the grain relative to the ferromagnetic exchange length. Herzer estimates an exchange length of 35 nm for an Fe-based compound. In

other words, FeCo crystals separated by much more than 35 nm will **not** be exchange coupled and will not have their magnetizations rotate together.

601. At no time does Dr. Coffey compare the grain sizes of the film to the exchange length, nor does he compute the averages over the exchange length (~35nm) as outlined in Herzer. Instead, Dr. Coffey implicitly assumes the exchange length is the size of the sample (over 5000nm)—essentially an infinite exchange length resulting in infinite exchange coupling—such that one can average all of the grains over *the entire sample*. There is no physical basis for this assumption.

602. In sum, both the '988 Patent and Dr. Coffey's calculation require that the bcc-d(110) crystals be exchange coupled. Dr. Coffey presents no evidence that the FeCo crystals in Seagate's write poles are exchange coupled. Just the opposite: he cites a paper (Herzer) explaining that the FeCo crystals in fact cannot be exchange coupled.

* * *

603. I have also considered Dr. Coffey's citations and characterizations of Seagate documents and deposition testimony on this issue (*see* Coffey ¶¶ 180-210) and find his characterizations of many of these documents to be flawed and unreasonable. Although Dr. Coffey string cites without explanation dozens of Seagate documents and testimony in ¶¶ 180-210 of his report, none actually support his conclusion that the FeCo layer forms a "uniaxial symmetry broken structure"—*i.e.*, "a structure that is uniaxial as a result of the structure being symmetry broken."

604. For all these reasons, Dr. Coffey's opinion that any FeCo layer in the accused [REDACTED] Products forms a "uniaxial symmetry broken structure" is flawed and unreasonable. None of the FeCo layers in the [REDACTED] layers form a "uniaxial symmetry broken structure," *i.e.*, "a structure that is uniaxial as a result of the structure being symmetry broken."

B. The Accused [REDACTED] Products Do Not Infringe Claims 1 and 27

605. In my opinion, the accused [REDACTED] products do not infringe claims 1 and 27 of the '988 Patent because the [REDACTED] write poles do not feature “at least one layer providing a (111) hexagonal atomic template.” (*See* Section IX.B.1, *infra*.)

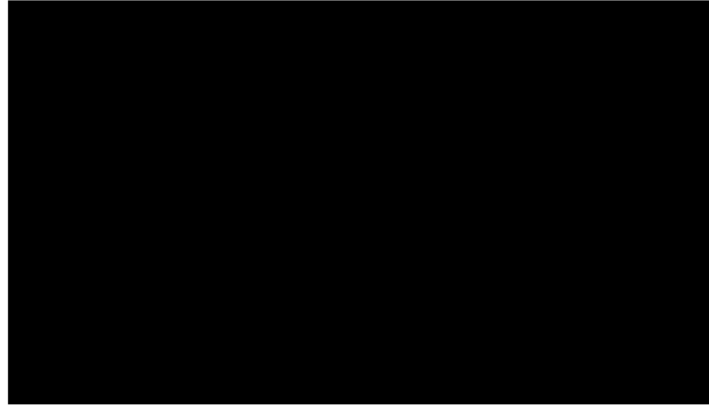
606. In my opinion, the accused [REDACTED] products do not infringe claims 1 and 27 of the '988 Patent because the [REDACTED] write poles do not feature “at least one bcc-d layer which is magnetic, forming a uniaxial symmetry broken structure.” (*See* Section IX.B.2, *infra*.)

1. The [REDACTED] products do not have “at least one layer providing a (111) textured hexagonal atomic template disposed between said substrate and said bcc-d layer”

Term	Court's Construction
atomic template	“an atomic pattern upon which material is grown and which is used to direct the growth of an overlying layer”
layer providing a (111) textured hexagonal atomic template	“layer that is predominately (111) hexagonal and that provides an atomic template”

607. Dr. Coffey argues in ¶¶ 370-383 of his report that the accused [REDACTED] products have “at least one layer providing a (111) textured hexagonal atomic template disposed between said substrate and said bcc-d layer.” I have carefully considered Dr. Coffey's arguments and find his conclusion to be unfounded. None of Dr. Coffey's data supports his conclusion that the [REDACTED] products have “a layer that is predominately (111) hexagonal and that provides an atomic template.”

608. As discussed above, the [REDACTED] write heads comprise several layers, including two layers of NiFe and two layers of FeCo, as depicted below:



609. I understand Dr. Coffey contends that the “lower layer of NiFe” is a “layer providing a (111) textured hexagonal atomic template disposed between said substrate and said bcc-d layer.” (*See, e.g.,* Coffey ¶ 373 (“I have concentrated my analysis on the lower (first-deposited) of the two layers of NiFe in the [REDACTED] Products . . .”).)

610. I disagree. The lower NiFe layer in the [REDACTED] write heads do not meet this claim limitation because the lower NiFe layer is not a “(111) textured hexagonal atomic template.” The [REDACTED] write heads contain no NiFe layer that is “predominately (111) hexagonal.” Moreover, the [REDACTED] write heads contain no NiFe layer that directs the growth of any overlying layer.

(a) “layer that is predominately (111) hexagonal”

611. In my opinion, none of the data Dr. Coffey cites shows a NiFe layer “that is predominately (111) hexagonal,” as required by the Court’s claim construction.

612. Dr. Coffey’s argument for the “(111) texture” of the NiFe is limited to a single paragraph in his report. Specifically, Dr. Coffey states in ¶ 378 of his report that “I understand that multiple FFTs were taken at various locations along the interface between the lower NiFe layers and FeCo layers of sample SBRD8K. I further understand that Dr. Clark was able to conclude that the lower fcc NiFe layer has a (111) texture and that it is evident that the lower NiFe layer is predominately or predominantly (111) fcc.” (Coffey, ¶ 378 (citing Clark ¶¶ 176-193 (SBRD8K sample)).)

613. I note that Dr. Coffey does not claim to have undertaken his own review of Dr. Clark's FFT data, but instead relies entirely on Dr. Clark's report for this claim limitation.

614. Because Dr. Coffey's only support for the "(111) texture" limitation comes from Dr. Clark's report, I now turn to ¶¶ 176-193 (SBRD8K) of Dr. Clark's report. I note that Dr. Clark's only basis for arguing that the lower NiFe layer is "(111) textured" comes from a handful of FFT images. (*See* Clark, ¶¶ 176-193.) In my opinion, none of Dr. Clark's FFT data supports his opinion that the NiFe layer is "(111) textured." If anything, Dr. Clark's FFT data shows that the imaged NiFe layers are not "(111) textured."

(i) Dr. Clark's FFT data for SBRD8K does not show a (111) textured NiFe layer

615. Dr. Clark sets out his basis for concluding that the SBRD8K samples contain a (111) textured NiFe layer in ¶¶ 176-193. Dr. Clark took FFT measurements from high resolution cross-section images of both the lower and upper NiFe layers of the S0GPPC sample. Specifically, Dr. Clark discusses the lower NiFe layer from ¶¶ 176-184 and the upper NiFe layer from ¶¶ 185-193. As I explain below, beginning with the lower NiFe layer, Dr. Clark has no basis for concluding that either NiFe layer of sample S0GPPC is "predominately (111) hexagonal."

616. **SBRD8K: Lower NiFe Layer.** Figure 102 of Dr. Clark's report purportedly shows "FFTs from the [lower] NiFe layer [] and [lower] FeCo layer." (Clark, p. 116.) According to Dr. Clark, "the two FFT patterns" shown in Figure 102 are "sufficient to determine the relative orientation of the lower NiFe layer and the lower FeCo layer above it. Therefore, the lower NiFe layer exhibits (111) texture, and the lower FeCo layer exhibits (110) texture." (Clark, ¶ 180.)

617. In my opinion, Dr. Clark's analysis of Figure 102 is flawed and unreasonable for at least three reasons.

618. First, Dr. Clark's analysis of Figure 102 is based on an erroneous premise—namely, that the FFTs correspond to standard diffraction patterns shown

below them. Dr. Clark's analysis hinges on the notion that Figure 102's NiFe FFT matches a $\{110\}_{\text{FCC}}$ diffraction pattern. (Clark, ¶ 178.) It does not.

619. I reproduce Figure 102 of Dr. Clark's report below:

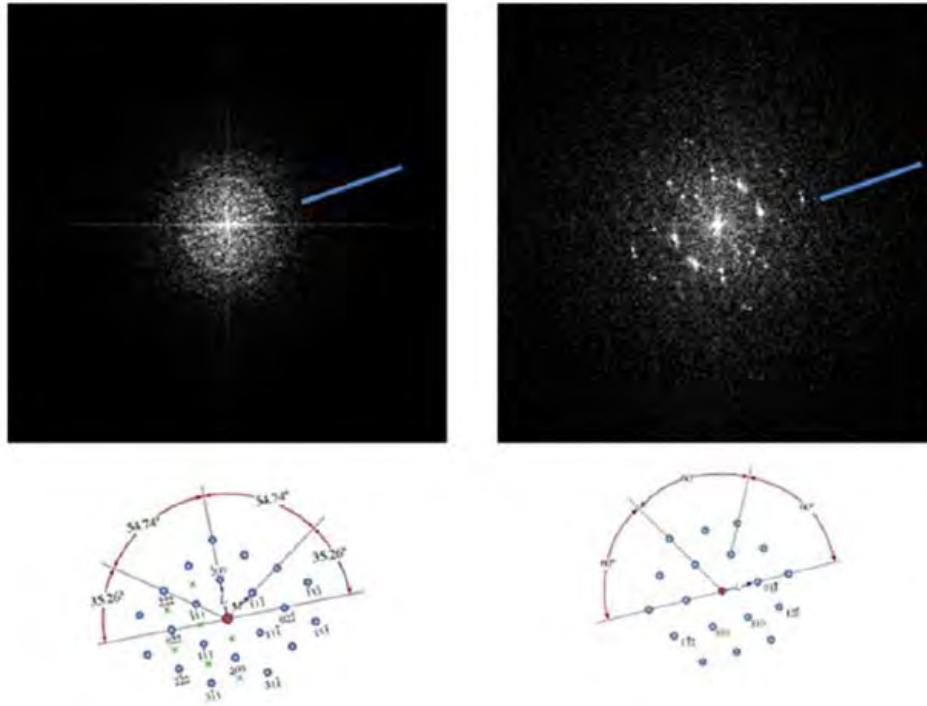
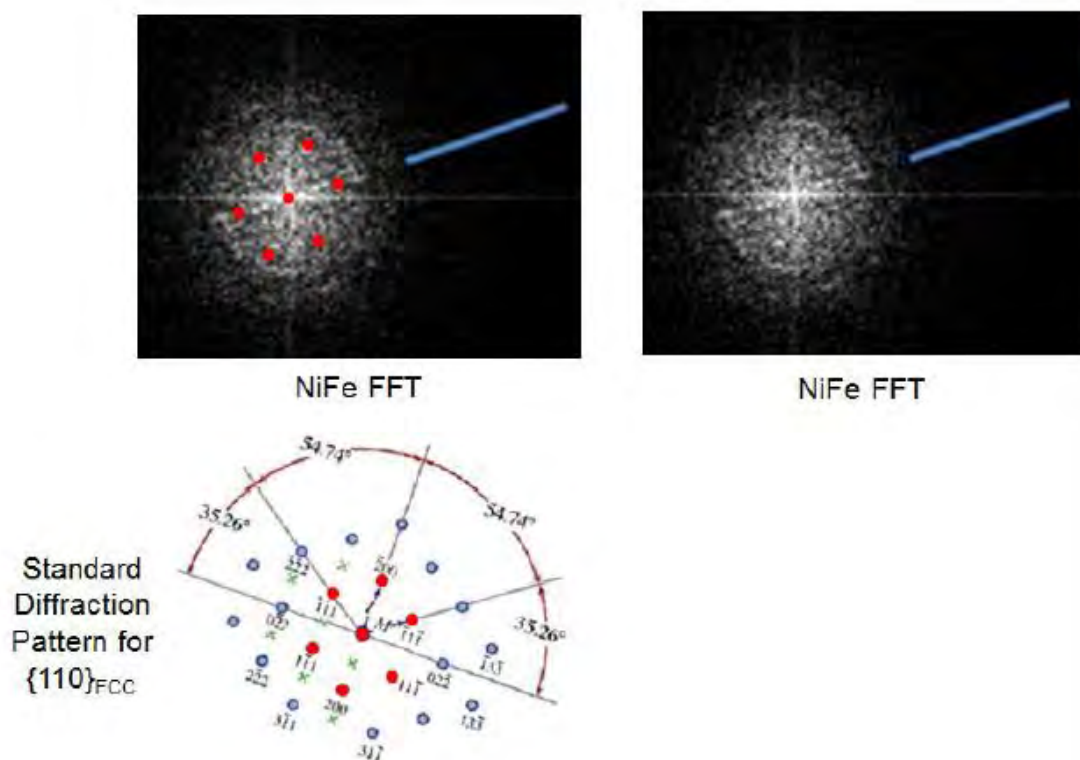


Figure 102: above: FFTs from the NiFe layer (left) and FeCo layer (right); below: standard diffraction patterns rotated into similar orientations as respective FFTs shown immediately above.

620. There is simply no basis for Dr. Clark's assertion that the NiFe FFT matches the $\{110\}_{\text{FCC}}$ diffraction pattern shown below it. Dr. Clark attempts to match the NiFe FFT to the $\{110\}_{\text{FCC}}$ diffraction pattern in order to argue that the NiFe layer contains one or more fcc crystals. (Clark, ¶ 178.) But the NiFe FFT in Figure 102 clearly does not match the $\{110\}_{\text{FCC}}$ diffraction pattern needed for Dr. Clark to argue for the existence of fcc NiFe crystals. In other words, Dr. Clark's own FFT data does not show fcc crystals in the NiFe layer (let alone a predominance of fcc(111) crystals in that layer). For this reason alone, Figure 102 does not support Dr. Clark's flawed and unreasonable conclusion that the lower NiFe layer is "predominately (111) hexagonal."

621. I note that Dr. Clark does not describe the methodology he used to compare the NiFe FFT to the $\{110\}_{\text{FCC}}$ diffraction pattern in Figure 102. For example, Dr. Clark does not attempt to identify the center diffraction peak, which is a critical step in this type of analysis (diffraction peak distances and angles are measured relative to the center diffraction peak). Nor does Dr. Clark attempt to overlay the $\{110\}_{\text{FCC}}$ diffraction pattern over the NiFe FFT—perhaps because doing so would make it even more clear that the NiFe FFT in no way matches any $\{110\}_{\text{FCC}}$ pattern. No reasonable scientist would agree with Dr. Clark's analysis of Figure 102, or the conclusions he draws from that flawed and unreasonable analysis.

622. When properly analyzes the NiFe FFT in Figure 102, one readily sees that the NiFe FFT does not match the $\{110\}_{\text{FCC}}$ diffraction as Dr. Clark claims. Below is a modified version of Dr. Clark's Figure 102 that illustrates the substantial misalignment between the NiFe FFT and the $\{110\}_{\text{FCC}}$ diffraction pattern:



623. I note it is not surprising that the NiFe FFT data in Figure 102 does not match the $\{110\}_{\text{FCC}}$ diffraction pattern given the thinness of the NiFe layer. The lower

624. In addition to Figure 102, Dr. Clark claims to have analyzed additional FFTs measured along other portions of the lower NiFe layer, apparently concluding that those additional FFTs match a $\{110\}_{\text{FCC}}$ diffraction pattern. (Clark, ¶ 183.) They do not.

625. I note that Dr. Clark does not depict—let alone analyze—any of these additional FFTs in his report. Nevertheless, I have studied these additional FFTs of the lower NiFe layer, and I conclude that, like the NiFe FFT in Figure 102, none remotely matches the $\{110\}_{\text{FCC}}$ diffraction pattern (or the $\{112\}_{\text{FCC}}$ diffraction pattern). Again, Dr. Stach has compiled an exhibit showing the extent of the mismatches between these FFTs and the standard diffraction patterns ($\{110\}_{\text{FCC}}$ and $\{112\}_{\text{FCC}}$). (See Ex. D.) I have closely reviewed Ex. D, and I agree with Dr. Stach that because none of these additional FFTs match either the $\{110\}_{\text{FCC}}$ or the $\{112\}_{\text{FCC}}$ pattern, none of these additional FFTs depict any fcc NiFe crystals.

626. I also note that Dr. Clark later appears to hedge by acknowledging that the NiFe FFTs of the lower NiFe layer do not match any $\{110\}_{\text{FCC}}$ diffraction pattern. Specifically, Dr. Clark asserts that “[t]o the extent that the FFT results for the lower NiFe layer are inconclusive, I conclude that the lower NiFe layer is FCC and exhibits a predominant (111) texture based further on the discussion of the upper NiFe / FeCo layers below.” (Clark, ¶ 184.) In my opinion, this argument is flawed and unreasonable because it purports to draw conclusions about the texture of the *lower* NiFe layer based on measurements of the *upper* NiFe layer—even though the lower and upper NiFe layer measurements do not match. (Compare Clark Figure 102, with Clark Figure 104.) Moreover, Dr. Clark’s analysis of the upper NiFe layer is also flawed and unreasonable for many of the same reasons. (See ¶¶ 639-652, *infra*.)

627. Second, Dr. Clark’s analysis of Figure 102 is further flawed and unreasonable because even assuming Dr. Clark’s NiFe FFT data actually matched the $\{110\}_{\text{FCC}}$ diffraction pattern (they clearly do not), merely matching a $\{110\}_{\text{FCC}}$

diffraction pattern is evidence of an fcc crystal in the NiFe layer—it is *not* evidence of a (111) crystal, and certainly not evidence of a predominance of fcc(111) crystals.

628. As I explained in the Technology Background, crystal structure (*e.g.*, fcc, bcc) is a property distinct from crystal orientation (*e.g.*, (111), (110)). An fcc(111) crystal describes (1) an fcc crystal (2) whose (111) plane is oriented parallel to the substrate. (*See, e.g.*, ¶ Section V.A.2, *supra* (depicting both (111) and non-(111) fcc crystals).)

629. Even if Dr. Clark’s NiFe FFTs matched a $\{110\}_{\text{FCC}}$ diffraction pattern (and they clearly do not), this would only be evidence of one or more fcc crystals in the NiFe layer. In order to properly conclude that any of these fcc crystals are fcc(111) crystals, the NiFe FFTs *must* not only (1) match the $\{110\}_{\text{FCC}}$ diffraction pattern *but also* (2) match the $\{110\}_{\text{FCC}}$ pattern such that the $\langle 111 \rangle_{\text{FCC}}$ direction is perpendicular to the substrate (a.k.a. the layer interface).

630. Dr. Clark acknowledges this requirement and simply asserts it—even though the NiFe FFT data of Figure 102 plainly contradicts him. In particular, Dr. Clark asserts that “when analyzing the pattern from the spot spacing and distribution, it can be seen that a $\langle 111 \rangle_{\text{FCC}}$ direction”—shown by the yellow line in Figure 102’s NiFe FFT— “[is] also perpendicular to the lower NiFe/lower FeCo interface. . . . These mutual relationships are sufficient to determine the relative orientation of the lower NiFe layer and the lower FeCo layer above it. Therefore, the lower NiFe layer exhibits (111) texture” (Clark, ¶ 180.)

631. Dr. Clark’s assertion that the yellow line in Figure 102’s NiFe FFT—the $\langle 111 \rangle_{\text{FCC}}$ direction—is “perpendicular to the lower NiFe/lower FeCo interface” is contradicted by his own data. The $\langle 111 \rangle_{\text{FCC}}$ direction Dr. Clark draws in Figure 102 is not perpendicular to the interface shown in Figure 101, as demonstrated by the image below:

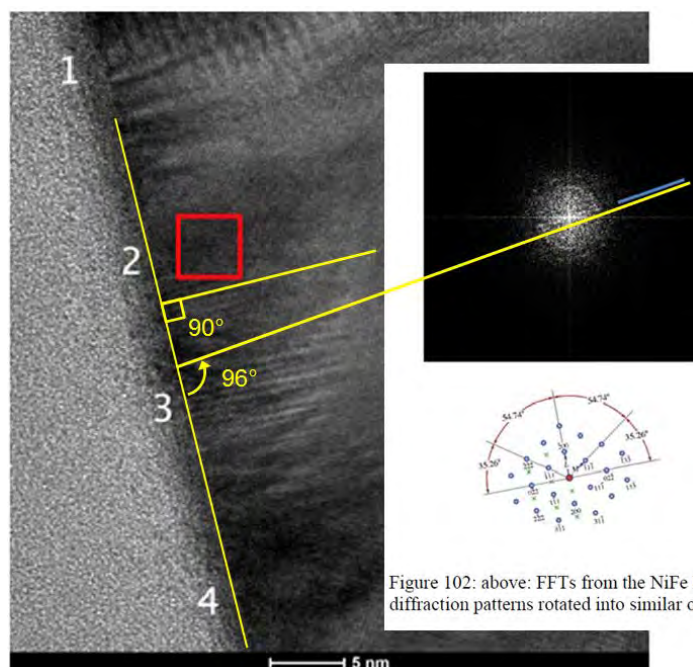


Figure 102: above: FFTs from the NiFe k diffraction patterns rotated into similar or

632. This comparison belies Dr. Clark’s claim that the $\langle 111 \rangle_{\text{FCC}}$ direction is “perpendicular to the lower NiFe/lower FeCo interface.” (Clark, ¶ 180.) The $\langle 111 \rangle_{\text{FCC}}$ direction is not perpendicular to the interface—as required of an fcc(111) crystal—but is instead about 96 degrees relative to the interface. Dr. Clark is wrong to assert in ¶ 180 that the $\langle 111 \rangle_{\text{FCC}}$ direction is perpendicular to the interface.

633. In sum, Dr. Clark’s NiFe FFT data does not match the $\{110\}_{\text{FCC}}$ diffraction pattern. But even assuming the NiFe FFT data matched the $\{110\}_{\text{FCC}}$ pattern as Dr. Clark claims, that match is inconsistent with a (111) crystal. The $\langle 111 \rangle_{\text{FCC}}$ direction is not perpendicular to the interface; Dr. Clark’s assertion that it is perpendicular contradicts the actual data. Dr. Clark’s analysis of Figure 102, and his conclusion that the FFT data somehow shows a (111) crystal (let alone a predominance of (111) crystals) in the lower NiFe layer, is therefore flawed and unreasonable for this reason as well.

634. Third, Dr. Clark’s analysis of Figure 102 and other FFT data is further flawed and unreasonable because, even if any of his FFT data actually matched a $\{110\}_{\text{FCC}}$ pattern with its $\langle 111 \rangle_{\text{FCC}}$ direction perpendicular to the NiFe/FeCo interface (which is not remotely the case), such limited FFT data does not reasonably allow Dr.

Clark to draw broad conclusions about the predominant crystal orientation (*i.e.*, texture) of the NiFe layer.

635. Dr. Clark's attempt to argue (111) texture based on a handful of FFT images is flawed and unreasonable because Dr. Clark's FFT data corresponds to a tiny fraction—less than 1%—of the overall NiFe layer. Accordingly, there is no scientific basis for Dr. Clark to assert that the NiFe layer has any “predominate” crystal orientation (let alone a predominately (111) crystal orientation) after having measured less than 1% of the overall layer. Such a conclusion is akin to a person concluding that a beach predominately comprises grains of black sand based on the fact that a single sample grain from that beach was found to be black.

636. In my opinion, it is scientifically unreasonable to conclude that a layer has any predominate crystal orientation based on a handful of select FFT measurements that correspond to less than 1% of the total layer. I am not aware of any scientific publication in which the authors inferred a layer's predominant crystal orientation based on such a limited number of FFT measurements. In my opinion, no reasonable scientist would conclude anything about a layer's predominant crystal orientation based on a handful of FFT measurements spanning less than 1% of the layer.

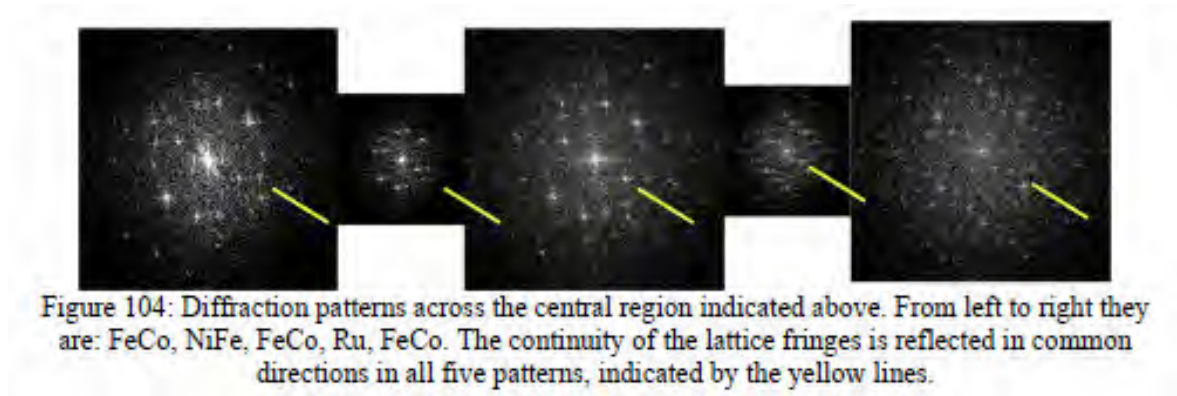
637. In sum, Dr. Clark argues that the lower NiFe layer is “(111) textured” based on a handful of FFT measurements of that layer. Because those FFT measurements do not match any $\{110\}_{\text{FCC}}$ diffraction pattern, do not feature any $\langle 111 \rangle_{\text{FCC}}$ direction perpendicular to the NiFe/FeCo interface, and comprise less than 1% of the entire lower NiFe layer, those FFT measurements do not support Dr. Clark's conclusion that the lower NiFe layer features a “(111) texture.” If anything, Dr. Clark's FFT data contradicts, rather than supports, his claim that the lower NiFe layer is “predominately (111) hexagonal.”

638. For all these reasons, it is my opinion that Dr. Clark's FFT data completely fails to show that the lower NiFe layer of the [REDACTED] write heads are “predominately (111) hexagonal.”

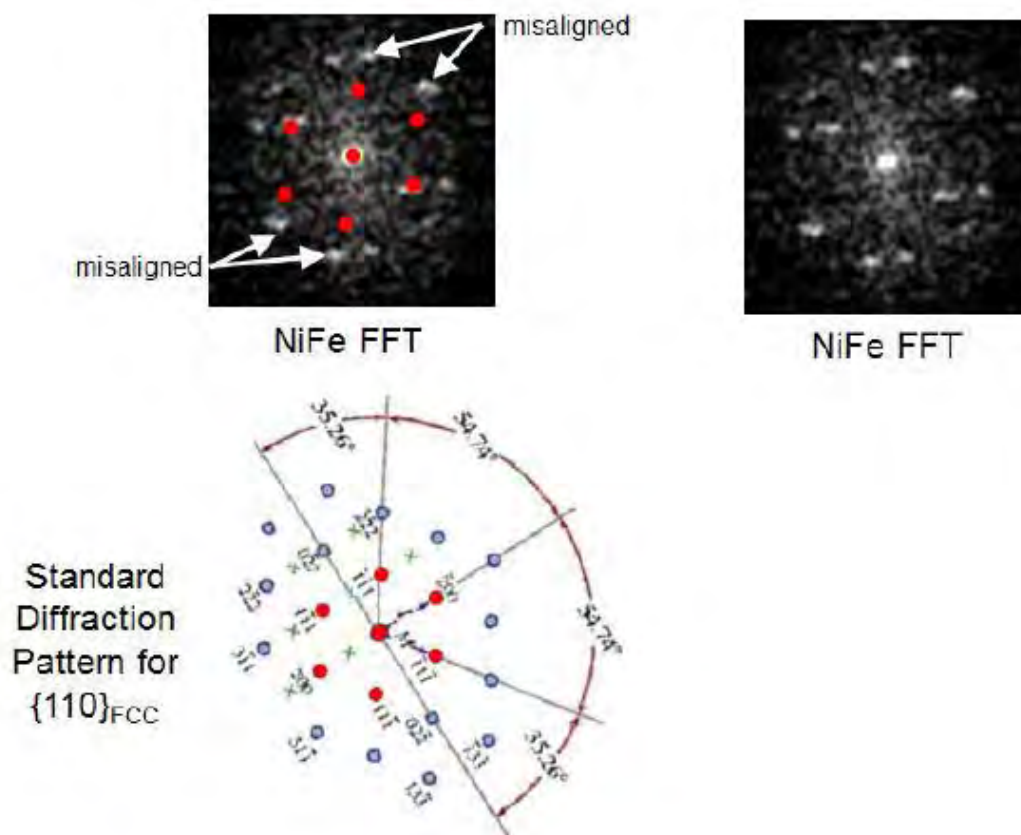
639. **SBRD8K: Upper NiFe Layer.** Dr. Clark next proceeds to discuss FFT measurements purportedly done on the upper NiFe layer. Figure 104 purportedly shows

“FFTs” from “(a) the upper FeCo layer,” “(b) in the upper NiFe layer,” and “(c) the lower FeCo layer.” (Clark, Figure 104 (p. 120).) According to Dr. Clark, Figure 104 “shows that the upper NiFe layer has a predominant (111) texture, and the upper FeCo layer has a predominant (110) texture.” (Clark, ¶ 189.)

640. In my opinion, Dr. Clark’s analysis of Figure 104 is flawed and unreasonable. I reproduce Figure 104 of Dr. Clark’s report below:



641. First, unlike the other NiFe FFTs he presents elsewhere in his report, here Dr. Clark does not even pretend that these NiFe FFTs match a $\{110\}_{\text{FCC}}$ diffraction pattern. (See, e.g., Clark, ¶ 197 (“[T]he FFTs as specific directions in the layers are not all readily ascertainable.”) Dr. Clark does not contend that the NiFe FFT matches a $\{110\}_{\text{FCC}}$ diffraction pattern—and they do not, as shown by the misalignment in the image below.



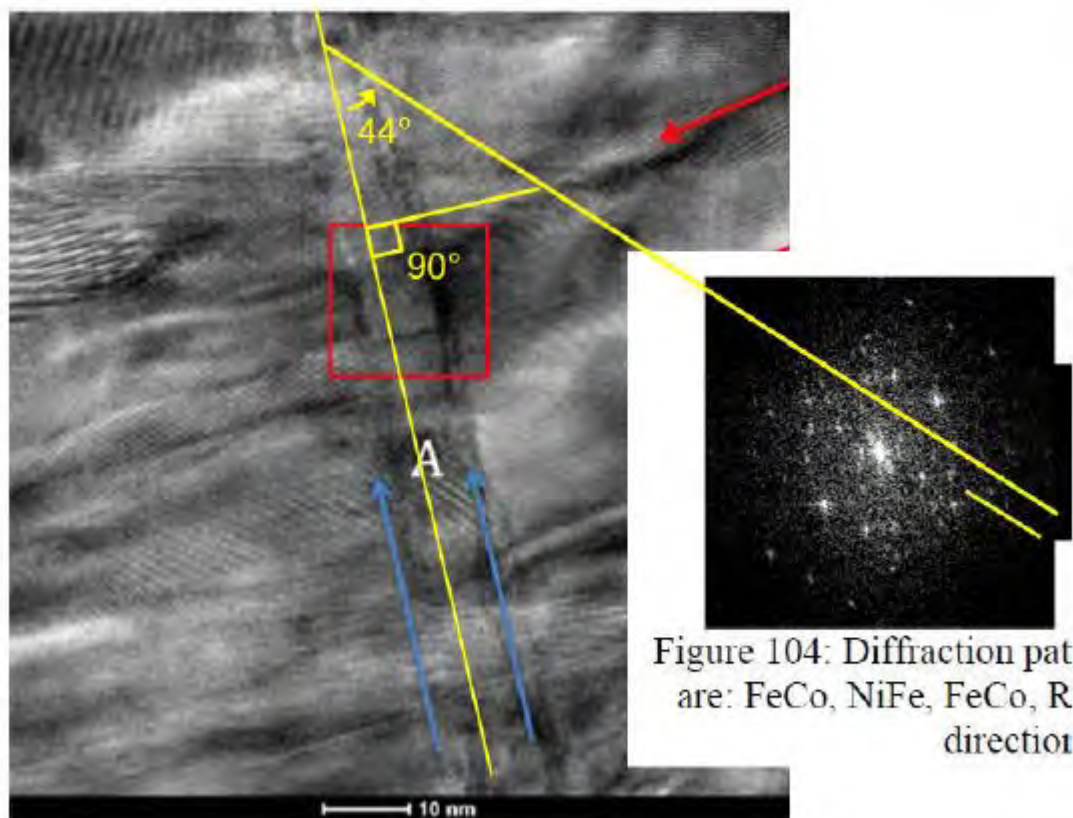
642. Because this NiFe FFT clearly does not match a $\{110\}_{\text{FCC}}$ (or $\{112\}_{\text{FCC}}$) pattern, this NiFe FFT is not evidence of any fcc NiFe crystals.

643. Second, Dr. Clark makes the unsupported claim that “[w]hen analyzing the pattern from the spot spacing and distribution, it can be seen that a $\langle 111 \rangle_{\text{FCC}}$ direction in the NiFe is parallel to a $\langle 110 \rangle_{\text{BCC}}$ in the FeCo . . . [and] [t]he directions are also perpendicular to the upper NiFe/FeCo interfaces Therefore, the lower NiFe layer exhibits (111) texture.” (Clark, ¶ 190.)

644. Dr. Clark’s “analysis” in ¶ 190 is nothing but a recycled copy-and-paste of his earlier FFT analyses (*compare, e.g.,* Clark, ¶ 101 with Clark, ¶ 190), which as I explained are flawed and unreasonable. The difference between Clark’s ¶ 101 and ¶ 190, however, is that Dr. Clark does not pretend to match Figure 104 to any diffraction pattern. Without trying to match the NiFe FFT of Figure 104 to a diffraction pattern, it makes no sense for Dr. Clark to opine about $\langle 111 \rangle_{\text{FCC}}$ directions (which, without a

diffraction pattern to reference them to, do not exist)—let alone a $\langle 111 \rangle_{\text{FCC}}$ direction “perpendicular to the upper NiFe/FeCo interface.” (Clark, ¶ 190.) In short, Dr. Clark has not shown any $\langle 111 \rangle_{\text{FCC}}$ direction perpendicular to the NiFe/FeCo interface, and he has absolutely no basis for asserting that any $\langle 111 \rangle_{\text{FCC}}$ direction is perpendicular to the NiFe/FeCo interface.

645. Nevertheless, if one assumes that the yellow lines in Figure 104 represent what Dr. Clark is referring to as the $\langle 111 \rangle_{\text{FCC}}$ direction, it is clear that this direction is not perpendicular to the NiFe/FeCo interface, as shown in the image below.



646. This comparison belies Dr. Clark’s claim that the $\langle 111 \rangle_{\text{FCC}}$ direction is “perpendicular to the upper NiFe/FeCo interface.” (Clark, ¶ 190.) The $\langle 111 \rangle_{\text{FCC}}$ direction is not perpendicular to the interface—as required of an fcc(111) crystal—but is instead about 106 degrees relative to the interface. Dr. Clark is wrong to assert in ¶ 190 that the $\langle 111 \rangle_{\text{FCC}}$ direction is perpendicular to the interface.

647. In sum, Dr. Clark's NiFe FFT data does not match any $\{110\}_{\text{FCC}}$ diffraction pattern. But even assuming the NiFe FFT data matched the $\{110\}_{\text{FCC}}$ pattern (which even Dr. Clark does not contend), that match is inconsistent with a (111) crystal. The $\langle 111 \rangle_{\text{FCC}}$ direction is not perpendicular to the interface; Dr. Clark's assertion that it is perpendicular contradicts the actual data. Dr. Clark's analysis of Figure 104, and his conclusion that the FFT data somehow shows a (111) crystal (let alone a predominance of (111) crystals) in the upper NiFe layer, is therefore flawed and unreasonable for this reason as well.

648. Third, Dr. Clark's analysis of Figure 104 and other FFT data is further flawed and unreasonable because even if any of his FFT data actually matched a $\{110\}_{\text{FCC}}$ pattern with its $\langle 111 \rangle_{\text{FCC}}$ direction perpendicular to the NiFe/FeCo interface (which is not remotely the case), such limited FFT data does not reasonably allow Dr. Clark to draw broad conclusions about the predominant crystal orientation (*i.e.*, texture) of the NiFe layer.

649. Dr. Clark's attempt to argue (111) texture based on a handful of FFT images is flawed and unreasonable because Dr. Clark's FFT data corresponds to a tiny fraction—less than 1%—of the overall NiFe layer. Accordingly, there is no scientific basis for Dr. Clark to assert that the NiFe layer has any “predominate” crystal orientation (let alone a predominately (111) crystal orientation) after having measured less than 1% of the overall layer. Such a conclusion is akin to a person concluding that a beach predominately comprises grains of black sand based on the fact that a single sample grain from that beach was found to be black.

650. In my opinion, it is scientifically unreasonable to conclude that a layer has any predominate crystal orientation based on a handful of select FFT measurements corresponding to less than 1% of the total layer. I am not aware of any scientific publication in which the authors inferred a layer's predominant crystal orientation based on a small number of FFT measurements. In my opinion, no reasonable scientist would conclude anything about a layer's predominant crystal orientation based on a handful of FFT measurements spanning less than 1% of the layer.

651. In sum, Dr. Clark argues that the upper NiFe layer is “(111) textured” based on a handful of FFT measurements of that layer. Because those FFT measurements do not match any $\{110\}_{\text{FCC}}$ diffraction pattern, do not feature any $\langle 111 \rangle_{\text{FCC}}$ direction perpendicular to the NiFe/FeCo interface, and comprise less than 1% of the entire upper NiFe layer, those FFT measurements do not support Dr. Clark’s conclusion that the upper NiFe layer features a “(111) texture.” If anything, Dr. Clark’s FFT data contradicts, rather than supports, his claim that the upper NiFe layer is “predominately (111) hexagonal.”

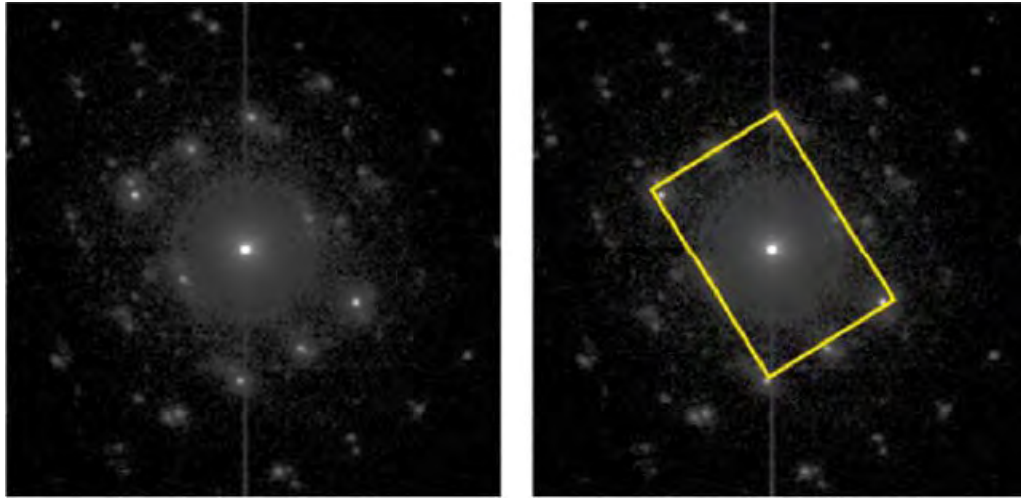
652. For all these reasons, it is my opinion that Dr. Clark’s FFT data completely fails to show that the upper NiFe layer of the [REDACTED] write heads are “predominately (111) hexagonal.”

(ii) Dr. Clark’s other measurements are inconsistent with a (111) textured NiFe layer

653. As explained above, none of Dr. Clark’s FFT data supports the conclusion the NiFe layers in the [REDACTED] write heads are predominately (111) hexagonal. In addition, none of Dr. Clark’s other TEM measurements suggest any (111) texture to the NiFe layer(s). I note that, aside from the FFTs discussed above, Dr. Clark does not contend that any of his other TEM measurements show a (111) texture for either NiFe layer.

654. **Dr. Clark’s Microbeam Diffraction Data Is Inconsistent With a (111) Textured NiFe Layer.** Dr. Clark also took thousands of microbeam diffraction measurements (most of which he did not produce). These microbeam diffraction measurements also undermine Dr. Clark’s claim that a “(111) textured” NiFe layer exists in the accused [REDACTED] products.

655. For example, one of Dr. Clark’s microbeam diffraction patterns (from Figure 107) is shown below:



656. As I explained in the Technology Background, a (111) hexagonal crystal would, when measured with plan-view microbeam diffraction, produce a specific hexagonal diffraction pattern. Yet no such hexagonal diffraction pattern can be found in any of Dr. Clark’s microbeam diffraction measurements—further indicating that no (111) hexagonal crystals exist.

657. Despite taking 1,600 microbeam diffraction measurements on the SBRD8K sample, Dr. Clark never attempts to identify any such hexagonal pattern in any of his 1,600 microbeam diffraction measurements. (*Cf.* LMS’s Infringement Contentions (served on Toshiba on Oct. 9, 2015, at 9).)

658. It is not possible to fit this hexagonal diffraction pattern to any of the microbeam diffraction measurements Dr. Clark produced. No matter how you position the hexagonal template, it is not possible to align the diffraction peaks to the vertices of the hexagon.

659. It is therefore my opinion that Dr. Clark’s microbeam diffraction data contradicts his opinion that the NiFe layers in the [REDACTED] write heads are “(111) textured.” It is my opinion that Dr. Clark’s microbeam diffraction data contradicts his opinion that the NiFe layers in the [REDACTED] write heads are “predominately (111) hexagonal.”

(iii) The extreme thinness of the NiFe layers prevents a predominate crystallographic orientation from forming

660. As I explained in the Technology Background, layers that are only a few atomic layers thick generally exhibit no crystal structure, as a crystal structure tends to develop and evolve as a layer grows in thickness. As a result, very thin layers often feature no crystal structure—and therefore no predominant crystallographic orientation. (See, e.g., '416 Patent at 11:6-9 (“The wetting layer 18 can be an amorphous material or a film too thin to have developed a crystalline texture, or a film whose texture provides a gross lattice mismatch for the ensuing layer.”); Patent Owner’s Preliminary Response to IPR2016-00013, at 42 (“One common feature in deposition of ultrathin films is that in many cases pseudomorphic growth occurs over several monolayers before the film converts into its usual crystal structure.”); *id.* at 43 (“In other words, an epitaxially grown ultrathin film will commonly have a pseudomorphic or metastable non-equilibrium crystalline structure for the first several monolayers. Such crystalline structures will not have formed into stable fcc or bcc structures. . . . Dr. Sinclair chose to ignore the fact that the layers at issue are ultrathin and therefore could not have formed equilibrium crystalline structures.”); *id.* at 43-44 (distinguishing prior art: “Dill never described the crystalline structure of the interface layer . . . but the thickness of that interface layer (i.e., 0.4-2 nm) indicates that it was pseudomorphic fcc and could not have been in equilibrium crystalline phase.”); D. Lambeth et al., *Magnetic Media Performance: Control Methods for Crystalline Texture and Orientation*, Mat. Res. Soc. Symp. Proc. Vol. 517, p. 185 (1998) (“However, below 5 nm the Cr is so thin that little or no crystalline texture has evolved . . .”); M. Ohring, MATERIALS SCIENCE OF THIN FILMS 529, 562 (“Sometimes, texture evolves from random in initial deposits to strong orientation of low-energy planes parallel to the film surface, and finally, to changes in preferred texture as the film thickens further.”).)

661. In addition, I note that another method of measuring a layer’s texture (if any) is x-ray diffraction (XRD)—indeed this is how Dr. Lambeth measured texture in both the '988 Patent and the '416 Patent. (See, e.g., '988 Patent at 38:17-19 (“First we

provide a perspective for the degree of texture obtained by observing a θ - 2θ x-ray diffraction scan”); ’416 Patent at FIG. 14, FIG. 21, FIG. 23, FIGs. 26-30.) I note that Dr. Clark and Dr. Coffey not analyze any XRD data in their reports.

662. I have also considered Dr. Coffey’s citations and characterizations of Seagate documents and deposition testimony on this issue (*see* Coffey ¶¶ 370-383) and find his characterizations of many of these documents to be flawed and unreasonable. Although Dr. Coffey string cites without explanation dozens of Seagate documents and testimony from ¶¶ 370-383 of his report, none actually support his conclusion that the NiFe layer is (111) textured. None of the cited Seagate documents or testimony support Dr. Coffey’s conclusion that any NiFe layer is “predominately (111) hexagonal.”

663. For all these reasons, it is my opinion that the accused [REDACTED] products do not meet this claim limitation. None of the NiFe layers in the [REDACTED] write heads are “(111) textured.” None of the NiFe layers in the [REDACTED] write heads are “predominately (111) hexagonal.”

(b) layer that provides “an atomic pattern upon which material is grown and which is used to direct the growth of an overlying layer”

664. In my opinion, the NiFe layers in the [REDACTED] write heads do not provide an “atomic template,” *i.e.*, “an atomic pattern . . . which is used to direct the growth of an overlying layer.” Each of the NiFe layers in the [REDACTED] write heads are so thin that they have not developed any long-range crystal structure needed for epitaxial growth—they therefore cannot and do not “direct the growth of an overlying layer.”

665. In addition, I note that Dr. Clark himself provides examples of FeCo crystals growing irrespective of the NiFe layer. For example, Dr. Clark states that “[s]everal sets of lattice fringes are seen [in Figure 100], as are the FeCo/NiFe/Ru interfaces. The fringes are present on both sides of the NiFe layer, in the NiFe layer itself, and on both sides of the Ru layer, *indicating that the orientation of the FeCo is maintained on both sides of the NiFe.*” (Clark, ¶ 175 (interpreting Figure 100).) In other words, the crystals in the lower FeCo layer continue into the upper FeCo layer—the

lower FeCo crystals are “growing through” the NiFe layer as if the NiFe layer was not there. This shows that the NiFe layer is not acting as an atomic template for the FeCo—*i.e.*, it is not “used to direct the growth of an overlying layer.”

666. For all these reasons, it is my opinion that the accused [REDACTED] products do not meet this claim limitation. None of the NiFe layers in the [REDACTED] write heads provide an “atomic template.” None of the NiFe layers in the [REDACTED] write heads are “used to direct the growth of an overlying layer.”

2. The [REDACTED] products do not have “at least one bcc-d layer which is magnetic, forming a uniaxial symmetry broken structure”

Term	Court’s Construction
uniaxial	“having an anisotropy energy density function with only a single maximum and a single minimum as the magnetization angle is rotated by 180 degrees from a physical axis”
symmetry broken structure	“a structure consisting of unequal volumes or unequal amounts of the bcc-d variants of a six variant system”
variant / orientational variant	“one of a set of possible crystal orientations”
variants / orientational variants	“two or more of a set of possible crystal orientations”
uniaxial symmetry broken structure	“a structure that is uniaxial as a result of the structure being symmetry broken”

667. Dr. Coffey argues in ¶¶ 318-332 of his report that the accused [REDACTED] products have “at least one bcc-d layer which is magnetic, forming a uniaxial symmetry broken structure.” I have carefully considered Dr. Coffey’s arguments and find his conclusion to be unfounded. Dr. Coffey’s data and analyses are flawed and unreasonable with respect to multiple claim limitations. Dr. Coffey’s data does not

support his conclusion that the [REDACTED] products have “at least one bcc-d layer which is magnetic, forming a uniaxial symmetry broken structure.”

668. As discussed above, the [REDACTED] write heads comprise several layers, including two layers of NiFe and two layers of FeCo, as depicted below:



669. I understand Dr. Coffey contends that “the lower (first-deposited) of the two layers of FeCo in the [REDACTED] Products” is “at least one bcc-d layer which is magnetic, forming a uniaxial symmetry broken structure.” (Coffey, ¶ 320.)

670. I disagree. Although the FeCo layers are magnetic bcc-d layers, neither the lower nor upper FeCo layers meet the remainder of this claim limitation. Neither the lower nor upper FeCo layers form a “symmetry broken structure.” (*See* Section IX.B.2(a).) Neither the lower nor upper FeCo layers are “uniaxial.” (*See* Section IX.B.2(b).) Neither the lower nor upper FeCo layers form a “uniaxial symmetry broken structure.” (*See* Section IX.B.2(c).)

671. I understand that Dr. Coffey analyzes the “uniaxial symmetry broken structure” limitation as a single claim limitation.¹⁹ (*See* Coffey, ¶¶ 333-361.) As I understand the Court’s claim construction order, however, “symmetry broken structure,”

¹⁹ Dr. Coffey ostensibly addresses the “uniaxial” limitation separately for purposes of asserting the doctrine of equivalents, but even here he appears to conflate multiple claim limitations in his analysis (namely, “uniaxial” and “uniaxial symmetry broken structure”). (*See* Coffey, ¶¶ 362-369.)

“uniaxial,” and “uniaxial symmetry broken structure” each represents a claim limitation, and all three must be met for there to be infringement.

672. Because I understand that infringement requires a limitation-by-limitation analysis of each claim limitation, I separately analyze each claim limitation—“symmetry broken structure,” “uniaxial,” and “uniaxial symmetry broken structure”—below.

**(a) “a structure consisting of unequal volumes or unequal amounts of the bcc-d variants of a six variant system”
(symmetry broken structure)**

673. In my opinion, the FeCo layers in the [REDACTED] products do not form a “symmetry broken structure”—*i.e.*, they do not form “a structure consisting of unequal volumes or unequal amounts of bcc-d variants of a six variant system.”

**(i) Drs. Coffey & Clark fail to show the existence of
any “variants” in the FeCo layers**

674. In my opinion, neither Dr. Coffey nor Dr. Clark offer any data showing that the FeCo layers in [REDACTED] form a six-variant system as taught by the '988 Patent and required by the Court's claim construction order. As I discuss above, the '988 Patent's six variants refers to bcc-d(110) crystals oriented in one of six ways relative to an underlying (111) hexagonal template crystal. Neither Dr. Coffey nor Dr. Clark offer data showing the existence of any such variants.

675. A “variant” in the context of the '988 Patent refers to a bcc-d(110) crystal with a particular orientation relative to the underlying (111) hexagonal template crystal. The Court construed “variants” to mean “two or more of a set of possible crystal orientations.” Whether two bcc-d crystals are the same variant or two different variants depends on their orientations relative to their underlying template crystals. If two bcc-d crystals have the same orientation relative to their underlying template crystals, they are the same “variant” (*i.e.*, they are “one of a set of possible orientations”). If two bcc-d crystals have different orientations relative to their underlying template crystal, they are two different variants (*i.e.*, they are “two . . . of a set of possible orientations”).

676. Because a “bcc-d variant” refers to a bcc-d(110) crystal with a particular orientation relative to an underlying (111) hexagonal template crystal, identifying a “bcc-d variant” requires identifying three things: (1) a bcc-d(110) crystal; (2) the underlying (111) hexagonal template crystal on which that bcc-d(110) crystal was grown; and (3) the orientation of the bcc-d(110) crystal relative to the template crystal.

677. Dr. Coffey and Dr. Clark fail to identify any “variants” (let alone variants of a six variant system) in any of the [REDACTED] layers.

678. Dr. Clark does attempt to identify bcc-d(110) crystals in the FeCo layers via microbeam diffraction measurements. But nowhere do Dr. Coffey or Dr. Clark attempt to identify any underlying (111) hexagonal template crystals—indeed, Dr. Clark’s own microbeam diffraction measurements show that no underlying (111) hexagonal template crystals exist. And nowhere do Dr. Coffey or Dr. Clark attempt to identify the orientation of any bcc-d crystal relative to an underlying (111) hexagonal template crystal (which, again, do not exist).

679. Because Dr. Coffey and Dr. Clark fail to identify any “bcc-d variants,” they fail to show that any [REDACTED] FeCo layer forms a “symmetry broken structure.”

a) Dr. Clark’s microbeam diffraction data does not show any “bcc-d variants of a six variant system”

680. Dr. Coffey argues that: “I understand that microbeam diffraction analysis of representative samples of the [REDACTED] Products shows that the lower layer of FeCo in the write pole contains multiple (110) bcc crystalline grains that are members of the Kurdjumov-Sachs six variant system.” (Coffey, ¶ 336.) Dr. Coffey erroneously contends that Dr. Clark’s microbeam diffraction analysis is evidence of a Kurdjumov-Sachs six variant system. In fact, Dr. Clark’s microbeam diffraction data shows no variants because they consistently show that no (111) hexagonal template crystals exist.

681. Dr. Clark took 1,600 microbeam diffraction measurements of the [REDACTED] FeCo layers. (*See, e.g.*, Clark, ¶ 194.) Of those 1,600 microbeam diffraction measurements, Dr. Clark contends that a few show one, two, or three bcc-d(110) crystals (depending on the measurement) in the FeCo layer. But Dr. Clark never contends that

any of these 1,600 microbeam diffraction measurements shows a (111) hexagonal template crystal (which I note is also compelling evidence that no (111) textured hexagonal atomic template exists in the accused [REDACTED] products). As a result, none of Dr. Clark's microbeam diffraction measurements shows the existence of any "bcc-d variants"—let alone "bcc-d variants of a six variant system."

682. Dr. Clark took 1,600 microbeam diffraction measurements of the SBRD8K sample. (Clark, ¶ 194.) According to Dr. Clark: "100 out of the 1600 diffraction patterns were selected using a random number generator. These 100 were categorized as either a) showing no recognizable pattern, b) showing a single {110} patterns, c) showing two or three {110} patterns, d) showing {110} twins, or e) showing a pattern other than {110}. The results show the following numbers in each category – a) 71, b) 5, c) 0 d) 0 e) 24." (Clark, ¶ 200.)

683. This is precisely the point. Dr. Clark never contends that any of these microbeam diffraction measurements includes anything resembling a fcc{111} pattern—*i.e.*, a pattern corresponding to a (111) hexagonal template crystal. I summarize in the table below Dr. Clark's own summary of his microbeam diffraction measurements:²⁰

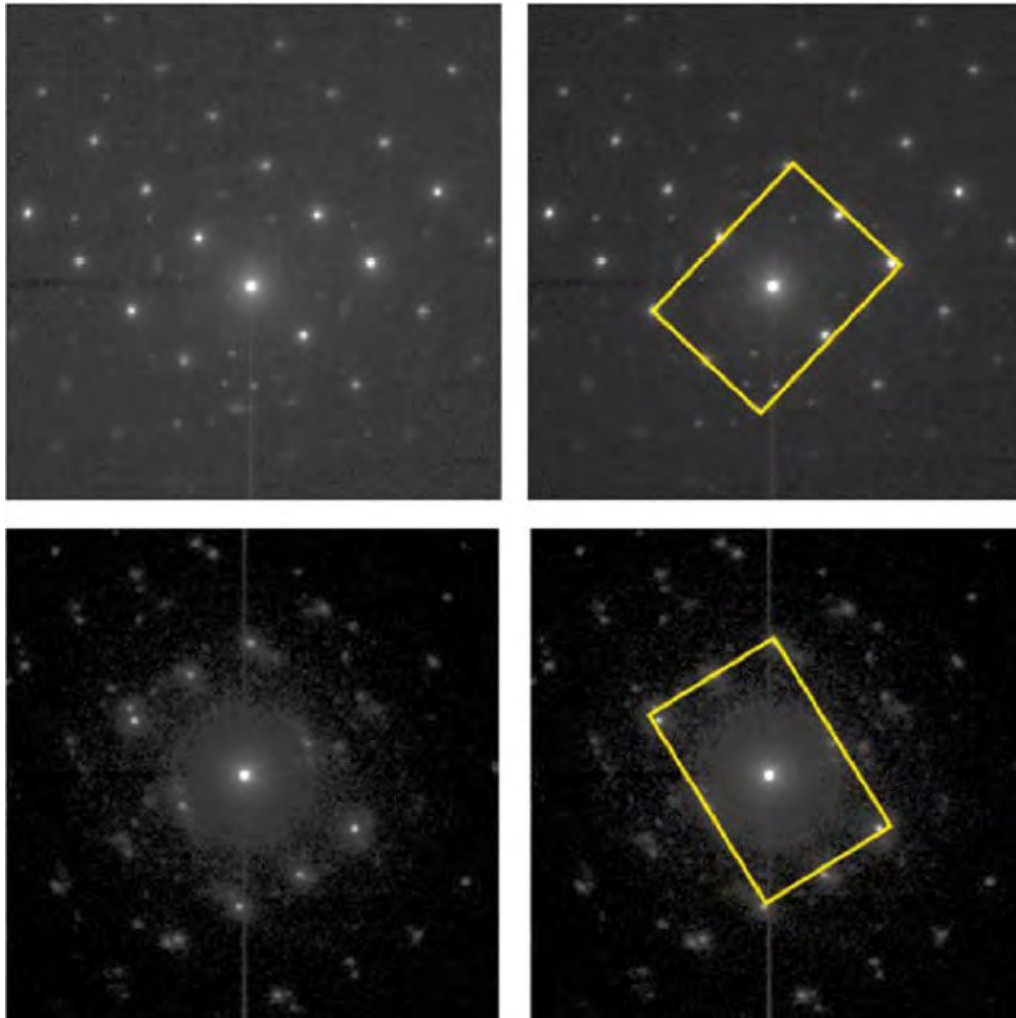
Summary of Microbeam Diffraction Measurements on Hybrid_X		
<u># of Images</u>	<u>Pattern Dr. Clark Contends Exists</u>	<u>Meaning</u>
71	No Recognizable Pattern	71/100 microbeam diffraction measurements show no recognizable crystal structure
5	Single bcc{110} Pattern	30/100 microbeam diffraction measurements show a single (110) crystal

²⁰ I note that Dr. Clark never produced most of the 1,600 microbeam diffraction patterns he purportedly took for sample SBRD8K. Indeed, of the 1,600 microbeam diffraction patterns Dr. Clark purportedly took, he produced just 8 in Appendix C to his report.

0	Two or Three bcc{110} Patterns	44/100 microbeam diffraction measurements show two or three (110) crystals
0	fcc{111} Pattern	0/100 microbeam diffraction measurements show any (111) hexagonal template crystal(s)

684. Of the 1,600 microbeam diffraction measurements of the S0GPPC sample, Dr. Clark depicts five of them in his report as Figures 107-110. Dr. Clark does not contend that a single one of these shows a (111) hexagonal crystal. And for good reason: they clearly do not. As a result, Figures 107-110 do not identify any “bcc-d variants” because none of those Figures show any (111) hexagonal template crystal.

685. As an example, I reproduce Figure 107 of Clark’s report:



686. Figure 107 clearly does not contain hexagonal pattern corresponding to a (111) hexagonal template crystal. Dr. Clark does not contend otherwise. As a result, Figure 107 does not identify “bcc-d variants” because it does not show any (111) hexagonal template crystal.

687. Figures 108, 109, and 110 also clearly do not contain any hexagonal pattern corresponding to a (111) hexagonal template crystal. Dr. Clark does not contend otherwise. As a result, Figures 108, 109, and 110 do not identify any “bcc-d variants” because they do not show any (111) hexagonal template crystal.

688. To the extent Dr. Clark contends that Figures 107-110 show “variants in a Kurdjumov-Sachs orientation,” that interpretation of Figures 107-110 is flawed and unreasonable. None of the crystallites identified in Figures 107-110 are “variants”

because none of the crystallites are grown on any underlying (111) hexagonal template crystal. Because none of the crystallites is a variant, the orientations of the crystallites relative to one another is *irrelevant* (what would be relevant is the orientation of each crystallite relative to an underlying (111) hexagonal template crystal—which does not exist). Without any evidence of the bcc-d crystallites’ orientations relative to any underlying (111) hexagonal template crystals—indeed, without any evidence that any (111) hexagonal template crystals even exist—it is incorrect and unreasonable for Dr. Clark to claim that Figures 107-110 show any “variants.”

689. I note that in addition to failing to show the presence of any (111) hexagonal template crystals in his microbeam diffraction patterns, Dr. Clark’s contention that his images show the presence of particular bcc(110) crystals is also not supported for many of his examples. Dr. Stach and I have identified and analyzed some of these examples in Exhibit E, attached to this report.

690. In sum, *none* of Dr. Clark’s microbeam diffraction images show any (111) hexagonal template crystals. As a result, none of Dr. Clark’s microbeam diffraction images show any “bcc-d variants”—let alone “bcc-d variants of a six variant system.” If “bcc-d variants of a six-variant system” actually existed in the measured SBRD8K sample, Dr. Clark’s microbeam imaging would have detected (111) hexagonal crystals underlying each of the bcc(110) crystallites. Contentions (served on Toshiba on Oct. 9, 2015), at 9.) No such evidence of a “bcc-d variant” exists in any of Dr. Clark’s microbeam diffraction data.

691. In my opinion, the fact that Dr. Clark took 1,600 microbeam diffraction measurements of the SBRD8K sample yet found no evidence of (111) hexagonal template crystals shows that the SBRD8K sample’s FeCo layers do not consist of the “bcc-d variants of a six variant system” and therefore do not form any “symmetry broken structure.”

b) Dr. Clark's FFT data does not show "bcc-d variants of a six variant system"

692. Dr. Coffey argues that: "I further understand that there are unequal amounts of variants from the Kurdjumov-Sachs six-variant system in the lower layer of FeCo in sample SBR8DK based on high resolution cross-sectional imaging. Dr. Clark used FFTs to analyze a cross-section sample from sample SBR8DK to confirm that the FeCo grains in the lower layer of FeCo and the lower layer of NiFe have an epitaxial (111)NiFe|| (110)FeCo orientation relationship with the in-plane directions $\langle 111 \rangle_{\text{bcc}} || \langle 110 \rangle_{\text{fcc}}$, which confirms that the FeCo grains are composed of variants from the Kurdjumov-Sachs six-variant system." (Coffey, ¶ 337.)

693. As I explained above, Dr. Clark's interpretation of his FFTs is flawed, unreasonable, and incorrect for multiple reasons. (See Section IX.B.1(a)(i), *supra*.)

694. First, contrary to Dr. Clark's claims, *none* of the FFT images for any NiFe layer even remotely matches the $\{110\}_{\text{FCC}}$ diffraction pattern. (See Section IX.B.1(a)(i), *supra*.)

695. Second, none of the FFT images show an epitaxial (111)NiFe|| (110)FeCo orientation relationship because none of the FFTs purport to show any NiFe crystals with their $\langle 111 \rangle_{\text{FCC}}$ direction perpendicular to the NiFe/FeCo interface. In other words, even assuming Dr. Clark's FFTs matched the diffraction patterns he claims they do (they do not), none of those FFTs show (111) NiFe crystals (*i.e.*, a NiFe crystal with its $\langle 111 \rangle_{\text{FCC}}$ direction perpendicular to the interface). (See Section IX.B.1(a)(i), *supra*.)

696. Third, there is no valid scientific basis for Dr. Clark to make sweeping conclusions about the predominant crystallographic orientation of a NiFe layer based on a handful of FFT images that span less than 1% of the layer. (See Section IX.B.1(a)(i), *supra*.)

697. In sum, Dr. Clark's argument that his FFT data shows a "(111)NiFe|| (110)FeCo orientation relationship with the in-plane directions $\langle 111 \rangle_{\text{bcc}} || \langle 110 \rangle_{\text{fcc}}$ " is unreasonable and simply not supported by his FFT data. Dr. Clark's FFTs show nothing of the sort, as is made plain when one actually examines the FFT data. (See Section IX.B.1(a)(i), *supra*.)

698. Dr. Coffey nevertheless relies on Dr. Clark's deeply flawed FFT analysis, and does not purport to offer any additional or independent analysis of his own. Dr. Coffey's opinion that "there are unequal amounts of variants from the Kurdjumov-Sachs six-variant system" is therefore based on nothing other than Dr. Clark's deeply flawed and unreliable FFT analysis.

* * *

699. In sum, neither Dr. Coffey nor Dr. Clark offer any evidence of a (111) hexagonal template. Although Dr. Clark provides microbeam diffraction images, some of which show the existence of one, two, or three bcc-d(110) crystals, none of those microbeam diffraction images indicate that any (111) hexagonal template crystal underlies any of these bcc-d(110) crystals. As for Dr. Clark's FFT data, none of that data remotely shows any (111) hexagonal crystal.

700. I have also considered Dr. Coffey's citations and characterizations of Seagate documents and deposition testimony on this issue (*see* Coffey ¶¶ 333-361) and find his characterizations of many of these documents to be flawed and unreasonable. Although Dr. Coffey string cites without explanation dozens of Seagate documents and testimony from ¶¶ 333-361 of his report, none actually support his conclusion that the FeCo layer forms a symmetry broken structure—*i.e.*, "a structure consisting of unequal volumes or unequal amounts of the bcc-d variants of a six variant system." For example, none of the cited Seagate documents or deposition testimony show any evidence of "bcc-d variants" because none show that any underlying (111) hexagonal template crystals exist in any accused Seagate products.

701. Because neither Dr. Coffey nor Dr. Clark offers any evidence of any (111) hexagonal template crystals underlying bcc-d(110) FeCo crystals, they have failed to show any "bcc-d variants"—let alone "bcc-d variants of a six variant system." Without the "bcc-d variants of a six variant system," neither FeCo layer can form a "symmetry broken structure."

c) Dr. Clark's microbeam diffraction and dark field image data consistently show FeCo layers with many non-(110) crystals

702. Dr. Coffey and Dr. Clark fail to provide any evidence of bcc-d variants of a six variant system in any of Seagate's FeCo layers. Indeed, Dr. Clark's own data repeatedly shows that Seagate's FeCo layers do not consist of six bcc(110) variants, and so do not form a "symmetry broken structure."

703. Dr. Clark obtained microbeam diffraction patterns for the lower FeCo layer of sample SBRD8K. Dr. Clark claims he randomly selected and characterized 100 of those patterns. Assuming Dr. Clark's characterization of those samples is correct (he did not include the images of those patterns in his report), he reports that for the first sample 95% of the diffraction patterns for the lower FeCo layer were not recognizable as bcc(110) crystals. (Clark, ¶ 200.) This indicates that many—likely *most*—of the crystals in the lower FeCo layer Dr. Clark measured are *not* bcc(110).

704. Moreover, Dr. Clark's dark field imaging data show that most of the crystals in the FeCo layers he analyzed are not bcc(110) crystals. The crystallites he identified that are bcc(110) make up little more than 36% of the layers according to his own area-fraction data. (*See* Clark, Table 3 (pp. 132-133).)

705. The presence of these many non-(110) crystals in the FeCo layers is inconsistent with the FeCo layers forming a symmetry broken structure. Non-(110) crystals cannot form a six-variant system under the '988 Patent. (*E.g.*, '988 Patent at 12:66-13:2 ("this invention deals with a structure to achieve uniaxial magnetocrystalline orientation via the use of the (110) texture of body centered cubic (BCC) or body centered cubic derivative crystal thin film structures.")) Because Seagate's FeCo layers contain many (if not mostly) non-(110) crystals, the FeCo layers do not consist of the bcc-d variants of a six variant system. Because Seagate's FeCo layers contain many (if not mostly) non-(110) crystals, they do not form a symmetry broken structure.

706. In my opinion, the fact that Seagate's FeCo layers all contain a substantial number of non-(110) crystals—as consistently shown across multiple different measurements by Dr. Clark—is further evidence that the FeCo layers in

Seagate's [REDACTED] products do not form a "symmetry broken structure" and therefore do not infringe the Asserted Claims of the '988 Patent.

707. For all these reasons, it is my opinion that none of the FeCo layers in the [REDACTED] write heads form "a structure consisting of unequal volumes or unequal amounts of the bcc-d variants of a six variant system" (*i.e.*, "a symmetry broken structure").

(ii) Under LMS's erroneous construction of "variant," the FeCo layers contain many more than six bcc-d variants

708. As I explained above, identifying a "bcc-d variant" requires identifying three things: (1) a bcc-d(110) crystal; (2) the underlying (111) hexagonal template crystal on which that bcc-d(110) crystal was grown; and (3) the orientation of the bcc-d(110) crystal relative to the template crystal.

709. Unable to show any underlying (111) hexagonal template crystals, Drs. Coffey and Clark ignore this requirement. Drs. Coffey and Clark implicitly—and incorrectly—construe "variant" so as to not require proof of any underlying (111) hexagonal template crystal. In particular, Drs. Coffey and Clark apparently have taken the position that *any* bcc-d(110) crystal is a "variant" (whether grown on an underlying (111) hexagonal template crystal or not), and two bcc-d(110) crystals with different orientations relative to each other are two different "variants." (*See, e.g.*, Clark, ¶ 198; Coffey, ¶ 336.)

710. Although I disagree that a "bcc-d variant" merely refers to any bcc-d(110) crystal, in this section (IX.B.2(a)(ii)) I will apply Dr. Coffey's and Dr. Clark's flawed understanding of "variant" to show that, under their erroneous interpretation of "variant," more than six bcc-d variants exist in the accused FeCo layers based on their own data.

a) Microbeam Diffraction Data

711. In describing Figure 109, Dr. Clark states that "Figure 109 shows an example diffraction pattern with **two crystallites both in the (110)_{BCC} orientation**,

rotated about their common $[110]_{\text{BCC}}$ direction by $\sim 70.53^\circ$. This is also the separation of two variants in the Kurdjumov-Sachs orientation.” (Clark, ¶ 198.)

712. Dr. Clark apparently contends that Figure 109 shows two variants because it shows two $(110)_{\text{BCC}}$ crystallites. He contends that these two variants—these two $(110)_{\text{BCC}}$ crystallites—have a Kurdjumov Sachs-orientation because they are oriented roughly 70.53 degrees from one another. (*But see, e.g.*, Clark, ¶ 111 (claiming that 11 degrees “is also the separation of two variants in the Kurdjumov-Sachs orientation”); *id.* at ¶ 154 (claiming that 12 degrees is “the separation of two variants in the Kurdjumov-Sachs orientation”).)

713. Dr. Clark’s analysis therefore posits that each of these $(110)_{\text{BCC}}$ crystallites is a “variant.” As I explained above, this is an erroneous understanding of “variant,” because not all $(110)_{\text{BCC}}$ crystallites are variants. Specifically, in order to identify a “variant,” one *must* identify both a $(110)_{\text{BCC}}$ crystallite *and* the underlying (111) hexagonal template crystal.

714. Nevertheless, if one applies Dr. Clark’s understanding that any $(110)_{\text{BCC}}$ crystallite in a microbeam diffraction pattern is a “variant,” then Dr. Clark’s own microbeam diffraction patterns show more than six $(110)_{\text{BCC}}$ crystallites with different orientations—and therefore more than six “variants.” To the extent Dr. Clark contends that each $(110)_{\text{BCC}}$ crystallite is a “variant,” Dr. Clark’s own microbeam diffraction patterns show more than six “variants” in each FeCo layer. Because a “symmetry broken structure” requires a “six variant system,” a layer containing more than six “variants” cannot form a “symmetry broken structure.”

715. Indeed, Figures 107-110 alone show more than six $(110)_{\text{BCC}}$ crystallites—and therefore more than six “variants” under Dr. Coffey’s and Dr. Clark’s erroneous interpretation of that term.

716. I note Dr. Clark’s dark field image data measurements, which I discuss below, also show more than six variants under his erroneous interpretation of “variant.”

717. Because Dr. Clark’s own microbeam diffraction data shows that the FeCo layers of the measured SBR8DK sample contain more than six $\text{bcc}(110)$ crystallites

(“variants,” according to him), the FeCo layers cannot form a “symmetry broken structure.”

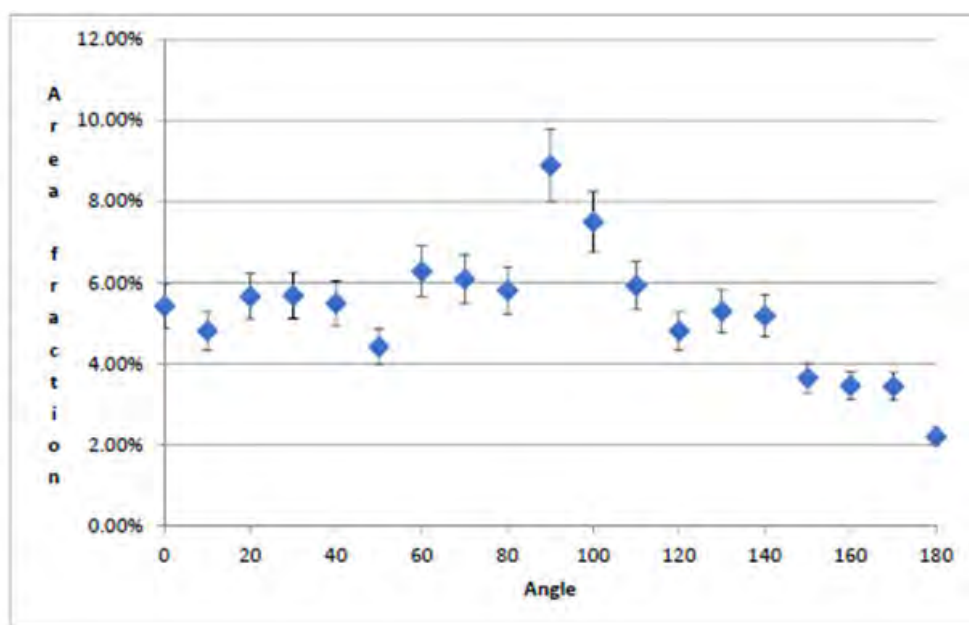
b) Dark Field Image Data

718. Dr. Coffey argues that “I also understand that dark field image analysis of samples SBRD8K show symmetry breaking in the lower layer of FeCo in the write pole.” (Coffey, ¶ 339.)

719. Dr. Clark took dark field image measurements on the SBR8DK write head sample. Specifically, Dr. Clark states that “a dark field image of an area of the lower FeCo layer is obtained . . . Where crystallites show up bright in the dark field image, in indicates that their {200} planes are oriented so as to diffract into the direction enclosed by the objective aperture.” (Clark, ¶ 203.)

720. For sample SBRD8K, Dr. Clark plots the “area fraction of white crystallites vs. angle” in Table 3 and Figure 117, which I reproduce below:

Angle	%Area
0	1.994
10	1.769
20	2.08
30	2.089
40	2.018
50	1.624
60	2.308
70	2.238
80	2.134
90	3.271
100	2.758
110	2.18
120	1.769
130	1.947
140	1.905
150	1.341
160	1.27
170	1.264
180	0.807



721. Dr. Coffey argues that Dr. Clark’s “dark field imaging analysis provides information on the fraction of crystallites with their easy axes substantially aligned toward each measured orientation and, *consequently, shows the presence of unequal amounts of variants* . . . because a greater amount of bcc-d crystallites are composed of

variants with their easy axis aligned perpendicular to the long-axis of the write head (parallel to the ABS) than in other directions.” (Coffey, ¶ 340.)

722. According to Dr. Clark’s Figure 117 (his dark field imaging data), there appears to be a greater amount of bcc-d crystallites aligned at 0 and 180 degrees than in other directions. Dr. Coffey argues that this shows that bcc-d crystallites of different orientations—“variants”—exist in unequal amounts in the FeCo layer. (Coffey, ¶ 340.) Dr. Coffey takes the position that these bcc-d crystallites with different orientations are “variants” and that Figure 59 shows these “variants” exist in unequal amounts. (*Id.*)

723. But Figure 117 shows bcc-d crystallites with more than six different orientations. Because none of the area fractions is “0,” Figure 117 indicates that there exist FeCo crystallites with their $\langle 200 \rangle$ directions aligned at 0 degrees, 10 degrees, 20 degrees, 30 degrees, 40 degrees, 50 degrees, 60 degrees, 70 degrees, 80 degrees, 90 degrees, 100 degrees, 110 degrees, 120 degrees, 130 degrees, 140 degrees, 150 degrees, 160 degrees, and 170 degrees. Under Dr. Clark and Dr. Coffey’s expansive and erroneous interpretation of “variants,” each of these crystallites is oriented differently and thus is a different “variant.” Under Dr. Clark and Dr. Coffey’s expansive interpretation and erroneous of “variants,” Figure 117 shows far more than six variants in the measured FeCo layer.

724. Because Dr. Clark’s own dark field imaging data show that the measured FeCo layer in the SBRD8K sample contains more than six “variants” (under Dr. Clark’s and Dr. Coffey’s erroneous and expansive definition of “variants”), the FeCo layer cannot and does not form a “symmetry broken structure.”

725. I also note that Dr. Clark’s dark field imaging is not a reliable technique for determining unequal amounts or unequal volumes of variants. According to the ’988 Patent, the proper technique for assessing a symmetry broken structure is a *pole figure*. (See, e.g., ’988 Patent, FIG. 14.) Nowhere does the ’988 Patent contemplate or even mention assessing a “symmetry broken structure” using dark field imaging techniques. Nowhere does Dr. Clark or Dr. Coffey perform (let alone analyze) any pole figure data for any of the accused Seagate products.

726. Dr. Clark's dark field imaging is also flawed because it is overinclusive in the crystallites it measures. Specifically, Dr. Clark's dark field image data is only meaningful to the extent it records the orientation of bcc(110) crystallites—and not other bcc-d crystallites. That is not the case here. Due to how Dr. Clark ran his dark field image measurement (namely, by selecting to focus on the 200 ring), he counts not only bcc(110) crystallites *but also* bcc(100) crystallites (as well as other possible crystallite orientations such as (012) and (013)).

727. In other words, both the bcc(110) and bcc(100) crystallite orientations will necessarily contribute scattering to the 200 ring. As a result, Dr. Clark's dark field imaging is flawed, and it is unreasonable to argue that there exists unequal amounts of bcc(110) crystallites when the data inherently counts both bcc(110) and bcc(100) crystallites.

728. Dr. Clark's dark field imaging is flawed in several other respects as well. These flaws cast doubt on the accuracy and reliability of his dark field image data, and also invalidate many of Dr. Clark's and Dr. Coffey's conclusions based on the dark field data. For example, Dr. Clark double counts certain pixels (*i.e.*, the same pixels are counted as "white" for multiple different angles within 180 degrees).

729. Moreover, the area fraction of crystallites at 0 and 180 degrees should be the same, yet they are not. (*See, e.g.*, Clark, Figure 117 (1.994% area at 0 degrees vs. 0.807% area at 180 degrees).) The pronounced discrepancy between the area fraction of crystallites at 0 and the area fraction of crystallites at 180 suggests serious flaws with how Dr. Clark performed his dark field measurements.

730. In addition, the aperture Dr. Clark used to generate his dark field image data was not limited to the 200 ring (as Dr. Clark claims), but appears to have picked up diffraction from other rings. (*See, e.g.*, Clark, Figure 113 (clearly depicting multiple rings in the aperture).) By including additional rings in the aperture, the resulting dark field image will include crystallites besides those that contribute to the 200 ring.

731. This is *another* reason why Dr. Clark's dark field image data inherently counts more than just bcc(110) crystals. As discussed above, Dr. Clark's decision to focus on the 200 ring already results in him counting non-(110) crystals in the dark field

data. But due to his flawed aperture, Dr. Clark in fact focused on multiple rings (not just the 200 ring), leading him to count *even more* non-(110) crystals in the dark field data.

732. It is unreasonable to argue that there exists unequal amounts of bcc(110) crystallites based on data that inherently counts non-(110) crystallites. I note this also renders all of Dr. Coffey’s magnetic calculations mathematically flawed and incorrect, because those calculations assume that Dr. Clark’s dark field image data counts only bcc(110) crystals, when in fact they do not. (*See* Section IX.B.2(c)(ii), *infra*.)

(b) “having an anisotropy energy density function with only a single maximum and a single minimum as the magnetization angle is rotated by 180 degrees from a physical axis” (uniaxial)

733. Dr. Coffey argues that “it is my opinion that the lower FeCo layer in the [REDACTED] Products is uniaxial as a result of the structure therein being symmetry broken, in accordance with the Court’s claim construction of claim 1 of the ‘988 patent.” (Coffey, ¶ 341.)

734. In my opinion, Dr. Coffey fails to show that any FeCo layer in the [REDACTED] Products is “uniaxial”—*i.e.*, that any FeCo layer “ha[s] an anisotropy energy density function with only a single maximum and a single minimum as the magnetization angle is rotated by 180 degrees from a physical axis.”

(i) Dr. Coffey cites no magnetic data whatsoever in his report

735. The ‘988 Patent defines “uniaxial” as follows:

Here, we define a “uniaxial” anisotropy to exist if the anisotropy energy density function only contains a single maximum and a single minimum as the magnetization angle, θ , is rotated by 180 degrees from a physical axis.

(‘988 Patent at 1:56-60.)

736. The Court construed “uniaxial” to mean “having an anisotropy energy density function with only a single maximum and a single minimum as the magnetization angle is rotated by 180 degrees from a physical axis.”

737. According to the '988 Patent, uniaxial materials and uniaxial thin films have various useful applications. (*See, e.g.*, '988 Patent at 2:8-19 (“[T]he device is constructed so that the applied field is directed along the hard magnetic axis of a uniaxial magnetic material.”); *id.* at 3:9-10 (criticizing non-uniaxial materials: “Multi-axis anisotropy materials always switch via wall motion and so suffer losses”); *id.* at 3:64-65 (“Uniaxial anisotropy is needed in such a device to achieve low losses.”).)

738. In describing its invention, the '988 Patent claims that “[m]aterials and device processing to achieve a desired orientation or anisotropy is commonly difficult and sometimes impossible, perhaps because heretofore the mechanism for achieving anisotropic orientation has not been well understood.” ('988 Patent at 1:62-66.) The '988 Patent purports to solve the problem of creating uniaxial thin films as follows: “[b]y the selection and growth of a very special exchange coupled subset of these six orientational variants a symmetry broken *uniaxial magnetic thin film* is obtained.” ('988 Patent at 14:52-55.) Thus, the '988 Patent purports to have invented a mechanism for achieving uniaxial magnetic anisotropy in certain materials—specifically, magnetic bcc-d layers. (*See* '988 Patent, Claim 1.)

739. “Uniaxial” is a magnetic property. Assessing whether a magnetic bcc-d layer is “uniaxial” requires magnetic testing and analysis of magnetic data. Assessing whether a magnetic bcc-d layer forms a “uniaxial” structure requires magnetic testing and analysis of magnetic data.

740. For example, the '988 Patent describes taking magnetic measurements of certain samples to assess whether those samples featured a uniaxial magnetic layer: “Magnetic response curve measurements were made for these samples. . . . FIG. 15 shows the M_x and M_y versus H_x response of one of the two variant exchange coupled, uniaxial symmetry broken samples” ('988 Patent at 43:49-50, 43:58-61.) The '988 Patent further states that “FIG. 15 clearly shows a non-linear uniaxial type of response function when the sample was driven into saturation and uniaxial result similar to the ideal of FIG. 2.” ('988 Patent at 44:15-18; *see also id.* at 14:24-28 (“FIG. 15 shows a uniaxial magnetic hard axis response, M_x, function, and easy axis response function,

My, data to an applied field along the hard axis, Hx, for an Fe ($K_1 > 0$) sample prepared with the easy axis along the hexagonal template $\langle 112 \rangle$ direction.”.)

741. FIG. 15 of the '988 Patent is data in the form of a “magnetic response curve measurement” (commonly referred to as a hysteresis loop) that was generated using a vibrating sample magnetometer (VSM). FIG. 15 of the '988 Patent is shown below:

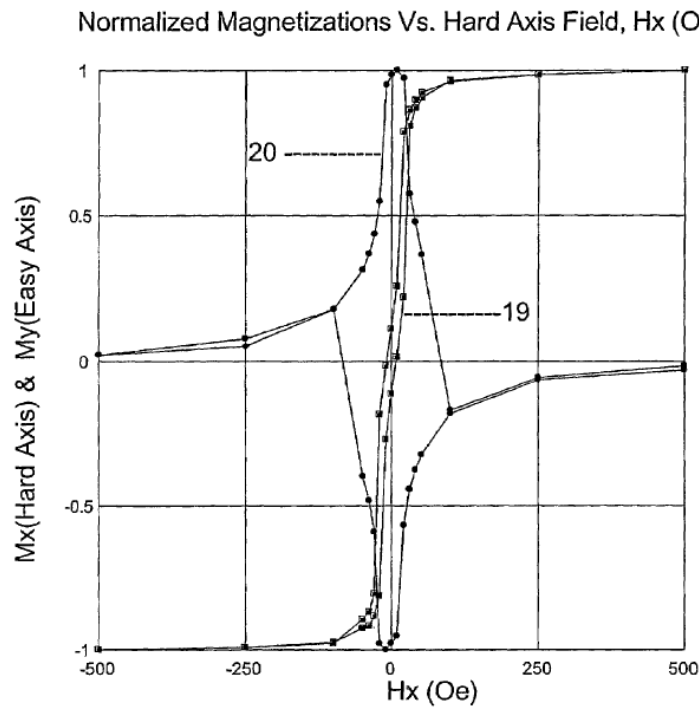


Figure 15

742. Because “uniaxial” is a *magnetic* property, assessing whether a structure has uniaxial anisotropy necessarily requires *magnetic* measurements and an analysis of *magnetic* data. The '988 Patent took magnetic measurements (VSM) to generate the magnetic data (hysteresis loop) seen in FIG. 15.

743. Neither Dr. Coffey nor Dr. Clark cites, discusses, or analyzes *any actual magnetic measurements whatsoever* in their reports.

744. The '988 Patent is a *magnetic* patent. It bears the title “*Magnetic Material Structures, Devices, and Methods.*” The first sentence of the specification states: “*This invention is directed to magnetic material structures, methods for making*

magnetic material structures, and devices made from *magnetic* material structures.”
(’988 Patent 1:8-10.) The “uniaxial” limitation of claim 1 is a *magnetic* claim limitation.

745. Yet neither Dr. Coffey nor Dr. Clark cites, discusses, nor analyzes *any magnetic measurements whatsoever* in their reports. Without such magnetic measurements, Dr. Coffey has no basis to conclude that the accused Seagate products meet the “uniaxial” limitation of claim 1. In my opinion, no reasonable scientist would accept Dr. Coffey’s conclusions about “uniaxial”—a *magnetic* claim limitation—without any magnetic measurements or data in his report.

746. Indeed, LMS apparently knew that magnetic testing was required to assess the “uniaxial” claim limitation—yet neither Dr. Coffey nor Dr. Clark cite any such magnetic testing in their reports. In its Amended Infringement Contentions against Seagate—dated November 29, 2017²¹—LMS wrote that:

[I]t is anticipated that magneto-optic Kerr effect (“MOKE”) measurements of plan-view samples of the FeCo-based layer of the write head will yield M-H loops at various angles of measurements. Upon obtaining multiple measurements at regular angular intervals, the magnetic anisotropy energy density function associated with the FeCo-based layer can be calculated and will confirm only a single maximum and a single minimum as the magnetization angle is rotated by 180 degrees from a physical axis.

(LMS’s Amended Infringement Contentions Ex. 2A, at 27.)

747. “MOKE” is a type of magnetic measurement that can be used to generate M-H loops (a.k.a. hysteresis loops or magnetization response curves). Had Dr. Coffey’s report contained the MOKE measurements LMS described in its amended infringement contentions, one might reasonably analyze them to assess whether they correspond to a uniaxial magnetic layer in the accused Seagate products. But Dr. Coffey’s report contained no MOKE measurements—or any magnetic measurements for that matter. It is unreasonable for Dr. Coffey to conclude that the accused Seagate products have a

²¹ I note that LMS served its Amended Infringement Contentions *after* the Court issued its claim construction order construing, among other things, the term “uniaxial.”

“uniaxial” FeCo layer when he conducts no magnetic measurements and analyzes no magnetic data to support that conclusion.

748. I understand that LMS asked Seagate to produce monitor wafers containing the accused [REDACTED] write heads, purportedly so that LMS could perform magnetic testing on those [REDACTED] write head materials. I understand that Seagate produced the monitor wafers to LMS as requested before the close of fact discovery. I understand this gave LMS over two months in which to perform magnetic measurements on these monitor wafers. Either Dr. Coffey did not take any magnetic measurements of the accused FeCo layers, or he took magnetic measurements and omitted them from his report.

749. In sum, it is not appropriate, reliable, or scientifically valid to conclude that an FeCo layer is uniaxial, or that an FeCo layer forms a “uniaxial” structure, without measuring the FeCo layer’s actual magnetic properties. Dr. Coffey and Dr. Clark do not cite any magnetic measurements of any FeCo layers—let alone magnetic measurements showing an FeCo layer having an anisotropy energy density function with only a single maximum and a single minimum as the magnetization angle is rotated by 180 degrees from a physical axis.

750. Dr. Coffey and Dr. Clark therefore fail to show that any FeCo layer in the accused [REDACTED] Products is “uniaxial.” Dr. Coffey and Dr. Clark fail to show that any FeCo layer in the accused [REDACTED] Products forms a “uniaxial” structure.

(ii) **Dr. Coffey erroneously conflates “uniaxial” with “uniaxial symmetry broken structure”—completely ignoring all other sources of magnetic anisotropy**

751. Rather than take magnetic measurements of the accused FeCo layers, Dr. Coffey instead purports to theoretically model a single source of magnetic anisotropy in the FeCo layers—namely, the layers’ magnetocrystalline anisotropy. Dr. Coffey concludes that because the FeCo layers purportedly have a uniaxial magnetocrystalline anisotropy (they do not), that is somehow the same as showing that the FeCo layers are uniaxial. In my opinion, Dr. Coffey inappropriately conflates the Court’s construction of “uniaxial” with “uniaxial symmetry broken structure.”

752. As I explain in the Technology Background—and as Dr. Coffey acknowledges—there are many sources of magnetic anisotropy, including shape anisotropy, strain anisotropy, magnetocrystalline anisotropy, and atomic pair ordering.

753. Whether a material is “uniaxial” involves the interaction of these different sources of magnetic anisotropy. In other words, “uniaxial” refers to a material where *the* anisotropy energy density function of the material contains only a single minimum and a single maximum as the magnetization is rotated by 180 degrees. A material has only one anisotropy energy density function: the total anisotropy due to shape anisotropy, strain anisotropy, magnetocrystalline anisotropy, atomic pair ordering, among other things.

754. When one takes a magnetic measurement of a material one is measuring (directly or indirectly) the anisotropy energy density function of the material, *i.e.*, the total magnetic anisotropy. One can conclude that a material is “uniaxial” only if that anisotropy energy density function contains only a single minimum and a single maximum within a 180 degree rotation. Because Dr. Coffey never takes any magnetic measurements and never considers the anisotropy energy density function of any FeCo layer, his conclusion that any FeCo layer is “uniaxial” is flawed and unreasonable.

755. Rather than take magnetic measurements of the FeCo layers or consider the anisotropy energy density function of those layers, Dr. Coffey purports to theoretically model a single source of magnetic anisotropy in the FeCo layers—namely, the layers’ magnetocrystalline anisotropy. According to Dr. Coffey’s model, the FeCo layers feature a uniaxial magnetocrystalline anisotropy—a point on which he is mistaken. (*See* Section IX.B.2(c), *infra.*) But even assuming the FeCo layers featured a uniaxial magnetocrystalline anisotropy, it simply does not follow that the FeCo layers are therefore “uniaxial.” Because the anisotropy energy density function of the FeCo layers involves multiple components—multiple sources of anisotropy—one cannot ignore these other components when opining about whether the FeCo layers form a “uniaxial” structure. Yet that is what Dr. Coffey does.

756. A simple analogy exposes the flaw in Dr. Coffey’s reasoning. Dr. Coffey’s reasoning is analogous to reasoning that a paint mixture containing several

different colors must be blue because one of the component paint colors is blue. That reasoning is flawed because one cannot ignore the other color components if one is to validly conclude anything about the color of the paint mixture. For example, if the paint mixture contains equal parts blue and yellow, the mixture is not blue, but green.

757. Shape anisotropy, in particular, plays a major role in the magnetic anisotropy of many thin film materials, including the FeCo layers at issue here. I note that Dr. Coffey concedes this fact. In discussing shape anisotropy, Dr. Coffey writes: “[F]or films having in-plane dimensions only 100 times greater than their thickness, the in-plane shape dependent demagnetization effects can be significant. . . . In this range of dimensions and for thin films that are not circular, the in-plane anisotropy effects can be significant to the magnetization directions of an object.” (Coffey, ¶ 50.)

758. The FeCo layers at issue here are “films having in-plane dimensions only 100 times greater than their thickness.” (Coffey, ¶ 50.) As Dr. Coffey acknowledges, “[i]n this range of dimensions and for thin films that are not circular, the in-plane shape anisotropy effects can be significant to the magnetization directions of an object.” (*Id.*)

759. Despite acknowledging the “significant” impact of shape on the magnetic anisotropy of the FeCo layers, Dr. Coffey’s report contains no analysis or consideration of those layers’ shape anisotropy—or for that matter, any source of magnetic anisotropy other than magnetocrystalline anisotropy.

760. Thus, to the extent Dr. Coffey concludes that the FeCo layers are “uniaxial” without considering any of these other sources of magnetic anisotropy, that conclusion is flawed and unreasonable. To the extent Dr. Coffey concludes that the FeCo layers form a “uniaxial” structure without considering any of these other sources of magnetic anisotropy, that conclusion is flawed and unreasonable.

761. I note that it would have been relatively straightforward for Dr. Coffey to have considered all these different sources of anisotropy—namely, by taking actual magnetic measurements of the accused FeCo layers. Such magnetic measurements would have measured (directly or indirectly) the magnetic anisotropy of the layers from all sources. That is how the ’988 Patent assessed the magnetic anisotropy of its samples: by taking VSM measurements and analyzing the resulting M-H loops. (*See, e.g.*, ’988

Patent, FIG. 15.) That is how LMS previously intended to assess the magnetic anisotropy of the FeCo layers, according to its amended infringement contentions: by taking MOKE measurements and analyzing the resulting M-H loops. (LMS's Amended Infringement Contentions Ex. 2A, at 27.) Yet that is not what Dr. Coffey has done.

762. In sum, Dr. Coffey attempts to theoretically model the magnetocrystalline anisotropy of the FeCo layers and argues that according to his (deeply flawed) calculations, the magnetocrystalline anisotropy is uniaxial. In a leap of logic he then argues that because the magnetocrystalline anisotropy is uniaxial, the FeCo layers must be uniaxial. That simply does not follow. Shape anisotropy exerts a significant influence on the magnetic anisotropy of the FeCo layers. It is therefore flawed and unreasonable for Dr. Coffey to conclude that the magnetic anisotropy energy density function of the FeCo layers contains only a single minimum and maximum within 180 degrees without having considered, *e.g.*, shape anisotropy, strain anisotropy, and atomic pair ordering. Moreover, both the '988 Patent and LMS's latest infringement contentions in this case make clear that the "uniaxial" limitation should have been assessed with magnetic measurements, none of which appear anywhere in Dr. Coffey's report. Either Dr. Coffey did not take any magnetic measurements of the accused FeCo layers, or he took magnetic measurements and omitted them from his report.

763. For all these reasons, Dr. Coffey's opinion that any FeCo layer in the accused [REDACTED] Products exhibits "uniaxial" anisotropy is flawed and unreasonable. For all these reasons, Dr. Coffey's opinion that any FeCo layer in the accused [REDACTED] Products forms a "uniaxial" structure is flawed and unreasonable.

(iii) In lieu of relying on any magnetic data, Dr. Coffey erroneously relies on the doctrine of equivalents

764. According to Dr. Coffey: "That the lower FeCo layer may have other contributors to its magnetic anisotropy, such as shape anisotropy or stress anisotropy, does not change the fact that the [REDACTED] Products achieve uniaxial magnetic properties as a result of symmetry breaking in the FeCo layer." (Coffey, ¶ 366.)

765. As I explained above, that is incorrect. It is unreasonable for Dr. Coffey to conclude that the “[REDACTED] Products achieve uniaxial magnetic properties” without any magnetic measurements or data to suggest that [REDACTED] Products are in fact uniaxial. Attempting to cloak this shortcoming under the guise of the doctrine of equivalents does not alter the basic fact that to prove “uniaxial magnetic properties” (Coffey, ¶ 366), one necessarily must perform magnetic measurements and analyze magnetic data.

766. According to Dr. Coffey: “I understand that Seagate may argue that, contrary to the Court’s construction of ‘uniaxial,’ claim 1 requires that the bcc-d layer must exhibit uniaxial magnetic anisotropy due to symmetry breaking that dominates any other anisotropy that may be present or is the sole source of anisotropy.” (Coffey, ¶ 363.)

767. To be clear: that is not my opinion, nor is it Seagate’s position. My opinion simply is that one cannot reasonably conclude that a bcc-d layer exhibits “uniaxial” anisotropy without actually measuring the layer’s magnetic properties. One cannot reasonably conclude that a bcc-d layer exhibits “uniaxial anisotropy” solely by modeling a single source of anisotropy (magnetocrystalline anisotropy) to the exclusion of all others. Doing so is contrary to the well-accepted physics of magnetic anisotropy. (See, e.g., B.D. Cullity and C.D. Graham, INTRODUCTION TO MAGNETIC MATERIALS, 2ND EDITION (2009), at 197-98.) Doing so also improperly conflates the Court’s construction of “uniaxial” with the Court’s construction of “uniaxial symmetry broken structure” (causation).

768. In my opinion, Dr. Coffey fails to show that any FeCo layer in any [REDACTED] Product is “uniaxial.” Dr. Coffey fails to show that any FeCo layer in any [REDACTED] Product forms a “uniaxial” structure. In my opinion, an FeCo layer that is not uniaxial does not perform substantially the same function in substantially the same way to achieve substantially the same result as an FeCo layer that is uniaxial. I note that although Dr. Coffey appears to contend otherwise, his contention is entirely conclusory. (See Coffey, ¶ 364.) For example, Dr. Coffey does not identify or explain how an FeCo

layer that is not uniaxial serves substantially the same function in substantially the same way to achieve substantially the same result as an FeCo layer that is uniaxial.

769. Indeed, the '988 Patent draws a sharp distinction between uniaxial and non-uniaxial materials, criticizing the latter's use in certain applications as leading to energy losses. (*See, e.g.*, '988 Patent at 2:20-22 ("For example, a material, which has bi-axial anisotropy . . . will exhibit hysteresis and losses."); *id.* at 3:9-10 ("Multi-axis anisotropy materials always switch via wall motion and so suffer losses.").) The '988 Patent itself therefore contradicts Dr. Coffey's claim that non-uniaxial materials are somehow equivalent to uniaxial materials.

770. I have also considered Dr. Coffey's citations and characterizations of Seagate documents and deposition testimony on this issue (*see* Coffey ¶¶ 333-369) and find his characterizations of many of these documents to be flawed and unreasonable. Although Dr. Coffey string cites without explanation dozens of Seagate documents and testimony in ¶¶ 333-369 of his report, none actually support his conclusion that the FeCo layer forms a "uniaxial" structure—*i.e.*, a structure "having an anisotropy energy density function with only a single maximum and a single minimum as the magnetization angle is rotated by 180 degrees from a physical axis." For example, none of the cited Seagate documents and deposition testimony show any anisotropy energy density function for any FeCo layer, let alone an FeCo layer having an anisotropy energy density function with only a single maximum and a single minimum as the magnetization angle is rotated by 180 degrees from a physical axis.

771. For all these reasons, Dr. Coffey's opinion that any FeCo layer in the accused [REDACTED] Products meets the "uniaxial" claim limitation, either literally or under the doctrine of equivalents, is unreasonable, unsupported, and incorrect.

(c) “a structure that is uniaxial as a result of the structure being symmetry broken” (uniaxial symmetry broken structure)

772. In my opinion, the FeCo layers in the [REDACTED] products do not form a “uniaxial symmetry broken structure”—*i.e.*, they do not form “a structure that is uniaxial as a result of the structure being symmetry broken.”

773. Dr. Coffey states that “it is my opinion that the lower FeCo layer of FeCo in the [REDACTED] Products is uniaxial because the anisotropy energy density function I calculated solely due to the measured broken symmetry in representative samples of the [REDACTED] Products has a single maximum and a single minimum as the magnetization angle is rotated by 180 degrees from a physical axis.” (Coffey, ¶ 334.)

774. In my opinion, Dr. Coffey’s theoretical anisotropy calculation is severely flawed and unreliable in multiple respects.

775. First, although Dr. Coffey claims that he calculated “the anisotropy energy density function [I] solely due to the measured broken symmetry,” that statement is factually incorrect. (Coffey, ¶ 334.)

776. A “symmetry broken structure” consists of unequal amounts or unequal volumes of the bcc-d variants of a six-variant system. These six bcc-d variants refer to bcc-d(110) crystals oriented in one of six orientations relative to an underlying (111) hexagonal template crystal. Moreover, any crystals that are not (110) are not “variants” and do not comprise the “symmetry broken structure” of the ’988 Patent. Dr. Clark’s diffraction measurements consistently show that the measured FeCo layers include substantial amounts of non-(110) crystals—including, for example, bcc-d(100) crystals and bcc-d(211) crystals. (*See* Section IX.B.2(a)(i).c, *supra*.) The magnetic anisotropy associated with these non-(110) crystals would not be magnetic anisotropy that results from a “symmetry broken structure.”

777. In order for Dr. Coffey to claim that “the anisotropy energy density function [he] calculated solely due to the measured broken symmetry . . . has a single maximum and a single minimum as the magnetization angle is rotated by 180 degrees

from a physical axis,” he would have needed to calculate the anisotropy energy density function from only bcc-d(110) crystals—and *no other bcc-d crystals*. But Dr. Coffey’s calculations in fact count non-(110) bcc-d crystals, uprooting the entire premise of his theoretical calculations. (*See* Section IX.B.2(c)(ii), *infra*.)

778. Second, in addition to erroneously counting non-(110) bcc-d crystals in his anisotropy calculation, Dr. Coffey also ignores the empirical data as measured by Dr. Clark. Although Dr. Coffey purports to rely on Dr. Clark’s dark field image measurements, he ultimately disregards those measurements. Specifically, when Dr. calculates anisotropy he does not use any of Dr. Clark’s empirically measured data. Rather than use actual measured data as the input to his anisotropy calculation, Dr. Coffey substitutes in data that Dr. Coffey wished Dr. Clark had measured—not what Dr. Clark actually measured. (*See* Section IX.B.2(c)(iii), *infra*.)

779. Third, there are many serious additional flaws with Dr. Coffey’s anisotropy model. Dr. Coffey makes unwarranted assumptions, errors in calculation, and unfounded conclusions. I discuss the other errors in Dr. Coffey’s anisotropy model in Section IX.B.2(c)(iv).

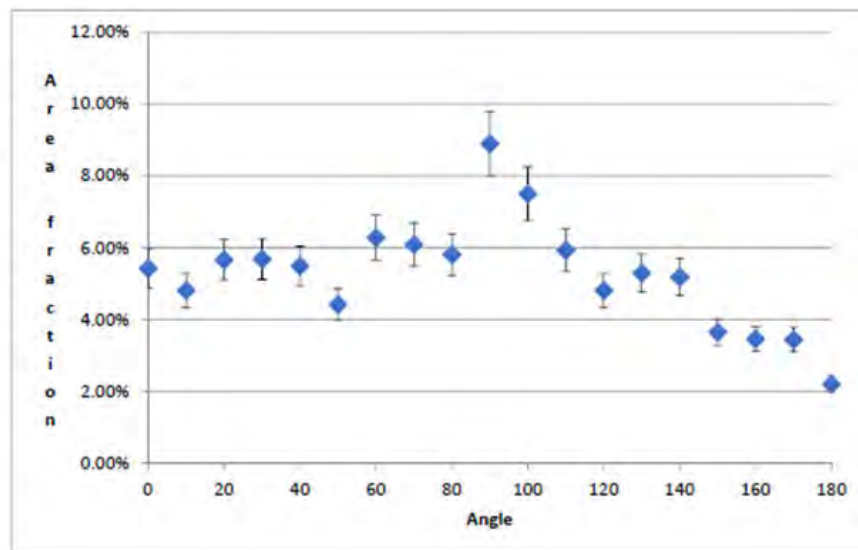
780. Dr. Coffey’s anisotropy calculation is flawed and unreliable for all these reasons. In my opinion, Dr. Coffey’s theoretical methodology for calculating anisotropy appears to be created solely for the purposes of this litigation. In my opinion, Dr. Coffey’s theoretical methodology for calculating anisotropy contains no testable hypothesis, has never been subject to peer review, has no known or potential rate of error, is not controlled by any scientific standards, is based on flawed and unreliable data, and is not reasonably grounded in established scientific methods.

(i) Overview of Dr. Coffey’s method of calculating anisotropy

781. Before discussing the numerous flaws with Dr. Coffey’s anisotropy calculation in more detail, I will summarize Dr. Coffey’s method for calculating what he erroneously claims to be the anisotropy caused by symmetry breaking. Dr. Coffey’s method can be broken down into a three-step process.

782. **Step 1.** Dr. Coffey plots the dark field image data from Dr. Clark, an example of which is shown below:

Angle	%Area
0	1.994
10	1.769
20	2.08
30	2.089
40	2.018
50	1.624
60	2.308
70	2.238
80	2.134
90	3.271
100	2.758
110	2.18
120	1.769
130	1.947
140	1.905
150	1.341
160	1.27
170	1.264
180	0.807



783. Dr. Coffey erroneously contends that this plot of the dark field image data shows that “[t]he area fraction for the (110) bcc, six-variant crystallites is not independent of direction, rather it shows a pronounced variation as a function of angle.” (Coffey, ¶ 342.) In other words, Dr. Coffey believes, erroneously, that this graph plots the relative amounts of bcc(110) crystal orientations in the measured FeCo layer when in fact it does not. (See Section IX.B.2(c)(ii), *infra*.)

784. **Step 2.** Given what he believes to be the relative amounts of bcc(110) crystal orientations, Dr. Coffey attempts to calculate the magnetocrystalline anisotropy of these crystals. Dr. Coffey states that “the anisotropy energy density function for bcc-d crystals in the (110) plane is set forth in Chikazumi and referenced in the ‘988 patent. . . . Specifically, the equation is:”

$$E_{110}(\theta) = K_1\left\{\left(\frac{1}{4}\right)\sin^4(\theta) + \sin^2(\theta)\cos^2(\theta)\right\} + K_2\left\{\left(\frac{1}{4}\right)\sin^4(\theta)\cos^2(\theta)\right\} \\ + \text{higher } K \text{ terms}$$

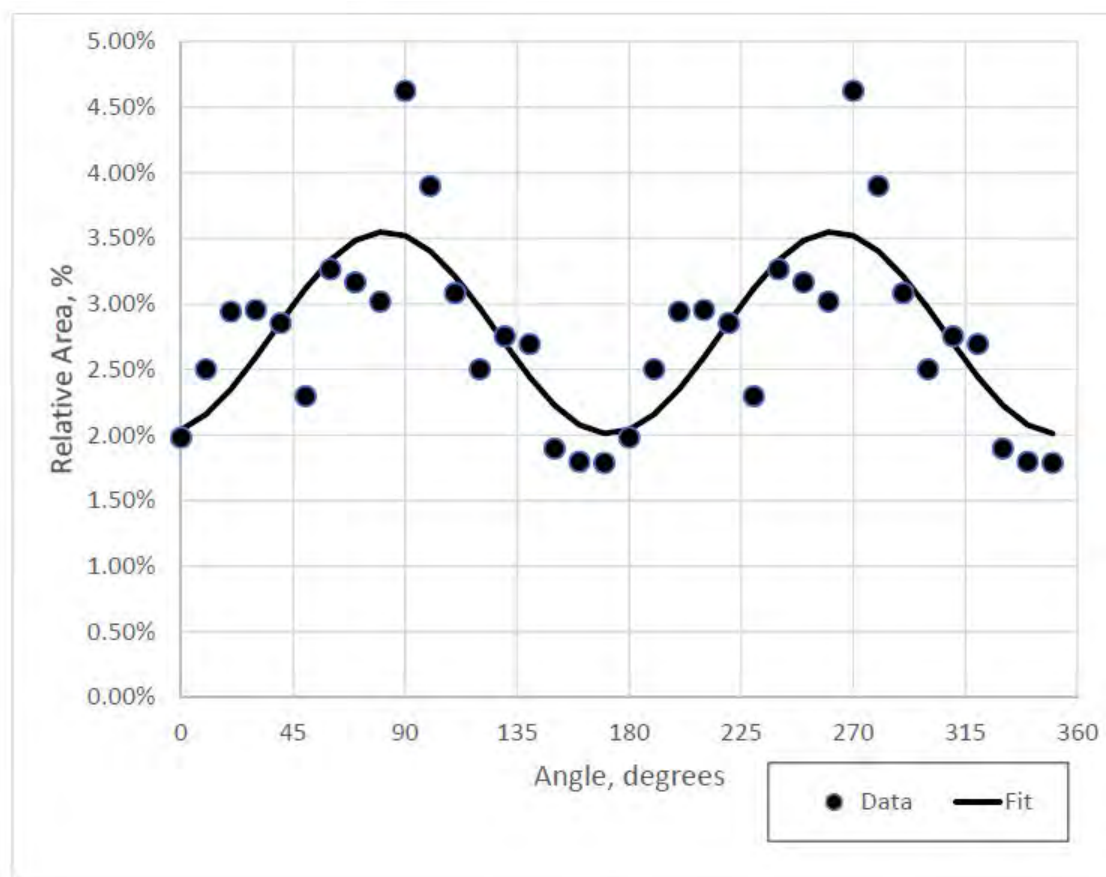
(Coffey, ¶ 343.)

785. Dr. Coffey relates the Chikazumi Equation to the dark field image data from Dr. Clark by writing that: “to determine the overall anisotropy energy density due

to the symmetry breaking evidenced in the lower FeCo layer in the [REDACTED] Products it is necessary to calculate the anisotropy energy density as an average over all the crystallites at different orientations in the sample.” (Coffey, ¶ 345.)

786. **Step 3.** With the dark field image data (which Dr. Coffey mistakenly believes to show the amounts of bcc(110) crystal orientations) and the Chikazumi Equation specifying the magnetocrystalline anisotropy of bcc(110) crystals, Dr. Coffey proceeds to calculate the anisotropy using the Chikazumi Equation. But rather than use the dark field image data from Dr. Clark as the input to the Chikazumi Equation, Dr. Coffey *discards* Dr. Clark’s measured data and replaces it with data forced to fit a perfect sinusoidal function. (Coffey, ¶¶ 342-347.)

787. The graph below is from Dr. Coffey’s report:

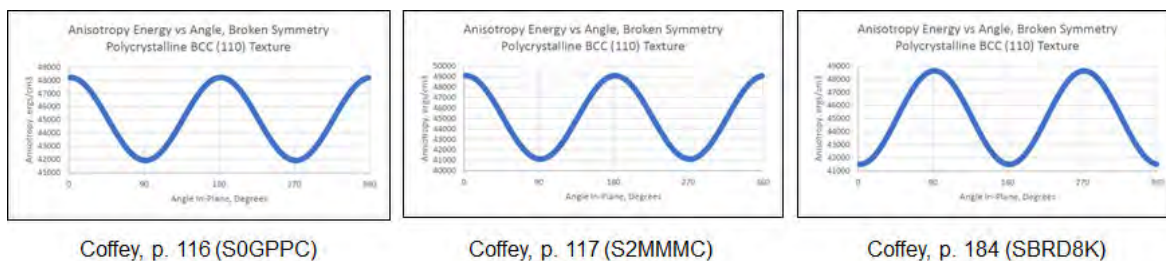


(Coffey, ¶ 342.)

788. The dots represent the empirical data as measured by Dr. Clark's dark field image experiments. But those dots are not the values Dr. Coffey uses to calculate the anisotropy. Instead, Coffey calculates anisotropy assuming that the crystal orientations fit *exactly* the superimposed sinusoidal curve shown above.

789. Dr. Coffey provides no reasonable justification for discarding Dr. Clark's empirical data in favor of conveniently smooth, perfect sinusoidal fit. (See Coffey, ¶ 342.) I have shown mathematically that any set of data, if forced to fit Dr. Coffey's perfectly smooth sinusoidal function, will *always* generate a uniaxial result when plugged into the Chikazumi Equation. (Ex. F.) In other words, by discarding Dr. Clark's empirically measured crystal distribution data and substituting in a sinusoidal crystal distribution, Dr. Coffey *guarantees* a uniaxial outcome.

790. Dr. Coffey then performs the anisotropy calculation using the Chikazumi Equation and plots the result. (Coffey, ¶ 347.) Because Dr. Coffey's methodology of substituting sinusoidal values for actual measured values guarantees him a uniaxial result, it comes as no surprise that Dr. Coffey's calculation yields a perfectly smooth, uniaxial energy density function for each of the samples "analyzed":



791. I note that all three energy density functions, although ostensibly calculated from three different samples, all fit a *perfect* \sin^2 function—*i.e.*, not only uniaxial, but uniaxial in the theoretical Stoner-Wohlfarth sense. (See, *e.g.*, '988 Patent at 2:63-66 ("Materials exhibiting the $\sin^2(\theta)$ energy density functional form are often referred to as having Stoner-Wohlfarth behavior after the famous ideal uniaxial single domain magnetization theory.")) This is not surprising since Dr. Coffey did not use any *actual* measured data for his analysis, but instead used data forced to fit a sinusoidal

function, such that his calculations were guaranteed to generate perfectly uniaxial energy density functions.

792. Having summarized Dr. Coffey's method for purportedly calculating the anisotropy from symmetry breaking, I now explain in more detail the numerous flaws with his analysis.

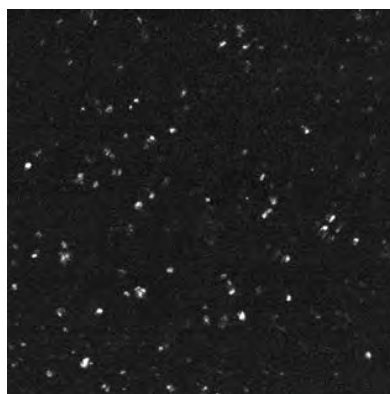
(ii) Dr. Coffey erroneously assumes that Dr. Clark's dark field image data depicts only bcc-d(110) crystals

793. Dr. Coffey's anisotropy calculation incorrectly assumes that the only crystals measured in Dr. Clark's dark field image data are bcc-d(110) crystals. Dr. Coffey calculates anisotropy using the Chikazumi Equation, which is an equation that describes the magnetic anisotropy energy density function of bcc-d(110) crystals—*but not any other kind of crystal*. The anisotropy energy density function of crystals with other orientations—such as a bcc-d(100) crystal—is *not* represented by the Chikazumi Equation. If one measured a sample containing bcc-d(100) crystals and calculated the anisotropy by applying the Chikazumi Equation, the result would be mathematically incorrect. Yet that is what Dr. Coffey does.

794. By focusing on the 200 ring in his dark field image measurements, Dr. Clark's dark field image data necessarily includes not only bcc-d(110) crystals but also bcc-d(100) crystals (as well as a number of other possible bcc-d crystal orientations). Put another way, the pixels that “light up” in the dark field image data correspond to both bcc-d(110) and bcc-d(100) crystals.²²

795. For example, the white pixels in the following dark field image data from Dr. Clark include both bcc-d(110) and bcc-d(100) crystals:

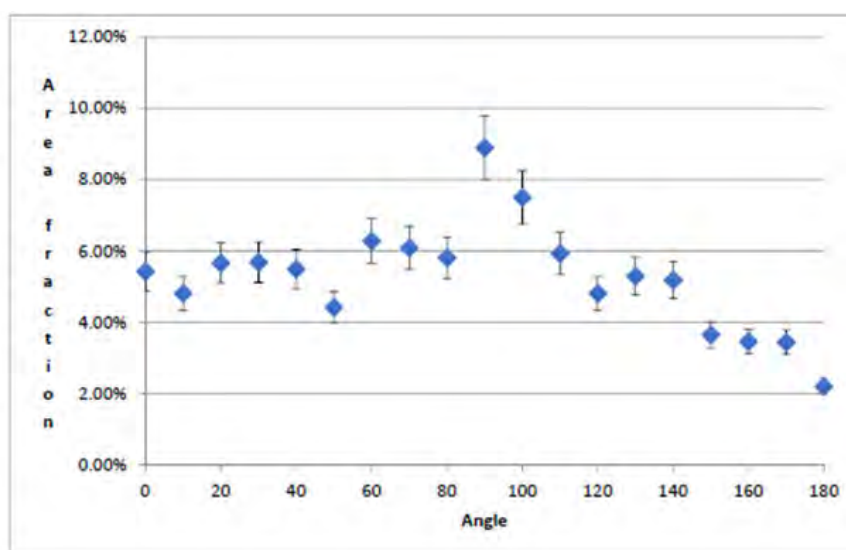
²² And likely other crystal orientations as well. As I note above, the aperture Dr. Clark used for his dark field imaging includes more than just the 200 ring. (*See* Section IX.B.2(a)(i)c, *supra*.) This results in even more non-(110) crystals being measured by Dr. Clark's dark field imaging. (*Id.*)



SBRD8K – 320-1

796. Dr. Clark's dark field image analysis plots the total amounts of bcc-d(110) crystals *and* bcc-d(100) crystals as a function of angle. The plot for SBRD8K is shown below:

Angle	%Area
0	1.994
10	1.769
20	2.08
30	2.089
40	2.018
50	1.624
60	2.308
70	2.238
80	2.134
90	3.271
100	2.758
110	2.18
120	1.769
130	1.947
140	1.905
150	1.341
160	1.27
170	1.264
180	0.807

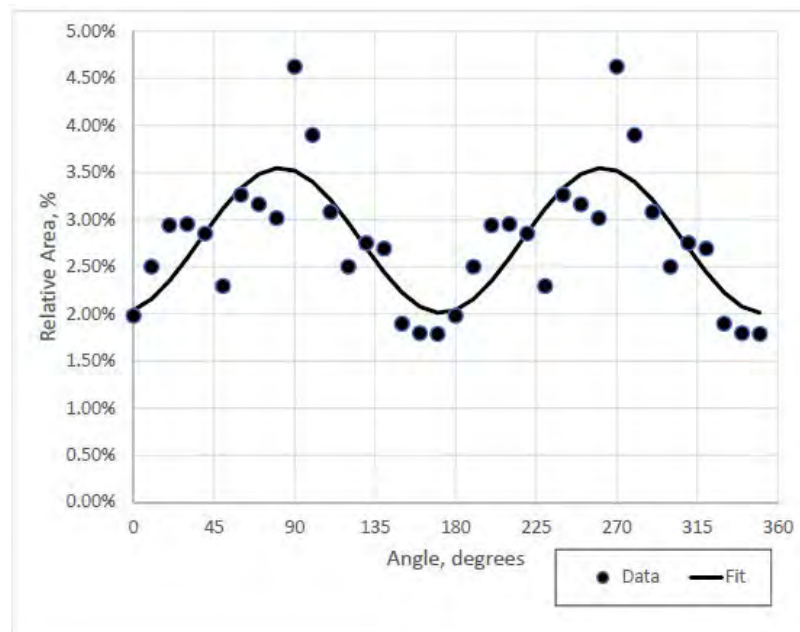


797. Although the plot says that 1.994% of the pixels “light up” at 0 degrees, that 1.994% of pixels includes *both* bcc-d(110) and bcc-d(100) crystals. For example, the 1.994% could be 1.5% bcc-d(110) and 0.494% bcc-d(100). Or it could be 0.494% bcc-d and 1.5% bcc-d(100). Based on the dark field image data alone, it is not possible to quantify the breakdown of bcc-d(100) and bcc-d(110) crystals at any given angle. What is clear, however, is that there exists significant amounts of bcc-d(100) crystals

throughout the accused FeCo layers—this is confirmed both by Dr. Clark’s microbeam diffraction data. (*See, e.g.*, Section IX.B.2(a)(i)c, *supra.*)

798. I also note that the sum of the total area from 0-170 degrees (or 10-180 degrees) is approximately 36%. This means that Dr. Clark’s dark field imaging counts only about 36% of the crystals in the layer (and of those 36%, some will be bcc(100), not bcc(110)). This is significant for two reasons. First, it shows that the majority of the FeCo layer (64%+) is in fact not bcc(110). (*See, e.g.*, Section IX.B.2(a)(i)c, *supra.*) Second, it means that about 64% of the crystals in the layer are *never accounted for* in any of Dr. Coffey’s calculations, making his calculation of the magnetocrystalline anisotropy of the FeCo layer incomplete, unreliable, and incorrect.

799. In sum, significant amounts of bcc-d(100) crystals exist throughout the accused FeCo layers, and Dr. Clark’s dark field image data necessarily includes those bcc-d(100) crystals in its measurement. Yet Dr. Coffey mistakenly calculates the anisotropy assuming that the only crystals represented in the dark field image data are bcc-d(110) crystals. This mistaken assumption is made explicit by Dr. Coffey himself when he refers to the dark field image plots, as well as when he performs his anisotropy calculation.



800. Dr. Coffey mistakenly describes the dark field image plot above as showing “[t]he area fraction for the (110) bcc, six-variant crystallites is not independent of direction, rather it shows a pronounced variation as a function of angle.” (Coffey, ¶ 342.) But the plotted values include non-bcc(110) crystals (such as bcc(100) crystals) and so this interpretation of the dark field image data is incorrect.

801. Dr. Coffey’s mistaken interpretation of Dr. Clark’s dark field image data—namely, his mistaken assumption that the dark field image plots contain only bcc-d(110) crystals—is further made clear by how Dr. Coffey calculates the anisotropy energy density function. He writes that “the anisotropy energy density function *for bcc-d crystals in the (110) plane* is set forth in Chikazumi,” and then cites the Chikazumi Equation. (Coffey, ¶ 343.) But the Chikazumi Equation applies only to bcc-d(110) crystals—not bcc-d(100) crystals, or any other kind of crystal.

802. It would be proper to apply the Chikazumi Equation to a set of dark field image data only if the dark field image data measured *only* bcc-d(110) crystals. But because Dr. Clark’s dark field image data includes other bcc-d crystals—including for example bcc-d(100) crystals—Dr. Coffey’s application of the Chikazumi Equation to calculate anisotropy based on Dr. Clark’s dark field image data is flawed, unreasonable, and leads to mathematically invalid results.

803. An analogy may help illustrate this critical flaw in Dr. Coffey’s calculation. Suppose one has two kinds of socks: cotton socks and wool socks. There is an equation that says each cotton sock contains 10g of cotton. But this equation does not apply to wool socks (each wool socks contains only 1g of cotton). We know through measurements that we have a total of 500 socks—but these measurements do *not* tell us how many of those 500 socks are cotton and how many are wool. Nevertheless, we proceed by assuming that all 500 socks are cotton—erroneously applying the cotton sock equation to all 500 socks, and erroneously concluding that the 500 socks collectively contain $500 \times 10\text{g} = 5,000\text{g}$ of cotton.

804. Rather than socks, Dr. Coffey does this with bcc-d crystals. The Chikazumi Equation describes the anisotropy energy density function of bcc-d(110) crystals (cotton socks) *but not* bcc-d(100) crystals (wool socks). The dark field image

data from Dr. Clark plots the total amount of bcc-d(110) and bcc-d(100) crystals as a function of angle (the amount of cotton and wool socks)—but does not distinguish how many of those crystals are bcc-d(110) and how many are bcc-d(100). Nevertheless, Dr. Coffey proceeds by assuming that all the crystals are bcc-d(110)—he therefore erroneously applies the Chikazumi Equation to all the crystals, leading to a mathematically absurd outcome.

805. In sum, Dr. Coffey’s anisotropy calculation explicitly assumes that Dr. Clark’s dark field image data measures only bcc-d(110) crystals. (Coffey, ¶¶ 342-343.) Because Dr. Clark’s dark field image data measures additional bcc-d crystals—including bcc-d(100) crystals—this fundamental assumption underlying Dr. Coffey’s anisotropy calculation does not hold. This is a critical flaw in Dr. Coffey’s anisotropy calculation that, in my opinion, renders his conclusions about the anisotropy energy density function of the accused FeCo layers flawed, unreasonable, and mathematically incorrect.

(iii) Dr. Coffey ignores the actual empirical data, and instead calculates anisotropy using made up data that guarantees a uniaxial outcome

806. Although Dr. Coffey purports to rely on the dark field image data from Clark, he ends up discarding Dr. Clark’s data in favor of another set of data—data that Dr. Coffey made up to guarantee a uniaxial energy density function. (*See* Ex. F.)

807. Dr. Coffey’s methodology is therefore flawed and unreliable because it puts the cart before the horse. Rather than a methodology designed to measure the magnetic anisotropy of crystals, Dr. Coffey’s methodology is designed to consistently give one and only one result: uniaxial magnetic anisotropy. (*Id.*)

808. In engineering and computer science, there is a maxim that states “garbage in, garbage out.” This expresses the idea that if one inputs flawed and unreliable data (“garbage”) into a formula, the formula will give you flawed and unreliable data (“garbage”) as output. In other words, a calculation yields an invalid result if the input to that calculation is invalid.

809. That is the case here. Although Dr. Coffey claims to rely on Dr. Clark’s empirically measured dark field image data, he does not actually use it as the input to his

anisotropy calculations. Instead, Dr. Coffey discards Clark's empirical measurements, using as the input to his anisotropy calculation perfect sinusoidal data *guaranteed* to produce a uniaxial result. (*Id.*)

810. In my opinion, Dr. Coffey's use of made-up sinusoidal data is unreasonable and scientifically unjustified—*i.e.*, “garbage” input. In my opinion, this renders Dr. Coffey's calculations invalid, unreasonable, and scientifically incorrect—*i.e.*, “garbage” output.

(iv) Dr. Coffey makes additional errors in his anisotropy calculation, which is purely theoretical

811. Unreasonable Simplifications to the Chikazumi Equation. Dr. Coffey relies on the Chikazumi Equation from the '988 Patent to theoretically calculate energy density functions. As I explained above, use of the Chikazumi Equation is inappropriate here because that equation pertains *only* to bcc-d(110) crystals, not the bcc-d(100) and other crystals present in Dr. Clark's dark field measurements.

812. Dr. Coffey's application of the Chikazumi Equation is flawed for another reason as well: namely, the equation Dr. Coffey applies is not the actual Chikazumi Equation, but rather a simplified form of the equation.

813. This is the actual Chikazumi Equation as it appears in the '988 Patent:

$$E_{110}(\theta) = K_1 \left\{ (1/4) \sin^4(\theta) + \sin^2(\theta) \cos^2(\theta) \right\} + K_2 \left\{ (1/4) \sin^4(\theta) \cos^2(\theta) \right\} + \text{higher } K \text{ terms.}$$

814. This is also the equation Dr. Coffey cites in his report:

$$E_{110}(\theta) = K_1 \left\{ (1/4) \sin^4(\theta) + \sin^2(\theta) \cos^2(\theta) \right\} + K_2 \left\{ (1/4) \sin^4(\theta) \cos^2(\theta) \right\} + \text{higher } K \text{ terms}$$

(Coffey, ¶ 343.)

815. But that is not the equation Dr. Coffey applies. Dr. Coffey simplifies the actual Chikazumi equation by assuming that $K_2=0$. (Coffey, ¶ 350.) He further assumes

that all higher order anisotropy terms (e.g., K_3 , K_4) are also all also zero. (*Id.*) These simplifying assumptions are not justified or reasonable here.

816. The '988 Patent posits that K_2 and higher order anisotropy terms can be ignored (assumed to be zero) in instances where K_1 is many times larger than K_2 . Both the '988 Patent and Dr. Coffey fail to consider, however, that there are many instances where it is not appropriate to assume $K_1 \gg K_2$ —including cases involving FeCo alloys. Although pure Fe has a $K_1 > K_2$, as one adds Co to the Fe to create an FeCo alloy, the value of K_1 dramatically diminishes, as seen in the graph below:

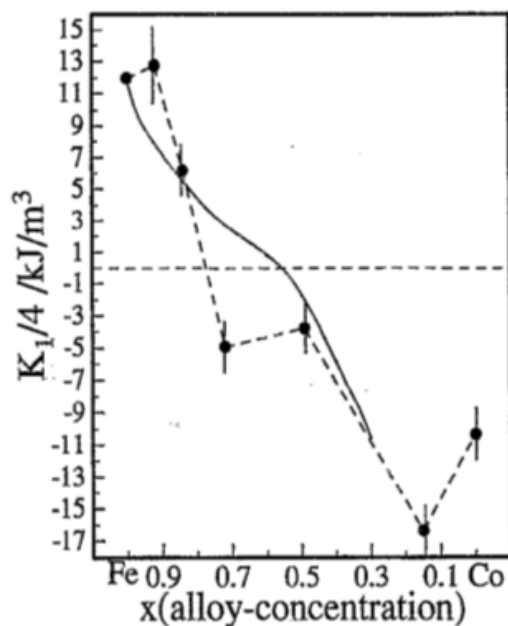


FIG. 7. Cubic anisotropy constant K_1 vs alloy concentration for $\text{Fe}_x\text{Co}_{1-x}$ films on $\text{MgO}(001)$ substrates, as obtained from the MOKE hysteresis curves. A change of sign of the anisotropy constant occurs at an alloy concentration of $x=0.8$. The solid line reproduces the bulk behavior (Ref. 14).

817. As seen in the graph, K_1 rapidly decreases with increasing Co content. Eventually, K_1 reaches 0 and goes negative with increasing Co content—this happens around 60% Fe based on the previous research on bulk materials, and around 80% Fe for this study of FeCo films.

818. [REDACTED]

(See, e.g., Seagate's First Supplemental Response to LMS's Interrogatory

No. 10 at 14-15.) This ratio of Fe and Co results in a small, positive or negative K_1 —indeed, it is very near where K_1 goes to zero. Any calculation that assumes that the magnitude of K_1 is many times greater than K_2 is therefore flawed and unreasonable.

819. Moreover, in many systems it is observed that K_1 and K_2 have very different temperature and composition dependence. The plot below shows the measured anisotropy for Co versus temperature:

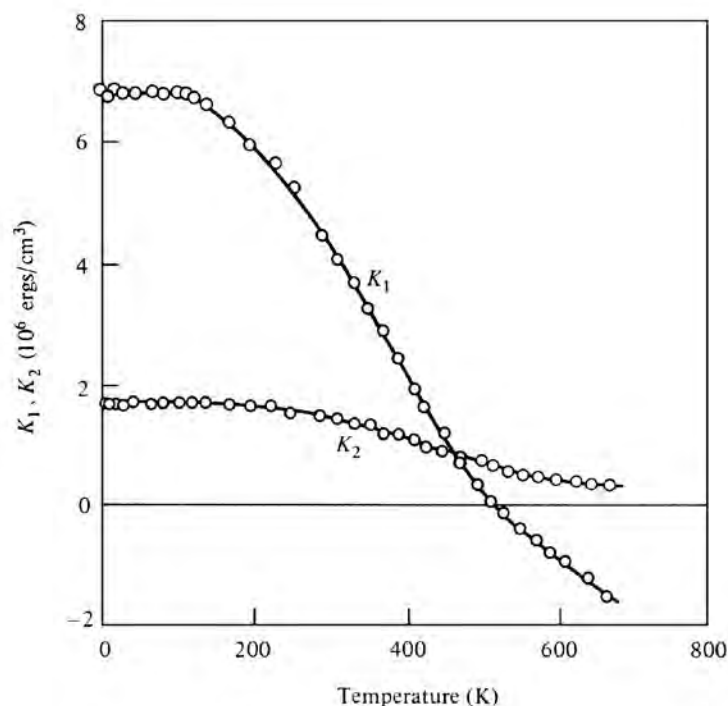


Fig. 7.25 Temperature dependence of anisotropy constants of cobalt [Y. Barnier, R. Pauthenet, and G. Rimet, *Cobalt*, 15 (1962) p. 1].

820. As can be seen, at elevated temperatures when K_1 changes sign, the magnitude of K_2 exceeds K_1 . [REDACTED]

[REDACTED] MAGNETISM AND MAGNETIC

MATERIALS by J.M.D. Coey gives the following anisotropy constants for an alloy of Fe₆₅Co₃₅: $K_1 \approx 20 \text{ kJm}^{-3}$ and $K_2 \approx -35 \text{ kJm}^{-3}$ ($K_1 \approx 2 \times 10^5 \text{ erg cm}^{-3}$ and $K_2 \approx -3.5 \times 10^5 \text{ erg cm}^{-3}$)—so that the magnitude of K_2 is nearly twice that of K_1 .

821. [REDACTED]

[REDACTED] Any calculation that

assumes that K_1 is positive and many times greater in magnitude than K_2 is therefore flawed, unreasonable, and incorrect.

822. No Evidence or Mention of Exchange Coupling. I note that according to the '988 Patent, even when the correct variants of a six-variant system dominate (which is not remotely the case here), that alone is not enough to result in a “uniaxial symmetry broken structure” because “in order to achieve a uniaxial magnetic behavior the appropriate set of variants must be exchanged coupled.” ('988 Patent 22:62-66; *see also id.* at 41:14-15 (“exchange coupling [is] needed to cause uniaxial M-H curves”).) Nowhere does Dr. Coffey even consider—let alone show—that any purported “variants” are magnetically exchange coupled.

823. Moreover, Dr. Coffey states that the approach to calculate the “[t]he averaging of the anisotropy energy of individual crystals to determine an effective average anisotropy energy for a polycrystalline sample is described by G. Herzer, ‘Grain size dependence of coercivity and permeability in nanocrystalline ferromagnets,’ IEEE Trans. Magn., vol. 26, no. 5, pp. 1397-1402, Sept. 1990 (produced by Seagate at SEA01974948).” (Coffey, ¶ 346.)

824. Although Dr. Coffey cites Herzer as purported support for his methodology, Herzer in fact undermines Dr. Coffey’s average anisotropy calculation, which implicitly assumes that the crystals are all exchange coupled (*i.e.*, all the crystals’ magnetizations will rotate together in unison).

825. Herzer’s article goes on to state “For large grains the magnetization can follow the easy magnetic directions in the single grains and domains can be formed within the grains. The magnetization process, thus, is determined by the magneto-crystalline anisotropy K_1 of the crystallites.

826. Herzer states that “[f]or very small grains . . . ferromagnetic exchange interaction more and more forces the magnetic moments to align parallel, thus, impeding the magnetization to follow the easy directions of each individual grain. As a consequence the effective anisotropy for the magnetic behavior is an average over several grains and, thus, reduced in magnitude.” But “[f]or large grains the magnetization can follow the easy magnetic directions in the single grains and domains

can be formed within the grains.” Thus Herzer states that the way one averages the anisotropy depends on the size of the grain relative to the ferromagnetic exchange length. Herzer estimates an exchange length of 35 nm for an Fe-based compound. In other words, FeCo crystals separated by much more than 35 nm will **not** be exchange coupled and will not have their magnetizations rotate together.

827. At no time does Dr. Coffey compare the grain sizes of the film to the exchange length, nor does he compute the averages over the exchange length (~35nm) as outlined in Herzer. Instead, Dr. Coffey implicitly assumes the exchange length is the size of the sample (over 5000nm)—essentially an infinite exchange length resulting in infinite exchange coupling—such that one can average all of the grains over *the entire sample*. There is no physical basis for this assumption.

828. In sum, both the '988 Patent and Dr. Coffey's calculation require that the bcc-d(110) crystals be exchange coupled. Dr. Coffey presents no evidence that the FeCo crystals in Seagate's write poles are exchange coupled. Just the opposite: he cites a paper (Herzer) explaining that the FeCo crystals in fact cannot be exchange coupled.

* * *

829. I have also considered Dr. Coffey's citations and characterizations of Seagate documents and deposition testimony on this issue (*see* Coffey ¶¶ 333-361) and find his characterizations of many of these documents to be flawed and unreasonable. Although Dr. Coffey string cites without explanation dozens of Seagate documents and testimony in ¶¶ 333-361 of his report, none actually support his conclusion that the FeCo layer forms a “uniaxial symmetry broken structure” —*i.e.*, “a structure that is uniaxial as a result of the structure being symmetry broken.”

830. For all these reasons, Dr. Coffey's opinion that any FeCo layer in the accused [REDACTED] Products forms a “uniaxial symmetry broken structure” is flawed and unreasonable. None of the FeCo layers in the [REDACTED] layers form a “uniaxial symmetry broken structure,” *i.e.*, “a structure that is uniaxial as a result of the structure being symmetry broken.”

C. The Accused [REDACTED] Products Do Not Infringe Claims 1 and 27

831. The accused [REDACTED] products do not infringe claims 1 and 27 of the '988 Patent because the [REDACTED] write poles do not feature “at least one layer providing a (111) hexagonal atomic template.” (*See* Section IX.C.1, *infra*.)

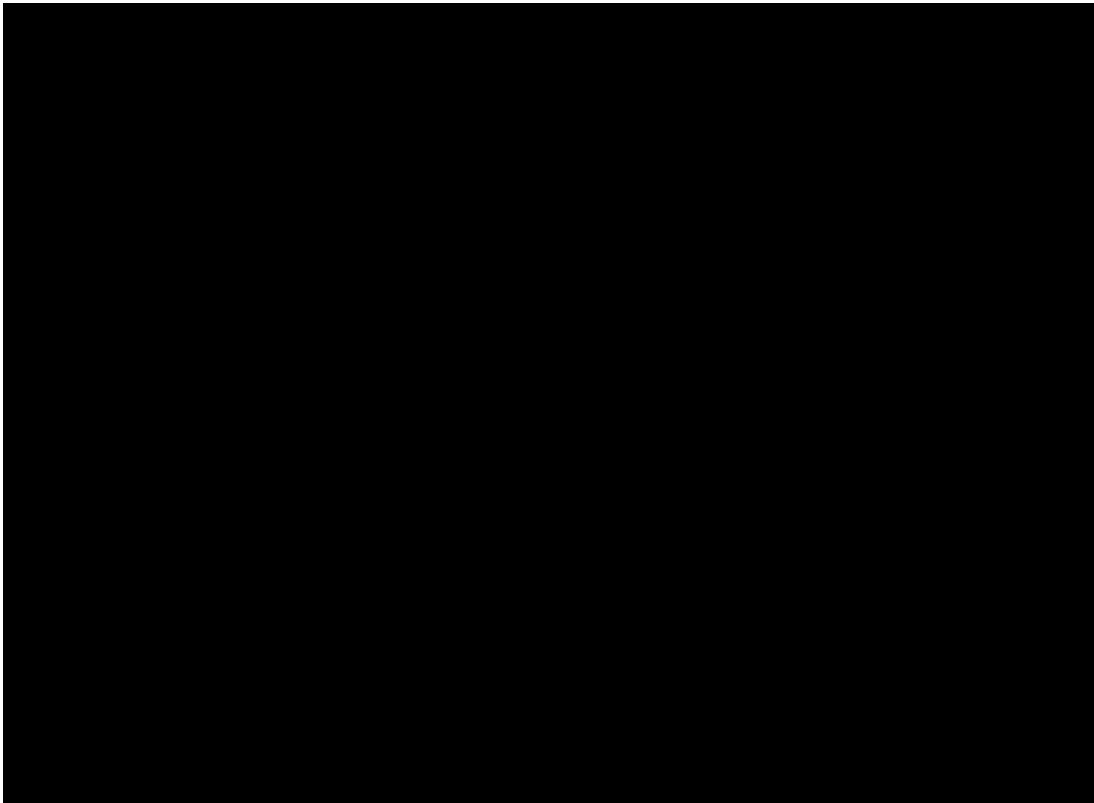
832. The accused [REDACTED] products do not infringe claims 1 and 27 of the '988 Patent because the [REDACTED] write poles do not feature “at least one bcc-d layer which is magnetic, forming a uniaxial symmetry broken structure.” (*See* Section IX.C.2, *infra*.)

1. The [REDACTED] products do not have “at least one layer providing a (111) textured hexagonal atomic template disposed between said substrate and said bcc-d layer”

Term	Court's Construction
atomic template	“an atomic pattern upon which material is grown and which is used to direct the growth of an overlying layer”
layer providing a (111) textured hexagonal atomic template	“layer that is predominately (111) hexagonal and that provides an atomic template”

833. Dr. Coffey argues in ¶¶ 488-498 of his report that the accused [REDACTED] products have “at least one layer providing a (111) textured hexagonal atomic template disposed between said substrate and said bcc-d layer.” I have considered Dr. Coffey's arguments and find his conclusion to be utterly unfounded. Dr. Coffey provides no data whatsoever to support his conclusion that the [REDACTED] products have “a layer that is predominately (111) hexagonal and that provides an atomic template.”

834. As discussed above, the [REDACTED] write heads comprise layers of NiFe and FeCo, repeated eight times as depicted below:



835. I understand Dr. Coffey contends that the “lower layer of NiFe” is a “layer providing a (111) textured hexagonal atomic template disposed between said substrate and said bcc-d layer.” (*See, e.g.*, Coffey ¶ 498.)

836. I disagree. The lowermost NiFe layer in the [REDACTED] write heads does not meet this claim limitation because the lowermost NiFe layer is not a “(111) textured hexagonal atomic template.” In fact, the [REDACTED] write heads contain no NiFe layer that is “predominately (111) hexagonal.” Moreover, the [REDACTED] write heads contain no NiFe layer that directs the growth of any overlying layer.

837. Dr. Coffey cites *no data whatsoever* showing that a NiFe layer in the [REDACTED] write poles “that is predominately (111) hexagonal,” as required by the Court’s claim construction. Dr. Coffey argument for the “(111) texture” of the NiFe is limited to a single paragraph in his report. Specifically, Dr. Coffey states in ¶ 493 that: “I further understand that the lower NiFe layer is substantially similar to the lower NiFe layers in the [REDACTED] products. Accordingly, Dr. Clark’s analysis showing that the lower NiFe layer in representative products of the [REDACTED] Products has an fcc crystal structure with its (111) planes parallel to the lower FeCo layer deposited

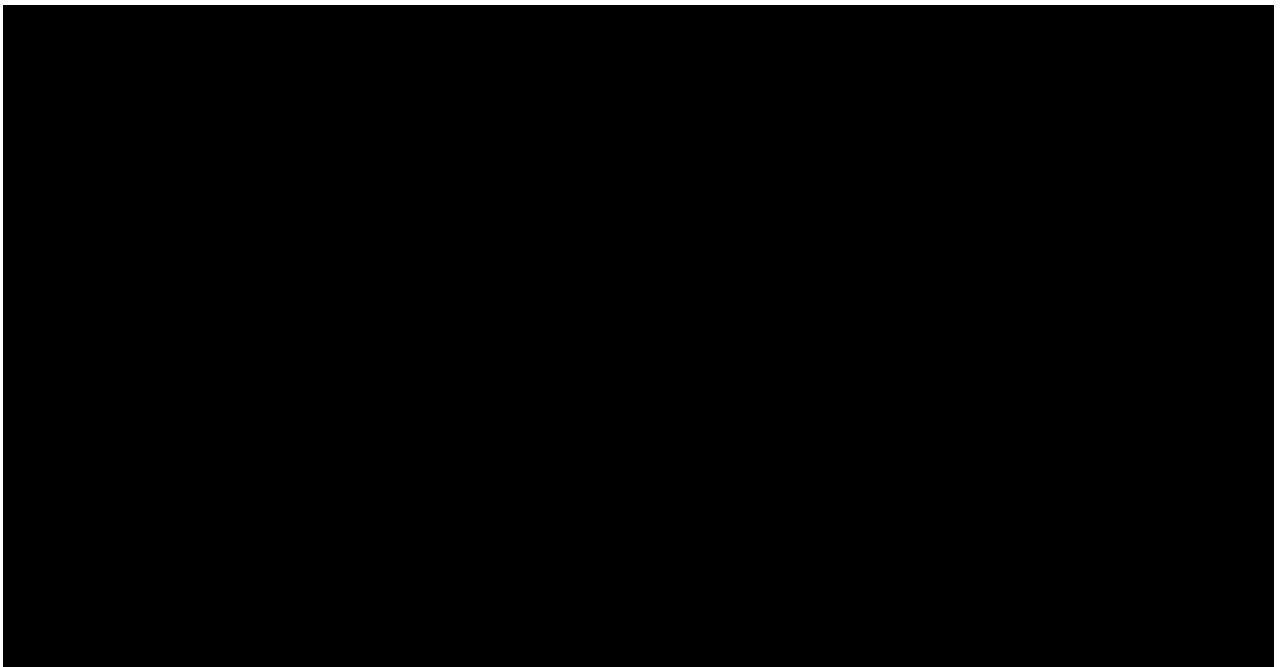
above it . . . also supports that the lower NiFe layer in the [REDACTED] Products has a (111) oriented fcc crystal structure.” (Coffey, ¶ 493 (citing Clark ¶¶ 87-105 ([REDACTED] sample), ¶¶ 133-150 ([REDACTED] sample), ¶¶ 176-193 ([REDACTED] sample))).)

838. In other words, because Dr. Coffey “understands” that Dr. Clark took FFT data for the [REDACTED] NiFe layers, and because Dr. Coffey “understands” the [REDACTED] NiFe layer is “substantially similar” to the [REDACTED] NiFe layers, Dr. Coffey purports to draw conclusions about the [REDACTED] NiFe layers entirely from measurements of the *non* [REDACTED] write heads.

839. This line of reasoning is flawed and unreasonable on its face.

840. First, it is clearly unreasonable to conclude anything about the predominate crystal orientation of the NiFe layers in an [REDACTED] write pole based on FFT measurements of the [REDACTED] write poles.

841. Second, contrary to Dr. Coffey’s “understanding,” the [REDACTED] NiFe layers are not “substantially similar” to the [REDACTED] write poles. (*See, e.g.*, Seagate’s First Supplemental Response to Interrogatory No. 10.) One only need look at the layers of [REDACTED] (right) compared to the layers of [REDACTED] (left) to see that the layer stacks are not “substantially similar”:



842. Third, as I described above in Sections IX.A.1 and IX.B.1, *supra*, Dr. Clark’s FFT data for the [REDACTED] write poles in fact do not show any (111) textured NiFe layers in either of those write poles. It is simply erroneous for Dr. Coffey to conclude that the [REDACTED] NiFe layer is (111) textured based on FFT data of [REDACTED] [REDACTED] NiFe layers—especially when that FFT data does not show any (111) textured NiFe layer in the [REDACTED] write poles.

843. Fourth, as I explained in the Technology Background, layers that are only a few atomic layers thick often exhibit no crystal structure, as a crystal structure tends to develop and evolve as a layer grows in thickness. As a result, very thin layers often feature no crystal structure—and therefore no predominant crystallographic orientation. That is the case here.

844. For all these reasons, Dr. Clark and Dr. Coffey completely fail to show that any NiFe layer in any [REDACTED] write head is “(111) textured.” In my opinion, the [REDACTED] write heads do not feature any NiFe layer that is “predominately (111) hexagonal.”

2. The [REDACTED] products do not have “at least one bcc-d layer which is magnetic, forming a uniaxial symmetry broken structure”

Term	Court’s Construction
uniaxial	“having an anisotropy energy density function with only a single maximum and a single minimum as the magnetization angle is rotated by 180 degrees from a physical axis”
symmetry broken structure	“a structure consisting of unequal volumes or unequal amounts of the bcc-d variants of a six variant system”
variant / orientational variant	“one of a set of possible crystal orientations”
variants / orientational variants	“two or more of a set of possible crystal orientations”

Term	Court's Construction
uniaxial symmetry broken structure	“a structure that is uniaxial as a result of the structure being symmetry broken”

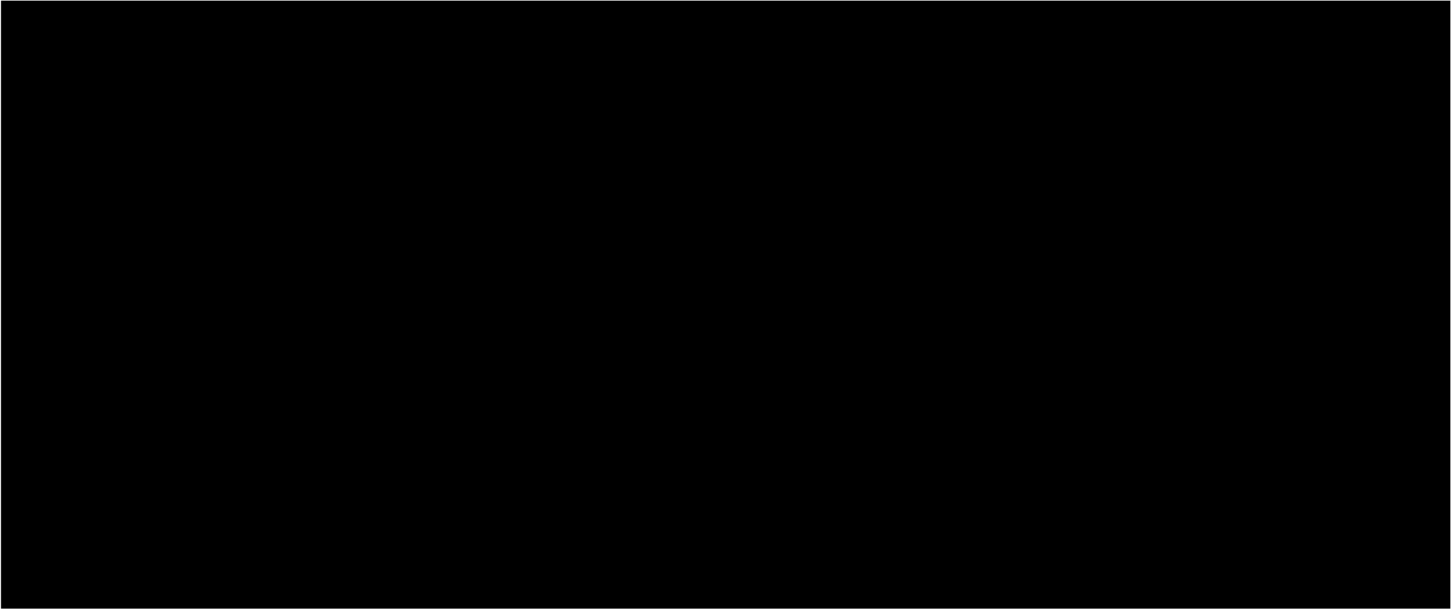
845. Because neither Dr. Coffey nor Dr. Clark took any measurements whatsoever on any [REDACTED] write head, their infringement arguments for the [REDACTED] write heads all boil down to one conclusory argument: this claim limitation is present in the accused 8X write heads because it is present in the accused [REDACTED] write heads and/or the accused [REDACTED] write heads. (*See, e.g.*, Coffey, ¶ 460 (“[B]ecause of the substantial similarities between the lowest NiFe layer and the lowest FeCo layer in each of the 8X, [REDACTED] Products, I am able to rely on the same reverse engineering of these layers in the [REDACTED] Products in support of my infringement analysis for the [REDACTED] Products.”).) Given the unreasonableness of such a claim, I respond with two high level points.

846. First, as I explained above, Dr. Coffey is incorrect to contend that the [REDACTED] write heads meet the limitations of “symmetry broken structure,” “uniaxial,” and “uniaxial symmetry broken structure.” Thus, to the extent Dr. Coffey argues that the [REDACTED] write heads meet a given claim limitation because the [REDACTED] write heads meet that claim limitation, that is incorrect.

847. Neither the [REDACTED] write heads have an FeCo layer that forms a “symmetry broken structure.” Neither the [REDACTED] write heads have an FeCo layer that is “uniaxial.” Neither the [REDACTED] write heads have an FeCo layer that forms a “uniaxial symmetry broken structure.” I hereby incorporate by reference my analysis of the [REDACTED] write heads into this section.

848. It is therefore incorrect for Dr. Coffey to argue that the [REDACTED] write heads meet any of these limitations based on these limitations purportedly existing in the [REDACTED] write heads (because they do not).

849. Second, Dr. Coffey purports to infer complex crystallographic and magnetic properties about the [REDACTED] write heads based on the [REDACTED] write heads because Dr. Coffey asserts—without a shred of analysis or reasoning—that the [REDACTED] write heads are “substantially similar” to [REDACTED]. They are not. (*See, e.g.*, Seagate’s Response to Interrogatory No. 10.) Indeed, one only need look at the layers of [REDACTED] (right) compared to the layers of [REDACTED] to debunk Coffey’s unreasoned and baseless claim that the write heads are “substantially similar.”



850. For all these reasons, Dr. Clark and Dr. Coffey completely fail to show that any FeCo layer in any [REDACTED] write head forms a “symmetry broken structure.” Dr. Coffey’s opinion to the contrary has no factual basis and is completely unreliable.

851. For all these reasons, Dr. Clark and Dr. Coffey completely fail to show that any FeCo layer in any [REDACTED] write head is “uniaxial.” For all these reasons, Dr. Clark and Dr. Coffey completely fail to show that any FeCo layer in any [REDACTED] write head forms a “uniaxial” structure. Dr. Coffey’s opinion to the contrary has no factual basis and is completely unreliable.

852. For all these reasons, Dr. Clark and Dr. Coffey completely fail to show that any FeCo layer in any [REDACTED] write head forms a “uniaxial symmetry broken structure.” Dr. Coffey’s opinion to the contrary has no factual basis and is completely unreliable.

D. The Accused Products Do Not Infringe the Other Asserted Claims of the '988 Patent

853. For all the reasons above, I conclude that none of the Accused Seagate Products infringe either independent claims 1 or 27 of the '988 Patent. The other asserted claims are all dependent claims that depend either on claim 1 or 27.

854. Because I understand there cannot be infringement of a dependent claim if the independent claim on which it depends is not infringed, it is my opinion that none of the Accused Seagate Products infringe any of the other asserted claims of the '988 Patent.

X. ANALYSIS REGARDING INDIRECT INFRINGEMENT

855. As discussed above, none of the Accused Products directly infringe any of the Asserted Claims. I understand that without direct infringement, there can be no indirect infringement.

856. I note that Dr. Coffey makes assertions about activities of Seagate that allegedly induced third parties to directly infringe the '988 Patent. (*See* Coffey, ¶¶ 121-124.) Dr. Coffey does not describe how his experience in the field of magnetic materials and magnetic recording qualifies him to give opinions on Seagate's alleged sales activities. Dr. Coffey also does not describe what expertise he has regarding the legal issue of induced infringement, or the basis for his opinion on induced infringement, other than citing to some Seagate web pages and deposition testimony without any analysis or explanation of what activities Seagate allegedly took to induce others to infringe the '988 Patent with knowledge that such activities would result in infringement.

857. I further note that Dr. Coffey does not refer to or cite any facts of which he has personal knowledge or expertise relating to the issue of when or how Seagate had knowledge that any of its activities induced acts of others with knowledge that the acts of others would constitute infringement of the '988 Patent.

XI. ANALYSIS REGARDING DAMAGES ISSUES

A. PMR

858. In his report, Dr. Coffey opines that the alleged invention of the '988 Patent was “critical” to enabling Seagate and other HDD manufacturers to commercialize PMR HDDs using write heads capable of writing to higher areal density media. (*See* Coffey, ¶¶ 118-119.) I disagree with Dr. Coffey’s opinions, which I find conclusory and unsubstantiated. Even a basic PMR HDD requires the use, coordination, and optimization of many components—each of which typically includes sub-components that must themselves be integrated and optimized to work with the other components of the HDD. Further, in my opinion, there is no connection between the alleged invention of the '988 Patent and Seagate’s development of PMR write heads.

859. I provide below a non-exhaustive review of some of the many components required for a PMR HDD to function. This discussion does not attempt to address all the components—or all the issues such as manufacturing, integration, and optimization of components—needed to create a high areal density PMR HDD.

860. PMR was first championed by Japanese professor Shun-ichi Iwasaki in the 1970s, was further developed and optimized in the proceeding decades, and was commercialized by the HDD industry in the early 2000s. PMR technology continues to be developed and optimized by the HDD industry through significant R&D investments.

861. As I explain in the Technology Background, data is stored on disks in the form of magnetic transitions. “The use of perpendicular media [*i.e.*, PMR disks] instead of conventional longitudinal media [*i.e.*, LMR disks] is the main reason why perpendicular recording is considered to be the technology capable of deferring the superparamagnetic limited to areal densities much beyond 100 Gbit/in².” (SAKHRAT KHIZROEV & DMITRI LITVINOV, PERPENDICULAR MAGNETIC RECORDING 127 (Kluwer Academic Publishers 2004).) PMR disks store magnetic bits as either “up” or “down” (perpendicular to the disk surface) while LMR disks store magnetic bits parallel to the disk surface.

862. The magnetic bits (whose transitions represent data in the form of “0s” and “1s”) are stored on a magnetic storage layer in the PMR disk. PMR disks also require a soft underlayer underneath the magnetic storage layer. The soft underlayer forms a magnetic circuit with the write head. (H.J. Richter, *The Transition from Longitudinal to Perpendicular Recording*, J. Phys. D. 40, R149-R177 (2007).) To write data, the PMR write head generates magnetic flux, which induces magnetic transitions in the magnetic storage layer, disperses through the soft underlayer, and then returns to the write head through return poles. (*Id.*) The soft underlayer, in tandem with the return poles of the write head, dilute the returning magnetic flux exiting the magnetic storage layer so that magnetic transitions are not written to unintended areas of the magnetic storage layer as the magnetic flux returns to the write head.

863. The media’s magnetic storage layer and soft underlayer require careful optimization to create a functioning PMR HDD. Although the magnetic storage layer bears certain similarities to LMR disks, several non-trivial technological challenges had to be solved to create PMR media. (*See, e.g.*, SAKHRAT KHIZROEV & DMITRI LITVINOV, PERPENDICULAR MAGNETIC RECORDING 128.) Moreover, LMR disks did not use any soft underlayer, which was “[o]ne of the key features of perpendicular recording that makes it superior compared to longitudinal recording with respect to [] superparamagnetic instabilities.” (*Id.* at 144.) Developing a suitable soft underlayer posed several technical challenges and issues that needed to be resolved before PMR was realized. (*See, e.g., id.* at 145.) Resolving these challenges and issues included optimizing various material properties of the soft underlayer, including various magnetic properties. Optimization of these properties involved optimizing material compositions, dimensions, and processing parameters and conditions. (*See, e.g., id.* at 153 (“A not properly optimized [soft underlayer] material can introduce a significant amount of noise into the playback signal.”).)

864. In addition to the magnetic storage layer and soft underlayer, PMR disks include a substrate, one or more seed layers, one or more interlayers, an overcoat layer, and lubricants. Each of these layers must work with other disk layers and/or the read

and write heads to create a functioning PMR HDD, with each layer having carefully calibrated material properties.

865. In addition to the many layers and components of a PMR disk, a large suite of electronics is needed to write to and read from the PMR disk. These electronics are responsible for executing various algorithms—such as positioning of the read heads and write heads, controlling the gap between the sliders and the PMR disks, timing of read and write operations, processing and communicating data represented by perpendicularly-stored magnetic transitions, and degaussing the write pole, among many others. The electronics executing these algorithms are a combination of hardware and software components; the software alone comprises many thousands of lines of code.

866. In addition to optimizing the PMR disk and associated electronics, sliders and slider components (*e.g.*, read heads, heaters, air bearing surfaces, write heads) need to be optimized to write to and read from the PMR disk. For read heads, the materials, magnetic shields, and dimensions had to be optimized to sense the smaller, perpendicular magnetic transitions. For heaters and air bearing surfaces, the materials, positions, and dimensions had to be optimized such that the gap between the slider and the PMR disks was maintained at a desirable distance.

867. PMR write heads include several components (*e.g.*, yokes, coils, top shields, bottom shields, side shields, write poles) that need to be optimized and coordinated to work together. As mentioned above, writing magnetic transitions in PMR media is done by magnetic flux created by the write pole of the write head. The magnetic flux is generated by current applied to coils, and is concentrated in the write head via the yoke and write pole. The concentrated magnetic flux emanates from the tip of the write pole, travels through the magnetic storage layer to the soft underlayer where it is diluted before returning to side or return shields. For this magnetic circuit to work effectively, the materials, dimensions, positions, and other properties of each component need to be carefully calibrated and matched to the properties of the media. For example, Seagate monitors and controls over fifteen parameters and properties just for the front shield and the side shields. (*See, e.g.*, SEA03052381.)

868. Dr. Coffey’s conclusory opinions fail to account for the careful calibration, optimization, and coordination of the dozens of HDD components required for a functioning PMR HDD.

869. According to Dr. Coffey, in order to store data on the smaller domains of the media used in perpendicular magnetic recording, the media had to be made of higher coercivity materials. This, in turn, required that write heads for PMR use higher magnetization materials in order to create sufficiently strong magnetic fields to change the magnetization of this higher coercivity media. (*See, e.g., id.* at ¶ 66-67; *see also* ¶ 119.) I note this greatly oversimplifies the issue—there are many other ways to achieve higher density without using higher coercivity media.

870. Nevertheless, Dr. Coffey suggests that materials such as FeCo were looked upon favorably because of their high saturation magnetization (up to 2.4 Tesla), but “traditionally using 2.4T thin film materials in bcc form was difficult because these materials had inherent isotropic magnetic properties with high coercivity.” (*Id.* at ¶ 67.) Dr. Coffey argues that having a write head with soft, uniaxial properties, was necessary to prevent “Erase After Write” (“EAW”) issues, “a problem wherein previously-written data would be inadvertently erased by the write head due to the errant presence of a magnetic field emitted from the write head.” (*Id.* at ¶ 73 (“[H]aving uniaxial anisotropy as a material property is favorable for mitigating EAW—when the sole easy axis . . . is in the cross track direction of the head, then that will be the preferred direction for the magnetization of the material to lie when there is no current through the coils.”).)

871. Dr. Coffey acknowledges that the “shape of the write pole material away from the media aids this magnetization direction,” but contends that “as the pole is shaped to become narrower as it reaches the surface facing the head in the small pole tip region, the shape promotes an up and down magnetization along the material’s in-plane hard axis . . . that can result in Erase After Write.” (*Id.* at ¶ 73.) He then asserts that the ’988 Patent discloses an invention that “contribute[s] to uniaxial anisotropy in the write head through symmetry breaking, therefore permitting the presence of higher magnetization materials in the write pole of the write head.” (*Id.* at 119.) According to Dr. Coffey, “[t]he ’988 patented invention, by mitigating EAW in PMR write heads,

therefore played a critical role in enabling Seagate to commercialize HDDs with PMR functionality.” (*Id.* at ¶ 118.)

872. There are multiple problems with Dr. Coffey’s argument. First, Dr. Coffey does not cite any evidence that Seagate or any other HDD manufacturer was aware of, relied on, or used the ’988 Patent in developing PMR technology. In fact, as explained above, it is my opinion that none of the accused Seagate products use the invention claimed in the ’988 Patent.

873. In Seagate’s case, the evidence I have reviewed demonstrates that Seagate independently developed PMR technology beginning in the 1990s, resulting in prototypes no later than 2001—including those using FeCo in the write heads—well before the publication or issuance of the ’988 Patent. (*See, e.g.*, SEA01043275 at SEA01043282.) Furthermore, to my knowledge, the ’988 Patent has never been mentioned in any publication as a critical advance necessary to—or even contributing to—the commercialization of PMR HDDs. (*See, e.g.*, Lambeth 30b1 Dep. Tr. at 264:15-266:6.) In fact, I am not aware of any peer-reviewed publication that has discussed, recognized, or given accolades to the ’988 Patent in connection with any technology.

874. Furthermore, even if Dr. Coffey was correct that the invention claimed in the ’988 patent would “contribute” to uniaxial anisotropy, he never quantifies the extent of that contribution. My own analysis confirms that any such contribution would be negligible at best—on the order of a few Oersteds—and certainly in no way “critical” to having a viable write head for PMR media. Indeed, the other sources of magnetic anisotropy in the write head—such as shape and stress—dwarf any anisotropy arising from having a symmetry broken magnetic layer in the write head.

875. Dr. Coffey also provides no evidence that a uniaxial anisotropy contribution from the alleged invention of the ’988 Patent would be necessary or sufficient for addressing EAW. Nor is there any support for Dr. Coffey’s claim that EAW presented a bottleneck in the development and commercialization of PMR drives. In truth, EAW issues continued to persist even years after HDD manufacturers had successfully commercialized PMR HDDs. (*See, e.g.*, U.S. Pat. No. 7,914,916, filed in 2008 (“A consistent issue with perpendicular head recording is erase after write, (EAW)

which is due to a delayed relaxation of the magnetization once the write current in the head is switched off.”); SEA03129091 (discussing techniques for eliminating EAW such as degaussing).)

876. In my opinion, Dr. Coffey grossly overstates the value of uniaxial anisotropy in write heads for PMR HDDs, and never explains why uniaxial anisotropy—as opposed to something else—would be necessary or critical to avoiding EAW. Indeed, Seagate’s write heads are not uniaxial, and Seagate has chosen to effectively deal with EAW in a completely different way. In particular, Seagate uses a technique known as *degaussing* to effectively eliminate EAW. (See, e.g., SEA03129091.) Degaussing, which has nothing to do with uniaxial anisotropy, describes a technique where after the write head is done writing, rather than remove the write current entirely, a small alternating current is briefly applied at the end of the writing process. (*Id.*) Applying this alternating current helps the write head demagnetize faster than if the current was removed entirely. Seagate has found that this “Deguass feature of preamp [is] typically very effective in eliminating [conventional] EAW” and “Response to degauss is relatively strong.” (*Id.*) Degaussing is commonly used to deal with EAW since it is both effective at eliminating EAW and has no significant drawbacks. I note that there are still other techniques for avoiding EAW as well, including for example using antiferromagnetically coupled layers and/or optimizing write head geometry (neither of which have anything to do with uniaxial magnetic anisotropy). (See, e.g., D. Bai et. al, *Writer Pole Tip Remanence in Perpendicular Recording*, IEEE Transactions on Magnetics Vol. 42, No. 3 (March 2006), at 473-480 (discussing use of laminated and/or antiferromagnetically coupled poles to combat remanent erasure, *i.e.*, EAW); X. Shen and R.H. Victora, *Effect of Pole Tip Geometry on Remnant Field*, Journal of Applied Physics 103, 07F542-1 (2008) (discussing pole tip geometry design that “reduces the remnant field dramatically”).)

877. For all of these reasons, Dr. Coffey’s opinion that the invention of the ‘988 Patent was critical to Seagate’s ability to commercialize PMR HDDs is incorrect, unreasonable, and has no factual basis.

B. Comparability of Certain Licensed Patents to the '988 Patent

878. I understand that in considering damages issues the parties may evaluate licenses for use of other patents comparable to the patent-in-suit, and that the other patents or technology should be sufficiently comparable, related or have a discernible link to the claimed technology. I have been asked to provide my opinions regarding the technical comparability of technology described and claimed in certain patents owned or licensed by Seagate with that of the alleged invention of the '988 Patent. I express those opinions in this section.

1. "Jülich" Patent

879. I understand that in July 1997, Seagate received a license from the Jülich Research Centre ("Jülich") in Germany to U.S. Patent No. 4,949,039 ("the '039 Patent") and its foreign counterparts. The patent is entitled "Magnetic Field Sensor with Ferromagnetic Thin Layers Having Magnetically Antiparallel Polarized Component," and issued in 1990. The '039 Patent names Peter Grünberg as the inventor. Dr. Grünberg, along with Albert Fert, received the 2007 Nobel Prize in Physics for discovering the giant magnetoresistance ("GMR") effect in 1988.

880. I have reviewed the '039 Patent. It describes and claims GMR structures in magnetic field sensors. In addition to being the subject of a Nobel Prize, the GMR effect claimed in the '039 Patent is widely acknowledged as the basis for dramatically improving the sensitivity of read heads in HDDs and allowing for greatly enhanced areal density.

881. The '039 Patent specifically describes and broadly claims a magnetic field sensor having at least three layers, including a nonmagnetic layer positioned between two magnetic layers with the magnetic layers having anti-parallel magnetic directions. The magnetic field sensor claimed with this layer structure exploits the GMR effect—resulting in a sensor with increased sensitivity to magnetic fields. Accordingly, the '039 Patent covers the foundational elements (*i.e.*, a nonmagnetic layer positioned between two magnetic layers) of GMR sensors for read heads in HDDs.

882. In my opinion, the '039 Patent relates to technology that is comparable to the '988 Patent, to the extent that both (i) are generally directed to HDDs and other magnetic storage devices; (ii) are directed to thin-film subcomponents in HDDs; (iii) are focused on a key sub-component in an HDD, the read/write head; (iv) involve thin-film magnetic structures that purportedly can be used in the read/write head of an HDD; and (v) are intended to increase areal density for data storage in HDDs.

883. The invention claimed in the '039 Patent, however, is a vastly greater improvement than the invention claimed in the '988 Patent. In particular, the GMR technology of the '039 Patent constituted a foundational shift in HDD technology by significantly increasing the performance over prior magnetic field sensors such as anisotropic magneto-resistive (AMR) sensors. GMR sensors have much greater sensitivity to magnetic fields compared to single-magnetic-layer structures used in AMR sensors. As such, GMR sensors are substantially more effective than AMR sensors while also being smaller than AMR sensors. The commercialization cycle for GMR heads was approximately half as long as that for AMR heads, meaning they were brought to market in half the time. (Christopher H. Bajorek, "Magnetoresistive (MR) Heads and the Earliest MR Head-Based Disk Drives: Sawmill and Corsair," Computer History Museum, November 2014, p. 2 of 11, *available at* <http://s3.computerhistory.org/groups/magnetoresistive-heads.pdf>.)

884. As noted above, the GMR technology claimed by the '039 Patent resulted in significant improvements in areal density. Areal density is a measure of the amount of data that can be stored in a given area on the disk in an HDD, typically expressed as gigabits or terabits per square inch (Gb/in² or Tb/in²). Since the diameter of an HDD media disk is fixed in order to fit within a given enclosure, the higher the areal density, the larger the storage capacity of a given HDD. Thus areal density is a key metric used to evaluate the storage capacity of an HDD technology, and the '039 Patent and the GMR effect claimed in that patent allowed compounded annual growth of 100% percent for HDD areal density. (*See, e.g.,* E. Grochowski, *The Continuing Evolution of Magnetic Hard Disk Drives*, in HOLOGRAPHIC DATA STORAGE 448 (H.J. Coufal et al. eds., Springer 2000); "Without the discovery and improvement of GMR materials,

magnetic recording at a density of $> 10 \text{ Gb/in.}^2$ would be unthinkable.” SHAN X. WANG & ALEXANDER M. TARATORIN, *MAGNETIC INFORMATION STORAGE TECHNOLOGY* 171 (Academic Press 1999).) Prior to the advent of GMR technology, the compounded annual growth for areal density was approximately 60%. (E. Hirota, H. Sakakima, K. Inomata, *GIANT MAGNETO-RESISTANCE DEVICES* 99, (Dr. G. Ertl et al. eds., Springer 2002).)

885. GMR technology, and the innovation of the Grünberg patent in particular, has resulted in intensive research, publishing of papers, lectures, text books, and industry activity. The Grünberg patent and GMR were considered revolutionary. As noted by the Nobel Prize Committee in 2007: “The discovery of giant magnetoresistance immediately opened the door to a wealth of new scientific and technological possibilities, including a tremendous influence on the technique of data storage and magnetic sensors. Thousands of scientists all around the world are today working on magnetoelectronic phenomena and their exploration.” (The Discovery of Giant Magnetoresistance, *NobelPrize.org*, Oct. 9, 2007, p. 2, available at https://www.nobelprize.org/nobel_prizes/physics/laureates/2007/advanced-physicsprize2007.pdf.)

886. It is not surprising that GMR technology was widely adopted by the industry, because it “revolutionized the hard disk drive (HDD) industry, enabling manufacturers to make dramatic improvements in the amount of data HDDs can hold, and paving the way for powerful PCs and new products such as Apple’s iPod.” (Jason Dedrick, Kenneth L. Kraemer, “Who Captures the Value in Technological Innovation? The distribution of benefits in the GMR-based global storage industry,” *Penn State University*, September 2013, p. 8, available at <http://citeseerx.ist.psu.edu/viewdoc/download?doi=10.1.1.405.2326&rep=rep1&type=pdf>.)

887. In contrast, the purported invention of the ’988 Patent at most had an incremental effect in improving uniaxial anisotropy in write heads, not a fundamental shift like GMR. As noted above (*see* Section V.D and Section XI.A, *supra*) any such improvement would be *de minimis* at best, and uniaxial anisotropy could be derived

from multiple other prior art sources, including from shape, pair ordering, and strain. In addition, in stark contrast to the voluminous quantity of research, papers, and industry focus following the grant of the Grünberg patent, to my knowledge there have been no papers, research, or interest following the publishing of the '988 Patent. The Grünberg patent resulted in the pinnacle of scientific achievement—the Nobel Prize—while again to my knowledge, no awards have been granted as a result of the purported discovery of the '988 Patent.

2. “Censtor” Patents

888. I understand that in March 2002, Seagate received a license from Censtor Corporation (“Censtor”) to Censtor’s patent portfolio consisting of over thirty U.S. patents and applications, and in July 2003, Seagate acquired Censtor’s patent portfolio. The issuance dates of the patents in the portfolio range from 1983 to 2004. Censtor has been credited as being one of the first HDD companies to research and produce heads and disks for PMR. (*See, e.g.*, Sakhrat Khizroev & Dmitri Litvinov, PERPENDICULAR MAGNETIC RECORDING 1 (Kluwer Academic Publishers 2004).)

889. The licensed and later-acquired patent portfolio includes patents broadly directed to various read/write head designs including PMR write heads, suspensions, sliders, and special surface treatments for disks that allow sliders to directly contact disks during operation:

	Patent / Publication Number	Technology	Publication Date
1	US5453315A	Suspensions	9/26/1995
2	US5476131A	Suspensions	12/19/1995
3	US5483025A	Suspensions	1/9/1996
4	US5490027A	Suspensions	2/6/1996
5	US5557488A	Suspensions	9/17/1996
10	US4636894A	Slider	1/13/1987
6	US6320725B1	PMR write heads and media	11/20/2001
7	US20020093761A1	PMR write heads and media	7/18/2002
8	US4423450A	PMR write heads	12/27/1983
9	US4860139A	PMR write heads	8/22/1989
11	US4751598A	PMR write heads	6/14/1988
12	US5632669A	Manufacturing	5/27/1997
13	US5885131A	Manufacturing	3/23/1999
14	US4757402A	Heads, generally	7/12/1988
15	US5041932A	Heads, generally	8/20/1991
16	US5073242A	Heads, generally	12/17/1991
17	US5111351A	Heads, generally	5/5/1992
18	US5163218A	Heads, generally	11/17/1992
19	US5174012A	Heads, generally	12/29/1992
20	US6493191B1	Contact recording	12/10/2002
21	US20020176210A1	Contact recording	11/28/2002
22	US5063712A	Contact recording	11/12/1991
23	US5550691A	Contact recording	8/27/1996
24	US5822153A	Contact recording	10/13/1998
25	US5909340A	Contact recording	6/1/1999
26	US5949612A	Contact recording	9/7/1999
27	US6160685A	Contact recording	12/12/2000
28	US6198607B1	Contact recording	3/6/2001
29	US6212047B1	Contact recording	4/3/2001
30	US6411470B1	Contact recording	6/25/2002
31	US6535361B2	Contact recording	3/18/2003
32	US6600631B1	Contact recording	7/29/2003
33	US6804085B1	Contact recording	10/12/2004
34	US5625515A	Actuators	4/29/1997

890. In general, the patents in this portfolio relate to HDD technology and or improvements for components of HDDs. More specifically, a number of these patents are directed toward enhancing PMR heads and media, including U.S. Patent Nos. 6,320,725; 4,423,450; 4,860,139; 4,751,598; and U.S. patent application publication number 2002/0093761. For example, U.S. Patent No. 4,423,450 (“the ’450 Patent”) is generally directed toward an improved read/write head for perpendicular recording techniques. The ’450 Patent is entitled “Magnetic Head and Multitrack Transducer for Perpendicular Recording and Method for Fabricating,” and issued in 1983. It claims a transducer with a magnetic path constructed for perpendicular recording, and includes a

flux gate that may selectively open or close the magnetic path for either reading or writing.

891. As another example of a PMR patent in the Censtor portfolio licensed to Seagate, U.S. Patent number 4,860,139 (“the ’139 Patent”) is generally directed toward a PMR read/write head that includes a flux-return portion and a planar pole portion that is spaced from the flux-return portion but magnetically coupled to the flux-return portion. The ’139 Patent is entitled “Planarized Read/Write Head and Method,” and issued in 1989. It claims a flux-return portion, an insulated coil, a pole portion with a magnetic film that forms a yoke, with the coil and pole portion residing in parallel planes.

892. U.S. Patent Number 4,751,598 (“the ’598 Patent”) is also part of the Censtor portfolio licensed to Seagate. The ’139 Patent is entitled “Thin-film, Cross-Field, Closed-Flux, Anisotropic Electromagnetic Field Device,” and issued in 1988. It is generally directed toward PMR read/write heads. In particular, it claims a thin film, cross-field, closed-flux anisotropic read/write head, including a pair of orthogonally related current conductors, and a magnetically permeable structure. Portions of the magnetic structure are inductively coupled to the conductors and extend completely around the cross-sectional perimeter of one of the conductors, with an easy axis of magnetization substantially parallel to the current flow in the conductors and normal to the recording surface.

893. In another example, U.S. Patent No. 6,320,725, entitled “Hard disk drive having ring head with predominantly perpendicular media fields” describes and claims approaches for writing perpendicular magnetic fields using write heads shaped similar to LMR write heads (e.g., write heads with a magnetic gap near the recording media).

894. At the time of the portfolio license and subsequent acquisition, these patents described above claimed read/write head and media designs that the HDD industry was investigating for commercial applications of PMR.

895. In my opinion, the Censtor portfolio patents relate to technology that is comparable to the ’988 Patent to the extent that both are (i) directed generally to HDDs and magnetic devices; (ii) relate to structures for components in HDDs; (iii) directed to

magnetic thin film components affecting the reading and writing of data in HDDs; and (iv) related to increasing areal density for data storage in HDDs.

896. The inventions claimed by the Censtor patents directed toward PMR read/write heads, in particular, offer a significantly greater improvement than the invention claimed in the '988 Patent. Specifically, the inventions claimed in the Censtor patents directed toward PMR read/write heads covered multiple aspects of the entire read/write head and media. For example, the '450 Patent describes the geometry of the entire read/write head, including many magnetic thin film layers, and also describes the process for manufacturing these many layers. In contrast, the '988 Patent is directed to a de minimis improvement of a single magnetic property via the crystal structure of a minor portion of the write head – just two thin film layers. As noted above, the magnetic property the '988 Patent purports to allow, uniaxial anisotropy, could also be derived from multiple other prior art sources, including from shape, pair ordering, and strain.

3. Carnegie Mellon University Patents

897. I understand that in 1997 Seagate received a license from the Data Storage Systems Center ("DSSC") at Carnegie Mellon University to a number of U.S. Patents covering HDD technology. Seagate was a member of the DSSC from 1997 through 2003, and provided funding to the DSSC to support research into HDD technology. In exchange for this funding, Seagate received a license to many patents, including U.S. Patent No. 6,248,416 ("the '416 Patent"). The '416 Patent was invented by Dr. Lambeth, and is generally directed toward certain thin film crystalline structures for use in read/write heads and the media of HDDs. In particular, the '416 Patent claims a recording medium comprising a substrate, a magnetic layer made of Co or a Co alloy film with a (1010) crystalline texture, and a two layer underlayer structure having a first underlayer with an fcc(110) crystal texture and a second underlayer having a bcc(112) crystal texture, such that the second underlayer is disposed between the first underlayer and the magnetic layer.

898. In my opinion, the '416 Patent relates to technology that is comparable to the '988 Patent to the extent that both (i) are generally directed to HDDs and other

magnetic storage devices; (ii) are directed to thin-film based subcomponents in the HDDs; (iii) involve thin-film magnetic structures in an HDD; (iv) involve multiple thin film layers with specific crystalline textures that are intended to induce beneficial magnetic properties; and (v) are intended to increase areal density for data storage in HDDs.

899. In addition, during the prosecution of the '988 Patent, the '416 Patent was cited by the patent examiner as invalidating prior art, demonstrating that at minimum, the Patent Office thought both patents share many claim elements. This is further indicia that the '416 Patent is technically comparable to the '988 Patent.

900. An additional patent covered by Seagate's license with the DSSC is U.S. Patent No. 5,693,426 ("the '426 Patent"). The '426 Patent is entitled "Magnetic Recording Medium with B2 Structured Underlayer and a Cobalt-Based Magnetic Layer," and issued in 1997. Dr. Lambeth is an inventor of this Patent. The '426 Patent is generally directed toward thin film magnetic layers in media with particular crystalline orientations. Specifically, the '426 Patent claims a substrate, a Cobalt or Cobalt-alloy magnetic layer, and an underlayer with a B2-ordered crystalline structure that is disposed between the substrate and magnetic layer.

901. In my opinion, the '426 Patent relates to technology that is comparable to the '988 Patent to the extent that both (i) are generally directed to HDDs and other magnetic storage devices; (ii) are directed to thin-film based subcomponents in the HDDs; (iii) involve thin-film magnetic structures in an HDD; (iv) involve multiple thin film layers with specific crystalline textures that are intended to induce beneficial magnetic properties; and (v) are intended to increase areal density for data storage in HDDs.

902. The invention claimed by the '426 Patent offers a significantly greater improvement than the invention claimed in the '988 Patent. Specifically, the inventions claimed in the '426 Patent allowed a significant increase in coercivity of the media and smaller grain sizes, which in turn allowed for higher areal density. These improvements to the media were adopted by industry. (Thomas W. Peterson, "Creating an Innovation Ecosystem," National Science Foundation, 2009, Slide 16 of 28, available at

http://www.nseresearch.org/2009/presentations/Day2_Peterson.ppt (Slide 16: “Nickel Aluminum Underlayer Enables High-capacity Memory Storage”); “NSF Engineering Research Centers – Creating New Knowledge, Innovators and Technologies For Over 30 Years,” National Science Foundation, October 2015, p. 6, available at <http://ercassoc.org/sites/default/files/download-files/ERC%2030th%20anniversary%20brochure.pdf>.) In contrast, the ’988 Patent is directed to a de minimis improvement of a single magnetic property via the crystal structure of a minor portion of the write head – just two thin film layers. As noted above, the magnetic property the ’988 Patent purports to allow, uniaxial anisotropy, could also be derived from multiple other prior art sources, including from shape, pair ordering, and strain.

903. Seagate’s license with the DSSC also covered U.S. Patent No. 4,825,318 (“the ’318 Patent”). The ’318 Patent is generally directed toward a magnetic thin film read/write head for PMR. Specifically, the ’318 Patent claims an inductive read/write head with three magnetic poles, each insulated from one another, and electrical coils positioned about the three poles in order to induce magnetic flux in the flux paths within the magnetic poles.

904. In my opinion, the ’318 Patent relates to technology that is comparable to the ’988 Patent to the extent that both (i) are generally directed to HDDs and other magnetic storage devices; (ii) are directed to thin-film based subcomponents in the HDDs; (iii) are focused on a key sub-component in an HDD, the write head; (iv) involve thin-film magnetic structures that purportedly can be used within the write head of an HDD; and (v) are intended to increase areal density for data storage in HDDs.

4. Syndia License

905. I understand that Seagate signed a license agreement with Syndia in 2001. This license covered thirty-three U.S. Patents, including several patents directed toward diamond coatings used in heads and media in HDDs. Several of the Syndia patents licensed to Seagate also include processes for using chemical vapor deposition to deposit diamond coatings. These diamond coatings provided crucial protection to heads and

media in HDDs, and allowed the use of thin film media. Specifically, the diamond coatings provide corrosion resistance, shock resistance, and sliding wear durability.

906. These protections are critical to prevent damage from occurring to both the head and the media in the event that an HDD is jarred and the head comes into contact with the rapidly spinning media beneath it. The long term durability of the head and media is also critical to enabling the head to fly as close to the disk as possible, which in turn is critical to enabling higher areal density. Higher areal density requires smaller bits, meaning the head must fly closer to the disk in order to detect the smaller magnetic field emitted by smaller bits. Thus because diamond coating is “one of the major contributors to [head media] spacing,” it is critical to improving areal density. (S. N. Piramanayagam, M. Shakerzadeh, B. Varghese, H. Tan, “Effect of Carbon Overcoat Implantation on the Magnetic and Structural Properties of Perpendicular Recording Media,” IEEE Transactions on Magnetics, Vol. 51, Issue 11, Nov. 2015.)

907. For example, U.S. Patent No. 4,702,808 (“the ’808 Patent”) is generally directed toward chemical vapor deposition by utilizing one or more lasers to vaporize metal within a process chamber and to cause such metal to be selectively deposited on a substrate, such as microelectronic circuit chips. In particular, the ’808 Patent claims a chemical reaction apparatus with a stream of matter and a beam of collimated coherent radiation (e.g., a laser), with a means for directing said beam at the stream of matter to effect a chemical change in the matter, and finally a means for transferring the chemically changed matter to a select location.

908. In my opinion, the ’808 Patent relates to technology that is comparable to the ’988 Patent to the extent that both (i) are generally related to thin films in HDDs; (ii) relate to use of certain thin films in HDDs; and (iii) relate to increasing areal density for data storage in HDDs.

5. White License

909. I understand that Seagate signed a license with Dr. James White in 1999. This license covered all patents owned by Dr. White that have an effective filing date prior to January 1, 2000. These patents are generally directed toward sliders used in

HDDs. For example, U.S. Patent No. 4,673,996 (“the ’996 patent”) is directed toward an air bearing slider assembly with a transverse pressurization contour along the sides of the slider. These contours create a pressure distribution across the slider such that the slider fly height about the media does not vary based on which track the slider is above (inner-most or outer-most) or the velocity of the media beneath the slider. This enabled HDDs to have sliders fly much closer to the media, which in turn allowed for read heads to function more effectively in accurately detecting the magnetic fields of the bits they fly over. Magnetic bits in the media could be reduced in size, as the smaller magnetic field of each media bit could still be detected by a read head that flew closer to the media. Thus the areal density of HDD media is closely related to the fly height of the slider. (Bruno Marchon, Thomas Pitchford, Yiao-Tee Hsia, Sunita Gangopadhyay, “The Head-Disk Interface Roadmap to an Areal Density of 4 Tbit/in²,” *Advances in Tribology*, vol. 2013, Article ID 521086, 2013, available at <https://www.hindawi.com/journals/at/2013/521086/>.)

910. In my opinion, the ’996 Patent relates to technology that is comparable to the ’988 Patent to the extent that both are related to (i) subcomponents in HDDs; (ii) a component in HDDs, the transducer head; and (iii) increasing areal density for data storage in HDDs.

6. “Dual Stripe MR Technology”

911. I understand that the only patents or technology that Dr. Coffey opines are comparable to the ’988 Patent are certain Censtor patents (Coffey, ¶ 108) and what Dr. Coffey calls “Dual Stripe MR technology” (Coffey, ¶ 109). The section of Dr. Coffey’s report on “Dual Stripe MR technology,” however, does not list or cite to any patents and does not in any way explain the “Dual Stripe MR technology” that he generally refers to. Accordingly, it is not clear what (if any) patents or technology Dr. Coffey contends are comparable to the ’988 Patent. I reserve the right to comment on or supplement my opinion to address any further detail provided by Dr. Coffey regarding “Dual Stripe MR technology.”

912. In general, dual stripe magneto-resistive technology is a modified form of a magneto-resistive (“MR”) read head. An MR head relies on the fact that when an electric current is exposed to a magnetic field in a certain direction, the magnetic field tends to increase the resistance in the electric current. A dual stripe MR head adds a second MR sensor in order to allow the read head to detect and reject noise.

Signed: 
Eric E. Fullerton, Ph.D.

Dated: July 16, 2018

EXHIBIT A

Eric Edward Fullerton

*Center for Memory and Recording Research, 0401
University of California, San Diego
9500 Gilman Drive
La Jolla, CA 92093-0401*

*Telephone: (858) 534-9639 FAX: (858) 534-2720
e-mail: efullerton@ucsd.edu*

Personal: US Citizen, Date of birth: May 7, 1962

Education: B.S. in Physics - Harvey Mudd College, Claremont, CA - 1984.
M.S. in Physics, University of California, San Diego - 1986.
Ph.D. in Physics, University of California, San Diego - 1991.

Employment:

Professor:	Department of Electrical and Computer Engineering
Professor:	Department of NanoEngineering
Endowed Chair & Director	Center for Memory and Recording Research University of California, San Diego (2007-present)
Senior Manager:	Hitachi Global Storage Technologies (2005-2006)
Research Staff Member	Hitachi Global Storage Technologies (2003-2006)
Research Staff Member	IBM Almaden Research Center (1997-2003)
Physicist	Argonne National Laboratory (1996-1997).
Assistant Physicist	Argonne National Laboratory (1993-1996).
Postdoctoral Appointee	Argonne National Laboratory (1991-1993).
Research Assistant	Argonne National Laboratory (1987-1990).
Research Assistant	University of California, San Diego (1985-1991).

Awards: Alfred B. Focke Award, Harvey Mudd College - 1984.
Argonne's Exceptional Performance Award, Argonne National Laboratory 1996.
Fellow of the American Physical Society – 1998.
IBM Outstanding Technical Achievement Award – 2002.
Hitachi GST Gold Patent Award – Patent # 6,537,684 – 2003.
IBM Fourth Plateau Invention Achievement Award – 2004.
Hitachi GST Gold Patent Award – Patent # 6,773,834 – 2004.
Docteur Honoris Causa from Université Henri Poincaré, Nancy France – 2011.
Fellow of the IEEE – 2011
AIP Industrial Application of Physics Prize – 2012
Lorraine University D'excellence Programme Professor@Lorraine – 2106-2020
Fulbright-Tocqueville Distinguished Chair Award – 2017-18
Member of the National Academy of Engineering – 2018

Professional Societies: American Physical Society (Fellow), IEEE Magnetics (Fellow), Materials Research Society, American Vacuum Society

Research Areas: Thin film and superlattice growth, interfacial and thin-film magnetism; magnetic recording and nano-technologies; spin-based electronics, x-ray and neutron scattering

EXHIBIT A

Students and post-docs

Post-doctoral advisor for:	Kentaro Takano	1997-1999 (HGST Research)
	Olav Hellwig	2000-2003 (HGST Research)
	Ioan Tudosa	2007-2009 (SLAC National Accelerator Laboratory)
	Vojtech Uhlir	2011-2015 (Brno University of Technology)
	Matthias Gottwald	2011-2013 (IBM)
	Dokyun Kim	2014 –2016 (Applied Materials)
	Rajasekhar Medapalli,	2014 – present
	Conrad Rizal	2014 – 2015 (Baylor University)
	Roopali Kukreja	2014 – 2015 (UC Davis)
	Mohammed El Hadri	2016 - present
	Igor Vaskivskyi	2017 – present
Graduate students:	Keith Chan (2011, currently Samsung), Erik Shipton (2011, currently GeneralAtomic), Jimmy Kan (2013, currently Qualcomm), Marko Lubarda (2013, currently Assistant Professor at the University of Donja Gorica in Montenegro), Nasim Eibagi (2016, currently Tokyo Electron), Sohini Manna, Jonathan Sapan, Richard Choi, Sergio Montoya, R. Tolley, S. Patel, T. Hensen, H. Ren, Y. Xian, UC San Diego	
Visiting professors hosted:	Aletta Prinsloo, Rand Afrikaans University, 2001. Stephane Mangin, U.H.P-Nancy, 2004-2005. Aletta Prinsloo, University of Johannesburg, 2006 Young Kim, Korea University 2010 Stephane Mangin, U.H.P-Nancy, 2013-2013 Yukiko Takahashi, NIMS, Japan, 2014	

Conference/professional society participation

Program co-chair	Intermag 2009, Sacramento, CA 2009
Co-organizer:	4 th Int. Conf. on the Physics of X-ray Multilayer Structures, Breckenridge, CO 1998.
	Focus sessions on magnetic nanostructures and heterostructures, APS March Meeting 1997.
	Tutorial on Magnetic and magneto-transport properties of metallic thin films and superlattices, APS March Meeting 1997.
	Symposium on synchrotron radiation and materials science, E-MRS, Strasbourg, 2005.
	Physics by the Bay IV conference, UC Berkeley, Oct. 1, 2005.
	International Workshop on Spin Transfer (IWSST 2006), Nancy, France 2006.
	Focus session: Nanomagnetic Particles and Structures for Information Storage Applications, APS March Meeting 2007.
	Symposium I, MRS Fall Meeting 2007, Boston MA.
	Focus session: Spin Transport & Magnetization Dynamics in Metal Based Systems, APS March Meeting 2008
	Focus session: Novel Magnetic Devices, APS March Meeting 2010.
	Nano-Magnetism and Beyond Symposium, Oct. 10, 2009, Chicago, IL
	International Workshop on Spin Transfer (IWSST 2011), Nancy, France 2011.
	International Workshop on Advanced Micromagnetics (IWAM), La Jolla, CA 2012
	International French-US Workshop: Toward low-power spintronic devices, La Jolla, CA 2013
Executive committee	APS Division of Materials Physics, 2001-2003
	APS GMAG, 2009-2011
	APS GMAG 2017 - present
Selection committee	Vice Chair: selection committee for the David Adler Lectureship Award 2005.
	Chair: selection committee for the David Adler Lectureship Award 2006.
Fellowship committee	APS Division of Materials Physics, 2002
	APS GMAG, 2009-2011
Advisory Committee:	Conference on Magnetism and Magnetic Materials AdComm committee 2007-2013
	The Magnetic Recording Conference (TMRC) Adcomm committee 2010-present
Program committee:	Workshop on Magnetism in Lower Dimensional Systems, Argonne, June 19-24, 1995.
	3 rd Int. Conf. on the Physics of X-ray Multilayer Structures, Breckenridge, CO 1996.
	5 th Int. Conf. on the Physics of X-ray Multilayer Structures, Chamonix, France 2000.
	4 th Int. Symposium on Metallic Multilayers (MML '04), Boulder, CO 2004.

	9 th Joint MMM/Intermag Conference, Anaheim, CA January 2004
	Intermag 2008, Madrid Spain
	Intermag 2011, Taipei, Taiwan
	12 th Joint MMM/Intermag Conference, Chicago, IL, January 2013
	IEEE Intermag 2014 Conference, Dresden Germany
	International Conference on Magnetism, 2015, Barcelona, Spain
	61 st Annual Conference on Magnetism and Magnetic Materials, 2016 New Orleans, LA
	International Conference on Magnetism, 2018, San Francisco, CA
	International Conference on Nanoscience + Technology 2018 (ICN+T 2018), Brno, Czech Rep.
Steering committee	The 8 th Joint MMM-Intermag Conference, San Antonio TX, 2001.
	46 th Conference on Magnetism and Magnetic Materials, Seattle WA, 2001.
	47 th Conference on Magnetism and Magnetic Materials, Tampa Bay FL, 2002.
Nominating committee	APS Topical Group on Magnetism and its Applications, 1997-1999
	APS Division of Materials Physics, 2000
Panelist	NSF FY 2003 Nanoscale Interdisciplinary Research Teams (NIRT) review panel.
	NSF FY 2005 Nanoscale Interdisciplinary Research Teams (NIRT) review panel.
	NSF Site Visit of the Materials Research Science and Engineering Center at the University of Alabama, Nov. 15-16, 2005
	NSF ECCS Division, FY 2008 Unsolicited Panel B-March 6-7, 2008 review panel
	APS ITGAP Proposal Review Committee 2010-2011
	NSF DMR-Condensed Matter Physics Review Panel, 2011
	NSF-ECCS-EPMD Unsolicited Proposal Panel on January 23-24, 2012
	NSF-ECCS-EPMD Unsolicited Proposal Panel on March 18-19, 2013
	DOE – review of the Materials Sciences programs at Ames Laboratory
	NSF Magnetic Materials SBIR/STTR Phase I Panel, March 6, 2013
	National Academy of Sciences Panel for Review of the Material Measurement Laboratory at the National Institute of Standards and Technology, June 17-19, 2014
	DOE – review of the Materials Sciences programs at Ames Laboratory, July 27-30, 2015
	BES workshop on Basic Research Needs (BRN) for Quantum Materials for Energy Relevant Technology February 8-10, 2016 Gaithersburg, MD.
	NRC Research Associateship Programs (RAP) review panels, Irvine CA, March 6-7, 2017
Judge/Chair	MRS graduate student awards, 2001-2003 MRS Spring meeting

Journal activity

Publications:	>340 published articles, including 23 Phys. Rev. Lett., 64 Phys. Rev. B and 54 Appl. Phys. Lett., Nature, 2 Science, 3 Nature Materials, 2 Nature Nanotechnology, Phys. Rev. X and Nature Physics (<i>h-index</i> =61 ISI Web of Science and 72 Google Scholar).
Advisory Editor:	Journal of Magnetism and Magnetic Materials, 2004-2008
Referee:	Nature, Science Phys. Rev. Lett., Nature Materials, Nature Physics, Nature Nanotechnology, Phys. Rev. B, Appl. Phys. Lett., J. Appl. Phys., J. Magn. Magn. Mater., IEEE Trans. Mag., Thin Solid Films, J. Mater. Res., J. Phys.: Condens. Matter, J. Vac. Sci. Technol., Appl. Phys., etc.
Books and Chapters:	Magnetic superlattices , E. E. Fullerton, <i>Handbook of Thin Film Process Technology</i> , edited by D. A. Glocker and S. I. Shah, (Bristol, IOP Publishing, 1997). X-ray scattering studies of ultrathin metallic structures , E. E. Fullerton and S. K. Sinha, in <i>Ultrathin Magnetic Structures III Fundamentals of Nanomagnetism</i> ed. by J. A. C. Bland and B. Heinrich, (Springer-Verlag, Berlin 2005). pages 285-313. <i>Nanoscale Magnetic Materials and Applications</i> ed. by JP Liu, E Fullerton, O Gutfleisch, DJ Sellmyer, (Springer Science+ Business Media, LLC, 233 Spring Street, New York, NY 10013, USA).

Issued US patents

US Patent # 6,280,813	Magnetic recording media with antiferromagnetically coupled ferromagnetic films as the recording layer Selected one of the "Five Patents to Watch" by MIT's Technology Review magazine.
US Patent # 6,372,330	Laminated magnetic recording media with antiferromagnetically coupled layers as the individual magnetic layers in the laminate
US Patent # 6,383,597	Magnetic recording media with magnetic bit regions patterned by ion irradiation
US Patent # 6,383,598	Patterned magnetic recording media with regions rendered nonmagnetic by ion irradiation
US Patent # 6,383,668	Magnetic recording media with antiferromagnetically-coupled host layer for the magnetic recording layer
US Patent # 6,391,430	Patterned magnetic recording media with discrete, magnetic regions separated by
RE40,726	regions of antiferromagnetically coupled films
US Patent # 6,440,589	Magnetic media with ferromagnetic overlay materials for improved thermal stability
US Patent # 6,537,684	Antiferromagnetically coupled magnetic recording media with boron-free first ferromagnetic film as nucleation layer.
US Patent # 6,567,236	Antiferromagnetically coupled thin films for magnetic recording
US Patent # 6,594,100	Method for recording magnetic transitions on recording layer having antiferromagnetically coupled ferromagnetic films
US Patent # 6,631,057	Magnetic device with ferromagnetic layer contacting specified yttrium or rare earth element oxide antiferromagnetic layer
US Patent # 6,650,513	Magnetic devices with a ferromagnetic layer having perpendicular magnetic anisotropy and an antiferromagnetic layer for perpendicularly exchange biasing the ferromagnetic layer.
US Patent # 6,723,450	Magnetic recording medium with antiparallel coupled ferromagnetic films as the recording layer
US Patent # 6,773,834	Laminated magnetic recording media with antiferromagnetically coupled layer as one of the individual magnetic layers in the laminate
US Patent # 6,834,026	Method for thermally-assisted recording on a magnetic recording disk
US Patent # 6,835,476	Antiferromagnetically coupled magnetic recording media with CoCrFe alloy first ferromagnetic film
US Patent # 6,836,392	Stability-enhancing underlayer for exchange-coupled magnetic structures, magnetoresistive sensors, and magnetic disk drive systems
US Patent # 6,893,741	Magnetic device with improved antiferromagnetically coupling film
US Patent # 6,992,866	Exchange-coupled magnetoresistive sensor with a coercive ferrite layer and an oxide underlayer having a spinel lattice structure
US Patent # 7,081,309	Magnetic recording disk with antiferromagnetically-coupled magnetic layer having multiple ferromagnetically-coupled lower layers
US Patent # 7,116,532	Stability-enhancing underlayer for exchange-coupled magnetic structures, magnetoresistive sensors, and magnetic disk drive systems
US Patent # 7,125,616	Magnetic recording disk with antiferromagnetically-coupled magnetic layer having multiple lower layers
US Patent # 7,360,299	Method for manufacturing a magnetic read sensor employing oblique etched underlayers for inducing uniaxial magnetic anisotropy in a hard magnetic in-stack bias layer
US Patent # 7,360,300	Method for manufacturing a magnetic read sensor employing oblique etched underlayers for inducing uniaxial magnetic anisotropy in a hard magnetic pinning layer
US Patent # 7,363,699	Method for manufacturing a magnetic read sensor employing oblique etched underlayers for inducing uniaxial magnetic anisotropy in hard magnetic bias layers
US Patent # 7,372,116	Heat assisted switching in an MRAM cell utilizing the antiferromagnetic to ferromagnetic transition in FeRh
US Patent # 7,382,590	MR sensor and thin film media having alloyed Ru antiparallel spacer layer for enhanced antiparallel exchange coupling
US Patent # 7,425,377	Incoherently-reversing magnetic laminate with exchange coupled ferromagnetic layers
US Patent # 7,457,085	Magnetic read sensor employing oblique etched underlayers for inducing uniaxial magnetic anisotropy in hard magnetic bias layers

US Patent # 7,460,343	Magnetic read sensor employing oblique etched underlayers for inducing uniaxial magnetic anisotropy in a hard magnetic in-stack bias layer
US Patent # 7,479,332	Method and apparatus for improving signal-to-noise ratio in longitudinal recording media
US Patent # 7,488,545	Perpendicular magnetic recording medium with laminated recording layers formed of exchange-coupled ferromagnetic layers
US Patent # 7,514,162	Perpendicular magnetic recording medium with metamagnetic antiferromagnetically-coupled layer between the soft underlayer and recording layer
US Patent # 7,529,065	Laminated magnetic thin films with weak antiferromagnetic coupling for perpendicular magnetic recording
US Patent # 7,550,210	Perpendicular magnetic recording medium with multiple exchange-coupled magnetic layers having substantially similar anisotropy fields
US Patent # 7,556,870	Antiferromagnetically coupled media for magnetic recording with weak coupling layer
US Patent # 7,572,526	Perpendicular magnetic recording medium with exchange-spring structure having multiple exchange-spring layers and recording system for the medium
US Patent # 7,572,527	Perpendicular magnetic recording medium with improved antiferromagnetically-coupled recording layer
US Patent # 7,588,841	Perpendicular magnetic recording exchange-spring type medium with a lateral coupling layer for increasing intergranular exchange coupling in the lower magnetic layer
US Patent # 7,615,771	Memory array having memory cells formed from metallic material
US Patent # 7,670,696	Perpendicular magnetic recording medium with patterned magnetic islands and nonmagnetic trenches and manufacturing method for suppressing surface diffusion of trench material
US Patent # 7,672,090	Magnetic read sensor employing oblique etched underlayers for inducing uniaxial magnetic anisotropy in a hard magnetic pinning layer
US Patent # 7,687,157	Perpendicular recording media having an exchange-spring structure
US Patent # 7,732,071	Perpendicular magnetic recording system with patterned medium and manufacturing process for the medium
US Patent # 7,846,563	Perpendicular magnetic recording exchange-spring type medium with a lateral coupling layer for increasing intergranular exchange coupling in the lower magnetic layer
US Patent # 7,846,565	Perpendicular magnetic recording disk drive with patterned disk having capping layer for suppression of surface diffusion of trench material
US Patent # 7,976,964	Disk drive with laminated magnetic thin films with sublayers for magnetic recording
US Patent # 7,989,096	Perpendicular recording media having an exchange-spring structure
US Patent # 8,021,769	Patterned perpendicular magnetic recording medium with exchange coupled recording layer structure and magnetic recording system using the medium
US Patent # 8,263,239	Laminated magnetic thin films for magnetic recording with weak ferromagnetic coupling,

Patent Awards:

IBM Invention Achievement Award - Patent # 6,280,813 ranked among top 10% most valuable IBM Patents.

IBM First Plateau Invention Achievement Award 2001.

IBM Second Plateau Invention Achievement Award 2002.

IBM Third Plateau Invention Achievement Award 2002.

IBM Fourth Plateau Invention Achievement Award 2003.

Hitachi GST Gold Patent Award – Patent # 6,537,684 ranked one of the most valuable HGST patents of 2003.

Hitachi GST Gold Patent Award – Patent # 6,773,834 ranked one of the most valuable HGST patents of 2004

Invited Talks (conferences and workshops)

120. **Materials Challenges of Data (Keynote speaker)**
The Material World Forum, Nancy, France, June 27-29, 2018
119. **Challenges of big data: Handling bits in a modern world**
Fulbright Conférence Inaugurale, Nancy, France, April 9, 2018
118. **Skymion formation and current control in Pt/Co/Os/Pt heterostructures**
One Day Workshop: Nanomagnetism, Nancy, France, Feb. 7, 2018.
117. **Interplay of structure and magnetism during ultrafast optical excitations**
International Workshop on Ultrafast Dynamics and Metastability, Washington, DC, Nov. 12-15, 2017
116. **Role of magnetic correlations on the antiferromagnetic-to-ferromagnetic phase transition in FeRh**
The 62nd Annual Conference on Magnetism and Magnetic Materials, Pittsburgh, PA, Nov. 6-10, 2017
115. **Materials Optimization to Form Skymions and Skymion lattices**
Workshop on Magnetic Nano-objects, Nancy, France, Oct. 2, 2017
114. **Materials Optimization to Form Skymion and Skymion lattices**
Skymionics: Materials, Phenomena and Applications Workshop, Santa Fe, NM, Aug. 7-10, 2017
113. **Role of microstructures on all-optical switching and THz emission**
The 28th Magnetic Recording Conference, Tsukuba, Japan, Aug. 2-4, 2017
112. **All-optical control of magnetic thin films and nanostructures**
Frontiers in Theoretical and Applied Physics | UAE 2017 (FTAPS 2017), Sharjah, UAE, Feb. 22-25, 2017
111. **All-optical switching and spin-lattice coupling in granular FePt films**
International Workshop & School on Spin Transfer (IWST 2016), Nancy, France, Sept. 19-23, 2016
110. **Controlled magnetic phase transitions and transition asymmetry in mesoscale FeRh stripes**
SPIE Optics + Photonics 2016, San Diego, CA Aug. 31, 2016
109. **Strain-induced modification of nanoscale ceramic material properties**
NSF-sponsored Ceramics for Energy Workshop, La Jolla, CA, 6/3-4/2016.
108. **Emergent phenomena in FeRh films and mesoscale wires**
International Workshop on Spintronic Memory and Logic, Beihang University, Beijing, China, 4/ 30-5/2, 2016
107. **Interplay of structure and magnetism during ultrafast optical excitations**
New Opportunities for Magnetic Dynamics and Materials using synchrotron facilities, Vail, CO, Mar. 21-14, 2016
106. **Optical control of ferromagnetic films and nanostructures**
Materials Science Joint Workshop between Korea University and UCSD, Seoul, South Korea, Feb. 2, 2016
105. **Controlled optical switching of ferromagnetic thin films and nanostructures**
20th International Conference on Magnetism, Barcelona, Spain, July 10, 2015
104. **Optical control of magnetic films and nanostructures**
Conference on Light and Nanomagnetism, July 2, 2015, Nancy France
103. **Future of big data: the challenges of more data using less energy**
World Materials Forum, 23 & 24 June 2015, Nancy, France
102. **All optical control of magnetic thin films and nanostructures**
79th Annual Meeting of the DPG and DPG Spring Meeting, p. MA 41.2, Berlin, Germany, Mar. 15-20
101. **Shining light on magnetism: controlled magnetic switching with optical laser pulses**
IEEE Magnetics Society Rocky Mountain Chapter Technical Presentation, Boulder CO, Jan. 14, 2015.
100. **Magnetic recording: 116 years of progress and the challenges ahead**
59th Annual Magnetism and Magnetic Materials Conference, Honolulu, HI, Nov. 3-7, 2014.
99. **All optical control of magnetic thin films and nanostructures**
Magnetic Single Nano-Object Workshop (M-SNOW 14), Nancy, France, Sept. 9-12, 2014.
98. **All optical control of magnetic thin films and nanostructures**
Magnetic Single Nano-Object Workshop (M-SNOW 14), Nancy, France, Sept. 9-12, 2014.
97. **All optical control of magnetic thin films and nanostructures**
SPIE Optics + Photonics 2015, San Diego, CA, Aug. 17-12, 2014.
96. **All optical control of magnetic thin films and nanostructures**
The 25th Magnetic Recording Conference (TMRC 2014), Berkeley, CA, Aug 11-13, 2014
95. **Bits of the Future: Emergent Physics for Advanced Magnetic Information Technologies (Plenary speaker)**
The 59th Annual Conference of the South African Institute of Physics, Johannesburg South Africa, July 7-11, 2014
94. **Bits of the Future: Emergent Physics for Advanced Magnetic Information Technologies (Keynote speaker)**
23rd ASME Annual Conference on Information Storage and Process Systems, Santa Clara CA June 23, 2014

93. **Engineered materials for all-optical helicity-dependent magnetic switching**
2014 March Meeting of the American Physical Society, Denver, Co, Mar. 3 – Mar. 8, 2014.
92. **Engineered materials for all-optical helicity-dependent magnetic switching**
58th annual conference on Magnetism and Magnetic Materials (MMM), Denver, Co, Nov. 8-12, 2013
91. **Characterization of engineered magnetic materials at nanometer spatial scales and ultra-fast time scales**
The ALS Cross-Cutting Review of Magnetism and Spintronics, Berkeley, CA, Oct. 21-22, 2013
90. **Materials challenges for advanced magnetic storage and memory applications (Plenary speaker)**
XXII International Materials Research Congress 2013, Cancun, Mexico, Aug. 11-15, 2013
89. **Light-induced magnetization reversal of high-anisotropy TbCo alloy films**
1st Int. Workshop on Spin-Orbit Induced Torque, KAUST, Thuwal, Saudi Arabia, Feb. 24-27, 2012
88. **The physics of perpendicular anisotropy devices**
The 16th Joint Inter-laboratory Workshop on Nano-Magnetics, Jeju Island, Korea Sept. 19-20, 2012.
87. **Field and current reversal of perpendicular spin-torque devices**
Int. Conf. on Electronic Materials and Nanotechnologies for Green Environment, Jeju Isl., Korea Sept. 16-19, 2012.
86. **Magnetic nanostructures for advanced storage and memory applications (Plenary speaker)**
Int. Conf. on Electronic Materials and Nanotechnologies for Green Environment, Jeju Isl., Korea Sept. 16-19, 2012.
85. **Energy-assisted writing of high-anisotropy nanostructures**
The Magnetic Recording Conference (2012), San Jose, CA, Aug. 19-22, 2012
84. **Spin Transfer Torque Phenomena in Perpendicular Anisotropy Devices**
2012 Materials Research Society Spring Meeting, San Francisco, CA, April 9 – 24, 2012
83. **AIP Prize for Industrial Applications of Physics Lecture: Controlled exchange in recording media and spintronic devices**, 2012 March Meeting of the American Physical Society, Boston, MA, Feb. 27 – Mar. 2, 2012.
82. **Controlled growth and magnetic properties of CVD grown Ni nanostructures**
Magnetic Single Nano-Object Workshop & School (M-SNOWS '12, Feb. 5-10, 2012, Les Houches, France
81. **Spin-torque phenomena in high-anisotropy magnetic nanostructures**
Symposium: Physics at the nanoscale, Madrid Spain, Oct. 18-21, 2011.
80. **X-ray imaging of structure and magnetism in thin films and nanowires**
COSMIC at the ALS: New Frontiers in Soft X-Ray Coherent Scattering and Imaging Workshop, Berkeley, CA Aug. 2-3, 2011.
79. **Spin-torque phenomena in high-anisotropy magnetic nanostructures**
MORIS-2011 Conference, Nijmegen, the Netherlands, June 21-24 2011.
78. **Current induced modification of the hard layer in perpendicular anisotropy spin valves**
IWST '11, International Workshop on Spin Torque 2011, Nancy France, Jan. 19 2011.
77. **Bits of the future: Impact of GMR on magnetic information storage**
Colloque 2010 de l'Institut Jean Lamour – Nanosciences, Nancy University, Jan. 14 2011
76. **Magnetic information technologies: Challenges and research opportunities.**
The 55th Magnetism and Magnetic Materials Conference, Atlanta, GA, Nov. 14-18, 2010.
75. **Spin-torque phenomena in high-anisotropy magnetic nanostructures (Plenary speaker)**
IEEE 7th International Symposium on Metallic Multilayers (MML2010) Berkeley CA, Sept. 19-24, 2010
74. **Magnetic spectroscopy**
National School on Neutron and X-ray Scattering, Argonne, IL, June 17, 2010.
73. **Spin-torque behavior of perpendicular anisotropy nanopillar devices**
AVS 56th International Symposium and Exhibition, San Jose, CA, Nov. 8-13, 2009.
72. **Spin transfer torques in high anisotropy magnetic nanostructures**
Nanoscale Magnetism, 2009 Advanced Light Source User's Meeting, Berkeley, CA, Oct. 15-17, 2009.
71. **Spin transfer torques in high anisotropy magnetic nanostructures (Keynote speaker)**
Trends in Nanotechnology TNT 2009, Barcelona, Spain, Sept. 7-11, 2009.
70. **Magnetic spectroscopies**
National School on Neutron and X-ray Scattering, Argonne, IL, June 11, 2009.
69. **Materials requirements for next-generation magnetic storage and memory applications: Part II**
International School on Magnetic Single Nano-Object, Nancy France, Nov. 23, 2008.
68. **Materials requirements for next-generation magnetic storage and memory applications: Part I**
International School on Magnetic Single Nano-Object, Nancy France, Nov. 23, 2008.
67. **Influence of spin transfer torques on the Stoner-Wohlfarth astroid**
53rd conference on Magnetism and Magnetic Materials, Austin, TX 2008.
66. **Spin torque devices with perpendicular magnetic anisotropy**

Workshop on "Materials for spin transfer torque MRAM", Univ. of Alabama, Tuscaloosa AL, Oct. 15, 2008.

65. **Magnetic multilayers**
National School on Neutron and X-ray Scattering, Argonne, IL, Oct. 8, 2008.
64. **Current and field induced reversal of magnetic islands with perpendicular anisotropy spintronics** Symposium of the SPIE Optics & Photonics Conference, San Diego, CA, August 10-14, 2008.
63. **Exchange spring reversal in high anisotropy composite materials**
52nd Magnetism and Magnetic Materials Conference, Tampa, FL, Nov. 5-9, 2007.
62. **Spin-torque-induced reversal in nanopillars containing perpendicularly magnetized layers**
2007 March Meeting of the American Physical Society, Denver CO, 2007.
61. **Magnetism at the Nanoscale: Applications**
Tutorial, 2007 March Meeting of the American Physical Society, Denver CO, 2007
60. **Magnetic reversal and domain structure in perpendicular AF-coupled films**
Plenary speaker, 5th Int. Conf. on Synchrotron Radiation in Materials Science, Chicago, IL July 31, 2006.
59. **Current-induced magnetization reversal and domain formation in nanopillars with perpendicular anisotropy**
California Symposium on Nanomagnetism, UC Irvine, CA April 10-11, 2006
58. **Probing magnetism at the nanoscale: new physics and emerging technologies**
Workshop on Soft X-ray Scattering from Hard and Soft Matter, LBNL, Berkeley, CA Sept. 31, 2005.
57. **Nano-structured magnetic materials: novel physics and emerging technologies**
National Nanotechnology Initiative Workshop on X-rays and Neutrons: Essential Tools for Nanoscience Research, Washington D.C. June 16-17, 2005.
56. **Resonant x-ray scattering from nano-structured magnetic recording materials**
The 2nd US-Japan Workshop on Synchrotron Radiation and Nanoscience, San Diego, CA April 4-6, 2005.
55. **Nano-structured magnetic materials for high-density recording**
Workshop on nanomagnetism using x-ray techniques, Lake Geneva, WI, Aug. 29 – Sept. 1, 2004.
54. **Soft x-ray techniques for characterizing magnetic nanostructures**
LANSCE Neutron Scattering Winter School, Los Alamos National Laboratory, Jan. 14, 2004.
53. **Antiferromagnetically-coupled perpendicular anisotropy films**
DOE CSP Nanocomposite magnetic materials 2003 annual workshop, Monterey, CA, Oct. 19-21, 2003.
52. **Resonant magnetic x-ray imaging and scattering as probes of heterogeneous thin films**
International Symposium on Advanced Magnetic Materials-2003, Yokohama, Japan, Oct. 8-13, 2003.
51. **Antiferromagnetically-coupled magnetic media layers for high-density recording**
5th Joint UK Magnetism Workshop, University of Glasgow, July 2-4, 2003.
50. **Thermal energy and the potential limits of magnetic nanostructures**
Nanoscience: Controlling Interactions in Complex Materials, Workshop, Argonne, IL, May 1, 2003.
49. **Domain and domain wall structure in antiferromagnetic films with perpendicular anisotropy**
2003 March Meeting of the American Physical Society, Austin TX, March 4, 2003.
48. **Soft x-ray characterization of perpendicular recording media**
North American Perpendicular Magnetic Recording Conference, Monterey, CA, Jan. 7-9, 2003.
47. **Magnetic small-angle soft x-ray scattering as a probe of nanocomposite magnetic films**
Fall MRS meeting, Boston, MA (2002).
46. **Magnetic x-ray scattering from nanocomposite magnetic films used for high-density recording**
The 7th International Conf. on Surface X-ray & Neutron Scattering, Lake Tahoe, CA Sept. 23-27 (2002).
45. **Coupled magnetic media: the promises and the pitfalls**
The Magnetic Recording Conference 2002, Santa Clara, CA, August 28-30 (2002).
44. **Magnetic x-ray scattering as a probe of recording media**
European Materials Research Society Meeting. Strasbourg, June 18-21, 2002
43. **Nanotechnology in magnetic data storage**
4th EC/NSF Workshop on Nanotechnology, Grenoble, June 12-14, 2002.
42. **Soft x-ray characterization of perpendicular recording media**
North American Perpendicular Magnetic Recording Conference, Coral Gables, FL, Jan. 7-9, 2002.
41. **Domain structure in LaFeO₃ thin films and its role on exchange coupling**
46th Conference on Magnetism and Magnetic Materials, Seattle WA, Nov. 15, 2001.
40. **Critical issues in magnetic recording technologies**
Workshop on Spectroscopies of Electronic Materials: Correlated Electrons and Nanoscale Phenomena
Advanced Light Source, Lawrence Berkeley National Laboratory, Oct. 16, 2001.
39. **Antiferromagnetically-coupled magnetic media layers for thermally-stable high-density recording**

- IUVSTA 15th International Vacuum Congress, San Francisco, CA Oct. 28-Nov. 2, 2001.
38. **Antiferromagnetically-coupled recording media**
DISKCON 2001, San Jose, CA Sept. 19, 2001.
 37. **Advance magnetic recording media, beyond the superparamagnetic limit**
IEEE Magnetics Society Lecture, Santa Clara, Sept. 11, 2001.
 36. **Multilayers**
National School on Neutron and X-ray Scattering, Argonne, IL Aug. 24, 2001.
 35. **Antiferromagnetically-coupled magnetic media for thermally-stable high-density recording**
2001 Materials Research Society Spring meeting, San Francisco, CA April 18, 2001.
 34. **Thermally stable magnetic media based on antiferromagnetically coupled layers**
2001 March Meeting of the American Physical Society, Seattle, WA March 14, 2001.
 33. **Bits of the future, High-density magnetic recording media**
IEEE Magnetics Society Lecture, La Jolla, CA, Feb. 8, 2001.
 32. **Antiferromagnetically-coupled magnetic recording media**
The 8th joint MMM-Intermag conference, Jan. 7-11, 2001.
 31. **Incoherent and coherent scattering from nanocomposite magnetic films used for high-density magnetic recording**
Workshop on Soft X-Ray Speckle: Nanoscale Dynamics in Liquids and Solids, Stanford, Oct. 18 2000.
 30. **Growth, characterization and recording performance of Co-X/Pd multilayer record media**
The 5th Perpendicular Magnetic Recording Conference, Sendai, Japan, Oct. 23-26, 2000.
 29. **Thin film and multilayer structures**
National School on Neutron and X-ray Scattering, Argonne National Laboratory, Aug. 14-26, 2000.
 28. **Physical limits of magnetic thin film technologies (Plenary speaker).**
45th South African Inst. of Physics, Johannesburg, South Africa July 5, 2000.
 27. **Soft X-ray characterization of structural and magnetic heterogeneity in magnetic films and recording media**
44th Annual Conference on Magnetism and Magnetic Materials, San Jose, CA Nov. 15-19, 1999.
 26. **Multilayers**
Neutron and X-ray Scattering Summer School, Argonne National Laboratory, Aug. 26, 1999.
 25. **Neutron determination of Fe and Cr ordering in Fe/Cr(001) superlattices**
The Advanced Study Institute meeting on *Exploration of Subsurface Phenomena by Particle Scattering*
Naval Postgraduate School, Monterey, CA October 19-23, 1998
 24. **Magnetoresistance: Physics and Applications**
Tutorial, 1998 March Meeting of the American Physical Society, Los Angeles CA, March 15, 1998.
 23. **Exchange-spring behavior in epitaxial hard/soft magnetic heterostructures**
1998 March Meeting of the American Physical Society, Los Angeles, CA March 17, 1998.
 22. **X-Ray diffraction and reflectivity analysis**
4th international conference on the Physics of X-ray Multilayer Structures, Breckenridge CO.1998.
 21. **Exchange-spring behavior in epitaxial hard/soft magnetic heterostructures**
1998 March Meeting of the American Physical Society, Los Angeles, CA March 17, 1998.
 20. **General approach to the epitaxial growth of RE-TM thin films and heterostructures**
American Vacuum Society, Oct. 20-24, 1997 San Jose, CA
 19. **Structure and magnetism of epitaxial Fe/Cr superlattices**
Fourth International Conference on Composites Engineering, July 6-11, 1997, Hawaii.
 18. **Argonne's results on the magnetic state of Cr in Fe/Cr superlattices**
Workshop on the Magnetic State of Cr in Fe/Cr/Fe, NIST, Gaithersburg, MD Nov. 6, 1996.
 17. **Spin-density-wave antiferromagnetism of Cr in Fe/Cr(001) superlattices**
5th International Conference on the Physics of Transition Metals, Osaka Japan, Sept. 24-27, 1996.
 16. **Growth and magnetic ordering of epitaxial Fe/Cr superlattices**
American Vacuum Society-Rocky Mountain Chapter Meeting, Denver, CO Aug. 22, 1996.
 15. **Structure and magnetism of epitaxial rare-earth-transition-metal films**
NATO-ASI school on Magnetic Hysteresis in Novel Magnetic Materials, Mykonos, Greece, July 1-12, 1996.
 14. **The role of Cr ordering on the magnetic and transport properties of Fe/Cr superlattices**
Intermag, Seattle WA, April 9-12, 1996.
 13. **Fundamental magnetic and magneto-transport properties of ultrathin metallic structures**
Tutorial, 1996 March Meeting of the American Physical Society, St. Louis, March 17, 1996.
 12. **Suppression of biquadratic coupling at the Cr Néel temperature in Fe/Cr(001) superlattices**
40th Annual Conference on Magnetism and Magnetic Materials, Philadelphia, PA Nov. 6-9, 1995.

11. **New physics in epitaxial Fe/Cr superlattices**
1st Gordon Conference on Magnetic Nano-structures, Irsee, Bavaria Sept. 17-22, 1995.
10. **Quantitative x-ray diffraction from thin films and superlattices**
IV International Conference on Advanced Materials 1995, Cancun, Mexico, Aug. 27 - Sept. 1, 1995.
9. **Quantitative x-ray diffraction from thin films and superlattices**
1st Michigan State Univ. workshop on the structure of metallic multilayers, East Lansing, MI July 10, 1995.
8. **Magnetic ordering transition at the Cr Néel temperature in Fe/Cr(001) superlattices**
IV International Conference on Surface X-Ray and Neutron Scattering, Lake Geneva, WI, June 26-30, 1995.
7. **Magnetic phase transitions in epitaxial Fe/Cr superlattices**
XVIII Brazilian Meeting of Condensed Materials, Caxambú, Brazil, June 6-10, 1995.
6. **Magnetic phase transitions in epitaxial Fe/Cr superlattices**
1995 Spring Meeting of the Material Research Society, San Francisco, CA, April 17-21, 1995.
5. **Interlayer coupling in novel superlattice structures**
1994 March Meeting of the American Physical Society, Bull. Am. Phys. Soc. **39**, 556 (1994).
4. **Characterization of interface structure in multilayers using specular x-ray reflectance**
Physics of X-ray Multilayer Structures, Optical Society of America, Jackson Hole, WY, March 14-17, 1994.
3. **Structure and magnetism of sputtered superlattices**
New Horizons: A workshop on the state of the art in neutron reflectometry, Gaithersburg, MD, Dec. 9, 1993.
2. **Quantitative structural and chemical analysis of thin films and superlattices**
Tutorial, 1992 March Meeting of the American Physical Society, Indianapolis Indiana, March 15, 1992.
1. **Magnetic properties of Fe/Cr and Fe/Cu superlattices**
35th Annual Conference on Magnetism and Magnetic Materials Fall 1990.

Journal publications

348. **Periodic chiral magnetic domains in single-crystal nickel nanowires**
J. J. Kan, M. V. Lubarda, K. T. Chan, V. Uhlir, A. Scholl, V. Lomakin, and E. E. Fullerton, *Phys. Rev. Mater.* **2**, 064406 (2018).
347. **Microstructure and magneto-optical surface plasmon resonance of Co/Au**
C. Rizal, S. Pisana, I. Hrvoic and E. E. Fullerton, *J. Phys. Comm.* **2**, 055010 (2018).
346. **Bragg coherent diffractive imaging of ferromagnetic Nickel nanoparticles**
J. W. Kim, S. Manna, R. Harder, J. Wingert, E. E. Fullerton, and O. G. Shpyrko, *J. Appl. Phys.* **123**, 204302 (2018)
345. **Laser induced phase transition in epitaxial FeRh layers studied by pump-probe valence band photoemission**
F. Pressacco, V. Uhlir, M. Gatti, A. Nicolaou, A. Bendounan, J. A. Arregi, S. K. K. Patel, E. E. Fullerton, D. Krizmanic, F. Sirotti, *Structural Dynamics* **5**, 034501 (2018).
344. **Observation of all-optical switching in He⁺-irradiated Co/Pt multilayers: influence of the domain wall energy**
M. S. El Hadri, M. Hehn, G. Malinowski, C. Beigne, E. E. Fullerton, D. Ravelosona and S. Mangin, *J. Phys. D: Appl. Phys.* **51**, 215004 (2018).
343. **A Wearable Colorimetric Dosimeter to Monitor Sunlight Exposure**
J. Wang, A. S. Jeevarathinam, A. Jhunjhunwala, H. Ren, J. Lemaster, Y. Luo, D. P. Fenning, E. E. Fullerton, and J. V. Jokerst, *Adv. Mater. Technol.* **5**, 1800037 (2018).
342. **Room-temperature observation and current control of skyrmions in Pt/Co/Os/Pt thin films**
R. Tolley, S. A. Montoya, and E. E. Fullerton, *Phys. Rev. Mater.* **2**, No. 4 (Apr. 2018) pp 044404 (2018).
341. **Residual Stress in Cr₉₉Al₁ Polycrystalline Thin Films**
Z. P. Mudau, C. J. Sheppard, A. R. E. Prinsloo, A. M. Venter, T. P. Ntsoane, and E. E. Fullerton, *Acta Physica Polonica A* **133**, 578-581 (2018).
340. **Room-temperature observation and current control of skyrmions in Pt/Co/Os/Pt thin films.**
R Tolley, S. A. Montoya, and E. E. Fullerton, *Phys. Rev. Mater.* **2**, 044404 (2018)
339. **Nanostructuring multilayer hyperbolic metamaterials for ultrafast and bright green InGa_N quantum wells**
D. Lu, H. Qian, K. Wang, H. Shen, F. Wei, Y. Jiang, E. E. Fullerton, P. K. L. Yu, and Z. Liu, *Adv. Mater.* **30**, 1706411 (2018).
338. **Magnetization reversal and confinement effects across the metamagnetic phase transition in mesoscale FeRh structures**
J. A. Arregi, M. Horký, K. Fabianová, R. Tolley, E. E. Fullerton, and V. Uhlir, *J. Phys. D: Appl. Phys.* **51**, 105001 (2018).
337. **Helicity-dependent all-optical domain wall motion in ferromagnetic thin films**
Y. Quessab, R. Medapalli, M.S. El Hadri, M. Hehn, G. Malinowski, E.E. Fullerton, S. Mangin, *Phys. Rev. B* **97**, 054419 (2018).
336. **Spin transfer torque magnetization reversal in a hard/soft composite structures**
M. Kuteifan, C.-H. Lambert, M. V. Lubarda, V. Lomakin, E.E. Fullerton, and S. Mangin, *AIP Advances* **8**, 015024 (2018).
335. **Phase coexistence and kinetic arrest in the magnetostructural transition of the ordered alloy FeRh**
D. J. Keavney, Y. Choi, M. V. Holt, V. Uhlir, D. Arena, E. E. Fullerton, P. J. Ryan and J.-W. Kim, *Scientific Reports* **8**, 1778 (2018).
334. **Beyond a phenomenological description of magnetostriction**
A. H. Reid, X. Shen, P. Maldonado, T. Chase, E. Jal, P. Granitzka, K. Carva, R. K. Li, J. Li, L. Wu, T. Vecchione, T. Liu, Z. Chen, D. Higley, N. Hartmann, R. Coffe, J. Wu, G. L. Dakowski, W. Schlotter, H. Ohldag, Y.K. Takahashi, V. Mehta, O. Hellwig, A. Fry, Y. Zhu, J. Cao, E. E. Fullerton, J. Stöhr, P. M. Oppeneer, X. J. Wang & H.A. Dürr, *Nature Communications*, **9**, 388 (2018).
333. **Characterization of strain and its effects on ferromagnetic nickel nanocubes**
S. Manna, J. W. Kim, M. V. Lubarda, J. Wingert, R. Harder, F. Spada, V. Lomakin, O. Shpyrko and E. E. Fullerton, *AIP Advances* **7**, 125025 (2017).
332. **Mechanism of all-optical control of ferromagnetic multilayers with circularly polarized light**
R. Medapalli, D. Afanasiev, D. K. Kim, Y. Quessab, S. Manna, S. Montoya, A. Kirilyuk, Th. Rasing, A. V. Kimel, E. E. Fullerton, *Phys. Rev. B* **96**, 224421 (2017).
331. **Pair distribution function analysis applied to decahedral gold nanoparticles,**
H. Nakotte, C. Silkwood, K. L. Page, H.W. Wang, D. Olds, B. Kiefer, S. Manna, D. Karpov, E. Fohtung and E. E. Fullerton, *Physica Scripta* **92**, 114002 (2017).
330. **Manipulating exchange bias using all-optical helicity-dependent switching**

- P. Vallobra, T. Fache, Y. Xu, L. Zhang, G. Malinowski, M. Hehn, J.-C. Rojas-Sánchez, E.E. Fullerton and S. Mangin, *Phys. Rev. B* **96**, 144403 (2017).
329. **Electronic metamaterials with tunable second-order optical nonlinearities**
H.-H. Lin, F. Vallini, M.-H. Yang, R. Sharma, M. W. Puckett, S. Montoya, C. D. Wurm, E. E. Fullerton, and Y. Fainman, *Scientific Reports*, **7**, 9983 (2017).
 328. **3D Bragg coherent diffractive imaging of five-fold multiply twinned gold nanoparticle**
J. W. Kim, A. Ulvestad, S. Manna, R. Harder, E.E. Fullerton, and O. G. Shpyrko, *Nanoscale* **9**, 13153-13158 (2017).
 327. **The 2017 Magnetism Roadmap**
D. Sander, S. Valenzuela, D. Makarov, C. Marrows, E. E. Fullerton, P. Fischer, J. McCord, P. Vavassori, S. Mangin, P. Pirro, B. Hillebrands, A. Kent, T. Jungwirth, O. Gutfleisch, C.-G. Kim, and A. Berger, *J. Phys. D: Appl. Phys.* **50**, 363001 (2017).
 326. **Perpendicular magnetic anisotropy and microstructure properties of nanoscale Co/Au multilayers**
C. Rizal and E. E. Fullerton, *J. Phys. D: Appl. Phys.* **50**, 355002 (2017).
 325. **Nanosecond x-ray photon correlation spectroscopy on magnetic skyrmions**
M. H. Seaberg, B. Holladay, J. C. T. Lee, M. Sikorski, A. H. Reid, S. A. Montoya, G. L. Dakovski, J. D. Koralek, G. Coslovich, S. Moeller, W. F. Schlotter, R. Streubel, S. D. Kevan, P. Fischer, E. E. Fullerton, J. L. Turner, F.-J. Decker, S. K. Sinha, S. Roy, and J. J. Turner, *Phys. Rev. Lett.* **119**, 067403(2017).
 324. **Visualizing Spin Selectivity in DNA Mediated Charge Transfer via Fluorescence Microscopy**
J. M. Abendroth, N. Nakatsuka, M. Ye, D. K. Kim, E. E. Fullerton, A. M. Andrews, and P. S. Weiss, *ACS Nano* **11**, 7516-7526 (2017).
 323. **Resonant properties of dipole skyrmions in amorphous Fe/Gd multilayers**
S. A. Montoya, S. Couture, J. J. Chess, J. C. T Lee, N. Kent, M.-Y. Im, S.D. Kevan, P. Fischer, B. J. McMorran, S. Roy, V. Lomakin, and E.E. Fullerton, *Phys. Rev. B* **95**, 224405 (2017).
 322. **Static and Dynamic Interfacial Effects in Magnetism**
F. Hellman, A. Hoffmann, Y. Tserkovnyak, G. S. D. Beach, E. E. Fullerton, C. Leighton, A. H. MacDonald, D. C. Ralph, D. A. Arena, H. A. Dürr, P. Fischer, J. Grollier, J. P. Heremans, T. Jungwirth, A. V. Kimel, B. Koopmans, I. N. Krivorotov, S. J. May, A. K. Petford-Long, J. M. Rondinelli, N. Samarth, I. K. Schuller, A. N. Slavin, M. D. Stiles, O. Tchernyshyov, A. Thiaville and B. L. Zink, *Rev. Mod. Phys.* **89**, 025006/1-79 (2017).
 321. **Increased magnetic damping in ultrathin films of Co₂FeAl with perpendicular anisotropy**
Y.K. Takahashi, Y. Miura, R. Choi, T. Ohkubo, Z.C. Wen, K. Ishioka, R. Mandal, R. Medapalli, H. Sukegawa, S. Mitani, E. E. Fullerton and K. Hono, *Appl. Phys. Lett.* **110**, 252409 (2017).
 320. **Magnetic switching in granular FePt layers promoted by near-field laser enhancement**
P. W. Granitzka, E. Jal, L. Le Guyader, M. Savoini, D. J. Higley, T. Liu, Z. Chen, T. Chase, H. Ohldag, G. L. Dakovski, W. Schlotter, S. Carron, M. Hoffman, P. Shafer, E. Arenholz, O. Hellwig, V. Mehta, Y. K. Takahashi, S. L. Johnson, E. E. Fullerton, J. Stöhr, A. H. Reid and H. A. Dürr, *Nano Letters* **17**, 2426-2432 (2017).
 319. **A streamlined approach to mapping the magnetic induction of skyrmionic materials**
J. J. Chess, S. A. Montoya, T. R. Harvey, C. Ophus, S. Couture, V. Lomakin, E. E. Fullerton, and B. J. McMorran, *Ultramicroscopy* **177**, 78-83 (2017).
 318. **Synthesis of second-order nonlinearities in dielectric-semiconductor-dielectric metamaterials**
H.-H. Lin, M.-H. Yang, R. Sharma, M. W. Puckett, S. Montoya, C. D. Wurm, F. Vallini, E. E. Fullerton, and Y. Fainman, *Appl. Phys. Lett.* **110**, 113103 (2017).
 317. **Determination of domain wall chirality using in-situ Lorentz transmission electron microscopy**
J. J. Chess, S. A. Montoya, E. E. Fullerton, and B. J. McMorran, *AIP Advances* **7**, 056807 (2017).
 316. **Tailoring magnetic energies to form skyrmions and skyrmion lattices**
S. A. Montoya, S. Couture, J. J. Chess, J. C. T Lee, N. Kent, D. Henze, M.-Y. Im, S.D. Kevan, P. Fischer, B. J. McMorran, V. Lomakin, S. Roy, and E.E. Fullerton, *Phys. Rev. B* **95**, 024415 (2017).
 315. **Phase coexistence and pinning of charge density waves by interfaces in chromium**
A. Singer, S. K. K. Patel, V. Uhlir, R. Kukreja, A. Ulvestad, E. M. Dufresne, A. R. Sandy, E. E. Fullerton, and O. G. Shpyrko, *Phys. Rev. B* **94**, 174110 (2016).
 314. **Observation of x-ray radiation pressure effects on nanocrystals**
J. W. Kim, A. Ulvestad, S. Manna, R. Harder, E. Fohtung, A. Singer, L. Boucheron, E. E. Fullerton, and O. G. Shpyrko, *J. Appl. Phys.* **120**, 163102 (2016).
 313. **Universal domain wall dynamics under electric field in Ta/CoFeB/MgO devices with perpendicular anisotropy**
W. Lin, N. Vernier, G. Agnus, K. Garcia, B. Ocker, W. Zhao, E. E. Fullerton and D. Ravelosona, *Nature Communications* **7**, 13532 (2016).
 312. **Luminescent hyperbolic metasurfaces**

- J. Smalley, F. Valini, S. Montoya, L. Ferrari, S. Shahin, C. T. Riley, B. Kanté, E. E. Fullerton, Z. Liu, and Y. Fainman, *Nature Communications* **8**, 13793 (2016).
311. **Accumulative magnetic switching of ultra-high-density recording media by circularly polarized light**
Y.K. Takahashi, R. Medapalli, S. Kasai, J. Wang, K. Ishioka, S.H. Wee, O. Hellwig, K. Hono, and E.E. Fullerton, *Phys. Rev. Appl.* **6**, 054004 (2016).
 310. **Colossal magnetic phase transition asymmetry in mesoscale FeRh stripes**
V. Uhlíř, J. A. Arregi and E. E. Fullerton, *Nature Communications* **7**, 13113 (2016).
 309. **Domain size criterion for the observation of all-optical helicity-dependent switching in magnetic thin films**
M. S. El Hadri, M. Hehn, P. Pirro, C.-H. Lambert, G. Malinowski, E. E. Fullerton, and S. Mangin, *Phys. Rev. B* **94**, 064419 (2016).
 308. **Enhancement of charge ordering by dynamic electron-phonon interaction**
A. Singer, S. K. K. Patel, R. Kukreja, V. Uhlíř, J. Wingert, S. Festersen, D. Zhu, J. M. Glowina, H. Lemke, S. Nelson, M. Kozina, K. Rossnagel, M. Bauer, B. M. Murphy, O. M. Magnussen, E. E. Fullerton, and O. G. Shpyrko, *Phys. Rev. Lett.* **117**, 056401 (2016).
 307. **Synthesizing Skyrmion Molecules in Fe-Gd Thin Films**
J. C. T. Lee, J. Chess, S. A. Montoya, X. Shi, N. Tamura, S. K. Mishra, D. H. Parks, P. Fischer, B. McMorran, S. K. Sinha, E. E. Fullerton, S. D. Kevan, and S. Roy, *Appl. Phys. Lett.* **109**, 022402 (2016).
 306. **Torque magnetometry of perpendicular anisotropy exchange-spring heterostructures**
P. Vallobra, T. Hauet, F. Montaigne, E.G Shipton, E.E. Fullerton, S. Mangin, *J. Appl. Phys.* **120**, 013903 (2016).
 305. **Current-induced pinwheel oscillations in perpendicular magnetic anisotropy spin valve nanopillars**
R. Choi, J. A. Katine, S. Mangin, and E. E. Fullerton, *IEEE Trans. Mag.* **52**, 1300705 (2016).
 304. **Spintronics, magnetoresistive heads, and the emergence of the digital world**
E. E. Fullerton and J. R Childress, *Proc. of the IEEE* **104**, 1787-1795 (2016).
 303. **All-optical switching in granular ferromagnets caused by magnetic circular dichroism**
M.O.A. Ellis, E. E. Fullerton, R. W Chantrell, *Scientific Reports* **6**, 30522 (2016).
 302. **Synthesis of single-crystalline anisotropic Au nano-crystals via chemical vapor deposition**
S. Manna, J. W. Kim, Y. Takahashi, O. G. Shpyrko, and E. E. Fullerton, *J. Appl. Phys.* **119**, 174301 (2016).
 301. **Photo-spintronics: Magnetic field controlled photoemission and light controlled spin transport in hybrid chiral oligopeptides-nanoparticles structures**
P. C. Mondal, P. Roy, D. K. Kim, E. E. Fullerton, H. Cohen, and R. Naaman, *Nano Lett.* **16**, 2806-2811 (2016)
 300. **Shaping nanoscale magnetic domain memory by field cooling**
K. Chesnel, A. Safsten, M. Rytting and E. E. Fullerton, *Nature Comm.*, **7**, 11648 (2016).
 299. **Large exchange-dominated domain wall velocities in antiferromagnetically coupled nanowires**
M. Kuteifan, M. V. Lubarda, S. Fu, R. Chang, M. A. Escobar, S. Mangin, E. E. Fullerton, and V. Lomakin, *AIP Advances* **6**, 045103 (2016).
 298. **Demonstration of a highly-tunable hybrid NMOS-magnetic-tunnel-junction ring oscillators**
R. Choi, J. J. Kan, S. H. Kang, and E. E. Fullerton, *IEEE Trans. Elect. Devices* **53**, 1668 (2016).
 297. **Stable room-temperature ferromagnetic phase at the FeRh(100) surface**
F. Pressacco, V. Uhlíř, M. Gatti, A. Bendounan, E. E. Fullerton, and F. Sirotti, *Scientific Reports* **6** 22383 (2016).
 296. **Electrical characterization of all-optical helicity-dependent switching in ferromagnetic Hall crosses**
M. S. El Hadri, P. Pirro, C. H. Lambert, N. Bergeard, S. Petit-Watelot, M. Hehn, G. Malinowski, Y. Quessab, R. Medapalli, E. E. Fullerton, and S. Mangin, *Appl. Phys. Lett.* **108**, 092405 (2016).
 295. **Bright circularly polarized soft X-ray high harmonics for X-ray magnetic circular dichroism**
T. Fan, P. Gychtol, R. Knut, C. Hernández-García, D. D. Hickstein, D. Zusin, C. Gentry, F. Dollar, C. Mancuso, C. Hogle, O. Kfir, D. Legut, K. Carva, J. Ellis, K. Dorney, C. Chen, O. Shpyrko, E. E. Fullerton, O. Cohen, P. M. Oppeneer, D. B. Milošević, A. Becker, A. Jaron-Becker, T. Popmintchev, M. Murnane, and H. Kapteyn, *Proceedings of the National Academy of Sciences* **112**, 14206-14211 (2015).
 294. **Generation and manipulation of domain walls using a thermal gradient in a ferrimagnetic TbCo wire**
R. Tolley, T. Liu, S. Le Gall, Y. Xu, M. Gottwald, T. Hauet, M. Hehn, F. Montaigne, E. E. Fullerton, S. Mangin, *Appl. Phys. Lett.* **106**, 242403 (2015)
 293. **Anomalous weak scattering in metal-semiconductor multilayer hyperbolic metamaterials**
H. Shen, D. Lu, B. Van Saders, J. J. Kan, H. Xu, E. E. Fullerton, and Z. Liu, *Phys. Rev. X* **5**, 021021-1-9 (2015).
 292. **Condensation of collective charge ordering in chromium**
A. Singer, M. J. Marsh, S. H. Dietze, V. Uhlíř, Y. Li, D. A. Walko, E. M. Dufresne, G. Srajer, M. P. Cosgri, P. G. Evans, E. E. Fullerton, and O. G. Shpyrko, *Phys. Rev. B* **91**, 115134-1-8 (2015).
 291. **Exchange bias mediated by interfacial nanoparticles**
A.E. Berkowitz, S.K. Sinha, E.E. Fullerton and D.J. Smith, *J. Appl. Phys.*, **117**, 172607-1-6 (2015).

290. **Dynamics and efficiency of magnetic vortex circulation reversal**
M. Urbánek, V. Uhlíř, C.-H. Lambert, J. J. Kan, N. Eibagi, M. Vaňatka, L. Flajšman, R. Kalousek, M.-Y. Im, P. Fischer, T. Šikola, and E. E. Fullerton, *Phys. Rev. B* **91**, 094415-1-11 (2015).
289. **Testing spin-flip scattering as a possible mechanism of ultrafast demagnetization in ordered magnetic alloys**
S. Günther, C. Spezzani, R. Ciprian, C. Grazioli, B. Ressel, M. Coreno, L. Poletto, P. Miotti, Maurizio Sacchi, Giancarlo Panaccione, V. Uhlir, E. E. Fullerton, G. De Ninno, and C. H. Back, *Phys. Rev. B* **90**, 180407 (2014).
288. **Curvature-induced and thermal strain in polyhedral gold nanocrystals**
J.W. Kim, S. Manna, S.H. Dietze, A. Ulvestad, R. Harder, E. Fohtung, E.E. Fullerton, and O.G. Shpyrko, *Appl. Phys. Lett.* **105**, 173108-1-5 (2014).
287. **All-optical control of ferromagnetic thin films and nanostructures**
C.-H. Lambert, S. Mangin, B. S. D. Ch. S. Varaprasad, Y.K. Takahashi, M. Hehn, M. Cinchetti, G. Malinowski, K. Hono, Y. Fainman, M. Aeschlimann, and E.E. Fullerton, *Science* **345**, 1337-1340 (2014).
286. **Switching field distributions with spin transfer torques in perpendicularly magnetized spin-valve nanopillars**
D. B. Gopman, D. Bedau, S. Mangin, E. E. Fullerton, J.A. Katine, and A.D. Kent, *Phys. Rev. B* **89**, 134427 (2014).
285. **Subpicosecond magnetization dynamics in TbCo alloys**
S. Alebrand, U. Bierbrauer, M. Hehn, M. Gottwald, O. Schmitt, D. Steil, E. E. Fullerton, S. Mangin, M. Cinchetti, and M. Aeschlimann, *Phys. Rev. B* **89**, 144404-1-7 (2014).
284. **Ultralow thermal conductivity of multilayers with highly dissimilar Debye temperatures**
E. Dechaumphai, D. Lu, J. J. Kan, J. Moon, E. E. Fullerton, and Z. Liu, and R. Chen, *Nano Letters* **14**, 2448-2455 (2014).
283. **Investigating the role of super diffusive currents in laser induced demagnetization of ferromagnets with nanoscale magnetic domains**
N. Moisan, G. Malinowski, J. Mauchain, B. Vodungbo, J. Lüning, M. Hehn, S. Mangin, E. E. Fullerton, and A. Thiaville, *Scientific Reports* **4**, 4658 (2014).
282. **Temperature dependent nucleation, propagation, and annihilation of domain walls in all-perpendicular spin-valve nanopillars**
D. B. Gopman, D. Bedau, S. Mangin, E. E. Fullerton, J. A. Katine, and A. D. Kent, *J. Appl. Phys.* **115**, 113910 (2014).
281. **Nonswitchable magnetic moments in polycrystalline and (111)-epitaxial permalloy/CoO exchange-biased bilayers**
S.-W. Chen, X. Lu, E. Blackburn, V. Lauter, H. Ambaye, K. T. Chan, E. E. Fullerton, A. E. Berkowitz, and S. K. Sinha, *Phys. Rev. B* **89**, 094419 (2014).
280. **Dynamics of spin torque switching in all-perpendicular spin valve nanopillars**
H. Liu, D. Bedau, J. Z. Sun, S. Mangin, E. E. Fullerton, J. A. Katine, and A. D. Kent
J. Magn. Mater. **358-359**, 233, (2014).
279. **Understanding improved electrochemical properties of NiO-doped NiF₂-C composite conversion materials by X-ray absorption spectroscopy and pair distribution function analysis**
D. H. Lee, K. J. Carroll, K. W. Chapman, O. J. Borkiewicz, S. Calvin, E. E. Fullerton and Y. S. Meng, *Phys. Chem. Chem. Phys.* **16**, 3095 (2014).
278. **Bimodal switching field distributions in all-perpendicular spin-valve nanopillars**
D. B. Gopman, D. Bedau, S. Mangin, E. E. Fullerton, J. A. Katine, and A. D. Kent, *J. Appl. Phys.* **115**, 17C707 (2014).
277. **Low depinning fields in Ta-CoFeB-MgO ultrathin films with perpendicular magnetic anisotropy**
C. Burrowes, N. Vernier, J-P. Adam, L.Herrera Diez, K.Garcia, I. Barisic, G. Agnus, S. Eimer, J-V Kim, T. Devolder, A. Lamperti, R. Mantovan, B. Ockert, E.E Fullerton, and D. Ravelosona
Appl. Phys. Lett. **103**, 182401 (2013).
276. **Engineered materials for all-optical helicity-dependent magnetic switching**
S. Mangin, M. Gottwald, C.-H. Lambert, D. Steil, V. Uhlíř, L. Pang, M. Hehn, S. Alebrand, M. Cinchetti, G. Malinowski, Y. Fainman, M. Aeschlimann, and E.E. Fullerton, *Nature Materials* **13**, 286–292, (2014).
275. **Enhancing spontaneous emission rates by nano-patterned multilayer hyperbolic metamaterials**
D. Lu, J. J. Kan, E. E. Fullerton and Z. Liu, *Nature Nanotechnology* **9**, 48-53 (2014).
274. **Temperature dependence of the switching field in all-perpendicular spin-valve nanopillars**
D. B. Gopman, D. Bedau, G. Wolf, S. Mangin, E. E. Fullerton, J. A. Katine, and A. D. Kent, *Phys. Rev. B – Rapid Communications* **88**, 100401-1-5 (2013).
273. **Low-temperature magnetic characterization of optimum and etch-damaged in-plane magnetic tunnel junctions**

- J. J. Kan, K. Lee, S. H. Kang, and E. E. Fullerton, *J. of Appl. Phys.* **114**, 114506-1-4 (2013).
272. **Paramagnetic $\text{Fe}_x\text{Ta}_{1-x}$ alloys for engineering of perpendicularly magnetized tunnel junctions**
M. Gottwald, J. J. Kan, K. Lee, S. H. Kang, and E. E. Fullerton, *APL Materials* **1**, 022102-1-5 (2013).
 271. **Phase transition in iron-rhodium thin films probed by ferromagnetic resonance**
E. Mancini, F. Pressacco, M. Hartiger, E. E. Fullerton, T. Suzuki, G. Woltersdorf, and C. H. Back, *J. Physics-Cond. Matter* **46**, 245302 (2013).
 270. **Strong perpendicular magnetic anisotropy at the Fe-MgO(001) interface**
C.-H. Lambert, A. Rajanikanth, T. Hauet, S. Mangin, E.E. Fullerton, and S. Andrieu, *Appl. Phys. Lett.* **102**, 122410 (2013).
 269. **Dynamic switching of the spin circulation in tapered magnetic nanodisks**
V. Uhlíř, M. Urbánek, L. Hladík, J. Spousta, M.-Y. Im, P. Fischer, N. Eibagi, J. J. Kan, E. E. Fullerton and T. Šikola, *Nature Nanotechnology* **8**, 341 (2013).
 268. **Ultra-thin Co/Pd multilayers with enhanced high-temperature annealing stability**
M. Gottwald, K. Lee, J. J. Kan, B. Ocker, J. Langer, S. H. Kang, and E.E. Fullerton
Appl. Phys. Lett. **102**, 052405 (2013).
 267. **Tunable resonant properties of perpendicular anisotropy [Co/Pd]/Fe/[Co/Pd] multilayer**
J. Dou, M. J. Pechan, E. Shipton, N. Eibagi and E. E. Fullerton, *J. Appl. Phys.* **113**, 17C115 (2013).
 266. **Domain wall motion in nanopillar spin-valves with perpendicular anisotropy driven by spin-transfer torques**
J. Cucchiara, S. Le Gall, E. E. Fullerton, J.-V. Kim, D. Ravelosona, Y. Henry, J. A. Katine, A. D. Kent, D. Bedau, D. Gopman, and S. Mangin, *Phys. Rev. B* **86**, 214429 (2012).
 265. **Thermodynamic Measurements of Fe-Rh Alloys**
D. W. Cooke, F. Hellman, C. Baldasseroni, C. Bordel, S. Moyerman, and E. E. Fullerton, *Phys. Rev. Lett.* **109**, 117201 (2012).
 264. **Field mapping and temperature dependence of magnetic domain memory induced by exchange couplings**
K. Chesnel, B. Wilcken, M. Rytting, S. D. Kevan and E. E. Fullerton, *New J. Phys.*, **15**, 023016, (2013).
 263. **Write Error Rate Slopes of In-Plane Magnetic Tunnel Junctions**
K. Lee, J. J. Kan, E. E. Fullerton, and S. H. Kang, *IEEE Magn. Lett.* **3**, 3000604 (2012).
 262. **Light-induced magnetization reversal of high-anisotropy TbCo alloy films**
S. Alebrand, M. Gottwald, M. Hehn, D. Steil, M. Cinchetti, D. Lacour, E. E. Fullerton, M. Aeschlimann, and S. Mangin, *Appl. Phys. Lett.* **101**, 162408 (2012).
 261. **Fe spin reorientation across the metamagnetic transition in strained FeRh thin films**
C. Bordel, J. Juraszek, D. W. Cooke, C. Baldasseroni, S. Mankovsky, J. Minár, H. Ebert, S. Moyerman, E.E. Fullerton and F. Hellman, *Phys. Rev. Lett.* **109**, 117201 (2012).
 260. **Role of dipolar interactions on the thermal stability of high-density bit-patterned media**
N. Eibagi, J. J. Kan, F. E. Spada and E. E. Fullerton, *IEEE Magn. Lett.* **3**, 4500204 (2012).
 259. **Probing the three-dimensional strain inhomogeneity and equilibrium elastic properties of single crystal Ni nanowires**
E. Fohtung, J. W. Kim, K. T. Chan, R. Harder, E.E. Fullerton & O.G. Shpyrko, *Appl. Phys. Lett.* **101**, 033107 (2012).
 258. **State diagram of nanopillar spin valves with perpendicular magnetic anisotropy**
S. Le Gall, J. Cucchiara, M. Gottwald, C. Berthelot, and C.-H. Lambert, Y. Henry, D. Bedau, D. B. Gopman, H. Liu, and A. D. Kent, J. Z. Sun, W. Lin and D. Ravelosona, J. A. Katine, E. E. Fullerton, S. Mangin, *Phys. Rev. B* **86**, 014419 (2012).
 257. **Co/Ni(111) superlattices studied by microscopy, x-ray absorption, and ab initio calculations**
M. Gottwald, S. Andrieu, F. Gimbert, E. Shipton, L. Calmels, C. Magen, E. Snoeck, M. Liberati, T. Hauet, E. Arenholz, S. Mangin, E. E. Fullerton, *Phys. Rev. B* **86**, 014425 (2012).
 256. **Electronic structure changes across the metamagnetic transition in FeRh via hard x-ray photoemission**
A. X. Gray, D. W. Cooke, P. Krüger, C. Bordel, A. M. Kaiser, S. Moyerman, E. E. Fullerton, S. Ueda, Y. Yamashita, A. Gloskovskii, C. M. Schneider, W. Drube, K. Kobayashi, F. Hellman, and C. S. Fadley, *Phys. Rev. Lett.* **108**, 257208 (2012).
 255. **Domain wall motion in magnetically frustrated nanorings**
M. V. Lubarda, M. A. Escobar, S. Li, R. Chang, E. E. Fullerton, V. Lomakin, *Phys. Rev. B* **85**, 214428 (2012).
 254. **Time-resolved magnetic relaxation of a nanomagnet on subnanosecond time scales**
H. Liu, D. Bedau, J. Z. Sun, S. Mangin, E.E. Fullerton, J. A. Katine, A. D. Kent
Phys. Rev. B **85**, 220405(R) (2012).

253. **Transport and switching behaviors in magnetic tunnel junctions consisting of CoFeB/FeNiSiB hybrid free layers**, D. H. Kim, D. K. Kim, J. U. Cho, S. Y. Park, S. Isogami, M. Tsunoda, M. Takahashi, E. E. Fullerton, and Y. K. Kim, *J. Appl. Phys.* **111**, 093913 (2012)
252. **Structural and Magnetic Dynamics of a Laser Induced Phase Transition in FeRh**
S. O. Mariager, F. Pressacco, G. Ingold, A. Caviezel, E. Möhr-Vorobeve, P. Beaud, S. L. Johnson, C. J. Milne, E. Mancini, S. Moyerman, E. E. Fullerton, R. Feidenhans'l, C. H. Back, and C. Quitmann
Phys. Rev. Lett. **108** 087201-1-5 (2012).
251. **Thermal stability of patterned Co/Pd nanodot arrays**
I. Tudosa, Marko V. Lubarda, K. T. Chan, M. A. Escobar, V. Lomakin and E. E. Fullerton
Appl. Phys. Lett. **100**, 102401 (2012).
250. **Asymmetric switching behavior in perpendicularly magnetized spin-valve nanopillars due to the polarizer dipole field**
D. B. Gopman, D. Bedau, S. Mangin, C. H. Lambert, E. E. Fullerton, J. A. Katine, and A. D. Kent
Appl. Phys. Lett. **100**, 062404 (2012).
249. **Controlled growth behavior of chemical vapor deposited Ni nanostructures**
K. T. Chan, J. J. Kan, C. Doran, L. Ouyang, D.J. Smith, and E.E. Fullerton
Philosophical Magazine **92**, 2173 (2012).
248. **Emergent rotational symmetries in disordered magnetic domain patterns**
R. Su, K. A. Seu, D. Parks, J. J. Kan, E. E. Fullerton, S. Roy, and S. D. Kevan,
Phys. Rev. Lett. **107**, 257204 (2011).
247. **Cargo-towing fuel-free magnetic nanomotors for targeted drug delivery**
W. Gao, D. Kagan, O. S. Pak, C. Clawson, S. Campuzano, E. Chuluun-Erdene, E. Shipton, E. E. Fullerton, L. Zhang, E. Lauga, and J. Wang, *Small* **8**, 460 (2012).
246. **Current-induced magnetization reversal in terms of power dissipation**
J. Cucchiara, E. E. Fullerton, A. D. Kent, J.Z. Sun, Y. Henry, and S. Mangin, *Phys. Rev. B* **84**, 100405 (2011).
245. **Spin-transfer-torque reversal in perpendicular anisotropy spin valves with composite free layers**
I. Yulaev, M. Lubarda, S. Mangin, V. Lomakin, and E. E. Fullerton, *Appl. Phys. Lett.* **99**, 132502 (2011).
244. **Dichroic coherent diffractive imaging**
A. Tripathi, J. Mohanty, S. H. Dietze, O. G. Shpyrko, E. Shipton, E. E. Fullerton, S. S. Kim, and I. McNulty, *Proc. Natl. Acad. Sci.* **108**, 13393-13398 (2011).
243. **Effect of microwave irradiation on spin-torque-driven magnetization precession in nanopillars with magnetic perpendicular anisotropy**
N. Reckers, J. Cucchiara, O. Posth, C. Hassel, F. M. Römer, R. Narkowicz, R. A. Gallardo, P. Landeros, H. Zähres, S. Mangin, J. A. Katine, E. E. Fullerton, G. Dumpich, R. Meckenstock, J. Lindner, and M. Farle,
Phys. Rev. B **83**, 184427 (2011).
242. **Tunable surface plasmon polaritons in Ag composite films by adding dielectrics or semiconductors**
D. Lu, J. Kan, E. E. Fullerton, and Z. Liu, *Appl. Phys. Lett.* **98**, 243114 (2011).
241. **Asymmetric domain wall depinning under current in spin valves with perpendicular anisotropy**
S.-H. Park, N.-M. Nguyen, C. Burrowes, L. Prejebeanu, E. E. Fullerton, C. Chappert, and D. Ravelosona,
Appl. Phys. Lett. **98**, 232512 (2011).
240. **Perpendicular magnetization of CoFeB on single-crystal MgO**
K. Lee, S. H. Kang, J. J. Sapan, and E. E. Fullerton, *J. Appl. Phys.* **109**, 123910 (2011).
239. **Calorimetry of epitaxial thin films**
D.W. Cooke, F. Hellman, J.R. Groves, B.M. Clemens, S. Moyerman, and E.E. Fullerton,
Rev. Sci. Instr. **82**, 023908 (2011).
238. **Magnetotransport properties of epitaxial MgO(001)/FeRh films across the antiferromagnet to ferromagnet transition**, M. Sharma, H.M. Aarbogh, J.-U. Thiele, S. Maat, E.E. Fullerton and C. Leighton
J. Appl. Phys. **109**, 083913 (2011).
237. **Momentum transfer resolved memory in a magnetic system with perpendicular anisotropy**
K. A. Seu, S. Roy, R. Su, D. Parks, E. Shipton, E. E. Fullerton, and S. Kevan, *Appl. Phys. Lett.* **98**, 122505 (2011).
236. **Ferromagnetic resonance study of Co/Pd/Co/Ni multilayers with perpendicular anisotropy irradiated with helium ions**
J.-M. L. Beaujour, A.D. Kent, D. Ravelosona, I. Tudosa and E.E. Fullerton, *J. Appl. Phys.* **109**, 033917 (2011).
235. **Reversal in bit patterned media with vertical and lateral exchange**
M. V. Lubarda, S. Li, B. Livshitz, E. E. Fullerton, and V. Lomakin, *IEEE Trans. Magn.* **47**, 18 (2011).
234. **Antiferromagnetically coupled capped bit patterned media for high-density magnetic recording**
M. V. Lubarda, S. Li, B. Livshitz, E. E. Fullerton, and V. Lomakin, *Appl. Phys. Lett.* **98**, 012513 (2011).

233. **Oscillating spatial dependence of domain memory in ferromagnetic films mapped via x-ray speckle correlation**
K. Chesnel, J. Nelson, S. D. Kevan, M. J. Carey, and E. E. Fullerton, Phys. Rev. B **83**, 054436 (2011).
232. **Spin-transfer pulse switching: From the dynamic to the thermally activated regime**
D. Bedau, H. Liu, J. Z. Sun, J. A. Katine, E. E. Fullerton, S. Mangin and A. D. Kent, Appl. Phys. Lett. **97**, 262502 (2011).
231. **Oriented growth of single-crystal Ni nanowires onto amorphous SiO₂**
K. T. Chan, J. J. Kan, C. Doran, L. Ouyang, D. J. Smith, and E. E. Fullerton, Nano Lett. **10**, 5070 (2010).
230. **Exchange bias and domain evolution at 10 nm scales**
I. Schmid, M. A. Marioni, P. Kappenberger, S. Romer, M. Parlinska-Wojtan, H. J. Hug, O. Hellwig, M. J. Carey, and E. E. Fullerton, Phys. Rev. Lett. **105**, 197201 (2010).
229. **Investigation of Fe–Si–N films as magnetic overcoat for high density recording disk drives**
M. Gauvin, E. E. Fullerton, and F. E. Talke, J. Appl. Phys. **108**, 063925 (2010).
228. **Cumulative minor loop growth in Co/Pt- and Co/Pd-multilayers**
A. Berger, S. Mangin, J. McCord, O. Hellwig, and E. E. Fullerton, Phys. Rev. B **82**, 104423 (2010).
227. **Electric-field modification of magnetism in a thin CoPd film**
M. Zhernenkova, M. R. Fitzsimmons, J. Chlistunoff, J. Majewski, I. Tudosa, and E. E. Fullerton, Phys. Rev. B **82**, 024420 (2010).
226. **Magnetic susceptibility measurements as a probe of spin transfer driven magnetization dynamics**
W. Lin, J. Cucchiara, C. Berthelot, T. Hauet, Y. Henry, J. A. Katine, E. E. Fullerton, and S. Mangin Appl. Phys. Lett. **96**, 252503 (2010).
225. **Perpendicular spin-torque switching with a synthetic antiferromagnetic reference layer**
I. Tudosa, J. A. Katine, S. Mangin, and E. E. Fullerton, Appl. Phys. Lett. **96**, 212504 (2010).
224. **Current induced switching of the hard layer in perpendicular magnetic nanopillars**
I. Tudosa, J. A. Katine, S. Mangin, and E. E. Fullerton, IEEE Trans. Mag. **46**, 2328 (2010).
223. **Thickness and temperature effects on magnetic properties and roughness of ordered FePt films**
C. S. Kim, J. J. Sapan, S. Moyerman, K. Lee, E. E. Fullerton, and M. H. Kryder IEEE Trans. Mag. **46**, 2282 (2010).
222. **Core-shell structured nanowire spin valves**
K. T. Chan, C. Doran, E. G. Shipton, and E. E. Fullerton, IEEE Trans. Mag. **46**, 2209 (2010).
221. **Microscopic return point memory in Co/Pd multilayer films**
K. A. Seu, R. Su, S. Roy, D. Parks, E. Shipton, E. E. Fullerton, S. D. Kevan, New J. Phys. **12**, 035009 (2010).
220. **Influence of growth morphology on the Neel temperature of CrRu thin films and heterostructures**
A. R. E. Prinsloo, H. A. Derrett, O. Hellwig O, E. E. Fullerton, H. L. Alberts, and N. van den Berg J. Magn. Magn. Mater. **322**, 1126-1129 (2010).
219. **Ultrafast spin-transfer switching in spin valve nanopillars with perpendicular anisotropy**
D. Bedau, H. Liu, J.-J. Bouzaglou, A. D. Kent, J. Z. Sun, J. A. Katine, E. E. Fullerton, and S. Mangin Appl. Phys. Lett. **96**, 022514 (2010).
218. **Coercivity tuning in Co/Pd multilayer based bit patterned media**
O. Hellwig, T. Hauet, T. Thomson, E. Dobisz, J. D. Risner-Jamtegaard, D. Yaney, B. D. Terris, and E. E. Fullerton, Appl. Phys. Lett. **95**, 232505 (2009).
217. **Ferromagnetic resonance linewidth in ultrathin films with perpendicular magnetic anisotropy**
J.-M. Beaujour, D. Ravelosona, I. Tudosa, E. E. Fullerton, and A. D. Kent, Phys. Rev. B **80**, 180415(R) (2009).
216. **Nonadiabatic spin-torques in narrow magnetic domain walls**
C. Burrowes, A. P. Mihai, J.-P. Attané, L. Vila, A. Marty, J.-V. Kim, F. Garcia-Sanchez, L.D. Buda-Prejbeanu, C. Chappert, Y. Samson, I. Tudosa, E.E. Fullerton, and D. Ravelosona, Nature Phys. **6**, 17 (2009).
215. **Suppression of the perpendicular anisotropy at the CoO Néel temperature in exchange-biased CoO/[Co/Pt] multilayers**
E. Shipton, K. Chan, T. Hauet, O. Hellwig, and E. E. Fullerton, Appl. Phys. Lett. **95**, 132509 (2009).
214. **Frustration driven stripe domain formation in Co/Pt multilayer films**
J. E. Davies, O. Hellwig, E. E. Fullerton, M. Winklhofer, R. D. Shull, and K. Liu Appl. Phys. Lett. **95**, 022505 (2009).
213. **Strong perpendicular magnetic anisotropy in Ni/Co(111) single crystal superlattices**
S. Girod, M. Gottwald, S. Andrieu, S. Mangin, J. McCord, E. E. Fullerton, J.-M. L. Beaujour, B. J. Krishnatreya, and A. D. Kent, Appl. Phys. Lett. **94**, 262504 (2009).
212. **Distortion of the Stoner-Wohlfarth astroid by a spin-polarized current**
Y. Henry, S. Mangin, J. Cucchiara, J. A. Katine, and E. E. Fullerton, Phys. Rev. B, **79**, 214422 (2009).

- Selected PRB Editors' Suggestion and for the Virtual Journal of Nanoscale Science & Technology
211. **Microwave assisted magnetization reversal in composite media**
S. Li, B. Livshitz, H. N. Bertram, M. Schabes, T. Schrefl, E. E. Fullerton, and V. Lomakin, Appl. Phys. Lett. **94**, 202509 (2009).
 210. **Microwave-assisted magnetization reversal and multilevel recording in composite media**
S. J. Li, B. Livshitz, H.N. Bertram, E. E. Fullerton, and V. Lomakin, J. Appl. Phys. **105**, 07B909 (2009).
 209. **Capped bit patterned media for high density magnetic recording**
S. Li, B. Livshitz, H. N. Bertram, A. Inomata, E. E. Fullerton, and V. Lomakin, J. Appl. Phys. **105**, 07C121 (2009)
 208. **Telegraph noise magnetization switching driven by spin transfer in perpendicularly magnetized nanopillars**
J. Cucchiara, Y. Henry, D. Ravelosona, D. Lacour, E. E. Fullerton, J. A. Katine and S. Mangin, Appl. Phys. Lett. **94**, 102503 (2009).
 207. **Reducing the critical current for spin-transfer switching of perpendicularly magnetized nanomagnets**
S. Mangin, Y. Henry, D. Ravelosona, J. A. Katine and E. E. Fullerton, Appl. Phys. Lett. **94**, 012502 (2009).
Selected for Virtual Journal of Nanoscale Science & Technology
 206. **Spin transfer torque effects in devices with perpendicular anisotropy**
S. Mangin, D. Ravelosona, Y. Henry, J. A. Katine and E. E. Fullerton, AAAPPS Bulletin **18**, 41 (2008).
 205. **Magnetic memory in ferromagnetic thin films via exchange coupling**
K. Chesnel, E. E. Fullerton, M. J. Carey, J. B. Kortright, and S. D. Kevan, Phys. Rev. B **78**, 132409 (2008).
 204. **Suppression of magnetic trench material in bit patterned media fabricated by blanket deposition onto pre-patterned substrates**
O. Hellwig, A. Moser, E. Dobisz, Z. Z. Bandic, H. Yang, D. S. Kercher, J. D. Risner-Jamtgaard, D. Yaney, and E. E. Fullerton, Appl. Phys. Lett. **93**, 192501 (2008).
 203. **Improved media performance in optimally-coupled exchange spring layer media**
A. Berger, N. Supper, Y. Ikeda, B. Lengsfeld, A. Moser and E. E. Fullerton, Appl. Phys. Lett. **93**, 122502 (2008).
 202. **Mechanism of chirality reversal for planar interface domain walls in exchange-coupled hard/soft magnetic bilayers**
J. McCord, Y. Henry, T. Hauet, F. Montaigne, E. E. Fullerton, and S. Mangin, Phys. Rev. B **78**, 094417 (2008).
 201. **Non-Linear and hysteretic exchange bias in antiferromagnetically coupled ferromagnetic bilayers**
A. Berger, O. Hovorka, G. Friedman, and E. E. Fullerton, Phys. Rev. B **78**, 224407 (2008).
 200. **Field and current driven domain wall motion in wires with perpendicular magnetic anisotropy**
C. Burrowes, D. Ravelosona, C. Chappert, S. Mangin, E. E. Fullerton, J. A. Katine, and B. D. Terris., Appl. Phys. Lett. **93**, 172513 (2008).
 199. **Monodispersed MnO nanoparticles with epitaxial Mn₃O₄ shells**
A. E. Berkowitz, G.F. Rodriguez, J. I. Hong, K. An, T. Hyeon, N. Agarwal, D. J. Smith, and E. E. Fullerton, J. Physics D **41**, 134007 (2008).
 198. **Influence of interface exchange coupling in perpendicular anisotropy [Pt/Co]₅₀/TbFe bilayers**
S. Mangin, T. Hauet, P. Fischer, D.H. Kim, J.B. Kortright, K. Chesnel, E. Arenholz and E. E. Fullerton Phys. Rev. B **78**, 024424 (2008).
 197. **Interfacial magnetic domain wall formation in perpendicular-anisotropy, exchange-spring films**
S.M. Watson, T. Hauet, J.A. Borchers, S. Mangin, E. E. Fullerton, Appl. Phys. Lett. **92**, 202507 (2008).
 196. **Origin of the magneto-thermoelectric voltage in cluster-assembled metallic nanostructures**
E. E. Fullerton and S. Mangin, Nature Materials **7**, 257 (2008).
 195. **Device implications of spin transfer torques**
J. A. Katine and E. E. Fullerton, J. Magn. Magn. Mater **320**, 1217 (2008).
 194. **Temperature-dependent magnetization reversal in (Co/Pt)/Ru multilayers**
J. E. Davies, O. Hellwig, E. E. Fullerton, and K. Liu, Phys. Rev. B **77**, 014421 (2008).
 193. **Antiferromagnetic LaFeO₃ thin films and their effect on exchange bias**
J. W. Seo, E. E. Fullerton, F. Nolting, A. Scholl, J. Fompeyrine, and J.-P. Locquet J. Phys: Cond. Matter **20**, 264014 (2008).
 192. **Antiferromagnetic MnO nanoparticles with ferrimagnetic Mn₃O₄ shells: Doubly inverted core-shell system**
A. E. Berkowitz, G. F. Rodriguez, J. I. Hong, K. An, T. Hyeon, N. Agarwal, D. J. Smith, and E. E. Fullerton, Phys. Rev. B **77**, 024403 (2008).
 191. **Tailoring magnetism in CoNi films with perpendicular anisotropy by ion irradiation**
D. Stanescu, D. Ravelosona, V. Mathet, C. Chappert, Y. Samson, C. Beigné, N. Vernier, J. Ferré, J. Gierak, E. Bouhris, and E. E. Fullerton, J. Appl. Phys. **103**, 07B529 (2008).
 190. **The role of uncompensated spins in exchange biasing**

- I. Schmid, P. Kappenberger, O. Hellwig, M. J. Carey, E. E. Fullerton and H. J. Hug
Europhys. Lett. **81**, 17001 (2008).
189. **Editorial: Topical issue on new trends in spin transfer physics**
E. Fullerton, A. Mougin, D. Ravelosona, and S. Mangin, Eur. Phys. J. B **59**, 413 (2007).
 188. **Exchange-bias training effect in TbFe/GdFe: micromagnetic mechanism**
T. Hauet, S. Mangin, J. McCord, F. Montaigne, E. E. Fullerton, Phys. Rev. B **76**, 144423 (2007).
 187. **Domain structure and magnetization reversal of antiferromagnetically coupled perpendicular anisotropy films**
O. Hellwig, A. Berger, J. B. Kortright and E. E. Fullerton, J. Magn. Magn. Mater. **319**, 13 (2007).
 186. **The 2007 Nobel Prize in Physics: magnetism and transport at the nanoscale**
E. E. Fullerton and I. K. Schuller, ACS Nano **1**, 384 (2007).
 185. **Separating dipolar broadening from the intrinsic switching field distribution in perpendicular patterned media**, O. Hellwig, A. Berger, T. Thomson, E. Dobisz, Z. Bandic, H. Yang, and D. S. Kercher and E. E. Fullerton, Appl. Phys. Lett. **90**, 162516 (2007).
 184. **Disorder-induced magnetic memory: Experiments and theories**
M. S. Pierce, C. R. Buechler, L. B. Sorensen, S. D. Kevan, E. A. Jagla, J. M. Deutsch, T. Mai, O. Narayan, J. E. Davies, Kai Liu, G. T. Zimanyi, H. G. Katzgraber, O. Hellwig, E. E. Fullerton, P. Fischer, and J. B. Kortright, Phys. Rev. B **75**, 144406 (2007).
 183. **Magnetic phase separation in artificial A-type antiferromagnetic films**
O. Hellwig, A. Berger and E. E. Fullerton, Phys. Rev. B **75**, 134416 (2007).
 182. **Ultrafast magnetization dynamics in high perpendicular anisotropy [Co/Pt]*n* multilayers**
A. Barman, S. Wang, O. Hellwig, A. Berger, E. E. Fullerton, and H. Schmidt, J. Appl. Phys. **101**, 09D102 (2007).
 181. **Threshold currents to move domain walls in films with perpendicular anisotropy**
D. Ravelosona, S. Mangin, J. A. Katine, E. E. Fullerton and B.D. Terris, Appl. Phys. Lett. **90**, 072508 (2007).
 180. **Current induced domain wall states in CPP nanopillars with perpendicular anisotropy**
D. Ravelosona, S. Mangin, Y. Henry, Y. Lemaho, J. Katine, B. Terris and E. E. Fullerton
J. Phys. D: Appl. Phys. **40** 1253–1256 (2007).
 179. **Advances in nanomagnetism via X-ray techniques**
G. Srajer, L.H. Lewis, S.D. Bader, A.J. Epstein, C.S. Fadley, E.E. Fullerton, A. Hoffmann, J.B. Kortright, Kannan M. Krishnan, S.A. Majetich, T.S. Rahman, C.A. Ross, M.B. Salamon, I.K. Schuller, T.C. Schulthess, and J.Z. Sun, J. Magn. Magn. Mater. **307**, 1-36 (2006).
 178. **Experimental study of longitudinal exchange spring media**
N. F. Supper, D. T. Margulies, A. Moser, A. Berger, H. Do and E. E. Fullerton
J. Appl. Phys. **99**, 08S310 (2006).
 177. **Domain wall creation in nanostructures driven by a spin-polarized current**
D. Ravelosona, S. Mangin, Y. Lemaho, J. A. Katine, B. D. Terris and E. E. Fullerton,
Phys. Rev. Lett. **96**, 186604 (2006).
 176. **State-of-the-art magnetic hard disk drives**
I. R. McFadyen, E. E. Fullerton and M. J. Carey, MRS Bulletin **31**, 379 (2006).
 175. **Influence of lateral domains and interface domain walls on exchange-bias phenomena in TbFe/GdFe bilayers**
S. Mangin, T. Hauet, Y. Henry, F. Montaigne and E. E. Fullerton, Phys. Rev. B **74**, 024414 (2006).
 174. **Current-induced magnetization reversal in nanopillars with perpendicular anisotropy**
S. Mangin, D. Ravelosona, J. A. Katine, M. J. Carey, B. D. Terris and E. E. Fullerton,
Nature Materials **5**, 210 (2006).
 173. **Reversible hysteresis loop tuning**
A. Berger, Ch. Binek, D. T. Margulies, A. Moser and E. E. Fullerton, Physica B **372**, 168 (2006).
 172. **Temperature and field hysteresis of the antiferromagnetic-to-ferromagnetic phase transition in epitaxial FeRh films**, S. Maat, J.-U. Thiele and E. E. Fullerton, Phys. Rev. B **72**, 214432 (2005).
 171. **Writability enhancement using exchange spring media**
N. Supper, D.T. Margulies, A. Moser, A. Berger, H. Do and E. E. Fullerton,
IEEE Trans. Mag. **41**, 3238 (2005).
 170. **$\Delta H(M, \Delta M)$ -method for the determination of intrinsic switching field distributions in perpendicular media**
A. Berger, Y. Xu, B. Lengsfeld, Y. Ikeda and E. E. Fullerton, IEEE Trans. Mag. **41**, 3178 (2005).
 169. **Anisotropy dependence of irreversible switching in Fe/SmCo and FeNi/FePt exchange spring magnet films**
J. E. Davies, O. Hellwig, E. E. Fullerton, J. S. Jiang, S. D. Bader, G. T. Zimányi and Kai Liu

- Appl. Phys. Lett. **86**, 262503 (2005).
168. **Magnetization profiles in antiferromagnetically-coupled recording media**
M. F. Toney, J. A. Borchers, K. V. O'Donovan, C. F. Majkrzak, D. T. Margulies, and E. E. Fullerton, Appl. Phys. Lett. **86**, 162506 (2005).
 167. **Noise subtraction in antiferromagnetically-coupled recording media**
A. Moser, N.F. Supper, A. Berger, D.T. Margulies, and E.E. Fullerton, Appl. Phys. Lett. **86**, 262501 (2005).
 166. **Understanding and optimizing laminated recording media**
D.T. Margulies, N. Supper, H. Do, M. E. Schabes, A. Berger, A. Moser, P. Rice, P. Arnett, M. Madison, B. Lengsfeld, H. Rosen, K. Tang, A. Polcyn, and E. E. Fullerton, J. Appl. Phys. **97**, 10N109 (2005).
 165. **Magnetic reversal and domain structure in perpendicular antiferromagnetically-coupled films**
O. Hellwig, A. Berger and E. E. Fullerton, J. Magn. Mater. **290-291**, 1 (2005).
 164. **Laminated antiferromagnetically-coupled media: Optimization and extendibility.**
K. Tang, D. Margulies, A. Polcyn, N. Supper, H. Do, M. Mirzamaani, M. Doerner, X. Bian, M. Mercado, L. Tang, H. Rosen, E. E. Fullerton, C. Tsang, R. Nimmagadda and Q.-F. Xiao, IEEE Trans. Mag. **41**, 642 (2005).
 163. **Interparticle magnetic correlations in dense Co nanoparticle assemblies**
J. B. Kortright, O. Hellwig, S. Sun, and E. E. Fullerton, Phys. Rev. B **71**, 012402 (2005).
 162. **Disorder induced microscopic magnetic memory**
M. S. Pierce, C. R. Buechler, L. B. Sorensen, J. J. Turner, S. D. Kevan, E. A. Jagla, J. M. Deutsch, T. Mai, O. Narayan, J. E. Davies, K. Liu, J. Hunter Dunn, K. M. Chesnel, J. B. Kortright, O. Hellwig, and E. E. Fullerton., Phys. Rev. Lett. **94**, 017202 (2005).
 161. **Magnetization reversal of Co/Pt multilayers: Microscopic origin of high field magnetic irreversibility**
J. E. Davies, O. Hellwig, E. E. Fullerton, G. Denbeaux, J. B. Kortright and K. Liu, Phys. Rev. B **70**, 224434 (2004).
 160. **The origin of signal-to-noise ratio improvements in laminated recording media**
D.T. Margulies, M. E. Schabes, N. Supper, H. Do, A. Berger, A. Moser, P. Arnett, M. Madison, B. Lengsfeld, H. Rosen, and E. E. Fullerton, Appl. Phys. Lett. **85**, 6200 (2004).
 159. **Antiferromagnetic phase transitions in an ordered Pt₃Fe(111) film studied by neutron diffraction**
V. V. Krishnamurthy, I. Zoto, G. J. Mankey, J. L. Robertson, S. Maat, E. E. Fullerton, I. Nwagwu and J. K. Akujieze, Phys. Rev. B **70**, 024420 (2004).
 158. **Film optimization of laminated antiferromagnetically coupled media**
K. Tang, C. Tsang, M. Mirzamaani, M. Doerner, A. Polcyn, X. Bian, D. T. Margulies, E. E. Fullerton, L. Tang, N. Supper and M. Mercado, IEEE Trans. Mag. **40**, 3548 (2004).
 157. **Biquadratic coupling in antiferromagnetically-coupled recording media**
A. Moser, A. Berger, D. T. Margulies, and E. E. Fullerton, J. Appl. Phys. **95**, 6657 (2004).
 156. **Magnetic and structural properties of FePt/FeRh exchange spring films for thermally assisted magnetic recording media**, J.-U. Thiele, S. Maat J. L. Robertson and E. E. Fullerton, IEEE Trans. Mag. **40**, 2537 (2004).
 155. **Direct imaging and determination of the uncompensated spin density in exchange-biased CoO/(Co/Pt) multilayers**
P. Kappenberger, S. Martin, Y. Pellmont, H. J. Hug, J. B. Kortright, O. Hellwig, and E. E. Fullerton Phys. Rev. Lett. **91**, 267202 (2003).
 154. **Hysteretic spin-density-wave ordering in confined geometries**
E. E. Fullerton, J. L. Robertson, A. E. R. Prinsloo, H. L. Alberts, and S. D. Bader Phys. Rev. Lett. **91**, 237201 (2003).
 153. **Magnetic domain size tuning of biquadratic exchange coupling in magnetic thin films**
A. Moser, A. Berger, D. T. Margulies, and E. E. Fullerton, Phys. Rev. Lett. **91**, 097203 (2003).
 152. **Domain walls in antiferromagnetically-coupled multilayer films**
O. Hellwig, A. Berger, and E.E. Fullerton, Phys. Rev. Lett. **91**, 197203 (2003).
 151. **The energy barriers in antiferromagnetically coupled media**
D.T. Margulies, A. Berger, A. Moser, M.E. Schabes and E. E. Fullerton, Appl. Phys. Lett. **82**, 3201 (2003).
 150. **Polarization effects in coherent scattering from magnetic specimen: Implications for x-ray holography, lensless imaging, and correlation spectroscopy**
S. Eisebitt, M. Lörger, W. Eberhardt, J. Lüning, J. Stöhr, O. Hellwig, C. Rettner, E. E. Fullerton, G. Denbeaux, Phys. Rev. B **68**, 104419 (2003).
 149. **X-ray studies of aligned magnetic stripe domains in perpendicular multilayers**
O. Hellwig, G. Denbeau, J. B. Kortright, and E. E. Fullerton, Physica B **336**, 136 (2003).
 148. **Antiferromagnetically-coupled magnetic recording media (invited)**
E. E. Fullerton, D. T. Margulies, N. Supper, H. Do, M. Schabes, A. Berger, and A. Moser

- IEEE Trans. Mag. **39**, 639 (2003).
147. **Ferromagnetism of FePt₃ films induced by ion beam irradiation**
S. Maat, A. Kellock, D. Weller, J. E. E. Baglin and E. E. Fullerton, J. Magn. Magn. Mater. **265**, 1 (2003).
 146. **A new phase diagram for layered antiferromagnetic films**
O. Hellwig, T. L. Kirk, J. B. Kortright, Andreas Berger, and E. E. Fullerton, Nature Mater. **2**, 112 (2003).
 145. **Magnetism in heterogeneous thin film systems: resonant x-ray scattering studies**
J. B. Kortright, J. S. Jiang, S. D. Bader, O. Hellwig, D. T. Margulies, and E. E. Fullerton
Nucl. Inst. and Methods B **199**, 301 (2003).
 144. **Soft x-ray magnetic scattering as a probe of recording media (invited)**
E. E. Fullerton, O. Hellwig, K. Takano, and J. B. Kortright, Nucl. Inst. and Methods B **200**, 202 (2003).
 143. **Quasistatic x-ray speckle metrology of microscopic magnetic return point memory**
M. S. Pierce, R. G. Moore, L. B. Sorensen, S. D. Kevan, O. Hellwig, E. E. Fullerton and J. B. Kortright,
Phys. Rev. Lett., **90**, 175502 (2003).
 142. **FeRh/FePt exchange spring films for thermally assisted magnetic recording media**
J.-U. Thiele, S. Maat and E. E. Fullerton, Appl. Phys. Lett. **82**, 2859 (2003).
 141. **Thermal relaxation in antiferromagnetically coupled granular magnetic media**
A. Moser, D. T. Margulies, and E. E. Fullerton, Phys. Rev. B **66**, 092410 (2002).
 140. **Thermal activation and reversal times in antiferromagnetically-coupled media**
D. T. Margulies, A. Moser, M. E. Schabes, and E. E. Fullerton, Appl. Phys. Lett. **81**, 4631 (2002).
 139. **Rotational hysteresis of exchange-spring magnets**
J. S. Jiang, S. D. Bader, H. Kaper, G. K. Leaf, R. D. Schull, A. J. Shapiro, V. S. Gornakov, V. I. Nikitenko, C. L. Platt, A. E. Berkowitz, S. David and E. E. Fullerton, J. Phys. D: Appl. Phys. **35**, 2359 (2002).
 138. **Magnetic Recording: Advancing into the future**
A. Moser, K. Takano, D. T. Margulies, M. Albrecht, Y. Sonobe, Y. Ikeda, S. Sun, and E. E. Fullerton
J. Phys. D: Appl. Phys. **35**, R157 (2002).
 137. **Cobalt-oxide underlayers for cobalt-ferrite pinned spin valves**
S. Maat, M. J. Carey, E. E. Fullerton, T.X. Le, P. M. Rice, and B. A. Gurney, Appl. Phys. Lett. **81**, 520 (2002).
 136. **Probing the magnetic transitions in exchange-biased FePt₃/Fe bilayers**
R. L. Compton, M. J. Pechan, S. Maat, and Eric E. Fullerton, Phys. Rev. B **66**, 054411 (2002).
 135. **Coercivity mechanisms in positive exchange biased Co films and Co/Pt multilayers**
T. L. Kirk, O. Hellwig, and Eric E. Fullerton, Phys. Rev. B **65**, 224426 (2002).
 134. **Signal decay and amplitude measurements of antiferromagnetically coupled magnetic recording media**
A. Moser, D. T. Margulies, C. T. Rettner, and E. E. Fullerton, Appl. Phys. Lett. **81**, 2815 (2002).
 133. **Polymer mediated self-assembly of magnetic nanoparticles**
S. Sun, S. Anders, H. F. Hamann, Jan-U. Thiele, J. E. E. Baglin, T. Thomson, E. E. Fullerton, C. B. Murray, and B. D. Terris, J. Am. Chem. Soc. **124**, 2885 (2002).
 132. **Soft x-ray characterization of perpendicular recording media**
E. E. Fullerton, O. Hellwig, Y. Ikeda, B. Lengsfeld, K. Takano and J. B. Kortright,
IEEE Trans. Mag. **38**, 1693 (2002).
 131. **Magnetic reversal of perpendicularly-biased Co/Pt multilayers**
O. Hellwig, S. Maat, J. B. Kortright, E. E. Fullerton, Phys. Rev. B **64**, 144418 (2002).
 130. **Role of B on grain sizes and magnetic correlation lengths in recording media as determined by soft x-ray scattering**
O. Hellwig, J.B. Kortright, D. T. Margulies, B. Lengsfeld, and E. E. Fullerton, Appl. Phys. Lett. **80**, 1234 (2002).
 129. **Lithography and self-assembly for nanometer scale magnetism**
S. Anders, S. Sun, C. B. Murray, C. T. Rettner, M. E. Best, T. Thomson, M. Albrecht, J.-U. Thiele, E. E. Fullerton, and B. D. Terris, Microelectronic Engineering **61**, 569 (2002).
 128. **Interlayer coupling and magnetic reversal of antiferromagnetically coupled media**
D. T. Margulies, M. E. Schabes, W. McChesney, and Eric E. Fullerton, Appl. Phys. Lett. **80**, 91 (2002).
 127. **A model of the magnetic properties of FePt granular media**
R. W. Chantrell, D. Weller, T. J. Klemmer, S. Sun and E. E. Fullerton, J. Appl. Phys. **91**, 6866 (2002).
 126. **Exchange bias in Fe_xZn_{1-x}F₂/Co bilayers**
H. Shi, D. Lederman and E. E. Fullerton, J. Appl. Phys. **91**, 7763 (2002).
 125. **Stokes anti-Stokes Brillouin intensity asymmetry of spin modes in ferromagnetic films and multilayers.**
R. Zivieri, P. Vavassori, L. Giovannini, F. Nizzoli, E. E. Fullerton, M. Grimsditch, and V. Metlushko
Phys. Rev. B **65**, 165406 (2002).
 124. **Pinpointing chiral structures with front/back neutron reflectometry**

- K. V. O'Donovan, J. A. Borchers, C. F. Majkrzak, O. Hellwig, and E. E. Fullerton, *Phys. Rev. Lett.* **88**, 067201 (2002).
123. **Stokes anti-Stokes peak intensity interchange across a first-order transition**
Z. Rivieri, P. Vavassori, L. Giovannini, F. Nizzoli, E. E. Fullerton, and M. Grimsditch, *Surf. Science* **507**, 502 (2002).
 122. **Magnetization temperature dependence in Fe/Cr superlattices**
A. A. R. Fernandes, C. A. Ramos, A. Macedo Teixeira, and E. E. Fullerton, *Physica B* **320**, 175 (2002).
 121. **Extracting buried twists with polarized neutron reflectometry**
K. V. O'Donovan, J.A. Borchers, C.F. Majkrzak, O. Hellwig, and E. E. Fullerton, *Appl. Phys. A* **74**, S1544 (2002).
 120. **Antiferromagnetically coupled magnetic medium structure extends areal density for hard disk drives**
D. Margulies, E. E. Fullerton, M. Schabes, H. Do, E. Grochowski, M. Carey, B. Gurney, A. Moser, M. Best, K. Rubin, H. Rosen, M. Doerner, M. Mirzamaani, K. Tang, Datatech, Seventh Edition, 9 (2001).
 119. **Preisach analysis of epitaxial hard/soft bilayer**
D. R. Cornejo, F. M. Rhen, F. P. Missell, and E. E. Fullerton, *J. Magn. Magn. Mater.* **226-230**, 11251 (2001).
 118. **FMR study of the crystalline anisotropy of [Fe(t)Cr(38 Å)]_N superlattices grown on MgO(100) and (110)**
A. M. Teixeira, C. A. Ramos, A. A. R. Fernandes, and E. E. Fullerton, *J. Magn. Magn. Mater.* **226-230**, 1788 (2001).
 117. **Reversal modes of exchange-spring magnets revealed by torque magnetometry**
C. L. Platt, A. E. Berkowitz, S. David, E. E. Fullerton, J. S. Jiang and S. D. Bader, *Appl. Phys. Lett.* **79**, 3991 (2001).
 116. **Resolving magnetic and chemical correlations in CoPtCr films using soft x-ray resonant scattering**
J.B. Kortright, O. Hellwig, D. T. Margulies, and E. E. Fullerton, *J. Magn. Magn. Mater.* **240**, 325 (2001).
 115. **Advanced magnetic recording media for high-density data storage (invited)**
E. E. Fullerton, D. T. Margulies, A. Moser, K. Takano, *Solid State Tech.* **44 (9)** (2001).
 114. **Growth, structural, and magnetic properties of high coercivity Co/Pt multilayers**
D. Weller, L. Folks, M. Best, E. E. Fullerton, B. D. Terris, G. J. Kusinski, K. M. Krishnan, and G. Thomas, *J. Appl. Phys.* **89**, 7525 (2001).
 113. **Magnetic patterning of chemically ordered CrPt₃ films**
O. Hellwig, D. Weller, A. J. Kellock, J. E. E. Baglin, and E. E. Fullerton, *Appl. Phys. Lett.* **79**, 1151 (2001).
 112. **Perpendicular exchange bias of Co/Pt multilayers**
S. Maat, K. Takano, S. S. P. Parkin, E. E. Fullerton, *Phys. Rev. Lett.* **87**, 087202 (2001).
 111. **Dynamic coercivity measurements of antiferromagnetically coupled magnetic media layers**
J. Lohau, A. Moser, D.T. Margulies, E. E. Fullerton and M.E. Schabes, *Appl. Phys. Lett.* **78**, 2748 (2001).
 110. **Biquadratic exchange coupling in an unequal Fe/Cr/Fe(100) trilayer**
P. Vavassori, M. Grimsditch and Eric E. Fullerton, *J. Magn. Magn. Mater.* **223**, 284 (2001).
 109. **Soft x-ray small-angle scattering as a sensitive probe of magnetic and charge heterogeneity**
J. B. Kortright, S.-K. Kim, G. P. Denbeaux, G. Zeltzer, K. Takano, and E. E. Fullerton
Phys. Rev. B **64**, 092401 (2001).
 108. **Coherent soft x-ray magnetic scattering (invited)**
B. Hu, P. Geissbuhler, L. B. Sorensen, S. D. Kevan, J. B. Kortright, E. E. Fullerton
Synch. Rad. News **14**, 11 (2001).
 107. **Compositional controlled FePt nanoparticle materials (invited)**
S. Sun, Eric E. Fullerton, D. Weller, and C. B. Murray, *IEEE Trans. Mag.* **37**, 1239 (2001).
 106. **Theory of antiferromagnetically coupled magnetic recording media**
M. E. Schabes, E. E. Fullerton, and D. Margulies, *IEEE Trans. Mag.* **37**, 1432 (2001).
 105. **Medium noise and grain size analysis of CoCrPt/Ti perpendicular media with NiAl seed layers.**
Y. Ikeda, Y. Sonobe, G. Zeltzer, B. K. Yen, K. Takano, H. Do, E. E. Fullerton, and P. Rice,
IEEE Trans. Mag. **37**, 1583 (2001).
 104. **Antiferromagnetic structure of FePt₃ films studied by neutron scattering**
S. Maat, O. Hellwig, G. Zeltzer, E. E. Fullerton, G. Mankey, M. L. Crow, J. L. Robertson,
Phys. Rev. B **63**, 134426 (2001).
 103. **X-ray magneto-optic Kerr effect studies of spring magnet heterostructures**
J. B. Kortright, S.-K. Kim, E. E. Fullerton, J. S. Jiang, and S. D. Bader,
Nucl. Inst. and Methods. A **467-468**, 1396 (2001).
 102. **Demonstration of 35 Gbits/in² using media on glass substrates**
M. Madison, M. Doerner, K. Tang, Q. Peng, A. Polcyn, T. Arnoldussen, M.F. Toney, K. Takano, X. Bian, E. Fullerton, D. Margulies, K. Rubin and D. Weller, *IEEE Trans. Mag.* **37**, 1052 (2001).

101. **Epitaxial hard-soft magnetic heterostructures as model exchange-spring magnets**
J. S. Jiang, E. E. Fullerton, M. Grimsditch, C. H. Sowers, J. Pearson, S. D. Bader, *Philos. Mag. B* **80**, 247 (2000).
100. **Brillouin light scattering study of an exchange coupled asymmetric trilayer of Fe/Cr**
P. Vavassori, M. Grimsditch, E. E. Fullerton, L. Giovannini, R. Zivieri, and F. Nizzoli, *Surf. Sci.* **454-456**, 880 (2000).
99. **Antiferromagnetically-coupled magnetic media layers for thermally-stable high-density recording**
E. E. Fullerton, D. Margulies, M. Schabes, M. Doerner, M. Carey, B. Gurney, A. Moser, M. Best, G. Zeltzer, K. Rubin, and H. Rosen, *Appl. Phys. Lett.* **77**, 3806 (2000).
98. **Preisach analysis of epitaxial hard/soft bilayers**
D. R. Cornejo, F. M. Rhen, F. P. Missell, and E. E. Fullerton, *J. Magn. Magn. Mater.* **226**, 1251 (2001).
97. **Writing and detecting bits at 100 Gbit/in² in longitudinal magnetic recording media**
A. Moser, C.T. Rettner, M.E. Best, E. E. Fullerton, D. Weller, M. Parker, and M.F. Doerner, *IEEE Trans. Mag.* **36**, 2137 (2000). correction *IEEE Trans. Mag.* **37**, 3078 (2001).
96. **The switching behavior of Fe₅₅Pt₄₅/Ni₈₀Fe₂₀ exchange-spring magnets studied by resonant soft x-ray magneto-optical Kerr effect**
O. Hellwig, J. B. Kortright, K. Takano, and E. E. Fullerton, *Phys. Rev. B* **62**, 11694 (2000).
95. **Direct observation of the alignment of ferromagnetic spins by antiferromagnetic spins**
F. Nolting, J. Stohr, A. Scholl, J. W. Seo, J. Fompeyrine, H. Siegert, J.-P. Locquet, S. Anders, J. Luening, E. E. Fullerton, M. Toney, M. R. Scheinfein, H. A. Padmore, *Nature* **405**, 767 (2000).
94. **Design tradeoffs for beyond 20 Gb/in²: Using a merged-notched head on advanced low-noise media**
M. Madison, T. Arnoldussen, M. Pinarbasi, M. Parker, M. Doerner, C. S. Bhatia, D. Call, J. Li, L. Dorius, K. Tang, L. Ingall, E. Lee, S. Yuan, R. Schwenker, J. Tabib, L. Lauchlan, J. Raniseski, R. Smith, W.-C. Hsiao, T. Lin, D. Mauri, E. Marinero, D. Margulies, K. Rubin, E. Fullerton, D. Weller, and A. Moser, *J. Appl. Phys.* **87**, 6364, (2000).
93. **Observation of antiferromagnetic domains in epitaxial LaFeO₃ by means of x-ray magnetic linear dichroism spectromicroscopy**
A. Scholl, J. Stohr, J. Luening, J.-P. Locquet, J. Fompeyrine, J. W. Seo, H. Siegert, F. Nolting, S. Anders, E. E. Fullerton, M. R. Scheinfein, H. A. Padmore, *Science* **287**, 1014 (2000).
92. **Co_xCr_{1-x}/Pt multilayers as perpendicular recording media**
K. Takano, G. Zeltzer, D. Weller, and E. E. Fullerton, *J. Appl. Phys.* **87**, 6364 (2000).
91. **Anisotropy determination in epitaxial Sm-Co/Fe exchange springs**
M. J. Pechan, N. Teng, J.-D. Stewart, J. Z. Hilt, E. E. Fullerton, J. S. Jiang, C. H. Sowers, S. D. Bader, *J. Appl. Phys.* **87**, 6686 (2000).
90. **Spring magnet films (invited)**
J. S. Jiang, E. E. Fullerton, C. H. Sowers, A. Inomata, S. D. Bader, V. I. Nikitenko, and R. D. Schull, *IEEE Trans. Magn.* **35**, 3229 (1999).
89. **Hard/soft magnetic heterostructures: Model exchange-spring magnets (invited)**
E. E. Fullerton, J. S. Jiang, S. D. Bader, *J. Magn. Magn. Mater.* **200**, 392 (1999).
88. **Exchange-spring systems: Coupling of hard and soft ferromagnets as measured by magnetization and Brillouin light scattering (invited)**
M. Grimsditch, R. Camley, E. E. Fullerton, J. S. Jiang, S. D. Bader, and C. H. Sowers
J. Appl. Phys. **85**, 5901 (1999).
87. **Magnetic profile in Nb/Si superconducting multilayers**
S. M. Yusuf, R. M. Osgood III, J. S. Jiang, C. H. Sowers, S. D. Bader, E. E. Fullerton, G. P. Felcher, *J. Magn. Magn. Mater.* **198-199**, 564 (1999).
86. **Symmetry influence on interlayer coupling in epitaxial Co/Cr trilayers grown on MgO (100) and (110) substrates**
J. Z. Hilt, J. J. Picconatto, A. O'Brien, M. Pechan, and E. E. Fullerton, *J. Magn. Magn. Mater.* **198-199**, 387 (1999).
85. **Ferromagnetic resonance in Co hcp and fcc single crystal films on MgO**
in *Magnetism, Magnetic Materials and their Applications*, Materials Science Forum **302-3**, 76 (1999).
84. **Depth-dependent diamagnetism of layered superconductors: Nb/Si**
S.M. Yusuf, E. E. Fullerton, R. M. Osgood, and G. Felcher, *J. Appl. Phys.* **83**, 6801 (1998).
83. **Exchange-spring behavior in epitaxial hard/soft magnetic bilayer films**
J. S. Jiang, E. E. Fullerton, M. Grimsditch, C. H. Sowers, and S. D. Bader, *J. Appl. Phys.* **83**, 6238 (1998).
82. **Magnetic anisotropy and its microstructural origin in epitaxially grown SmCo thin films**
M. Benaissa, K. M. Krishnan, E. E. Fullerton, and J. S. Jiang, *IEEE Trans. Mag.* **34**, 1204 (1998).
81. **Structure and magnetic properties of exchange-spring Sm-Co/Co superlattices**

- E. E. Fullerton, J. Samuel Jiang, C. H. Sowers, J. E. Pearson, and S. D. Bader, Appl. Phys. Lett. **72**, 380 (1998).
80. **Infra-red spectra of giant magnetoresistance Fe/Cr/Cr trilayers**
S. Uran, M. Grimsditch, E. E. Fullerton, and S. D. Bader, Phys. Rev. B **57**, 2705 (1998).
79. **Sources of interface magnetization and interface anisotropy in Fe/Cu multilayers as revealed by thermal behavior**
M. J. Pechan, E. E. Fullerton, and Ivan K. Schuller, J. Magn. Magn. Mater. **183** 19 (1998).
78. **Exchange-spring behavior in epitaxial hard/soft magnetic bilayers**
E. E. Fullerton, J. S. Jiang, M. Grimsditch, C. H. Sowers, S. D. Bader, Phys. Rev. B **58**, 12193 (1998).
77. **Low frequency dynamic response and hysteresis in magnetic superlattices**
S. Rakhmanova, D. L. Mills, and E. E. Fullerton, Phys. Rev. B **57**, 476 (1998).
76. **Enhanced Co orbital moments in Co-rare-earth permanent magnet films**
D. J. Keavney, E. E. Fullerton, D. Li, C.H. Sowers, S. D. Bader, K. Goodman, J. G. Tobin, and R. Carr
Phys. Rev. B **57**, 5291 (1998).
75. **High-coercivity, epitaxial Sm-Co films with uniaxial in-plane anisotropy**
E. E. Fullerton, J. S. Jiang, Ch. Rehm, C. H. Sowers, S. D. Bader, J. B. Patel, and X. Z. Wu
Appl. Phys. Lett. **71**, 1579 (1997).
74. **Temperature-dependent study of ion-channeling in Fe/Cr superlattices**
F. Rüders, L. E. Rehn, P. M. Baldo, E. E. Fullerton, and S. D. Bader, Nucl. Inst. and Meth. B **121**, 30 (1997).
73. **Interplay between biquadratic coupling and the Néel transition in Fe/Cr₉₄Fe₆(001) superlattices**
Eric E. Fullerton, C. H. Sowers and S. D. Bader, Phys. Rev. B **56**, 5468 (1997).
72. **High-coercivity, c-axis oriented Nd₂Fe₁₄B films grown by molecular beam**
D. J. Keavney, E. E. Fullerton, J. E. Pearson, and S.D. Bader, J. Appl. Phys. **81**, 4441 (1997).
71. **Structure and magnetism of epitaxial rare-earth-transition-metal films**
E. E. Fullerton, C. H. Sowers, J. P. Pearson, S. D. Bader, J. B. Patel, X.Z. Wu, and D. Lederman
J. Appl. Phys. **81**, 5637 (1997).
70. **Magnetic anisotropy, coupling, and transport properties of epitaxial Co/Cr superlattices on MgO (100) and (110),** J. Johanna Picconatto, M. J. Pechan, and E. E. Fullerton, J. Appl. Phys. **81**, 5058 (1997).
69. **Exchange and anisotropy effects on spin waves in epitaxial Co films**
M. Grimsditch, E. E. Fullerton and R. L. Stamps, Phys. Rev. B **56**, 2617 (1997).
68. **Spin-density-wave antiferromagnetism of Cr in Fe/Cr(001) superlattices (invited)**
E. E. Fullerton, S. D. Bader, and J. L. Robertson, Physica B **237-238**, 234 (1997).
67. **Perpendicular conductance and magnetic coupling in epitaxial Fe/MgO/Fe(100) trilayers**
D. J. Keavney, E. E. Fullerton, and S. D. Bader, J. Appl. Phys. **81**, 795 (1997).
66. **Structure and magnetism of epitaxial rare-earth-transition-metal films (invited)**
E. E. Fullerton, C. H. Sowers, J. P. Pearson, X.Z. Wu, D. Lederman, and S. D. Bader in *Magnetic Hysteresis in Novel Magnetic Materials*, edited by G.C. Hadjipanayis, (Kluwer Acad. Press, Netherlands, 1997), p. 467-478.
65. **Phase diagram of imperfect ferromagnetic/antiferromagnetic bilayers**
A. Berger and E. E. Fullerton, J. Magn. Magn. Mater. **165**, 471 (1997).
64. **Unusual vortex dynamics in Nb- α Si multilayers with strong interlayer coupling**
J.D. Hettinger, B.R. Washburn, N.B. Remmes, D.G. Steel, K.E. Gray, E. E. Fullerton, and C.H. Sowers
Phys. Rev. Lett. **77**, 5280 (1996).
63. **A general approach to the epitaxial growth of rare-earth-transition-metal films**
E. E. Fullerton, C. H. Sowers, J. P. Pearson, X.Z. Wu, D. Lederman, and S. D. Bader
Appl. Phys. Lett. **69**, 2438 (1996).
62. **Magnetization studies of Ho/Y superlattices: Role of magnetoelastic coupling**
M. J. Conover, E. E. Fullerton and S. D. Bader, Phys. Rev. B **54**, 1100 (1996).
63. **A general approach to the epitaxial growth of rare-earth-transition-metal films**
E. E. Fullerton, C. H. Sowers, J. P. Pearson, X.Z. Wu, D. Lederman, and S. D. Bader
Appl. Phys. Lett. **69**, 2438 (1996).
62. **Magnetization studies of Ho/Y superlattices: Role of magnetoelastic coupling**
M. J. Conover, E. E. Fullerton and S. D. Bader, Phys. Rev. B **54**, 1100 (1996).
61. **Magnetic properties of c-axis textured Nd₂Fe₁₄B thin films**
D. J. Keavney, E. E. Fullerton, J. E. Pearson, and S.D. Bader, IEEE Trans. Mag. **32**, 4440 (1996).
60. **Growth of oriented rare-earth-transition-metal thin films**
E. E. Fullerton, C. H. Sowers, X. Z. Wu, and S.D. Bader, IEEE Trans. Mag. **32**, 4434 (1996).
59. **Brillouin light scattering study of Fe/Cr/Fe (211) and (100) trilayers**
M. Grimsditch, S. Kumar, and E. E. Fullerton, Phys. Rev. B **54**, 3385 (1996).

58. **Resonant x-ray reflectivity study of Fe/Cr superlattices**
J. Bai, E. E. Fullerton, and P. Montano, *Physica B* **221**, 411 (1996).
57. **Spin-density-wave antiferromagnetism of Cr in Fe/Cr(001) superlattices**
E. E. Fullerton, S. D. Bader, and J. L. Robertson, *Phys. Rev. Lett.* **77**, 1382 (1996).
56. **Temperature-dependent biquadratic coupling in antiferromagnetically coupled Fe/FeSi multilayers**
E. E. Fullerton and S. D. Bader, *Phys. Rev. B-Brief Reports* **53**, 5112 (1996).
55. **Neutron diffraction and reflectivity studies of the Cr Néel transition in Fe/Cr(001) superlattices (invited)**
E. E. Fullerton, S. Adenwalla, G. P. Felcher, K. T. Riggs, C. H. Sowers, S. D. Bader, and J. L. Robertson
Physica B **221**, 370 (1996).
54. **Magnons in antiferromagnetically coupled superlattices**
R. W. Wang, D. L. Mills, E. E. Fullerton, S. Kumar, and M. Grimsditch, *Phys. Rev. B* **53**, 2627 (1996).
53. **Polarized neutron reflectivity confirmation of 90° magnetic structure in Fe/Cr(001) superlattices**
S. Adenwalla, G. P. Felcher, E. E. Fullerton and S. D. Bader, *Phys. Rev. B* **53**, 2474 (1996).
52. **Magnetic phase transitions in epitaxial Fe/Cr superlattices (invited)**
E. E. Fullerton, K. T. Riggs, C. H. Sowers, S. D. Bader, and A. Berger, in *Magnetic Ultrathin Films, Multilayers and Surfaces*, edited by A. Fert, H. Fujimori, G. Guntherodt, B. Heinrich, W.F. Egelhoff, Jr., E.E. Marinero, and R.L. White, MRS Symp. Proc. No. 384 (Materials Research Society, Pittsburgh, 1995) p 145.
51. **X-ray Fraunhofer diffraction patterns from a thin-film waveguide**
Y. P. Feng, S. K. Sinha, E. E. Fullerton, G. Grübel, D. Abernathy, D. P. Siddons, and J. B. Hastings
Appl. Phys. Lett. **67**, 3647 (1995).
50. **Suppression of biquadratic interlayer coupling in Fe/Cr(001) superlattices below the Néel transition of Cr**
E. E. Fullerton, K. T. Riggs, C. H. Sowers, S. D. Bader, and A. Berger, *Phys. Rev. Lett.* **75**, 330 (1995).
49. **Magnetic and structural properties of Fe/Pd multilayers studied by magnetic x-ray dichroism and x-ray absorption spectroscopy**, S. M. Mini, E. E. Fullerton, A. Fontaine, C.H. Sowers, A. S. Bommannavar, A. Traverse, F. Baudalet, and S. Pizzini, in *Applications of Synchrotron Radiation Techniques to Materials Science II*, edited by L.J. Terminello *et al.*, MRS Symposia Proceedings No. 375 (Materials Research Society, Pittsburgh, 1995) p 87.
48. **Observation of pure nuclear diffraction from an Fe/Cr antiferromagnetic multilayer**
T. Toellner, W. Sturhalm, R. Röhlberger, E. E. Alp, C. H. Sowers, and E. E. Fullerton
Phys. Rev. Lett. **74**, 3475 (1995).
47. **Enhanced magnetic moments in epitaxial bcc Fe/Ag(001) films overcoated with Ag, Au, Cu and Pd**
J. A. C. Bland, D. Daboo, B. Heinrich, Z. Celinski, E. E. Fullerton, K. Ounadjela, and D. Stoeffler
J. Magn. Magn. Mater. **148**, 85 (1995).
46. **Epitaxial growth of ultrathin MgO films on an Fe(001) seed layers**
Y. Park, E. E. Fullerton, and S. D. Bader, *J. Vac. Sci. Technol. A* **13**, 301 (1995).
45. **Interlayer magnetic coupling in epitaxial Fe/Cr(211) and (100) superlattices**
E. E. Fullerton, J. E. Mattson, C. H. Sowers, and S. D. Bader, *Acta Metallurgica et Materialia* **33**, 1637 (1995).
44. **Structure and magnetism of epitaxially-strained Pd(001) films on Fe(001): Experiment and theory**
E. E. Fullerton, D. Stoeffler, K. Ounadjela, B. Heinrich, Z. Celinski, and J. A. C. Bland
Phys. Rev. B **51**, 6364 (1995).
43. **Determination of magnetic anisotropy in Fe/Cu multilayers: equivalence of dynamic and static measurements**
M. J. Pechan, E. E. Fullerton, W. Robertson, M. Grimsditch, and I. K. Schuller, *Phys. Rev. B*, **52**, 3045 (1995).
42. **Epitaxial growth of bcc transition metal films and superlattices onto MgO(111), (011), and (001) substrates**
J. E. Mattson, E. E. Fullerton, C. H. Sowers, and S. D. Bader, *J. Vac. Sci. Technol. A* **13**, 276 (1995).
41. **A simple, closed-form expression for the x-ray reflectivity from multilayers with cumulative roughness**
D. M. Kelly, E. E. Fullerton, J. Santa-Maria, and I. K. Schuller, *Acta Met. et Mater.* **33**, 1603 (1995).
40. **Growth-induced uniaxial in-plane magnetic anisotropy for ultrathin Fe deposited on MgO(001) by oblique-incidence molecular beam epitaxy**
Y. Park, E. E. Fullerton, and S. D. Bader, *Appl. Phys. Lett.* **66**, 2140 (1995).
39. **Characterization of interface structure in multilayers using specular x-ray reflectance (invited)**
E. E. Fullerton, in *Physics of X-ray Multilayer Structures*, 1994 Technical Digest Series, Vol. 6 (Optical Society of America, Washington DC, 1994) pp. 48-51.
38. **Surface spin-flop transition in Fe/Cr(211) superlattices: experiment and theory**
R. W. Wang, D. L. Mills, E. E. Fullerton, J.E. Mattson, and S.D. Bader, *Phys. Rev. Lett.* **72**, 920 (1994).
37. **Modulation wavelength dependence of ion mixing in metallic superlattices**
Dale E. Alexander, Eric E. Fullerton, P. M. Baldo, C. H. Sowers, and L. E. Rehn, in *Materials Synthesis and*

Processing Using Ion Beams, edited by R. J. Culbertson, O. W. Holland, K. S. Jones, and K. Maex, MRS Symposia Proceedings No. 316 (Materials Research Society, Pittsburgh, 1994) p 271.

36. **Photo-induced antiferromagnetic interlayer coupling in superlattices with iron silicide spacers (invited)**
J.E. Mattson, Eric E. Fullerton, Sudha Kumar, S.R. Lee, C.H. Sowers, M. Grimsditch, S.D. Bader, and F.T. Parker, J. Appl. Phys. **75**, 6169 (1994).
35. **Orientationally independent antiferromagnetic coupling in epitaxial Fe/Cr(211) and (100) superlattices**
E. E. Fullerton, M.J. Conover, J.E. Mattson, C.H. Sowers, and S.D. Bader, J. Appl. Phys. **75**, 6461 (1994).
34. **Photo- and thermal-induced antiferromagnetic interlayer coupling in Fe/(Fe-Si) superlattices**
J.E. Mattson, E. E. Fullerton, Sudha Kumar, S.R. Lee, C.H. Sowers, M. Grimsditch, S.D. Bader, and F.T. Parker, in *New Trends in Magnetic Materials and their applications*, edited by J. L. Morán-López and J. M. Sanchez, (Plenum Press, New York, 1994) p. 157.
in *Thin Films: Stresses and Mechanical Properties IV*, edited by P. H. Townsend, T. P. Weihs, J.E. Sanchez Jr., P. Børgesen, MRS Symposia Proceedings No. 308 (Materials Research Society, Pittsburgh, 1993) p 685.
33. **Neutron-induced collision cascade mixing in Nb/V superlattices**
D. E. Alexander, E. E. Fullerton, P. M. Baldo, C. H. Sowers, and L. E. Rehn, Nucl. Inst. and Meth. B **90**, 344 (1994).
32. **Oscillatory interlayer coupling and giant magnetoresistance in epitaxial Fe/Cr(211) and (100) superlattices**
E. E. Fullerton, M.J. Conover, J.E. Mattson, C.H. Sowers, and S.D. Bader, Phys. Rev. B **48**, 15 755 (1993).
31. **150% magnetoresistance in sputtered Fe/Cr(100) superlattices**
E. E. Fullerton, M.J. Conover, J.E. Mattson, C.H. Sowers, and S.D. Bader, Appl. Phys. Lett. **63**, 1699 (1993).
30. **Phenomenological explanation of the elastic anomalies in superlattices (invited)**
M. Grimsditch, E. E. Fullerton, and Ivan K. Schuller
29. **Interfacial structure of lattice mismatched bcc(110)/bcc(110) transition metal superlattices**
E. E. Fullerton, S.M. Mini, A.S. Bommannavar, C.H. Sowers, S. N. Ehrlich, S.D. Bader
in *Applications of Synchrotron Radiation Techniques to Materials Science*, edited by D. L. Perry, N. D. Shinn, R. L. Stockbauer, K.L. D'Amico, L.J. Terminello, MRS Symposia Proceedings No. 307 (Materials Research Society, Pittsburgh, 1993) p 131.
28. **Interfacial roughness of sputtered superlattices: Nb/Si**
E. E. Fullerton, J. Pearson, C.H. Sowers, S.D. Bader, X.Z. Wu, and S.K. Sinha, Phys. Rev. B **48**, 17 432 (1993).
27. **Photo-induced antiferromagnetic interlayer coupling in Fe/(Fe-Si) superlattices**
J. E. Mattson, S. Kumar, E. E. Fullerton, S.R. Lee, C.H. Sowers, M. Grimsditch, S.D. Bader, and F.T. Parker, Phys. Rev. Lett. **71**, 185 (1993).
26. **X-ray diffraction characterization and sound velocity measurements of W/Ni multilayers**
E. E. Fullerton, S. Kumar, M. Grimsditch, D. M. Kelly, and I. K. Schuller, Phys. Rev. B **48**, 2560 (1993).
25. **Quantitative characterization of epitaxial superlattices by x-ray diffraction and high-resolution electron microscopy**
E. E. Fullerton, W. Cao, M. J. Carey, I. K. Schuller, G. Thomas, and A. E. Berkowitz, Appl. Phys. Lett. **63**, 482 (1993).
24. **Relationship between structural phase transitions and elastic anomalies in metallic superlattices**
E. E. Fullerton, I. K. Schuller, F. T. Parker, K. Svinarich, G. Eesley, R. Bhadra, M. Grimsditch
J. Appl. Phys. **73**, 7370 (1993).
23. **Interface structure in high T_C superlattices**
J. Guimpel, E. E. Fullerton, O. Nakamura, Ivan K. Schuller, J. Phys.: Condens. Matter **5**, A383 (1993).
22. **Magnetic excitations in antiferromagnetically coupled superlattices: Fe/Mo and Fe/Cr**
M. Grimsditch, S. Kumar, and E. E. Fullerton, J. Phys.: Condens. Matter **5**, A369 (1993).
21. **Breakdown of Possion's effect in Cu/Nb superlattices**
A. Fartash, M. Grimsditch, E. E. Fullerton, and Ivan K. Schuller, Phys. Rev. B **47**, 12 813 (1993).
20. **Oscillatory interlayer magnetic coupling of sputtered Fe/Nb superlattices**
J. E. Mattson, E. E. Fullerton, C.H. Sowers, Y.Y. Huang, G. Felcher, S.D. Bader, J. Appl. Phys. **73**, 5969 (1993).
19. **Magnetic decoupling in sputtered Fe/Si multilayers and superlattices**
Eric E. Fullerton, J. E. Mattson, S.R. Lee, C.H. Sowers, Y.Y. Huang, G. Felcher, S.D. Bader, and F.T. Parker, J. Appl. Phys. **73**, 6335 (1993).
18. **Connection between giant magnetoresistance and roughness in sputtered Fe/Cr superlattices**
David M. Kelly, Eric E. Fullerton, F.T. Parker, J. Guimpel, Y. Bruynseraede, and Ivan K. Schuller
Inter. J. Mod. Phys. B **7**, 419 (1992).
17. **Quantitative x-ray diffraction from superlattices (invited)**
Eric E. Fullerton, Ivan K. Schuller, and Y. Bruynseraede, MRS Bulletin **XVII** (12), 33 (1992).

16. **Non-oscillatory antiferromagnetic coupling in sputtered Fe/Si superlattices**
Eric E. Fullerton, J. E. Mattson, S.R. Lee, C.H. Sowers, Y.Y. Huang, G. Felcher, S.D. Bader, and F.T. Parker, *J. Magn. Magn. Mater.* **117**, L301 (1992).
15. **Structure of high T_C superlattices**
Eric E. Fullerton, O. Nakamura, J. Guimpel, Ivan K. Schuller, *Phys. Rev. Lett.* **69**, 2859 (1992).
14. **Effect of structure on the mechanical properties of metallic superlattices (invited)**
Ivan K. Schuller, A. Fartash, Eric E. Fullerton, and M. Grimsditch, in *Thin Films: Stresses and Mechanical Properties III*, edited by W.D. Nix *et al.*, MRS Symp. Proc. No. 239 (MRS, Pittsburgh, 1992) p. 499.
13. **Structural refinement of superlattices from x-ray diffraction**
Eric E. Fullerton, Ivan K. Schuller, H. Vanderstraeten, Y. Bruynseraede, *Phys. Rev. B* **45**, 9292 (1992).
12. **Roughness and giant magnetoresistance in Fe/Cr multilayers**
Eric E. Fullerton, D. M. Kelly, J. Guimpel, I.K. Schuller, Y. Bruynseraede, *Phys. Rev. Lett.* **68**, 859 (1992).
11. **High-Tc thin films with roughness smaller than one unit cell**
O. Nakamura, E. E. Fullerton, J. Guimpel, and Ivan K. Schuller, *Appl. Phys. Lett.* **60**, 120 (1992).
10. **Disorder and superconductivity in YBaCuO/GdBaCuO superlattices**
O. Nakamura, E. E. Fullerton, J. Guimpel, and Ivan K. Schuller, *Physica C* **185-189**, 2069 (1991).
9. **Quantitative x-ray structure determination of superlattices and interfaces (invited)**
I. K. Schuller, E. E. Fullerton, H. Vanderstraeten, Y. Bruynseraede
in *Structure/Property Relationships for Metal/Metal Interfaces*, edited by A.D. Romig, D.E. Fowler, and P.D. Bristowe, MRS Symposia Proceedings No. 229 (Materials Research Society, Pittsburgh, 1991) p. 41.
8. **Evidence for the supermodulus effect and enhanced hardness in metallic superlattices**
A. Fartash, E. E. Fullerton, Ivan K. Schuller, S. Bobbin, R. C. Cammarata, M. Grimsditch, *Phys. Rev. B* **44**, 13 760 (1991).
7. **Low angle x-ray diffraction of multilayered structures**
H. Vanderstraeten, D. Neerincx, K. Temst, Y. Bruynseraede, E. E. Fullerton, I. K. Schuller
J. Appl. Cryst. **24**, 571 (1991).
6. **Structural and elastic property changes in Ag/Co superlattices induced by high energy ion irradiation**
E. Fullerton, Ivan K. Schuller, R. Bhadra, Marcos Grimsditch, and Steven M. Hues
Mater. Science and Eng., A **126**, 19 (1990).
5. **Light scattering by surface acoustic waves on corrugated metal surfaces**
W. M. Robertson, M. Grimsditch, A. L. Moretti, R. G. Kaufman, G. R. Hulse, E. Fullerton, and Ivan K. Schuller, *Phys. Rev. B* **41**, 4986 (1990).
4. **Mössbauer effect determination of chemical segregation in sputtered Co-Cr films**
F.T. Parker, H. Oesterreicher, and E. Fullerton, *J. Appl. Phys.* **66**, 5988 (1989).
3. **Brillouin scattering from corrugated Ag films: Surface-plasmon-mediated enhancement and relaxed wave-vector conservation**
W. M. Robertson, M. Grimsditch, A. L. Moretti, R. G. Kaufman, G. R. Hulse, E. Fullerton, and Ivan K. Schuller, *Phys. Rev. B* **40**, 4153 (1989).
2. **Reexamination of the surface plasma wave technique for determining the dielectric constant and thickness of metal films**
W. M. Robertson and E. Fullerton, *J. Opt. Soc. Am. B* **6**, 1584 (1989).
1. **Effect of high-energy ion irradiation on the elastic moduli of Ag/Co superlattices**
Steven M. Hues, R. Bhadra, M. Grimsditch, E. Fullerton, and Ivan K. Schuller, *Phys. Rev. B - Rapid Comm.* **39**, 12966 (1989).

EXHIBIT B

List of Materials Considered by Eric Fullerton

Patents

U.S. Patent No. 7,128,988 (“the ’988 Patent”)

’988 Patent -- U.S. file history

File history for EP 1435091 (related to ’988 Patent)

U.S. Patent No. 6,248,416

U.S. Patent No. 7,914,916

U.S. Patent No. 4,949,039

U.S. Patent No. 5,453,315A

U.S. Patent No. 5,476,131A

U.S. Patent No. 5,483,025A

U.S. Patent No. 5,490,027A

U.S. Patent No. 5,557,488A

U.S. Patent No. 6,320,725B1

U.S. Patent Application Pub. No. US20020093761A1

U.S. Patent No. 4,423,450A

U.S. Patent No. 4,860,139A

U.S. Patent No. 4,636,894A

U.S. Patent No. 4,751,598A

U.S. Patent No. 5,632,669A

U.S. Patent No. 5,885,131A

U.S. Patent No. 4,757,402A

U.S. Patent No. 5,041,932A

U.S. Patent No. 5,073,242A

U.S. Patent No. 5,111,351A

U.S. Patent No. 5,163,218A

U.S. Patent No. 5,174,012A

U.S. Patent No. 6,493,191B1

U.S. Patent Application Pub. No. US20020176210A1

U.S. Patent No. 5,063,712A

U.S. Patent No. 5,550,691A

U.S. Patent No. 5,822,153A

U.S. Patent No. 5,909,340A

U.S. Patent No. 5,949,612A

U.S. Patent No. 6,160,685A

U.S. Patent No. 6,198,607B1

U.S. Patent No. 6,212,047B1

U.S. Patent No. 6,411,470B1

U.S. Patent No. 6,535,361B2

U.S. Patent No. 6,600,631B1

U.S. Patent No. 6,804,085B1

U.S. Patent No. 5,625,515A

U.S. Patent No. 5,693,426

U.S. Patent No. 4,825,318

U.S. Patent No. 4,702,808

U.S. Patent No. 4,673,996

Books / Articles

Y. Barneir et al., *Cobalt* 15 (1962)

Bruno Marchon, Thomas Pitchford, Yiao-Tee Hsia, Sunita Gangopadhyay, *The Head-Disk Interface Roadmap to an Areal Density of 4 Tbit/in²*, *Advances in Tribology*, vol. 2013, Article ID 521086, 2013, available at <https://www.hindawi.com/journals/at/2013/521086/>

S. N. Piramanayagam, M. Shakerzadeh, B. Varghese, H. Tan, *Effect of Carbon Overcoat Implantation on the Magnetic and Structural Properties of Perpendicular Recording Media*, *IEEE Transactions on Magnetics*, Vol. 51, Issue 11, Nov. 2015

E. Grochowski, *The Continuing Evolution of Magnetic Hard Disk Drives*, in *HOLOGRAPHIC DATA STORAGE 448* (H.J. Coufal et al. eds., Springer 2000)

Shan X. Wang & Alexander M. Taratorin, *MAGNETIC INFORMATION STORAGE TECHNOLOGY* (Academic Press 1999)

E. Hirota, H. Sakakima, K. Inomata, *GIANT MAGNETO-RESISTANCE DEVICES 99*, (Dr. G. Ertl et al. eds., Springer 2002)

S. Khizroev & D. Litvinov, *PERPENDICULAR MAGNETIC RECORDING* (Kluwer Academic Publishers 2004)

Jason Dedrick, Kenneth L. Kraemer, “Who Captures the Value in Technological Innovation? The distribution of benefits in the GMR-based global storage industry,” *Penn State University*, September 2013, available at <http://citeseerx.ist.psu.edu/viewdoc/download?doi=10.1.1.405.2326&rep=rep1&type=pdf>

H.J. Richter, *The Transition from Longitudinal to Perpendicular Recording*, *J. Phys. D.* 40, R149-R177 (2007)

J.M.D. Coey, *MAGNETISM AND MAGNETIC MATERIALS* (2010)

G. Herzer, *Grain Size Dependence of Coercivity and Permeability in Nanocrystalline Ferromagnets*, *IEEE Trans. on Magnetics*, Vol. 26, No. 5 (1990)

Th. Muhge et al., *Structural and Magnetic Studies of Fe_xCo_{1-x}(001) Alloy Films on MgO(001) Substrates*, *J. of Appl. Phy.* 77, 1055 (1995)

R. C. Hall, *Single Crystal Anisotropy and Magnetostriction Constants of Several Ferromagnetic Materials Including Alloys of NiFe, SiFe, AlFe, CoNi, and CoFe*, *J. of App. Phy.*, Vol. 30 No. 6 (1959)

Dahmen, *Orientation Relationships in Precipitation Systems*, Acta Metallurgica, 30(1) 63-73 (1982)

Gotoh, *Interpretation of the Epitaxial Orientation Relationship at bcc(110)/fcc(111) Interfaces*, Applied Surface Science 33/34 443-49 (1988)

KK Fung, *Identification and Determination of Crystal Structures and Orientations by Electron Diffraction* (Jan. 2001), available at:
<http://personal.cityu.edu.hk/~appkchu/AP5301/Electron%20Diffraction%20-%20Paper.pdf>

D. Lambeth et al., *Magnetic Media Performance: Control Methods for Crystalline Texture and Orientation*, Mat. Res. Soc. Symp. Proc., Vol. 517, p. 185 (1998)

B. Fultz and J. Howe, *Transmission Electron Microscopy and Diffractometry of Materials* (2013)

J.W. Edington, *Practical Electron Microscopy in Materials Science* (1976)

D.B. Williams and C.B. Carter, *Transmission Electron Microscopy*, Springer (2009)

Milton Ohring, *Materials Science of Thin Films* (1st ed. 1990)

Milton Ohring, *Materials Science of Thin Films* (2nd ed. 2002)

R. Lawrence Comstock, *Introduction to Magnetism and Magnetic Recording* (1999)

D. Jiles, *Magnetism and Magnetic Materials* (1998)

N. Sun & S. Wang, *Soft High Saturation Magnetization ($Fe_{0.7}Co_{0.3}$)_{1-x}N_x Thin Films for Inductive Write Heads*, IEEE Trans. on Mag., Vol. 36, No. 5 (Sept. 2000)

S. Chikazumi, *Physics of Ferromagnetism* (2nd ed. 1997) (Exhibit 2002 to IPR2016-00013)

R. O'Handley, *Modern Magnetic Materials: Principles and Applications* (2000)

Gong et al., *Epitaxial Growth of Quad-Crystal Co-Alloy Magnetic Recording Media*, IEEE Transactions on Magnetics, 35(5), 1999, pp. 2676-2663

Zangari et al., *Structure and Magnetic Properties of Sm-Co Thin Films on Cr/Ag/Si Templates*, Journal of Applied Physics, Vol. 85(8), Apr. 15, 1999, pp. 5759-5761

B.D. Cullity and C.D. Graham, INTRODUCTION TO MAGNETIC MATERIALS, 2nd Edition (2009)

D. Bai et. al, *Writer Pole Tip Remanence in Perpendicular Recording*, IEEE Transactions on Magnetics Vol. 42, No. 3 (March 2006), at 473-480

X. Shen and R.H. Victora, *Effect of Pole Tip Geometry on Remnant Field*, Journal of Applied Physics 103, 07F542-1 (2008)

Court Orders / Opinions / Transcripts

Markman Order (Dkt. No. 78)

Transcript of Markman Hearing

Deposition Transcripts and Exhibits

Transcript of 2/28/2018 Deposition of D. Lambeth and Exhibits

Transcript of 2/27/2018 Deposition of D. Lambeth and Exhibits

Transcript of 2/26/2018 Deposition of D. Lambeth and Exhibits

Transcript of 2/23/2018 Deposition of D. Lambeth and Exhibits

Transcript of 1/13/2017 Deposition of Dr. Coffey and Exhibits

Transcript of 1/11/2017 Deposition of Dr. Coffey and Exhibits

Transcript of 10/5/2017 Deposition of Venkat Inturi and Exhibits

Transcript of 2/9/2018 Deposition of Matthew Hadley and Exhibits

Transcript of 2/21/2018 Deposition of Michael Kautzky and Exhibits

Interrogatory Responses

LMS First Supplemental Response to Seagate Interrogatory No. 2

LMS Amended Response to Seagate Interrogatory No. 10

Seagate's First Supplemental Response to LMS's Interrogatory No. 10

Expert Reports

Initial Expert Report of Dr. William Alan Thomas Clark and attached appendices

Initial Expert Report of Dr. Kevin Coffey and attached appendices

Expert Report of Dr. Eric Stach and attached exhibits

Initial Expert Report of Dr. Caroline A. Ross

Seagate Documents

All Seagate documents cited in Dr. Coffey's Initial Expert Report

SEA03129091

SEA00026547

SEA00022942

SEA02887989

SEA01043275

SEA01043459

SEA01043148

SEA01044086

SEA01043618

SEA01043967

SEA01043614

SEA03052381

Other Materials

Patent Owner's Preliminary Response to IPR2016-00013

LMS Infringement Contentions (served on Toshiba on Oct. 9, 2015)
[Case No. 2:15-cv-07987-SJO-PLA Document 1-4]

LMS's Amended Infringement Contentions (served on Seagate Nov. 29, 2017)

The Discovery of Giant Magnetoresistance, *NobelPrize.org*, Oct. 9, 2007, available at https://www.nobelprize.org/nobel_prizes/physics/laureates/2007/advanced-physicsprize2007.pdf

Thomas W. Peterson, “Creating an Innovation Ecosystem,” National Science Foundation, 2009, available at http://www.nseresearch.org/2009/presentations/Day2_Peterson.ppt
“NSF Engineering Research Centers – Creating New Knowledge, Innovators and Technologies For Over 30 Years,” National Science Foundation, October 2015, available at <http://ercassoc.org/sites/default/files/download-files/ERC%2030th%20anniversary%20brochure.pdf>

EXHIBIT C

Table 1: Mechanics

1. Actuator designs, materials, and processes
2. Actuator bearings and lubricants
3. Air flow control
4. Internal air filtration
5. External air filtration
6. Pressure balancing
7. Hermetic sealing materials and processes
8. Enclosure materials and processes
9. Corrosion resistance under various temperatures and humidity levels
10. Component cleaning materials, methods, and tools

Table 2: Disk

1. Substrate type: aluminum or glass
2. Substrate dimensions: thickness and diameter
3. Substrate flatness
4. Magnetic alloys and processes
5. Film grain/crystallite size control and isolation
6. Orienting alloys and processes
7. Magnetic soft under layer design, alloys, and processes
8. Wear resistant and corrosion resistant overcoats
9. Lubricant materials and processes
10. Head burnish types and processes
11. Magnetic test types and processes
12. Optical test types and processes
13. Substrate and disc cleaning materials, methods, and tools
14. Electrostatic charging prevention methods and cassettes

Table 3: Spindle motor

1. Motor types
2. Bearing system
3. Labyrinth designs
4. Coil materials and processes
5. Hub materials and processes
6. Disk attachment designs, materials, and processes
7. Disk spacer designs, materials, and processes
8. Balancing designs and process
9. Component cleaning materials, methods, and tools

Table 4: Electronics
1. Electronic packaging at chip, module, card, and cable level: designs and processes
2. Interfaces (e.g., SATA, SCSI)
3. Data detection methods: <ul style="list-style-type: none"> a. Partial response maximum likelihood (PRML) or b. Enhanced PRML (EPRML)
4. Data formatting
5. Data encoding
6. Read head bias
7. Read head thermal asperity management
8. Servo formatting and writing
9. Error correction and recovery methods
10. HDD burn in and test
11. Servo control architectures and systems

Table 5: Arm assembly
1. Arm designs, materials, and processes
2. Arm to e-block attachment methods, materials, and processes
3. Preamp mounting and connections to HGAs
4. Attachment to actuator
5. Crash stop design and materials
6. Head ramp and head parking for dynamic head load-unload
7. Cleaning methods, tools, and materials
8. HGA designs, materials, and processes

Table 6: Slider
1. Slider designs, materials, and processes
2. Air bearing designs and processes
3. Slider overcoat designs, materials, and processes
4. Landing pad designs, materials, and processes
5. Preamp to head interconnections: designs, materials, and processes
5. Head fly height and head to medium spacing control methods
6. Head grounding and electro static discharge protection
7. Pole tip protrusion and recession: designs, control means, and processes
8. Means to actively control pole tip protrusion and recession
9. Thermal asperity reduction designs, materials, and processes
10. Head initialization methods

11. Head test methods
12. Cleaning methods, tools, and materials

Table 7: Read head
1. Read head shield designs, materials, and processes
2. Read head gap designs, materials, and processes
3. Read head width and placement relative to write head
4. Read head stripe height: designs, control means, and processes
5. Barkhausen noise reduction/control: designs, materials, and processes
6. Free and pinned layer placement and absolute as well as relative orientations of magnetizations
7. Materials and processes for pinning of the bias layer
8. Electrical lead designs, placement, materials, and processes
9. Magnetic materials in each layer and at interfaces
10. Insulating materials and processes for interlayers

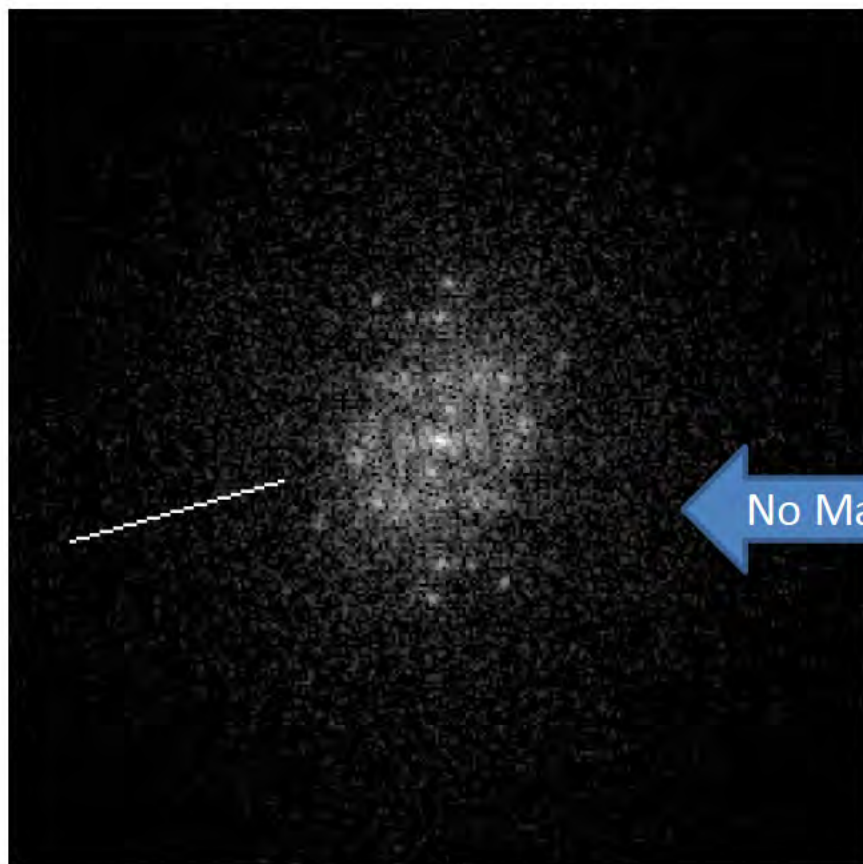
Table 8: Write head
1. Yoke designs, materials, and processes
2. Coil designs, materials, and processes
3. Write pole tip designs and processes
4. Top shield designs, materials, and processes
5. Bottom shield designs, materials, and processes
6. Side shields designs, materials, and processes
7. Throat height designs and processes
8. Gap designs, materials, and processes
9. Coil current timing and shapes
10. Degaussing methods
11. Write pole designs, materials, and processes

EXHIBIT D

FFT Diffraction Patterns in Dr. Clark's Appendix C

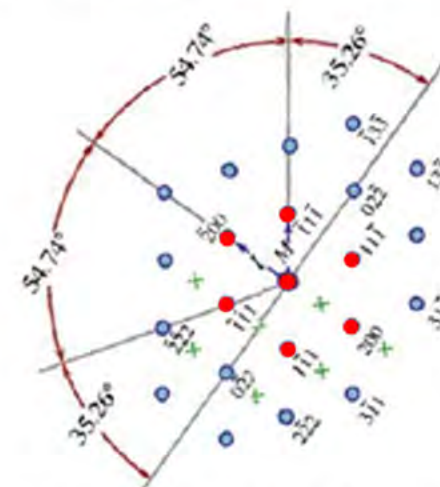
Sample	Position	Filename	No. of Points	No. of FFT's per point	Total No. of FFT's per file	Total No. of FFT's per Layer
S0GPPC	Upper	Middle1	4	3	12	42
		Middle2	3	3	9	
		Middle3	3	3	9	
		Middle4	3	3	9	
		Middle5	1	3	3	
	Lower	Frameright1	7	2	14	54
		Frameright2	7	2	14	
		Frameright3	5	2	10	
		Frameright4	5	2	10	
		Frameright5	3	2	6	
S2MMMC	Upper	18.10.05 CCD Acquire	1	3	3	3
	Lower	18.08.14 CCD Acquire	4	3	12	12
SBRD8K	Lower	18.21.37 CCD Acquire	4	3	12	12

Sample S0GPPC - Framerright1T FFT

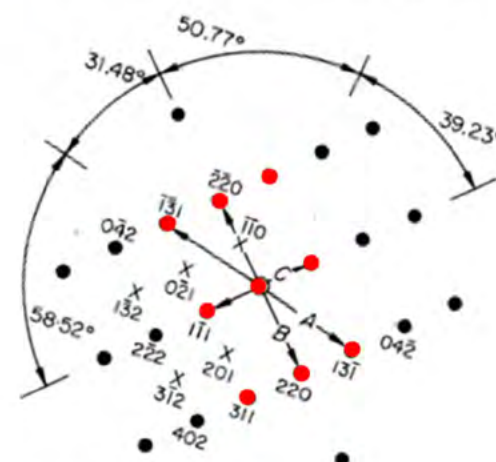


Framerright1T

No Match

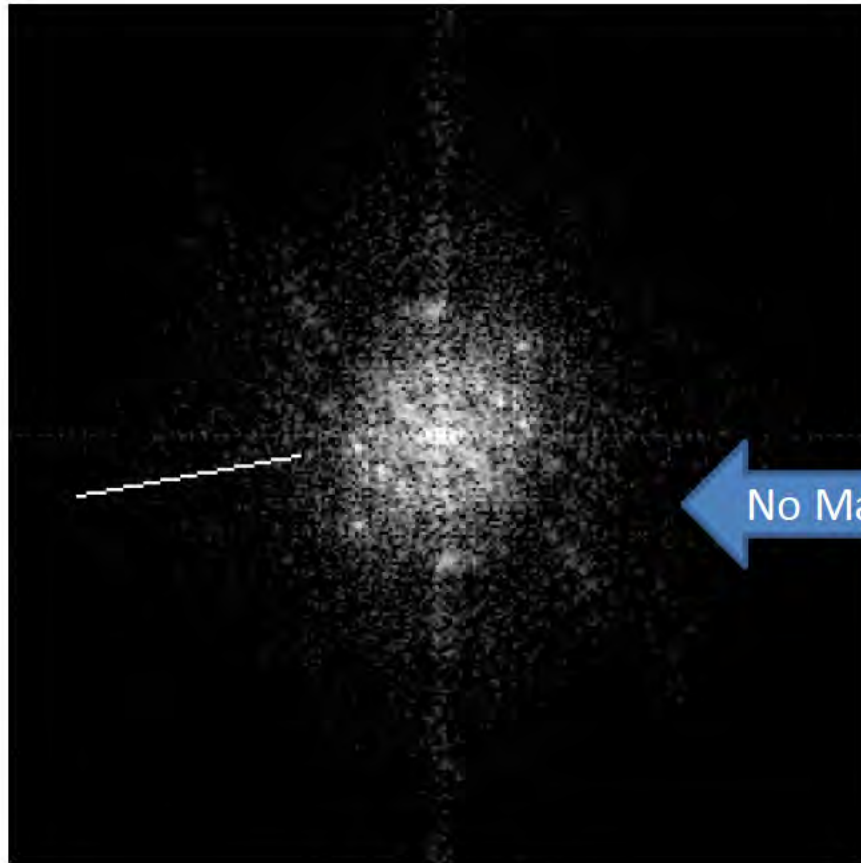


Standard Diffraction Pattern for {110}Fcc



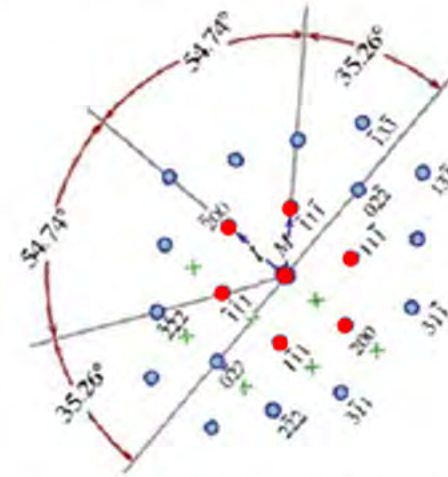
Standard Diffraction Pattern for {112}Fcc

Sample S0GPPC - Framerright2T FFT

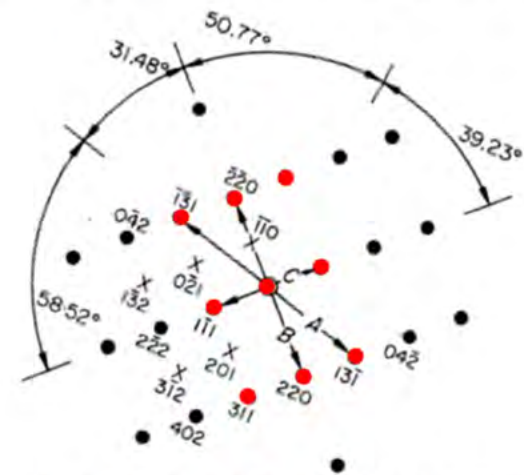


Framerright2T

No Match

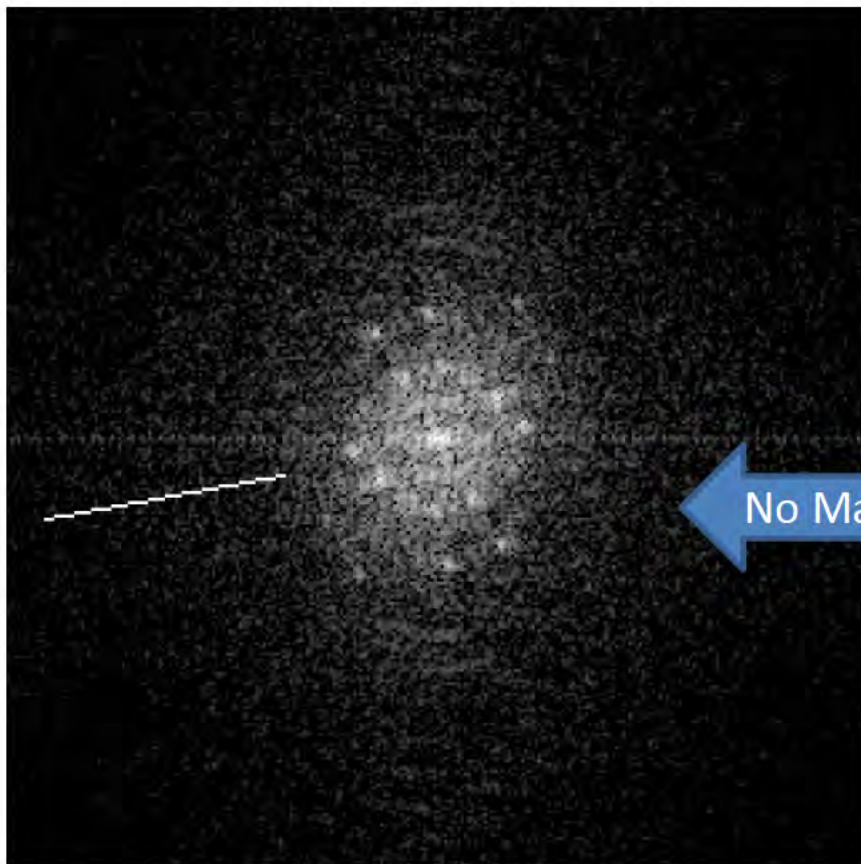


Standard Diffraction Pattern for {110}Fcc



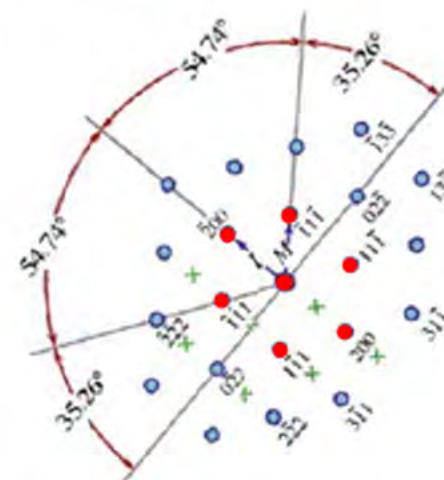
Standard Diffraction Pattern for {112}Fcc

Sample S0GPPC - Framerright3T FFT

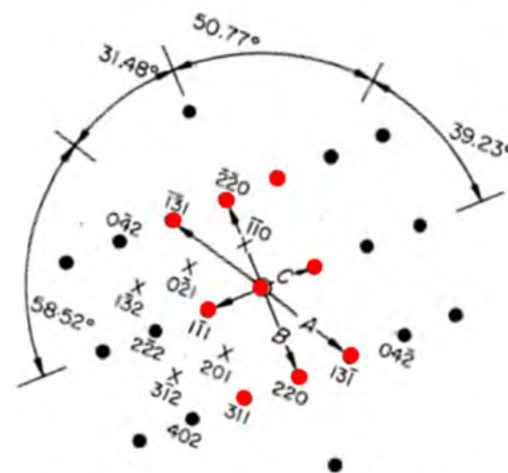


Framerright3T

No Match

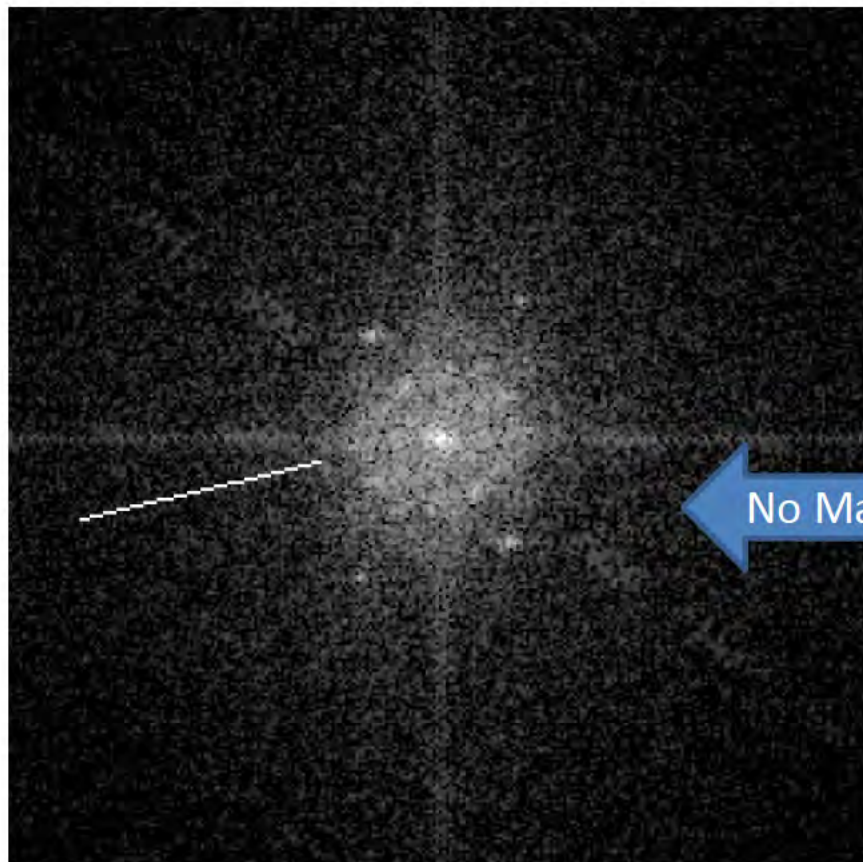


Standard Diffraction Pattern for {110}Fcc



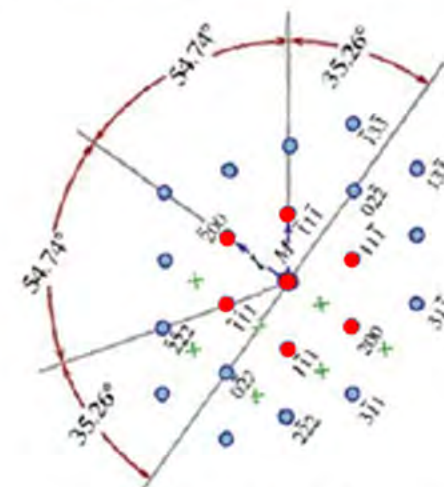
Standard Diffraction Pattern for {112}Fcc

Sample S0GPPC - Framerright4T FFT

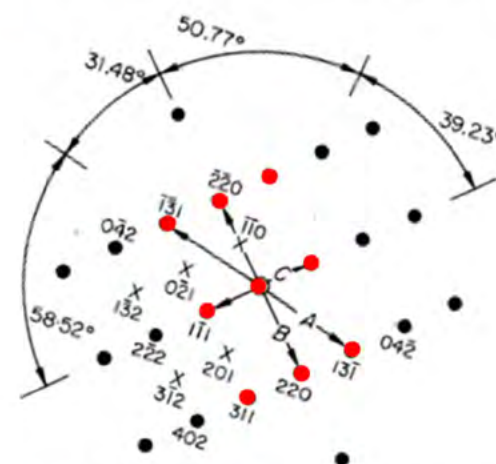


Framerright4T

No Match

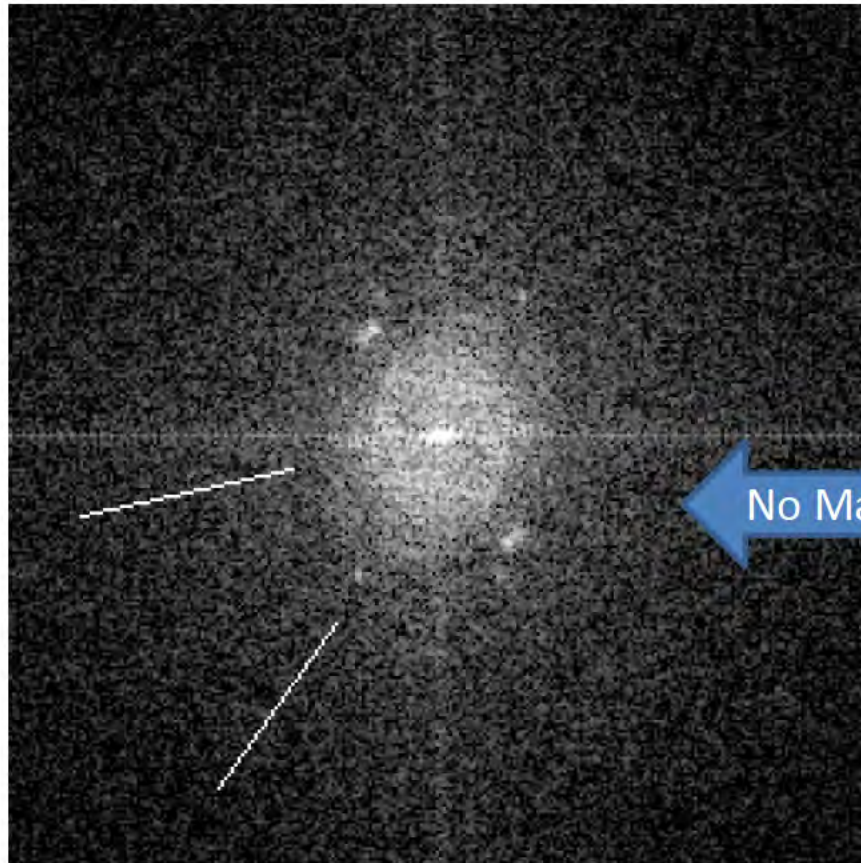


Standard Diffraction Pattern for {110}Fcc



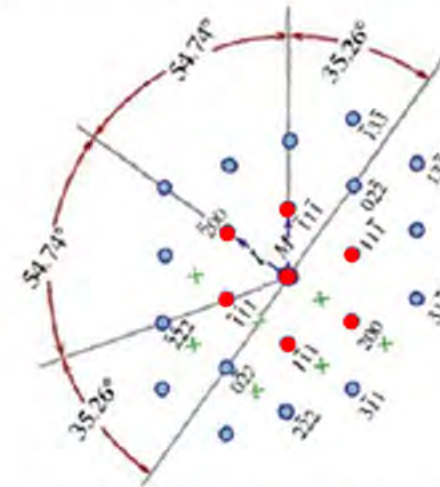
Standard Diffraction Pattern for {112}Fcc

Sample S0GPPC - Framerright5T FFT

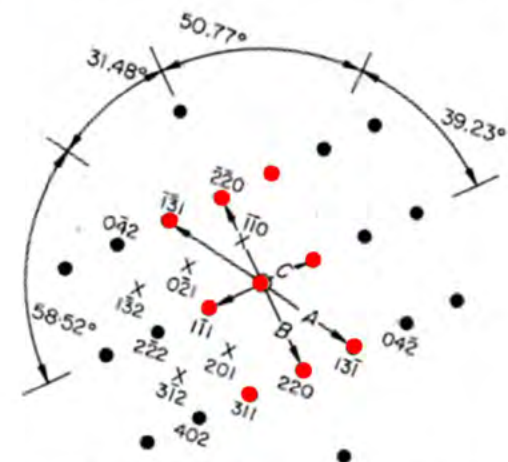


Framerright5T

No Match

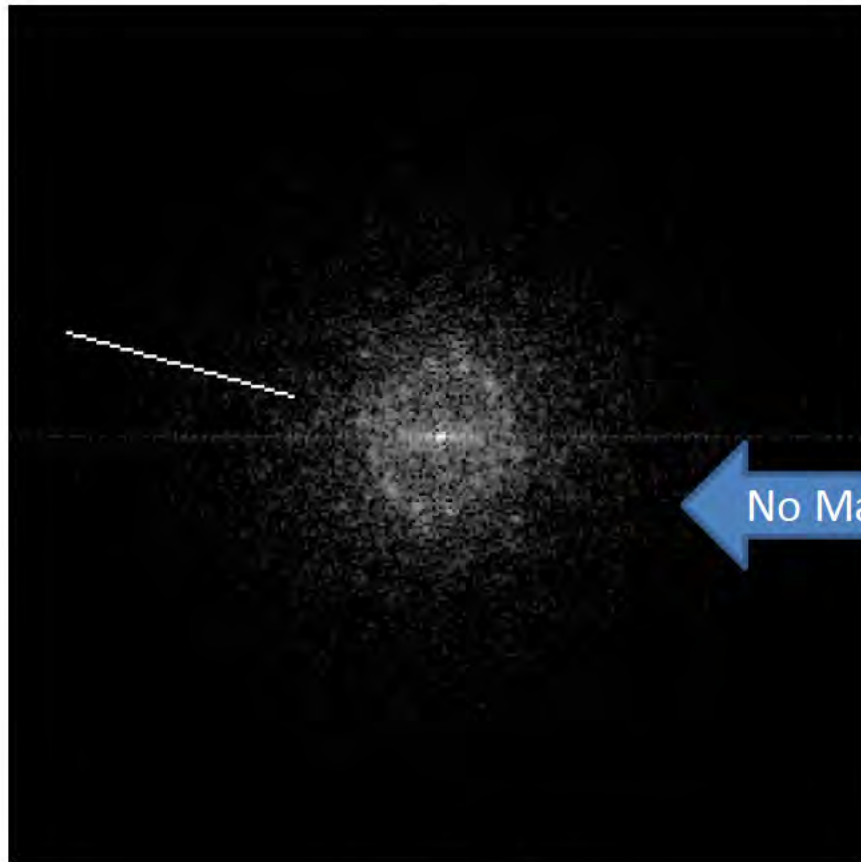


Standard Diffraction Pattern for {110}Fcc



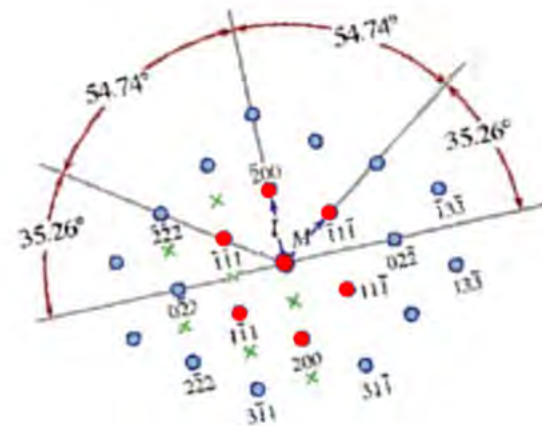
Standard Diffraction Pattern for {112}Fcc

Sample S0GPPC - Frameright6T FFT

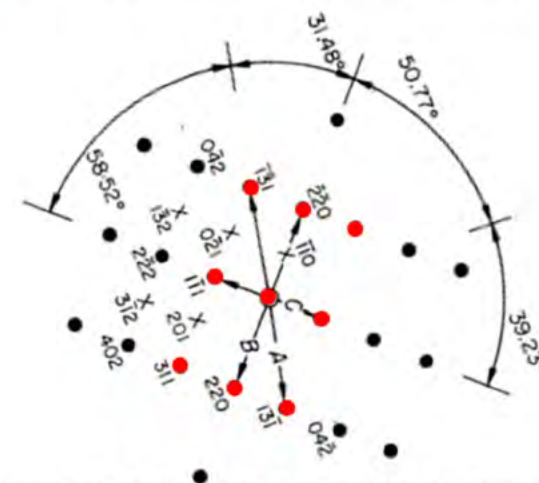


Frameright6T

No Match

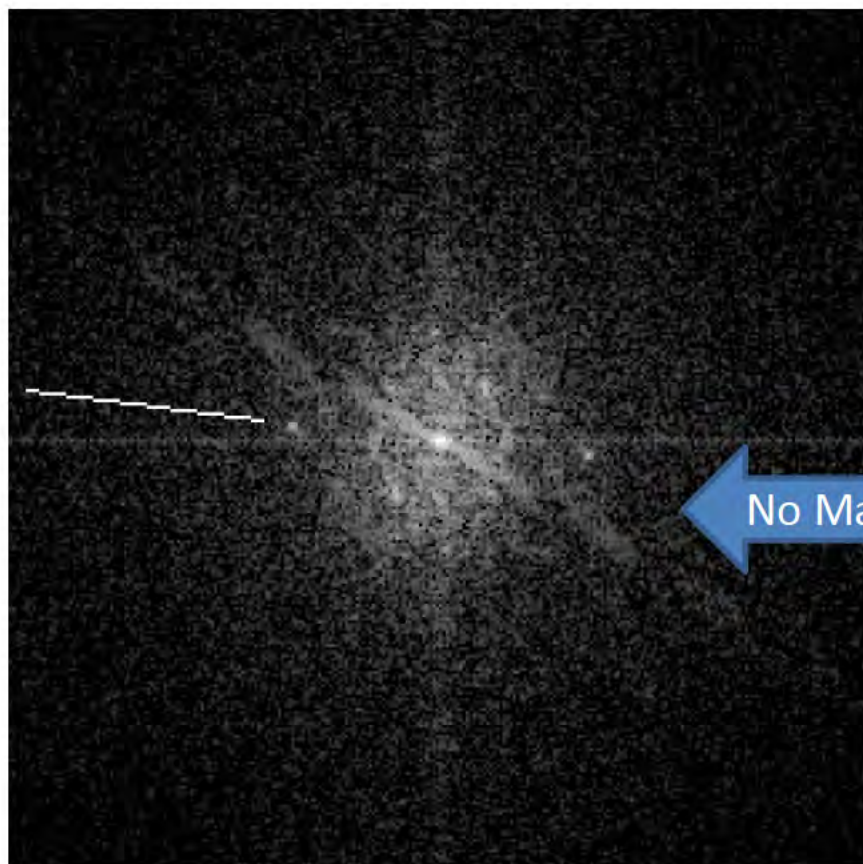


Standard Diffraction Pattern for {110}Fcc



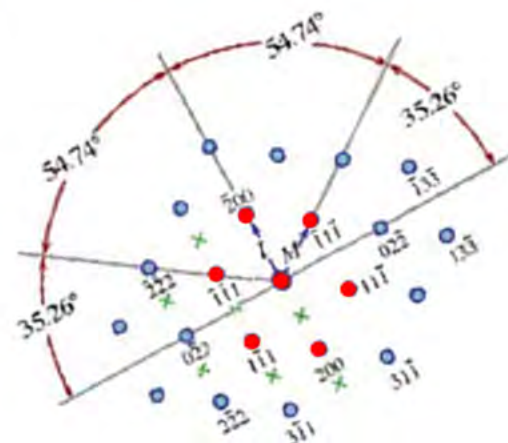
Standard Diffraction Pattern for {112}Fcc

Sample S0GPPC - Framerright7T FFT

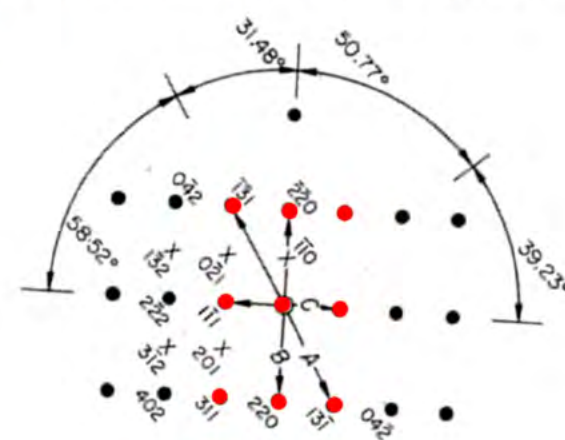


Framerright7T

No Match

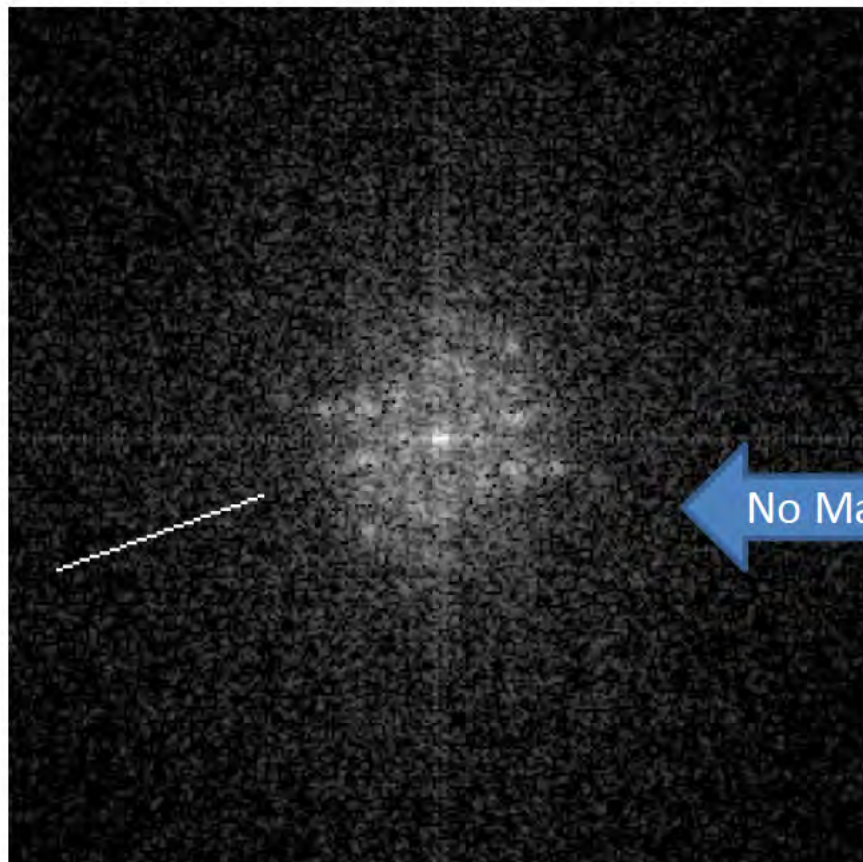


Standard Diffraction Pattern for {110}Fcc



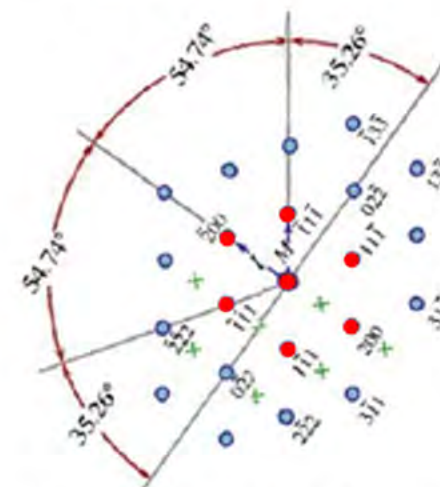
Standard Diffraction Pattern for {112}Fcc

Sample S0GPPC - Framerright21T FFT

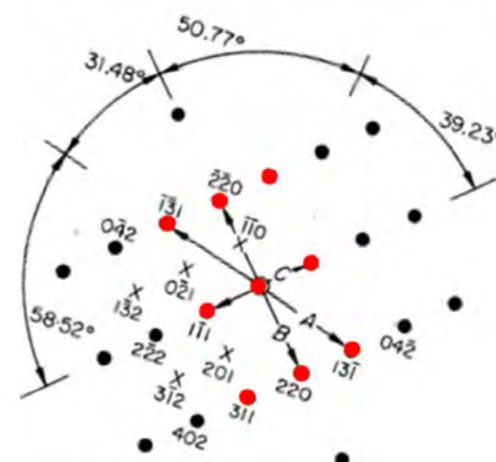


Framerright21T

No Match

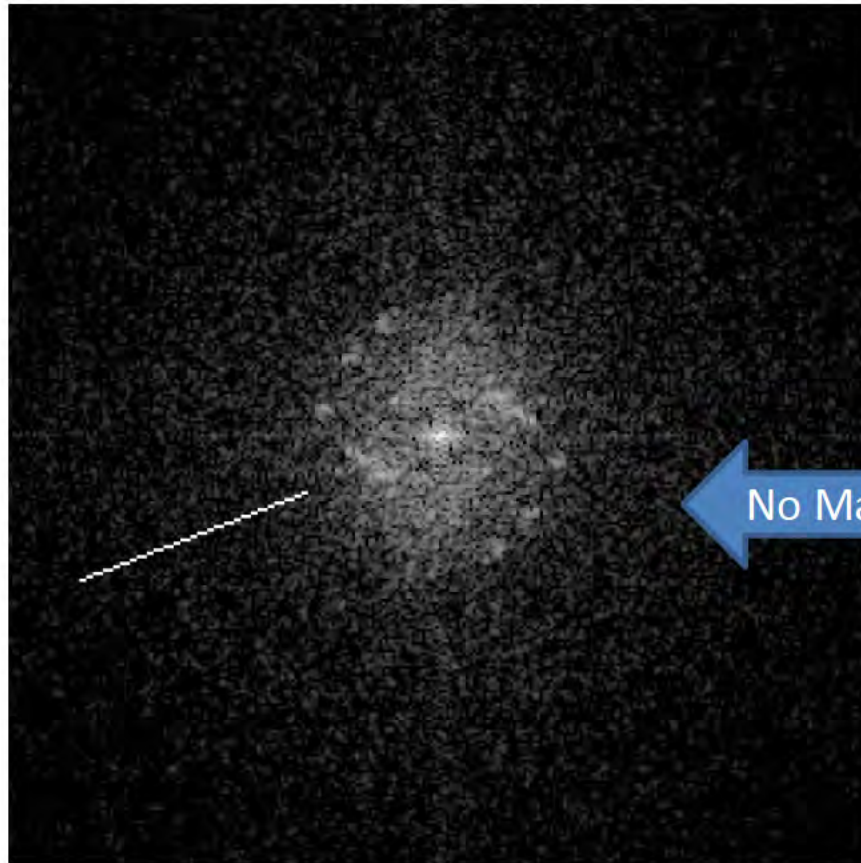


Standard Diffraction Pattern for {110}Fcc



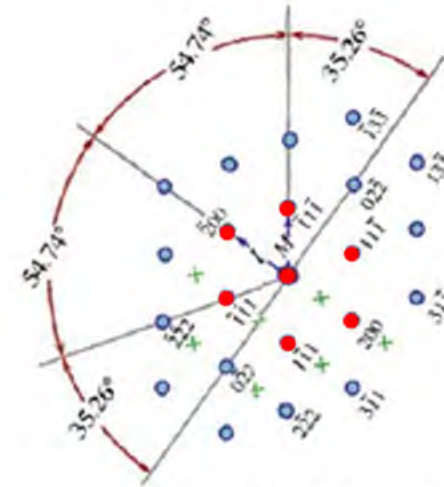
Standard Diffraction Pattern for {112}Fcc

Sample S0GPPC - Framerright22T FFT

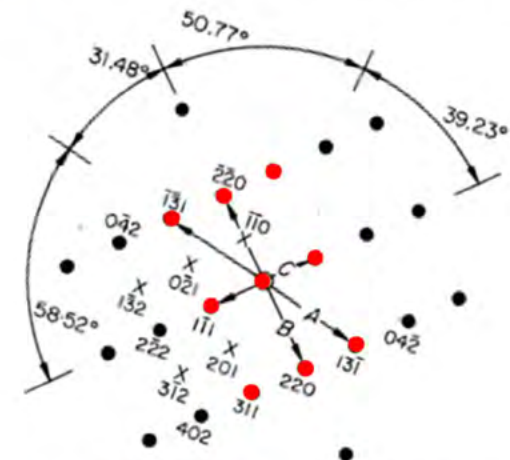


Framerright22T

No Match

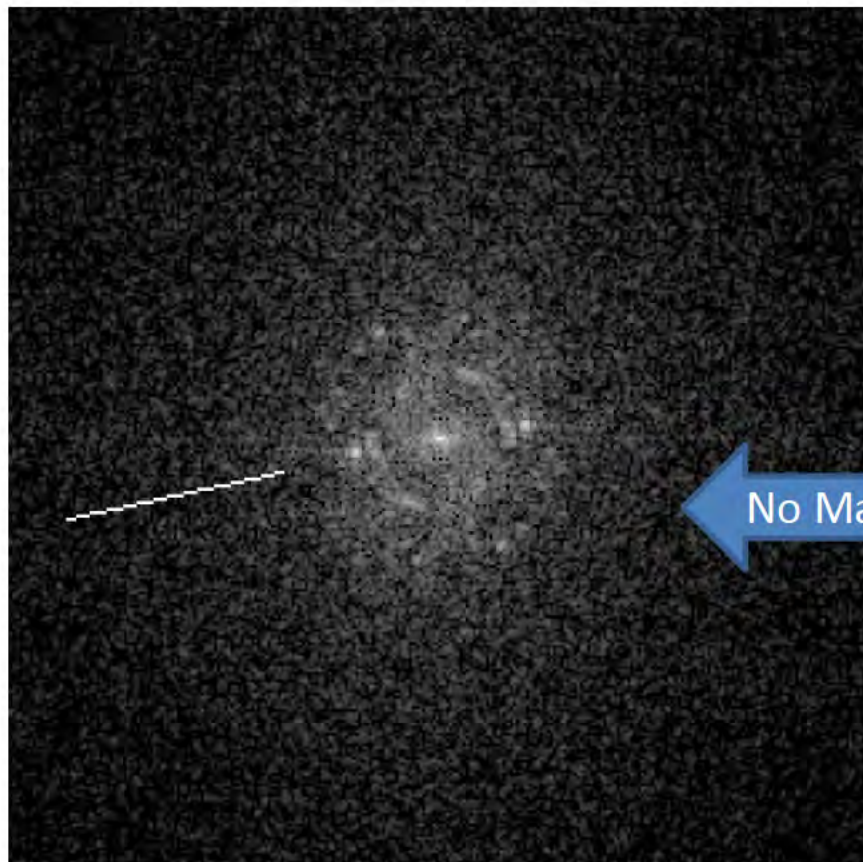


Standard Diffraction Pattern for {110}Fcc



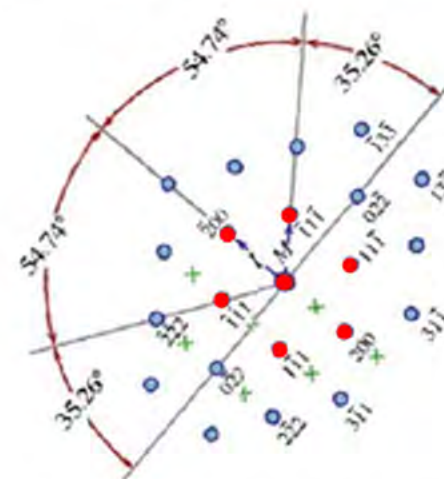
Standard Diffraction Pattern for {112}Fcc

Sample S0GPPC - Framerright23T FFT

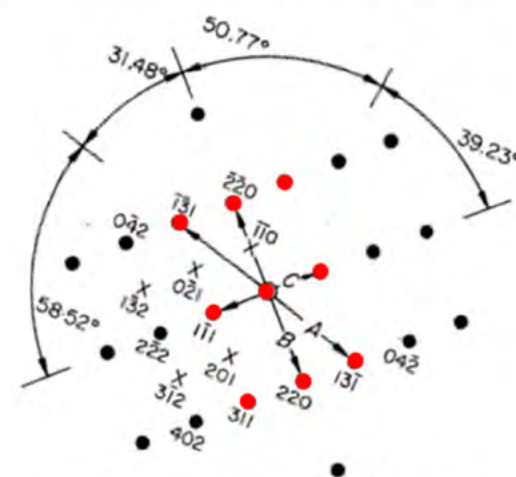


Framerright23T

No Match



Standard Diffraction Pattern for {110}Fcc



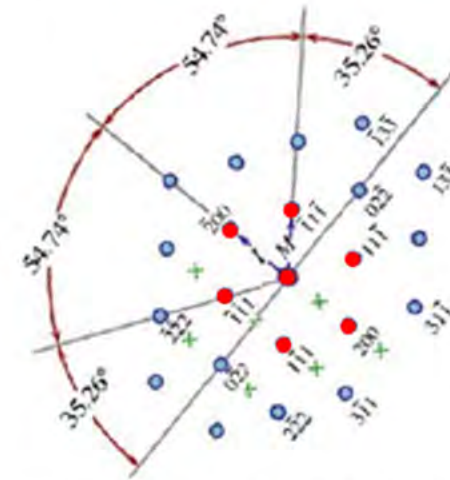
Standard Diffraction Pattern for {112}Fcc

Sample S0GPPC - Framerright24T FFT

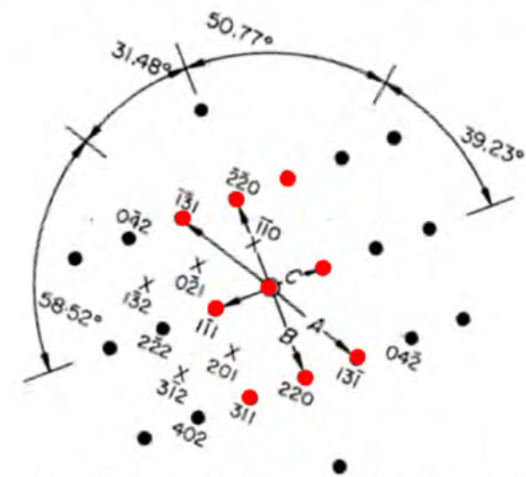


Framerright24T

No Match

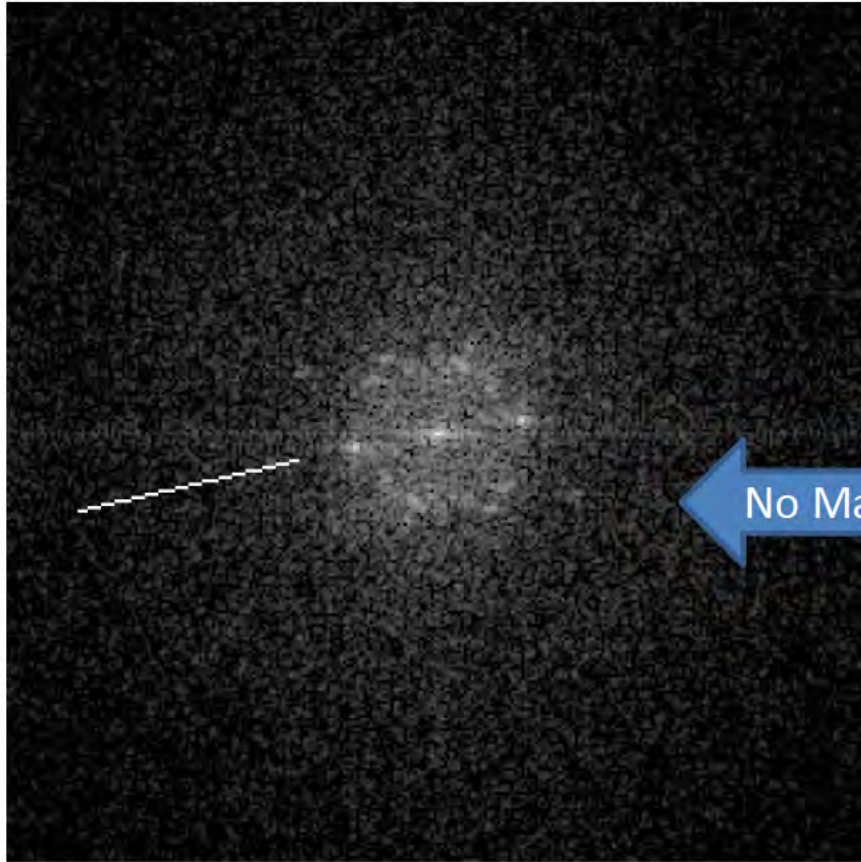


Standard Diffraction Pattern for {110}Fcc



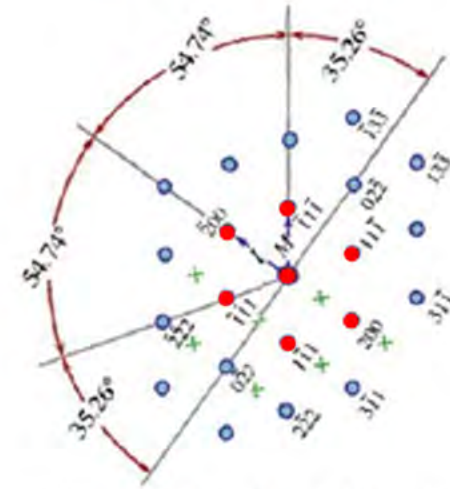
Standard Diffraction Pattern for {112}Fcc

Sample S0GPPC - Frameright25T FFT

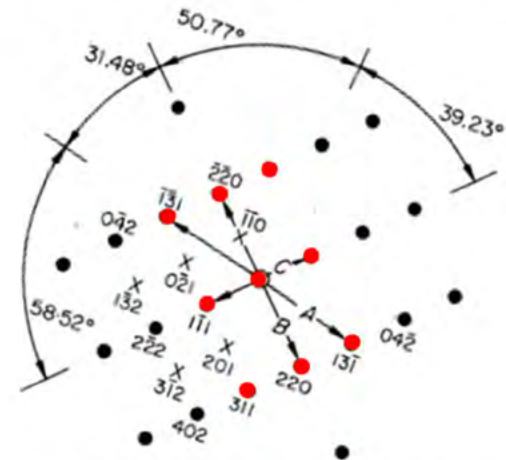


Frameright25T

No Match



Standard Diffraction Pattern for {110}Fcc



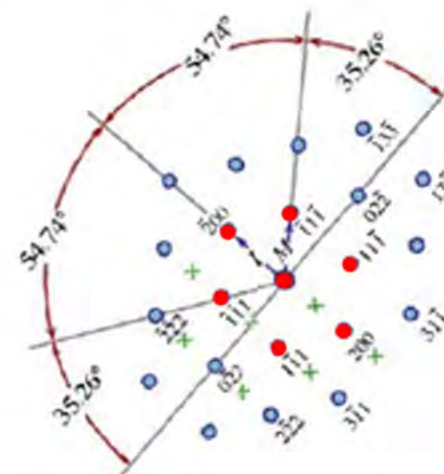
Standard Diffraction Pattern for {112}Fcc

Sample S0GPPC - Framerright26T FFT

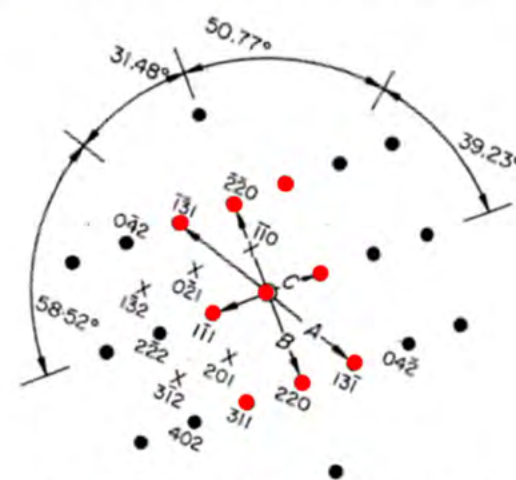


Framerright26T

No Match

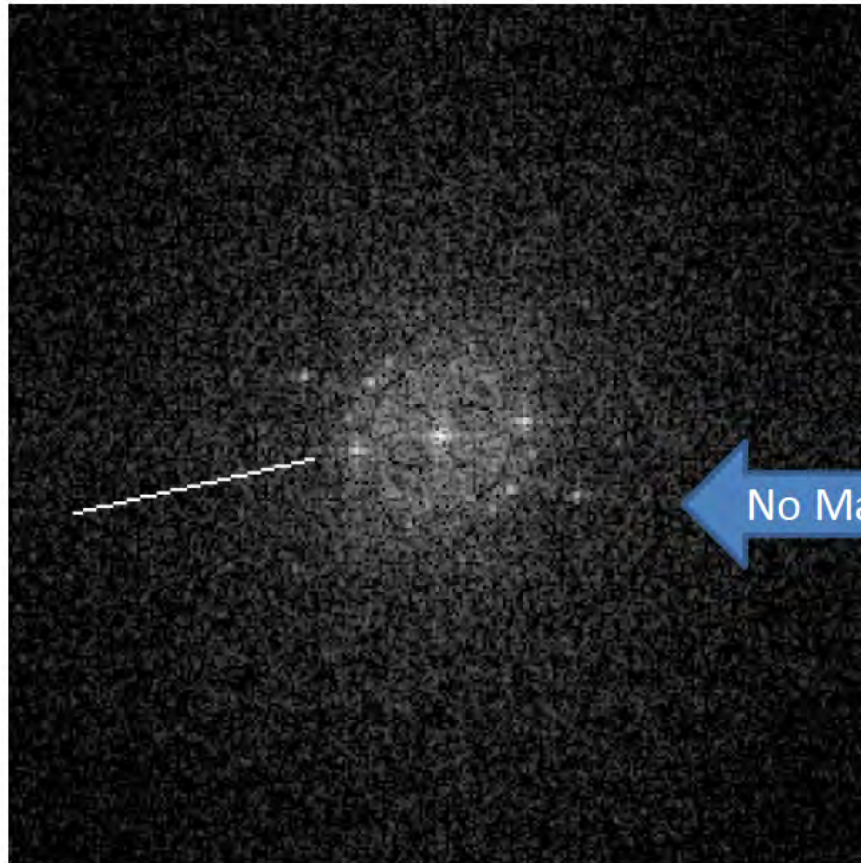


Standard Diffraction Pattern for {110}Fcc



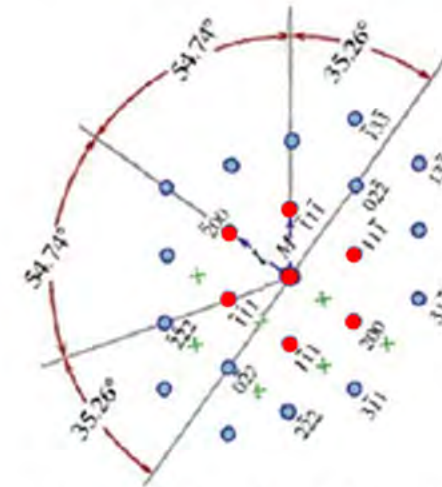
Standard Diffraction Pattern for {112}Fcc

Sample S0GPPC - Framerright27T FFT

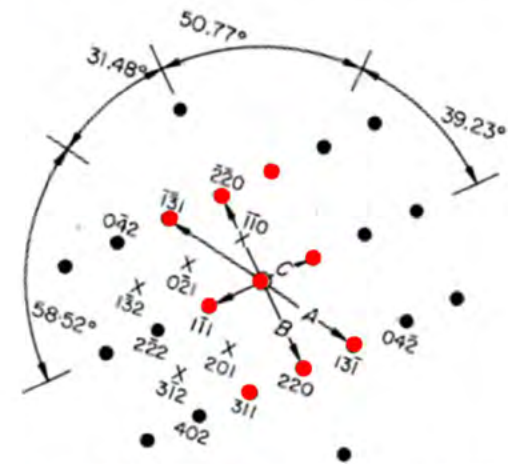


Framerright27T

No Match

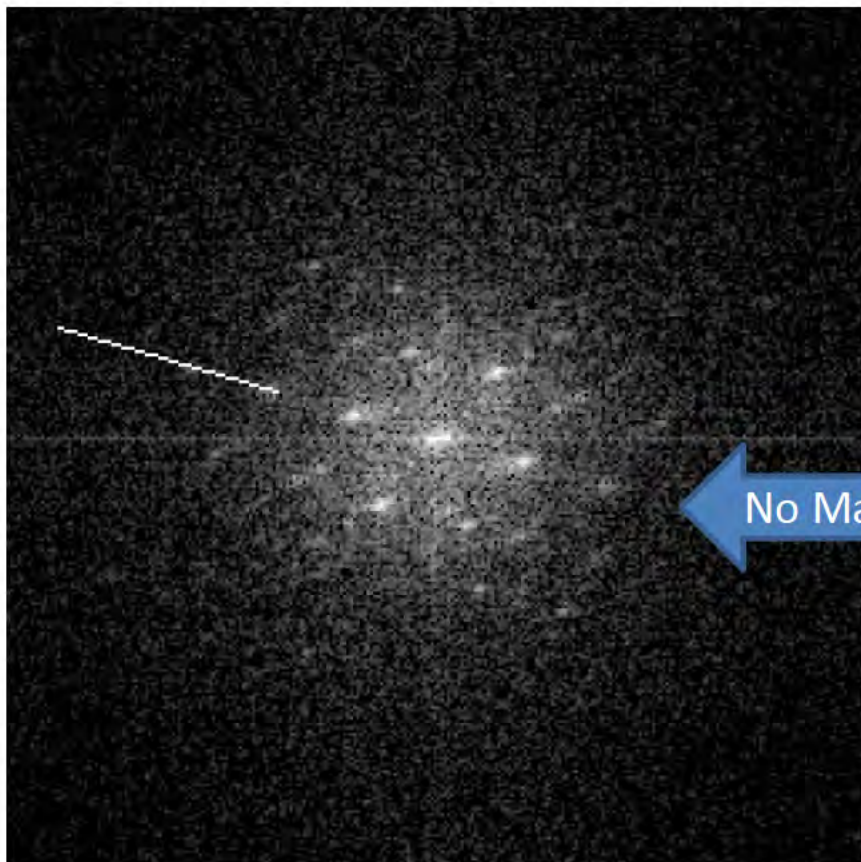


Standard Diffraction Pattern for {110}Fcc



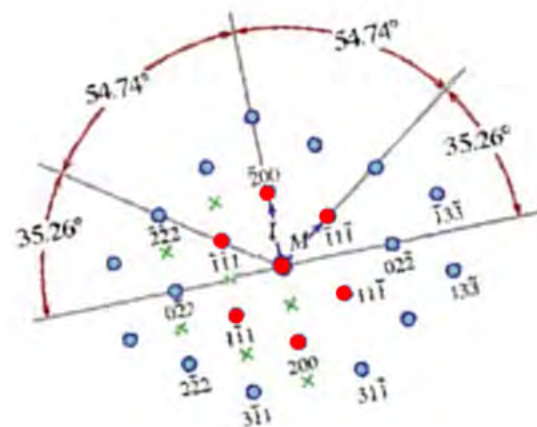
Standard Diffraction Pattern for {112}Fcc

Sample S0GPPC - Framerright31T FFT

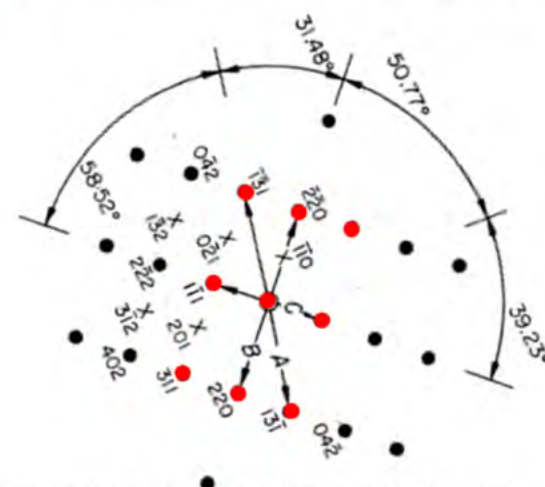


Framerright31T

No Match

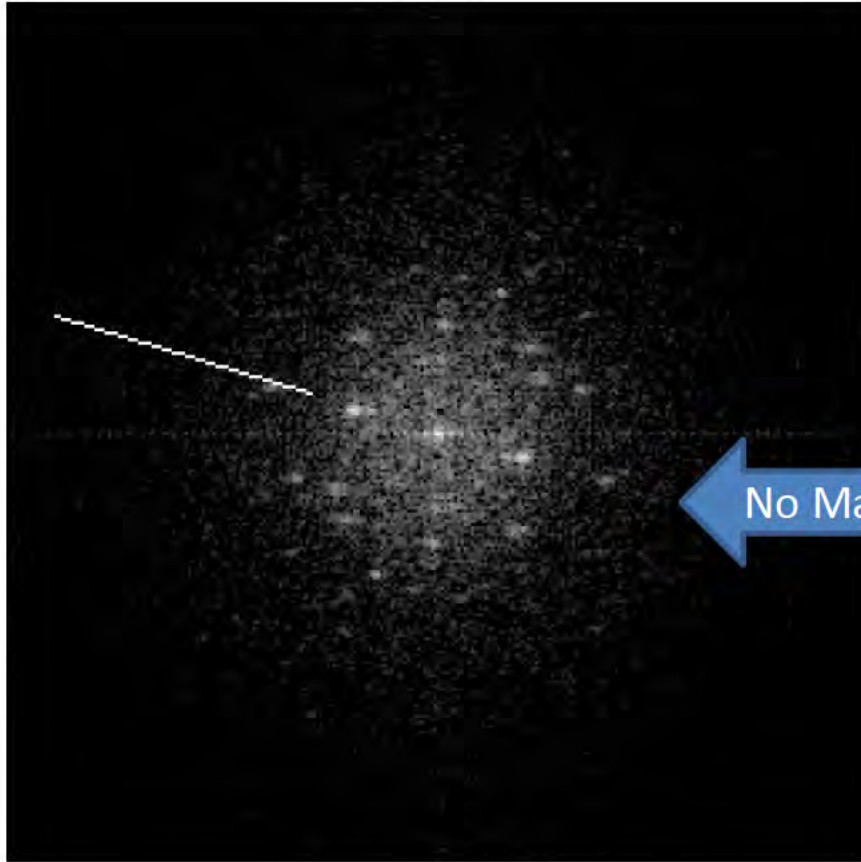


Standard Diffraction Pattern for {110}Fcc

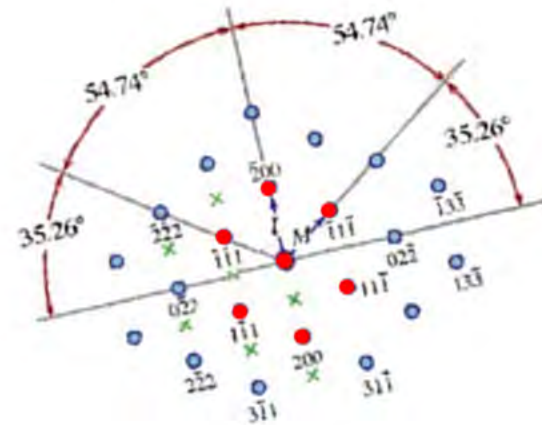


Standard Diffraction Pattern for {112}Fcc

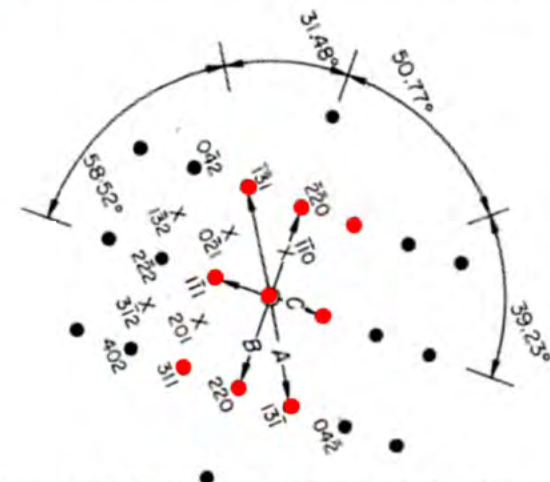
Sample S0GPPC - Frameright32T FFT



Frameright32T

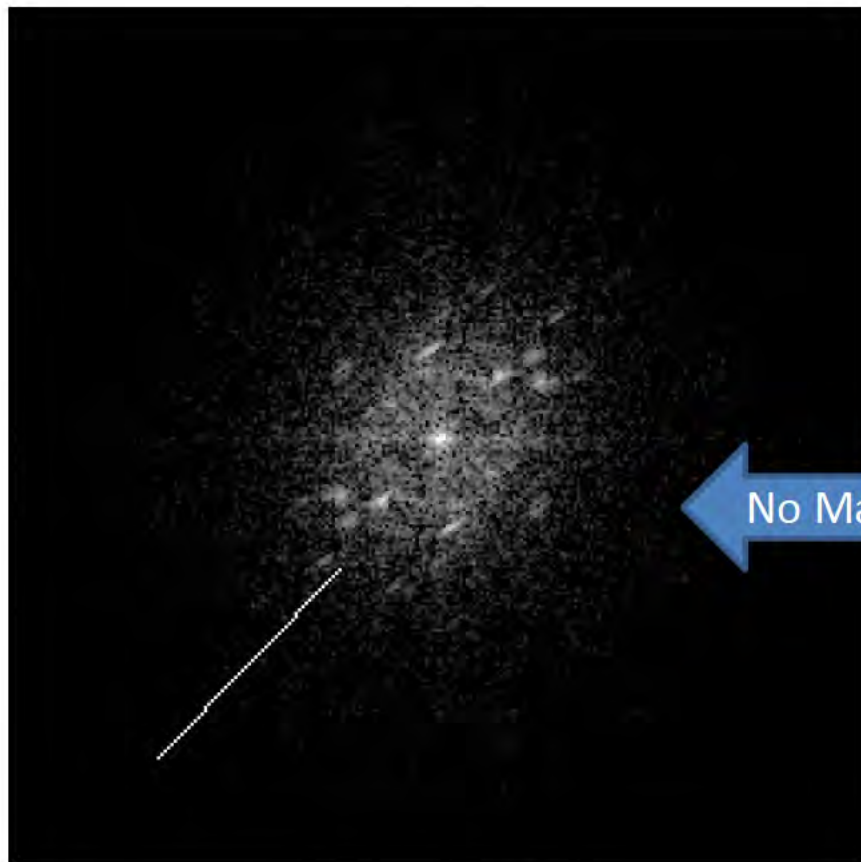


Standard Diffraction Pattern for {110}Fcc



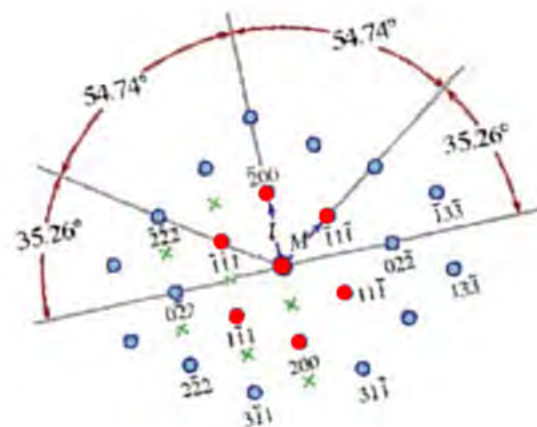
Standard Diffraction Pattern for {112}Fcc

Sample S0GPPC - Framerright33T FFT

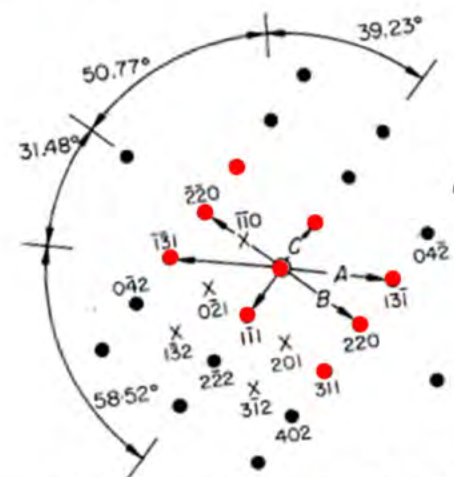


Framerright33T

No Match

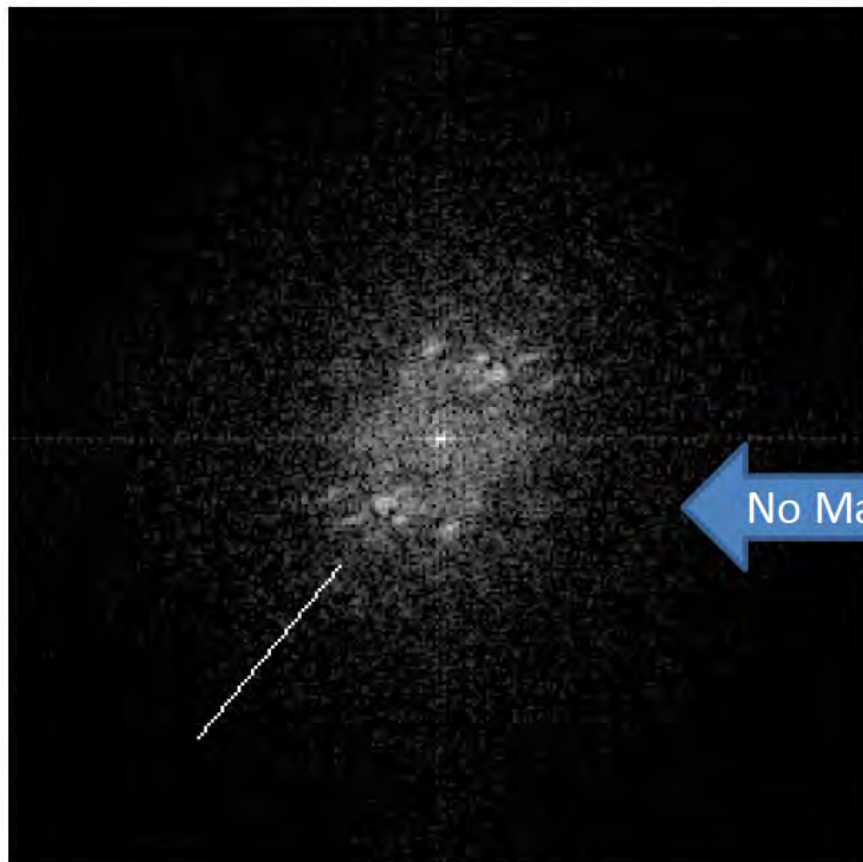


Standard Diffraction Pattern for {110}Fcc



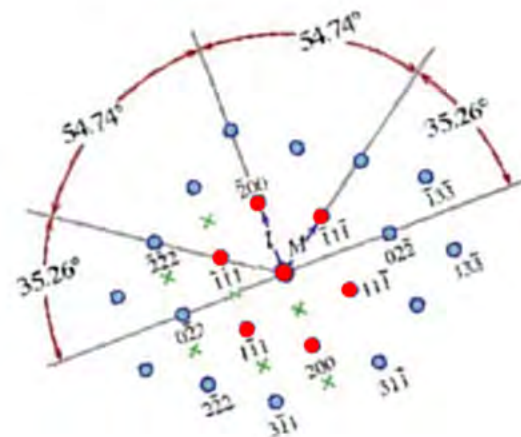
Standard Diffraction Pattern for {112}Fcc

Sample S0GPPC - Framerright34T FFT

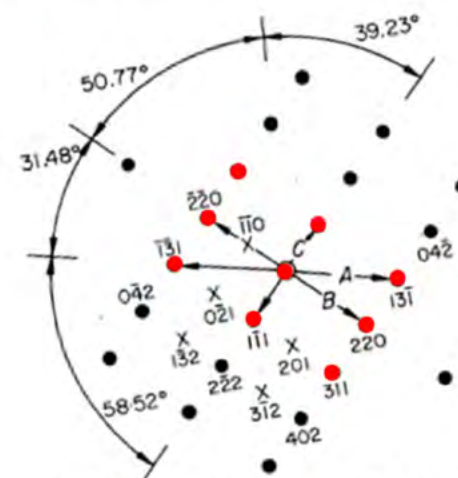


Framerright34T

No Match

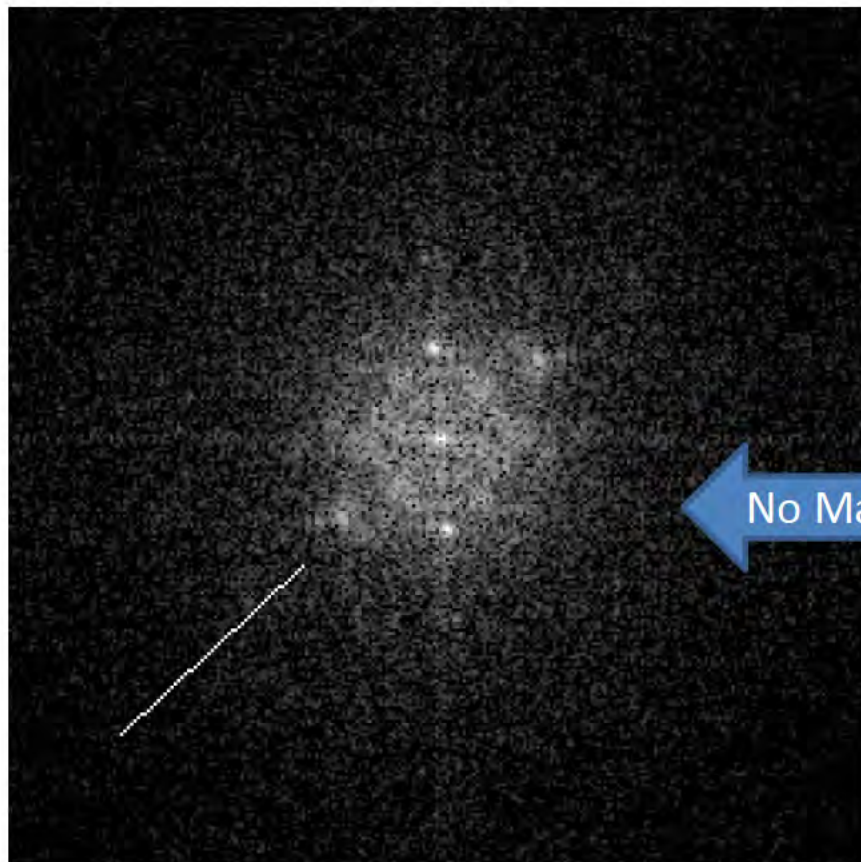


Standard Diffraction Pattern for {110}Fcc



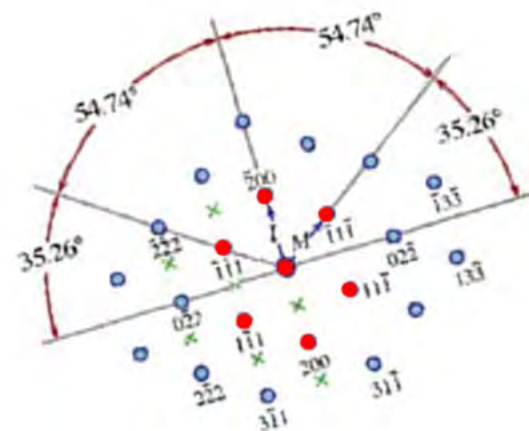
Standard Diffraction Pattern for {112}Fcc

Sample S0GPPC - Framerright35T FFT

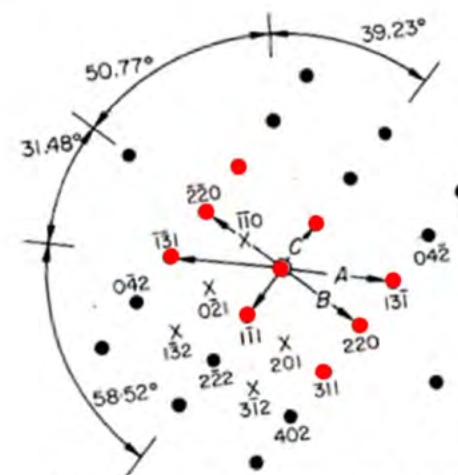


Framerright35T

No Match

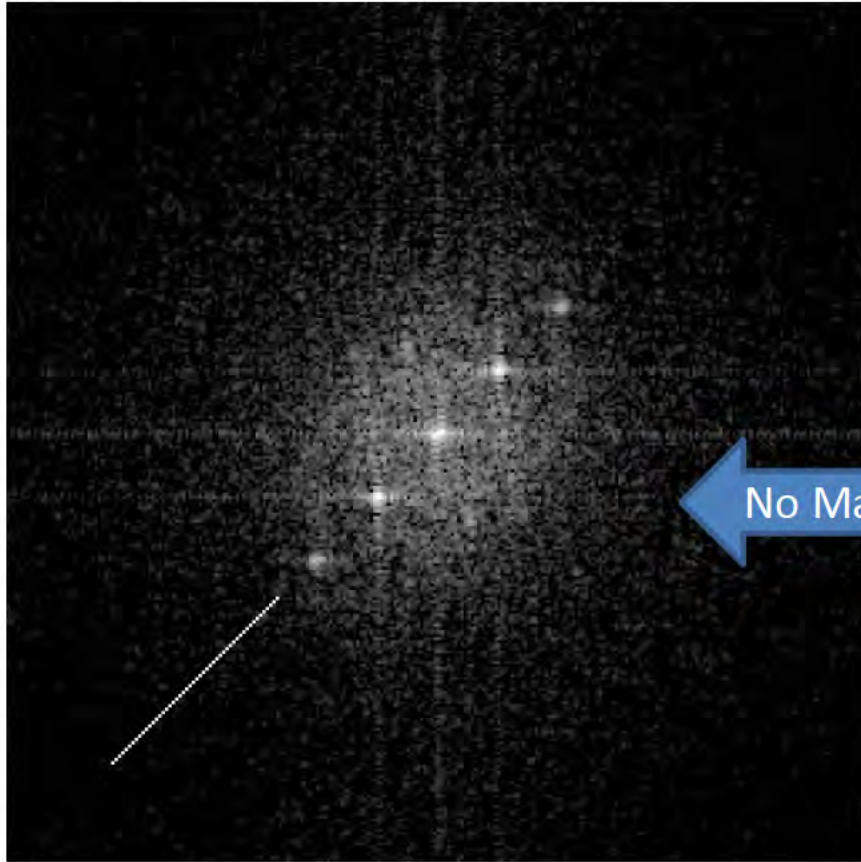


Standard Diffraction Pattern for {110}Fcc



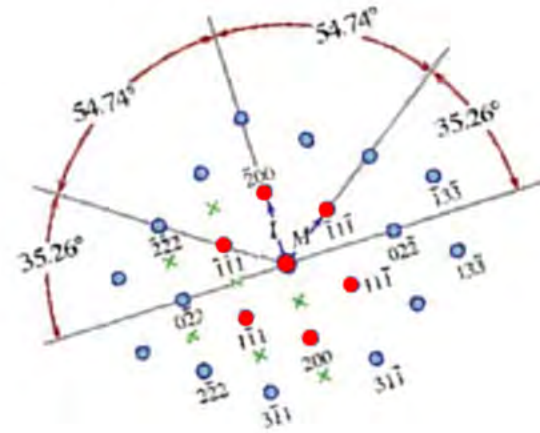
Standard Diffraction Pattern for {112}Fcc

Sample S0GPPC - Frameright41T FFT

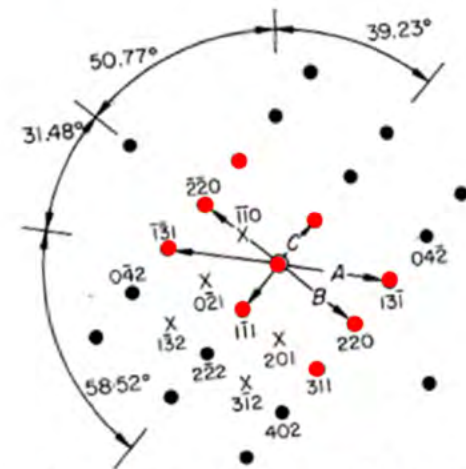


Frameright41T

No Match

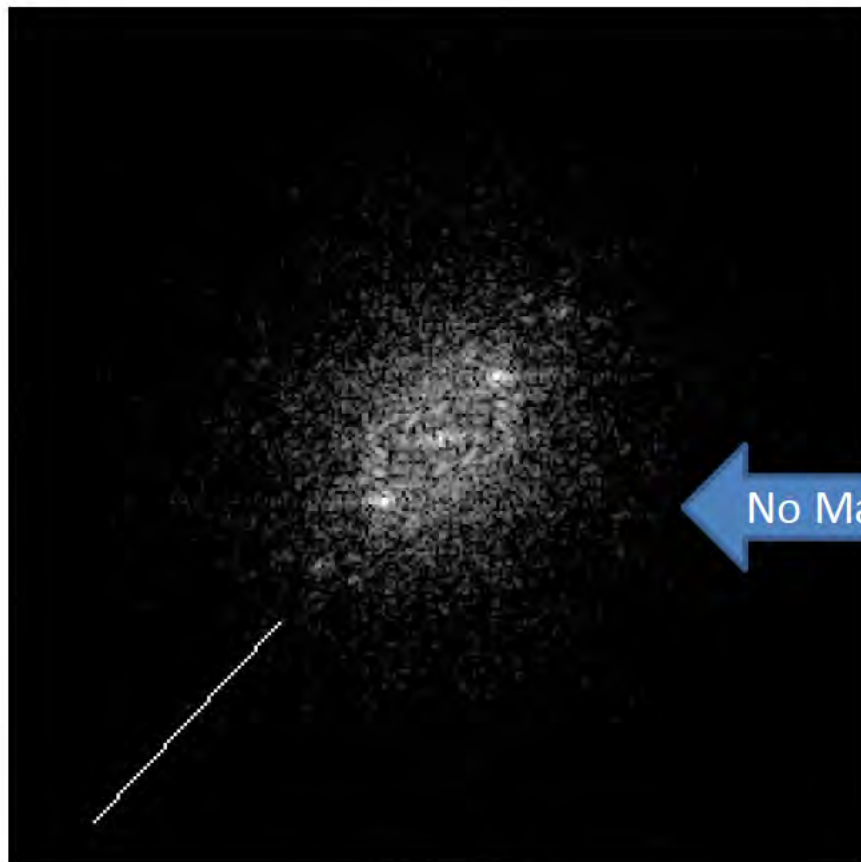


Standard Diffraction Pattern for {110}Fcc



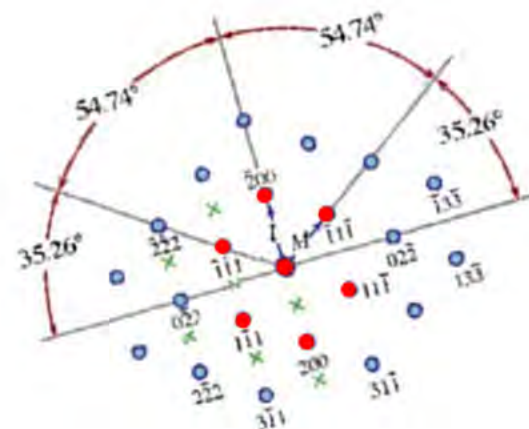
Standard Diffraction Pattern for {112}Fcc

Sample S0GPPC - Frameright42T FFT

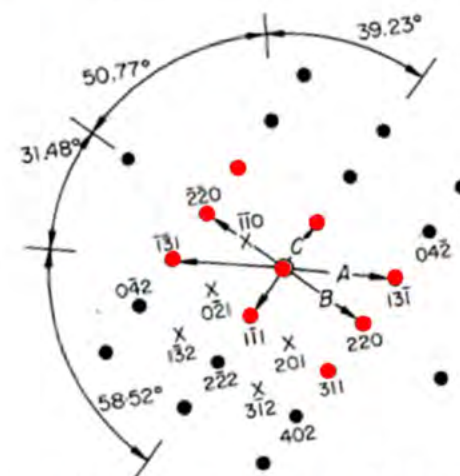


Frameright42T

No Match



Standard Diffraction Pattern for {110}Fcc



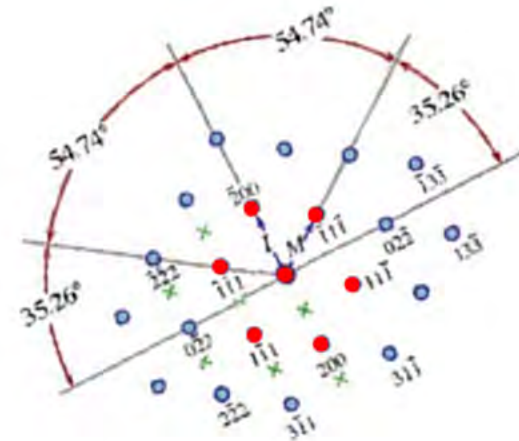
Standard Diffraction Pattern for {112}Fcc

Sample S0GPPC - Framerright43T FFT

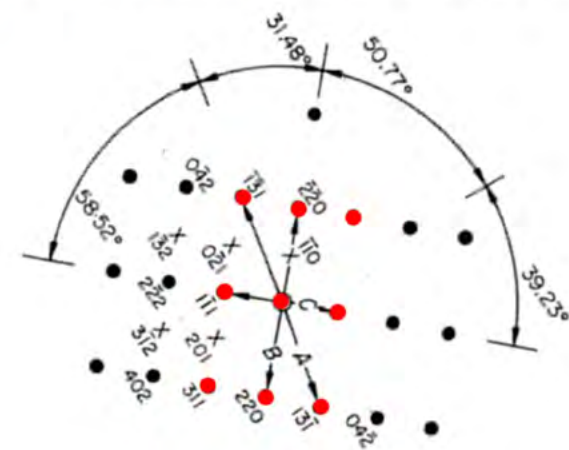


Framerright43T

No Match

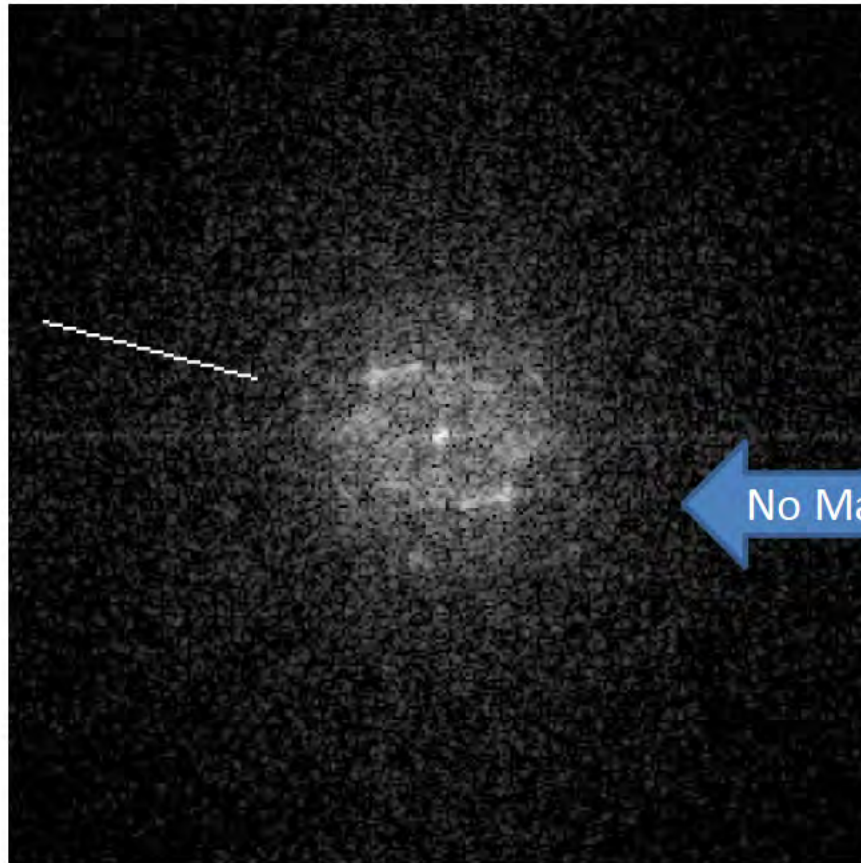


Standard Diffraction Pattern for {110}Fcc



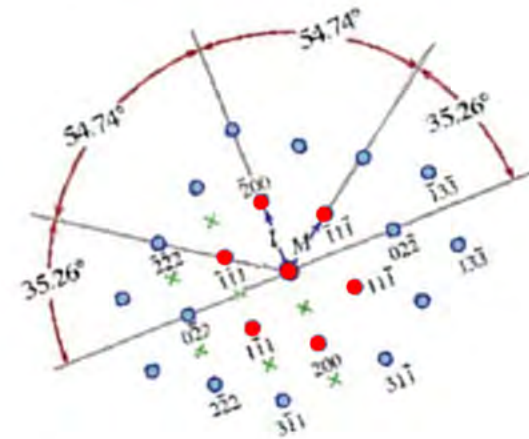
Standard Diffraction Pattern for {112}Fcc

Sample S0GPPC - Framerright44T FFT

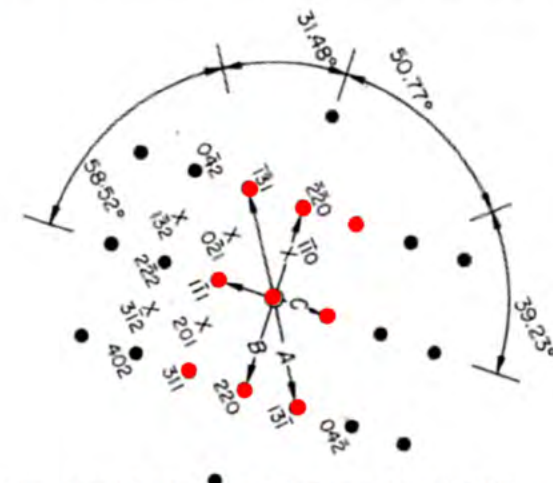


Framerright44T

No Match

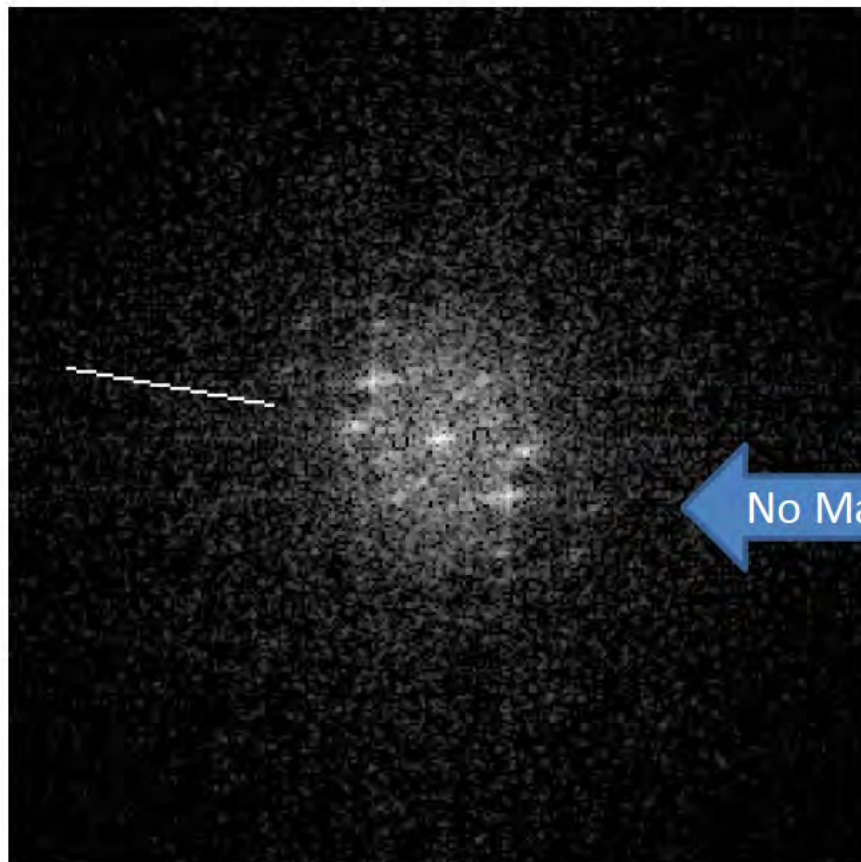


Standard Diffraction Pattern for {110}Fcc



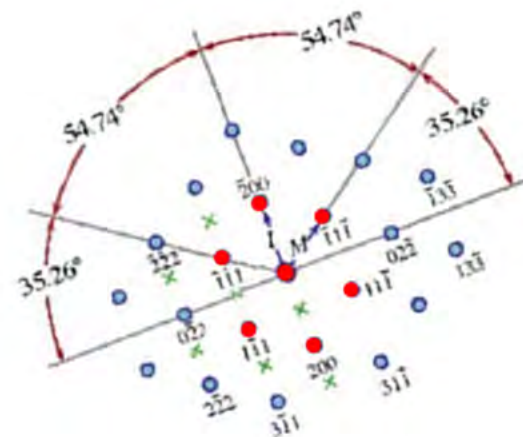
Standard Diffraction Pattern for {112}Fcc

Sample S0GPPC - Framerright45T FFT

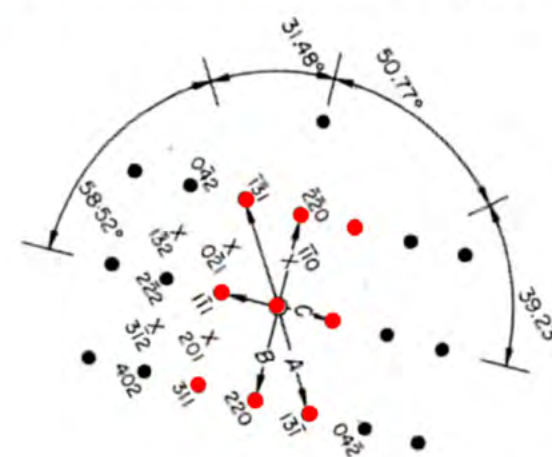


Framerright45T

No Match

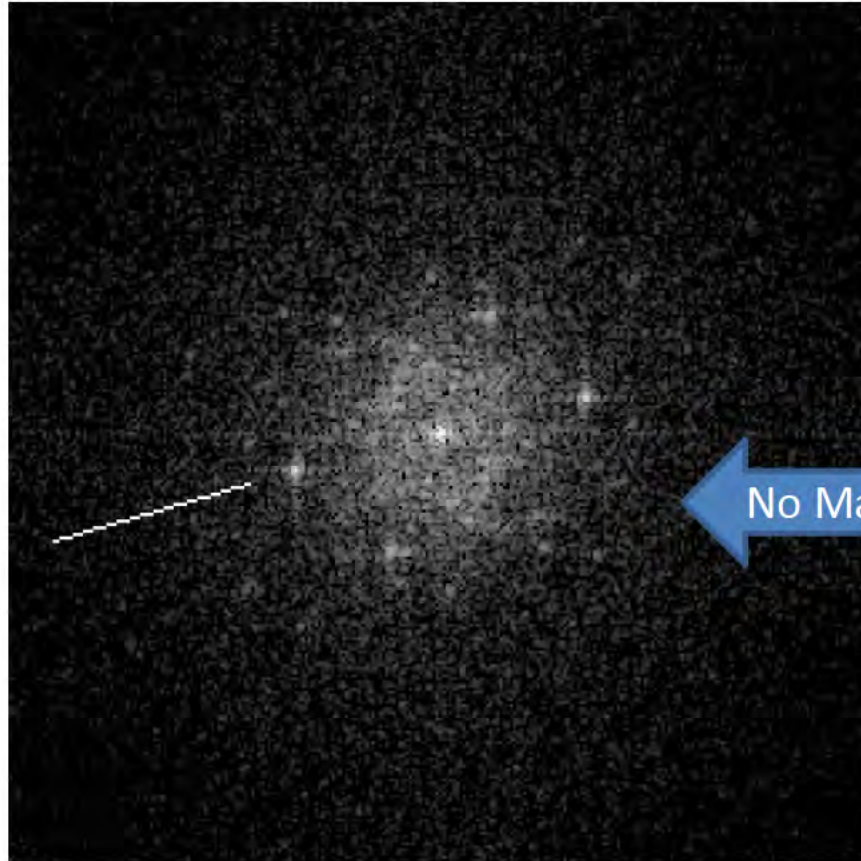


Standard Diffraction Pattern for {110}Fcc



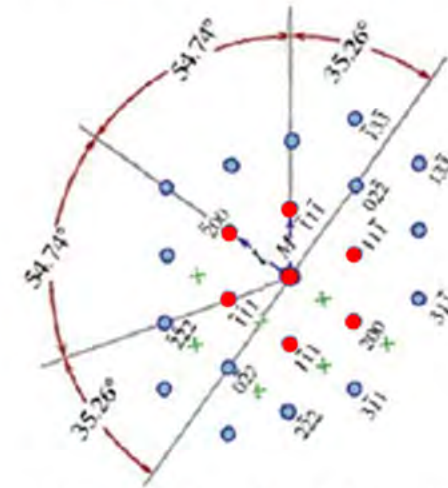
Standard Diffraction Pattern for {112}Fcc

Sample S0GPPC - Framerright51T FFT

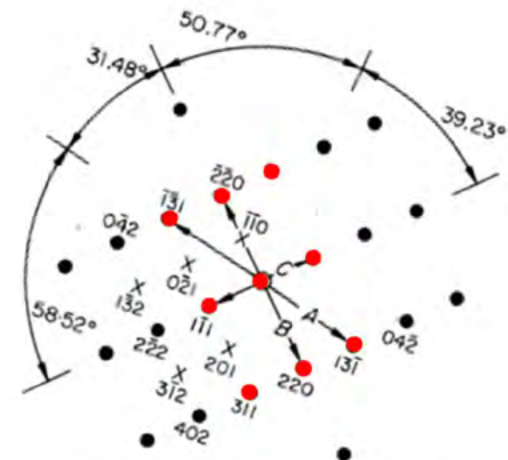


Framerright51T

No Match

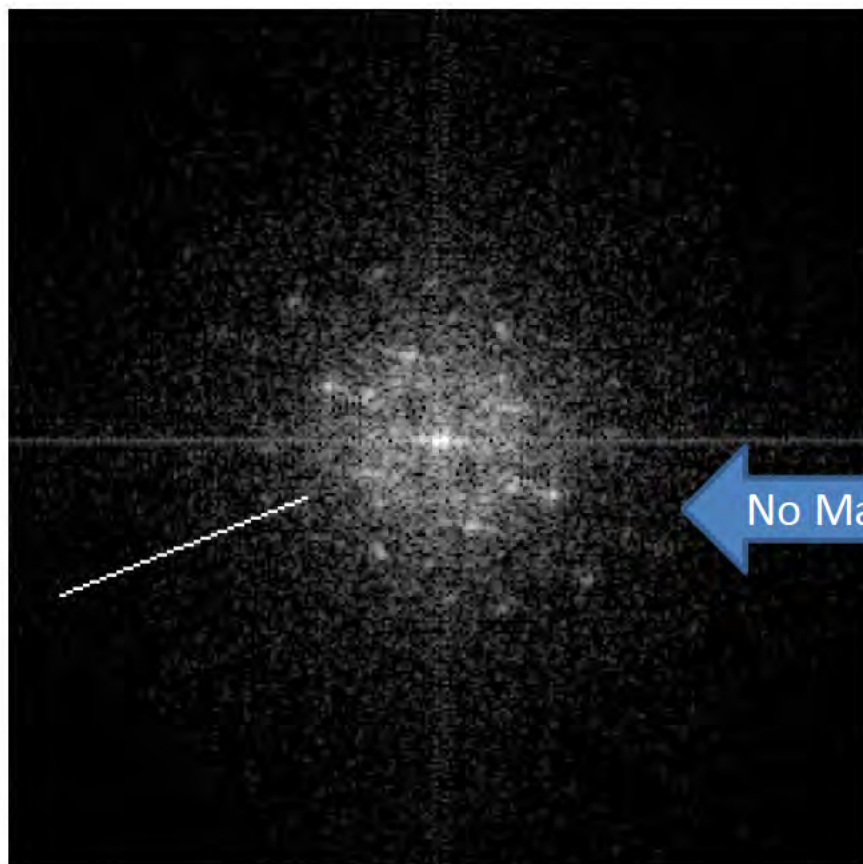


Standard Diffraction Pattern for {110}Fcc



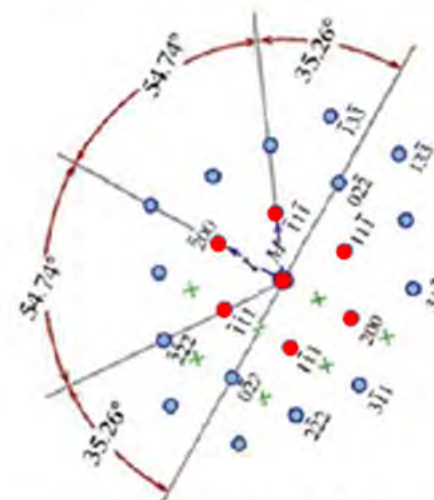
Standard Diffraction Pattern for {112}Fcc

Sample S0GPPC - Framerright52T FFT

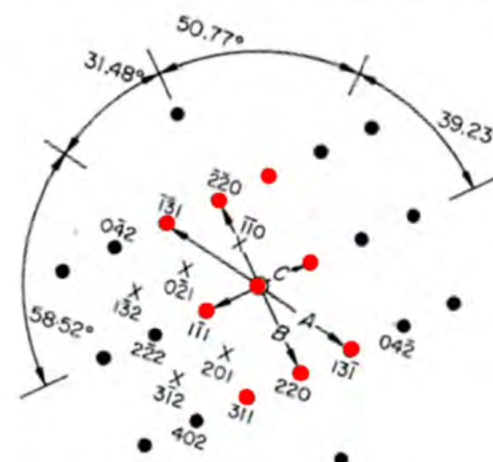


Framerright52T

No Match



Standard Diffraction Pattern for {110}Fcc



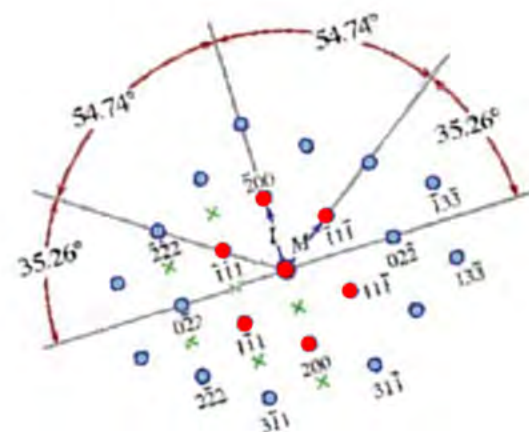
Standard Diffraction Pattern for {112}Fcc

Sample S0GPPC - Framerright53T FFT

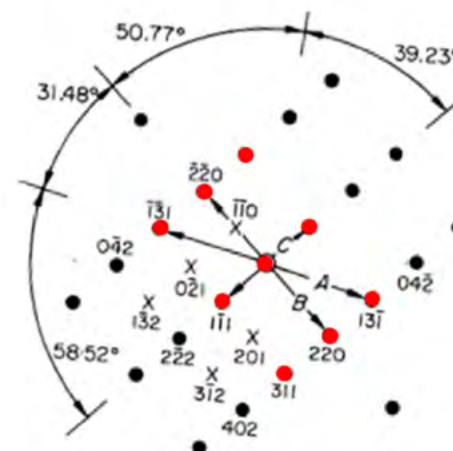


Framerright53T

No Match

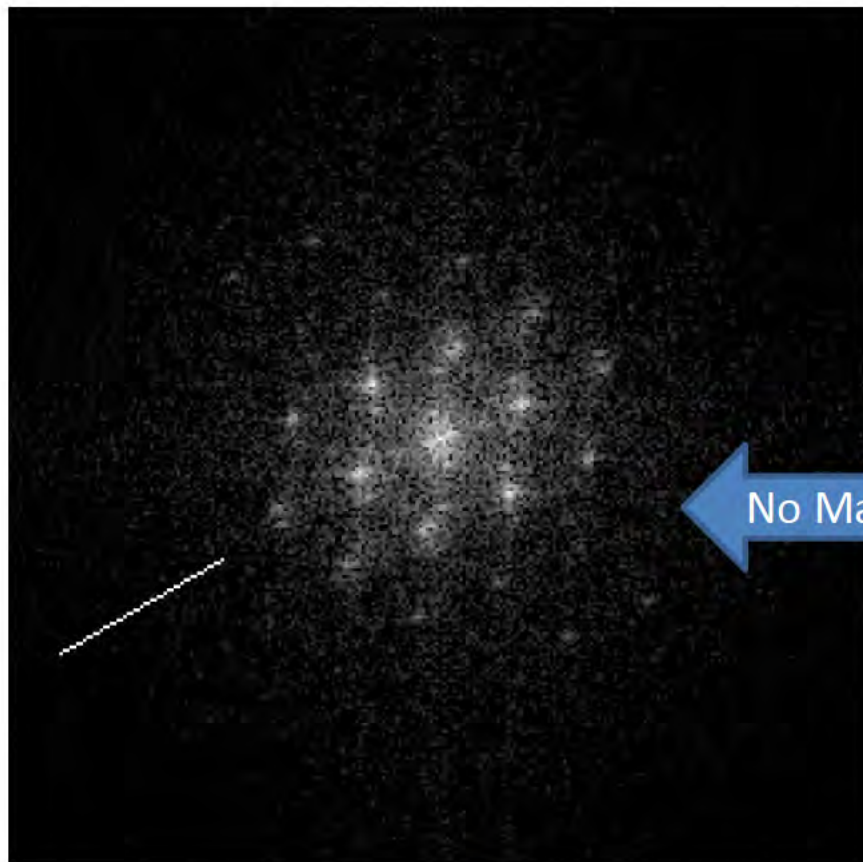


Standard Diffraction Pattern for {110}Fcc



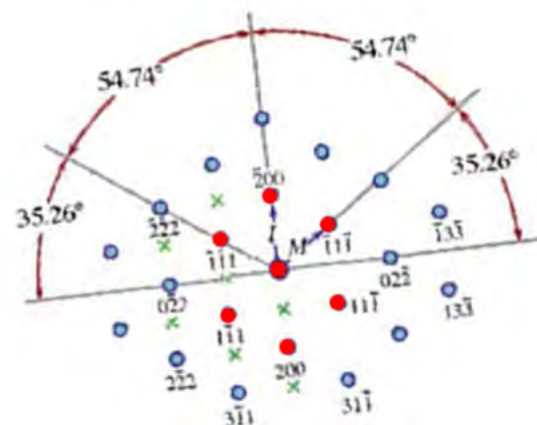
Standard Diffraction Pattern for {112}Fcc

Sample S0GPPC - Middle11T FFT

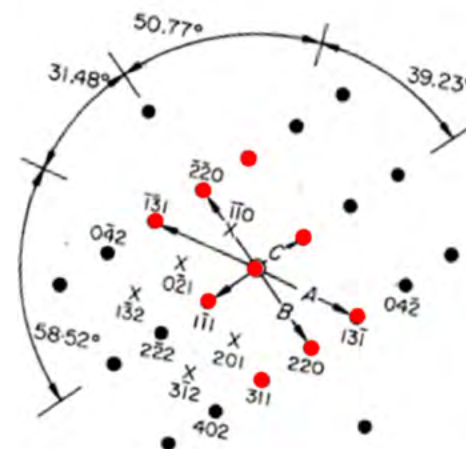


Middle11T

No Match



Standard Diffraction Pattern for {110}Fcc



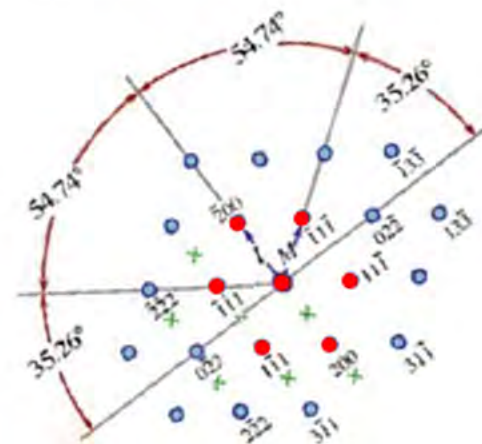
Standard Diffraction Pattern for {112}Fcc

Sample S0GPPC - Middle12T FFT

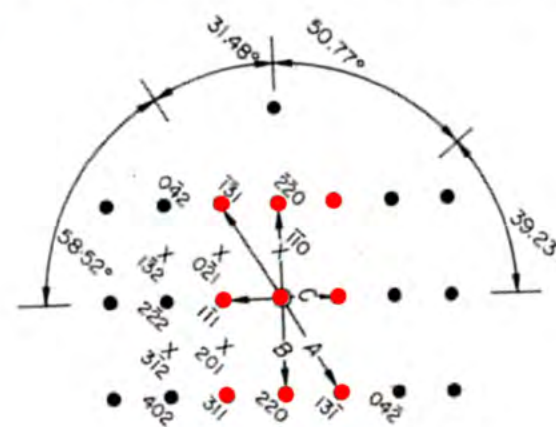


Middle12T

No Match

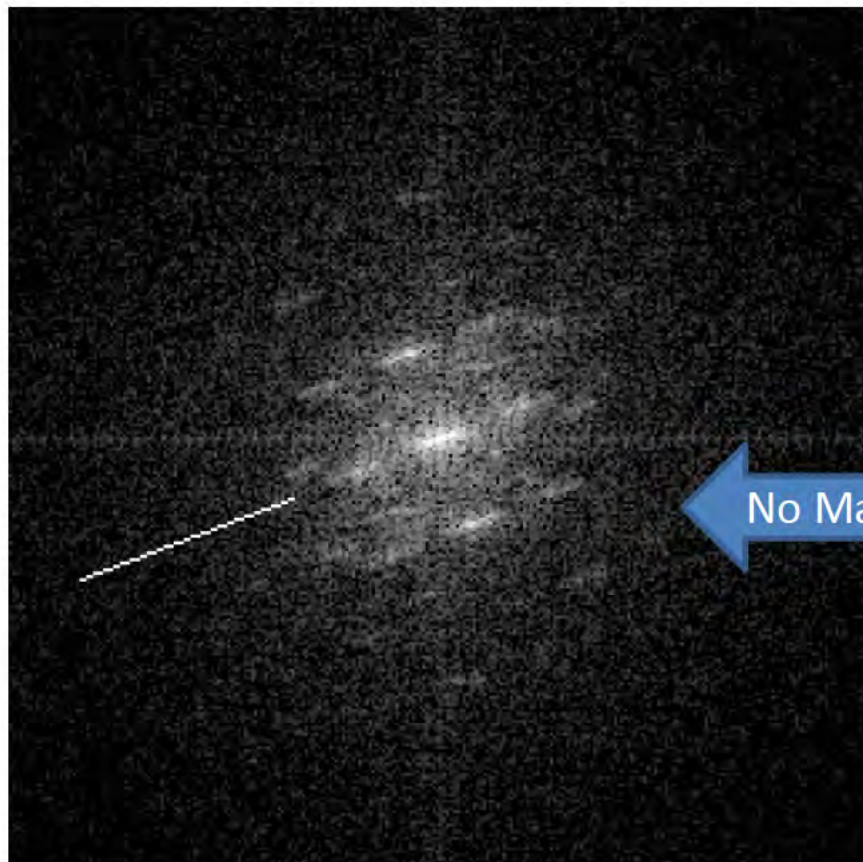


Standard Diffraction Pattern for {110}Fcc



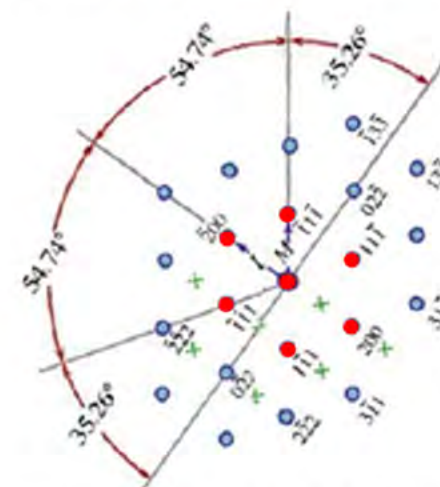
Standard Diffraction Pattern for {112}Fcc

Sample S0GPPC - Middle13T FFT

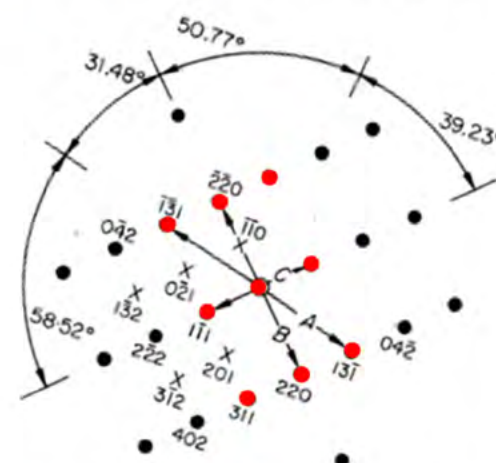


Middle13T

No Match

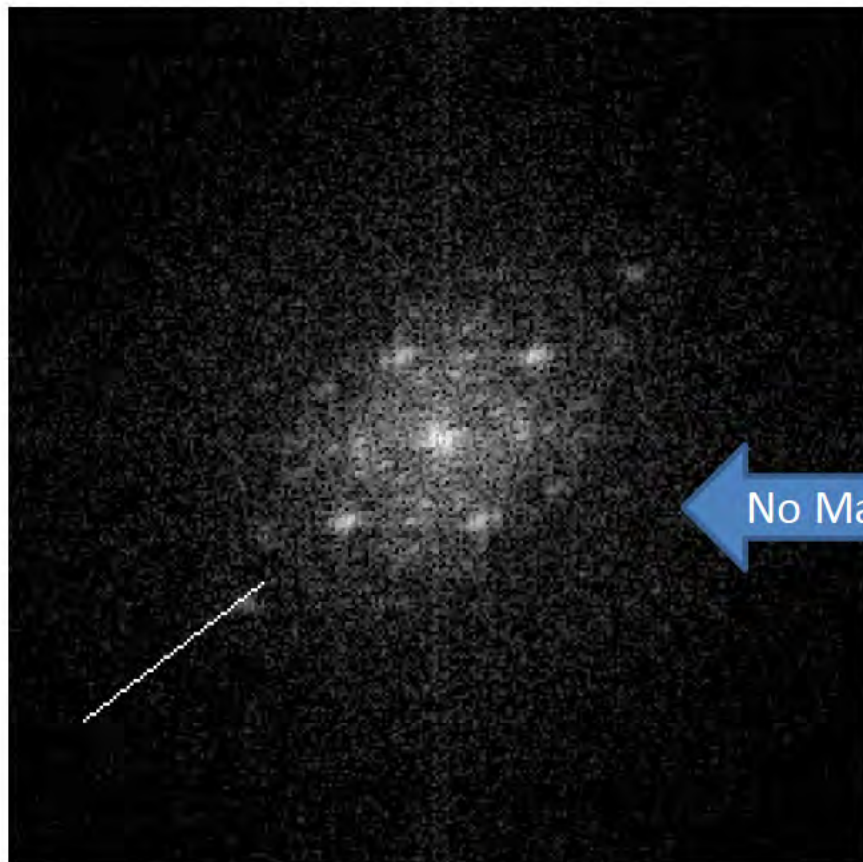


Standard Diffraction Pattern for {110}Fcc



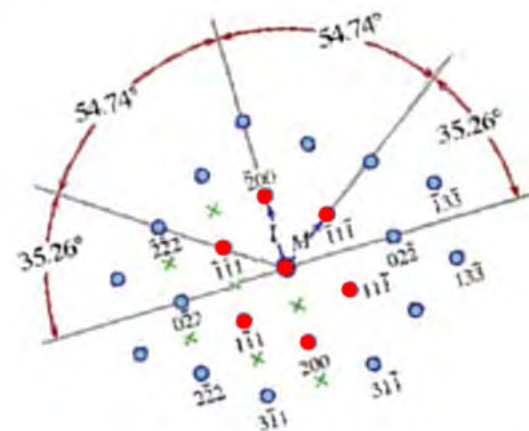
Standard Diffraction Pattern for {112}Fcc

Sample S0GPPC - Middle14T FFT

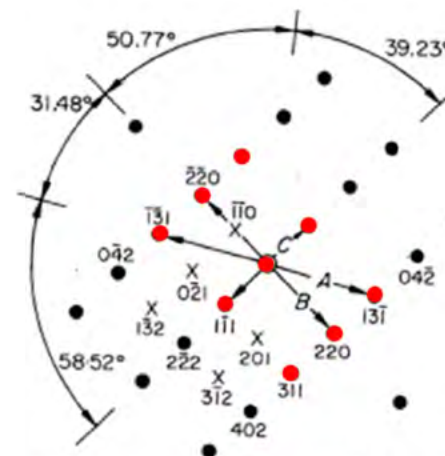


Middle14T

No Match

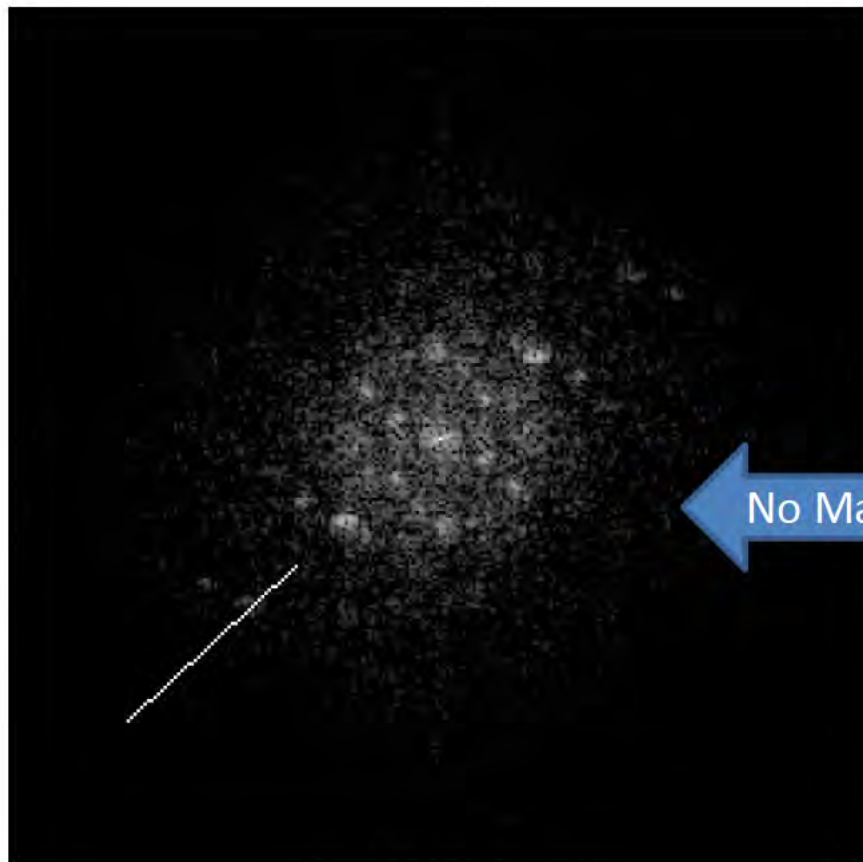


Standard Diffraction Pattern for {110}Fcc



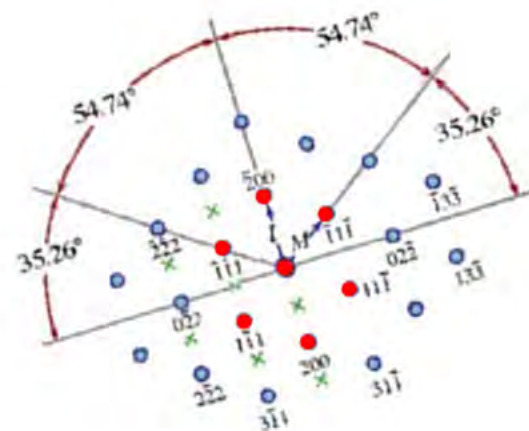
Standard Diffraction Pattern for {112}Fcc

Sample S0GPPC - Middle21T FFT

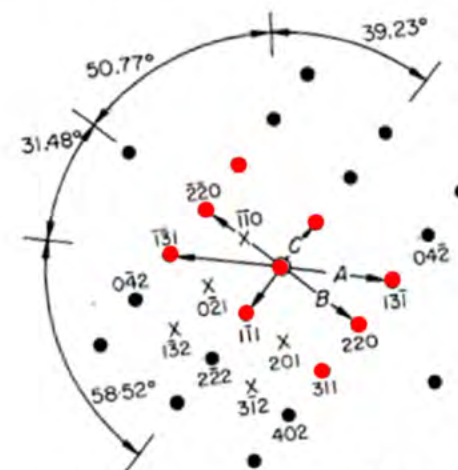


Middle21T

No Match

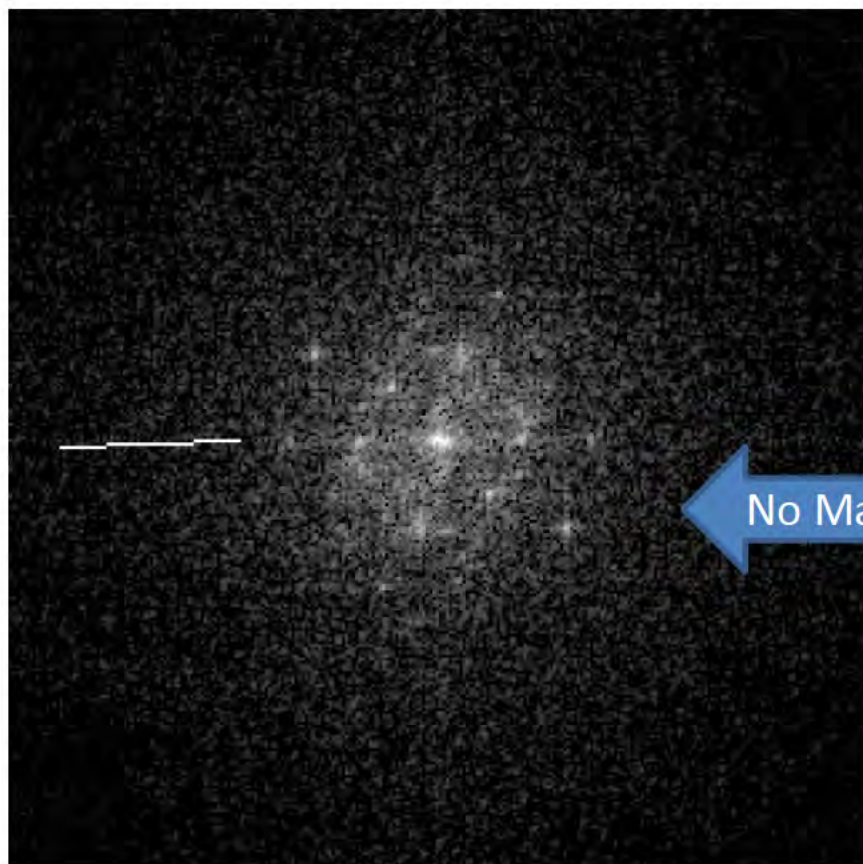


Standard Diffraction Pattern for {110}Fcc



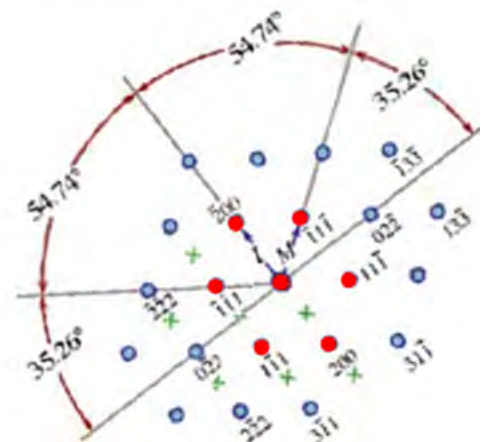
Standard Diffraction Pattern for {112}Fcc

Sample S0GPPC - Middle22T FFT

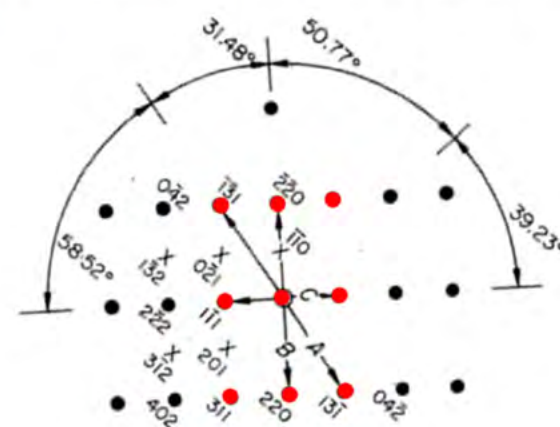


Middle22T

No Match



Standard Diffraction Pattern for {110}Fcc



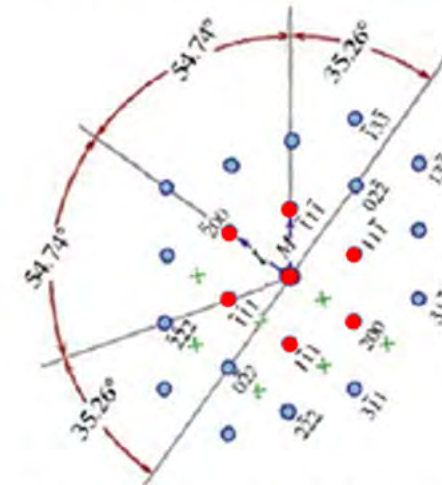
Standard Diffraction Pattern for {112}Fcc

Sample S0GPPC - Middle23T FFT

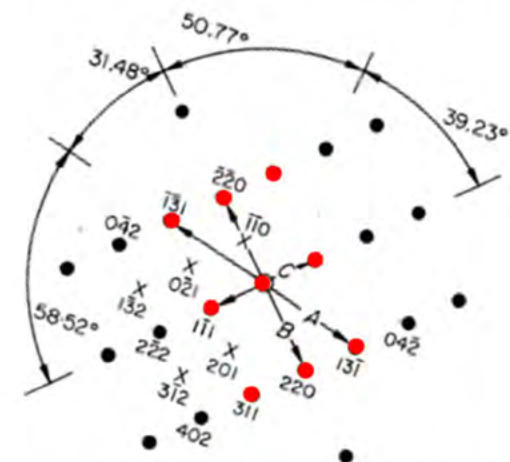


Middle23T

No Match



Standard Diffraction Pattern for {110}Fcc

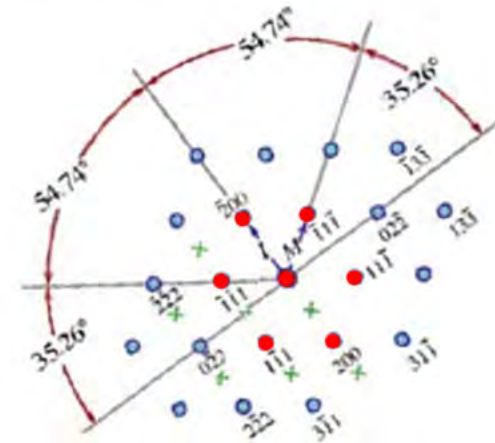


Standard Diffraction Pattern for {112}Fcc

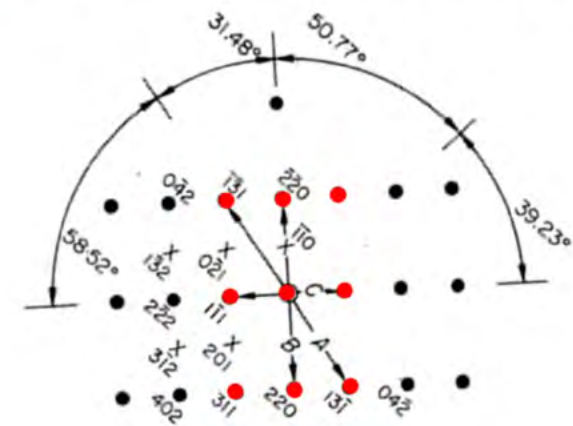
Sample S0GPPC - MiddleNi31T FFT



MiddleNi31T

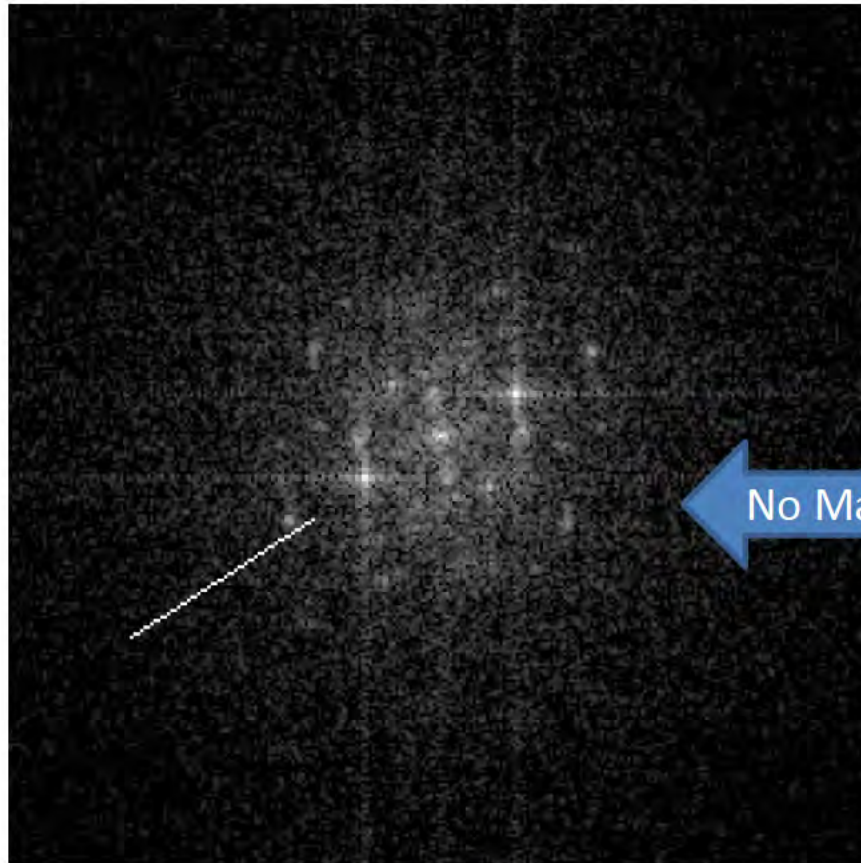


Standard Diffraction Pattern for {110}Fcc



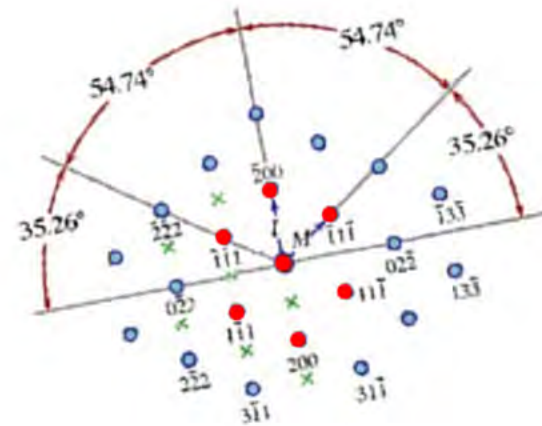
Standard Diffraction Pattern for {112}Fcc

Sample S0GPPC - MiddleNi32T FFT

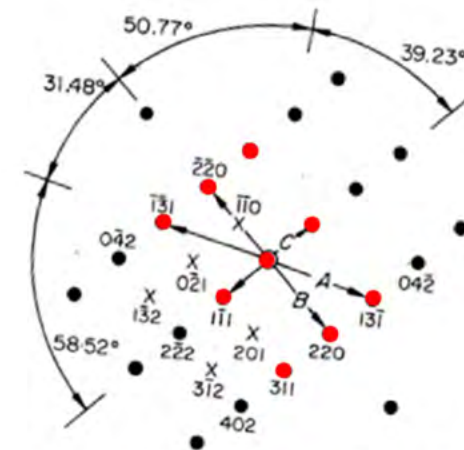


MiddleNi32T

No Match

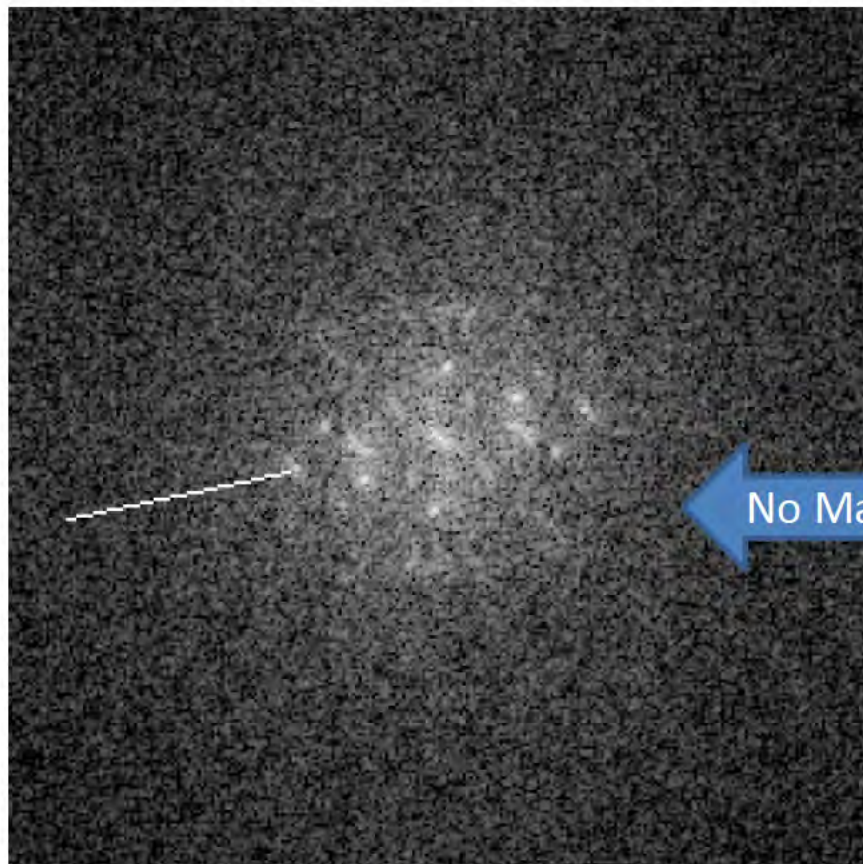


Standard Diffraction Pattern for {110}Fcc



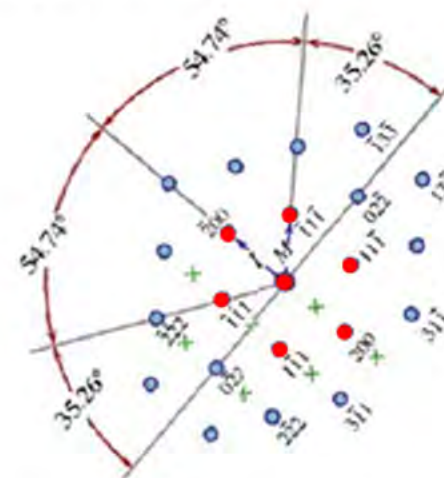
Standard Diffraction Pattern for {112}Fcc

Sample S0GPPC - MiddleNi33T FFT

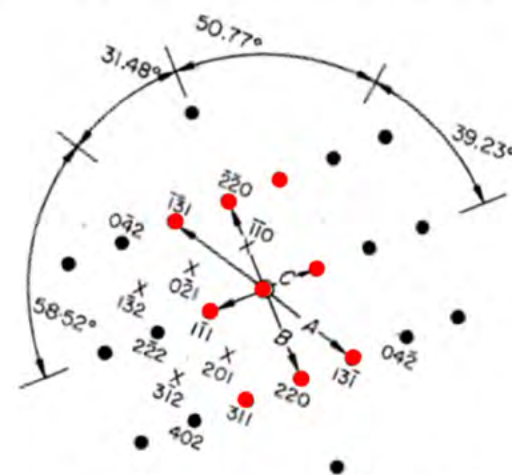


MiddleNi33T

No Match

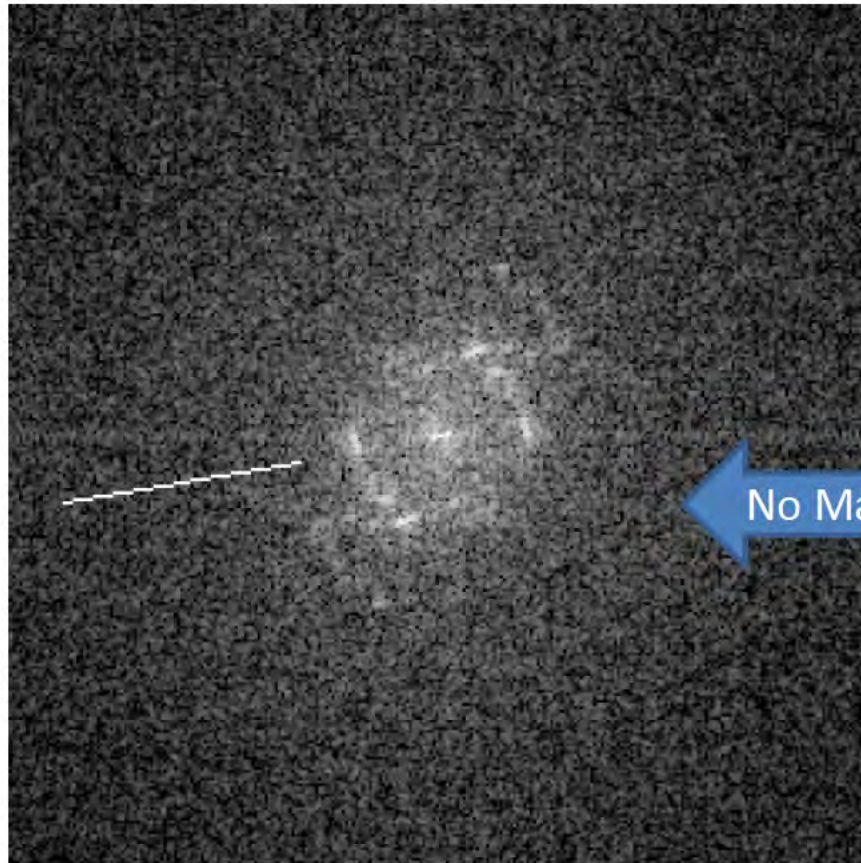


Standard Diffraction Pattern for {110}Fcc



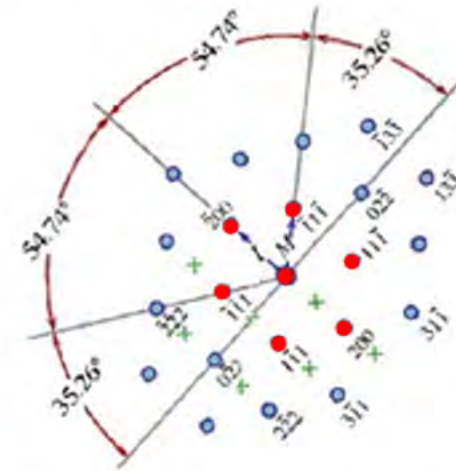
Standard Diffraction Pattern for {112}Fcc

Sample S0GPPC - MiddleNi41T FFT

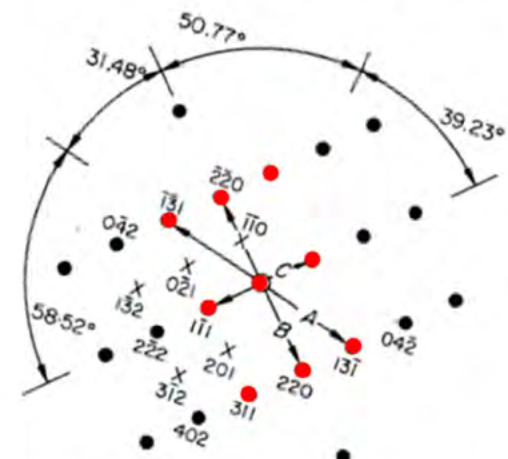


MiddleNi41T

No Match



Standard Diffraction Pattern for {110}Fcc



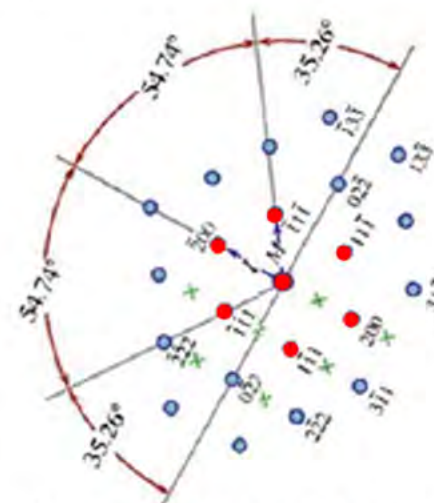
Standard Diffraction Pattern for {112}Fcc

Sample S0GPPC - MiddleNi42T FFT

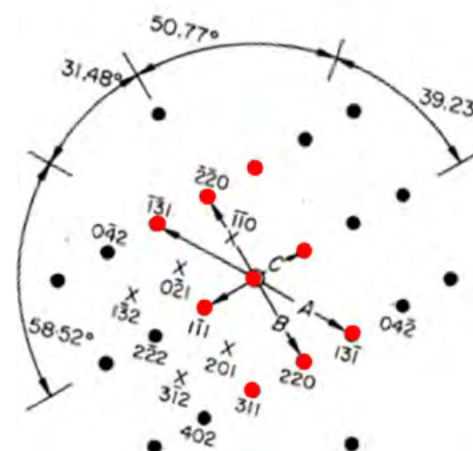


MiddleNi42T

No Match

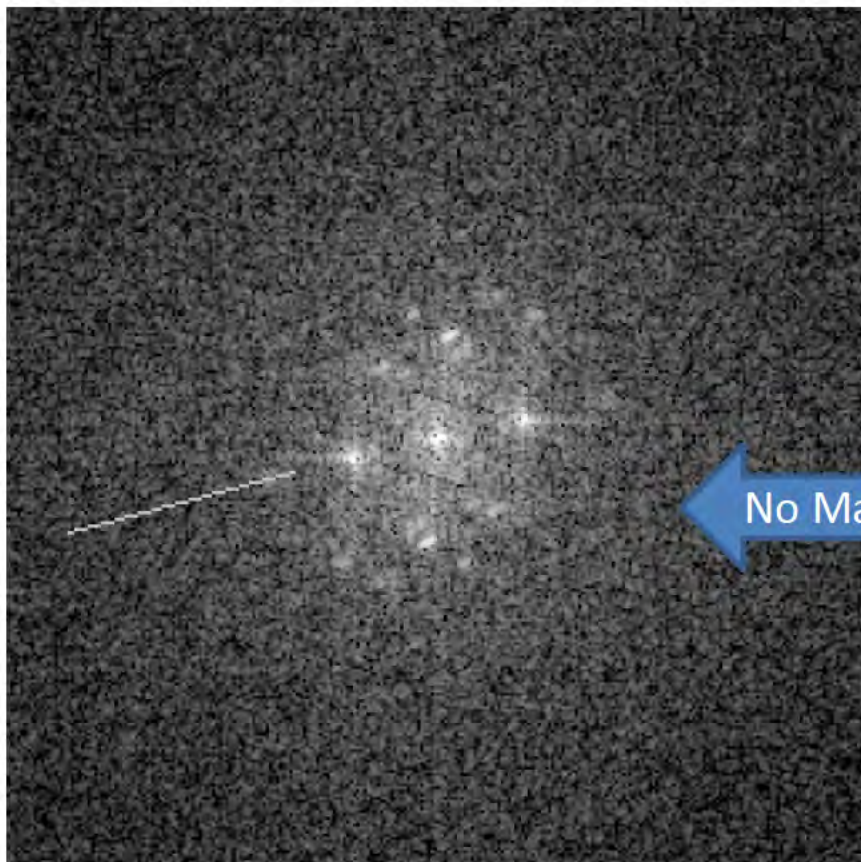


Standard Diffraction Pattern for {110}Fcc



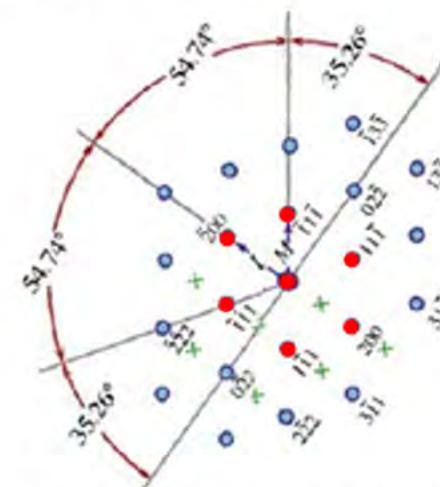
Standard Diffraction Pattern for {112}Fcc

Sample S0GPPC - MiddleNi43T FFT

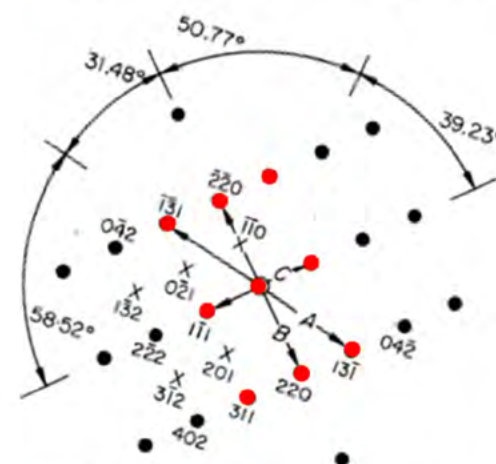


MiddleNi43T

No Match

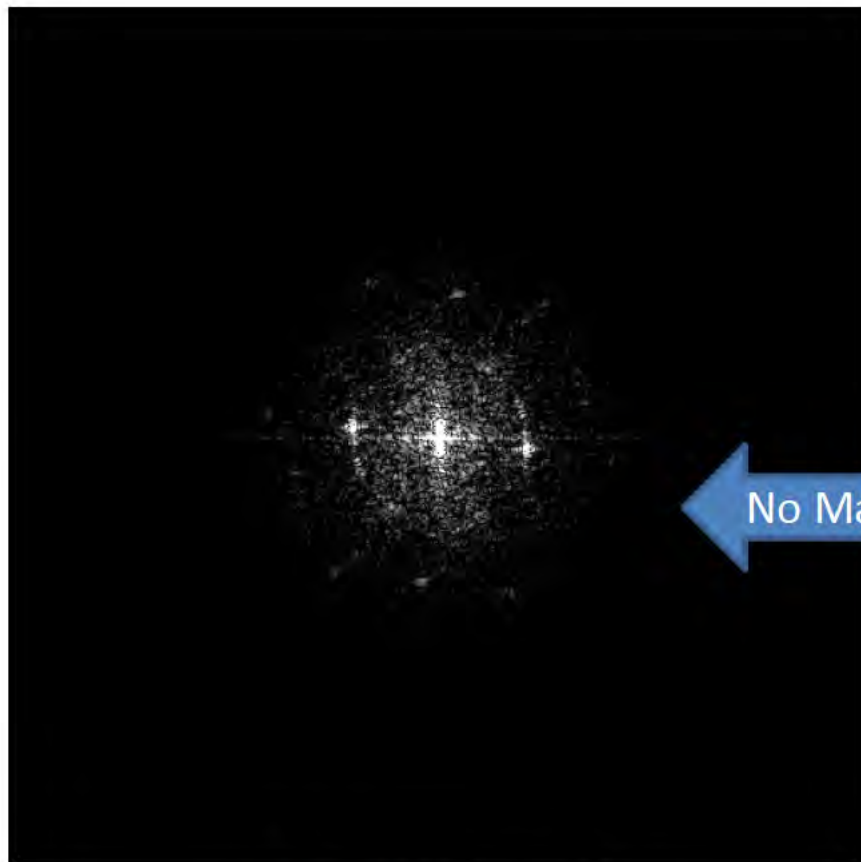


Standard Diffraction Pattern for {110}Fcc

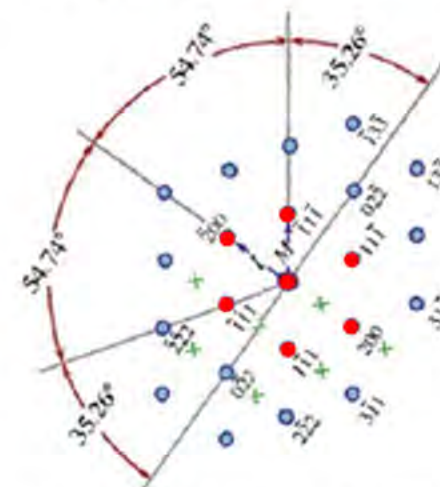
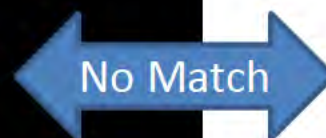


Standard Diffraction Pattern for {112}Fcc

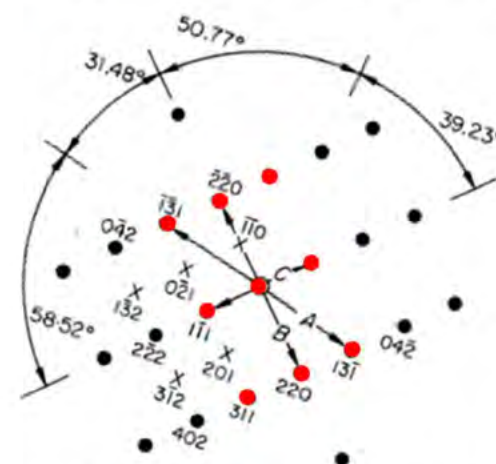
Sample S2MMMC - 18.08.14 CCD Acquire 1T FFT



18.08.14 CCD Acquire 1T

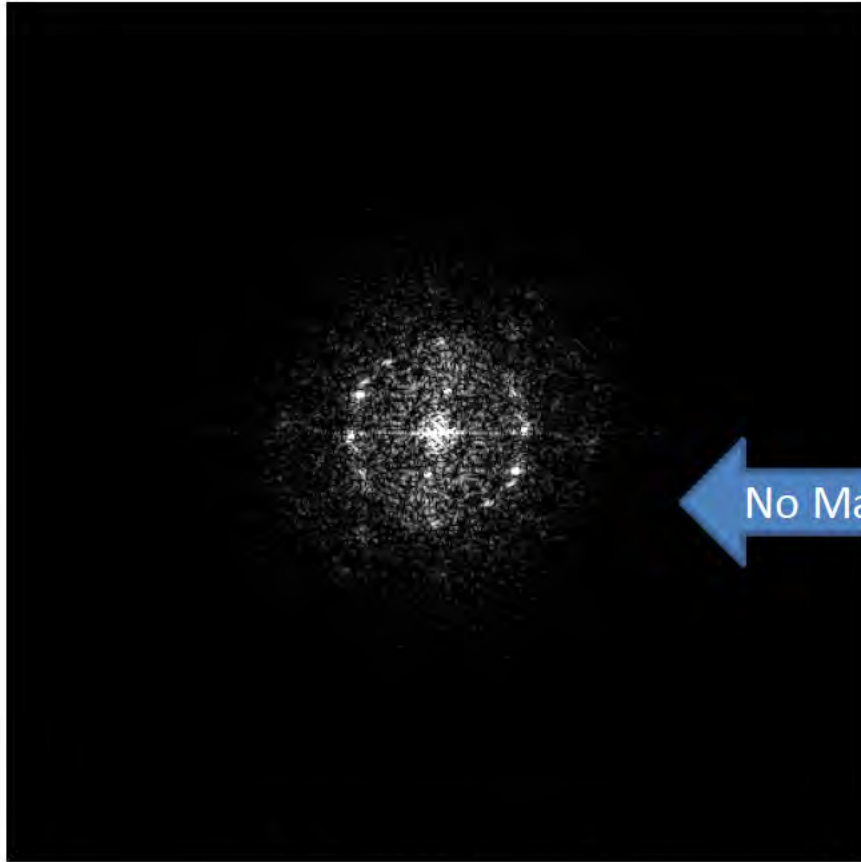


Standard Diffraction Pattern for {110}Fcc



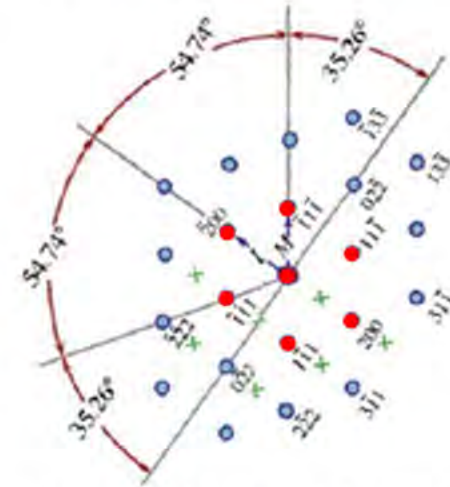
Standard Diffraction Pattern for {112}Fcc

Sample S2MMMC - 18.08.14 CCD Acquire 2T FFT

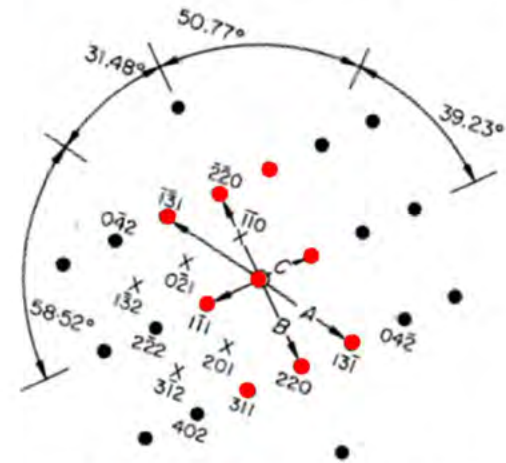


18.08.14 CCD Acquire 2T

No Match

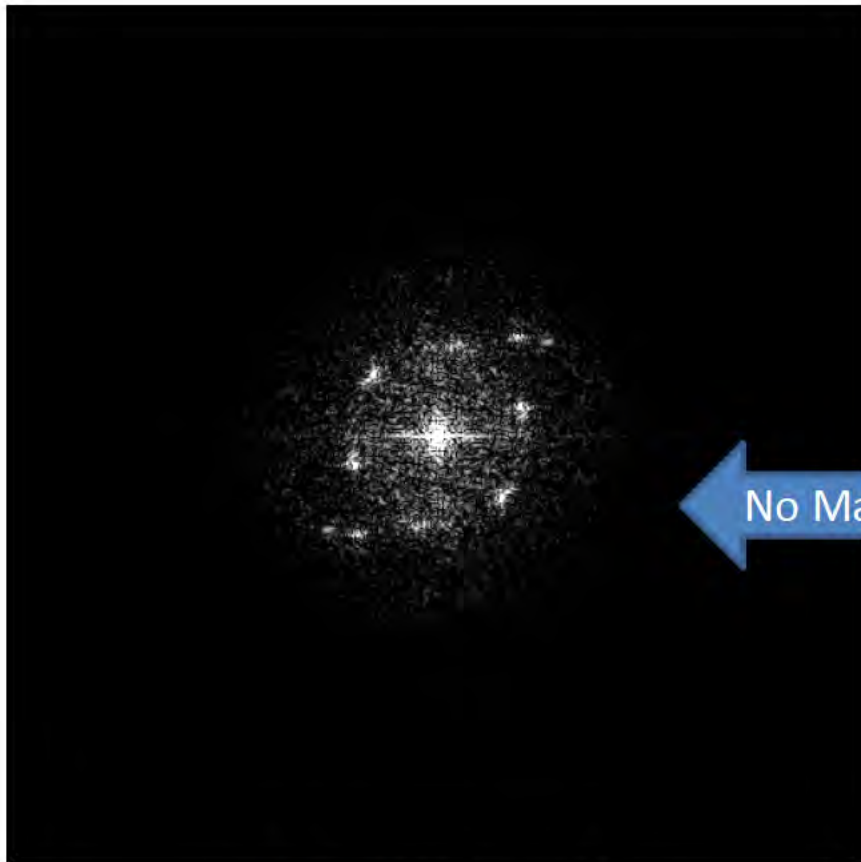


Standard Diffraction Pattern for {110}Fcc



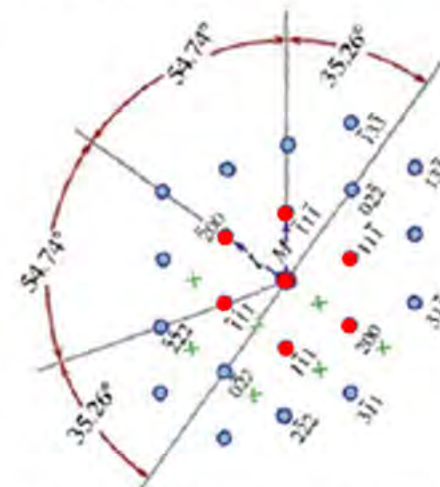
Standard Diffraction Pattern for {112}Fcc

Sample S2MMMC - 18.08.14 CCD Acquire 3T FFT

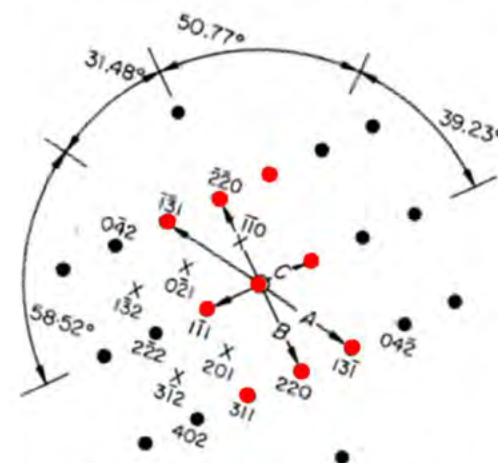


18.08.14 CCD Acquire 3T

No Match

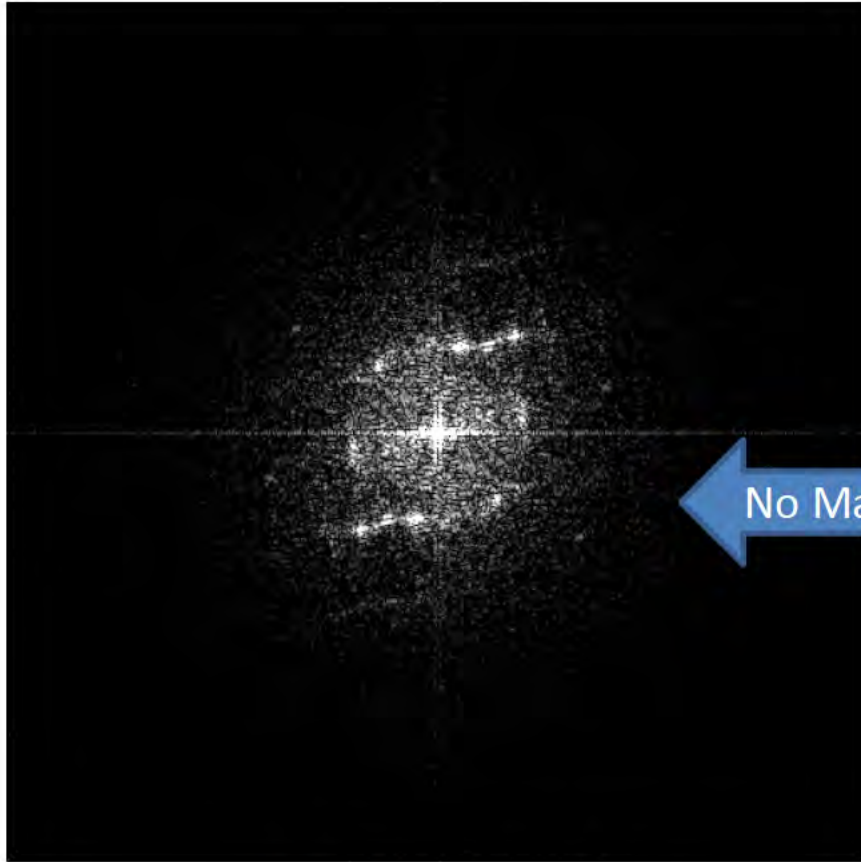


Standard Diffraction Pattern for {110}Fcc



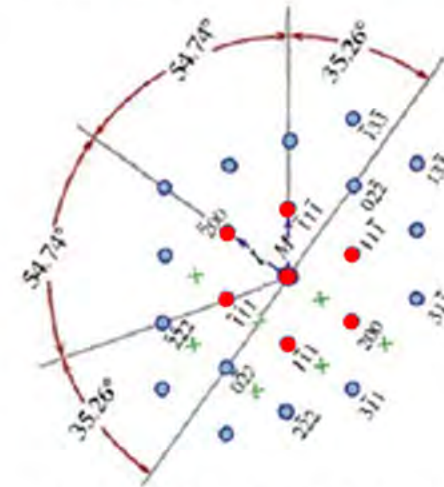
Standard Diffraction Pattern for {112}Fcc

Sample S2MMMC - 18.08.14 CCD Acquire 4T FFT

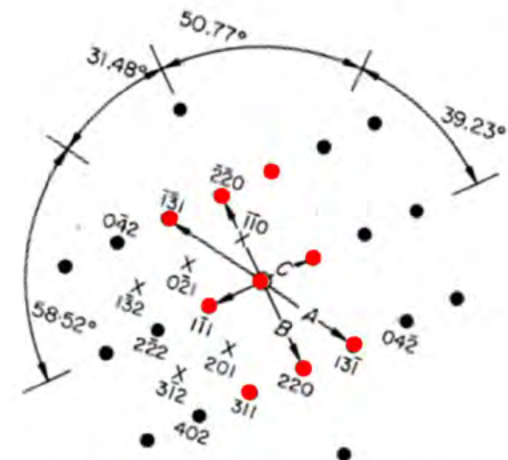


18.08.14 CCD Acquire 4T

No Match

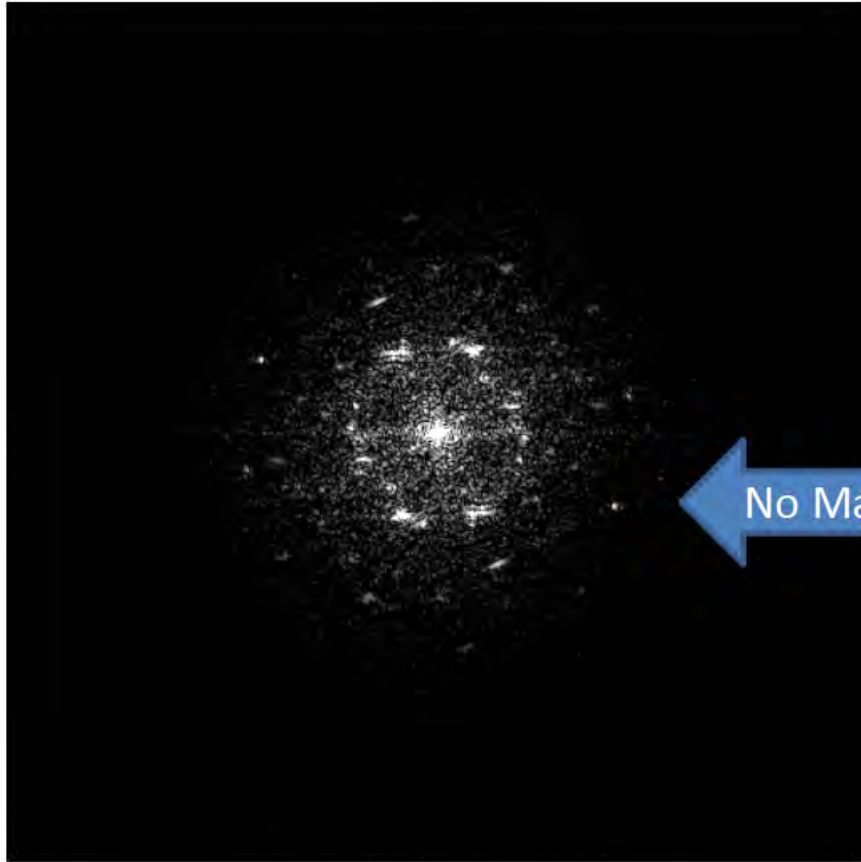


Standard Diffraction Pattern for $\{110\}$ Fcc



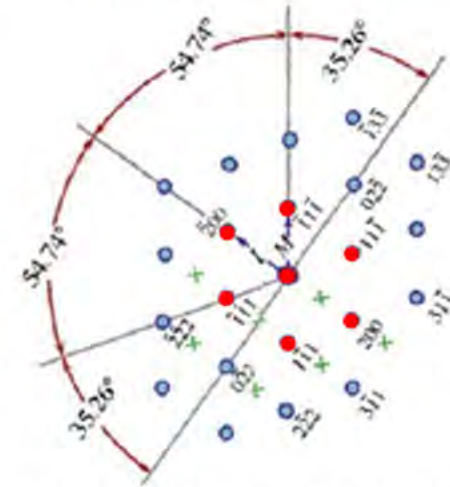
Standard Diffraction Pattern for {112}Fcc

Sample S2MMMC - 18.10.05 CCD Acquire 1T FFT

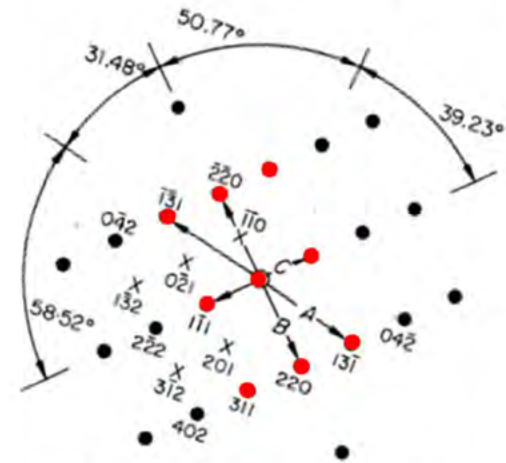


18.10.05 CCD Acquire 1T

No Match



Standard Diffraction Pattern for {110}Fcc



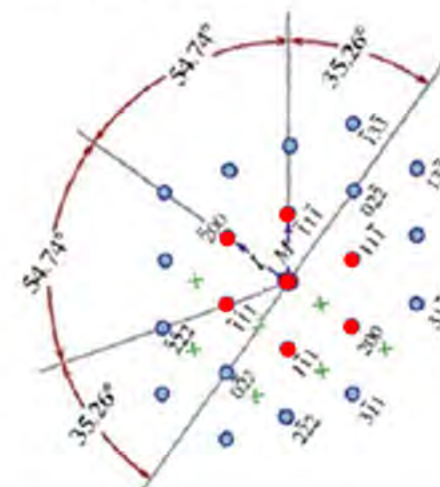
Standard Diffraction Pattern for {112}Fcc

Sample SBR8DK - 18.21.37 CCD Acquire 1T FFT

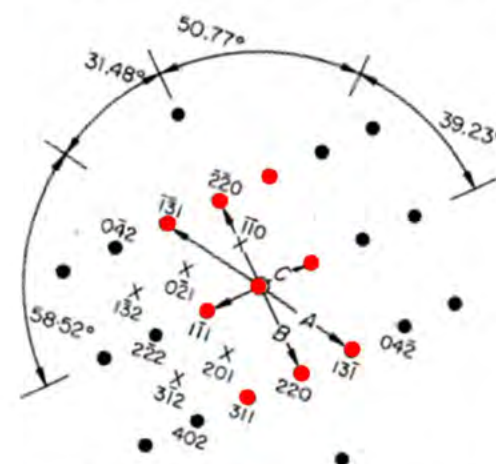


18.21.37 CCD Acquire 1T

No Match

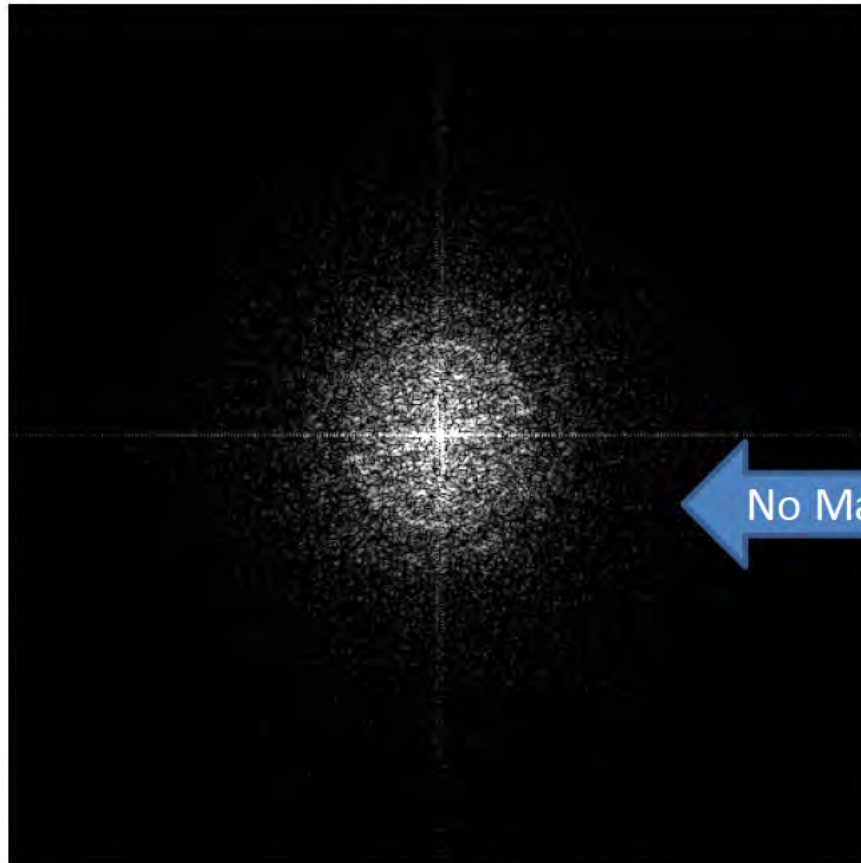


Standard Diffraction Pattern for {110}Fcc

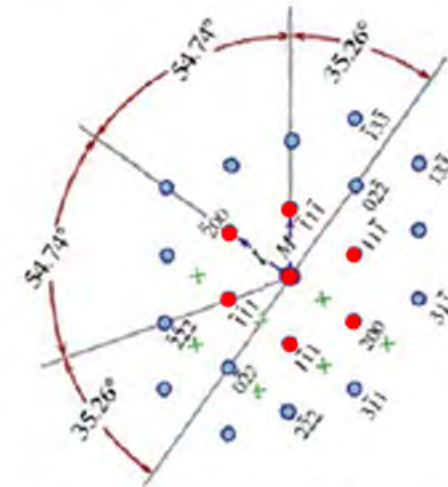
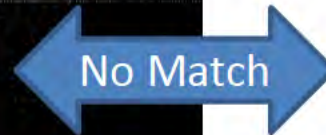


Standard Diffraction Pattern for {112}Fcc

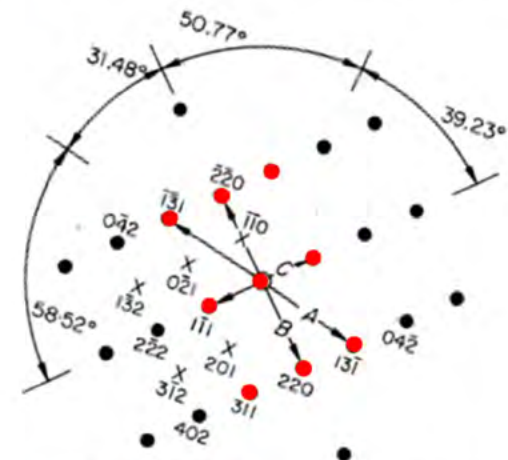
Sample SBR8DK - 18.21.37 CCD Acquire 2T FFT



18.21.37 CCD Acquire 2T



Standard Diffraction Pattern for {110}Fcc



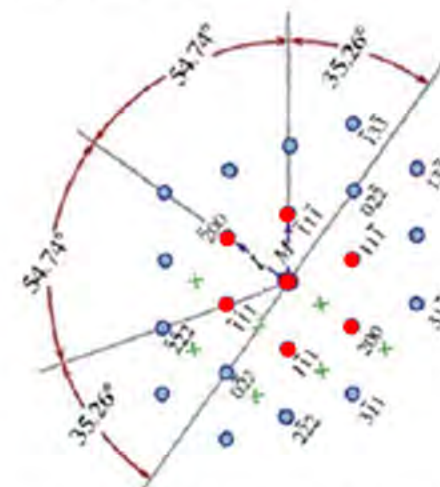
Standard Diffraction Pattern for {112}Fcc

Sample SBR8DK - 18.21.37 CCD Acquire 3T FFT

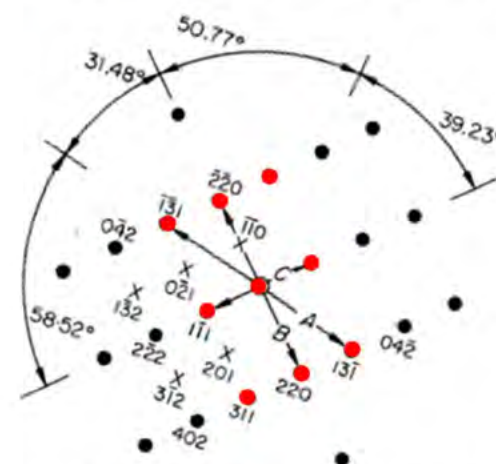


18.21.37 CCD Acquire 3T

No Match

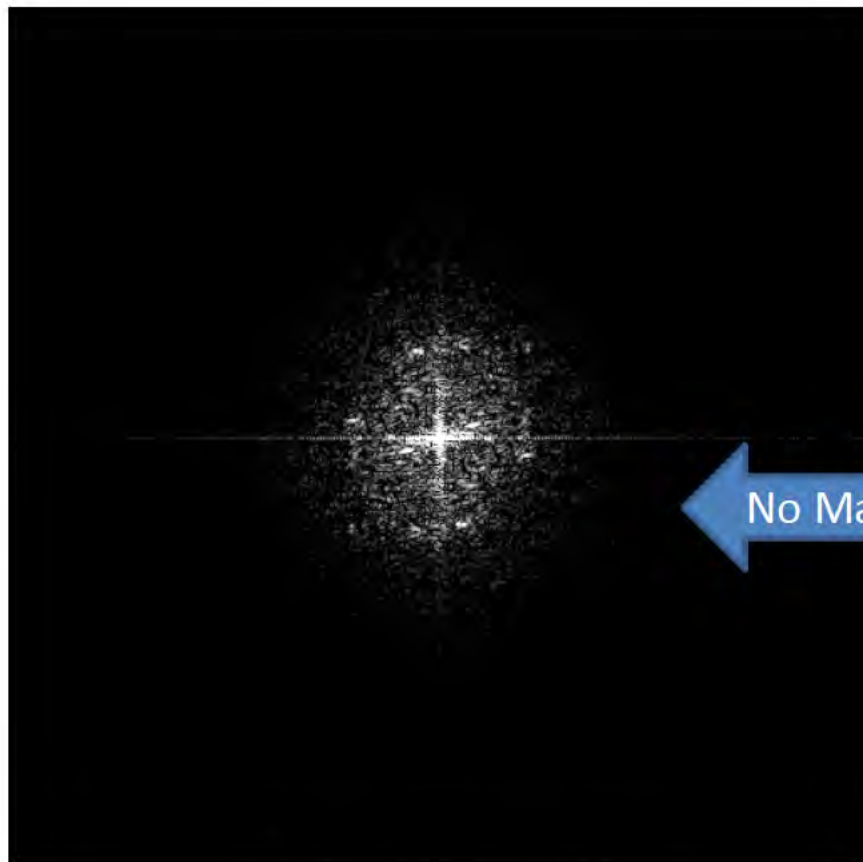


Standard Diffraction Pattern for {110}Fcc



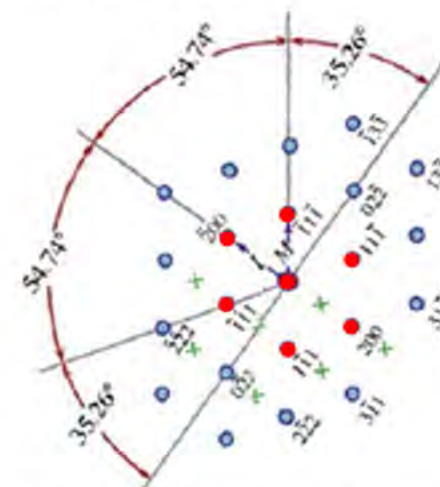
Standard Diffraction Pattern for {112}Fcc

Sample SBR8DK - 18.21.37 CCD Acquire 4T FFT

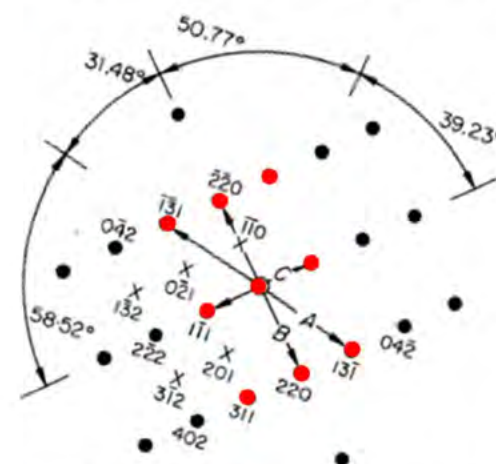


18.21.37 CCD Acquire 4T

No Match



Standard Diffraction Pattern for {110}Fcc

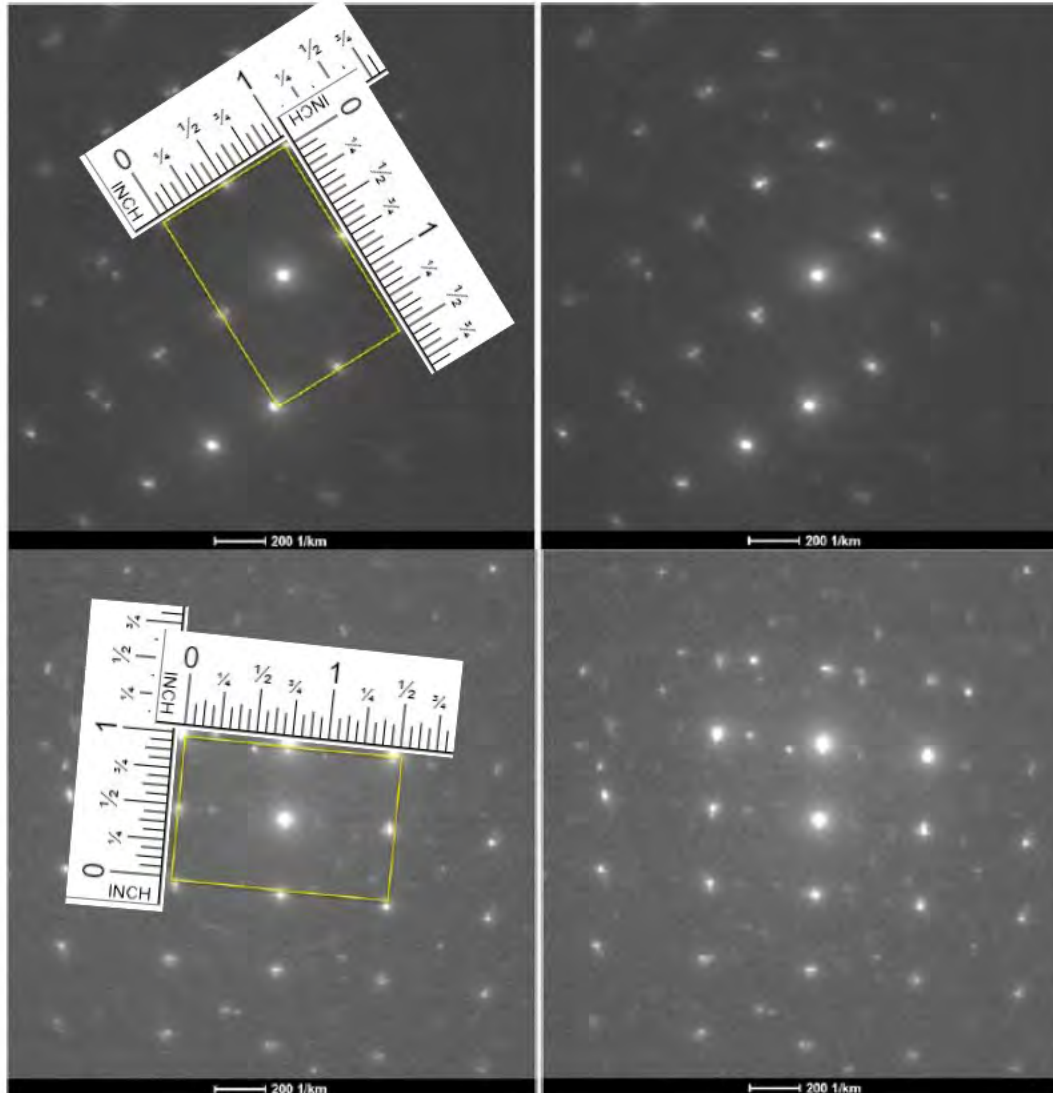


Standard Diffraction Pattern for {112}Fcc

EXHIBIT E

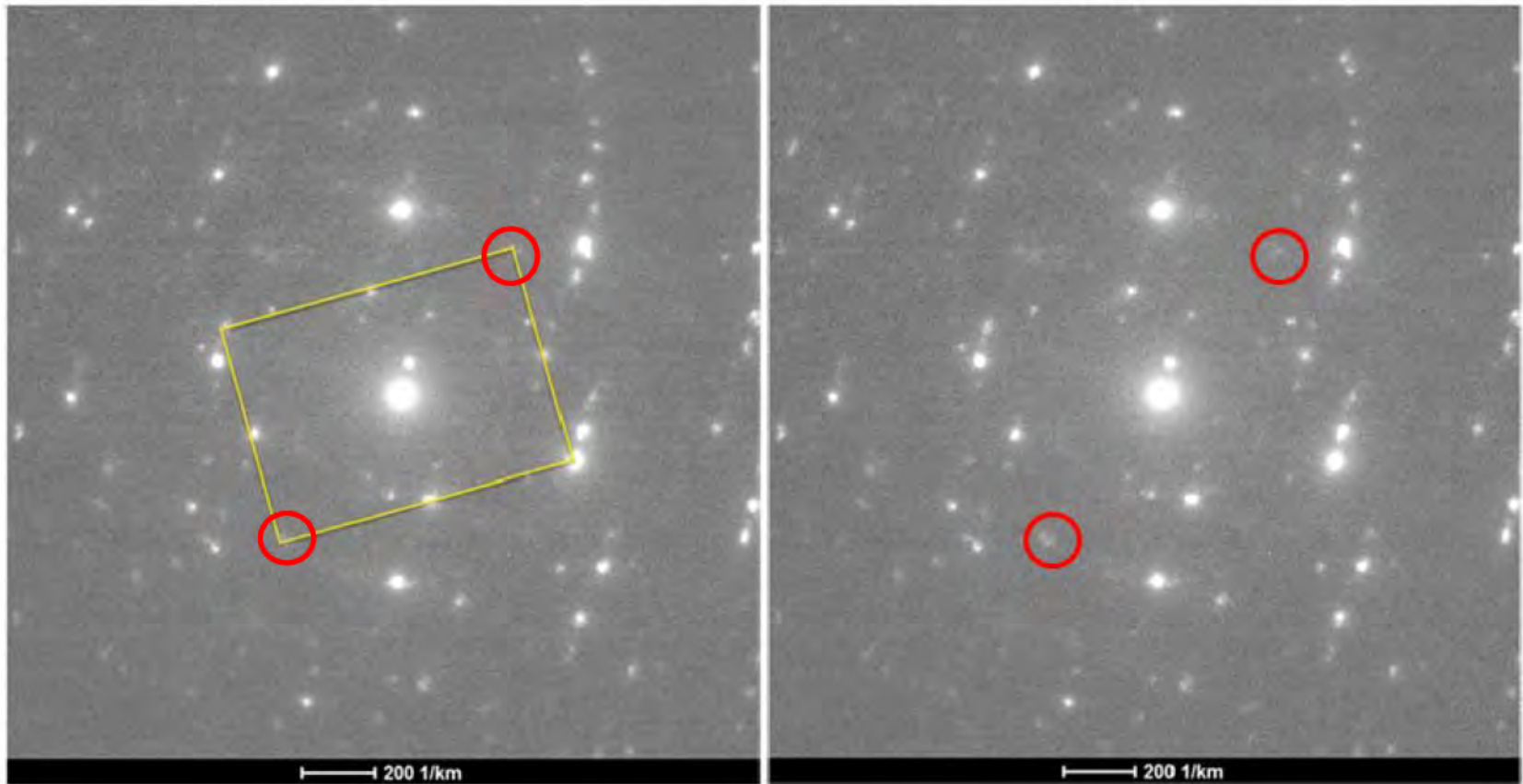
S0GPPC - Figure 47

Ratio = 1:1.5



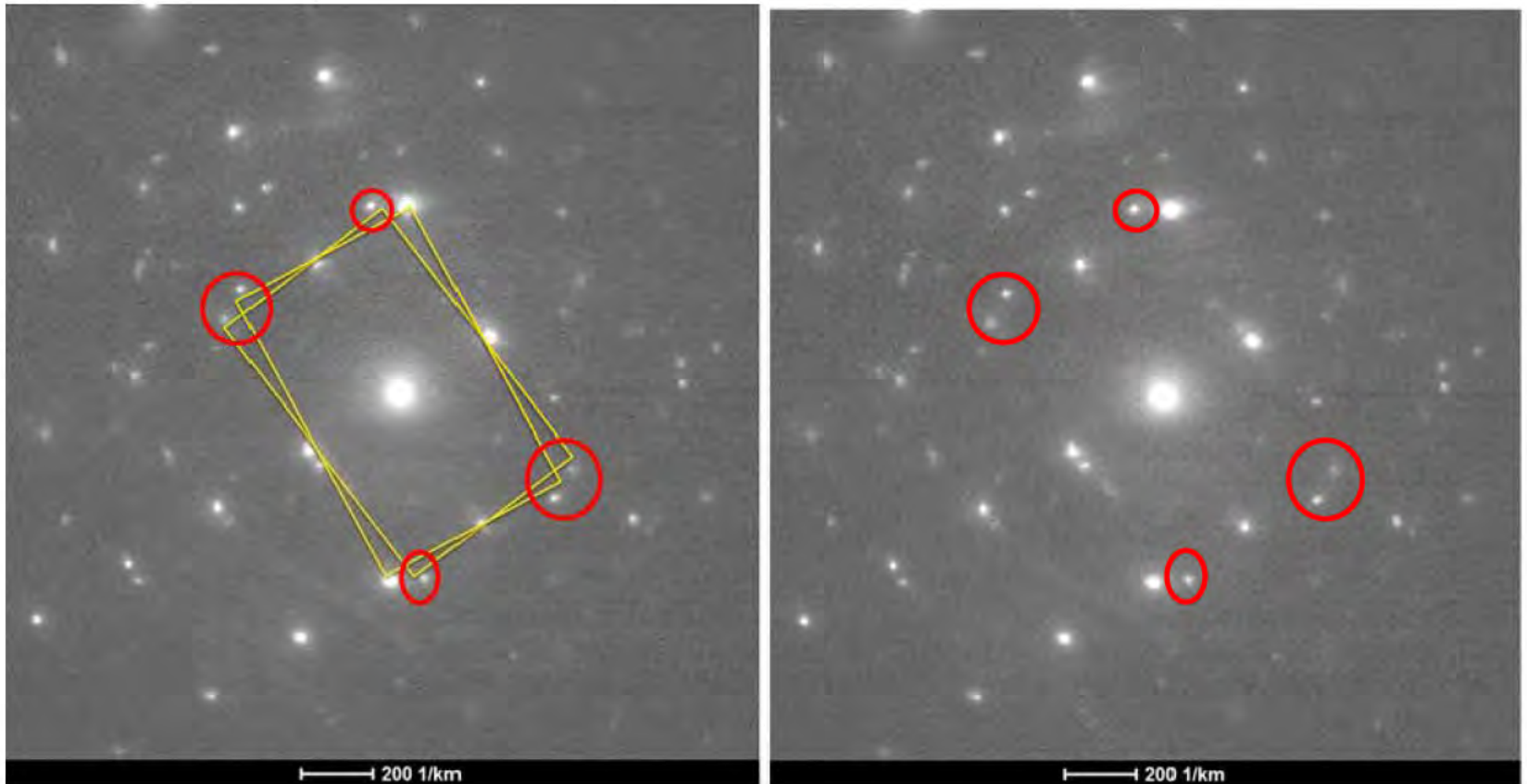
Ratio = 1:1.5

S0GPPC - Figure 48



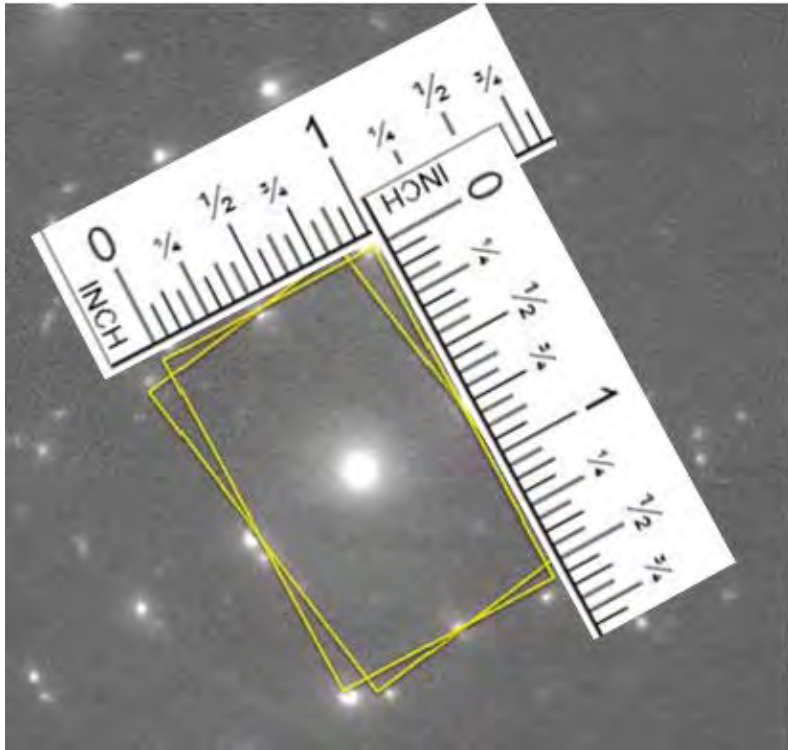
Red circles added by Dr. Stach to indicate spots that are weak, not clearly discernable or not present.

S0GPPC - Figure 49

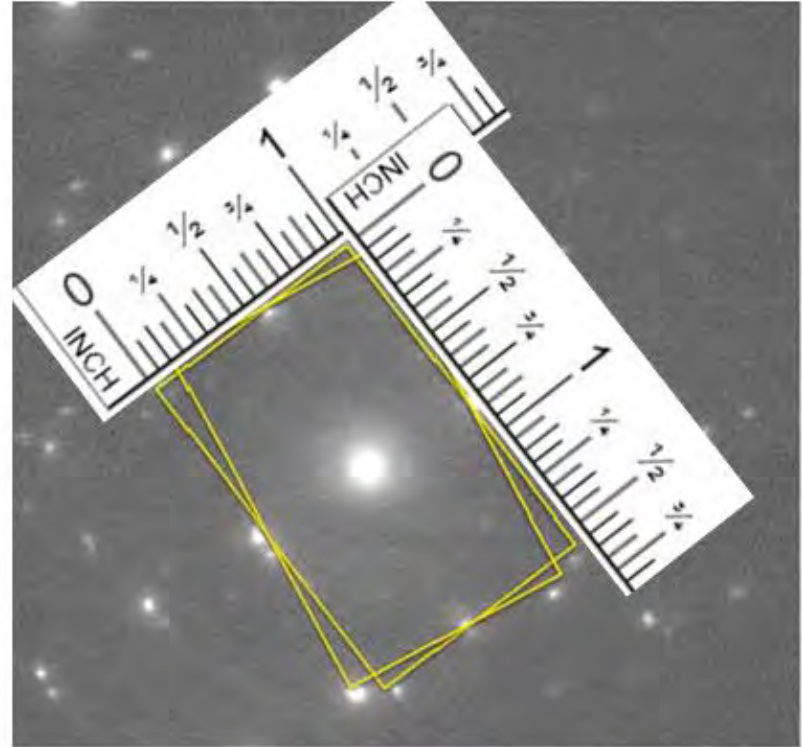


Red circles added by Dr. Stach to indicate spots that are not clearly discernable or not present. The lack of alignment with the box corners and nearby spots are significant enough to indicate that this interpretation is incorrect.

S0GPPC - Figure 49

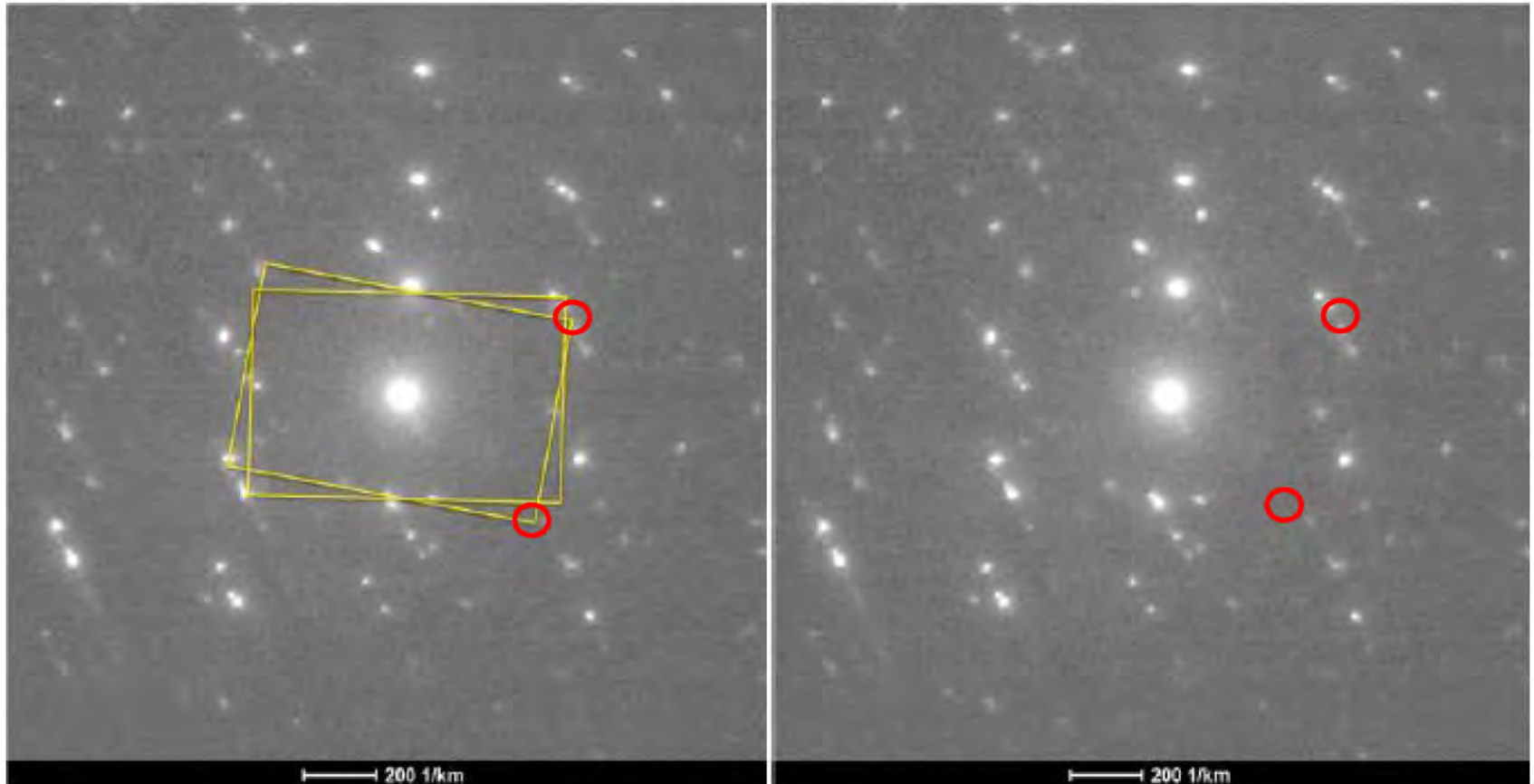


Ratio = 1:1.5625



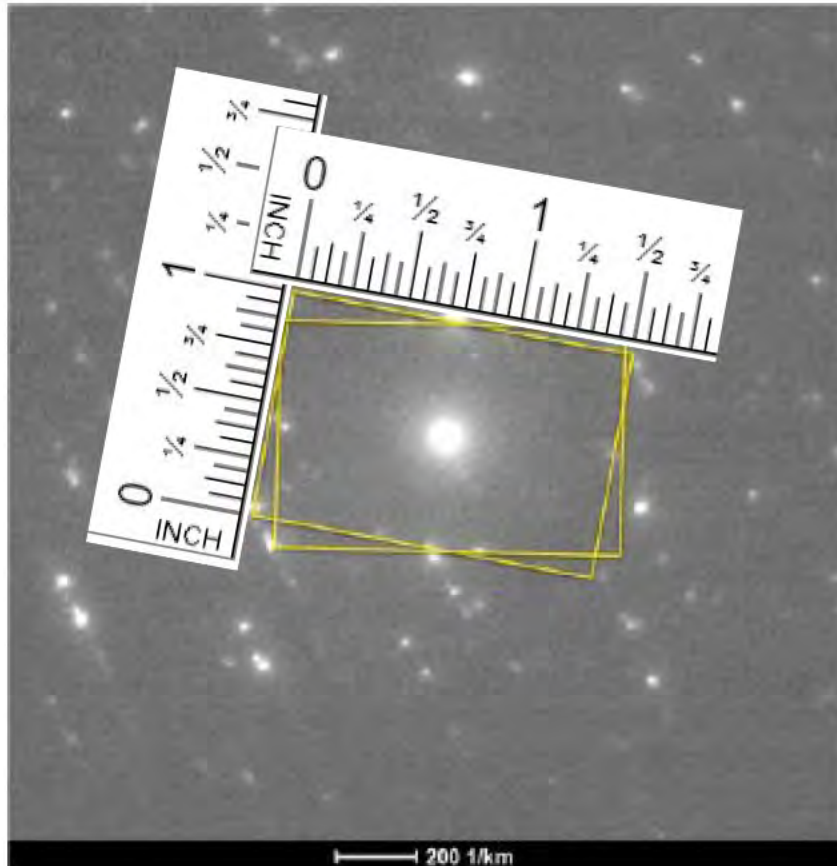
Ratio = 1:1.5625

S0GPPC - Figure 50

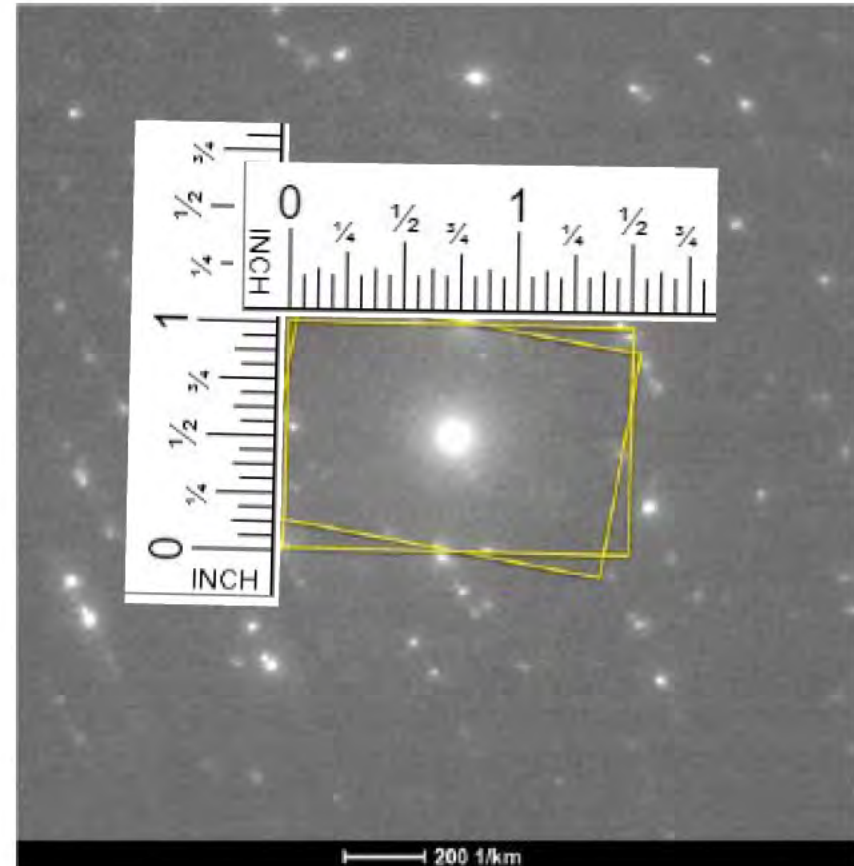


Red circles added by Dr. Stach to indicate spots that are not clearly discernable or not present. The lack of alignment with the box corners and nearby spots are significant enough to indicate that this interpretation is incorrect.

SOGPPC - Figure 50



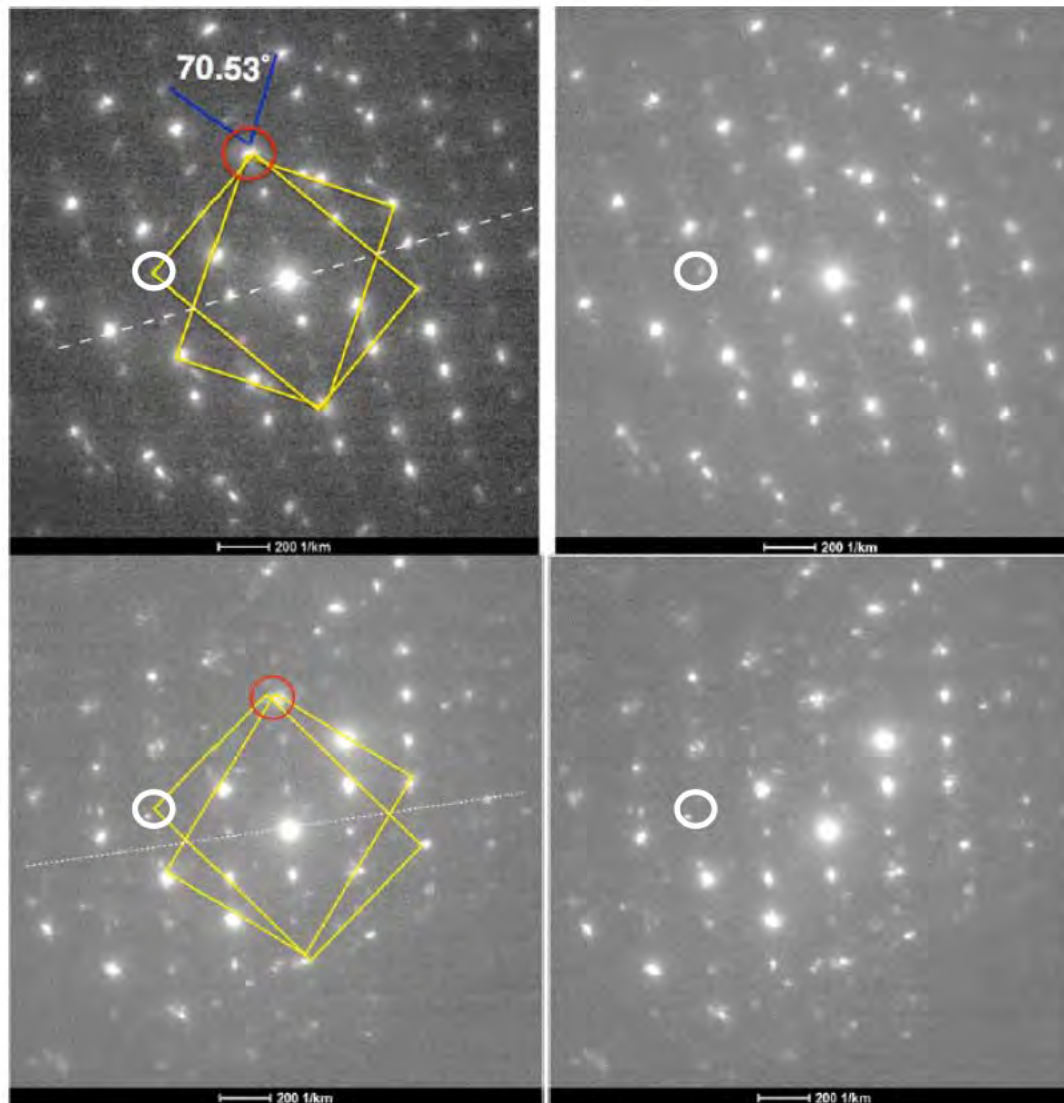
Ratio = 1:1.5



Ratio = 1:1.5

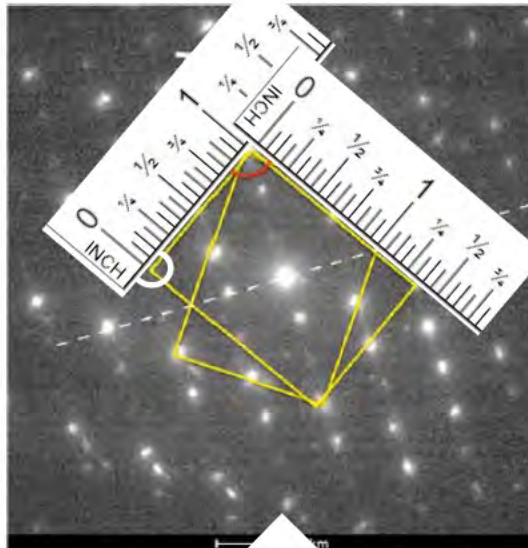
S0GPPC - Figure 51

- White rings inserted by Dr. Stach to show missing or not clearly discernable spots
- Red rings in original image
- The lack of alignment with the box corners and nearby spots are significant enough to indicate that this interpretation is incorrect.

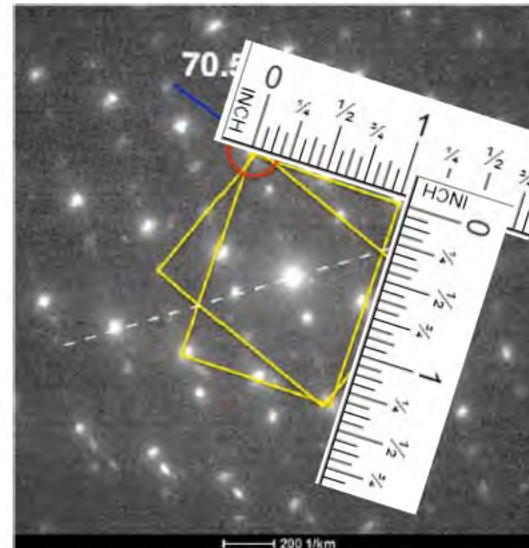


S0GPPC - Figure 51

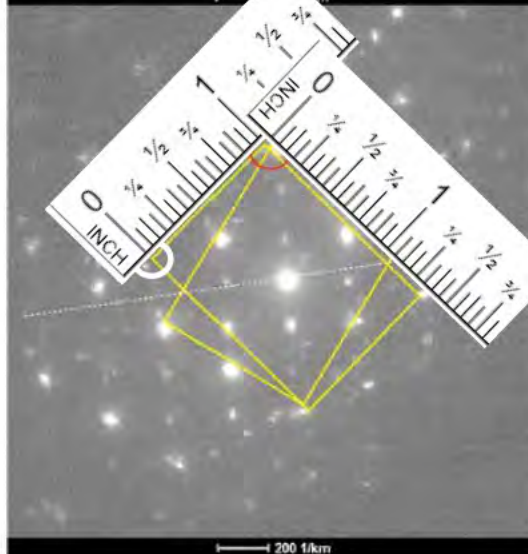
Ratio = 1.5:1



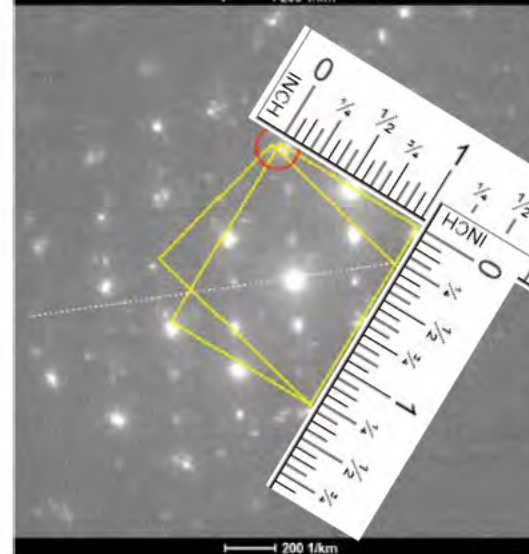
Ratio 1.375:1



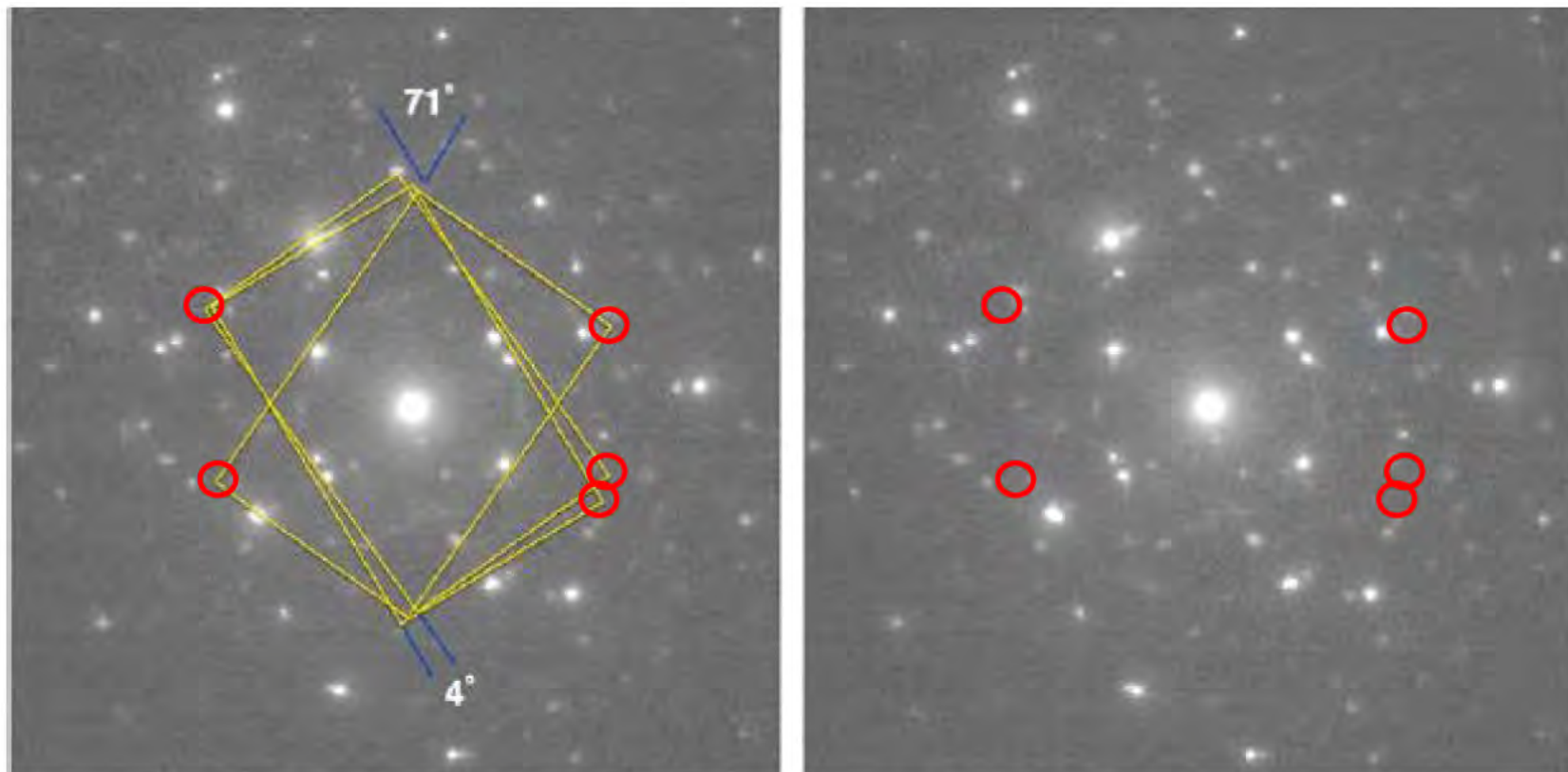
Ratio = 1.375:1



Ratio = 1.313:1

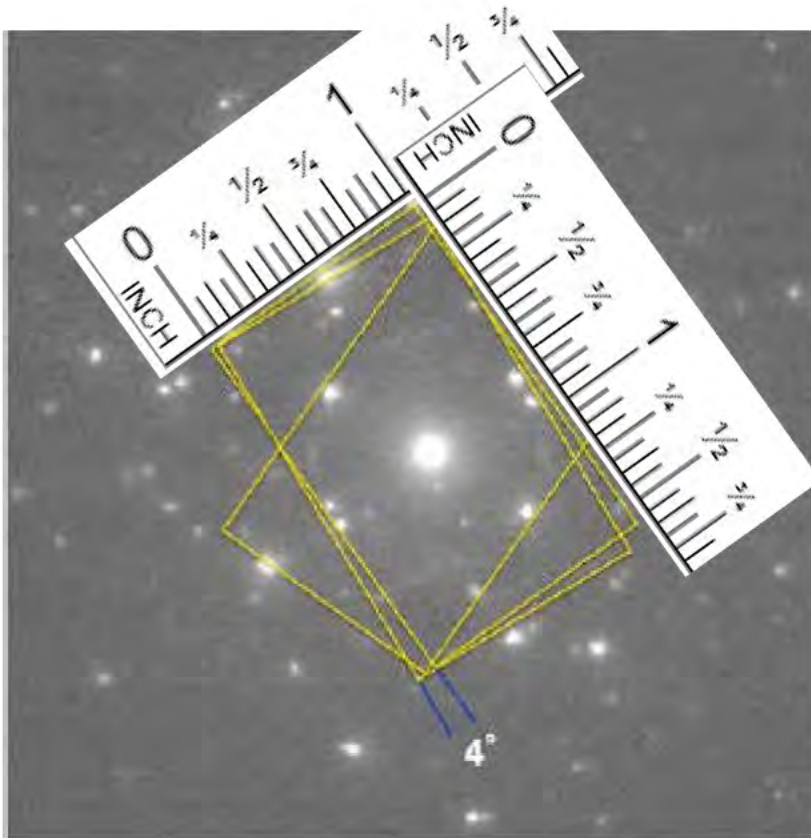


S0GPPC - Figure 52

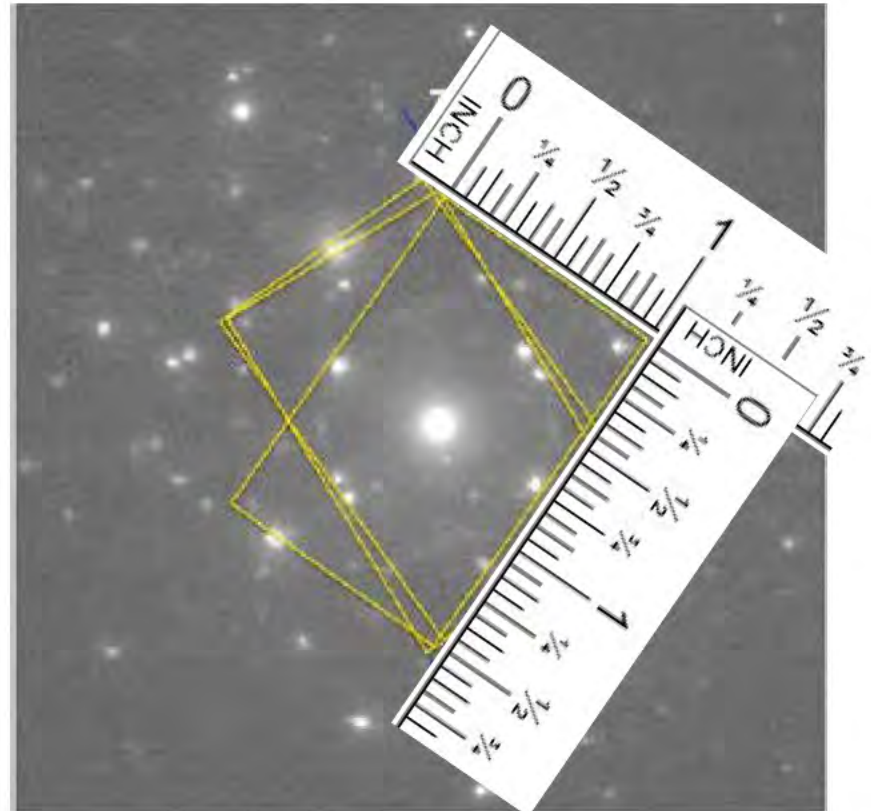


Red circles added by Dr. Stach to indicate spots that are not clearly discernable or not present. The lack of alignment with the box corners and nearby spots are significant enough to indicate that this interpretation is incorrect.

S0GPPC - Figure 52



Ratio = 1.563:1

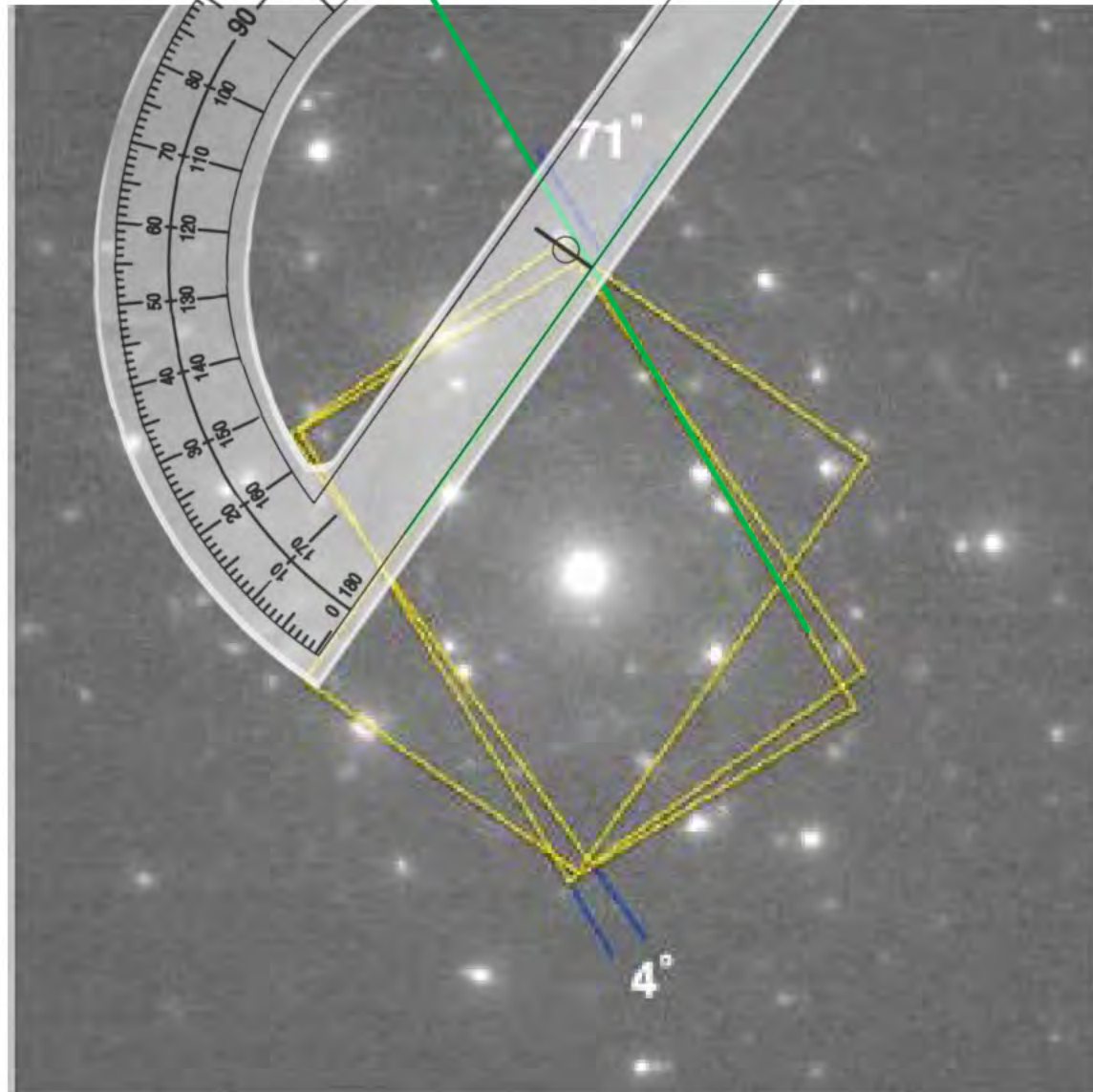


Ratio = 1.5:1

SOGPPC

66 degrees

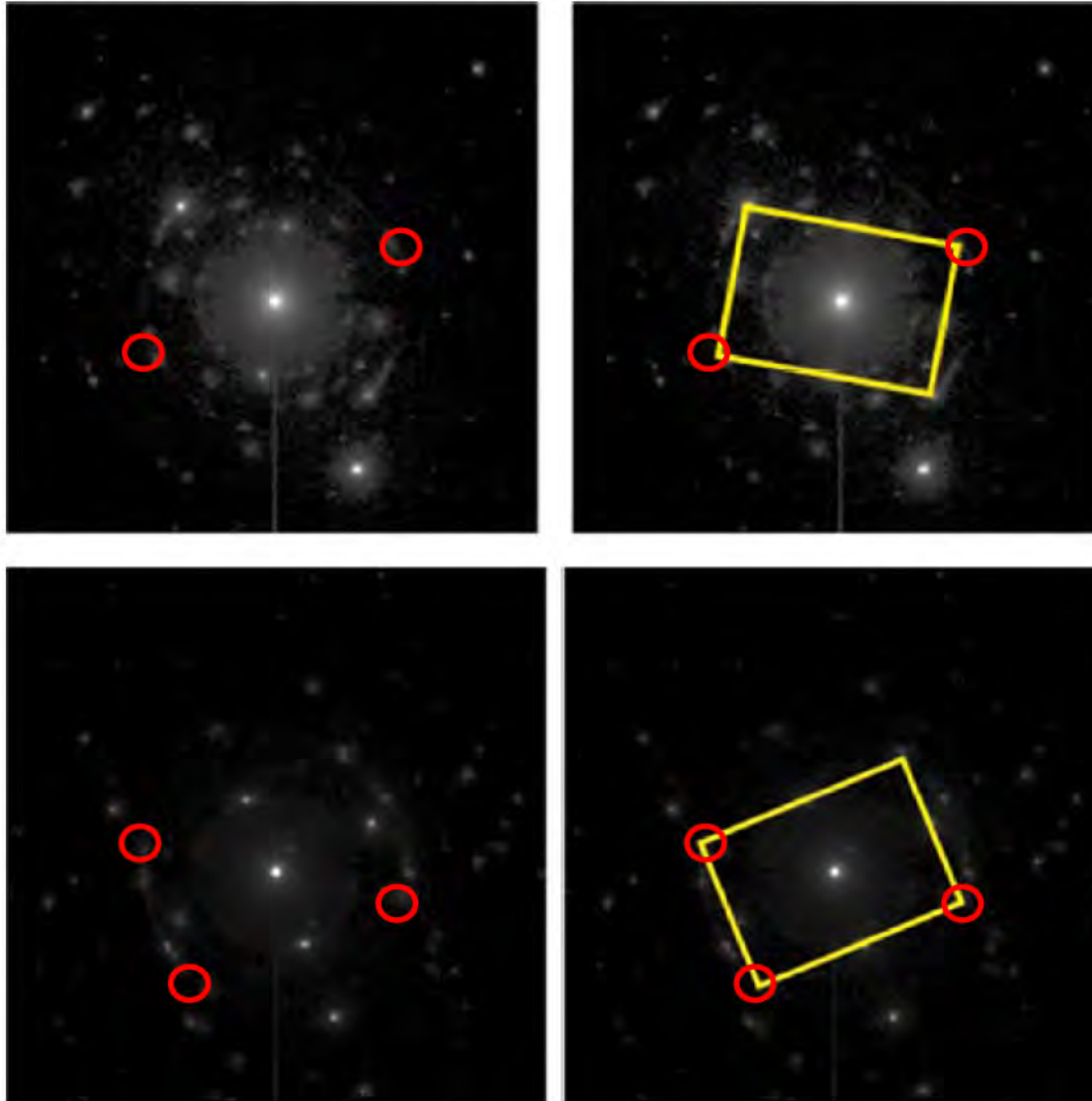
Fig. 52



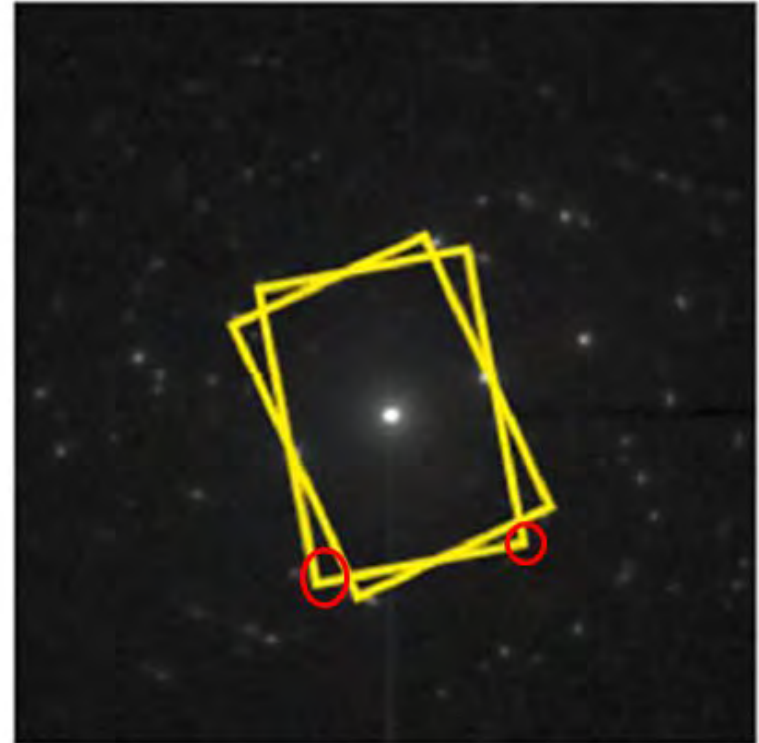
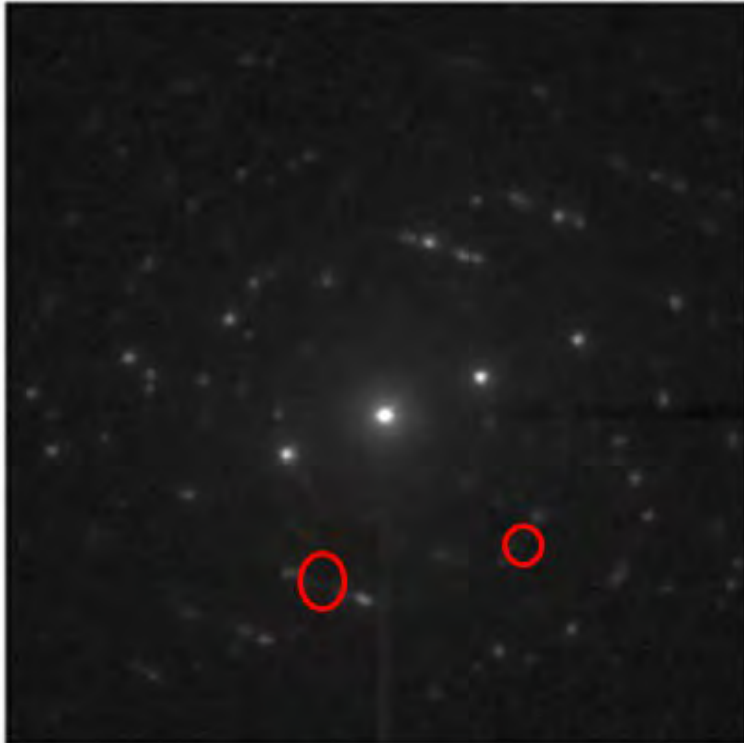
- Green lines and protractor added by Dr. Stach

S2MMMC - Figure 77

Red circles
added by Dr.
Stach to indicate
spots that are
not clearly
discernable or
not present.

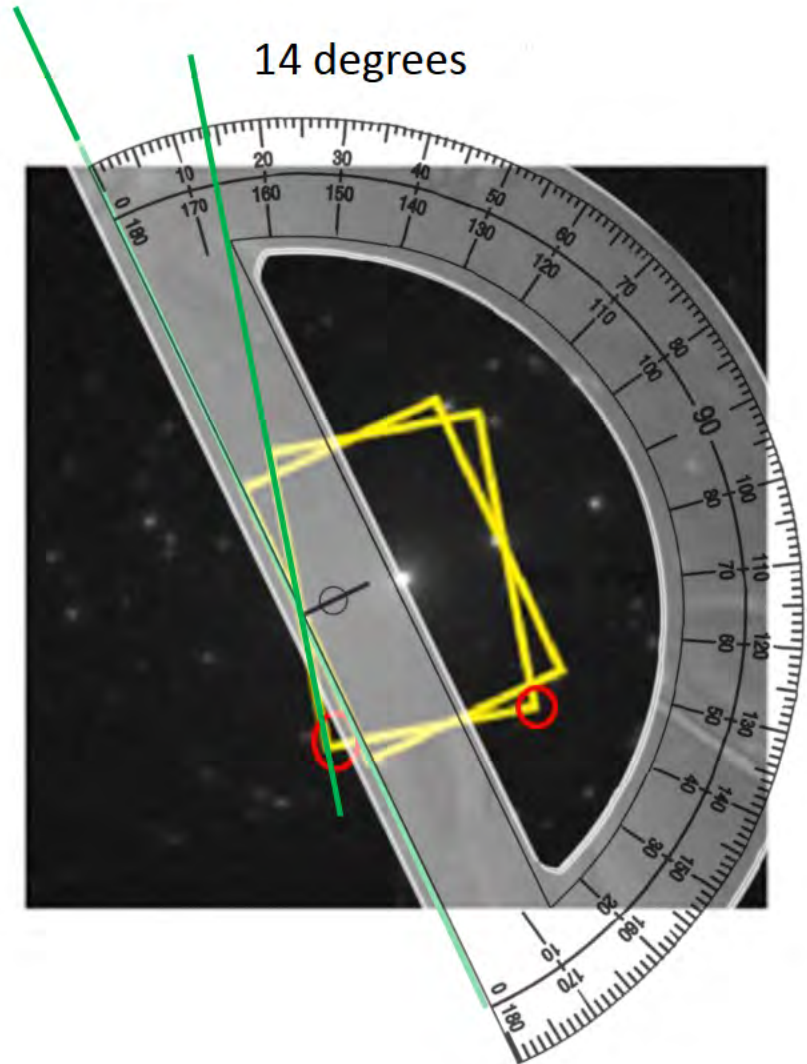
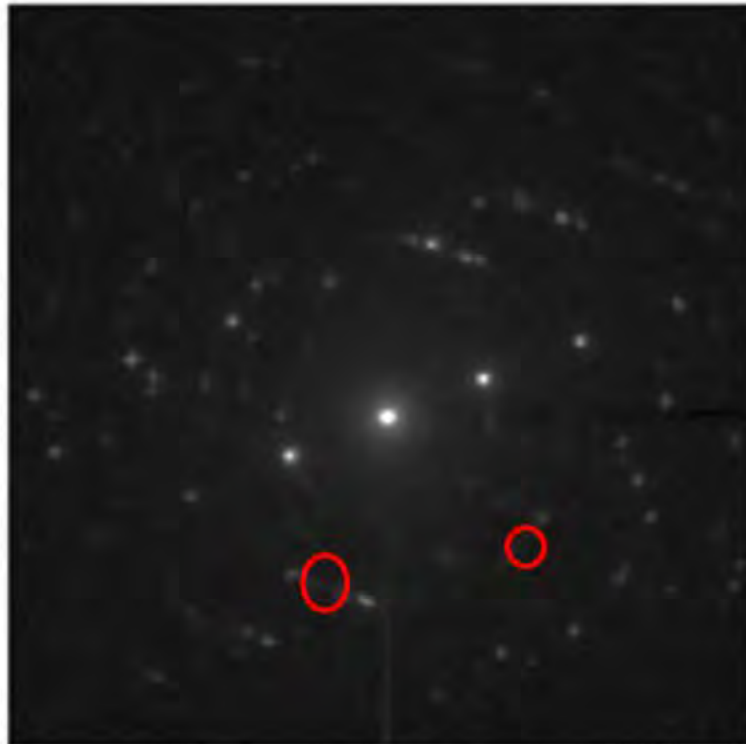


S2MMMC - Figure 78



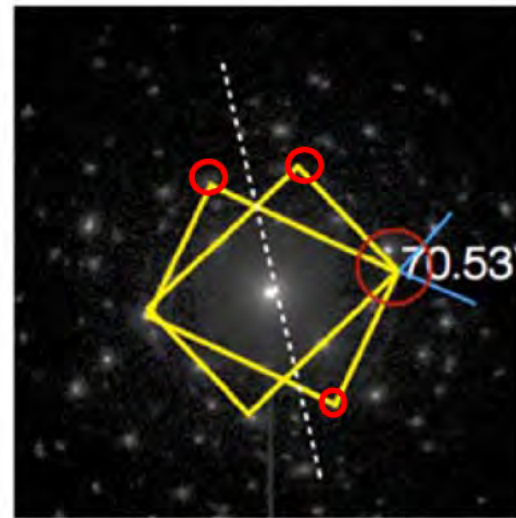
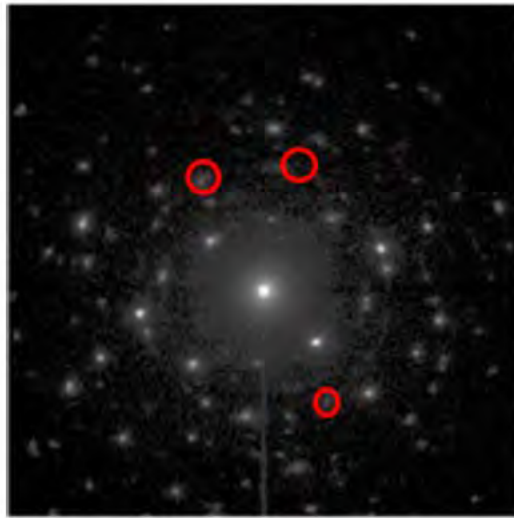
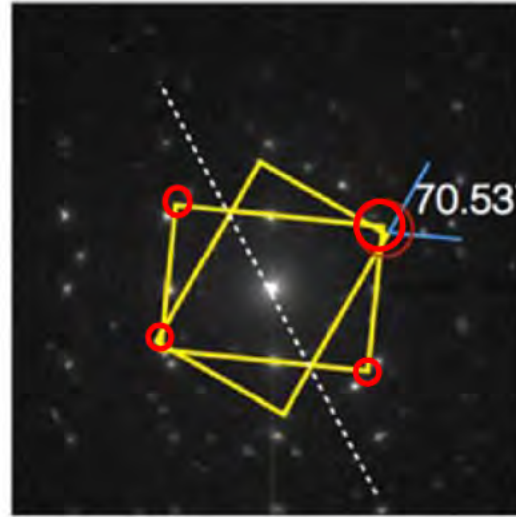
Red circles added by Dr. Stach to indicate spots that are not clearly discernable or not present. This interpretation is clearly incorrect.

S2MMMC - Figure 78

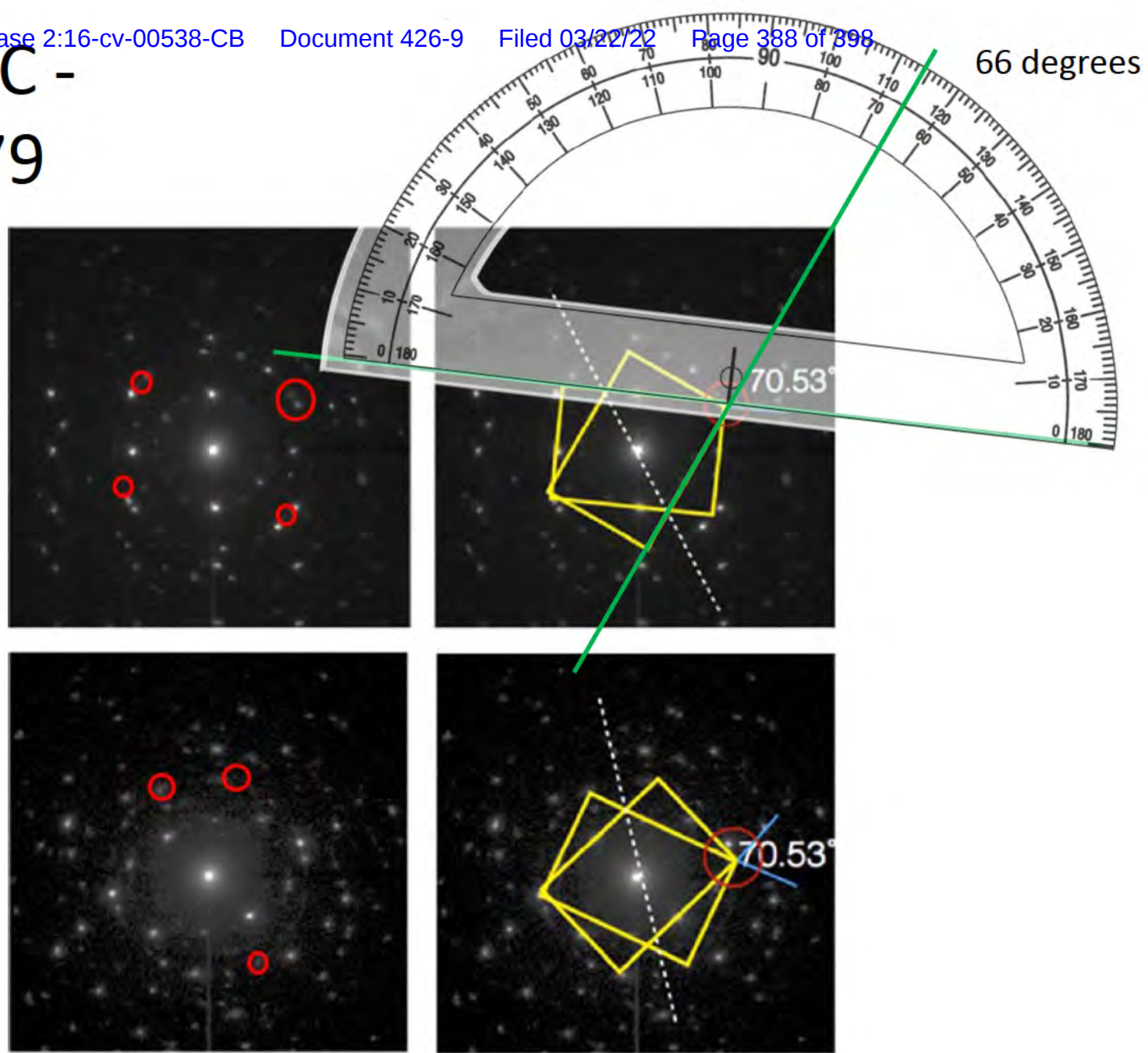


S2MMMC - Figure 79

Red circles
added by Dr.
Stach to indicate
spots that are
not clearly
discernable or
not present.

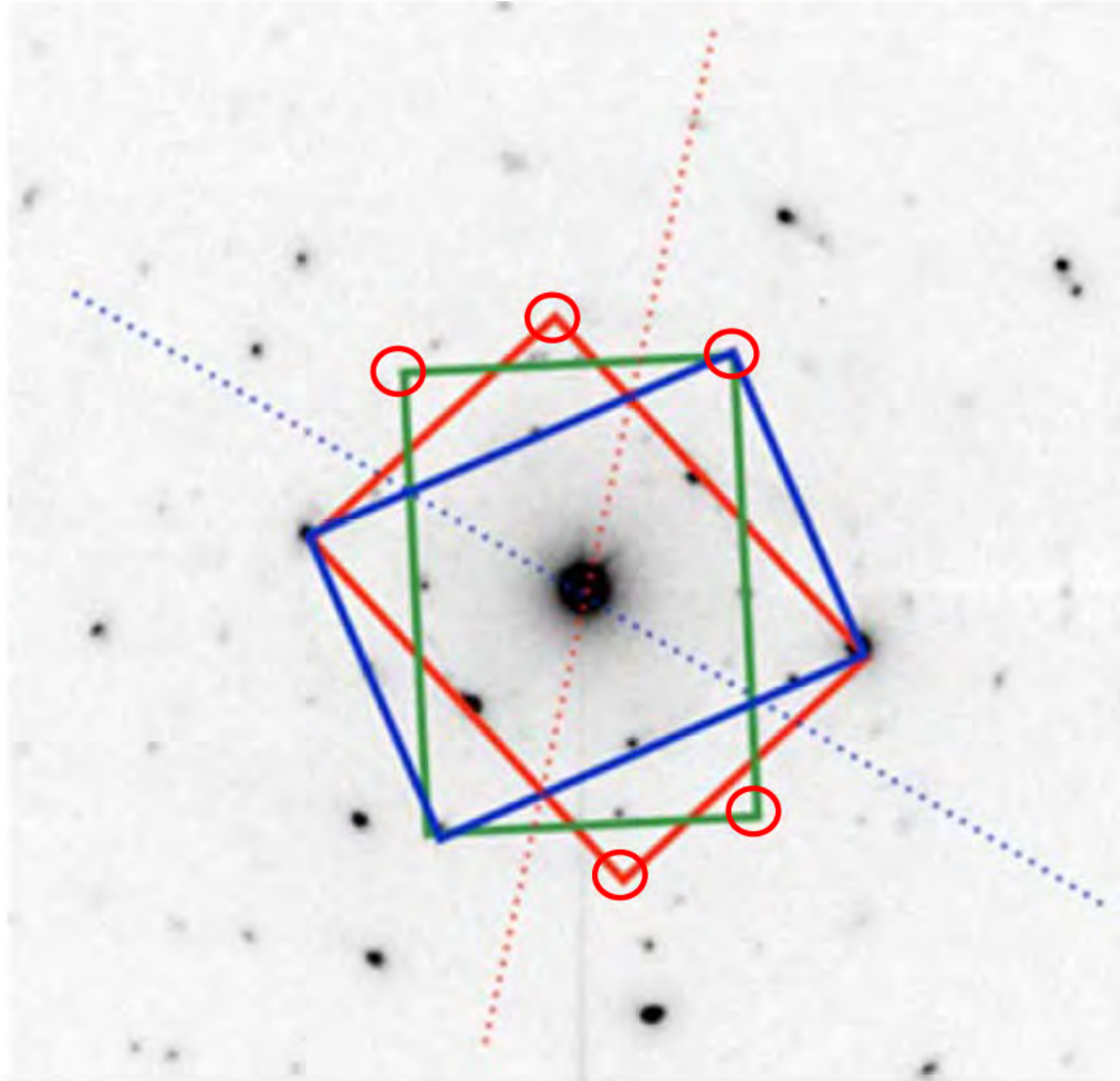


S2MMMC - Figure 79



S2MMMC - Figure 80

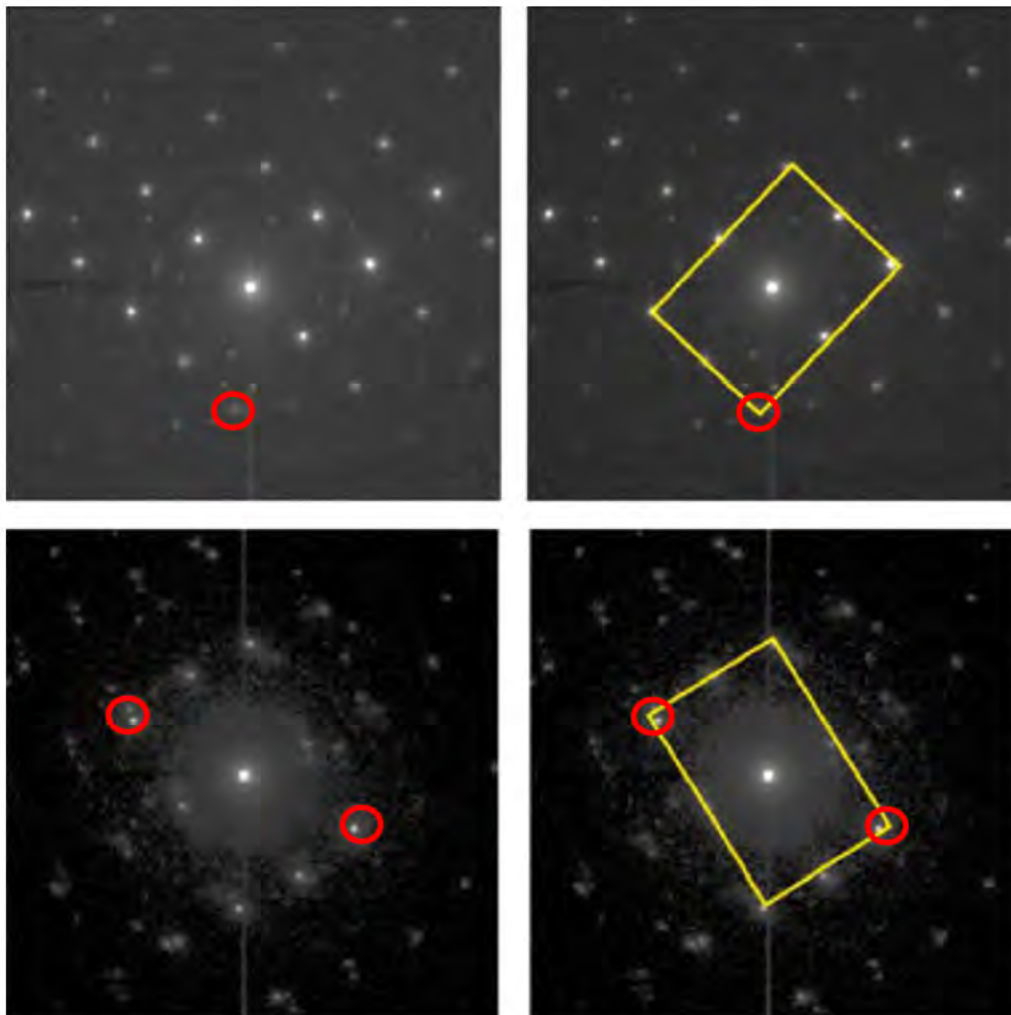
Red circles
added by Dr.
Stach to
indicate spots
that are not
clearly
discernable or
not present.



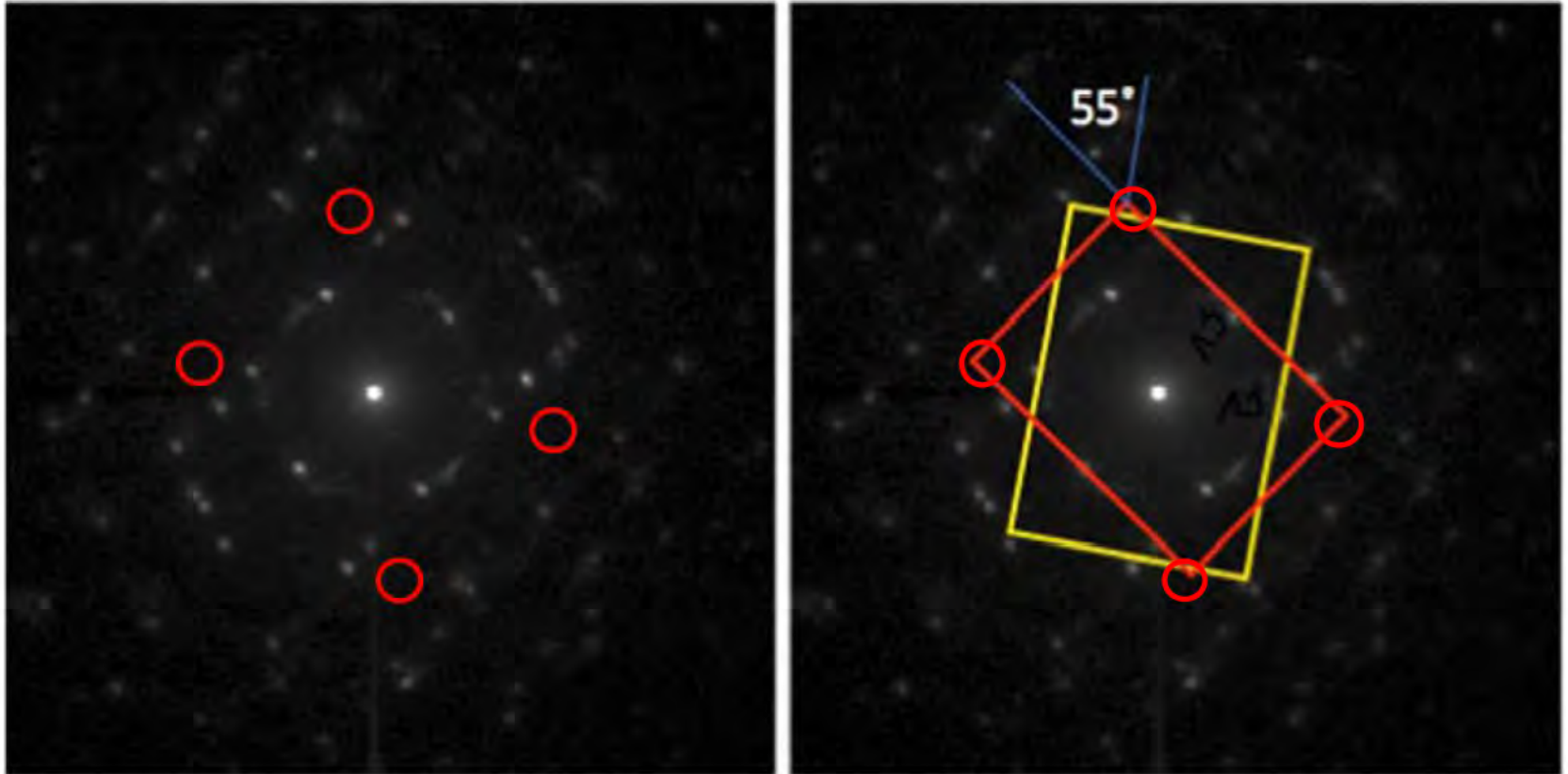
SBR8DK - Figure 107

Red circles added by Dr. Stach to indicate spots that are not clearly discernable or not present.

The lack of alignment with the box corners and nearby spots are significant enough to indicate that this interpretation is incorrect.

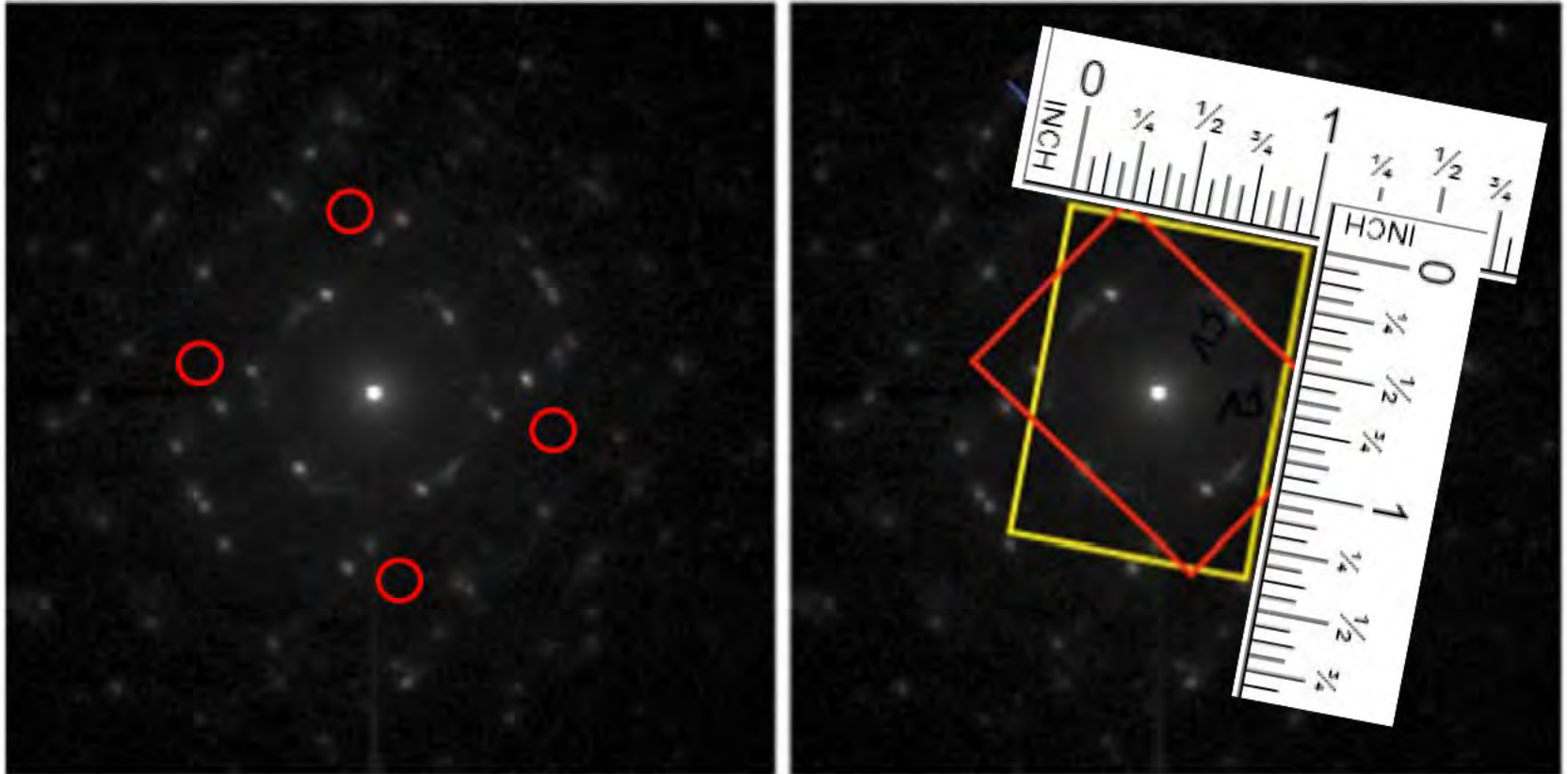


SBR8DK - Figure 108



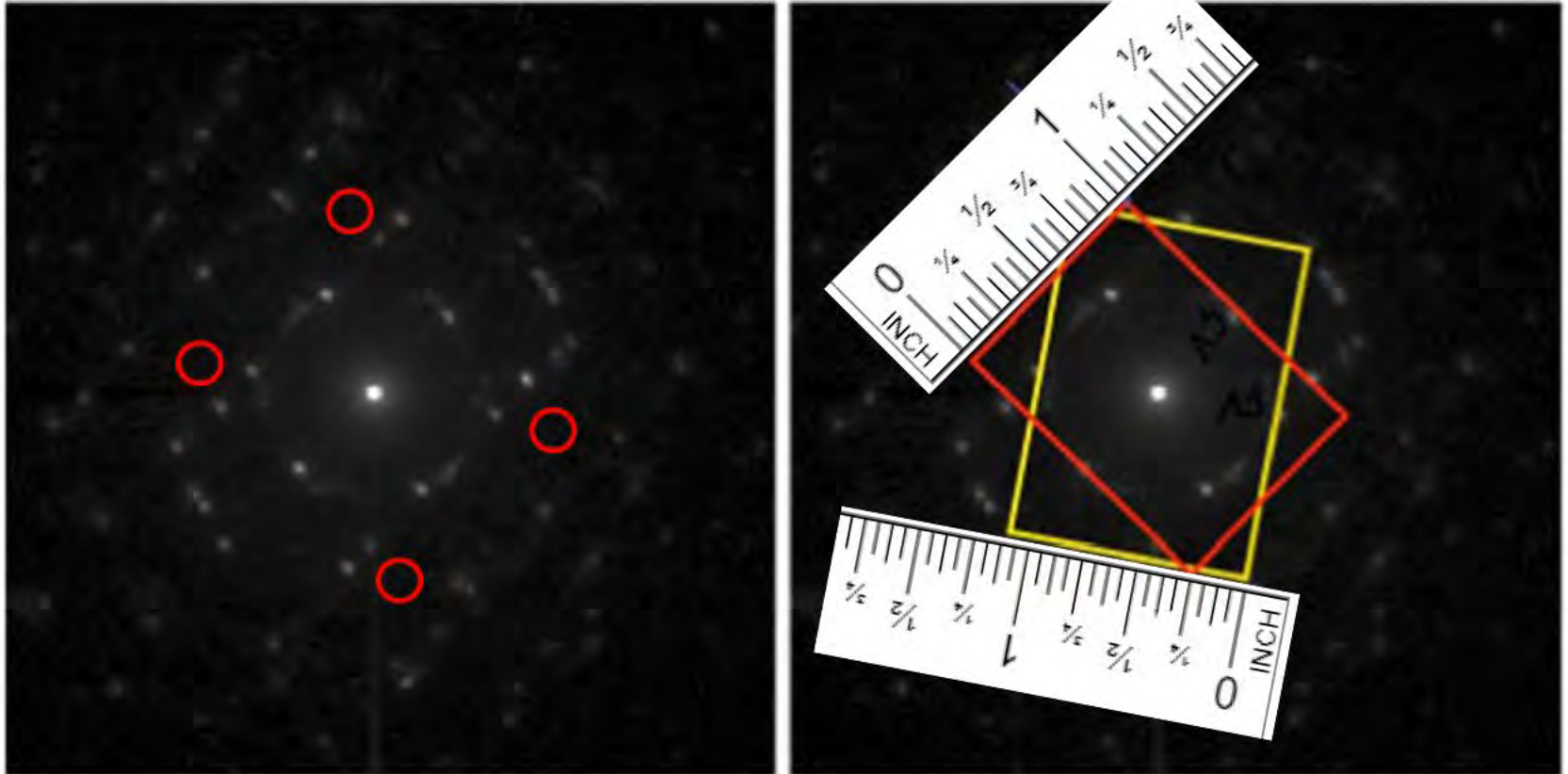
Red circles added by Dr. Stach to indicate spots that are not clearly discernable or not present. This interpretation is clearly incorrect.

SBR8DK - Figure 108



Ratio = 1:1.375

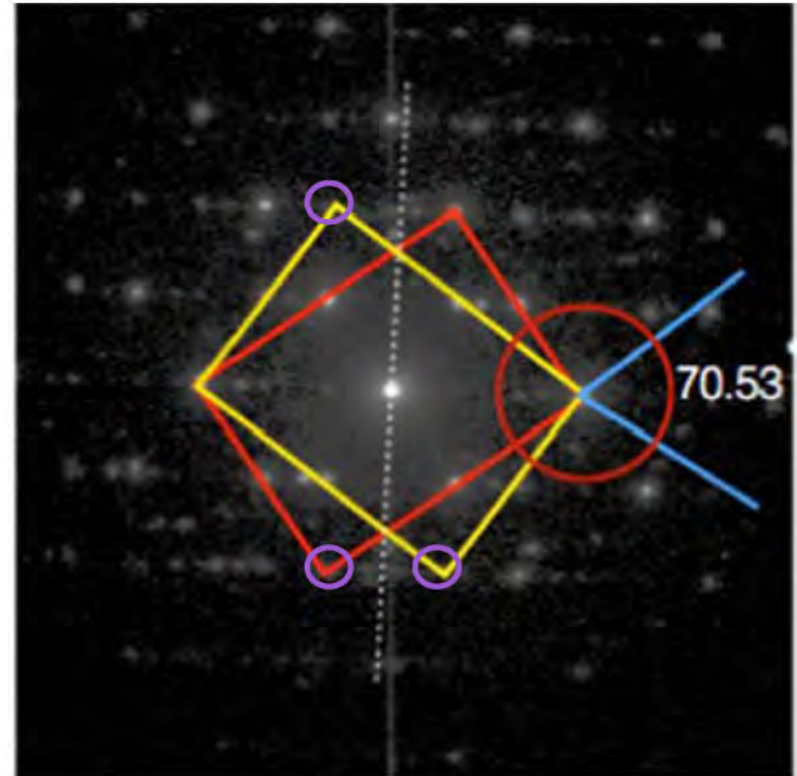
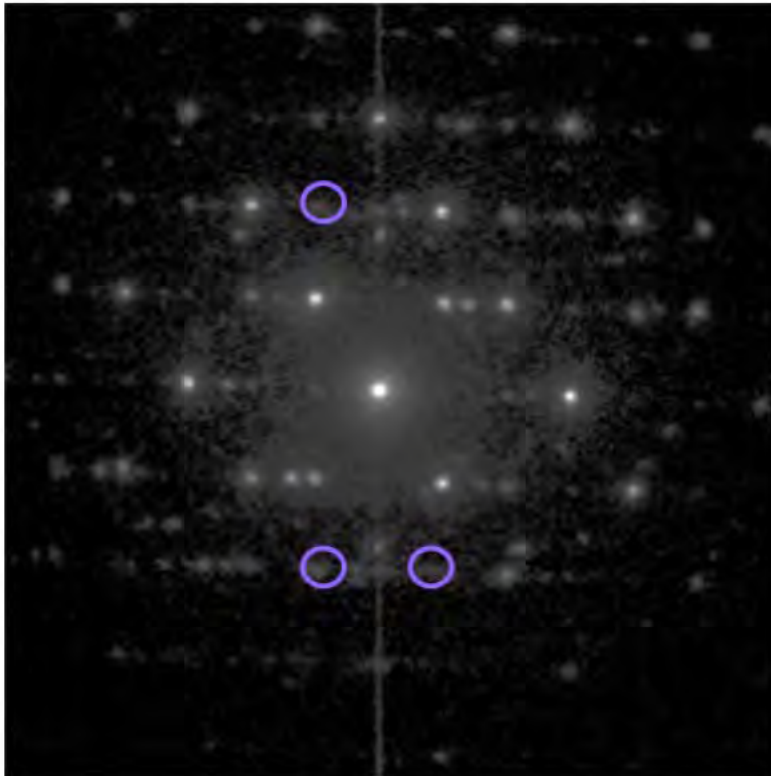
SBR8DK - Figure 108



Short side of red rectangle = 1 inch

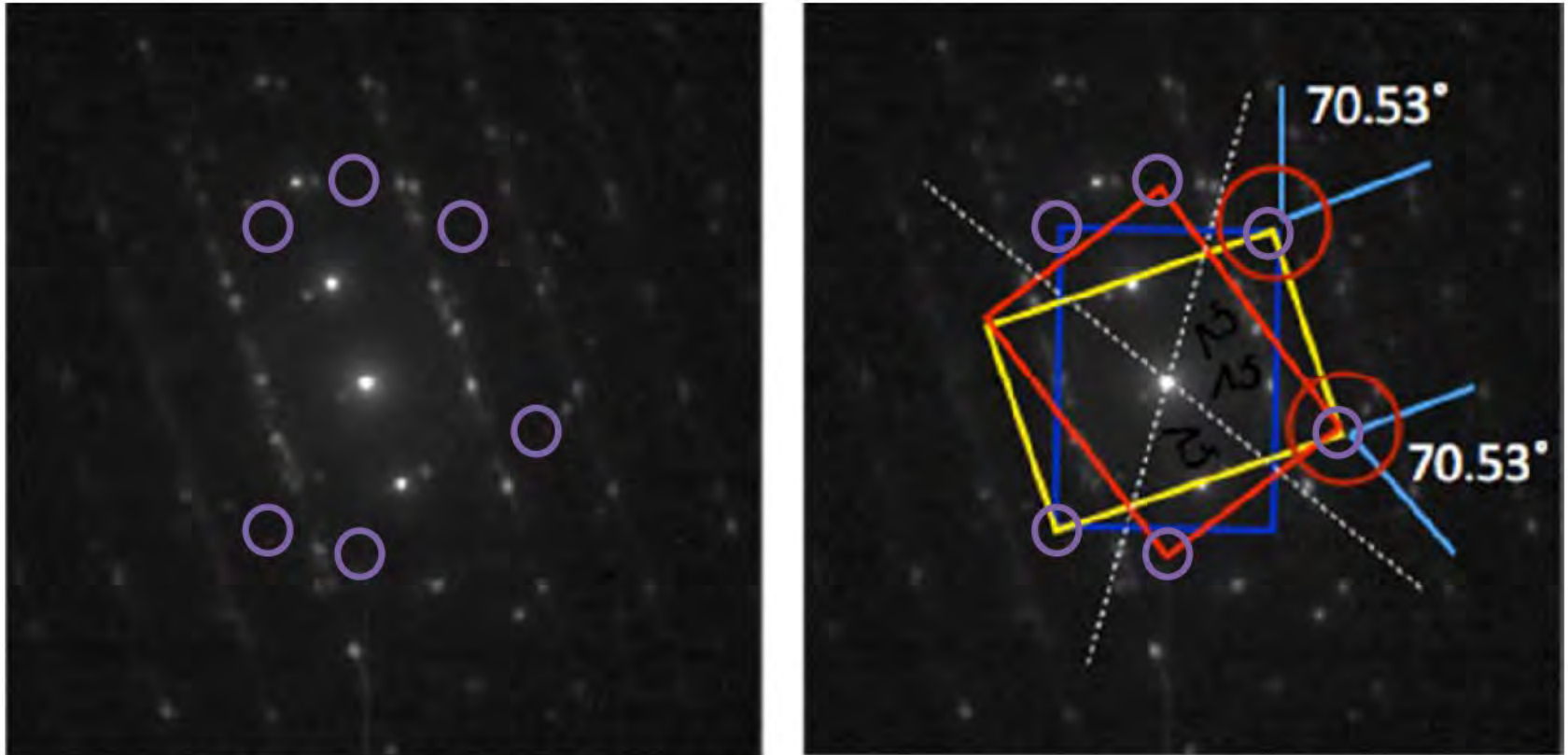
Short side of yellow rectangle = 1.12 inches

SBR8DK - Figure 109



Purple circles added by Dr. Stach to indicate spots that are weak, not clearly discernable or not present.

SBR8DK - Figure 110



Purple circles added by Dr. Stach to indicate spots that are not clearly discernable or not present. The blue box in particular has no match with any spot data.

EXHIBIT F

In Dr. Coffey's report he fits the area fraction distribution to a sinusoidal function of the form:

$$A \sin^2(\theta + \Delta) + B \cos^2(\theta + \Delta) \quad (1)$$

where θ is the in-plane angle relative to a direction in the write head, Δ is an offset angle, and A and B are fitting parameters. This sinusoidal function can be written equivalently as

$$(A - B) \sin^2(\theta + \Delta) + \text{constant} \quad (2)$$

In Dr. Coffey's report he then weights the $E_{110}(\theta)$ energy function by the area fraction distribution function. For the $E_{110}(\theta)$ energy function Dr. Coffey uses the Chikazumi Equation assuming $K_2=0$:

$$E_{110}(\theta) = K_1 \left(\frac{1}{4} \sin^4(\theta) + \sin^2(\theta) \cos^4(\theta) \right) \quad (3)$$

where K_1 is the first-order cubic anisotropy constant and θ is the in-plane angle measured from the [001] direction within the (110) plane. Using these equations an average magneto-crystalline anisotropy can be calculated by making the (very simplified) assumption that one can add the anisotropy of various grains at different angles weighted by their relative area. This can be done by integrating the $E_{110}(\theta)$ energy function (Eq. 3) weighted by the area distribution function (Eq. 2, ignoring the constant term):

$$\begin{aligned} \langle E(\theta) \rangle_{\text{Coffey}} &= \frac{\int_0^{180} E_{110}(\theta - \psi) (A - B) \sin^2(\psi + \Delta) d\psi}{\int_0^{180} \sin^2(\psi + \Delta) d\psi} \\ &= \frac{-K_1(A - B)}{8} \sin^2(\theta + \Delta) + \text{constant} \end{aligned} \quad (4)$$

where $\langle E(\theta) \rangle_{\text{Coffey}}$ is the average anisotropy energy density function using Dr. Coffey's approach. The result in Eq. 4 is a uniaxial \sin^2 function for the anisotropy energy density function.

Thus, using Dr. Coffey's methodology, any data that is forced to take the sinusoidal form of Eq. 1 ($A \neq B$) will always yield a uniaxial anisotropy energy density function. For example, I generated a **random distribution of numbers** from 1.0–2.0 to represent the area fractions every 10 degrees. These randomly generated numbers are represented by the red dots in Fig. 1. Applying the least square fit to the data proposed by Dr. Coffey (Eq. 2) results in a 'best fit' shown by the blue sinusoid in Fig. 1. Since the best fit results in a finite (A-B) value, this best fit, when used as an input to averaging the Chikazumi Equation, will output uniaxial anisotropy.

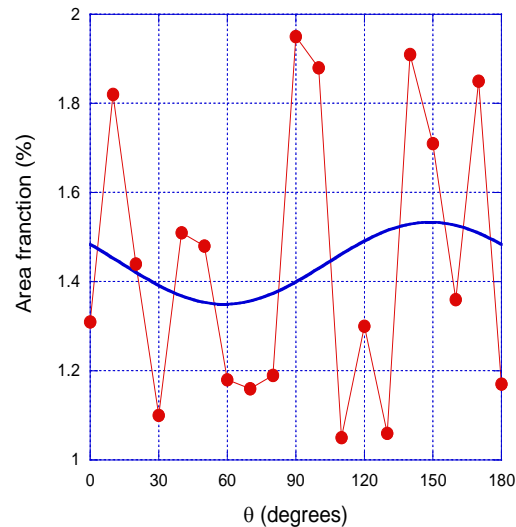


Figure 1 showing random area fractions with values between 1 and 2 percent. The blue line is a least square fit of the data to Eq. 2. The fit results are (A-B)=0.184, $\Delta=121.4$ degrees and constant=1.349.

The resulting uniaxial anisotropy is shown in Fig. 2 (in blue). Thus, using the methodology proposed by Dr. Coffey—*i.e.*, forcing Dr. Clark’s dark field image data to fit a sinusoidal function of the form of Eq. 1—yields a uniaxial anisotropy curve *even for randomly generated data*. In other words, applying Dr. Coffey’s method always results in a uniaxial energy density function of the form given in Eq. 4—even for randomly generated data.

